

EDITOR'S PICK 2021: HIGHLIGHTS IN CELL GROWTH AND DIVISION

EDITED BY: Philipp Kaldis

PUBLISHED IN: Frontiers in Cell and Developmental Biology



frontiers

Frontiers eBook Copyright Statement

The copyright in the text of individual articles in this eBook is the property of their respective authors or their respective institutions or funders. The copyright in graphics and images within each article may be subject to copyright of other parties. In both cases this is subject to a license granted to Frontiers.

The compilation of articles constituting this eBook is the property of Frontiers.

Each article within this eBook, and the eBook itself, are published under the most recent version of the Creative Commons CC-BY licence.

The version current at the date of publication of this eBook is CC-BY 4.0. If the CC-BY licence is updated, the licence granted by Frontiers is automatically updated to the new version.

When exercising any right under the CC-BY licence, Frontiers must be attributed as the original publisher of the article or eBook, as applicable.

Authors have the responsibility of ensuring that any graphics or other materials which are the property of others may be included in the CC-BY licence, but this should be checked before relying on the CC-BY licence to reproduce those materials. Any copyright notices relating to those materials must be complied with.

Copyright and source acknowledgement notices may not be removed and must be displayed in any copy, derivative work or partial copy which includes the elements in question.

All copyright, and all rights therein, are protected by national and international copyright laws. The above represents a summary only. For further information please read Frontiers' Conditions for Website Use and Copyright Statement, and the applicable CC-BY licence.

ISSN 1664-8714

ISBN 978-2-88976-805-9

DOI 10.3389/978-2-88976-805-9

About Frontiers

Frontiers is more than just an open-access publisher of scholarly articles: it is a pioneering approach to the world of academia, radically improving the way scholarly research is managed. The grand vision of Frontiers is a world where all people have an equal opportunity to seek, share and generate knowledge. Frontiers provides immediate and permanent online open access to all its publications, but this alone is not enough to realize our grand goals.

Frontiers Journal Series

The Frontiers Journal Series is a multi-tier and interdisciplinary set of open-access, online journals, promising a paradigm shift from the current review, selection and dissemination processes in academic publishing. All Frontiers journals are driven by researchers for researchers; therefore, they constitute a service to the scholarly community. At the same time, the Frontiers Journal Series operates on a revolutionary invention, the tiered publishing system, initially addressing specific communities of scholars, and gradually climbing up to broader public understanding, thus serving the interests of the lay society, too.

Dedication to Quality

Each Frontiers article is a landmark of the highest quality, thanks to genuinely collaborative interactions between authors and review editors, who include some of the world's best academicians. Research must be certified by peers before entering a stream of knowledge that may eventually reach the public - and shape society; therefore, Frontiers only applies the most rigorous and unbiased reviews.

Frontiers revolutionizes research publishing by freely delivering the most outstanding research, evaluated with no bias from both the academic and social point of view. By applying the most advanced information technologies, Frontiers is catapulting scholarly publishing into a new generation.

What are Frontiers Research Topics?

Frontiers Research Topics are very popular trademarks of the Frontiers Journals Series: they are collections of at least ten articles, all centered on a particular subject. With their unique mix of varied contributions from Original Research to Review Articles, Frontiers Research Topics unify the most influential researchers, the latest key findings and historical advances in a hot research area! Find out more on how to host your own Frontiers Research Topic or contribute to one as an author by contacting the Frontiers Editorial Office: frontiersin.org/about/contact

EDITOR'S PICK 2021: HIGHLIGHTS IN CELL GROWTH AND DIVISION

Topic Editor:

Philipp Kaldis, Lund University, Sweden

Citation: Kaldis, P., ed. (2022). Editor's Pick 2021: Highlights in Cell Growth and Division. Lausanne: Frontiers Media SA. doi: 10.3389/978-2-88976-805-9

Table of Contents

- 05 Editorial: Editor's Pick 2021: Highlights in Cell Growth and Division**
Philipp Kaldis
- 06 New Biological Insights on X and Y Chromosome-Bearing Spermatozoa**
Md Saidur Rahman and Myung-Geol Pang
- 25 Fzr/Cdh1 Promotes the Differentiation of Neural Stem Cell Lineages in Drosophila**
Phuong Thao Ly and Hongyan Wang
- 37 Human Derived Immortalized Dermal Papilla Cells With a Constant Expression of Testosterone Receptor**
Tomokazu Fukuda, Kouhei Takahashi, Shin Takase, Ai Orimoto, Takahiro Eitsuka, Kiyotaka Nakagawa and Tohru Kiyono
- 53 STAT3 Regulates Mouse Neural Progenitor Proliferation and Differentiation by Promoting Mitochondrial Metabolism**
Yixun Su, Wenjun Zhang, C. Pawan K. Patro, Jing Zhao, Tianhao Mu, Zhongnan Ma, Jianqiang Xu, Kenneth Ban, Chenju Yi and Yi Zhou
- 69 An Engineered Mouse to Identify Proliferating Cells and Their Derivatives**
Jihyun Jang, Kurt A. Engleka, Feiyan Liu, Li Li, Guang Song, Jonathan A. Epstein, and Deqiang Li
- 78 Dusp4 Contributes to Anesthesia Neurotoxicity via Mediated Neural Differentiation in Primates**
Jia Yan, Jingjie Li, Yanyong Cheng, Ying Zhang, Zhenning Zhou, Lei Zhang and Hong Jiang
- 86 Citicoline Protects Auditory Hair Cells Against Neomycin-Induced Damage**
Zhenhua Zhong, Xiaolong Fu, He Li, Jie Chen, Maohua Wang, Song Gao, Liyan Zhang, Cheng Cheng, Yuan Zhang, Peipei Li, Shasha Zhang, Xiaoyun Qian, Yilai Shu, Renjie Chai, and Xia Gao
- 101 Functional Versatility of the CDK Inhibitor p57^{Kip2}**
Justine Creff and Arnaud Besson
- 116 The Origins and Roles of Methylthiolated Cytokinins: Evidence From Among Life Kingdoms**
Maya Gibb, Anna B. Kisiala, Erin N. Morrison and R. J. Neil Emery
- 130 TULP2, a New RNA-Binding Protein, Is Required for Mouse Spermatid Differentiation and Male Fertility**
Meimei Zheng, Xu Chen, Yiqiang Cui, Wen Li, Haiqian Dai, Qiuling Yue, Hao Zhang, Ying Zheng, Xuejiang Guo and Hui Zhu
- 143 The Regulatory Role of Oxygen Metabolism in Exercise-Induced Cardiomyocyte Regeneration**
Bing Bo, Shuangshuang Li, Ke Zhou, and Jianshe Wei

160 *FOXC1 Negatively Regulates DKK1 Expression to Promote Gastric Cancer Cell Proliferation Through Activation of Wnt Signaling Pathway*

Jiang Jiang, Jianfang Li, Weiwu Yao, Wenfang Wang, Bowen Shi, Fei Yuan, Jingyan Dong and Huan Zhang

174 *Stepwise Induction of Inner Ear Hair Cells From Mouse Embryonic Fibroblasts via Mesenchymal- to-Epithelial Transition and Formation of Otic Epithelial Cells*

Qiong Yang, Haosong Shi, Yizhou Quan, Qianqian Chen, Wang Li, Li Wang, Yonghui Wang, Zhongzhong Ji, Shan-Kai Yin, Hai-Bo Shi, Huiming Xu and Wei-Qiang Gao



Editorial: Editor's Pick 2021: Highlights in Cell Growth and Division

Philipp Kaldis *

Department of Clinical Sciences, Lund University, Clinical Research Centre (CRC), Malmö, Sweden

Keywords: cell biology, developmental biology, cell growth, cell division, metabolism, neural development

Editorial on the Research Topic

Editor's Pick 2021: Highlights in Cell Growth and Division

The section “Cell Growth and Division” of Frontiers in Cell and Developmental Biology was started 6 years ago with the aim to capture exciting research in the broadest possible term of cell and developmental biology. This section has come a long way and after publishing approximately 900 manuscript, it is well established.

For the year 2021, we decided to launch a “research topic” named “*Editor's Pick 2021: Highlights in Cell Growth and Division*” to highlight some of the exciting manuscript that were published. The goal was to capture and highlight some of the exciting manuscripts, which reflect this section's goals in the broadest sense. Therefore, you should not be surprised to find topics like neural (stem cell) differentiation (Ly and Wang; Yan et al.), spermatogenesis (Rahman and Pang; Zheng et al.), hair development (Fukuda et al.), neural development (Su et al.), genetic mouse engineering (Jang et al.), hearing loss (Zhong et al.; Yang et al.), cell cycle (Creff and Besson; Jang et al.; Ly and Wang), cytokinins (Gibb et al.), gastric cancer (Jiang et al.), cardiomyocyte regeneration (Bo et al.), and metabolism (Su et al.; Bo et al.). Although all these topics are exciting and are well reflected in our section, we seek manuscripts also in other emerging research fields that are connected to cell and developmental biology.

I would like to thank all the authors of the manuscripts of the research topic “*Editor's Pick 2021: Highlights in Cell Growth and Division*” for their contribution to science, to their research field, and to our section. At the same time, I should highlight the efforts of all the associate editors and review editors without whom we could not run a successful journal.

Since we have now started a new year, I am looking forward to a lot of exciting research and hope that some of it will be published in our section.

OPEN ACCESS

Edited and reviewed by:

Song-Tao Liu,
University of Toledo, United States

*Correspondence:

Philipp Kaldis
philipp.kaldis@med.lu.se

Specialty section:

This article was submitted to
Cell Growth and Division,
a section of the journal
Frontiers in Cell and Developmental
Biology

Received: 21 January 2022

Accepted: 03 February 2022

Published: 07 March 2022

Citation:

Kaldis P (2022) Editorial: Editor's Pick
2021: Highlights in Cell Growth
and Division.
Front. Cell Dev. Biol. 10:859568.
doi: 10.3389/fcell.2022.859568

AUTHOR CONTRIBUTIONS

The author confirms being the sole contributor of this work and has approved it for publication.

Conflict of Interest: The author declares that the research was conducted in the absence of any commercial or financial relationships that could be construed as a potential conflict of interest.

Publisher's Note: All claims expressed in this article are solely those of the authors and do not necessarily represent those of their affiliated organizations, or those of the publisher, the editors and the reviewers. Any product that may be evaluated in this article, or claim that may be made by its manufacturer, is not guaranteed or endorsed by the publisher.

Copyright © 2022 Kaldis. This is an open-access article distributed under the terms of the Creative Commons Attribution License (CC BY). The use, distribution or reproduction in other forums is permitted, provided the original author(s) and the copyright owner(s) are credited and that the original publication in this journal is cited, in accordance with accepted academic practice. No use, distribution or reproduction is permitted which does not comply with these terms.



New Biological Insights on X and Y Chromosome-Bearing Spermatozoa

Md Saidur Rahman and Myung-Geol Pang*

Department of Animal Science and Technology and BET Research Institute, Chung-Ang University, Anseong, South Korea

OPEN ACCESS

Edited by:

Eiman Aleem,
University of Arizona, United States

Reviewed by:

Masayuki Shimada,
Hiroshima University, Japan
Alfonso Gutierrez Adan,
Instituto Nacional de Investigación y
Tecnología Agraria y Alimentaria
(INIA), Spain
George Seidel,
Colorado State University,
United States

*Correspondence:

Myung-Geol Pang
mgpang@cau.ac.kr

Specialty section:

This article was submitted to
Cell Growth and Division,
a section of the journal
Frontiers in Cell and Developmental
Biology

Received: 16 October 2019

Accepted: 23 December 2019

Published: 21 January 2020

Citation:

Rahman MS and Pang M-G
(2020) New Biological Insights on X
and Y Chromosome-Bearing
Spermatozoa.
Front. Cell Dev. Biol. 7:388.
doi: 10.3389/fcell.2019.00388

A spermatozoon is a male germ cell capable of fertilizing an oocyte and carries genetic information for determining the sex of the offspring. It comprises autosomes and an X (X spermatozoa) or a Y chromosome (Y spermatozoa). The origin and maturation of both X and Y spermatozoa are the same, however, certain differences may exist. Previous studies proposed a substantial difference between X and Y spermatozoa, however, recent studies suggest negligible or no differences between these spermatozoa with respect to ratio, shape and size, motility and swimming pattern, strength, electric charge, pH, stress response, and aneuploidy. The only difference between X and Y spermatozoa lies in their DNA content. Moreover, recent proteomic and genomic studies have identified a set of proteins and genes that are differentially expressed between X and Y spermatozoa. Therefore, the difference in DNA content might be responsible for the differential expression of certain genes and proteins between these cells. In this review, we have compiled our present knowledge to compare X and Y spermatozoa with respect to their structural, functional, and molecular features. In addition, we have highlighted several areas that could be explored in future studies in this field.

Keywords: X spermatozoa, Y spermatozoa, sperm function, proteome, genome

INTRODUCTION

A spermatozoon is a male reproductive cell that is produced in testis by highly orchestrated processes called spermatogenesis and spermiogenesis. During spermatogenesis, undifferentiated spermatogonia (stem cells) transform into type A₁ spermatogonia (differentiated cells). Eventually, by the process of several mitotic cell divisions, type A₁ spermatogonia become type B spermatogonia (Leblond and Clermont, 1952; Oakberg, 1956). Type B spermatogonia subsequently undergo a final round of mitosis to form the primary spermatocytes (only two cells are shown) that further proceed to meiosis (**Figure 1**). Through the first meiotic cell division, the primary spermatocyte yields two secondary spermatocytes, which then enter the second meiotic division and divides into four round spermatids that contain either the X or Y chromosomes (Leblond and Clermont, 1952). Finally, the haploid round spermatids differentiate to elongated spermatids and ultimately into spermatozoa by the process of spermiogenesis (Hendriksen, 1999). During this entire process, the spermatogenic cells migrate from the basement membrane toward the center of the seminiferous tubule and released into the lumen. It has been reported that cytokinesis is not complete during mitotic and meiotic divisions of these processes (Hendriksen, 1999). As shown in **Figure 1**, spermatogenic cells from the same type of A₁ spermatogonium form a syncytium and are connected by intercellular bridges that persist until the end of spermatogenesis (Braun et al., 1989). This intercellular bridge permits free cytoplasmic communication among the cells with different genotypes. Because ions

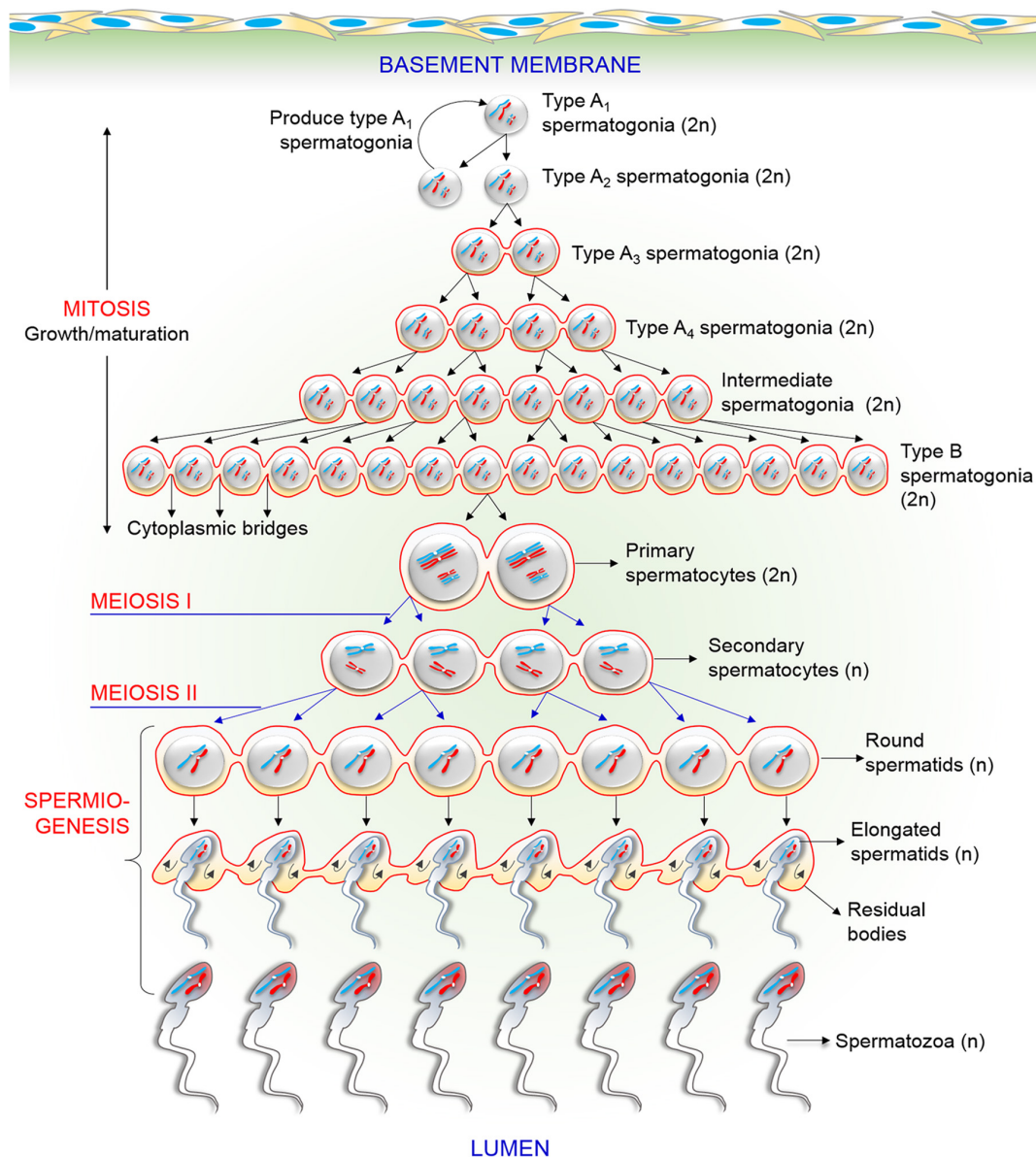


FIGURE 1 | Schematic drawing of the process of various events in male germ cells during spermatogenesis and spermiogenesis. The figure particularly displays the existence of intercellular bridges among spermatogenic cells. Each generation of cells is connected by intercellular bridges, thus, it divides synchronously in cohorts. See the main text for a detailed description.

and molecules (including genes and proteins) readily pass through these intercellular bridges, each cell containing either X or Y chromosome are matured synchronously (Braun et al., 1989; Jasin and Zalamea, 1992). Therefore, the origin, maturation, and functions of both X and Y chromosome-bearing spermatozoa are mostly identical.

Subsequently mature spermatozoa are released in semen during ejaculation, and is capable of fertilizing an oocyte, followed by contributing half of the genetic material to the offspring (Clapham, 2013; Rahman et al., 2013). Based on the chromosomal content, spermatozoa are of two types, that is, those bearing the X chromosome (X spermatozoa) and Y chromosome

(Y spermatozoa) (Shettles, 1960; Gellatly, 2009). If the X spermatozoon combines with the mother's X chromosome, the resulting offspring is a baby girl (XX), whereas if Y spermatozoon fertilizes the mother's oocyte, the resulting offspring is a baby boy (Gellatly, 2009). Certain preliminary studies reported several morphological differences between the X and Y spermatozoa using phase-contrast microscopy (Shettles, 1960; Cui and Matthews, 1993; Cui, 1997); however, most of the recent studies indicate that no major differences exist between the two sperm types (Hossain et al., 2001; You et al., 2017) except their DNA content. The discrepancy in these results, from the early and recent studies, is presumably due to relatively non-specific

methods used by the early investigators to differentiate between the X and Y spermatozoa (Hossain et al., 2001). Therefore, to understand the real differences between the two sperm types, a thorough discussion of both cells needs to be emphasized. In the present review, we summarized the existing scientific evidence to compare the X and Y spermatozoa considering their morphophysiological and molecular characteristics. In addition, we have highlighted the proteomics and genomics aspects of both cells, and investigated their clinical significance, in order to predict whether this difference could explain the occurrence of particular diseases in a sex-specific-manner.

SEARCH SCHEME AND ARTICLE SELECTION

PubMed search engine was used to thoroughly search the MEDLINE database for literature on X and/or Y spermatozoa using the following search terms: ratio, shape, size, gender selection, motility, swimming pattern, velocity, CASA, FISH, flow cytometric analysis, Percoll gradient, albumin gradient, swim-up method, viability, electrophobicity, electronegativity, pH tolerance, surface properties, Y-specific antigen, HY antigen, stress response, oxidative stress, endocrine disruptors, pesticide exposure, environmental toxicants, heat stress, DNA damage, chromosomal abnormality, aneuploidy, XX aneuploidy, XY aneuploidy, YY aneuploidy, proteomics, disease, gender-specific disease, and genomics. Full-text articles and abstracts in English language on X and Y spermatozoa published before December, 2019, were included in the review after screening their content. All article types such as original articles, reviews, letter to the editor, editorials, opinions, and debates were included in the review. Retracted papers were excluded by thoroughly checking the corresponding journal websites.

MORPHOPHYSIOLOGICAL CHARACTERISTICS OF X AND Y SPERMATOZOA

A mature mammalian spermatozoon comprises three distinct parts, namely, head, mid-piece, and tail (containing genetic material, mitochondria, and axial filament, respectively). Due to their unique organization, spermatozoa are different from the other cells. In this section, we will compare X and Y spermatozoa based on their morphological and physiological characteristics.

Ratio

During mammalian spermatogenesis, meiosis produces 50:50 ratio of X and Y spermatozoa according to Mendelian segregation. Therefore, the natural sex ratio during spermatogenesis is expected to be 1:1 (Umehara et al., 2019). An intensive literature search produced three major findings on the ratio of X and Y spermatozoa: (1) proportion of X spermatozoa was higher than that of Y spermatozoa (Martin et al., 1983; Bibbins et al., 1988), (2) proportion of Y spermatozoa was higher than that of X spermatozoa

(Landrum and Shettles, 1960; Shettles, 1960; Quinlivan and Sullivan, 1974), and (3) no difference existed in the proportion of the two sperm types (Van Kooij and Van Oost, 1992; Goldman et al., 1993; Han et al., 1993a).

It has been reported that an uncharacterized (unidentified) gene controlled the ratio of X and Y spermatozoa such that men with more brothers had a higher probability of having sons and those with more sisters had a higher probability of having daughters (Gellatly, 2009); however, these findings are mostly hypothetical, and presence of such a gene has not yet been confirmed. Moreover, a non-significant increase of Y spermatozoa in men with only sons (>3) or the X spermatozoa in men with only daughters (>3) has been reported in another investigation (Irving et al., 1999). Several previous studies from 1970 to 1980 suggested that paternal age differentially affected the ratio of X and Y spermatozoa, thus altering the secondary sex ratio of the offspring in a particular population (Erickson, 1976; James and Rostron, 1985; Ruder, 1985). Nevertheless, this finding was also proven to be imprecise by other contemporaries (Curtis et al., 1983; Martin et al., 1995a,b). Apart from the debate, it has been reported that an active gene transcription occurs selectively in the chromosomes (including sex chromosomes) of haploid round spermatids (Hu and Namekawa, 2015). Therefore, if the composition of sex chromosomes has changed due to the post-meiotic modifications in the gene expression and differential survival of spermatozoa during epididymal maturation, these may affect the expected ratio (Bean, 1990). In a recent study, Umehara et al. (2019) reported that ligand activation of Toll-like receptors 7/8 (TLR7/8), selectively encoded by the X chromosome, significantly suppress the motility of X spermatozoa without altering their ability of fertilization. This procedure allows producing over 90% of the male embryos following *in vitro* fertilization using ligand-selected highly motile spermatozoa. In another study using knockout (KO) mice model, Rathje et al. (2019) reported that partial deletions of the Y chromosome (Yqdel) in males produce an equal number of X and Y spermatozoa. Although both sperm types are equally capable of fertilizing oocytes once at the site of fertilization, they exhibit a functional (motility and morphology) difference from each other that potentially skewed offspring sex ratio. Consistent with these findings, Kruger et al. (2019) also showed that complete deletion of the X-linked Slx1 gene produced more male offspring by regulating post-meiotic germ cells transition (round spermatids to elongated spermatids).

An increased incidence of Y aneuploidy in spermatozoa was reported in another study, which selectively eliminated the Y spermatozoa and increased the proportion of X spermatozoa in mice and humans (Chaudhary et al., 2014). In accordance with this finding, we also reported that the viability of human Y spermatozoa is lower than that of X presumably due to the increased expression of apoptotic proteins in the live Y cells under stressful conditions, *in vitro*, thus, subsequently leading to shifts in the Y-to-X ratio (You et al., 2017). These findings indicate that functional properties of X and Y spermatozoa differ under certain *in vivo/in vitro* conditions due to the transcription of specific genes in particular cell types subsequently leading to the altered sex ratio at birth. Therefore, several factors, particularly

TABLE 1 | Summary of the ratio of mammalian X and Y spermatozoa.

| References | Species (spermatozoa) | Cells analyzed | Methods | Outcome measure | Hybridization efficacy | X:Y |
|---------------------------|------------------------------------|----------------|---|--|------------------------|--------------|
| Han et al., 1993b | Human (21–45 years) | 813,066 | Multicolor FISH | Fluorescence microscopy | NM | 1.07:1 |
| | Mouse (6–8 weeks) | 10,390 | | | | 1.24: 1 |
| Eisenberg et al., 2012 | Human | NM | Multicolor FISH | Epifluorescence microscopy (Zeiss Axiophot) | NM | 1:1.06 |
| | Oligospermic man | | | | | 1:1.03 |
| Smith et al., 2004 | Human (cryopreserved) | ~1000 | Multicolor FISH | Epifluorescence microscopy (Zeiss Axiophot) | 99 | ~1:1 |
| Hossain et al., 2001 | Human | 3300 | Multicolor FISH | Fluorescence microscopy | >98 | ~1:1 |
| Recio et al., 2001 | Human (18–47 years) | 9944–10,250 | Multicolor FISH | Epifluorescence microscopy (Zeiss Axiophot) | 99 | 1:1.03 |
| Szyda et al., 2000 | Bull | 2122 | | | | 1.15: 1 |
| Irving et al., 1999 | Man with only sons (>3) | NM | Multicolor FISH | Leitz Laborlux Ploemopak fluorescence microscopy | NM | 1.102:1 (NS) |
| | Man with only daughters (>3) | | | | | 1:1.17 (NS) |
| Hassanane et al., 1999 | Bull | >10,000 | Multicolor FISH | Fluorescence microscopy | NM | ~1:1 |
| Chandler et al., 1998 | Bull | ~100,000 | PCR | UV/VIS spectrophotometer | | 1≠1 |
| Halder and Tutschek, 1998 | Human | 4506 | Multicolor FISH | Epifluorescence microscopy (Zeiss Axiophot) | | 1.18:1 |
| Samura et al., 1997 | Human | >6000 | Multicolor FISH and Percoll separation | Epifluorescence microscopy (Zeiss Axiophot) | 99.8 | ~1:1.02 |
| | | | Multicolor FISH and swim-up/glass wool method | | | ~1:1 |
| Martin et al., 1996 | Human (21–52 years) | ~5000 | Multicolor FISH | Epifluorescence microscopy (Zeiss Axiophot) | | 1.02:1 |
| Griffin et al., 1996 | Human | >300,000 | Multicolor FISH | Epifluorescence microscopy (Zeiss Axiophot) | NM | ~1:1 |
| Spriggs et al., 1996 | Human (27–39 years) | 50,000 | Multicolor FISH | Epifluorescence microscopy (Zeiss Axiophot) | 98 | X Y |
| Chevret et al., 1995 | Human | 94,575 | Multicolor FISH and Percoll separation | Epifluorescence microscopy (Zeiss Axiophot) | NM | 1.03:1 |
| Martin et al., 1995a | Human (21–52 years) | >10,000 | Multicolor FISH | Epifluorescence microscopy (Zeiss Axiophot) | NM | 1.02:1 |
| Martin et al., 1995b | Lymphoma patient (human, 32 years) | >10,000 | Multicolor FISH | Epifluorescence microscopy (Zeiss Axiophot) | | ~1:1 |
| Williams et al., 1993 | Human | 2544–3860 | Multicolor FISH | Epifluorescence microscopy (Zeiss Axiophot) | 99 | 1:1.01 |
| Cui and Matthews, 1993 | Human | 233 | PCR | Direct microscopy | 93.1 | 1.06:1 |
| Lobel et al., 1993 | Human | | qPCR | | | ~1:1 |
| Goldman et al., 1993 | Human | 60,000 | Multicolor FISH | | | ~1:1 |
| Han et al., 1993a | Human | ~1263 | Multicolor FISH | Epifluorescence microscopy (Leitz microscope) | | ~1:1 |
| Benet et al., 1992 | Human | 505 | Leishman staining | Analyzing zona-free hamster oocytes | | 1.02:1 |

FISH, fluorescence in situ hybridization; NM, not mentioned; qPCR, real-time polymerase chain reaction; NS, non-significant.

genetic and environmental factors or both may differentially affect the ratio of X and Y spermatozoa by making one sperm type more sensitive to the external stress than that of the other. The ratio of X and Y spermatozoa in several animal species along with the methods used for differentiating between the two sperm types are summarized in **Table 1**. For some responses, there is a significant difference in means, but the difference is so small as to be of little or no biological significance because the distributions

overlap almost completely. This overlap, for example, is so great as to make the mean difference useless for sexing sperm.

Shape and Size

Despite the immense advancement in the field of developmental biology research, the basic idea of the spermatozoal structure remains unclear. As such, it is also unclear whether X and Y spermatozoa vary in their shape and size. By direct microscopic

examination, two distinct types of spermatozoa: one type with a small, round head (presumably Y spermatozoa) and other type with a comparatively larger, elongated head (presumably X spermatozoa) were proposed by the early studies (Shettles, 1960, 1961). Both X and Y spermatozoa possess identical autosomes and an X or a Y chromosome. Thus, the difference in the size of X and Y spermatozoa may be due to the variations between X and Y chromosomes. Nevertheless, several researchers have suggested that the size of a sperm is not exclusively associated with its chromosomal content and may also be associated with its cytoplasmic content, which may vary in a specific sperm population during spermatogenesis (Shannon and Handel, 1993; Lankenau et al., 1994; Cui, 1997). In addition, Hossain et al. (2001) suggested that variations in the cytoplasmic content of X and Y spermatozoa introduced by meiosis and/or spermatogenesis were greater than those introduced by the sex chromosomes itself.

Although the preliminary hypothesis that X and Y spermatozoa were different based on their size and shape (Shettles, 1960, 1961) was supported by other researchers (Cui and Matthews, 1993; Cui, 1997), they were refuted with forceful arguments by the findings of several recent studies that used more specific methods for differentiating between X and Y spermatozoa (Hossain et al., 2001; Grant, 2006; Zavaczki et al., 2006). In an important study, Carvalho et al. (2013) used atomic force microscopy (AFM) and demonstrated that no differences existed in the shape and size of bovine X and Y spermatozoa even though 23 structural features between X and Y spermatozoa were assessed. AFM is highly specific as it provides detailed three-dimensional information of cells and is suitable for imaging the cell surface. Therefore, it is tempting to speculate that no

or non-significant differences exist in the shape and size of X and Y spermatozoa. Previous studies mostly used non-specific comparative methods such as identification of Barr bodies and F bodies, which have low sensitivity in differentiating between X and Y spermatozoa, thus making the findings of these studies (i.e., X spermatozoa are larger than Y spermatozoa) less reliable. The findings of different studies on the shape and size of X and Y spermatozoa are summarized in **Table 2**.

Motility and Swimming Pattern

Owing to the high demand of sex preselection in animal reproduction, several studies have attempted to differentiate between X and Y spermatozoa over the past decades. Several researchers have used different methods to evaluate sex selection based on sperm motility; however, the efficacy of these methods is debatable. Additionally, it is unclear whether Y spermatozoa move faster than X spermatozoa. As an example, if Y spermatozoa move faster than X spermatozoa, a man should have a son, with an almost zero chance of having a daughter. Spermatozoa start swimming during the epididymal transition (Chang, 1951). Human spermatozoa travel at the rate of up to 3000 $\mu\text{m}/\text{min}$ (Smith and Braun, 2012); however, some spermatozoa move slowly at the rate of 1000/min. Thus, a 55 μm long spermatozoon efficiently covers 1000–3000 μm . During this journey, the morphology and chemotaxis of spermatozoa and ionic factors, protein phosphorylation (especially tyrosine), ATP, cyclic adenosine monophosphate, protein kinase-A (PKA), enzymatic factors, seminal plasma factors, and calcium ions present in spermatozoa play a dynamic role in keeping the spermatozoa motile (Kwon et al., 2014b; Rahman et al., 2017b, 2018). Simultaneously, certain fascinating physiological

TABLE 2 | Findings of several studies on the size and shape of X and Y spermatozoa of human and domestic animals.

| References | Spermatozoa | Cells analyzed | Parameters | Enrichment technique(s) | Outcome measured | Main findings |
|--|---|----------------|--|---|---------------------------|---------------|
| Carvalho et al., 2013 | Nellore bull | 400 | Sperm head shape and size | Flow cytometry | Atomic force microscopy | No difference |
| Zavaczki et al., 2006 | Healthy, oligozoospermic, and normozoospermic man | >2000 | Sperm head, perimeter, long and short axis, long or short axis, and tail length. | FISH | Phase-contrast microscopy | No difference |
| Hossain et al., 2001 | Human | 3300 | Head length and width and tail length | FISH | Fluorescence microscopy | No difference |
| Van Munster et al., 1999 | Bull | 520 | Cell size and diameter | | | No difference |
| Geraedts, 1997 | Human | >1298 | Sperm head volume | Flow cytometry | DIC microscopy | X > Y |
| Cui, 1997 | Human | NM | Sperm surface | Feulgen staining of the Y chromosome | Fluorescence microscopy | X (7%) > Y |
| Cui, 1997 | Human | 895 | Length, head perimeter, and length of the neck and tail | PCR identification of the Y chromosome | Light microscopy | X > Y |
| Cui and Matthews, 1993 | | 217 | | | | |
| Chandler et al., 1998 | Hereford bull | 2214 | Head areas | | DIC microscopy | X > Y |
| Landrum and Shettles, 1960; Shettles, 1960 | Human | NM | Head size and nuclear morphology | Dried unstained sperm observed directly | Phase-contrast microscopy | X > Y |

FISH, fluorescence in situ hybridization; DIC, differential interference contrast; NM, not mentioned.

processes such as capacitation and the acrosome reaction occur in spermatozoa (Visconti, 2009; Battistone et al., 2013; Rahman et al., 2017b). The difference in the ability of the X or Y spermatozoon to respond to these factors and processes will make it more active and motile than the other sperm type. Human X spermatozoa comprises 2.8% more genetic material (DNA) than Y spermatozoa; this difference is 3–4.2% between the X and Y spermatozoa of domestic livestock (Hendriksen et al., 1996). Several researchers have concluded that the variation in DNA content between X and Y spermatozoa may affect their motility and swimming pattern (Johnson et al., 1989; Johnson, 1994), however, the results of these studies are not conclusive.

Ericsson et al. (1973) used albumin gradient method and demonstrated that human Y spermatozoa (stained with quinacrine fluorochrome) reached the bottom of the gradient before X spermatozoa. These researches claimed that their method could identify >85% Y spermatozoa, of which 90–95% were motile. This finding was the first evidence of the difference in the swimming behavior of X and Y spermatozoa. The albumin gradient method has several advantages over other sperm sex preselection (methods for sperm selection along with their reliability status have been summarized in Table 3); however, detection of Y spermatozoa using quinacrine fluorochrome staining, as performed by Ericsson et al. (1973) was later proven to be non-specific (Flaherty and Matthews, 1996; Cui, 1997), thus leading to inappropriate results. In another study, Sarkar et al. (1984) reported that human X spermatozoa move slower (angular velocity decrease) than Y spermatozoa in the flow stream, however, the movement of both cells are similar in the stationary fluid.

The controversy regarding the motility of X and Y spermatozoa was mainly provoked in 1998, when Penfold and

coworker described their finding using flow cytometry and computer-assisted sperm analysis (CASA) for differentiating X and Y spermatozoa and measuring their motility parameters, respectively. They demonstrated that bull Y spermatozoa could not swim faster than X spermatozoa in a simple salt solution (Penfold et al., 1998). In accordance with the aforementioned findings, Alminana et al. (2014) reported a non-significant difference in the motility of X and Y spermatozoa. These findings indicate that no evidence is available that can help conclude whether Y spermatozoa are faster than X spermatozoa. This paradox becomes even more complex after considering the effect of oviductal fluid on the motility of X and Y spermatozoa (Zhu et al., 1994). In contrast, it has been confirmed that motility of X and Y spermatozoa vary under the certain condition *in vitro* (and presumably *in vivo*). For example, low pH, high temperature, and increased oxidative stress retarded motility in Y spermatozoa, whereas motility of X spermatozoa rapidly declined when spermatozoa are incubated in a high-pH condition (Shettles, 1970; Oyeyipo et al., 2017). In a recent study, Umehara et al. (2019) reported that ligand activation of TLR7/8 significantly decreased the motility of X spermatozoa (by altering ATP production) than that of Y. In addition, using the KO mice model, Rathje et al. (2019) reported that Yqdel males (XYRIIIqdel) produced less motile Y spermatozoa compared to X.

Viability

Sperm viability is the ability of spermatozoa to sustain an intact plasma membrane and acrosomal membrane and to survive during passage through the oviduct in order to reach and fertilize the egg. Shettles (1960) suggested that X spermatozoa were stronger and more robust than Y spermatozoa because they had higher DNA content than Y spermatozoa.

TABLE 3 | Acceptability of various methods for distinguishing between X and Y spermatozoa based on the difference in their motility, swimming pattern, and DNA content.

| References | Sample (spermatozoa) | Enrichment techniques | Base of separation | Target sperm | Sperm sorted (%) | Reliability |
|------------------------------|----------------------|---------------------------------|--|--------------|------------------|-------------|
| Erickson, 1976 | Human | Discontinuous albumin gradients | Y sperm has higher forward velocity than X sperm | Y | 85 | Unreliable |
| Evans et al., 1975 | | | | | 50 | Unreliable |
| Ross et al., 1975 | | | | | 50 | Unreliable |
| Quinlivan et al., 1982 | | | | | 52–74 | Unreliable |
| Brandriff et al., 1986 | | | | | 50 | Unreliable |
| Ueda and Yanagimachi, 1987 | | | | | 36.0–59.1 | Unreliable |
| Iizuka et al., 1987 | Human | Percoll gradients | Different motility of X and Y sperms | X | 94 | Unreliable |
| Wang et al., 1994 | | | | | 55.1 | Unreliable |
| Van Kooij and Van Oost, 1992 | | | | | 50 | Unreliable |
| Check et al., 1989 | Human | Swim-up method | Difference in swimming pattern | X | 81 | Unreliable |
| Han et al., 1993b | | | | X | 50 | Unreliable |
| Lobel et al., 1993 | | | | X | 41.9–56.7 | Unreliable |
| Yan et al., 2006 | | | | X and Y | 50 | Unreliable |
| Johnson et al., 1993 | Human | Flow cytometry | Difference in DNA mass | X and Y | X = 80, X = 75 | Reliable |
| Johnson, 2000 | Livestock | | | | X = 90 | Reliable |
| Umehara et al., 2019 | Mice | Swim-up method | TLR7/8 ligand activation | | Y = 90 X = 81 | Reliable |

This preliminary hypothesis is supported by other investigators (Cui and Matthews, 1993; Flaherty and Matthews, 1996; Carvalho et al., 2013). Carvalho et al. (2013) reported that in addition to higher DNA content, larger size and longer length of the X chromosome made X spermatozoa more viable than Y spermatozoa. Recently, we demonstrated that when spermatozoa were incubated at different temperatures/culture conditions (You et al., 2017) or in a media containing 2,3,7,8-tetrachlorodibenzo-p-dioxin (an endocrine disruptor) (You et al., 2018), the Y spermatozoa represent a compromised viability compared to X. Moreover, the similar effects of other endocrine disruptors, such as dibromochloropropane and diazinon (Diaz) on the viability of Y spermatozoa were reported in another study (Song et al., 2018). The decreased viability of Y spermatozoa was mostly associated with the increased expression of apoptotic proteins in live Y spermatozoa (You et al., 2017), which subsequently affects the overall lifespan (You et al., 2018).

In particular, viability of spermatozoa is also related to female investment. The environment in the female reproductive tract (mostly fluid composition, pH and ionic concentration, and transcriptomic responses) affects the viability of X and Y spermatozoa and helps in selecting the best spermatozoa for fertilization (Dominko and First, 1997; Holt and Fazeli, 2010). Van Dyk et al. (2001) performed *in vitro* experiments mimicking the *in vivo* setting in the female reproductive tract and reported that Y spermatozoa survived for a longer duration than X spermatozoa, and that Y spermatozoa were more proficient to bind with zona pellucida than X spermatozoa (binding ratio, Y:X = 1.15:1.02). Other studies have suggested that higher expression of certain proteins (such as those involved in energy metabolism, e.g., ATP synthase subunit) provides more energy to Y spermatozoa, thus increasing their viability (Chayko and Martin-Deleon, 1992; Aranha and Martin-Deleon, 1995; Hendriksen, 1999; Chen et al., 2012). Based on the aforementioned findings, two different hypotheses can be drawn: (1) due to higher DNA content, X spermatozoa are more stable/viable than Y spermatozoa at least in the *in vitro* condition or (2) certain properties of Y cells may ensure that their prolonged viability in the female reproductive tract (*in vivo*) subsequently affects the lifespan of both cells in a distinct manner.

Electrophobicity

Identification of subtle differences between X and Y spermatozoa is the only way to assess the preselection of a baby's sex. Various studies have attempted to identify the difference in the electrical charge between X and Y spermatozoa. Epididymal epithelium secretes sialic acid (glycoprotein) that provides a net negative surface charge to the spermatozoa (Hoffmann and Killian, 1981). The difference in cell surface charge between the two sperm types is due to the difference in their exposed sialic acid content (Kaneko et al., 1984). These findings suggest that X and Y spermatozoa may exhibit differences in their electrophobicity. Results of free-flow electrophoresis indicated that the electrophoretic mobility of human X spermatozoa was higher than that of Y spermatozoa, suggesting that X spermatozoa exhibited higher negative charge than Y spermatozoa (Kaneko et al., 1984; Kaneko et al., 1993).

In contrast, Engelmann et al. (1988) reported that human spermatozoa differentiated into X and Y fractions as they moved toward the anode, with the faster-moving and slower-moving fractions mainly comprising Y and X spermatozoa, respectively. The findings of Engelmann et al. (1988) were supported by those of another research group that used bovine spermatozoa (Blottner et al., 1994). The major limitation of these studies was the use of non-specific and unreliable quinacrine fluorescent staining to identify Y spermatozoa (F bodies) (Windsor et al., 1993), which led to inappropriate results. Recently, Ainsworth et al. (2011) observed that the use of CS-10 electrophoretic sperm isolation device did not skew the ratio of X and Y spermatozoa after their PCR-based differentiation. In particular, the device only isolated functional spermatozoa but was unable to specify their genotype. Thus, the movement of spermatozoa toward the anode might mainly depend on their surface sialic acid content, which allows them to comigrate with other spermatozoa during electrophoresis. Therefore, the findings of Ainsworth et al. (2011) clarified the unclear findings of the previous studies that reported a considerable difference in X and Y spermatozoa based on their electrophobicity.

pH Susceptibility

Mammalian spermatozoa are immotile in the testis and become motile in response to several external factors that are initiated during their transfer through the epididymis. Of these factors, ionic concentration, particularly pH, plays an integral role in regulating the functional maturation of the spermatozoa. During sperm storage in the cauda epididymis, a slightly acidic pH is maintained. In the domestic animals, this acidic pH in the cauda epididymis inhibits sperm motility (Hamamah and Gatti, 1998). The association between pH and sperm functions becomes more complicated once the spermatozoa are released into the female reproductive tract. An equilibrium is required between the pH of the medium/female reproductive tract and intracellular pH of spermatozoa for successful fertilization (Blomqvist et al., 2006). In this section, we will discuss whether X and Y spermatozoa present differential pH susceptibility.

The preliminary findings indicated that X spermatozoa are larger and stronger than Y spermatozoa, suggesting that they are more stable in an acidic pH than Y spermatozoa (Landrum and Shettles, 1960; Shettles, 1960). Limited studies have supported this preliminary hypothesis. Muehleis and Long (1976) reported that insemination of an ovulated female rabbit with semen diluted with buffers of pH 5.4, 6.9, and 9.6 produced 48, 63, and 49% male offspring, respectively. This result partly supports Shettles' hypothesis, which states that acidic pH (5.4) has deleterious effects on Y spermatozoa, thus affecting the probability (low probability of 48%) of conceiving male offspring; however, it is unclear whether an alkaline pH of 9.6 decreased the percentage (49%) of male offspring conceived particularly in comparison with the spermatozoa diluted with a buffer at pH 6.9. Pratt et al. (1987) reported a significant negative correlation between the vaginal pH and percentage of male offspring conceived in golden hamsters. Diasio and Glass (1971) reported that human X and Y spermatozoa could not be differentiated based on their pH affinity during their passage through a capillary tube containing

media of varying pH. By examining 58489 human spermatozoa, recently we demonstrated that incubation of human spermatozoa in different pH conditions, including 6.5, 7.5, and 8.5 for 0–5 days were incapable in altering the ratio of Y:X chromosome (You et al., 2017). Thus, majority of the recent findings do not provide any logical explanation for X and Y spermatozoa acting differently at various pH conditions.

Surface Properties (HY Antigen)

HY antigen is a male tissue-specific antigen. It is a fundamental part of the membrane of most male cells and is a specific antigen that controls the Y sperm-specific genes (Ohno and Wachtel, 1978). Here, we report evidence for the hypothesis that X and Y spermatozoa can be differentiated based on their surface HY antigen content.

Since the identification of a Y-linked histocompatibility antigen, scientists have believed that an immunological approach can be considered to control the sex ratio in mammals. This was initially demonstrated in a study by Bennett and Boyse (1973). They reported that the sex ratio of male offspring is significantly decreased (45.4%) when the female mice are inseminated with the spermatozoa treated with an anti-HY antibody compared with the untreated spermatozoa (53.4%). This study supported the hypothesis that the HY antigen could be used to distinguish between the X and Y spermatozoa; however, a minor shift in the male sex ratio after insemination with spermatozoa treated with the anti-HY antibody indicated only a small difference in the concentration of HY antigen between the two sperm types. Krco and Goldberg (1976) performed a 2-step cytotoxicity assay and identified the HY antigen in 8-celled mouse embryos, thus providing additional evidence of Y-chromosome expression of the HY antigen. Similar findings were obtained by other researchers by using several laboratory and domestic animal models (Silvers and Wachtel, 1977; Utsumi et al., 1993). Nevertheless, some researchers have found that the anti-HY antibody does not specifically bind to Y spermatozoa (Hoppe and Koo, 1984; Hendriksen et al., 1993; Sills et al., 1998). Sills et al. (1998) reported that the anti-HY antibody also binds to X spermatozoa and thus cannot be used to differentiate between X and Y spermatozoa. Besides, studies involving significant sex differentiation of human spermatozoa by using the surface antigen did not provide conclusive results (Jeulin et al., 1982; Sills et al., 1998).

MOLECULAR INSIGHTS OF X AND Y SPERMATOZOA

This section compares the molecular characteristics and biological activities of X and Y spermatozoa, with a special emphasis on the differences in their stress response, chromosomal abnormalities, and genomic/proteomic content.

Response to Stress

Several studies have examined the etiology of male infertility in the context of oxidative stress (Agarwal et al., 2014) and physical, environmental, and occupational stress (Aitken, 2014;

Barazani et al., 2014). Spermatozoa are the first cells that presented stress response (Gharagozloo and Aitken, 2011). In the MEDLINE database, the term “oxidative stress” has been mentioned in over 200,000 articles published between 2001 and to date, of which >1800 articles have focused on spermatozoa. Mechanisms underlying the response of X and Y spermatozoa during stress remain unclear. As X and Y spermatozoa differ in their genetic content, their response to stress may differs. Alminana et al. (2014) reported a non-significant difference while generating intracellular reactive oxygen species (ROS) by mitochondrial DNA in X and Y spermatozoa, and concluded that the tiny variations in DNA content between X and Y spermatozoa are unable to respond to stress differentially. A similar conclusion was drawn by other researchers (Ward and Coffey, 1991).

Mammalian spermatozoa cannot fertilize the oocyte before they are appropriately conditioned in the female reproductive tract even though they are motile and morphologically normal (Kwon et al., 2014b; Rahman et al., 2017b, 2019). Different parts of the female reproductive tract, such as the uterus, uterotubal junction, and oviduct, are specifically programmed to select only a functionally mature spermatozoon for fertilization (Holt and Fazeli, 2010). Once the spermatozoa reach the oviduct, they temporarily attach to the isthmus epithelium to undergo capacitation before ovulation (Rahman et al., 2015, 2016). Capacitation is a process during which complex molecular, biochemical, and physiological changes occur in spermatozoa in the female reproductive tract or in *in vitro* specialized media and is a prerequisite for fertilization (Salicioni et al., 2007; Visconti, 2012; Kwon et al., 2015). Therefore, preincubation of spermatozoa before fertilization is essential as capacitation duration might differ between X and Y spermatozoa depending on their genetic composition. Perez-Crespo et al. (2008) reported that mouse X and Y spermatozoa were differentially affected by elevated temperature. Moreover, they demonstrated that female mice mated with male mice that were exposed to scrotal heat stress on the day of mating produce more female pups. Altered sex ratio (i.e., increased number of female offspring) was also observed when the bovine spermatozoa incubated at 40°C for 4 h were used for insemination compared with those incubated at 38.5°C (Hendricks et al., 2009). Similarly, Lechniak et al. (2003) reported a significant increase in female blastocysts when bovine spermatozoa were preincubated for 24 h. In accordance with these findings, recently using an *in vitro* experimental design, we also demonstrated that human Y spermatozoa are more susceptible to stress than X *in vitro*, induced by variation of culture condition (You et al., 2017). In contrast, Iwata et al. (2008) reported that incubation of bovine spermatozoa with hyaluronic acid for 1 and 5 h produced 56.4 and 67.3% male embryos, respectively, thus skewing the expected 1:1 ratio. Therefore, it can be hypothesized that exposure of spermatozoa to external stress results in their differential survival; however, it is unclear whether stress provides selective survival advantage to X or Y sperms.

Recent studies have reported alterations in the sex ratio of human offspring exposed to increased levels of environmental chemicals, specifically endocrine-disrupting chemicals (EDs) (Van Larebeke et al., 2008; McDonald et al., 2014; Song et al., 2018; You et al., 2018). EDs interfere with the hormone

biosynthesis and metabolism and may affect cellular physiology and reproduction (Anway et al., 2005). Mocarelli et al. (2000) reported that an increase in the concentration of 2,3,7,8-tetrachlorodibenzo-*p*-dioxin (TCDD or dioxin) in the paternal serum elevated the probability of female births. Exposure of mice spermatozoa to TCDD *in vitro* also decreased the viability of Y spermatozoa (You et al., 2018), by potentially altering the embryonic male to female ratio. These findings were in accordance with another study (Ryan et al., 2002), where increased female births to men are documented following exposed to significantly high levels of TCDD. A similar effect of different EDs has been reported by several studies on humans and animals (Garry et al., 2002; Ikeda et al., 2005; Ishihara et al., 2007; Terrell et al., 2011). Despite few exceptions, for example, exposure to polychlorinated biphenyl was associated with an increase in the male births (Bonefeld-Jorgensen et al., 2001), the majority of the findings suggest that men exposed to a stressful environment are more likely to have girls (XX) than boys (XY) due to the higher DNA content in X spermatozoa than that in Y spermatozoa. Nevertheless, the particular stress response machineries between the two cell types remain unclear and need further investigation.

Difference in Chromosomal Content of X and Y Spermatozoa

Molecular characteristics of spermatozoa including the chromosomal content/abnormalities play a pivotal role in inducing infertility (Pang et al., 1999; Schmidt et al., 2000). Briefly, chromosomal abnormality is defined as the loss of or presence of an extra or irregular portion of a chromosome that results in atypical number of chromosomes or a structural abnormality in one or more chromosomes (Jurewicz et al., 2014). In general, chromosomal abnormalities in embryos are thought to be acquired from eggs (Hassold et al., 1996), however, these abnormalities in spermatozoa may also substantially affect the embryos (Tesarik and Mendoza, 1996; Bonduelle et al., 2002). Abnormalities in the sex chromosomes contribute to >5% of major chromosomal errors in embryos, with ~80% cases being of paternal origin (Hassold et al., 1996; Hassold and Hunt, 2001). In't Veld et al. (1995) and Hoegerman et al. (1995) were the first to report an increased risk of *de novo* chromosomal errors, particularly in the sex chromosomes, in spermatozoa. The frequency of sex chromosome aneuploidy in healthy human spermatozoa is 0.13–1.20% (Egozcue et al., 1997). Templado et al. (2005) reviewed 23 studies and found that the average sex chromosome disomy (presence of an extra chromosome in a haploid state) in human spermatozoa was 0.26%. Of the 23 chromosomes in human spermatozoa, chromosomes 13, 18, 21, X, and Y are important because higher incidence of abnormalities in these chromosomes can lead to miscarriages or live births (Pang et al., 1999, 2005, 2010; Rubio et al., 2001). In this section, we review the evidence of sex chromosome abnormalities or aneuploidy, which leads to male reproductive dysfunction.

A combination of recently developed FISH and multicolor chromosome-specific probes can be used to investigate the chromosomal content of spermatozoa in order to establish a relative aneuploidy rate (Chevret et al., 1995). A higher

percentage of sex chromosomal aneuploidy has been reported in oligoasthenoteratozoospermic patient spermatozoa compared to the autosomal aneuploidy in same individual, as well as sex chromosomal aneuploidy in healthy Y spermatozoa (Pang et al., 1999, 2010). In accordance with the aforementioned finding, Van Opstal et al. (1997) reported significantly higher errors in chromosomes X and Y than in chromosome 18 (autosome) in spermatozoa of azoospermic patients. In contrast, Pfeffer et al. (1999) reported higher incidence of chromosome 18 aneuploidy (0.7–10%) than sex chromosome aneuploidy (0–4.3%) in the swim-up sperm fraction of 10 infertile men with severe oligoasthenoteratozoospermia. Interestingly, the same study also reported higher sex chromosome aneuploidy, however, the aneuploidy was observed in the entire sperm pellet (Pfeffer et al., 1999). Therefore, different methods of sperm enrichment might also influence the incidence of aneuploidy.

Several studies have investigated the incidence of aneuploidy in X and Y chromosomes in human spermatozoa (Chevret et al., 1995; Martin et al., 1995a,b, 1996). Chevret et al. (1995) reported comparatively higher incidence of disomy in the X chromosome (0.04%) than that in the Y chromosome (0.009%) in normal male interphase spermatozoa, however, other studies have reported minute differences in the incidence of disomy in the X and Y chromosomes (Martin et al., 1995a,b; Samura et al., 1997). In contrast, Williams et al. (1993) reported higher incidence of disomy in the Y chromosome (YY, 0.11%) than that in the X chromosome (XX, 0.08%). This finding was further supported by another study that presented 0.18% (YY) and 0.07% (XX) disomy in the Y and X chromosomes, respectively (Martin et al., 1996). The difference between the reported aneuploidy rate in X and Y chromosomes remains unclear even though aneuploidy was detected using similar methods (i.e., 3-color FISH coupled with chromosome-specific probes and epifluorescence microscopy) in all the cases. Therefore, difference in the X and Y spermatozoa based on the frequency of aneuploidy in X and Y chromosomes remains unclear, which is in accordance with the other reported differences between these sperm types.

Recent studies have reported that exposure to certain EDs and pesticides induce sex chromosome abnormalities in spermatozoa (Smith et al., 2004; Xia et al., 2005; Perry, 2008). Epidemiological study revealed a significant association between exposure to two organochlorine chemicals and sex chromosome disomy in the spermatozoa collected from men who underwent infertility assessment at the Massachusetts General Hospital between January 2000 and May 2003 (Mcauliffe et al., 2012). They observed that higher serum levels of p,p'-dichlorodiphenyldichloroethylene (p,p'-DDE) significantly increased the frequency of XX (X sperm disomy), XY, and total sex chromosome disomy. Interestingly, men with higher serum levels of polychlorinated biphenyls (PCBs) presented a significant increase in the frequency of YY (Y sperm disomy), XY, and total sex chromosome disomy, however, this study did not provide further explanation of their findings, specifically on the mechanism by which the increased exposure to PCBs exerted protective effects against XX disomy and that in which the increased exposure to p,p'-DDE increased XX disomy. Therefore, possible mechanism(s) underlying the association

between exposure to toxic chemicals, including EDCs (for example PCBs and p, p'-DDE), and sex chromosome disomy should be investigated. Moreover, similar epidemiological studies are warranted to identify the effects of various environmental chemicals and their association with chromosomal aberrations in the spermatozoa.

Genomic and Proteomic Contents of X and Y Spermatozoa

Identification and quantification of genes/proteins in a cell provides fascinating insights regarding their cellular functions. Genomics deals with the structure, function, evolution, and mapping of genomes (Bader et al., 2003), whereas proteomics involves novel approaches for characterizing proteins by performing qualitative and quantitative analyses (Rahman et al., 2016, 2017a, 2018). A spermatozoon provides half of the nuclear genetic material to the diploid offspring via fertilization. Thus, examination of the genes and protein content in spermatozoa might provide potential insights on their functions. It has been reported that haploid spermatids are capable of active chromosomal (including sex chromosomes) transcription important for their growth and survival (Braun et al., 1989). As X and Y chromosome-bearing-spermatids express distinct genes encoded by each sex chromosome (Hendriksen, 1999), it might result in the proteomics difference between X and Y spermatozoa. Although the majority of the genes are shared between X and Y spermatids via the intracellular bridge (Braun et al., 1989), complete sharing has not occurred for all gene products (Hendriksen, 1999). Therefore, X and Y spermatozoa can be differentiated based on their gene/protein content. In this section, we review studies on the genomic and proteomic characteristics of X and Y spermatozoa and have elucidated their association with the morphophysiological characteristics of the two sperm types.

To date, very limited studies have identified and characterized genes that are differentially expressed in X and Y spermatozoa. Spermatozoa contain a minute amount of total RNA (human spermatozoon, 0.015 pg; bovine spermatozoon, 1.8×10^{-4} pg) compared to that in the somatic cells (1–3 pg). This small amount of RNA per spermatozoon is the major drawback for research on gene expression in these cells. Chen et al. (2014) used comprehensive genomic approaches and identified 31 differentially expressed genes in bovine X and Y spermatozoa (27 and 4 genes upregulated in X and Y spermatozoa, respectively). Using the RNA sequencing technology, it has been reported that the X chromosome encodes 492 genes, whereas the Y chromosome encodes only 15 genes in mouse spermatozoa. Some of these genes (particularly receptors) are also shown to be related to the growth, survivability, and functions of specific sperm types (Umehara et al., 2019). Therefore, differentially expressed genes might help in identifying the genetic background of stable differences between X and Y spermatozoa. Alminana et al. (2014) observed that spermatozoa revealed sex-specific gene expression in the oviduct of female pigs inseminated with either X or Y spermatozoa. When insemination was performed using Y spermatozoa, 271 transcripts were downregulated and 230

transcripts were upregulated in the oviduct. Thus, the oviduct might have special biological sensors for screening spermatozoa. Bermejo-Alvarez et al. (2010) reported significant differences in the mRNA levels of *GSTM3*, *DNMT3A*, and *PGRMC1* between bovine blastocysts produced by *in vitro* fertilization with X spermatozoa and those produced by *in vitro* fertilization with Y spermatozoa. This indicates that the oocyte might also regulate an identical mechanism for reorganizing the different spermatozoa. Recent advances in genomic studies have provided several improved techniques that allow complete lysis of spermatozoa and isolation of total RNA (Kirley, 1990; Meng and Feldman, 2010; Chen et al., 2014). Therefore, further studies are warranted to identify the genes expressed in the sexed spermatozoa of different species.

Mature spermatozoa undergo minimal transcription (there are few ribosomes, so translation is not possible) as well as protein synthesis (Kwon et al., 2014a, 2015). Therefore, these cells are extremely suitable for performing proteomic analysis. Direct comparison of protein levels in various cells can identify the markers responsible for differences between these cells (Park et al., 2013; Kwon et al., 2014a). Literature searches indicated that limited studies have been performed to evaluate the proteomic blueprint of X and Y spermatozoa to date. Hendriksen et al. (1996) reported a non-significant difference in the concentration of plasma membrane proteins in porcine X and Y spermatozoa. This study indicated that sexing of spermatozoa cannot be performed based on their surface properties. Chen et al. (2012) used two-dimensional electrophoresis along with mass spectrometry (2DE-MS/MS) and identified 42 differentially expressed proteins between X and Y spermatozoa. Of these, 11 proteins were upregulated and 4 were downregulated in X spermatozoa compared with those in the Y spermatozoa ($P < 0.05$). This finding was partly supported by other investigators (De Canio et al., 2014; Scott et al., 2018). Using label-free shotgun nUPLC-MS/MS De Canio et al. (2014) found that 15 and 2 proteins were upregulated in X and Y spermatozoa, respectively. In another recent study, Scott et al. (2018) identified the differential expression of eight proteins between X- and Y-bearing spermatozoa. Of these, the protein related to the embryo development (EF-hand domain-containing protein 1) was expressed abundantly in the Y spermatozoa, whereas majority of other detected proteins were abundant in the X spermatozoa. Since abundant proteins in Y spermatozoa help in post-fertilization embryo development and further in the survivability of male baby over female, which also support lightly higher males (105) than female (100) babies at birth. Despite differential expression of particular proteins between the two cell types, zinc ion binding structure of bovine heart cytochrome c (2EIN_R) is the only protein reported by Chen et al. (2012) with the characteristics unique expression in only X spermatozoa. Therefore, 2EIN_R could be considered as a novel biomarker for differentiating the two cell types/sex preselection purpose. In contrast, majority of these proteomics studies identified limited identical proteins despite the samples being collected from the same animal species (bull). Moreover, Chen et al. (2012) reported increased levels of tubulin isoforms $\alpha 3$ and $\beta 4B$ in X spermatozoa. In contrast, De Canio et al. (2014) reported different expression

TABLE 4 | List of differentially expressed proteins in X and Y chromosome bearing spermatozoa.

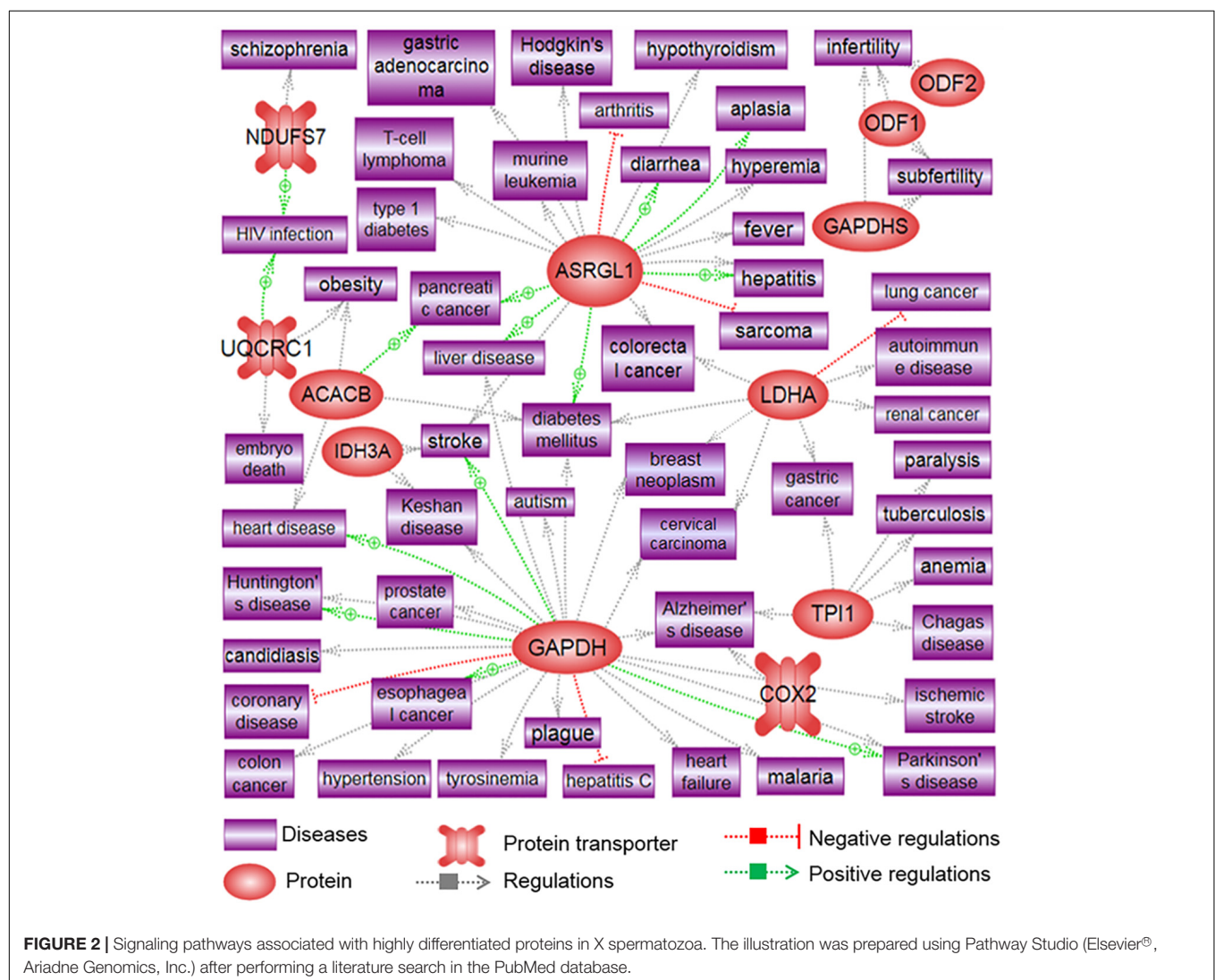
| Proteins (symbol) | Accession no | X/Y (intensity) | Proteomic technique | Related pathways ($P > 0.05$) | References |
|---|----------------|-----------------|---------------------|--|-----------------------|
| Upregulated proteins in X spermatozoa | | | | | |
| Seminal plasma protein PDC-109 (BSP1) | P02784 | 1.92 | nUPLC-MS/MS | | De Canio et al., 2014 |
| Glyceraldehyde 3-phosphate dehydrogenase (GAPDH) | P10096 | 1.69 | | Glucose metabolism, glycolysis | |
| Outer dense fiber protein 2 (ODF2) | Q2T9U2 | 1.63 | | | |
| Tubulin beta 4A (TUBB4A) | Q3ZBU7 | 1.58 | | | |
| L-Lactate dehydrogenase A (LDHA) | P19858 | 1.56 | | Glucose metabolism | |
| Outer dense fiber protein 1 (ODF1) | Q29438 | 1.53 | | | |
| A kinase anchor protein 3 (AKAP3) | Q77797 | 1.51 | | | |
| L-Asparaginase (ASRGL1) | Q32LE5 | 1.44 | | | |
| Tubulin beta 4B (TUBB4B) | Q3MHM5 | 1.42 | | | |
| Tubulin alpha 3 (TUBA3E) | Q32KN8 | 1.42 | | | |
| Outer dense fiber protein 3 (ODF3) | Q2TBH0 | 1.42 | | | |
| Glyceraldehyde 3-phosphate dehydrogenase, testis specific (GAPDHS) | Q2KJE5 | 1.40 | | Glucose metabolism | |
| Sperm acrosome membrane associated protein 1 (SPACA1) | Q2YDG7 | 1.36 | | | |
| Triosephosphate isomerase (TPI1) | Q5E956 | 1.36 | | Glucose metabolism, mTOR signaling | |
| Calmodulin (CALM) | P62157 | 1.36 | | | |
| FUN14 domain-containing protein 2 (FUNDC2) | NP_776763 | 2.612 | SWATH-MS | | Scott et al., 2018 |
| Acetyl-CoA carboxylase, type beta (ACACB) | CAI84638 | 2.149 | | | |
| NADH dehydrogenase [ubiquinone] iron-sulfur protein 7, mitochondrial (NDUFS7) | NP_001033111 | 1.502 | | | |
| Sorting and assembly machinery component 50 homolog (SAMM50) | NP_001040088 | 1.491 | | | |
| Cytochrome c oxidase subunit 2 (COX2) | QBH99117.1 | 1.399 | | mTOR signaling, TCA cycle, oxidative phosphorylation | |
| Protein FAN | NP_001179158 | 2.72 | MALDI-TOF-MS | | Chen et al., 2012 |
| Oxidase heme a, cytochrome | 771727A | 1.71 | | | |
| Cytochrome b-c1 complex subunit 1, mitochondrial (UQCRC1) | P31800 | 2.17 | | mTOR signaling, TCA cycle, oxidative phosphorylation | |
| 3-Hydroxyisobutyrate dehydrogenase (HIBADH) | AAI05544 | 1.58 | | | |
| Tubulin alpha-3 chain (TUBA3) | Q32KN8 | 1.68 | | | |
| Isocitrate dehydrogenase [NAD] subunit alpha, mitochondrial (IDH3A) | P41563 | 1.83 | | | |
| Chain A, the structure of crystalline profilin-beta-actin | 2BTF_A | 1.69 | | | |
| A Chain A, episelection: Novel Ki ~ nanomolar inhibitors of serine proteases | 1BTW_A | 1.8 | LC-MS | | |
| R Chain R, zinc ion binding structure of bovine heart cytochrome c | 2EIN_R | Only in X | | | |
| Tubulin beta-4B chain (TUBB4B) | NP_001029835 | 1.51 | | | |
| Isocitrate dehydrogenase 3 (NAD ⁺) alpha (IDH3A) | AAI18260 | 1.50 | | | |
| Upregulated proteins in Y spermatozoa | | | | | |
| Tubulin alpha 8 (TUBA8) | Q2HJB8 | 0.43 | nUPLC-MS/MS | Guanylate cyclase, and notch | De Canio et al., 2014 |
| Tubulin beta 2B (TUBB2B) | Q6B856 | 0.26 | | | |
| EF-hand domain-containing protein 1 (EFHC1) | NP_001179173.1 | 0.05 | SWATH-MS | | Scott et al., 2018 |
| Pyruvate dehydrogenase protein X component (PDHX) | NP_001069219.1 | 0.393 | | | |

(Continued)

TABLE 4 | Continued

| Proteins (symbol) | Accession no | X/Y (intensity) | Proteomic technique | Related pathways (P > 0.05) | References |
|---|----------------|-----------------|---------------------|---|-------------------|
| Dynein intermediate chain 2, axonemal (DNAI2) | XP_027374681.1 | 0.457 | | | |
| Chain A, crystal structure of bovine heart mitochondrial Bc1 with Jg144 inhibitor | 2FYU_A | 0.52 | MALDI-TOF-MS | | Chen et al., 2012 |
| ATP synthase subunit beta, mitochondrial (ATP5B) | P00829 | 0.48 | | | |
| F-actin-capping protein subunit beta (CAPZB) | P79136 | 0.50 | | Guanylate cyclase, notch, and actin cytoskeleton assembly | |
| lutathione S-transferase, mu 3 (brain) (GSTM3) | AAI12492 | 0.51 | LC-MS | Glutathione metabolism | |

Differentially expressed proteins in X and Y sperms were entered in the Pathway Studio program (Elsevier®) to identify the significantly correlated ($P < 0.05$) signaling pathways in these sperms. Briefly, protein names (symbols) were entered into the program to determine significantly matching pathways for each differentially expressed protein based on the information extracted from the NCBI PubMed database. Signaling pathways associated with the differentially expressed proteins were confirmed using a PubMed Medline hyperlink that was embedded in each node. Fisher's exact test was used to determine whether a pathway was statistically correlated with the target protein. $P < 0.05$ was considered as statistically significant.



profiles of two tubulin isoforms $\alpha 8$ and $\beta 2B$. Use of different proteomic approaches (i.e., 2DE-MS/MS, nUPLC-MS/MS, and SWATH-MS analysis) in these studies might have led to these

differences. Based on these findings, it is essential to speculate that X and Y spermatozoa can at least be different based on their protein content; however, further studies are warranted

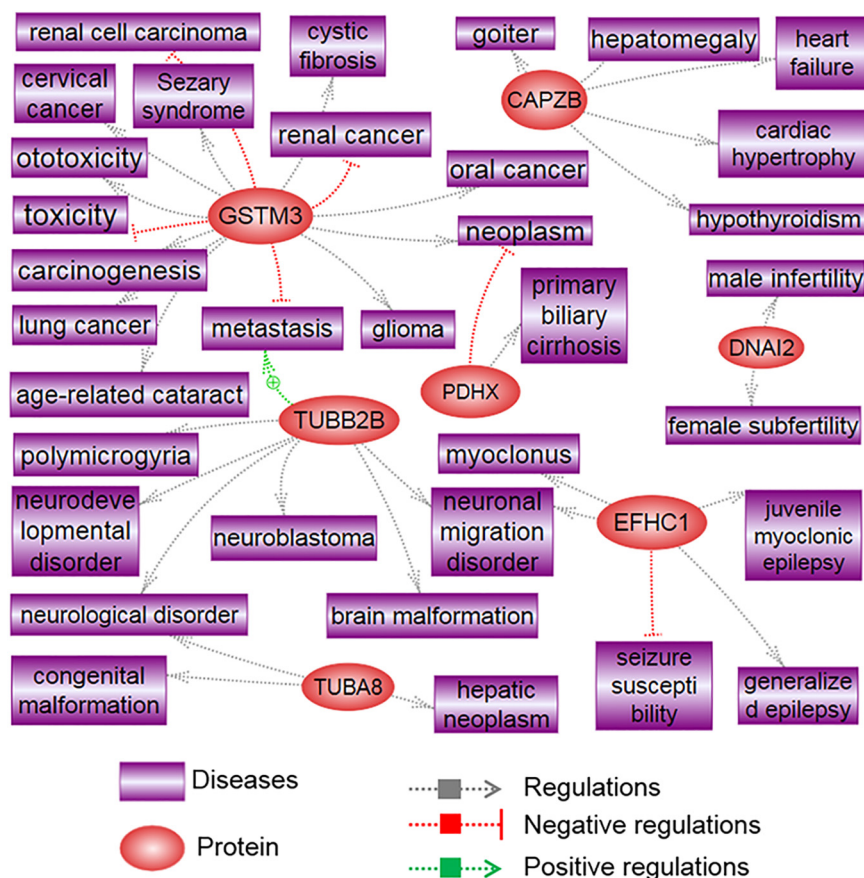


FIGURE 3 | Signaling pathways associated with highly differentiated proteins in Y spermatozoa. The illustration was prepared using Pathway Studio (Elsevier®, Ariadne Genomics, Inc.) after performing a literature search in the PubMed database.

to identify the validated markers that could differentiate these two cell types appropriately. In addition, proteomic analysis of X and Y spermatozoa from different animal species should be conducted for their practical application particularly for immunosexing techniques.

Proteins that are differentially expressed in X and Y spermatozoa are summarized in **Table 4** (data collected from published studies). We used the Pathway Studio program and found that proteins that were highly expressed in X spermatozoa were significantly ($P < 0.05$) correlated with five major canonical pathways/signaling, whereas proteins that were highly expressed in Y spermatozoa were correlated with four pathways/signaling (**Table 4**). The differences in the protein content and associated signaling pathways between X and Y spermatozoa might provide a theoretical basis to distinguish between these sperm types. Nevertheless, it is uncertain whether these differences are correlated with the biological aspect of X and Y spermatozoa. By using the same program, we determined the associated disease processes that were regulated by the differentially expressed proteins in X and Y spermatozoa. By using this simple illustration (**Figures 2, 3**), one may have a hypothetical presumption regarding the occurrence of specific diseases in men and women. For example, L-lactate

dehydrogenase A and testis-specific glyceraldehyde 3-phosphate dehydrogenase, which are highly expressed in X spermatozoa, are found to be functionally associated with breast neoplasm and cervical carcinoma (**Figure 2**). Both the cancers are the leading cause of cancer deaths in women (Siegel et al., 2015). In accordance, epidemiological investigation in humans revealed relatively higher incidence of anemia (Malhotra et al., 2004; Alvarez-Uria et al., 2014), Alzheimer's disease (Vina and Lloret, 2010), Huntington's disease (Panas et al., 2011), and trypanosoma (Pepin et al., 2002) in women. These diseases were also found to be associated with proteins that were highly expressed in X spermatozoa (**Figure 2**). Similarly, abundant proteins in Y spermatozoa, that is TUBA8 and GSTM3, were found to be associated with hepatic cancer and renal cancer, respectively, and the prevalence of both diseases were reported to be high in men compared to the women (Woldrich et al., 2008; Wu et al., 2018). However, few other diseases that are found to be related with the differentially expressed proteins either in the X and Y spermatozoa represent different results compared to the epidemiological data (**Figure 3**). For example, heart failure was found to be related with CAPZB that was highly expressed in Y spermatozoa, however, its incidence is lower in men than that in women. Consistently, tuberculosis was found to be related with

the altered functionality of TPI1 that was more highly expresses in X spermatozoa than in Y spermatozoa. However, the incidence of this disease is high in men than women. These inconsistencies presumably due to the Pathway Studio program, generated protein pathways by using information present in the PubMed database, which are incapable to explain every disease condition precisely. In addition, despite the differential expression of a particular protein between two cell types, the existence of majority of the proteins is constant between them. Therefore, the increased expression of a protein in the particular cell may not always represent their functional activation. Another major drawback of this hypothesis is that minor proteomic alterations (<2-fold) between X and Y spermatozoa may not necessarily display any significant differences in protein expression in the resulting offspring, and thus could predispose alternative conclusion.

CONCLUSION

Nature has developed many mechanisms to make genetically different sperm phenotypically identical within a male to avoid a fertilization advantage of one allele over another. Mendel's law of independent assortment would not be true if some alleles had a fertilization advantage. An example (very rare) where different alleles affect fertility is the T allele system on Chromosome 17 in mice, in which great infertility occurs (Colaco and Modi, 2018). Among the mechanisms employed by nature are intercellular bridges of clutches of 32 or more spermatogonia and spermatids so that RNA and proteins are exchanged in the clutches of the developing sperm with different genotypes, thus homogenizing the cytoplasm, cell membranes, and so on. Another mechanism is extremely limited post-meiotic gene expression during spermatogenesis/spermiogenesis. The Sertoli nurse cells take over many essential cellular molecular functions during this period to compensate. Additional mechanism is coating sperm with surface molecules during epididymal maturation to make sperm look alike. These mechanisms explain why sperm are so identical, including X and Y sperm (within a male). Indeed, differentiation between X and Y spermatozoa has been of immense interest to researchers, physicians, and breeders, since the beginning of recorded history. Various methods have

been used to distinguish between X and Y spermatozoa; however, the practical validity of these methods is questionable. The only consistent *de novo* difference identified between X and Y spermatozoon to date is in their DNA content, which might be responsible for the differential expression of some genes and proteins and the occurrence of certain diseases in a sex specific manner; however, it is unclear whether this difference in the DNA content results in other physical, chemical, and functional differences between X and Y spermatozoa. Moreover, the ambiguity in the existing findings might be due to the use of non-specific or less-specific methods for distinguishing between X and Y spermatozoa. Therefore, further studies using more specific, non-invasive (less injurious to cells) methods to distinguish between the two sperm types for the sex preselection of offspring are warranted.

AUTHOR CONTRIBUTIONS

MR and M-GP conceived the idea. MR drafted the manuscript and prepared the artworks. M-GP supervised the whole work. Both authors crucially revised the manuscript for important intellectual content and approved the final version to be published.

FUNDING

The authors thank the financial support provided by the Basic Science Research Program through the National Research Foundation of Korea (Project No. NRF-2018R1A6A1A03025159). MR was supported by the Korea Research Fellowship Program via the National Research Foundation of Korea funded by the Ministry of Science and ICT (Project No. 2017H1D3A1A02013844).

ACKNOWLEDGMENTS

We thank the funding agencies for supporting our study. We would also like to thank all present and former lab members for helpful discussions.

REFERENCES

- Agarwal, A., Sharma, R. K., Sharma, R., Assidi, M., Abuzenadah, A. M., Alshahrani, S., et al. (2014). Characterizing semen parameters and their association with reactive oxygen species in infertile men. *Reprod. Biol. Endocrinol.* 12:33. doi: 10.1186/1477-7827-12-33
- Ainsworth, C. J., Nixon, B., and Aitken, R. J. (2011). The electrophoretic separation of spermatozoa: an analysis of genotype, surface carbohydrate composition and potential for capacitation. *Int. J. Androl.* 34, e422–e434. doi: 10.1111/j.1365-2605.2011.01164.x
- Aitken, R. J. (2014). Age, the environment and our reproductive future: bonking baby boomers and the future of sex. *Reproduction* 147, S1–S11. doi: 10.1530/REP-13-0399
- Alminana, C., Caballero, I., Heath, P. R., Maleki-Dizaji, S., Parrilla, I., Cuello, C., et al. (2014). The battle of the sexes starts in the oviduct: modulation of oviductal transcriptome by X and Y-bearing spermatozoa. *BMC Genomics* 15:293. doi: 10.1186/1471-2164-15-293
- Alvarez-Uria, G., Naik, P. K., Midde, M., Yalla, P. S., and Pakam, R. (2014). Prevalence and severity of anaemia stratified by age and gender in rural India. *Anemia* 2014:176182. doi: 10.1155/2014/176182
- Anway, M. D., Cupp, A. S., Uzumcu, M., and Skinner, M. K. (2005). Epigenetic transgenerational actions of endocrine disruptors and male fertility. *Science* 308, 1466–1469. doi: 10.1126/science.1108190
- Aranha, I. P., and Martin-Deleon, P. A. (1995). Mouse chromosome 6 in Rb translocations: consequences in singly and doubly heterozygous males. *Cytogenet. Cell Genet.* 69, 253–259. doi: 10.1159/000133975
- Bader, G. D., Heilbut, A., Andrews, B., Tyers, M., Hughes, T., and Boone, C. (2003). Functional genomics and proteomics: charting a multidimensional map of the yeast cell. *Trends Cell Biol.* 13, 344–356. doi: 10.1016/s0962-8924(03)00127-2

- Barazani, Y., Katz, B. F., Nagler, H. M., and Stember, D. S. (2014). Lifestyle, environment, and male reproductive health. *Urol. Clin. North Am.* 41, 55–66. doi: 10.1016/j.ucl.2013.08.017
- Battistone, M. A., Da Ros, V. G., Salicioni, A. M., Navarrete, F. A., Krapf, D., Visconti, P. E., et al. (2013). Functional human sperm capacitation requires both bicarbonate-dependent PKA activation and down-regulation of Ser/Thr phosphatases by Src family kinases. *Mol. Hum. Reprod.* 19, 570–580. doi: 10.1093/molehr/gat033
- Bean, B. (1990). Progenitive sex ratio among functioning sperm cells. *Am. J. Hum. Genet.* 47, 351–353.
- Benet, J., Genesca, A., Navarro, J., Egozcue, J., and Templado, C. (1992). Cytogenetic studies in motile sperm from normal men. *Hum. Genet.* 89, 176–180.
- Bennett, D., and Boyse, E. A. (1973). Sex ratio in progeny of mice inseminated with sperm treated with H-Y antiserum. *Nature* 246, 308–309. doi: 10.1038/246308a0
- Bermejo-Alvarez, P., Rizados, D., Rath, D., Lonergan, P., and Gutierrez-Adan, A. (2010). Sex determines the expression level of one third of the actively expressed genes in bovine blastocysts. *Proc. Natl. Acad. Sci. U.S.A.* 107, 3394–3399. doi: 10.1073/pnas.0913843107
- Bibbins, P. E. Jr., Lipshultz, L. I., Ward, J. B. Jr., and Legator, M. S. (1988). Fluorescent body distribution in spermatozoa in the male with exclusively female offspring. *Fertil. Steril.* 49, 670–675. doi: 10.1016/s0015-0282(16)59838-0
- Blomqvist, S. R., Vidarsson, H., Soder, O., and Enerback, S. (2006). Epididymal expression of the forkhead transcription factor Foxl1 is required for male fertility. *EMBO J.* 25, 4131–4141. doi: 10.1038/sj.emboj.7601272
- Blottner, S., Bostedt, H., Mewes, K., and Pitra, C. (1994). Enrichment of bovine X and Y spermatozoa by free-flow electrophoresis. *Zentralbl. Veterinarmed. A* 41, 466–474. doi: 10.1111/j.1439-0442.1994.tb00113.x
- Bonduelle, M., Van Assche, E., Joris, H., Keymolen, K., Devroey, P., Van Steirteghem, A., et al. (2002). Prenatal testing in ICSI pregnancies: incidence of chromosomal anomalies in 1586 karyotypes and relation to sperm parameters. *Hum. Reprod.* 17, 2600–2614. doi: 10.1093/humrep/17.10.2600
- Bonefeld-Jorgensen, E. C., Andersen, H. R., Rasmussen, T. H., and Vinggaard, A. M. (2001). Effect of highly bioaccumulated polychlorinated biphenyl congeners on estrogen and androgen receptor activity. *Toxicology* 158, 141–153. doi: 10.1016/s0300-483x(00)00368-1
- Brandriff, B. F., Gordon, L. A., Haendel, S., Singer, S., Moore, D. H. II, and Gledhill, B. L. (1986). Sex chromosome ratios determined by karyotypic analysis in albumin-isolated human sperm. *Fertil. Steril.* 46, 678–685. doi: 10.1016/s0015-0282(16)49648-2
- Braun, R. E., Behringer, R. R., Peschon, J. J., Brinster, R. L., and Palmiter, R. D. (1989). Genetically haploid spermatids are phenotypically diploid. *Nature* 337, 373–376. doi: 10.1038/337373a0
- Carvalho, J. O., Silva, L. P., Sartori, R., and Dode, M. A. (2013). Nanoscale differences in the shape and size of X and Y chromosome-bearing bovine sperm heads assessed by atomic force microscopy. *PLoS One* 8:e59387. doi: 10.1371/journal.pone.0059387
- Chandler, J. E., Steinholt-Chenevert, H. C., Adkinson, R. W., and Moser, E. B. (1998). Sex ratio variation between ejaculates within sire evaluated by polymerase chain reaction, calving, and farrowing records. *J. Dairy Sci.* 81, 1855–1867. doi: 10.3168/jds.s0022-0302(98)75756-x
- Chang, M. C. (1951). Fertilizing capacity of spermatozoa deposited into the fallopian tubes. *Nature* 168, 697–698. doi: 10.1038/168697b0
- Chaudhary, I., Jain, M., and Halder, A. (2014). Sperm sex ratio (X: Y ratio) and its variations. *Austin J. Reprod. Med. Infertil.* 1:7.
- Chayko, C. A., and Martin-Deleon, P. A. (1992). The murine Rb(6.16) translocation: alterations in the proportion of alternate sperm segregants effecting fertilization in vitro and in vivo. *Hum. Genet.* 90, 79–85.
- Check, J. H., Shanis, B. S., Cooper, S. O., and Bollendorf, A. (1989). Male sex preselection: swim-up technique and insemination of women after ovulation induction. *Arch. Androl.* 23, 165–166. doi: 10.3109/01485018908986839
- Chen, X., Yue, Y., He, Y., Zhu, H., Hao, H., Zhao, X., et al. (2014). Identification and characterization of genes differentially expressed in X and Y sperm using suppression subtractive hybridization and cDNA microarray. *Mol. Reprod. Dev.* 81, 908–917. doi: 10.1002/mrd.22386
- Chen, X., Zhu, H., Wu, C., Han, W., Hao, H., Zhao, X., et al. (2012). Identification of differentially expressed proteins between bull X and Y spermatozoa. *J. Proteomics* 77, 59–67. doi: 10.1016/j.jpro.2012.07.004
- Chevret, E., Rousseaux, S., Monteil, M., Pelletier, R., Cozzi, J., and Sele, B. (1995). Meiotic segregation of the X and Y chromosomes and chromosome 1 analyzed by three-color FISH in human interphase spermatozoa. *Cytogenet. Cell Genet.* 71, 126–130. doi: 10.1159/000134090
- Clapham, D. E. (2013). Sperm BerserKers. *Elife*. 2:e01469. doi: 10.7554/eLife.01469
- Colaco, S., and Modi, D. (2018). Genetics of the human Y chromosome and its association with male infertility. *Reprod. Biol. Endocrinol.* 16:14. doi: 10.1186/s12958-018-0330-5
- Cui, K. H. (1997). Size differences between human X and Y spermatozoa and preferential fertilization diagnosis. *Mol. Hum. Reprod.* 3, 61–67. doi: 10.1093/molehr/3.1.61
- Cui, K. H., and Matthews, C. D. (1993). X larger than Y. *Nature* 366, 117–118.
- Curtsinger, J. W., Ito, R., and Hiraizumi, Y. (1983). A two-generation study of human sex-ratio variation. *Am. J. Hum. Genet.* 35, 951–961.
- De Canio, M., Soggiu, A., Piras, C., Bonizzi, L., Galli, A., Urbani, A., et al. (2014). Differential protein profile in sexed bovine semen: shotgun proteomics investigation. *Mol. Biosyst.* 10, 1264–1271. doi: 10.1039/c3mb70306a
- Diasio, R. B., and Glass, R. H. (1971). Effects of pH on the migration of X and Y sperm. *Fertil. Steril.* 22, 303–305. doi: 10.1016/s0015-0282(16)38224-3
- Dominko, T., and First, N. L. (1997). Relationship between the maturational state of oocytes at the time of insemination and sex ratio of subsequent early bovine embryos. *Theriogenology* 47, 1041–1050. doi: 10.1016/s0093-691x(97)00061-7
- Egozcue, J., Blanco, J., and Vidal, F. (1997). Chromosome studies in human sperm nuclei using fluorescence in-situ hybridization (FISH). *Hum. Reprod. Update* 3, 441–452. doi: 10.1093/humupd/3.5.441
- Eisenberg, M. L., Murthy, L., Hwang, K., Lamb, D. J., and Lipshultz, L. I. (2012). Sperm counts and sperm sex ratio in male infertility patients. *Asian J. Androl.* 14, 683–686. doi: 10.1038/aja.2012.58
- Engelmann, U., Krassnigg, F., Schatz, H., and Schill, W. B. (1988). Separation of human X and Y spermatozoa by free-flow electrophoresis. *Gamete Res.* 19, 151–160. doi: 10.1002/mrd.1120190205
- Erickson, J. D. (1976). The secondary sex ratio in the United States 1969–71: association with race, parental ages, birth order, paternal education and legitimacy. *Ann. Hum. Genet.* 40, 205–212. doi: 10.1111/j.1469-1809.1976.tb00182.x
- Ericsson, R. J., Langevin, C. N., and Nishino, M. (1973). Isolation of fractions rich in human Y sperm. *Nature* 246, 421–424. doi: 10.1038/246421a0
- Evans, J. M., Douglas, T. A., and Renton, J. P. (1975). An attempt to separate fractions rich in human Y sperm. *Nature* 253, 352–354. doi: 10.1038/253352a0
- Flaherty, S. P., and Matthews, C. D. (1996). Application of modern molecular techniques to evaluate sperm sex selection methods. *Mol. Hum. Reprod.* 2, 937–942. doi: 10.1093/molehr/2.12.937
- Garry, V. F., Harkins, M. E., Erickson, L. L., Long-Simpson, L. K., Holland, S. E., and Burroughs, B. L. (2002). Birth defects, season of conception, and sex of children born to pesticide applicators living in the Red River Valley of Minnesota, USA. *Environ. Health Perspect.* 110(Suppl. 3), 441–449. doi: 10.1289/ehp.02110s3441
- Gellatly, C. (2009). Trends in population sex ratios may be explained by changes in the frequencies of polymorphic alleles of a sex ratio gene. *Evol. Biol.* 36, 190–200. doi: 10.1007/s11692-008-9046-3
- Geraedts, J. P. (1997). X spermatozoa larger than Y in 1973. *Mol. Hum. Reprod.* 3, 545–546. doi: 10.1093/molehr/3.6.545
- Gharagozloo, P., and Aitken, R. J. (2011). The role of sperm oxidative stress in male infertility and the significance of oral antioxidant therapy. *Hum. Reprod.* 26, 1628–1640. doi: 10.1093/humrep/der132
- Goldman, A. S., Fomina, Z., Knights, P. A., Hill, C. J., Walker, A. P., and Hulten, M. A. (1993). Analysis of the primary sex ratio, sex chromosome aneuploidy and diploidy in human sperm using dual-colour fluorescence in situ hybridisation. *Eur. J. Hum. Genet.* 1, 325–334. doi: 10.1159/000472431
- Grant, V. J. (2006). Entrenched misinformation about X and Y sperm. *BMJ* 332:916.
- Griffin, D. K., Abruzzo, M. A., Millie, E. A., Feingold, E., and Hassold, T. J. (1996). Sex ratio in normal and disomic sperm: evidence that the extra chromosome 21 preferentially segregates with the Y chromosome. *Am. J. Hum. Genet.* 59, 1108–1113.

- Halder, A., and Tutscheck, B. (1998). Analysis of meiotic segregation in human noncondensed interphase spermatozoa by triple colour rapid direct fluorescent in situ hybridization. *Indian J. Med. Res.* 107, 94–97.
- Hamamah, S., and Gatti, J. L. (1998). Role of the ionic environment and internal pH on sperm activity. *Hum. Reprod.* 13(Suppl. 4), 20–30. doi: 10.1093/humrep/13.suppl_4.20
- Han, T. L., Flaherty, S. P., Ford, J. H., and Matthews, C. D. (1993a). Detection of X- and Y-bearing human spermatozoa after motile sperm isolation by swim-up. *Fertil. Steril.* 60, 1046–1051. doi: 10.1016/s0015-0282(16)56408-5
- Han, T. L., Ford, J. H., Webb, G. C., Flaherty, S. P., Correll, A., and Matthews, C. D. (1993b). Simultaneous detection of X- and Y-bearing human sperm by double fluorescence in situ hybridization. *Mol. Reprod. Dev.* 34, 308–313. doi: 10.1002/mrd.1080340311
- Hassanane, M., Kovacs, A., Laurent, P., Lindblad, K., and Gustavsson, I. (1999). Simultaneous detection of X- and Y-bearing bull spermatozoa by double colour fluorescence in situ hybridization. *Mol. Reprod. Dev.* 53, 407–412. doi: 10.1002/(sici)1098-2795(199908)53:4<407::aid-mrd6>3.0.co;2-o
- Hassold, T., Abruzzo, M., Adkins, K., Griffin, D., Merrill, M., Millie, E., et al. (1996). Human aneuploidy: incidence, origin, and etiology. *Environ. Mol. Mutagen.* 28, 167–175. doi: 10.1002/(sici)1098-2280(1996)28:3<167::aid-em2>3.3.co;2-v
- Hassold, T., and Hunt, P. (2001). To err (meiotically) is human: the genesis of human aneuploidy. *Nat. Rev. Genet.* 2, 280–291. doi: 10.1038/35066065
- Hendricks, K. E., Martins, L., and Hansen, P. J. (2009). Consequences for the bovine embryo of being derived from a spermatozoon subjected to post-ejaculatory aging and heat shock: development to the blastocyst stage and sex ratio. *J. Reprod. Dev.* 55, 69–74. doi: 10.1262/jrd.20097
- Hendriksen, P. J. (1999). Do X and Y spermatozoa differ in proteins? *Theriogenology* 52, 1295–1307. doi: 10.1016/s0093-691x(99)00218-6
- Hendriksen, P. J., Tieman, M., Van Der Lende, T., and Johnson, L. A. (1993). Binding of anti-H-Y monoclonal antibodies to separated X and Y chromosome-bearing porcine and bovine sperm. *Mol. Reprod. Dev.* 35, 189–196. doi: 10.1002/mrd.1080350213
- Hendriksen, P. J., Welch, G. R., Grootegoed, J. A., Van Der Lende, T., and Johnson, L. A. (1996). Comparison of detergent-solubilized membrane and soluble proteins from flow cytometrically sorted X- and Y-chromosome bearing porcine spermatozoa by high resolution 2-D electrophoresis. *Mol. Reprod. Dev.* 45, 342–350. doi: 10.1002/(sici)1098-2795(199611)45:3<342::aid-mrd11>3.3.co;2-s
- Hoegerman, S. F., Pang, M. G., and Kearns, W. G. (1995). Sex chromosome abnormalities after intracytoplasmic sperm injection. *Lancet* 346:1095. doi: 10.1016/s0140-6736(95)91768-3
- Hoffmann, D. S., and Killian, G. J. (1981). Isolation of epithelial cells from the corpus epididymidis and analysis for glycylphosphorylcholine, sialic acid, and protein. *J. Exp. Zool.* 217, 93–102. doi: 10.1002/jez.1402170110
- Holt, W. V., and Fazeli, A. (2010). The oviduct as a complex mediator of mammalian sperm function and selection. *Mol. Reprod. Dev.* 77, 934–943. doi: 10.1002/mrd.21234
- Hoppe, P. C., and Koo, G. C. (1984). Reacting mouse sperm with monoclonal H-Y antibodies does not influence sex ratio of eggs fertilized in vitro. *J. Reprod. Immunol.* 6, 1–9. doi: 10.1016/0165-0378(84)90036-6
- Hossain, A. M., Barik, S., and Kulkarni, P. M. (2001). Lack of significant morphological differences between human X and Y spermatozoa and their precursor cells (spermatids) exposed to different prehybridization treatments. *J. Androl.* 22, 119–123.
- Hu, Y. C., and Namekawa, S. H. (2015). Functional significance of the sex chromosomes during spermatogenesis. *Reproduction* 149, R265–R277. doi: 10.1530/REP-14-0613
- Iizuka, R., Kaneko, S., Aoki, R., and Kobayashi, T. (1987). Sexing of human sperm by discontinuous Percoll density gradient and its clinical application. *Hum. Reprod.* 2, 573–575. doi: 10.1093/oxfordjournals.humrep.a136591
- Ikedo, M., Tamura, M., Yamashita, J., Suzuki, C., and Tomita, T. (2005). Repeated in utero and lactational 2,3,7,8-tetrachlorodibenzo-p-dioxin exposure affects male gonads in offspring, leading to sex ratio changes in F2 progeny. *Toxicol. Appl. Pharmacol.* 206, 351–355. doi: 10.1016/j.taap.2004.11.019
- In't Veld, P., Brandenburg, H., Verhoeff, A., Dhont, M., and Los, F. (1995). Sex chromosomal abnormalities and intracytoplasmic sperm injection. *Lancet* 346:773. doi: 10.1016/s0140-6736(95)91531-1
- Irving, J., Bittles, A., Peverall, J., Murch, A., and Matson, P. (1999). The ratio of X- and Y-bearing sperm in ejaculates of men with three or more children of the same sex. *J. Assist. Reprod. Genet.* 16, 492–494.
- Ishihara, K., Warita, K., Tanida, T., Sugawara, T., Kitagawa, H., and Hoshi, N. (2007). Does paternal exposure to 2,3,7,8-tetrachlorodibenzo-p-dioxin (TCDD) affect the sex ratio of offspring? *J. Vet. Med. Sci.* 69, 347–352. doi: 10.1292/jvms.69.347
- Iwata, H., Shiono, H., Kon, Y., Matsubara, K., Kimura, K., Kuwayama, T., et al. (2008). Effects of modification of in vitro fertilization techniques on the sex ratio of the resultant bovine embryos. *Anim. Reprod. Sci.* 105, 234–244. doi: 10.1016/j.anireprosci.2007.03.006
- James, W. H., and Rostron, J. (1985). Parental age, parity and sex ratio in births in England and Wales, 1968–77. *J. Biosoc. Sci.* 17, 47–56. doi: 10.1017/s0021932000015467
- Jasin, M., and Zalamea, P. (1992). Analysis of *Escherichia coli* beta-galactosidase expression in transgenic mice by flow cytometry of sperm. *Proc. Natl. Acad. Sci. U.S.A.* 89, 10681–10685. doi: 10.1073/pnas.89.22.10681
- Jeulin, C., Wiels, J., Casanova, M., and Fellous, M. (1982). “Relationship between Y-chromosome and H-Y antigen expression in human spermatozoa,” in *The Sperm Cell*, ed. J. André (Dordrecht: Springer).
- Johnson, L. (1994). A new approach to study the architectural arrangement of spermatogenic stages revealed little evidence of a partial wave along the length of human seminiferous tubules. *J. Androl.* 15, 435–441.
- Johnson, L. A. (2000). Sexing mammalian sperm for production of offspring: the state-of-the-art. *Anim. Reprod. Sci.* 6, 93–107. doi: 10.1016/s0378-4320(00)00088-9
- Johnson, L. A., Flook, J. P., and Hawk, H. W. (1989). Sex preselection in rabbits: live births from X and Y sperm separated by DNA and cell sorting. *Biol. Reprod.* 41, 199–203. doi: 10.1095/biolreprod41.2.199
- Johnson, L. A., Welch, G. R., Keyvanfar, K., Dorfmann, A., Fugger, E. F., and Schulman, J. D. (1993). Gender preselection in humans? Flow cytometric separation of X and Y spermatozoa for the prevention of X-linked diseases. *Hum. Reprod.* 8, 1733–1739. doi: 10.1093/oxfordjournals.humrep.a137925
- Jurewicz, J., Radwan, M., Sobala, W., Radwan, P., Jakubowski, L., Hawula, W., et al. (2014). Lifestyle factors and sperm aneuploidy. *Reprod. Biol.* 14, 190–199. doi: 10.1016/j.repbio.2014.02.002
- Kaneko, S., Iizuka, R., Oshio, S., Nakajima, H., Oshio, S., and Mohri, H. (1993). Separation of human X- and Y-bearing sperm using free-flow electrophoresis. *Proc. Jpn. Acad. Ser. B* 59, 276–279. doi: 10.2183/pjab.59.276
- Kaneko, S., Oshio, S., Kobayashi, T., Iizuka, R., and Mohri, H. (1984). Human X- and Y-bearing sperm differ in cell surface sialic acid content. *Biochem. Biophys. Res. Commun.* 124, 950–955. doi: 10.1016/0006-291x(84)91050-7
- Kirley, T. L. (1990). Inactivation of (Na⁺,K⁺)-ATPase by beta-mercaptoethanol. Differential sensitivity to reduction of the three beta subunit disulfide bonds. *J. Biol. Chem.* 265, 4227–4232.
- Krcro, C. J., and Goldberg, E. H. (1976). H-Y male antigen: detection on eight-cell mouse embryos. *Science* 193, 1134–1135. doi: 10.1126/science.959826
- Kruger, A. N., Brogley, M. A., Huizinga, J. L., Kidd, J. M., de Rooij, D. G., Hu, Y. C., et al. (2019). A neofunctionalized X-linked ampliconic gene family is essential for male fertility and equal sex ratio in mice. *Curr. Biol.* 29, 3699–3706.e5. doi: 10.1016/j.cub.2019.08.057
- Kwon, W. S., Rahman, M. S., Lee, J. S., Kim, J., Yoon, S. J., Park, Y. J., et al. (2014a). A comprehensive proteomic approach to identifying capacitation related proteins in boar spermatozoa. *BMC Genomics* 15:897. doi: 10.1186/1471-2164-15-897
- Kwon, W. S., Rahman, M. S., and Pang, M. G. (2014b). Diagnosis and prognosis of male infertility in mammal: the focusing of tyrosine phosphorylation and phosphotyrosine proteins. *J. Proteome Res.* 13, 4505–4517. doi: 10.1021/pr500524p
- Kwon, W. S., Rahman, M. S., Lee, J. S., Yoon, S. J., Park, Y. J., and Pang, M. G. (2015). Discovery of predictive biomarkers for litter size in boar spermatozoa. *Mol. Cell. Proteomics* 14, 1230–1240. doi: 10.1074/mcp.M114.045369
- Landrum, B., and Shettles, L. B. (1960). Nuclear structure of human spermatozoa. *Nature* 188, 916–918. doi: 10.1038/188916a0
- Lankenau, S., Corces, V. G., and Lankenau, D. H. (1994). The *Drosophila* micropia retrotransposon encodes a testis-specific antisense RNA complementary to reverse transcriptase. *Mol. Cell. Biol.* 14, 1764–1775. doi: 10.1128/mcb.14.3.1764

- Leblond, C. P., and Clermont, Y. (1952). Definition of the stages of the cycle of the seminiferous epithelium in the rat. *Ann. N. Y. Acad. Sci.* 55, 548–573. doi: 10.1111/j.1749-6632.1952.tb26576.x
- Lechniak, D., Strabel, T., Bousquet, D., and King, A. W. (2003). Sperm pre-incubation prior to insemination affects the sex ratio of bovine embryos produced in vitro. *Reprod. Domest. Anim.* 38, 224–227. doi: 10.1046/j.1439-0531.2003.00410.x
- Lobel, S. M., Pomponio, R. J., and Mutter, G. L. (1993). The sex ratio of normal and manipulated human sperm quantitated by the polymerase chain reaction. *Fertil. Steril.* 59, 387–392. doi: 10.1016/s0015-0282(16)55682-9
- Malhotra, P., Kumari, S., Kumar, R., and Varma, S. (2004). Prevalence of anemia in adult rural population of north India. *J. Assoc. Physicians India* 52, 18–20.
- Martin, R. H., Balkan, W., Burns, K., Rademaker, A. W., Lin, C. C., and Rudd, N. L. (1983). The chromosome constitution of 1000 human spermatozoa. *Hum. Genet.* 63, 305–309. doi: 10.1007/bf00274750
- Martin, R. H., Rademaker, A. W., and Leonard, N. J. (1995a). Analysis of chromosomal abnormalities in human sperm after chemotherapy by karyotyping and fluorescence in situ hybridization (FISH). *Cancer Genet. Cytogenet.* 80, 29–32. doi: 10.1016/0165-4608(94)00162-5
- Martin, R. H., Spriggs, E., Ko, E., and Rademaker, A. W. (1995b). The relationship between paternal age, sex ratios, and aneuploidy frequencies in human sperm, as assessed by multicolor FISH. *Am. J. Hum. Genet.* 57, 1395–1399.
- Martin, R. H., Spriggs, E., and Rademaker, A. W. (1996). Multicolor fluorescence in situ hybridization analysis of aneuploidy and diploidy frequencies in 225,846 sperm from 10 normal men. *Biol. Reprod.* 54, 394–398. doi: 10.1095/biolreprod54.2.394
- Mcauliffe, M. E., Williams, P. L., Korrick, S. A., Altshul, L. M., and Perry, M. J. (2012). Environmental exposure to polychlorinated biphenyls and p,p'-DDE and sperm sex-chromosome disomy. *Environ. Health Perspect.* 120, 535–540. doi: 10.1289/ehp.1104017
- Mcdonald, E., Watterson, A., Tyler, A. N., McArthur, J., and Scott, E. M. (2014). Multi-factorial influences on sex ratio: a spatio-temporal investigation of endocrine disruptor pollution and neighborhood stress. *Int. J. Occup. Environ. Health* 20, 235–246. doi: 10.1179/2049396714Y.0000000073
- Meng, L., and Feldman, L. (2010). A rapid TRIzol-based two-step method for DNA-free RNA extraction from Arabidopsis siliques and dry seeds. *Biotechnol. J.* 5, 183–186. doi: 10.1002/biot.200900211
- Mocarelli, P., Gerthoux, P. M., Ferrari, E., Patterson, D. G. Jr., Kieszak, S. M., Brambilla, P., et al. (2000). Paternal concentrations of dioxin and sex ratio of offspring. *Lancet* 355, 1858–1863. doi: 10.1016/s0140-6736(00)02290-x
- Muehleis, P. M., and Long, S. Y. (1976). The effects of altering the pH of seminal fluid on the sex ratio of rabbit offspring. *Fertil. Steril.* 27, 1438–1445. doi: 10.1016/s0015-0282(16)42261-2
- Oakberg, E. F. (1956). Duration of spermatogenesis in the mouse and timing of stages of the cycle of the seminiferous epithelium. *Am. J. Anat.* 99, 507–516. doi: 10.1002/aja.1000990307
- Ohno, S., and Wachtel, S. S. (1978). On the selective elimination of Y-bearing sperm. *Immunogenetics* 7, 13–16. doi: 10.1007/BF01843982
- Oyeyipo, I. P., van der Linde, M., and du Plessis, S. S. (2017). Environmental exposure of sperm sex-chromosomes: a gender selection technique. *Toxicol. Res.* 33, 315–323. doi: 10.5487/TR.2017.33.4.315
- Panas, M., Karadima, G., Vassos, E., Kalfakis, N., Kladi, A., Christodoulou, K., et al. (2011). Huntington's disease in Greece: the experience of 14 years. *Clin. Genet.* 80, 586–590. doi: 10.1111/j.1399-0004.2010.01603.x
- Pang, M. G., Hoegerman, S. F., Cuticchia, A. J., Moon, S. Y., Doncel, G. F., Acosta, A. A., et al. (1999). Detection of aneuploidy for chromosomes 4, 6, 7, 8, 9, 10, 11, 12, 13, 17, 18, 21, X and Y by fluorescence in-situ hybridization in spermatozoa from nine patients with oligoasthenoteratozoospermia undergoing intracytoplasmic sperm injection. *Hum. Reprod.* 14, 1266–1273. doi: 10.1093/humrep/14.5.1266
- Pang, M. G., Kim, Y. J., Lee, S. H., and Kim, C. K. (2005). The high incidence of meiotic errors increases with decreased sperm count in severe male factor infertilities. *Hum. Reprod.* 20, 1688–1694. doi: 10.1093/humrep/deh817
- Pang, M. G., You, Y. A., Park, Y. J., Oh, S. A., Kim, D. S., and Kim, Y. J. (2010). Numerical chromosome abnormalities are associated with sperm tail swelling patterns. *Fertil. Steril.* 94, 1012–1020. doi: 10.1016/j.fertnstert.2009.04.043
- Park, Y. J., Kim, J., You, Y. A., and Pang, M. G. (2013). Proteomic revolution to improve tools for evaluating male fertility in animals. *J. Proteome Res.* 12, 4738–4747. doi: 10.1021/pr400639x
- Penfold, L. M., Holt, C., Holt, W. V., Welch, G. R., Cran, D. G., and Johnson, L. A. (1998). Comparative motility of X and Y chromosome-bearing bovine sperm separated on the basis of DNA content by flow sorting. *Mol. Reprod. Dev.* 50, 323–327. doi: 10.1002/(sici)1098-2795(199807)50:3<323::aid-mrdr8>3.0.co;2-l
- Pepin, J., Mpia, B., and Iloasebe, M. (2002). *Trypanosoma brucei gambiense* African trypanosomiasis: differences between men and women in severity of disease and response to treatment. *Trans. R. Soc. Trop. Med. Hyg.* 96, 421–426. doi: 10.1016/s0035-9203(02)90380-9
- Perez-Crespo, M., Pintado, B., and Gutierrez-Adan, A. (2008). Scrotal heat stress effects on sperm viability, sperm DNA integrity, and the offspring sex ratio in mice. *Mol. Reprod. Dev.* 75, 40–47. doi: 10.1002/mrd.20759
- Perry, M. J. (2008). Effects of environmental and occupational pesticide exposure on human sperm: a systematic review. *Hum. Reprod. Update* 14, 233–242. doi: 10.1093/humupd/dmm039
- Pfeffer, J., Pang, M. G., Hoegerman, S. F., Osgood, C. J., Stacey, M. W., Mayer, J., et al. (1999). Aneuploidy frequencies in semen fractions from ten oligoasthenoteratozoospermic patients donating sperm for intracytoplasmic sperm injection. *Fertil. Steril.* 72, 472–478. doi: 10.1016/s0015-0282(99)00279-4
- Pratt, N. C., Huck, U. W., and Lisk, R. D. (1987). Offspring sex ratio in hamsters is correlated with vaginal pH at certain times of mating. *Behav. Neural Biol.* 48, 310–316. doi: 10.1016/s0163-1047(87)90864-8
- Quinlivan, W. L., Preciado, K., Long, T. L., and Sullivan, H. (1982). Separation of human X and Y spermatozoa by albumin gradients and Sephadex chromatography. *Fertil. Steril.* 37, 104–107. doi: 10.1016/s0015-0282(16)45986-8
- Quinlivan, W. L., and Sullivan, H. (1974). The ratios and separation of X and Y spermatozoa in human semen. *Fertil. Steril.* 25, 315–318. doi: 10.1016/s0015-0282(16)40330-4
- Rahman, M. S., Kang, K. H., Arifuzzaman, S., Pang, W. K., Ryu, D. Y., Song, W. H., et al. (2019). Effect of antioxidants on BPA-induced stress on sperm function in a mouse model. *Sci. Rep.* 9:10584. doi: 10.1038/s41598-019-47158-9
- Rahman, M. S., Kwon, W. S., Karmakar, P. C., Yoon, S. J., Ryu, B. Y., and Pang, M. G. (2017a). Gestational exposure to bisphenol A affects the function and proteome profile of F1 spermatozoa in adult mice. *Environ. Health Perspect.* 125, 238–245. doi: 10.1289/EHP378
- Rahman, M. S., Kwon, W. S., and Pang, M. G. (2017b). Prediction of male fertility using capacitation-associated proteins in spermatozoa. *Mol. Reprod. Dev.* 84, 749–759. doi: 10.1002/mrd.22810
- Rahman, M. S., Kwon, W. S., Lee, J. S., Yoon, S. J., Ryu, B. Y., and Pang, M. G. (2015). Bisphenol-A affects male fertility via fertility-related proteins in spermatozoa. *Sci. Rep.* 5:9169. doi: 10.1038/srep09169
- Rahman, M. S., Kwon, W. S., Ryu, D. Y., Khatun, A., Karmakar, P. C., Ryu, B. Y., et al. (2018). Functional and proteomic alterations of F1 capacitated spermatozoa of adult mice following gestational exposure to bisphenol A. *J. Proteome Res.* 17, 524–535. doi: 10.1021/acs.jproteome.7b00668
- Rahman, M. S., Kwon, W. S., Yoon, S. J., Park, Y. J., Ryu, B. Y., and Pang, M. G. (2016). A novel approach to assessing bisphenol-A hazards using an *in vitro* model system. *BMC Genomics* 17:577. doi: 10.1186/s12864-016-2979-5
- Rahman, M. S., Lee, J. S., Kwon, W. S., and Pang, M. G. (2013). Sperm proteomics: road to male fertility and contraception. *Int. J. Endocrinol.* 2013:360986. doi: 10.1155/2013/360986
- Rathje, C. C., Johnson, E. E. P., Drage, D., Patinioti, C., Silvestri, G., Affara, N. A., et al. (2019). Differential sperm motility mediates the sex ratio drive shaping mouse sex chromosome evolution. *Curr. Biol.* 29, 3692–3698.e4. doi: 10.1016/j.cub.2019.09.031
- Recio, R., Robbins, W. A., Borja-Aburto, V., Moran-Martinez, J., Froines, J. R., Hernandez, R. M., et al. (2001). Organophosphorous pesticide exposure increases the frequency of sperm sex null aneuploidy. *Environ. Health Perspect.* 109, 1237–1240. doi: 10.1289/ehp.011091237
- Ross, A., Robinson, J. A., and Evans, H. J. (1975). Failure to confirm separation of X- and Y-bearing human sperm using BSA gradients. *Nature* 253, 354–355. doi: 10.1038/253354a0
- Rubio, C., Gil-Salom, M., Simon, C., Vidal, F., Rodrigo, L., Minguez, Y., et al. (2001). Incidence of sperm chromosomal abnormalities in a risk population:

- relationship with sperm quality and ICSI outcome. *Hum. Reprod.* 16, 2084–2092. doi: 10.1093/humrep/16.10.2084
- Ruder, A. (1985). Paternal-age and birth-order effect on the human secondary sex ratio. *Am. J. Hum. Genet.* 37, 362–372.
- Ryan, J. J., Amirova, Z., and Carrier, G. (2002). Sex ratios of children of Russian pesticide producers exposed to dioxin. *Environ. Health Perspect.* 110, A699–A701.
- Salicioni, A. M., Platt, M. D., Wertheimer, E. V., Arcelay, E., Allaire, A., Sosnik, J., et al. (2007). Signalling pathways involved in sperm capacitation. *Soc. Reprod. Fertil. Suppl.* 65, 245–259.
- Samura, O., Mihar, N., He, H., Okamoto, E., and Ohama, K. (1997). Assessment of sex chromosome ratio and aneuploidy rate in motile spermatozoa selected by three different methods. *Hum. Reprod.* 12, 2437–2442. doi: 10.1093/humrep/12.11.2437
- Sarkar, S., Jolly, D. J., Friedmann, T., and Jones, O. W. (1984). Swimming behavior of X and Y human sperm. *Differentiation* 27, 120–125. doi: 10.1111/j.1432-0436.1984.tb01416.x
- Schmidt, W., Jenderny, J., Hecher, K., Hackeloer, B. J., Kerber, S., Kochhan, L., et al. (2000). Detection of aneuploidy in chromosomes X, Y, 13, 18 and 21 by QF-PCR in 662 selected pregnancies at risk. *Mol. Hum. Reprod.* 6, 855–860. doi: 10.1093/molehr/6.9.855
- Scott, C., De Souza, F. F., Aristizabal, V. H. V., Hethrington, L., Krisp, C., Molloy, M., et al. (2018). Proteomic profile of sex-sorted bull sperm evaluated by SWATH-MS analysis. *Anim. Reprod. Sci.* 198, 121–128. doi: 10.1016/j.anireprosci.2018.09.010
- Shannon, M., and Handel, M. A. (1993). Expression of the Hprt gene during spermatogenesis: implications for sex-chromosome inactivation. *Biol. Reprod.* 49, 770–778. doi: 10.1095/biolreprod49.4.770
- Shettles, L. B. (1960). Nuclear morphology of human spermatozoa. *Nature* 186, 648–649. doi: 10.1038/186648a0
- Shettles, L. B. (1961). Human spermatozoa shape in relation to sex ratios. *Fertil. Steril.* 12, 502–508. doi: 10.1016/s0015-0282(16)34321-7
- Shettles, L. B. (1970). Factors influencing sex ratios. *Int. J. Gynecol. Obstet.* 8, 643–647. doi: 10.1002/j.1879-3479.1970.tb00029.x
- Siegel, R. L., Miller, K. D., and Jemal, A. (2015). Cancer statistics, 2015. *CA Cancer J. Clin.* 65, 5–29. doi: 10.3322/caac.21254
- Sills, E. S., Kirman, I., Colombero, L. T., Hariprashad, J., Rosenwaks, Z., and Palermo, G. D. (1998). H-Y antigen expression patterns in human X- and Y-chromosome-bearing spermatozoa. *Am. J. Reprod. Immunol.* 40, 43–47. doi: 10.1111/j.1600-0897.1998.tb00387.x
- Silvers, W. K., and Wachtel, S. S. (1977). H-Y antigen: behavior and function. *Science* 195, 956–960. doi: 10.1126/science.320662
- Smith, B. E., and Braun, R. E. (2012). Germ cell migration across Sertoli cell tight junctions. *Science* 338, 798–802. doi: 10.1126/science.1219969
- Smith, J. L., Garry, V. F., Rademaker, A. W., and Martin, R. H. (2004). Human sperm aneuploidy after exposure to pesticides. *Mol. Reprod. Dev.* 67, 353–359. doi: 10.1002/mrd.20022
- Song, W. H., Mohamed, E. A., Pang, W. K., Kang, K. H., Ryu, D. Y., Rahman, M. S., et al. (2018). Effect of endocrine disruptors on the ratio of X and Y chromosome-bearing live spermatozoa. *Reprod. Toxicol.* 82, 10–17. doi: 10.1016/j.reprotox.2018.09.002
- Spriggs, E. L., Rademaker, A. W., and Martin, R. H. (1996). Aneuploidy in human sperm: the use of multicolor FISH to test various theories of nondisjunction. *Am. J. Hum. Genet.* 58, 356–362.
- Szyda, J., Simianer, H., and Lien, S. (2000). Sex ratio distortion in bovine sperm correlates to recombination in the pseudoautosomal region. *Genet. Res.* 75, 53–59. doi: 10.1017/s0016672399004085
- Templado, C., Bosch, M., and Benet, J. (2005). Frequency and distribution of chromosome abnormalities in human spermatozoa. *Cytogenet. Genome Res.* 111, 199–205. doi: 10.1159/000086890
- Terrell, M. L., Hartnett, K. P., and Marcus, M. (2011). Can environmental or occupational hazards alter the sex ratio at birth? A systematic review. *Emerg. Health Threats J.* 4:7109. doi: 10.3402/ehth.v4i0.7109
- Tesarik, J., and Mendoza, C. (1996). Genomic imprinting abnormalities: a new potential risk of assisted reproduction. *Mol. Hum. Reprod.* 2, 295–298. doi: 10.1093/molehr/2.5.295
- Ueda, K., and Yanagimachi, R. (1987). Sperm chromosome analysis as a new system to test human X- and Y-sperm separation. *Gamete Res.* 17, 221–228. doi: 10.1002/mrd.1120170305
- Umehara, T., Tsujita, N., and Shimada, M. (2019). Activation of Toll-like receptor 7/8 encoded by the X chromosome alters sperm motility and provides a novel simple technology for sexing sperm. *PLoS Biol.* 17:e3000398. doi: 10.1371/journal.pbio.3000398
- Utsumi, K., Hayashi, M., Takakura, R., Utaka, K., and Iritani, A. (1993). Embryo sex selection by a rat male-specific antibody and the cytogenetic and developmental confirmation in cattle embryos. *Mol. Reprod. Dev.* 34, 25–32. doi: 10.1002/mrd.1080340105
- Van Dyk, Q., Mahony, M. C., and Hodgen, G. D. (2001). Differential binding of X- and Y-chromosome-bearing human spermatozoa to zona pellucida in vitro. *Andrologia* 33, 199–205. doi: 10.1046/j.1439-0272.2001.00427.x
- Van Kooij, R. J., and Van Oost, B. A. (1992). Determination of sex ratio of spermatozoa with a deoxyribonucleic acid-probe and quinacrine staining: a comparison. *Fertil. Steril.* 58, 384–386. doi: 10.1016/s0015-0282(16)55226-1
- Van Larebeke, N. A., Sasco, A. J., Brophy, J. T., Keith, M. M., Gilbertson, M., and Watterson, A. (2008). Sex ratio changes as sentinel health events of endocrine disruption. *Int. J. Occup. Environ. Health* 14, 138–143. doi: 10.1179/oeh.2008.14.2.138
- Van Munster, E. B., Stap, J., Hoebe, R. A., Te Meerman, G. J., and Aten, J. A. (1999). Difference in volume of X- and Y-chromosome-bearing bovine sperm heads matches difference in DNA content. *Cytometry* 35, 125–128. doi: 10.1002/(sici)1097-0320(19990201)35:2<125::aid-cyto3>3.0.co;2-h
- Van Opstal, D., Los, F. J., Ramlakhan, S., Van Hemel, J. O., Van Den Ouweland, A. M., Brandenburg, H., et al. (1997). Determination of the parent of origin in nine cases of prenatally detected chromosome aberrations found after intracytoplasmic sperm injection. *Hum. Reprod.* 12, 682–686. doi: 10.1093/humrep/12.4.682
- Vina, J., and Lloret, A. (2010). Why women have more Alzheimer's disease than men: gender and mitochondrial toxicity of amyloid-beta peptide. *J. Alzheimers Dis.* 20(Suppl. 2), S527–S533. doi: 10.3233/JAD-2010-100501
- Visconti, P. E. (2009). Understanding the molecular basis of sperm capacitation through kinase design. *Proc. Natl. Acad. Sci. U.S.A.* 106, 667–668. doi: 10.1073/pnas.0811895106
- Visconti, P. E. (2012). Sperm bioenergetics in a nutshell. *Biol. Reprod.* 87:72.
- Wang, H. X., Flaherty, S. P., Swann, N. J., and Matthews, C. D. (1994). Discontinuous Percoll gradients enrich X-bearing human spermatozoa: a study using double-label fluorescence in-situ hybridization. *Hum. Reprod.* 9, 1265–1270. doi: 10.1093/oxfordjournals.humrep.a138692
- Ward, W. S., and Coffey, D. S. (1991). DNA packaging and organization in mammalian spermatozoa: comparison with somatic cells. *Biol. Reprod.* 44, 569–574. doi: 10.1095/biolreprod44.4.569
- Williams, B. J., Ballenger, C. A., Malter, H. E., Bishop, F., Tucker, M., Zwingman, T. A., et al. (1993). Non-disjunction in human sperm: results of fluorescence in situ hybridization studies using two and three probes. *Hum. Mol. Genet.* 2, 1929–1936. doi: 10.1093/hmg/2.11.1929
- Windsor, D. P., Evans, G., and White, I. G. (1993). Sex predetermination by separation of X and Y chromosome-bearing sperm: a review. *Reprod. Fertil. Dev.* 5, 155–171.
- Woldrich, J. M., Mallin, K., Ritchey, J., Carroll, P. R., and Kane, C. J. (2008). Sex differences in renal cell cancer presentation and survival: an analysis of the National Cancer Database, 1993–2004. *J. Urol.* 179, 1709–1713; discussion 1713. doi: 10.1016/j.juro.2008.01.024
- Wu, E. M., Wong, L. L., Hernandez, B. Y., Ji, J. F., Jia, W., Kwee, S. A., et al. (2018). Gender differences in hepatocellular cancer: disparities in nonalcoholic fatty liver disease/steatohepatitis and liver transplantation. *Hepatoma Res.* 4:66. doi: 10.20517/2394-5079.2018.87
- Xia, Y., Cheng, S., Bian, Q., Xu, L., Collins, M. D., Chang, H. C., et al. (2005). Genotoxic effects on spermatozoa of carbaryl-exposed workers. *Toxicol. Sci.* 85, 615–623. doi: 10.1093/toxsci/kfi066
- Yan, J., Feng, H. L., Chen, Z. J., Hu, J., Gao, X., and Qin, Y. (2006). Influence of swim-up time on the ratio of X- and Y-bearing spermatozoa. *Eur. J. Obstet. Gynecol. Reprod. Biol.* 129, 150–154. doi: 10.1016/j.ejogrb.2006.02.020

- You, Y. A., Kwon, W. S., Saidur Rahman, M., Park, Y. J., Kim, Y. J., and Pang, M. G. (2017). Sex chromosome-dependent differential viability of human spermatozoa during prolonged incubation. *Hum. Reprod.* 32, 1183–1191. doi: 10.1093/humrep/dex080
- You, Y. A., Mohamed, E. A., Rahman, M. S., Kwon, W. S., Song, W. H., Ryu, B. Y., et al. (2018). 2,3,7,8-Tetrachlorodibenzo-p-dioxin can alter the sex ratio of embryos with decreased viability of Y spermatozoa in mice. *Reprod. Toxicol.* 77, 130–136. doi: 10.1016/j.reprotox.2018.02.011
- Zavaczki, Z., Celik-Ozenci, C., Ovari, L., Jakab, A., Sati, G. L., Ward, D. C., et al. (2006). Dimensional assessment of X-bearing and Y-bearing haploid and disomic human sperm with the use of fluorescence in situ hybridization and objective morphometry. *Fertil. Steril.* 85, 121–127. doi: 10.1016/j.fertnstert.2005.07.1295
- Zhu, J., Barratt, C. L., Lippes, J., Pacey, A. A., Lenton, E. A., and Cooke, I. D. (1994). Human oviductal fluid prolongs sperm survival. *Fertil. Steril.* 61, 360–366. doi: 10.1016/s0015-0282(16)56532-7
- Conflict of Interest:** The authors declare that the research was conducted in the absence of any commercial or financial relationships that could be construed as a potential conflict of interest.
- Copyright © 2020 Rahman and Pang. This is an open-access article distributed under the terms of the Creative Commons Attribution License (CC BY). The use, distribution or reproduction in other forums is permitted, provided the original author(s) and the copyright owner(s) are credited and that the original publication in this journal is cited, in accordance with accepted academic practice. No use, distribution or reproduction is permitted which does not comply with these terms.



Fzr/Cdh1 Promotes the Differentiation of Neural Stem Cell Lineages in *Drosophila*

Puong Thao Ly^{1†} and Hongyan Wang^{1,2,3*}

¹ Neuroscience & Behavioral Disorders Programme, Duke-NUS Medical School, Singapore, Singapore, ² Department of Physiology, Yong Loo Lin School of Medicine, National University of Singapore, Singapore, Singapore, ³ NUS Graduate School for Integrative Sciences and Engineering, National University of Singapore, Singapore, Singapore

OPEN ACCESS

Edited by:

Dominic C. Voon,
Kanazawa University, Japan

Reviewed by:

Makoto Sato,
Kanazawa University, Japan
Lucas Waltzer,
INSERM U1103 Génétique
Reproduction et Développement,
France

*Correspondence:

Hongyan Wang
hongyan.wang@duke-nus.edu.sg

†Present address:

Phuong Thao Ly,
School of Biological Sciences,
Nanyang Technological University,
Singapore, Singapore

Specialty section:

This article was submitted to
Cell Growth and Division,
a section of the journal
Frontiers in Cell and Developmental
Biology

Received: 25 September 2019

Accepted: 22 January 2020

Published: 11 February 2020

Citation:

Ly PT and Wang H (2020)
*Fzr/Cdh1 Promotes the Differentiation
of Neural Stem Cell Lineages
in *Drosophila*.*
Front. Cell Dev. Biol. 8:60.
doi: 10.3389/fcell.2020.00060

How stem cells and progenitors balance between self-renewal and differentiation is a central issue of stem cell biology. Here, we describe a novel and essential function of *Drosophila* Fzr/Cdh1, an evolutionary conserved protein, during the differentiation of neural stem cell (NSC) lineages in the central nervous system. We show that Fzr, a known co-activator of Anaphase Promoting Complex/Cyclosome (APC/C) ubiquitin ligase, promotes the production of neurons from neural progenitors called ganglion mother cells (GMCs). However, knockdown of APC/C subunit *Ida* or another APC/C co-activator *CDC20* does not similarly impair GMC-neuron transition. We also observe a concomitant loss of differentiation factor Prospero expression and ectopic accumulation of mitotic kinase Polo in *fzr* mutant clones, strongly supporting the impairment of GMC to neuron differentiation. Besides functioning in GMCs, Fzr is also present in NSCs to facilitate the production of intermediate neural progenitors from NSCs. Taken together, Fzr plays a novel function in promoting differentiation programs during *Drosophila* NSC lineage development. Given that human Fzr is inactivated in multiple types of human cancers including brain tumors and that Fzr regulates neurotoxicity in various models of neurodegenerative diseases, our study on the role of Fzr in turning off proliferation in neuronal cells may provide insights into how Fzr deficits may contribute to human neurodegenerative diseases and tumors.

Keywords: NSC, neuroblast, GMC, differentiation, Fzr/Cdh1

Abbreviations: APC/C, anaphase promoting complex/cyclosome; aPKC, atypical protein kinase C; Ase, asense; α -tub, alpha-tubulin; BAC, bacterial artificial chromosome; Baz, bazooka; BDSC, Bloomington *Drosophila* Stock Center; Bcd, bicoid; β -gal, β -galactosidase; Brm, Brahma; Cdc20, cell division cycle 20; Dcr2, Dicer 2; Dpn, deadpan; Elav, embryonic lethal abnormal visual system; EGFP, enhanced green fluorescent protein; Erm, Earmuff; Fzr, fizzy and cell division cycle 20 related; GFP, green fluorescent protein; GMC, Ganglion Mother Cell; Ida, imaginal discs arrested; INP, intermediate neural progenitor; Insc, inscuteable; Lola, longitudinal lacking; MARCM, mosaic analysis with a repressible cell marker; Mira, Miranda; Nerfin-1, nervous fingers 1; NSC, neural stem cell; ns, statistically non-significant; Phall, phalloidin; PH3, phospho-Histone H3; Polo, polo kinase; Pros, prospero; Repo, reversed polarity; Rca1, regulator of cyclin A1; RNAi, RNA interference; UAS, upstream activating sequence; VDRC, Vienna *Drosophila* Resource Center; Wor, Worniu.

INTRODUCTION

Understanding how stem cells maintain their self-renewal capacity and how their progeny differentiate into specific fates are essential to comprehend developmental processes as well as to exploit the therapeutic potential of stem cells for regenerative medicines and cancer treatments. The *Drosophila* larval brain NSCs, or neuroblasts, have emerged as a fertile model for studying stem cell self-renewal and differentiation *in vivo* (Li et al., 2014). In the *Drosophila* central nervous system, type I NSCs divide asymmetrically to self-renew and to generate a smaller daughter cell called the GMC that only divides once to give rise to two terminally differentiated neurons or glial cells (reviewed in Homem et al., 2015). Besides type I NSCs, 8 type II NSCs located bilaterally in the central brain divide asymmetrically to self-renew and generate intermediate neural progenitors (INPs), which can divide 4–6 times to give rise to GMCs and neurons (Bello et al., 2008; Boone and Doe, 2008; Bowman et al., 2008). Newly generated INPs need to differentiate into mature INPs before division. The transcription factor Earmuff (Erm), a homolog of the vertebrate Forebrain embryonic zinc-finger family, is required for INP maturation (Bowman et al., 2008; Weng et al., 2010). Erm works together with the SWI/SNF chromatin-remodeling complex Brahma (Brm) in immature INPs to restrain the developmental potential of INPs (Eroglu et al., 2014; Koe et al., 2014; Janssens et al., 2017; Liu et al., 2017). Several studies in both mammals and *Drosophila* have indicated that neuronal differentiation is actively maintained. To date, only a few factors have been implicated in maintaining *Drosophila* neuronal differentiation. These factors include the homeodomain transcription factor Prospero (Pros, human homolog Prox1) (Caussinus and Gonzalez, 2005; Choksi et al., 2006; Maurange et al., 2008), RNA splicing factor Midlife Crisis (Mlc) (Carney et al., 2013), BTB-zinc finger transcriptional factor longitudinals lacking (Lola) (Southall et al., 2014), and the zinc finger transcription factor Nervous fingers 1 (Nerfin-1) (Froldi et al., 2015). In the absence of Pros, GMCs revert to NSCs instead of committing to differentiation (Betschinger et al., 2006; Choksi et al., 2006; Lee et al., 2006). Mlc regulates expression and splicing of Pros and the loss of Mlc leads to the accumulation of ectopic NSC-like cells originating from dedifferentiated neurons, but these NSC-like cells are stalled during cell cycle and do not form tumors (Carney et al., 2013). Lola, on the other hand, acts redundantly with Pros. The loss of Lola is associated with neuron-to-NSC reversion and tumorigenesis in the optic lobes, but not in the central brain due to the compensatory functions of Pros (Southall et al., 2014). Recently, Nerfin-1 has been shown to function downstream of Pros to maintain neuronal differentiation. Neurons in *nerfin-1* mutants first increase their cellular size, then switch off neuronal program and start to express the NSC-identity program (Froldi et al., 2015). However, it remains elusive whether other cellular factors play a role in differentiation of NSC lineages.

Fzr (*fizzy-related*) or Rap (*retina aberrant in pattern*) or Cdh1, the *Drosophila* homolog of mammalian FZR1, is an evolutionarily conserved protein that functions as a positive regulator of Anaphase-Promoting Complex/Cyclosome

(APC/C), which regulates cell-cycle progression via ubiquitin-mediated proteolysis (Pines, 2011). While APC/C interacts with CDC20/Fizzy (Fzy) to mediate chromatid separation during metaphase-to-anaphase progression and drive mitotic exit, APC/C binds to Fzr/Cdh1 during mitotic exit and G1 phase to conclude mitotic exit as well as to participate in non-mitotic functions such as endoreplication, quiescence, and differentiation (Eguren et al., 2011). In *Drosophila*, Fzr has also been shown to promote mitotic exit (Meghini et al., 2016) and to regulate various non-mitotic functions, including glial migration (Silies and Klämbt, 2010) and glial cell number (Kaplow et al., 2008), synapse size and activity at neuromuscular junctions (van Roessel et al., 2004), terminal mitosis (Reber et al., 2006), endocycle and endoreplication (Sigrist and Lehner, 1997; Schaeffer et al., 2004; Narbonne-Reveau et al., 2008; Djabrayan et al., 2014), and in retinal differentiation (Martins et al., 2017). However, how Fzr functions in NSC lineages remains unknown.

Here, we describe a novel and essential role for *Drosophila* Fzr in GMC-to-neuron transition in both type I and type II NSC lineages of the developing larval brains. In *fzr*[−] mutant clones, GMC population expands at the expense of neurons. We also observe a concomitant loss of Pros expression and ectopic accumulation of Polo in mutant clones, suggesting the impairment of GMC to neuron differentiation. The localization of EGFP-Fzr^{BAC} in late GMCs is consistent with its novel function in GMCs. Moreover, Fzr also regulates NSC to INP transition, through genetic interaction with *Brm* and *Erm*.

MATERIALS AND METHODS

Fly Stocks and Genetics

FRT19A, *fzr*^A (#52384), FRT19A, *fzr*^B (#52385), and Dp(1;3)DC120 (#30265) were obtained from BDSC. FRT19A, *fzr*^{G0418} (#111943) was obtained from Kyoto Stock Center. UAS-Fzr-HA (#F000893) was obtained from FlyORF. UAS-HA-Rca1 is a gift from Dr. Frank Sprenger (Grosskortenhaus and Sprenger, 2002) and FRT19A, *fzr*^{8F3} (P{neoFRT}19A/FM7) was a gift from Dr. Christian Klämbt. EGFP-Fzr^{BAC} was generated in this study.

RNAi lines used in this study: *erm*_RNAi (BDSC #26778), *fzr*_RNAi (GD#25553), *cdc20*_RNAi_1 (GD#40500), *cdc20*_RNAi_2 (GD#44834), *ida*_RNAi (BDSC#34522), *brm*_RNAi (GD#37720), *β-gal*_RNAi (BDSC#50680), and *bcd*_RNAi (GD#48966).

Neural stem cell drivers included *insc*-Gal4 (BDSC#8751; 1407-Gal4) or *wor*-Gal4 (BDSC#56553). Glial driver was *repo*-Gal4 (BDSC#7415). Type I NSC driver (*ase*-Gal4; UAS-mCD8-GFP, T. Lee). Type II NSC driver (*w*; UAS-Dicer2, *wor*-Gal4, *ase*-Gal80; UAS-mCD8-GFP) (Bowman et al., 2008). INP driver (*erm*-Gal4/CyO) (Pfeiffer et al., 2008). Other drivers used in this study are: *nerfin-1*-Gal4, UAS-mCD8-GFP (Louis Y. Cheng), *pros*-Gal4 (BDSC#80572), and *elav*-Gal4 (BDSC#458). UAS-Dcr2 (BDSC#24650) or/and UAS-CD8-GFP (BDSC#32186) was used together with various Gal4 drivers or RNAi stocks.

Experiments with mutants were performed at 25°C, and experiments for RNAi-mediated knockdown or overexpression were carried out at 29°C.

Clonal Analysis

MARCM clones were generated as previously described (Lee et al., 1999). Briefly, the larvae were heat-shocked twice at 37°C for 2 hours (h) each, shortly after larval hatching (ALH) and at 10–16 h after the first heat shock. Larvae were further aged for another 3 days at 25°C before dissection.

MARCM driver used is *w^{hsFLP}, FRT19A, tubP-Gal80; UAS-nlsLac, UAS-mCD8-GFP; tub-Gal4* (Lee et al., 1999).

Immunocytochemistry

Wandering third instar larval brains were dissected in cold PBS and fixed in 4% EM-grade formaldehyde in PBS at room temperature (RT) for 22 minutes (min), following by three washes in 0.3% Triton-X in PBS (PBST). The sample was incubated with blocking buffer (3% BSA in PBST) for 45 min at RT, followed by incubation with primary antibody mixture overnight at 4°C. After three washes in PBST, larval brains were incubated with secondary antibody mixture for 90 min at RT, followed by two washes, and mounted in a glycerol based mounting medium (10 mg/ml of *p*-Phenylenediamine in PBS, 1:10 dilution with glycerol). For staining of DNA, additional incubation of the sample with diluted Topro-3 in PBST was performed just before adding mounting medium. Samples were imaged with Zeiss LSM 710 confocal microscopy and images were processed with Zeiss black software.

The following antibodies were used in this study: guinea pig anti-Dpn (1:1000, J. B. Skeath), rabbit anti-Ase (1:1000, Y. N. Jan), rabbit anti-Repo (1:500, W. Chia), rat anti-CD8 (1:250, Life technologies, Cat#MCD0800), rabbit anti-PH3 (1:200, Sigma, Cat#H9908-25UL: AB_260096), rat anti-Elav (1:40, DSHB, Cat#Rat-Elav-7E8A10), guinea pig anti-Nerfin-1 (1:1000, Louise Y. Cheng), mouse anti-Miranda (1:40, F. Matsuzaki), rabbit anti-aPKC ζ C20 (1:100, Santa Cruz Biotechnology Cat# sc-17781), guinea pig anti-Baz (1:500; A. Wodarz), mouse anti-Pros [1:10, DSHB, Cat# Prospero (MR1A)], rabbit anti-Polo (1:100, C. Sunkel), rabbit anti-GFP (Molecular Probes, Cat#A21311, 1:500), mouse anti- α -tub (1:200, Sigma-Aldrich, Cat#T6199-200UL), rabbit anti- β -gal (1:100, Invitrogen, A-11132), mouse anti- β -gal (1:1000, Promega, Cat#Z3781), rat anti-HA (1:2000; Roche, Cat #11867423001, Clone 3F10), rabbit anti-PntP1 [1:500, J. B. Skeath (Alvarez, 2003)]. DNA was labeled by ToPro-3 (1:5000, Invitrogen, Cat#T3605).

The secondary antibodies (Alexa 647, Alexa 568, and Alexa 488 or Alexa 405) were obtained from Jackson Immuno Research Laboratories, Inc. and used at 1:500 dilution. Phalloidin 488 (1:500, InvitrogenTM, A12379), was added together with secondary antibodies.

Generation of Transgenic Flies

BAC line (CH321-61L05) was used to generate *EGFP-Fzr^{BAC}* genomic construct according to the method described previously (Zhang et al., 2019). Briefly, a fragment containing enhanced GFP (EGFP) tag and Kanamycin-resistant gene was amplified from PL-452 EGFP vector and inserted to the N-terminus of *fzr* coding sequence by recombination using SW102 electrocompetent cells. The resulting cassette was then electroporated into *ara*-inducible

Cre carrying SW106 electrocompetent bacteria to remove the Kanamycin resistant gene. The correct clone carrying *EGFP-Fzr^{BAC}* was electroporated into EPI300 cells for amplification and the BAC DNA was purified using BACMAX kit (Epicentre Biotechnologies Cat# BMAX044). The *EGFP-Fzr^{BAC}* was sent to BestGene, Inc. for injection into $y^1 w^{67}c^{23}; P\{CaryP\}attP40$ (estimated cytosite 25C6) background. The primers used for recombination are listed in **Supplementary Table 1**.

Statistical Analysis

GraphPad Prism 6 software was used for statistical analysis. All data were presented as mean \pm SD. Unpaired two-tail *t*-tests were used for two sample comparisons and one-way ANOVA for comparison of more than two groups. In ANOVA, Dunnett's *post hoc* test was used to obtain the *P*-values for pairwise comparison. In this work, comparisons were performed against wild-type or control, unless otherwise indicated by a line between two genotypes. A value of $P \leq 0.05$ was considered as statistically significant, * indicated $P \leq 0.05$, ** indicates $P \leq 0.01$, *** indicates $P \leq 0.001$, and **** indicates $P \leq 0.0001$. $P > 0.05$ was considered as statistically non-significant (ns).

RESULTS

Loss of Fzr in NSC Lineages Results in Ectopic Progenitor GMCs

In order to evaluate the possible function of Fzr in NSC lineage development, we generated mosaic analysis with a repressible cell marker (MARCM) clones for two known mutant alleles of *fzr*, named *fzr^A* and *fzr^B*, which were isolated by ethyl methanesulfonate (EMS) mutagenesis on X-chromosome (Yamamoto et al., 2014). Both alleles failed to complement *fzr^{G0326}*, the hypomorphic allele with a *P{lacZ}* element inserted in the first intron of *fzr*, and were rescued by Dp(1;3)DC120 duplication regarding lethality (this study and Yamamoto et al., 2014). We have tried but failed to characterize the precise lesion of *fzr^A* and *fzr^B*. Whereas all the control type I NSC lineages ($n = 40$) contain a single Dpn⁺ Ase⁺ NSC and 4-5 Dpn⁻ Ase⁺ GMCs that undergo terminal division, *fzr^A* and *fzr^B* (collectively called *fzr⁻*) mutant clones contain a single NSC but a large number of ectopic GMCs (17.8 ± 6.38 and 19.6 ± 8.20 , respectively) (**Figures 1A,B**). The ectopic GMC phenotype observed in *fzr⁻* mutants were fully rescued by expressing an UAS- Fzr-HA transgene driven by *tub-Gal4* from MARCM driver as well as by the insertion of Dp(1;3)DC120, a genomic fragment containing the *fzr* locus (**Figures 1A,B**).

Next, we assessed whether ectopic GMCs were also observed in type II NSC lineages in *fzr⁻* mutants. There are 8 type II NSC lineages in each larval brain lobe. The defining characteristic of type II NSC clones is that they produce INPs, which can divide 4–6 times to generate GMCs. Within type II lineages, the NSCs can be recognized by their large size (10–14 μ m in diameter) and positive for Dpn but negative for Ase. INPs can be identified by their small size (3–4 μ m in diameter) and are either Dpn⁺ Ase⁺ (mature INPs) or Dpn⁻ Ase⁺ and Dpn⁻ Ase⁻ (immature INPs). We further analyzed the number of immature

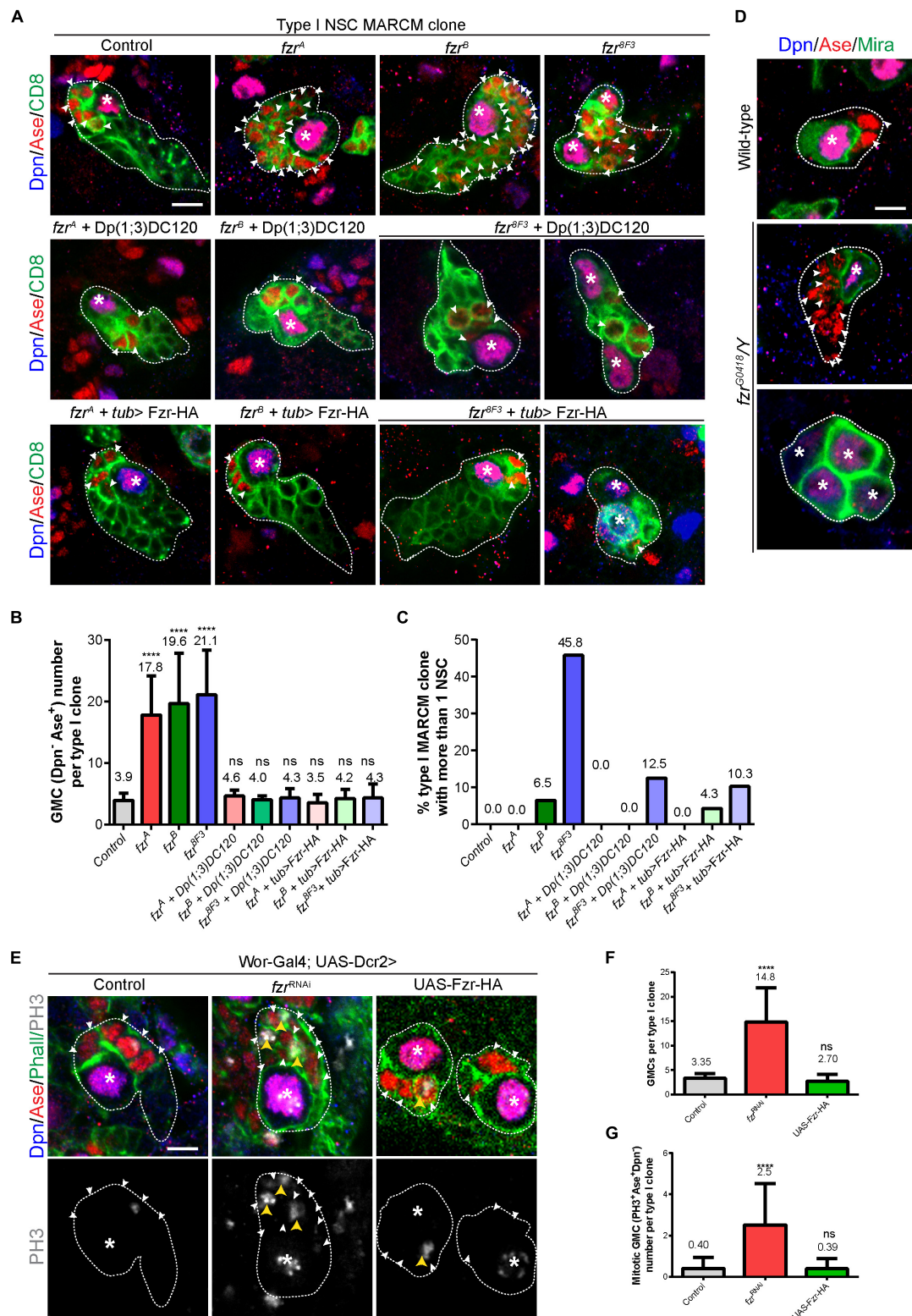


FIGURE 1 | Ectopic GMCs are generated upon Fzr deletion. **(A)** Type I NSC clones of MARCM driver control (FRT19A), *fzr^A*, *fzr^B*, *fzr^{8F3}*, *fzr^A + Dp(1;3)DC120*, *fzr^B + Dp(1;3)DC120*, *fzr^{8F3} + Dp(1;3)DC120*, *fzr^A + tub > Fzr-HA*, *fzr^B + tub > Fzr-HA*, and *fzr^{8F3} + tub > Fzr-HA* were labeled with Dpn, Ase and CD8. *tub > Fzr-HA* refers to UAS-Fzr-HA driven by *tub-Gal4* from MARCM driver, so Fzr-HA is expressed only in MARCM clones that lose *tub-Gal80* upon mitotic recombination. **(B,C)** Quantifications of GMC number **(B)** per type I MARCM clones and the percentage of MARCM clones with two or more NSCs **(C)** for **(A)**.

(Continued)

FIGURE 1 | Continued

Control, $n = 40$; fzr^A , $n = 46$; fzr^B , $n = 46$; fzr^{8F3} , $n = 24$; $fzr^A + \text{Dp}(1;3)\text{DC120}$, $n = 23$; $fzr^B + \text{Dp}(1;3)\text{DC120}$, $n = 20$; $fzr^{8F3} + \text{Dp}(1;3)\text{DC120}$, $n = 16$; $fzr^A + tub > Fzr\text{-HA}$, $n = 31$; $fzr^B + tub > Fzr\text{-HA}$, $n = 23$; $fzr^{8F3} + tub > Fzr\text{-HA}$, $n = 29$. **(D)** Type I NSC lineages of wild-type and hemizygous $fzr^{G0418/Y}$ larvae were labeled with Dpn, Ase, and Mira. Each genotype, $n > 30$ clones in at least five different brain lobes. **(E)** Type I NSC lineages of control ($\beta\text{-gal}^{RNAi}$), fzr^{RNAi} , or UAS-Fzr-HA with NSC-driver ($wor\text{-Gal4}$; UAS-Dcr2) were labeled with Dpn, Ase, Phall (Phalloidin, cortical actin), and PH3. **(F,G)** Quantifications of the number of GMCs **(F)** and mitotic GMCs **(G)** per type I clones for **(E)**. For **(F)**, control, $n = 20$; fzr^{RNAi} , $n = 50$; UAS-Fzr-HA, $n = 56$. For **(G)**, control, $n = 50$; fzr^{RNAi} , $n = 50$; UAS-Fzr-HA, $n = 41$. Data are presented as mean \pm SD. **** $P \leq 0.0001$. Asterisks, NSCs; white arrowheads, GMCs; yellow arrowheads, mitotic GMCs; white dotted lines, clone outline. Scale bars: 5 μm . n, number of quantified clones. Ase, Asense; Dcr2, Dicer 2; Dpn, Deadpan; Fzr, Fizzy and cell division cycle 20 related; GMC, Ganglion Mother Cell; MARCM, mosaic analysis with a repressible cell marker; Mira, Miranda; ns, statistically non-significant; NSC, neural stem cell; Phall, Phalloidin; PH3, phospho-Histone H3; UAS, upstream activating sequence; Wor, Worniu.

INPs in fzr^- type II clones by examining Ets domain-containing transcription factor Pointed P1 (PntP1), which is expressed in both type II NSCs and immature INPs (Zhu et al., 2011). The population of immature INPs are positive for PntP1 and can therefore be distinguished from GMCs. Similar to ectopic GMCs in fzr^- type I clones, the ectopic Dpn⁺ Ase⁺ cells, which include GMCs and immature INPs, are also observed in fzr^- mutant type II clones (**Supplementary Figures 1A,B**). Since we did not detect any change in the number of mature and immature INPs (**Supplementary Figures 1C,E–G**), ectopic Dpn⁺ Ase⁺ cells observed in type II fzr^- clones are most likely GMCs. Together, these results suggest that Fzr regulates the homeostasis of GMCs in both type I and type II NSC lineages.

Consistently, the knockdown of Fzr in NSCs (and their immediate progenies due to perdurance of Gal4 in progenies) using RNA interference (RNAi) with pan-NSC driver ($wor\text{-Gal4}$; UAS-Dcr2) resulted in ectopic GMCs (**Figures 1E,F**) that are often undergoing cell division (**Figures 1E,G**). Similarly, the knockdown of Fzr specifically in type I or type II NSCs (and immediate progenies of NSCs due to Gal4 protein perdurance) also leads to an increased number of GMCs (**Supplementary Figures 1H–K**).

Moreover, we also observed ectopic GMCs phenotype in clones from another fzr^- mutant, fzr^{8F3} as well as hemizygous mutant $fzr^{G0418/Y}$ (**Figures 1A–D**). The EMS fzr^{8F3} mutant contains a nonsense mutation (Trp214 > Stop) for fzr and likely produces short unstable peptides (Silies and Klämbt, 2010). The fzr^{G0418} has the $P\{lacW\}$ element inserted in the 5' end of fzr gene, and is hypomorphic allele of fzr (Jacobs et al., 2002). Besides having ectopic GMCs, a few fzr^B clones also contained ectopic small Dpn⁺Ase⁺ NSC-like cells (**Figure 1C**). Similarly, in fzr^{8F3} mutant clones, 45.8% ($n = 24$) and 80% ($n = 20$) of mutant type I and type II clones also contained ectopic NSCs (**Figures 1A,C** and **Supplementary Figures 1A,D**). While the ectopic GMC phenotype observed in fzr^{8F3} clone was completely rescued by the insertion of genomic fragment Dp(1;3)DC120, the ectopic NSC phenotype was only partially rescued (**Figures 1A,C** and **Supplementary Figures 1A,D**), suggesting an additional background mutation present in the fzr^{8F3} mutant might partially contribute to the ectopic NSC phenotype. Hereafter we focus on the function of Fzr in regulating GMC population in type I NSC clones.

In conclusion, Fzr plays an important role in NSC lineage progression in developing larval brains and that the Fzr loss results in the formation of ectopic GMCs.

Fzr[−] Neural Lineages Do Not Display Any Disturbance of NSC Asymmetric Division or Neuronal Dedifferentiation

To further characterize the cell fate of GMCs accumulated upon the loss of Fzr, we examined the expression of Nerfin-1, which is expressed in late GMCs and newly generated neurons. Whereas each control type I NSC clone contains only on average 1.09 ± 0.702 Ase⁺ Nerfin-1⁺ late GMCs and around 12.2 ± 4.82 Ase[−] Nerfin-1⁺ early neurons, there were 25.7 ± 8.52 and 24.0 ± 7.31 Ase⁺ Nerfin-1⁺ late GMCs and 2.26 ± 2.47 and 2.65 ± 3.42 Ase[−] Nerfin-1⁺ early neurons in fzr^A and fzr^B mutant clones, respectively (**Figures 2A–C**). Wild-type neurons express Embryonic lethal absnormal vision (Elav) but not Asense (**Figure 2D**). Strikingly, we observed a population of Elav⁺ Ase⁺ cells in fzr^- mutants with a concomitant reduction of Elav⁺ Ase[−] neurons (**Figures 2D–F**). Consistently, upon the loss of Fzr in type I MARCM clones, some of the Elav⁺ Ase⁺ cells are undergoing mitosis, as judged by the presence of phospho-Histone 3 (PH3) (**Figures 2D,G**). Altogether, these results indicate that loss of Fzr in NSC lineages results in the accumulation of dividing GMCs at the expense of generating neurons undergoing differentiation.

There are three non-mutually exclusive possibilities that could contribute to this interesting phenotype: (1) an ectopic production of GMCs from disrupted asymmetric divisions or extended NSC division; and/or (2) dedifferentiation of neurons to GMCs; and/or (3) failures during GMC differentiation that lead to their ectopic cell divisions.

To address the first possibility that the disturbance in NSC division results in production of excess GMCs, we examined the localization of polarity proteins that are essential for NSC division. We observed that the cellular localization of apically localized aPKC and basally localized Miranda (Mira) in fzr^{8F3} dividing NSCs are intact and similar to that of the control NSCs (**Figure 2H**). Similarly, Mira in both control as well as fzr^A and fzr^B NSCs are correctly localized (**Supplementary Figure 2A**). The localization of another apically localized protein Bazooka (Baz, *Drosophila* homolog of mammalian Par3) are also intact in fzr^{8F3} mutant NSCs (**Figure 2I**). In addition, the localization of mitotic kinase Polo in dividing NSCs seems unaffected in fzr^A and fzr^B NSCs (**Supplementary Figure 2B**). Besides, the number of progeny cells from a single NSC remains similar upon Fzr loss (**Supplementary Figure 1L**) and that no elevated cell-death, as judged by the

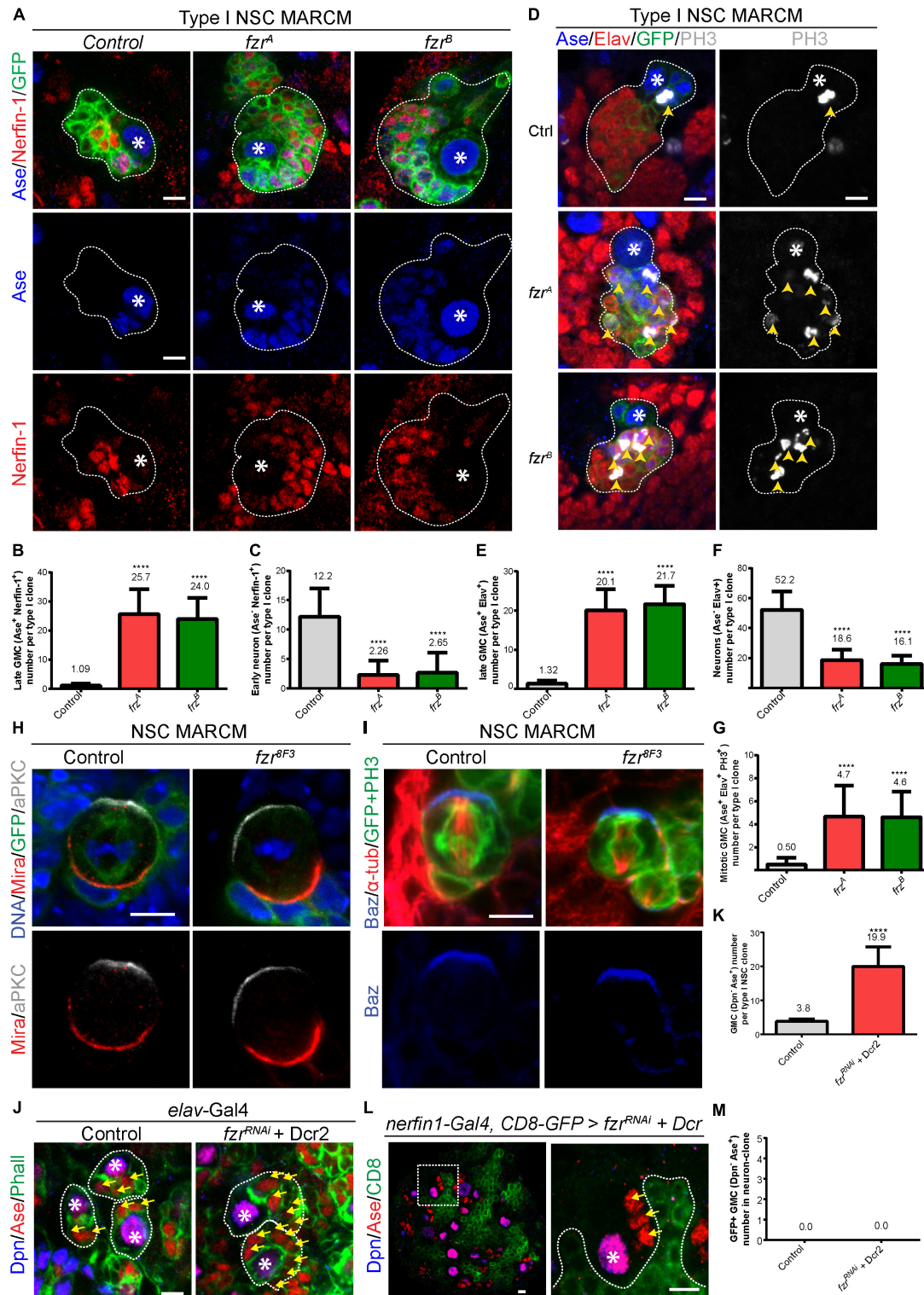


FIGURE 2 | Depletion of Fzr does not impair NSC division nor promote neuronal dedifferentiation. **(A)** Type I MARCM clones of MARCM driver control (FRT19A), *fzr^A* and *fzr^B* were labeled with Ase, Nerfin-1 and GFP. **(B,C)** Quantifications of the number of Ase⁺ Nerfin-1⁺ cells **(B)**, late GMCs and Ase⁺ Nerfin-1⁺ **(C)**, early neurons for **(A)**. For **(B,C)**, control, *n* = 35; *fzr^A*, *n* = 23; *fzr^B*, *n* = 20. **(D)** Type I MARCM clones of MARCM driver control (FRT19A), *fzr^A* and *fzr^B* were labeled with Ase, Elav, PH3, and GFP. **(E-G)** Quantifications of the number of Ase⁺ Elav⁺ cells **(E)**, Ase⁺ Elav⁺ **(F)**, neurons, and mitotic PH3⁺ Ase⁺ Elav⁺ **(G)** for **(D)**. For **(E,G)**, control, *n* = 22; *fzr^A*, *n* = 21; *fzr^B*, *n* = 23. For **(F)**, control, *n* = 21; *fzr^A*, *n* = 20; *fzr^B*, *n* = 21. **(H)** Mitotic NSCs in control (FRT19A MARCM control) and *fzr^{8F3}* MARCM clones **(Continued)**

FIGURE 2 | Continued

were labeled with DNA, Mira, aPKC, and GFP. Control, $n = 20$; fzr^{8F3} , $n = 20$. **(I)** Mitotic NSCs in control (FRT19A MARCM control) and fzr^{8F3} MARCM clones were labeled with Baz, α -tub, PH3, and GFP. Control, $n = 5$; fzr^{8F3} , $n = 7$. **(J)** Type I NSC lineages of control (β -gal^{RNAi} + Dcr2) or fzr^{RNAi} + Dcr2 with pan neuronal driver (*elav*-Gal4) were labeled with Dpn, Ase, and Phall. **(K)** Quantification of the number of Dpn⁺ Ase⁺ cells (GMCs) for **(J)** control, $n = 31$; fzr^{RNAi} + Dcr2, $n = 15$. **(L)** Type I NSC lineages of fzr^{RNAi} + UAS-Dcr2 with late-GMC and neuronal driver (*nerfin-1*-Gal4, UAS-CD8-GFP) was labeled with Dpn, Ase and GFP. Enlarged views of the white dotted boxes in the right panel is shown in left panel. **(M)** Quantifications of GMC number found within GFP⁺ neuron-clones for **(L)** control (β -gal^{RNAi} + Dcr2), $n = 50$; fzr^{RNAi} + Dcr2, $n = 50$. Data are presented as mean \pm SD. **** $P \leq 0.0001$. Asterisks, NSCs; yellow arrows, GMCs; yellow arrowheads, mitotic GMCs; white dotted lines, clone outline. Scale bars: 5 μ m. n, number of quantified clones. aPKC, atypical protein kinase C; Ase, Asense; α -tub, alpha-tubulin; Baz, Bazooka; Dcr2, Dicer 2; Dpn, Deadpan; Elav, embryonic lethal abnormal visual system; Fzr, Fizzy and cell division cycle 20 related; GMC, Ganglion Mother Cell; MARCM, mosaic analysis with a repressible cell marker; Mira, Miranda; Nerfin-1, Nervous finger 1; NSC, neural stem cell; Phall, Phalloidin; PH3, phospho-Histone H3; UAS, upstream activating sequence.

staining of cleaved caspase 3, was observed in fzr^A clones (**Supplementary Figure 2C**). Together, these results suggest that NSC division seems normal upon loss of Fzr and that disturbances in NSC division are unlikely the cause of GMC accumulation.

To test whether neuronal dedifferentiation accounts for the ectopic GMCs, we knocked down *Fzr* in different populations of NSCs lineages with fzr^{RNAi} with different Gal4 drivers. While the loss of *Fzr* in whole NSC lineage using *elav*-Gal4 or *pros*-Gal4 drivers resulted in ectopic GMCs (**Figures 2J,K** and **Supplementary Figure 2D**), the loss of *Fzr* in late GMCs and early neurons by *nerfin-1*-Gal4 driver did not result in ectopic GMCs within *nerfin-1* expressing clones (labeled by GFP) (**Figures 2L,M**). Moreover, using an enhancer trap in which beta-galactosidase (β -Gal) is inserted at *fzr* locus (fzr^{G0418}), we did not detect the expression of *Fzr* in *Elav*⁺ neurons (**Supplementary Figure 2E**), suggesting that *Fzr* does not function in neurons to maintain neuronal differentiation. In summary, our results indicate that neuronal dedifferentiation is unlikely the cause of GMC accumulation.

Interestingly, we observed a high expression of *Fzr* in glial cells (**Supplementary Figure 2F**). However, upon the knockdown of *Fzr* in glial cells by fzr^{RNAi} with glial driver (*repo*-Gal4), GMC number remains unchanged (**Supplementary Figures 2G–I**), indicating that GMC number is not regulated by *Fzr* in glial cells.

In summary, our results suggest that ectopic GMC accumulation upon the loss of *Fzr* is likely caused by the failed differentiation of GMCs that leads to ectopic GMC divisions.

Fzr[−] Neural Lineages Display Defects in GMC-to-Neuron Transition

To test if there are any defects during the transition of GMCs to neurons, we assessed the expression of differentiation factor Prospero (Pros) (Chu-Lagraff et al., 1991; Choksi et al., 2006) in fzr^{-} NSC clones. In most fzr^{-} clones, the expression of Pros is substantially reduced in comparison to those of control clones (**Figure 3A**). Moreover, the expression of Polo kinase, which promotes cell division and stemness (Sunkel and Glover, 1988; Glover, 2005), remained high in ectopic GMCs of fzr^{-} clones (**Figure 3B**). All these results suggest that the ectopic mutant GMCs maintain their undifferentiated states and are unable to differentiate into neurons.

In addition, *Fzr* displayed moderate staining in wild-type NSCs and weak staining in GMCs (**Figure 3C**, asterisks and yellow arrows, respectively), consistent with our model that *Fzr*

functions within GMCs to promote the transition of GMCs into neurons. To further characterize the expression pattern of endogenous *Fzr* in the nervous system, we attempted to generate anti-*Fzr* antibodies for immunostaining without success (data not shown). Next, we turned to labeling *Fzr* protein with enhanced GFP (EGFP) within its endogenous locus, hereafter called EGFP-*Fzr*^{BAC}. Consistent with the localization of *Fzr* shown by the enhancer trap, EGFP-*Fzr*^{BAC} displayed strong staining in glial cells, as judged by their glial morphology and cortical location (**Figure 3D**, white arrows) as well as being positive for the glial marker Repo (**Supplementary Figure 3A**). Besides, EGFP-*Fzr*^{BAC} also displayed strong localization in late GMCs (**Figure 3E**, yellow arrows), minimal level in early GMCs (**Figure 3E**, blue arrows, as judged by their small size, being Ase⁺ Mira^{weak} cells, and their immediate proximity to the big Ase⁺ Mira⁺ type I NSCs) and weak level in NSCs (**Figure 3E**, white asterisks).

Moreover, *Fzr* is known for its function as an activator of the ubiquitin ligase complex APC/C to promote the ubiquitination and degradation of various substrates during G1 (Sigrist and Lehner, 1997; Jacobs et al., 2002; Schaeffer et al., 2004). We wondered whether *Fzr* functions in NSC lineages might be mediated by APC/C^{Fzr} complex. To test this, we knocked down *ida*, a subunit of APC/C, in type II NSC driver. However, upon *ida* knockdown, no ectopic GMCs was observed, although other defects such as loss of NSCs, loss of NSC identity and mitotic arrest were observed (**Supplementary Figure 3B**). These phenotypes were also observed upon knockdown of *cdc20*, the co-activator of APC/C during mitosis (**Supplementary Figure 3B**). These phenotypes were consistent with known functions of APC/C in dividing cells and in agreement with the mitotic defects reported for *ida* and *cdc20* mutants (Dawson et al., 1993; Bentley et al., 2002), indicating the RNAi-mediated knockdown were efficient. Furthermore, upon the overexpression of HA tagged Rca1, the negative regulator of *Fzr*-dependence APC/C activity (Grosskortenhaus and Sprenger, 2002), no ectopic GMCs were observed in both type I and type II lineages (**Supplementary Figures 3D–H**), although HA-Rca1 protein was successfully over-expressed in type II NSCs and their immediate progenies (**Supplementary Figure 3C**). These results highlight a possibility that *Fzr* might function independently of APC/C in regulating GMC-to-neuron transition. Because the loss of function of APC/C blocks the mitotic progression of NSCs to generate GMCs, we are unable to completely rule out the potential involvement of APC/C in GMC-to-neuron differentiation.

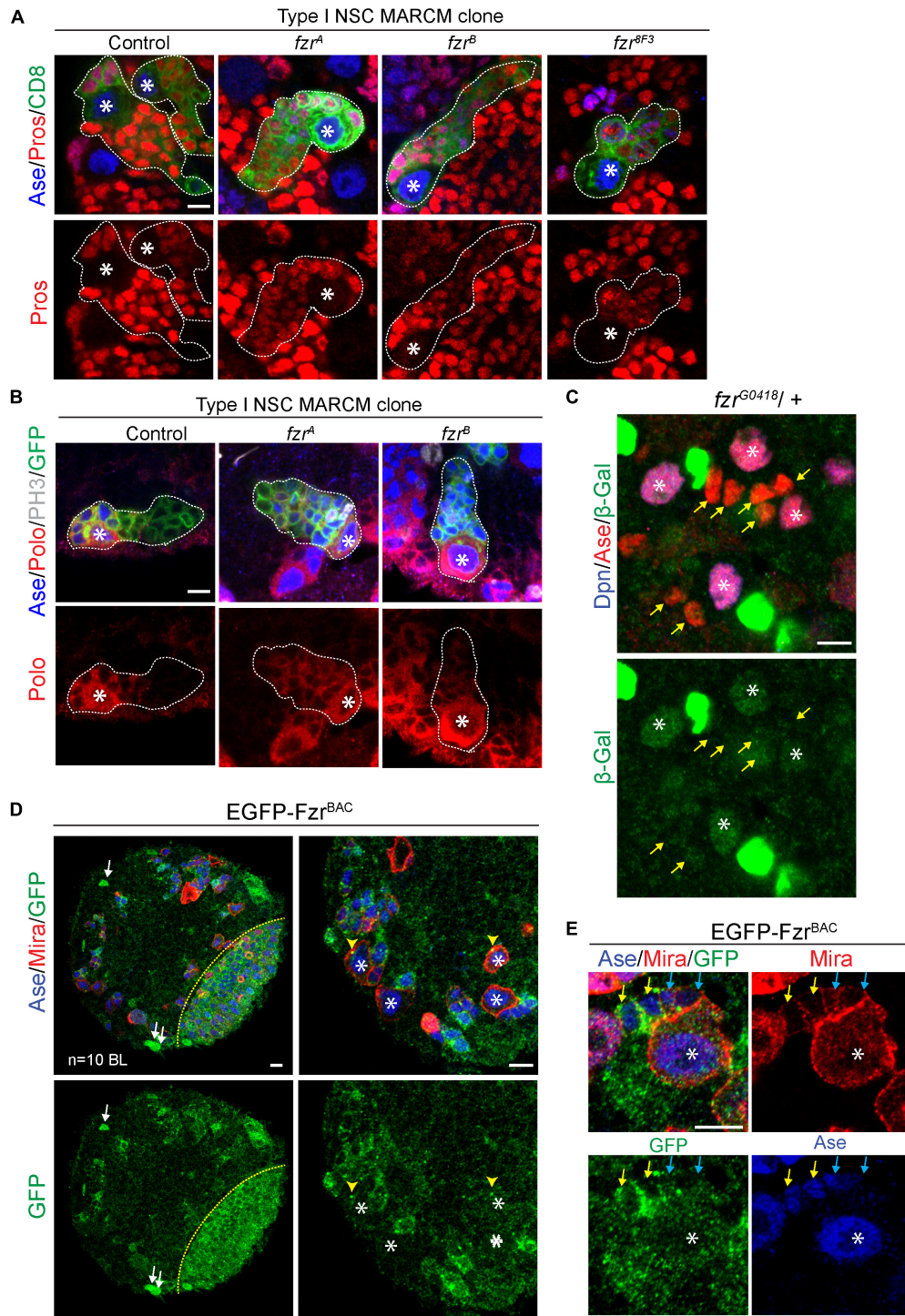


FIGURE 3 | Fzr promotes the transition from GMCs to neurons. **(A)** Type I MARCM clones of MARCM driver control (FRT19A), *fzr^A*, *fzr^B*, and *fzr^{8F3}* were labeled with Ase, Pros, and CD8. Control, $n = 22$; *fzr^A*, $n = 32$; *fzr^B*, $n = 27$; *fzr^{8F3}*, $n = 20$. **(B)** Type I MARCM clones of MARCM driver control (FRT19A) and *fzr^B* were labeled with Ase, Polo, PH3, and GFP. Control, $n = 30$; *fzr^A*, $n = 50$; *fzr^B*, $n = 50$. **(C)** NSC lineages in third instar larval brain of heterozygous *fzr^{G0418/+}* (*fzr-lacZ*)/+ were labeled with Dpn, Ase, and β-Gal, product of *lacZ* gene that is inserted in *fzr* locus. $n = 10$ brain lobes. Yellow arrows, GMCs. **(D,E)** Larval brains expressing genomic EGFP-Fzr^{BAC} were co-stained with Ase and Mira. $n = 10$ brain lobes. Yellow arrows, late GMCs; blue arrows, early GMCs; white arrows, glial like cells; yellow arrowhead, centrosome-like punctate; yellow dotted lines indicate boundary between the optic lobe and the central brain. Asterisks, NSCs; white dotted lines, clone outline. Scale bars: 5 μm. Ase, Asense; β-gal, β-galactosidase; Dcr2, Dicer 2; Dpn, Deadpan; EGFP, enhanced green fluorescent protein; Fzr, Fizzy and cell division cycle 20 related; GFP, green fluorescent protein; GMC, Ganglion Mother Cell; MARCM, mosaic analysis with a repressible cell marker; Mira, Miranda; NSC, neural stem cell; PH3, phospho-Histone H3; Polo, Polo kinase; Pros, Prospero.

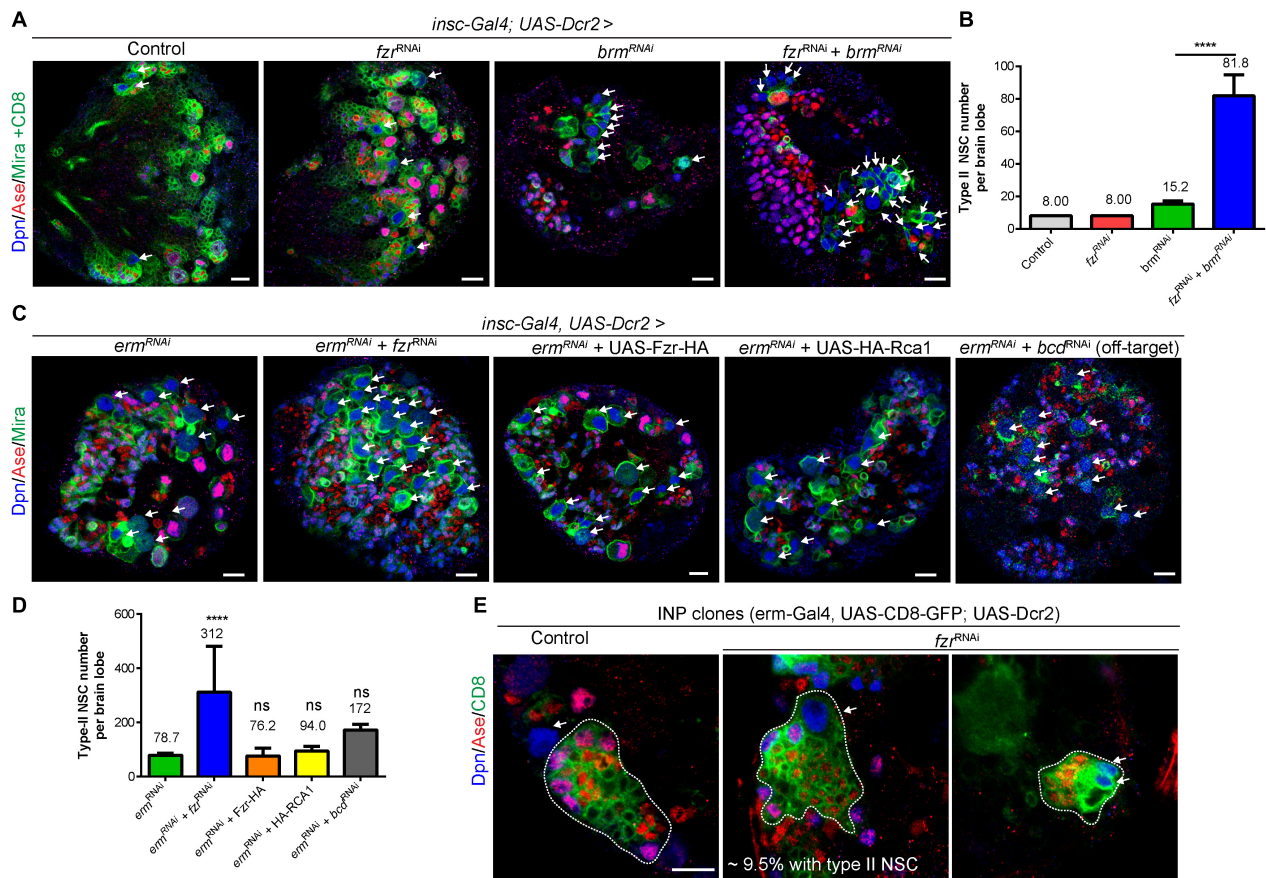


FIGURE 4 | Fzr genetically interacts with Brm and Erm to regulate NSC-INP transition. (A) Larval brains of control (β -gal^{RNAi} + UAS-CD8-GFP), *fzr^{RNAi}* (+ UAS-CD8-GFP), *brm^{RNAi}* (+ β -gal^{RNAi}) or *fzr^{RNAi} + brm^{RNAi}* with *insc-Gal4; UAS-Dcr2* were labeled with Dpn, Ase, Mira, and CD8. Note that to balance the number of UAS elements across different genotypes, additional control UAS line, β -gal^{RNAi} or UAS-CD8-GFP, were added to various RNAi lines, resulting in weaker phenotype in RNAi lines compared with those without additional UAS control shown earlier in this study. **(B)** Quantifications of type II NSC number per brain lobes for **(A)**. Control, $n = 10$; *fzr^{RNAi}*, $n = 10$; *brm^{RNAi}*, $n = 5$; and *fzr^{RNAi} + brm^{RNAi}*, $n = 6$. **(C)** Larval brains of *erm^{RNAi}* (+ β -gal^{RNAi}), *fzr^{RNAi} + erm^{RNAi}*, *erm^{RNAi} + Fzr-HA*, *erm^{RNAi} + HA-RCA1* or *bcd^{RNAi} + erm^{RNAi}* with *insc-Gal4; UAS-Dcr2* were labeled with Dpn, Ase, and Mira. **(D)** Quantification of type II NSC number per brain lobes for **(C)**. *erm^{RNAi}*, $n = 11$; *fzr^{RNAi} + erm^{RNAi}*, $n = 20$; *erm^{RNAi} + Fzr-HA*, $n = 21$; *erm^{RNAi} + HA-RCA1*, $n = 10$ and *bcd^{RNAi} + erm^{RNAi}*, $n = 10$. **(E)** INP clones of driver control (β -gal^{RNAi}) or *fzr^{RNAi}* under control of INP driver (*erm-Gal4; UAS-CD8-GFP; UAS-Dcr2*) were labeled with Dpn, Ase, and CD8. Control, $n = 90$; *fzr^{RNAi}*, $n = 105$. White dotted lines, INP clone outline. The middle and right panels displayed two different clones of *fzr^{RNAi}* under the control of INP driver. Respectively, one large and several small type-II NSCs were found within INP clones. Data are presented as mean \pm SD. **** $P \leq 0.0001$; ns for $P > 0.05$. White arrows, type II NSCs (~ 10 – $12 \mu\text{m}$ in diameter and Dpn⁺ Ase⁺). Scale bars: $10 \mu\text{m}$. Ase, Asense; β -gal, β -galactosidase; Bcd, bicoid; Brm, Brahma; Dcr2, Dicer 2; Dpn, Deadpan; Erm, Earmuff; Fzr, Fizzy and cell division cycle 20 related; GFP, green fluorescent protein; GMC, Ganglion Mother Cell; INP, intermediate neural progenitor; Insc, Inscuteable; Mira, Miranda; ns, statistically non-significant; NSC, neural stem cell; UAS, upstream activating sequence.

Fzr Loss Enhances Ectopic Type II NSCs Resulted From Downregulation of Differentiation Factors Erm or Brm

Our data shows that the loss of Fzr also results in the formation of ectopic NSCs in addition to excess GMCs (Figures 1A–C and Supplementary Figures 1A–D). Brahma (Brm) and Earmuff (Erm) are important to suppress dedifferentiation of INPs, and the loss of either *Brm* or *Erm* results in the reversion of INP to type II NSCs. Next we wondered if *Fzr* genetically interacted with *Brm* or *Erm* to suppress INP dedifferentiation. While *Fzr* knockdown alone using NSC-specific driver did not cause ectopic type II NSCs (8 type II NSCs per brain lobe similar to a control brain lobe, Figures 4A,B), the loss of *Brm* resulted in ectopic type

II NSCs (15.2 ± 1.92 NSC, $n = 5$). However, knockdown of *Fzr* dramatically enhanced dedifferentiation defects associated with *Brm* loss to 81.8 ± 12.8 NSCs per brain lobe (Figures 4A,B). Similarly, the knockdown of *Fzr* using NSC-specific driver (*insc-Gal4*) substantially enhanced the ectopic type II NSCs of *Erm* knockdown (Figures 4C,D, 78.7 ± 7.30 NSCs, $n = 11$ BLs in *erm^{RNAi} + control^{RNAi}* vs. 311.9 ± 169.6 NSCs, $n = 20$ BLs in *erm^{RNAi} + fzr^{RNAi}*). The overexpression of *Rca1*, negative regulator of Fzr-dependent functions of APC/C complex, as well as *Fzr* overexpression did not affect the severity of *Erm* loss, suggesting *Fzr* might function independent of APC/C complex in the regulation of INP-NSC homeostasis (Figures 4C,D). Interestingly, the knockdown of *Fzr* using INP driver (*erm-Gal4; UAS-CD8-GFP*) resulted in ectopic type II NSCs from 9.5% of

INP clones ($n = 105$), while none of the control INP clones contained any type II NSCs (Figure 4E). Due to the unavailability of independent RNAi lines targeting different *fzr* sequences and the lethality of homozygous *fzr* mutants in the early embryonic or larval stages, we were unable to confirm genetic relationship of *Fzr* and *Brm* or *Erm* in NSC-INP transition with additional RNAi lines or mutants. Moreover, knockdown of the potential off-target of *fzr*^{RNAi} (*GD#25553*), *bicoid* (*bcd*), by RNAi under the control of the same NSC-specific driver (*insc-Gal4*) did not lead to as strong enhancement of INP dedifferentiation associated with *Erm* loss, in comparison to the effect of *fzr*^{RNAi} (Figures 4C,D), suggesting that loss of *fzr* partially contributed to the genetic enhancement observed in the double knockdown *fzr*^{RNAi} and *erm*^{RNAi}.

Altogether, these results suggest that beside its roles in regulating GMC-to-neuron transition, *Fzr* genetically interacts with *Brm* and *Erm* to promote NSC-INP transition.

DISCUSSION

Here, we show that *Fzr*/Cdh1, an established co-activator of APC/C ubiquitin ligase known for its roles in regulating cell cycle or post-mitotic functions in terminally differentiated neurons or glial cells, promotes the commitment of neural progenitor GMCs to the production of terminally differentiated neurons (Figures 5A,B). In this study, we present multiple lines of evidence to support the function of *Fzr* in regulating GMC-to-neuron differentiation: (1) the presence of *Fzr* in late GMCs; (2) the accumulation of GMCs at the expense of neurons in *fzr*⁻ mutant NSC clones; and (3) the loss of differentiation factor Pros and ectopic accumulation of mitotic Polo kinase in NSC progenies upon loss of *fzr*. Beside functioning in GMCs, *Fzr* is also present in low level in NSCs to regulate NSC-to-INP transition of type II NSC lineages (Figures 5A,C).

In this study, we observed a strong expression of EGFP-*Fzr* in the optic lobe (Figure 3D). However, the function of *Fzr* in optic lobes is currently unclear. Recently, the APC/C^{*Fzr*} complex has been reported to promote retinal differentiation in *Drosophila* eye imaginal discs and thus the formation of adult eyes (Martins et al., 2017). In eye discs, *Fzr* modulates Wingless Signaling via Nek2 degradation, which is essential for progenitor cells to differentiate. As such, it would be interesting to examine if *Fzr* might regulate GMC differentiation in NSC lineages of the central brain through a similar mechanism.

In this study, we provide putative evidence that *Fzr* interacts with *Erm* and *Brm* to regulate NSC-INP balance. Interestingly, Ets2, the mammalian homolog of the master regulator of type II lineages PntP1, is stabilized upon Cdh1 deficiency and is proposed to be substrate of APC/C^{Cdh1} complex (Li et al., 2008). However, it remains to be determined how *Fzr*, *Erm*, or *Brm* cooperate to regulate NSC-INP transition in type II NSC lineages and if the underlining mechanisms for *Fzr*'s function in GMC-neuron and NSC-INP transitions are shared.

In mammals, Cdh1/*Fzr* and several core components of APC/C complex are highly expressed in post-mitotic neurons (Gieffers et al., 1999) and Cdh1/*Fzr* participates in the regulation of neuronal axonal and dendritic growth, synapses, metabolism

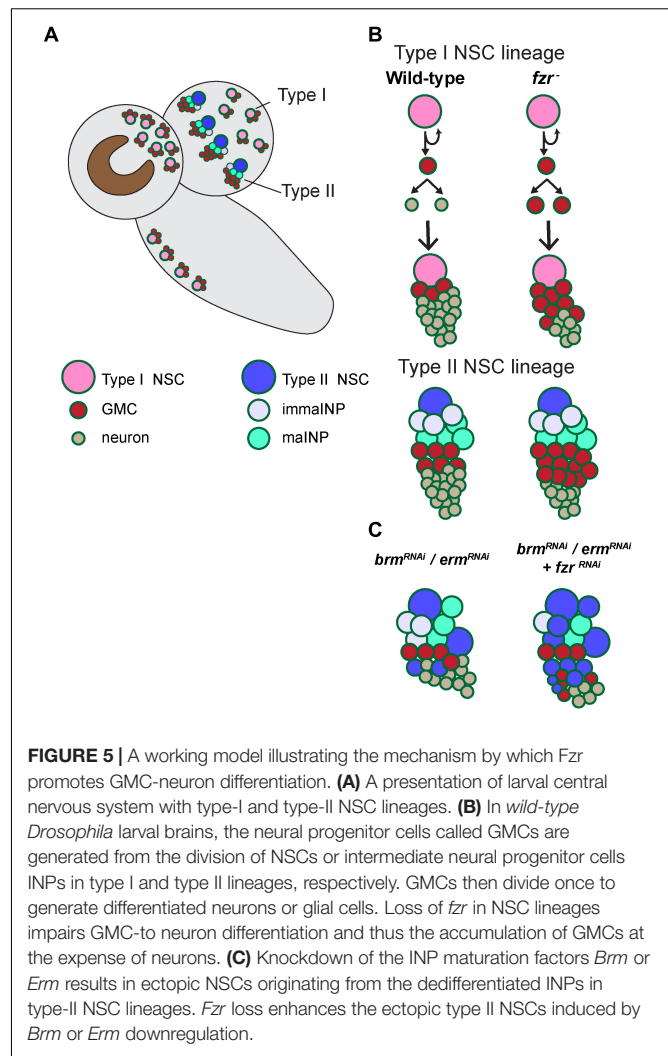


FIGURE 5 | A working model illustrating the mechanism by which *Fzr* promotes GMC-neuron differentiation. **(A)** A presentation of larval central nervous system with type-I and type-II NSC lineages. **(B)** In wild-type *Drosophila* larval brains, the neural progenitor cells called GMCs are generated from the division of NSCs or intermediate neural progenitor cells INPs in type I and type II lineages, respectively. GMCs then divide once to generate differentiated neurons or glial cells. Loss of *fzr* in NSC lineages impairs GMC-to neuron differentiation and thus the accumulation of GMCs at the expense of neurons. **(C)** Knockdown of the INP maturation factors *Brm* or *Erm* results in ectopic NSCs originating from the dedifferentiated INPs in type-II NSC lineages. *Fzr* loss enhances the ectopic type II NSCs induced by *Brm* or *Erm* downregulation.

and survival of neurons (Eguren et al., 2011). Besides, *Fzr*/Cdh1 functions to prevent replicative stress and p53-dependent cell death in neural progenitors (Eguren et al., 2013). In this study, we uncover a new role of *Fzr* in *Drosophila* nervous system: ensuring the commitment of neural progenitors to differentiation cascade. Large scale human cancer tissue arrays and prognostic analyses have indicated that loss of APC^{Cdh1} function correlates with various human carcinogenesis, including brain tumors (reviewed in Qiao et al., 2010). Besides, inactivation of Cdh1 has been implicated in excitation-mediated neuronal cell death in neurological disorders such as Alzheimer disease (Maestre et al., 2008). Our study on the role of *Fzr* in turning off proliferation in neuronal cells may provide insight into how *Fzr* deficit may contribute to human neurodegenerative diseases and tumors.

DATA AVAILABILITY STATEMENT

All datasets generated for this study are included in the article/Supplementary Material (see Supplementary Data Sheet S2 for the numerical data used in this study).

AUTHOR CONTRIBUTIONS

PL: conceptualization, data curation, formal analysis, investigation, methodology, writing – the original draft, and writing – review and editing. HW: conceptualization, funding acquisition, project administration, supervision, writing – review and editing the original draft, and writing – review and editing.

FUNDING

This work was supported by Duke-NUS Signature Research Program funded by Ministry of Health and Ministry of Education tier 2 (MOE2017-T2-2-025) to HW. The funders had no role in study design, data collection and analysis, decision to publish, or preparation of the manuscript.

REFERENCES

- Alvarez, A. D. (2003). pannier and pointedP2 act sequentially to regulate *Drosophila* heart development. *Development* 130, 3015–3026. doi: 10.1242/dev.00488
- Bello, B. C., Izergina, N., Caussinus, E., and Reichert, H. (2008). Amplification of neural stem cell proliferation by intermediate progenitor cells in *Drosophila* brain development. *Neural. Dev.* 3:5. doi: 10.1186/1749-8104-3-5
- Bentley, A. M., Williams, B. C., Goldberg, M. L., and Andres, A. J. (2002). Phenotypic characterization of *Drosophila* ida mutants: defining the role of APC5 in cell cycle progression. *J. Cell Sci.* 115, 949–961.
- Betschinger, J., Mechtler, K., and Knoblich, J. A. (2006). Asymmetric segregation of the tumor suppressor brat regulates self-renewal in *Drosophila* neural stem cells. *Cell* 124, 1241–1253. doi: 10.1016/j.cell.2006.01.038
- Boone, J. Q., and Doe, C. Q. (2008). Identification of *Drosophila* type II neuroblast lineages containing transit amplifying ganglion mother cells. *Dev. Neurobiol.* 68, 1185–1195. doi: 10.1002/dneu.20648
- Bowman, S. K., Rolland, V., Betschinger, J., Kinsey, K. A., Emery, G., and Knoblich, J. A. (2008). The tumor suppressors brat and numb regulate transit-amplifying neuroblast lineages in *Drosophila*. *Dev. Cell* 14, 535–546. doi: 10.1016/j.devcel.2008.03.004
- Carney, T. D., Struck, A. J., and Doe, C. Q. (2013). midlife crisis encodes a conserved zinc-finger protein required to maintain neuronal differentiation in *Drosophila*. *Development* 140, 4155–4164. doi: 10.1242/dev.093781
- Caussinus, E., and Gonzalez, C. (2005). Induction of tumor growth by altered stem-cell asymmetric division in *Drosophila melanogaster*. *Nat. Genet.* 37, 1125–1129. doi: 10.1038/ng1632
- Choksi, S. P., Southall, T. D., Bossing, T., Edoff, K., de Wit, E., Fischer, B. E., et al. (2006). Prospero acts as a binary switch between self-renewal and differentiation in *Drosophila* neural stem cells. *Dev. Cell* 11, 775–789. doi: 10.1016/j.devcel.2006.09.015
- Chu-Lagraff, Q., Wright, D. M., McNeil, L. K., and Doe, C. Q. (1991). The prospero gene encodes a divergent homeodomain protein that controls neuronal identity in *Drosophila*. *Dev. Suppl.* 2, 79–85.
- Dawson, I. A., Roth, S., Akam, M., and Artavanis-Tsakonas, S. (1993). Mutations of the fuzzy locus cause metaphase arrest in *Drosophila melanogaster* embryos. *Development* 117, 359–376.
- Djabrayan, N. J. V., Cruz, J., de Miguel, C., Franch-Marro, X., and Casanova, J. (2014). Specification of differentiated adult progenitors via inhibition of endocycle entry in the *Drosophila* trachea. *Cell Rep.* 9, 859–865. doi: 10.1016/j.celrep.2014.09.043
- Eguren, M., Machado, E., and Malumbres, M. (2011). Non-mitotic functions of the anaphase-promoting complex. *Semin. Cell Dev. Biol.* 22, 572–578. doi: 10.1016/j.semcdb.2011.03.010

ACKNOWLEDGMENTS

We thank F. Matsuzaki, J. B. Skeath, C. Doe, A. Sehgal, T. Lee, Y. N. Jan, L. Y. Cheng, A. Wodarz, C. Sunkel, and W. Chia, the Hybridoma Bank, the Bloomington *Drosophila* Stock Center, Vienna *Drosophila* RNAi Center, and the *Drosophila* Genomics Resource Center (DGRC) for fly stocks, antibodies, and cDNA clones, Dr. Chwee Tat Koe for discussion, and Ms. Ye Sing Tan for technical assistance.

SUPPLEMENTARY MATERIAL

The Supplementary Material for this article can be found online at: <https://www.frontiersin.org/articles/10.3389/fcell.2020.00060/full#supplementary-material>

- Eguren, M., Porlan, E., Machado, E., García-Higuera, I., Cañamero, M., Fariñas, I., et al. (2013). The APC/C cofactor Cdh1 prevents replicative stress and p53-dependent cell death in neural progenitors. *Nat. Commun.* 4:2880. doi: 10.1038/ncomms3880
- Eroglu, E., Burkard, T. R., Jiang, Y., Saini, N., Homem, C. C. F., Reichert, H., et al. (2014). SWI/SNF complex prevents lineage reversion and induces temporal patterning in neural stem cells. *Cell* 156, 1259–1273. doi: 10.1016/j.cell.2014.01.053
- Froldi, F., Szuperak, M., Weng, C.-F., Shi, W., Papenfuss, A. T., and Cheng, L. Y. (2015). The transcription factor Nerfin-1 prevents reversion of neurons into neural stem cells. *Genes Dev.* 29, 129–143. doi: 10.1101/gad.250282.114
- Gieffers, C., Peters, B. H., Kramer, E. R., Dotti, C. G., and Peters, J. M. (1999). Expression of the CDH1-associated form of the anaphase-promoting complex in postmitotic neurons. *Proc. Natl. Acad. Sci. U.S.A.* 96, 11317–11322. doi: 10.1073/pnas.96.20.11317
- Glover, D. M. (2005). Polo kinase and progression through M phase in *Drosophila*: a perspective from the spindle poles. *Oncogene* 24, 230–237. doi: 10.1038/sj.onc.1208279
- Grosskortenhaus, R., and Sprenger, F. (2002). Rca1 inhibits APC-Cdh1Fzr and is required to prevent cyclin degradation in G2. *Dev. Cell* 2, 29–40. doi: 10.1016/S1534-5807(01)00104-6
- Homem, C. C. F., Repic, M., and Knoblich, J. A. (2015). Proliferation control in neural stem and progenitor cells. *Nat. Rev. Neurosci.* 16, 647–659. doi: 10.1038/nrn4021
- Jacobs, H. W., Richter, D. O., Venkatesh, T. R., and Lehner, C. F. (2002). Completion of mitosis requires neither fzr/rap nor fzr2, a Male Germline-Specific *Drosophila* Cdh1 Homolog. *Curr. Biol.* 12, 1435–1441. doi: 10.1016/S0960-9822(02)01074-6
- Janssens, D. H., Hamm, D. C., Anhezini, L., Xiao, Q., Siller, K. H., Siegrist, S. E., et al. (2017). An Hdac1/Rpd3-poised circuit balances continual self-renewal and rapid restriction of developmental potential during asymmetric stem cell division. *Dev. Cell* 40, 367.e7–380.e7. doi: 10.1016/j.devcel.2017.01.014
- Kaplow, M. E., Korayem, A. H., and Venkatesh, T. R. (2008). Regulation of glia number in *Drosophila* by Rap/Fzr, an activator of the anaphase-promoting complex, and loco, an RGS protein. *Genetics* 178, 2003–2016. doi: 10.1534/genetics.107.086397
- Koe, C. T., Li, S., Rossi, F., Wong, J. J. L., Wang, Y., Zhang, Z., et al. (2014). The Brm-HDAC3-Erm repressor complex suppresses dedifferentiation in *Drosophila* type II neuroblast lineages. *Elife* 3:e01906. doi: 10.7554/eLife.01906
- Lee, C. Y., Wilkinson, B. D., Siegrist, S. E., Wharton, R. P., and Doe, C. Q. (2006). Brat is a miranda cargo protein that promotes neuronal differentiation and inhibits neuroblast self-renewal. *Dev. Cell* 10, 441–449. doi: 10.1016/j.devcel.2006.01.017
- Lee, T., Lee, A., and Luo, L. (1999). Development of the *Drosophila* mushroom bodies: sequential generation of three distinct types of neurons from a neuroblast. *Development* 125, 4065–4076.

- Li, M., Shin, Y.-H. H., Hou, L., Huang, X., Wei, Z., Klann, E., et al. (2008). The adaptor protein of the anaphase promoting complex Cdh1 is essential in maintaining replicative lifespan and in learning and memory. *Nat. Cell Biol.* 10, 1083–1089. doi: 10.1038/ncb1768
- Li, S., Wang, H., and Groth, C. (2014). *Drosophila* neuroblasts as a new model for the study of stem cell self-renewal and tumour formation. *Biosci. Rep.* 34, 401–414. doi: 10.1042/BSR20140008
- Liu, K., Shen, D., Shen, J., Gao, S. M., Li, B., Wong, C., et al. (2017). The super elongation complex drives neural stem cell fate commitment. *Dev. Cell* 40, 537.e6–551.e6. doi: 10.1016/j.devcel.2017.02.022
- Maestre, C., Delgado-Esteban, M., Gomez-Sanchez, J. C., Bolaños, J. P., and Almeida, A. (2008). Cdk5 phosphorylates Cdh1 and modulates cyclin B1 stability in excitotoxicity. *EMBO J.* 27, 2736–2745. doi: 10.1038/emboj.2008.195
- Martins, T., Meghini, F., Florio, F., and Kimata, Y. (2017). The APC / C coordinates retinal differentiation with G1 arrest through the Nek2-dependent modulation of wingless signaling. *Dev. Cell* 40, 67–80. doi: 10.1016/j.devcel.2016.12.005
- Maurange, C., Cheng, L., and Gould, A. P. (2008). Temporal transcription factors and their targets schedule the end of neural proliferation in *Drosophila*. *Cell* 133, 891–902. doi: 10.1016/j.cell.2008.03.034
- Meghini, F., Martins, T., Tait, X., Fujimitsu, K., Yamano, H., Glover, D. M., et al. (2016). of the APC / C at the centrosome during mitotic exit. *Nat. Commun.* 7, 1–17. doi: 10.1038/ncomms12607
- Narbonne-Reveau, K., Senger, S., Pal, M., Herr, A., Richardson, H. E., Asano, M., et al. (2008). APC/C Fzr/Cdh1 promotes cell cycle progression during the *Drosophila* endocycle. *Development* 135, 1451–1461. doi: 10.1242/dev.016295
- Pfeiffer, B. D., Jenett, A., Hammonds, A. S., Ngo, T.-T. B., Misra, S., Murphy, C., et al. (2008). Tools for neuroanatomy and neurogenetics in *Drosophila*. *Proc. Natl. Acad. Sci. U.S.A.* 105, 9715–9720. doi: 10.1073/pnas.0803697105
- Pines, J. (2011). Cubism and the cell cycle: the many faces of the APC/C. *Nat. Rev. Mol. Cell Biol.* 12, 427–438. doi: 10.1038/nrm3132
- Qiao, X., Zhang, L., Gamper, A. M., Fujita, T., and Wan, Y. (2010). APC/C-Cdh1: From cell cycle to cellular differentiation and genomic integrity. *Cell Cycle* 9, 3904–3912. doi: 10.4161/cc.9.19.13585
- Reber, A., Lehner, C. F., and Jacobs, H. W. (2006). Terminal mitoses require negative regulation of Fzr/Cdh1 by Cyclin A, preventing premature degradation of mitotic cyclins and String/Cdc25. *Development* 133, 3201–3211. doi: 10.1242/dev.02488
- Schaeffer, V., Althausen, C., Shcherbata, H. R., Deng, W., and Ruohola-Baker, H. (2004). Notch-Dependent Fizzy-related/Hec1/Cdh1 expression is required for the mitotic-to-endocycle transition in *Drosophila* Follicle Cells. *Curr. Biol.* 14, 630–636. doi: 10.1016/j.cub.2004.03.040
- Sigrist, S. J., and Lehner, C. F. (1997). *Drosophila* fizzy-related down-regulates mitotic cyclins and is required for cell proliferation arrest and entry into endocycles. *Cell* 90, 671–681. doi: 10.1016/S0092-8674(00)80528-0
- Silies, M., and Klämbt, C. (2010). APC/C(Fzr/Cdh1)-dependent regulation of cell adhesion controls glial migration in the *Drosophila* PNS. *Nat. Neurosci.* 13, 1357–1364. doi: 10.1038/nn.2656
- Southall, T. D., Davidson, C. M., Miller, C., Carr, A., and Brand, A. H. (2014). Dedifferentiation of neurons precedes tumor formation in lola mutants. *Dev. Cell* 28, 685–696. doi: 10.1016/j.devcel.2014.01.030
- Sunkel, C. E., and Glover, D. M. (1988). polo, a mitotic mutant of *Drosophila* displaying abnormal spindle poles. *J. Cell Sci.* 89, 25–38.
- van Roessel, P., Elliott, D. A., Robinson, I. M., Prokop, A., and Brand, A. H. (2004). Independent regulation of synaptic size and activity by the anaphase-promoting complex. *Cell* 119, 707–718. doi: 10.1016/j.cell.2004.11.028
- Weng, M., Golden, K. L., and Lee, C.-Y. Y. (2010). dFzf/Earmuff maintains the restricted developmental potential of intermediate neural progenitors in *Drosophila*. *Dev. Cell* 18, 126–135. doi: 10.1016/j.devcel.2009.12.007
- Yamamoto, S., Jaiswal, M., Charng, W.-L., Gambin, T., Karaca, E., Mirzaa, G., et al. (2014). Resource a *Drosophila* genetic resource of mutants to study mechanisms underlying human genetic diseases. *Cell* 159, 200–214. doi: 10.1016/j.cell.2014.09.002
- Zhang, Y., Koe, C. T., Tan, Y. S., Ho, J., Tan, P., Yu, F., et al. (2019). The Integrator complex prevents dedifferentiation of intermediate neural progenitors back into neural stem cells. *Cell Rep.* 27, 987.e3–996.e3. doi: 10.1016/j.celrep.2019.03.089
- Zhu, S., Barshow, S., Wildonger, J., Jan, L. Y., and Jan, Y.-N. (2011). Ets transcription factor pointed promotes the generation of intermediate neural progenitors in *Drosophila* larval brains. *Proc. Natl. Acad. Sci. U.S.A.* 108, 20615–20620. doi: 10.1073/pnas.1118595109

Conflict of Interest: The authors declare that the research was conducted in the absence of any commercial or financial relationships that could be construed as a potential conflict of interest.

Copyright © 2020 Ly and Wang. This is an open-access article distributed under the terms of the Creative Commons Attribution License (CC BY). The use, distribution or reproduction in other forums is permitted, provided the original author(s) and the copyright owner(s) are credited and that the original publication in this journal is cited, in accordance with accepted academic practice. No use, distribution or reproduction is permitted which does not comply with these terms.



Human Derived Immortalized Dermal Papilla Cells With a Constant Expression of Testosterone Receptor

Tomokazu Fukuda^{1,2*}, Kouhei Takahashi¹, Shin Takase¹, Ai Orimoto¹, Takahiro Eitsuka³, Kiyotaka Nakagawa³ and Tohru Kiyono^{4*}

¹ Graduate School of Science and Engineering, Iwate University, Morioka, Japan, ² Soft-Path Engineering Research Center, Iwate University, Morioka, Japan, ³ Graduate School of Agricultural Science, Tohoku University, Sendai, Japan, ⁴ Division of Carcinogenesis and Cancer Prevention and Department of Cell Culture Technology, National Cancer Center Research Institute, Tokyo, Japan

OPEN ACCESS

Edited by:

Dominic C. Voon,
Kanazawa University, Japan

Reviewed by:

Shang Li,
Duke-NUS Medical School,
Singapore
Ekaterina Vorotelyak,
Koltzov Institute of Developmental
Biology (RAS), Russia

*Correspondence:

Tomokazu Fukuda
tomofukuda009@gmail.com
Tohru Kiyono
tkiyono@ncc.go.jp

†ORCID:

Tomokazu Fukuda
orcid.org/0000-0001-8456-0483

Specialty section:

This article was submitted to
Cell Growth and Division,
a section of the journal
Frontiers in Cell and Developmental
Biology

Received: 13 December 2019

Accepted: 26 February 2020

Published: 18 March 2020

Citation:

Fukuda T, Takahashi K, Takase S,
Orimoto A, Eitsuka T, Nakagawa K
and Kiyono T (2020) Human Derived
Immortalized Dermal Papilla Cells
With a Constant Expression
of Testosterone Receptor.
Front. Cell Dev. Biol. 8:157.
doi: 10.3389/fcell.2020.00157

Androgenetic alopecia (AGA) is the most common type of hair loss, and is mainly caused by the biological effects of testosterone on dermal papilla cells (DPCs). *In vitro* culturing of DPCs might be a useful tool for the screening of target molecule of AGA. However, primary DPCs cannot continuously proliferate owing to cellular senescence and cell culture stress. In this study, we introduced mutant cyclin-dependent kinase 4 (CDK4), Cyclin D1, and telomerase reverse transcriptase (TERT) into DPCs. We confirmed protein expression of CDK4 and Cyclin D1, and enzymatic activity of TERT. Furthermore, we found the established cell line was free from cellular senescence. We also introduced the androgen receptor gene using a recombinant retrovirus, to compensate the transcriptional suppressed endogenous androgen receptor in the process of cell proliferation. Furthermore, we detected the efficient nuclear translocation of androgen receptor into the nucleus after the treatment of dihydrotestosterone, indicating the functionality of our introduced receptor. Our established cell line is a useful tool to identify the downstream signaling pathway, which activated by the testosterone.

Keywords: dihydrotestosterone, dermal papilla cells, immortalization, androgen receptor, nuclear localization

INTRODUCTION

Hair plays an important role in protecting the skin from mechanical damage. The hair follicle regulates hair growth through complex interactions between hormones, neuropeptides, and immune cells. The hair follicle consists of multiple cell types, including dermal papilla cells (DPCs), matrix cells, and melanocytes (Driskell et al., 2011). The process of hair growth can be classified into three stages: the growth stage (anagen), the regression stage (catagen), and the rest stage (telogen) (Milner et al., 2002). Hair growth occurs throughout the duration of the anagen phase until the hair enters the catagen phase, in which the hair follicle shrinks, and apoptosis occurs. During the telogen phase, the hair follicle remains dormant while new hair growth begins, eventually causing hair loss or “shedding” of the old hair. This hair growth and replacement process is known as the hair cycle (Davis, 1962). Hair growth and proliferation is mainly due to the hair matrix cell proliferation and

Abbreviations: AGA, Androgenetic alopecia; DPCs, dermal papilla cells; CDK, cyclin-dependent kinase 4; TERT, telomerase reverse transcriptase; DHT, dihydrotestosterone; TGFβ, transforming growth factor β; Dkk1, Dickkopf-related protein 1; DAPI, 4',6-diamidino-2-phenylindole; SA-β-Gal, senescence-associated β-galactosidase; AP, alkaline phosphatase.

differentiation into the hair shaft (comprising three layers: the medulla, cortex, and hair cuticle) and the inner root sheath (IRS, comprising three layers: the cuticle, Huxley's layer, and Henle's layer) (Detmar et al., 1993). The proliferation of hair matrix cells is regulated by growth stimulation from DPCs via insulin growth factor I (IGF-I) (Danilenko et al., 1996) and fibroblast growth factors 5 and 7 (FGF5 and FGF7) (Hébert et al., 1994; Guo et al., 1996).

Androgenetic alopecia (AGA) is the most common type of hair loss in men. Fifty eight percent of the 30–50-year-old men suffer from AGA (Shankar et al., 2009). AGA is characterized by hair loss from the top and front of the head. Although the molecular mechanisms of AGA are not fully understood, testosterone and its metabolic form, dihydrotestosterone (DHT), are considered to be the major causes of AGA (Kwack et al., 2008). DHT is produced from enzymatic catalysis of testosterone via the enzyme 5 α -reductase (Münster et al., 2003). DHT has a stronger affinity for the androgen receptor than does testosterone, and forms a DHT-androgen receptor complex, which then moves from the cytoplasm into the nucleus. Nuclear localization of the DHT-androgen receptor complex enhances the secretion of hair growth-suppressive factors from DPCs, such as transforming growth factor β (TGF β) or Dickkopf-related protein 1 (Dkk1) (Kwack et al., 2010). As a result, the duration of the hair growth period decreases, resulting in the loss of hair from the top and front of the head, which is characteristic of AGA.

The standard pharmaceutical product used to treat AGA is Finasteride (Gupta and Charrette, 2014). Finasteride is an inhibitor of the 5 α -reductase enzyme. By inhibiting the enzymatic activity of 5 α -reductase, Finasteride reduces the concentration of DHT, which prevents the progression of AGA and hair loss (Kaufman and Dawber, 1999). Although Finasteride is effective in preventing the progression of AGA, there are several major side effects. One example of the adverse effects of Finasteride is sexual dysfunction, such as erectile dysfunction or decreased libido (Coskuner et al., 2019). In addition to negative side effects, the cost of Finasteride therapy is relatively high. Consequently, the screening of new molecular target for the treatment AGA is worth investigating to reduce potential side effects and cost. Furthermore, owing to the large population of AGA patients, the discovery of new anti-AGA drugs could be very profitable.

In general, cell culture is more advantageous than traditional experimental animal models from view point of animal welfare and cost. As described previously, DPCs are the control center for regulating hair growth and are target cells for the biological effect of DHT (Kwack et al., 2008). Therefore, *in vitro* culture of DPCs would be useful to find out the molecular target and the screening of pharmaceutical products to treat AGA. DPCs can be prepared from primary cultures of human cells, but sampling and primary cell culture can produce wide variability depending on cell preparation (Topouzi et al., 2017). Furthermore, primary DPCs cannot continuously proliferate because of cellular senescence and the Hayflick limit. Owing to this limitation, the number of passages of primary DPCs could affect the results obtained.

Our research group previously reported that combined expression of R24C mutant cyclin-dependent kinase 4 (CDK4), Cyclin D1, and telomere reverse transcriptase (TERT) allowed

us to efficiently immortalize human- (Shiomi et al., 2011), cattle and pig- (Donai et al., 2014), prairie vole- (Katayama et al., 2016, 2017), monkey- (Kuroda et al., 2015a), midget buffalo- (Fukuda et al., 2016), and mega bat- (Tani et al., 2019), Tsushima wildcat-derived cells (Gouko et al., 2018). Furthermore, growth acceleration with mutant CDK4 and Cyclin D1 is conserved even in sea turtles, suggesting that the underlying cell cycle mechanism was well-conserved throughout animal evolution (Fukuda et al., 2018). Cells immortalized using this method maintain the cell differentiation and chromosome patterns of the original cells (Shiomi et al., 2011). In this study, we introduced an expression cassette of R24C mutant CDK4, Cyclin D1, and TERT into human DPCs via lentivirus. Immortalized DPCs could be shared with scientists worldwide as research materials, which would contribute to experimental reproducibility. Establishment of an immortalized cell line can also reduce the necessity for primary cell culture if the original nature of the cells is preserved. Owing to the nature of DPCs, the expression of androgen receptors decreases with increasing passage number. To overcome this limitation, we also introduced an androgen receptor expression cassette through retroviral expression. This study is the first to describe the establishment of immortalized DPCs with intact chromosome condition and androgen receptor expression.

MATERIALS AND METHODS

Cell Culture

Human follicle DPCs were obtained from PromoCell (C-12072, Heidelberg, Germany) through the local distributor, Takara Bio (Shiga, Japan). DPCs were cultured in follicle dermal papilla cell medium (cat. no, C-26500, PromoCell) supplemented with: a supplement mix containing 0.04 mL/mL fetal calf serum, 0.004 mL/mL bovine pituitary extract, 1 ng/mL basic fibroblast growth factor, and 5 μ g/mL insulin; and 1% antibiotic antimycotic mixed stock solution (cat. no, 09366-44, Nacalai Tesque, Kyoto, Japan). The cell culture conditions were as follows: DPCs were seeded in a six-well plate with 2 mL of medium per well. The cells were cultured at 37°C in a humidified atmosphere with 5% CO₂.

Preparation of Recombinant Viruses and Genetic Introduction

To immortalize primary DPCs, we prepared recombinant lentiviruses expressing mutant CDK4, Cyclin D1, and TERT. We made a mixture of lentivirus solution expressing mutant CDK4, Cyclin D1, and TERT. The packaging of recombinant lentiviruses was carried out via transient expression of CSII-CMV-hTERT, CSII-CMV-Cyclin D1, and CSII-CMV-hCDK4R24C using packaging plasmids (pCAG-HIV-gp, pCMV-VSV-G-Rsv-Rev, kindly provided by Dr. Hiroyuki Miyoshi, Keio University, Japan) in 293T cells. As a surrogate marker to monitor the efficiency of infection, we used pCSII-CMV-EGFP, which expresses a fluorescent marker. The preparation and recombination of lentiviruses was previously described in our past study (Fukuda et al., 2017). We named the cells transfected with R24C mutant CDK4, Cyclin D1, and TERT as K4DT cells, in reference to the

modified genes (Katayama et al., 2019). We similarly named the recombinant cells with R24C mutant CDK4 and Cyclin D1 as K4D cells. The recombinant cells were automatically selected by the growth advantage, we carried out the cell analysis based on the pooled cell population.

To express the androgen receptor in our established K4DT cells, we chemically synthesized an expression cassette of the androgen receptor, including hemagglutinin (HA) at the amino terminal end. HA was used as a tag for convenient detection of the introduced androgen receptor protein. We inserted the cDNA fragment encoding the androgen receptor with an HA tag into the multiple cloning site of QCXIN, a retroviral vector (Takara Bio). As a surrogate marker to monitor the efficiency of infection, we used QCXIN-EGFP, which expresses EGFP. The packaging of retrovirus was carried out in 293T cell under the transient expression of QCXIN-AR or QCXIN-EGFP, and packaging plasmids, pCL-gag pol, and pCMV-VSV-G-RSV-Rev (Dr. Hiroyuki Miyoshi, RIKEN BioResource Center, Tsukuba, Japan). The detailed packaging procedure was described in our previous report (Fukuda et al., 2018). We named immortalized DPCs with androgen receptor expression K4DT-AR, and immortalized DPCs with control EGFP expression K4DT-EGFP.

Western Blotting

We carried out western blotting to detect the expression of proteins encoded by the introduced genes, i.e., CDK4, Cyclin D1, and the androgen receptor. The cells were lysed in a solution containing 50 mM Tris-HCl (pH 7.4), 0.15 M NaCl, 1% Triton X-100, 2.5 mg/mL sodium deoxycholate, and a protease inhibitor cocktail. A detailed protocol for western blotting is described in our previous study (Fukuda et al., 2017).

A rabbit anti-human Cyclin D1 antibody (1:5000, code no. 553, Medical & Biological Laboratories Co., LTD., Nagoya, Japan), a mouse anti-human CDK4 antibody (1:200, cat. no. sc-56277, Santa Cruz Biotechnology, Dallas, TX, United States), and a mouse anti- α -tubulin antibody (1:1000, cat. no. sc-32293, Santa Cruz Biotechnology) were used as primary antibodies. An anti-HA high affinity antibody (cat. no. 11867423001, clone 3F10, 100 μ g/mL solution, Sigma Aldrich, St. Louis, MO, United States) was used for the western blotting at a finale concentration of 100 ng/mL. A sheep anti-mouse IgG-linked horseradish peroxidase (HRP) (1:2000, code no. NA931V, GE Healthcare, Buckinghamshire, United Kingdom), a donkey anti-rabbit IgG-linked HRP (1:2000, code no. NA934V, GE Healthcare), and an anti-rat IgG-linked HRP (1:2000, code no. 31470, Thermo Fisher Scientific, Waltham, MA, United States) were used as secondary antibodies. Signals from the target proteins were detected using Signal Enhancer HIKARI for Western Blotting and ELISA (code no. 02270-81, Nacalai Tesque), and the images were detected using an ImageQuant LAS-4000 Mini system (GE Healthcare).

Immunofluorescence Staining of HA Tag

To examine the localization of the androgen receptor in our established cells, we carried out immunofluorescence staining. Cells were cultured on a chamber slide (cat. No. 177473, Thermo Fisher Scientific). Forty-eight hours after seeding, we fixed the cells with 4% paraformaldehyde in phosphate-buffered saline

(PBS) (cat. no. 09154-85, Nacalai Tesque). Permeabilization was performed by incubating cells in PBS with 0.5% Triton X-100 for 15 min (cat. no. 35501-15, Nacalai Tesque). After washing with PBS with 0.1% Tween 20 for 5 min (lot. no. M8M7587, Nacalai Tesque), we incubated the cells in a 1% bovine serum albumin blocking solution (BSA, cat. no. 01863-06, Nacalai Tesque) on a rotary shaker (NR-2, TAITEC, Saitama, Japan) for 45 min. After blocking, cells were exposed to the primary antibody overnight. The anti-HA high affinity antibody (cat. no. 11867423001, clone 3F10, 100 μ g/mL solution, Sigma-Aldrich, St. Louis, MO, United States) was diluted at 1:20 in PBS with 1% BSA. After primary antibody incubation, cells were incubated with the second antibody, which acts as a fluorescent marker. A goat anti-rat IgG conjugated with Alexa Fluor 568 (cat. no. A11077, Thermo Fisher Scientific) was used as a secondary antibody to detect the HA-tag. DAPI (4',6-diamidino-2-phenylindole) was used as a counterstaining reagent.

Senescence-Associated β -Galactosidase (SA- β -Gal) Staining

At passage number 13, we carried out staining of senescence-associated β -galactosidase (SA- β -Gal) in K4DT cells, K4D cells, and primary DPCs. We conducted staining procedures based on the protocol described by Debacq-Chainiaux et al. (2009).

Genomic PCR

To extract genomic DNA from cells, we used the NucleoSpin Tissue Kit (cat. no. 740952, Takara Bio). PCR was performed with 100 ng of template DNA, 1X KOD-FX neo PCR buffer (KFX-201; Toyobo, Osaka, Japan), 0.4 mM dNTPs (KFX-201, Toyobo), 0.5 U KOD-FX neo (KFX-201, Toyobo), and 0.3 mM of each primer, in accordance with the manufacturer's protocol. PCR was carried out under the following conditions for 40 cycles: pre-denaturation at 94°C for 2 min, denaturation at 98°C for 10 s, and extension at 68°C for 1 min (two-step PCR). Tuberous sclerosis type II (TSC2) was used as an internal control since TSC2 does not have any pseudogenes in its genome. We analyzed the PCR products by electrophoresis in 0.8% agarose/Tris-acetate-EDTA (ethylenediaminetetraacetic acid) gels and stained with ethidium bromide (14603-64, Nacalai Tesque). We used the same forward primer for the detection of the Cyclin D1, CDK4, and TERT expression cassettes: 5'-GGCACAAAATCAA CGGACTTT-3'. The reverse primer for the detection of Cyclin D1 was 5'-TTCCTCGCAGACCTCCAGCA-3'. The reverse primer for the detection of CDK4 was TF808, 5'-ACGAAGTGTGCTGATGGGAAGGC-3'. The reverse primer for the detection of TERT was TF809, 5'-AGCTCCTTCAGGCAGGACACCT-3'. To detect TSC2, the forward primer 5'-AAACCGAGCCCCATTTGACC-3' and the reverse primer 5'-TGGTCGTAGCGGAATCGAGGAT-3' were used.

Cell Cycle Analysis

We performed cell cycle analysis of primary, K4D, and K4DT cells at passage number 5 using a Muse Cell Cycle Assay Kit (cat. no. MCH100106, Merck Millipore Corporation, Billerica,

MA, United States) and a Muse Cell Analyzer (cat. no. 0500-3115, Merck Millipore Corporation). The fixation and analysis procedures are described in the protocol provided by the manufacturer. The statistical significance of each cell cycle stage was evaluated using the non-parametric multiple comparison method (Steel test). A *p*-value < 0.05 was considered statistically significant (*n* = 6).

Alkaline Phosphatase Staining

Cells were fixed with 4% paraformaldehyde in phosphate-buffered saline (PBS) (09154-85; Nacalai Tesque) for 3 min and then incubated with an alkaline phosphatase staining solution at 37°C for 10–15 min. The staining solution consisted of 0.6 mg/mL Fast Red TR Salt [hemi(zinc chloride) salt, F8764; Sigma-Aldrich, St. Louis, MO, United States], 0.1 mg/mL naphthol phosphate (23821-24; Nacalai Tesque), 0.7 mM N,N-dimethylformamide (13016-65; Nacalai Tesque), 0.2 mM MgCl₂ (20908-65; Nacalai Tesque), and 0.1 mM Tris-HCl (pH 8.5). The staining reaction stopped after ~15 min due to fixation with the 4% paraformaldehyde solution. More details are described in our previous reports (Donai et al., 2013).

Population Doubling Assay

Primary, K4D, and K4DT cells were seeded at densities of 5×10^4 cells/well in 35 mm diameter dishes (Thermo Fisher Scientific). Experiments were carried out in triplicate. When the cells in one of the wells reached confluence, all the cells were passaged, and then the total number of cells in each well was counted using an automated cell counter (Countess, Thermo Fisher Scientific). Population doubling (PD) was a measure of cell growth rate. PD was calculated with the following formula: $PD = \log_2(a/b)$, where *a* is the total number of cells in the current passage and *b* is the number of seeded cells (Qin et al., 2012). The averages and standard deviations (SD) were calculated from triplicate samples.

Karyotype Analysis

Karyotype analysis was carried out in K4DT cells. K4DT cells were treated with 0.02 mg/mL colcemid (Sigma-Aldrich) overnight. After trypsinization, cells were exposed to a hypotonic solution and fixed in Carnoy's fluid. After fixing, cells were stained with Giemsa solution (Fukuda et al., 2012b). The chromosome number was determined from 50 mitotic cells, and the detailed chromosomal condition was evaluated using G-banding in 20 mitotic cells.

Detection of Endogenous Androgen Receptor Gene With Real Time PCR

To address the expression level of androgen receptor in cells, we carried out the detection of mRNA level of endogenous androgen receptor gene with real time PCR analysis. Total RNAs were extracted from cells at 80% confluent condition in 35 mm dishes. Total RNAs were obtained from wild type DPCs at passage 8, DPCs with K4DT expression at passage 12, human embryonic fibroblasts HE16 (RIKEN BioResource Research Center, Tsukuba, Japan) with NucleoSpin RNA

Plus (Takara Bio). As the positive control for detection, we purchased human prostate total RNA (Takara Bio, Z6550N). Five microgram of total RNAs were used for the reverse transcription reaction with PrimeScript RT reagent Kit with gDNA Eraser, Perfect Real Time (Takara Bio, RR047A) with random hexamer primer in 25 µL of volume. One microliter of cDNAs were applied into the real time PCR reaction with specific primers for androgen receptors (TF1007; 5'-CCAGCAGAAATGATTGCAC-3', and TF1008; 5'-ATTACCAAGTTTCTTCAGCTTC-3') with Thunderbird Sybr qPCR mix (Toyobo) and Thermal Cycler Dice® Real Time System II (Takara Bio, TP960). The expression level of androgen receptor was adjusted with the level of house keeping gene, glyceraldehyde-3-phosphate dehydrogenase (GAPDH) detected with specific primers (TF999; 5'-GAGGTGCACCACCAACTGCTTAGC-3' and TF1000; 5'-TCGGCATGGACTGTGGTCATGAG-3'). The average expression level and standard error of each samples were calculated from six replicates for each group.

F-Actin Distribution Detected by Fluorescence Phalloidin

We carried out the cell culture of wild type, K4DT, and AR expressing K4DT DPCs in 35 mm glass base dish (code 3970-035, Iwaki, Shizuoka, Japan) after the collagen treatment. Around 1.0×10^5 cells of wild type, K4DT, AR expressing K4DT DPCs cells were seeded into each glass base dish. After 2 days later, the cells were washed by 1X PBS, then fixed with 4% paraformaldehyde solution. After the permeabilized treatment with Triton X-100, we stained the cells with X40 diluted Rohodamine X conjugated Phalloidin solution (code 165-2164, FUJIFILM Wako Pure Chemical, Osaka, Japan, powder was dissolved into 1.5 mL of dimethylformamide, final concentration is 6.6 µmol/L). We detected the intensity of fluorescence images with imageJ software. The intensity was detected from the cytoplasm of 15 randomly selected cells.

Immunostaining of α-Smooth Muscle Actin (SMA)

For the characterization of DPCs, α-smooth muscle actin (SMA) is one of the marker genes. To detect the immune-staining, we used primary antibody against SMA (sc-32251, Santa Cruz Biotechnology, Dallas, TX, United States). The seeding condition is identical with that of F-actin in the previous section. Cells were washed by 1X PBS, then fixed with 4% paraformaldehyde solution. After the permeabilized treatment with Triton X-100, we did the blocking with 1% bovine serum albumin in PBS for 10 min. Next, X100 diluted primary antibody was exposed to the cell overnight at 4°C. After the wash with 1X PBS wash, the secondary antibody, Goat anti-Mouse IgG (H + L) with Alexa 488 (Thermo Fisher Scientific) was exposed to the cells with X 200 dilution for 1 h. DAPI (4',6-diamidino-2-phenylindole) was used as a counterstaining reagent. We detected the intensity of fluorescence images with imageJ software. The intensity was detected from the cytoplasm of 15 randomly selected cells.

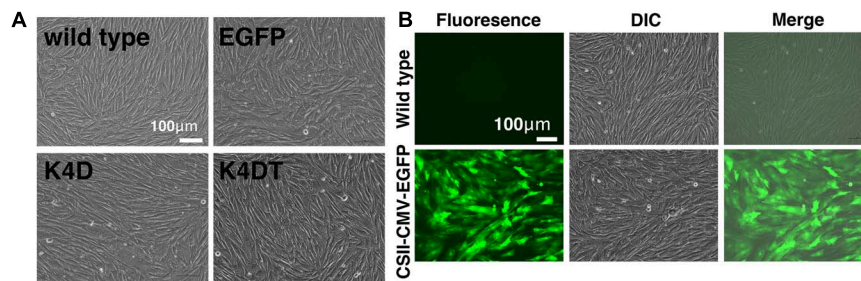


FIGURE 1 | The morphologies of wild type, EGFP-expressing, mutant CDK4 and Cyclin D (K4D cell)-expressing, and mutant CDK4, Cyclin D, and telomere reverse transcriptase (TERT)-expressing cells (K4DT cells). **(A)** Cell morphology of wild type (upper left), EGFP (upper right), CDK4 and Cyclin D (lower left), and mutant CDK4, Cyclin D, and TERT-expressing cells. **(B)** Detection of EGFP fluorescence after infection of DPCs with EGFP-expressing lentiviruses. Fluorescent, difference in contrast (DIC), and merge images are shown.

Protocol for DHT Treatment and Real Time PCR Detection of Dkk1 and TGFβ1

For the dihydrotestosterone treatment, cell culture medium for cell growth has replaced into DMEM/F12 medium (code 048-29785, FUJIFILM Wako Pure Chemical) without serum, with antibiotics for 48 h. The dihydrotestosterone (DHT) (Stanolone, code A0462, Tokyo Chemical Industry, Tokyo, Japan) was dissolved in Dimethyl sulfoxide at 100 μM concentration. 1/1000 volume of DHT solution was added to DMEM/F12 without serum and exposed to the cells for 48 h. We obtained total RNA with NucleoSpin RNA Plus (Takara Bio). Five microgram of total RNAs were used for the reverse transcription reaction with PrimeScript RT reagent Kit with gDNA Eraser, Perfect Real Time (Takara Bio, RR047A) with random hexamer primer in 25 μL of volume. One microliter of cDNAs were applied into the real time PCR reaction with specific primers for Dkk1 (TF1041; 5'-GCGGGAATAAGTACCAGAC-3', TF1042; 5'-CGCAGTACTCATCAGTGCC-3', Taqman probe; 5'-FAM-AACTACCAGCCGTACCCGTGC-3'-BHQ) with Thunderbird Probe qPCR mix (Toyobo) and Thermal Cycler Dice Real Time System II (Takara Bio, TP960). The expression level of Dkk1 was adjusted with the level of housekeeping gene, glyceraldehyde-3-phosphate dehydrogenase (GAPDH) detected with specific primers. The average expression level and standard error of each samples were calculated from six replicates for each group. For the detection of expression level of TGFβ1, specific primers were used for the detection (TF1075; 5'-CCGAGCCCTGGACACCAAC-3' and TF1076; 5'-CACTTCCAGCCGAGGTCCTT-3') with Thunderbird Syber qPCR mix (Toyobo).

The Detection of Nuclear Translocation of AR After the DHT Treatment

Presence and absence of DHT, we stained AR expressing K4DT DPCs with HA antibody. We obtained 16 cell images from each group. Based on the staining feature, we counted the number of cells, which is both positive for nuclear and cytoplasm. Furthermore, the number of cells, which is positive only within the nuclear was also counted in 16 images. Based on the number of positive cells, the ratio of cells, which both positive for nuclear

and cytoplasm, the ratio of cells, which only positive for nuclear, were calculated. MDV3100 (code 11596, Cayman Chemical, Ann Arbor, MI, United States) was dissolved in DMSO at 10 mM solution. The cell was exposed at 10 μM solution under the presence of 100 nM DHT.

Statistical Analysis

To evaluate statistical differences, we used the non-parametric method, Steel's test or Mann-Whitney *U*-test. *P*-values that were less than 0.05 were considered statistically significant.

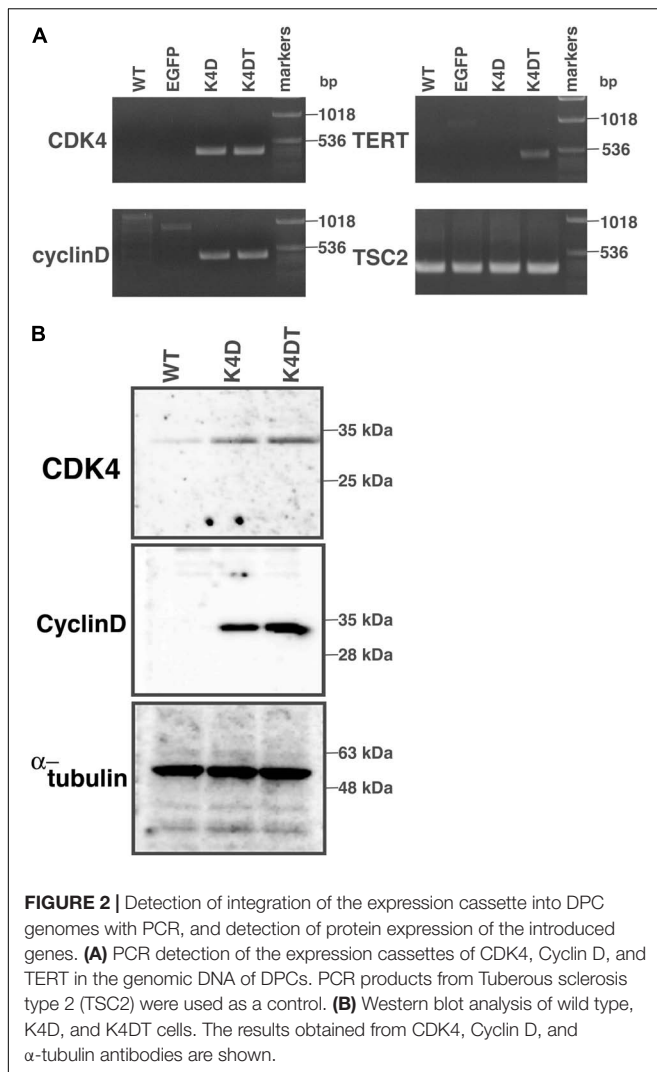
RESULTS

Transduction With CDK4, Cyclin D1, and TERT Resulted in Immortalized DPCs

We transduced EGFP or human CDK4, Cyclin D1, and TERT into primary DPCs using lentiviruses. We named the cells transfected with R24C mutant CDK4, Cyclin D1, and TERT as K4DT cells, in reference to the modified genes (Katayama et al., 2019). We similarly named the recombinant cells with R24C mutant CDK4 and Cyclin D1 as K4D cells. As shown in **Figure 1A**, we did not observe any differences among the cell morphologies of primary, K4D, K4DT, and EGFP cells, indicating that transduction of human CDK4, Cyclin D1, and TERT via lentiviruses did not cause any toxicity in these cells. We monitored the gene delivery efficiency of the lentiviruses in DPCs using the recombinant lentivirus CSII-CMV-EGFP as a surrogate marker. As shown in **Figure 1B**, cells transduced with EGFP-expressing lentiviruses showed a high level of green fluorescence, whereas wild type (uninfected control) DPCs did not. From these results, we estimated that transduction of these genes into DPCs by lentiviruses has an efficiency of 70–80%.

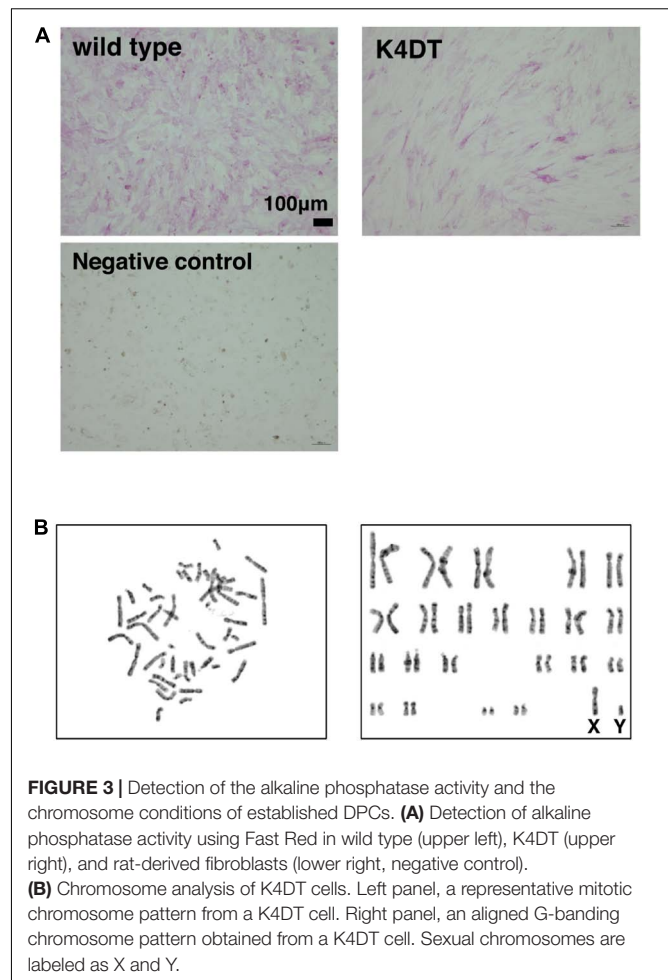
Detection of the Genomic Expression Cassettes With PCR, and Detection of Protein Expression

First, we carried out polymerase chain reaction (PCR) to detect integration of the genomic expression cassettes – CDK4, Cyclin D1, and TERT, introduced by lentiviral infection – into



the genomic DNA of primary DPCs. We analyzed four cell populations: wild type, EGFP, K4D, and K4DT cells. The results of the PCR are shown in **Figure 2A** and **Supplementary Figure S2**. As expected, although the primary and EGFP cells (Lanes 1 and 2) did not show any product, K4D and K4DT cells (Lanes 3 and 4) showed a strong band. We used TSC2 as a control. The results of control PCR amplification showed that all genomic DNA produced sufficient amplification products, indicating that the recovery of genomic DNA and the amplification reaction worked properly.

Next, we carried out western blotting to detect the expression of CDK4 and Cyclin D1 proteins with specific antibodies (**Figure 2B** and **Supplementary Figure S3**). K4D and K4DT cells showed specific bands at the expected molecular weight (Lanes 2 and 3), whereas primary cells showed a weak signal, which could be attributed to endogenous human-derived CDK4 protein (Lane 1). We used α -tubulin as a positive control. Taken together, these data show that exogenous genes were inserted into the genomic DNA of DPCs by lentiviral transduction, and the expression cassettes produced functional proteins.



K4DT Cells Retain the Characteristics of Primary Cells

To elucidate whether established K4DT cells retained the characteristics of primary cells, we assayed the activity of alkaline phosphatase (AP), one of the biological markers of dermal papilla cell, at around passage 5. As shown in **Figure 3A**, primary cells showed positive staining for AP (**Figure 3A**, upper left). In addition to primary cells, we also found that K4DT cells stained positive for AP activity (**Figure 3A**, right panel). We confirmed the negative staining of AP in rat-derived fibroblasts, supporting the specificity of the AP staining (**Figure 3A**, lower left). These results showed that K4DT cells retained characteristics of the original primary cells.

Karyotype Analysis

As shown in **Figure 3B**, we analyzed the chromosomal condition of K4DT cells at around passage 13 using the G-band method. We evaluated the number of chromosomes in 50 dividing K4DT cells. The karyotyping results revealed that K4DT cells were complete, normal 46XY diploids (100%, **Table 1**). In G-banding analysis, 19 cells showed a complete normal pattern of human chromosomes (95%), but one sample exhibited a chromosomal

TABLE 1 | Karyotype analysis of our established immortalized human follicle dermal papilla cells.

| Cell line | Total cell counts | Chromosome Number | | |
|-----------|-------------------|-------------------|----|----|
| | | 45 | 46 | 47 |
| K4DT | 50 | 0 | 50 | 0 |

abnormality in chromosome 1 at the P36 position. Thus, we concluded that the expression of CDK4, Cyclin D1, and TERT allows for cellular immortalization of DPC cells with an intact chromosomal pattern.

K4DT Cells Were Immortalized and Overcame Cellular Senescence

To evaluate the cell proliferation rate and measure the population doubling (PD) of the established cell lines, we carried out sequential passaging. As shown in **Figure 4A**, although primary cells showed a gradually decrease in cell proliferation ability, K4D and K4DT cells continued to proliferate without a decrease in cell growth. However, K4D cells tended to display slower rates of proliferation at around passage 12, which could be explained by cellular senescence. As shown in **Figure 4B**, we detected cellular senescence in each cell line at passage 14, after serial passage, using SA- β -Gal staining. While almost all the primary cells showed intense positive staining (**Figure 4B**, upper left), staining signals were much weaker in K4DT cells (**Figure 4B**, lower left). In K4D cells, although some cells showed positive staining, the incidence of positive cells was much lower than that in primary cells (**Figure 4B**, upper right). The cell size of primary cells at passage 14 became much larger than that of K4DT or K4D cells, indicating that K4DT cells do not exhibit an increase in cytoplasm, which is one of the characteristics of aged cells.

Cell Cycle Analysis

To compare the cell cycle distribution of cells, we performed cell cycle analysis using a Muse Cell Cycle Assay Kit (Merck Millipore Corporation) and a Muse Cell Analyzer (Merck Millipore Corporation). As shown in **Figure 4C**, while about 70% of primary cells exhibited and arrested at G0/G1 phases, the percentage of K4D and K4DT cells in G0/G1 phases was about 50% less. The representative histogram of wild type, K4D, and K4DT cells is shown in **Figure 4C**. The ratio of S and G2/M phases in K4D and K4DT cells was about 20% higher than in primary cells, which had around 15% S and G2/M phase cells. The results of the cell cycle analysis are summarized in **Table 2**, and the statistical difference was evaluated. As shown in **Table 2**, a decreased ratio of G0/G1 and increased ratio of S phase and G2/M phase cells were detected. From the results of cell cycle analysis, we concluded that K4DT cells showed accelerated turnover of the cell cycle due to the expression of CDK4 and Cyclin D1.

Real-Time PCR Detection of Androgen Receptor Expression

In our previous study, we showed that expression of the androgen receptor in DPCs was suppressed after several

passages, even in primary culture. Kwack et al. (2010) reported that the mRNA expression level of the androgen receptor dramatically decreases after passage six compared to the original cell culture. To determine whether our immortalized DPCs exhibited suppression of the androgen receptor, we used real-time PCR to detect the endogenous expression level of the androgen receptor. As shown in **Figure 4D**, total RNA from normal prostate tissue was used as a positive control. The human embryonic fibroblast line HE16 was used as a negative control. When the expression level of the androgen receptor in wild type DPCs at passage eight was set to 1.0, the relative expression level in HE16 cells was close to 1.0, while the relative expression level in normal prostate-derived RNA was more than 42. The expression level in immortalized K4DT DPCs at passage 12 was almost the same as that in primary DPCs and HE16 fibroblasts. Amplification plots of AR was shown in **Supplementary Figure S7**. These data indicated that primary DPCs exhibited suppression of the androgen receptor, probably due to the several passages performed during manufacturing. From these data, we concluded that our established immortalized DPCs are negative for androgen receptor expression.

Retroviral Introduction of the Androgen Receptor Into Immortalized DPCs

As shown in **Figure 4D**, original DPCs and immortalized DPCs showed low expression of the androgen receptor. To estimate the efficiency of gene introduction via retrovirus, retroviruses expressing EGFP were used to infect K4DT cells. As shown in the upper panels of **Supplementary Figure S1**, a small percentage of K4DT cells were infected. There was no obvious cell toxicity after infection with androgen receptor-expressing retroviruses (**Supplementary Figure S1**, lower panels), and we did not detect any morphological changes in infected cells. The efficiency of infection was not as high as described in the previous section. Due to the presence of a neomycin-resistance gene downstream of the EGFP or androgen receptor-expressing retrovirus (QCXIN retrovirus, Takara Bio, Shiga, Japan), we were able to perform selection using G418 antibiotics to purify the EGFP or androgen receptor-expressing cells. As shown in **Figure 5A**, DPCs expressing K4DT with no additional infection showed complete cell death after G418 selection (700 μ g/mL) (**Figure 5A**, upper panels). However, the K4DT DPCs successfully infected by QCXIN-EGFP or QCXIN-AR showed resistance to G418 selection (**Figure 5A**, middle and lower panels). Furthermore, after infection with QCXIN-EGFP, the surviving cells selected for by administration of 700 μ g/mL of G418 were all positive for EGFP expression (**Figure 5A**, middle panel), indicating that antibiotic selection worked properly. To verify androgen receptor expression in DPCs with K4DT, we carried out western blotting using an HA antibody. As shown in **Figure 5B**, although α -tubulin did not show any difference in signal intensity (**Figure 5B**, right panel and **Supplementary Figure S4**), DPCs infected with QCXIN-AR showed a specific signal at 100 kDa in the western blot for HA antibody (**Figure 5B**, Left panel, lane 2 and **Supplementary Figure S4**). From these data, we concluded

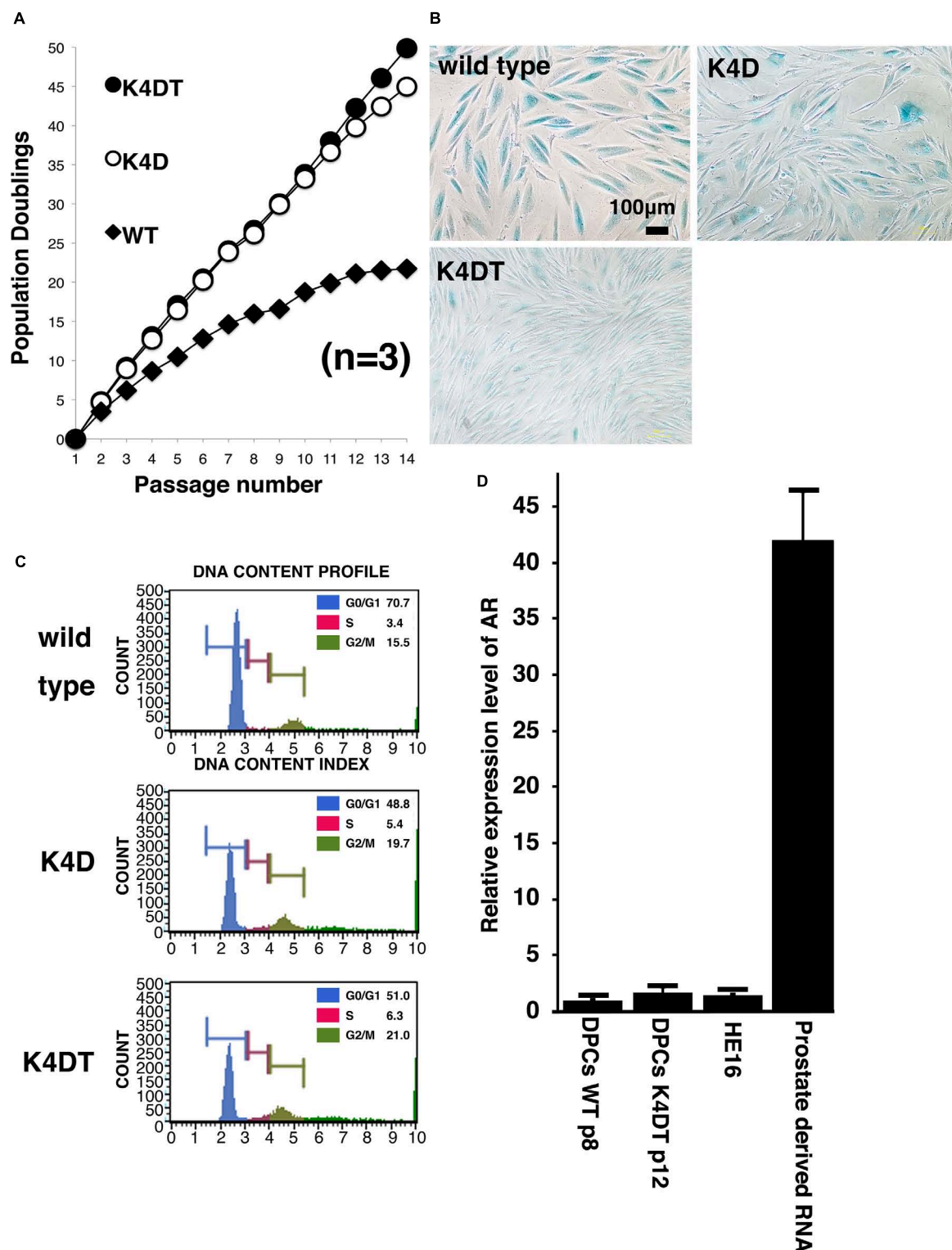
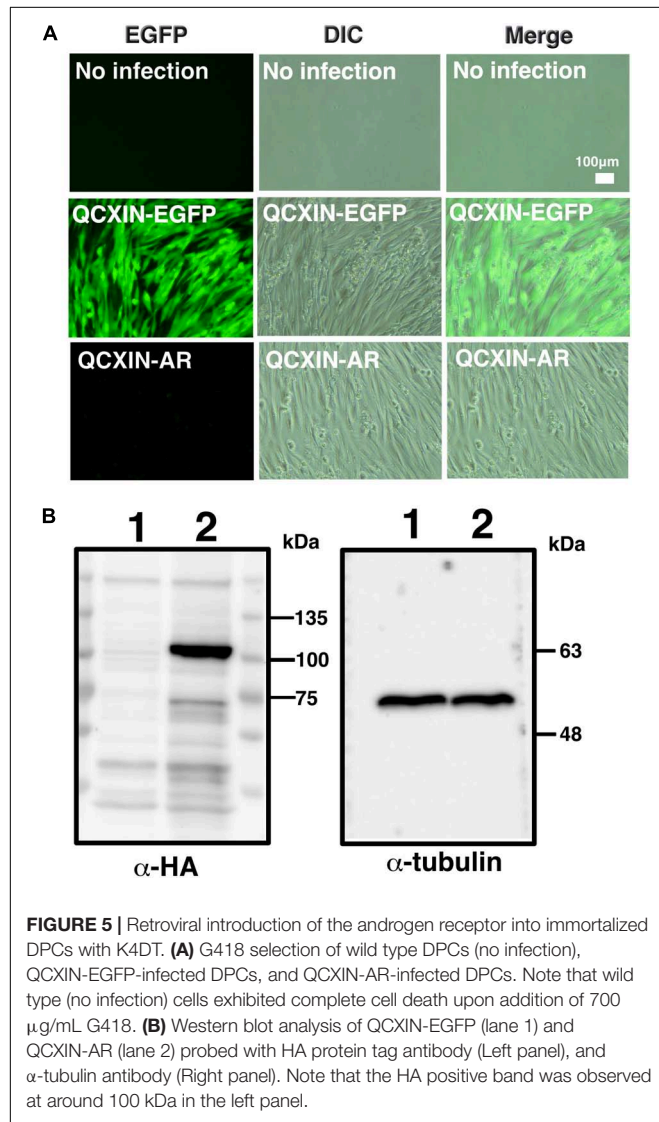


FIGURE 4 | Results of sequential passaging, detection of cellular senescence, and expression levels of the androgen receptor. **(A)** Sequential passaging and cumulative population doubling of wild type, K4D, and K4DT cells. Averages and standard deviations were obtained from triplicate samples. **(B)** Detection of cellular senescence using SA- β -gal staining in wild type, K4D, and K4DT cells. The bar indicates 100 μ m. **(C)** Cell cycle histogram of representative results obtained from wild type, K4D, and K4DT cells. **(D)** Detection of the androgen receptor gene in wild type DPCs at passage 8, immortalized K4DT DPCs at passage 12, HE12 human fibroblasts, and adult human prostate-derived RNA. Wild type DPC expression levels were set to 1.0, and the relative amount of AR was detected using real-time PCR. Six samples were analyzed for each group. The averages and standard deviations are shown.

TABLE 2 | Cell cycle analysis of wild type, K4D and K4DT cells.

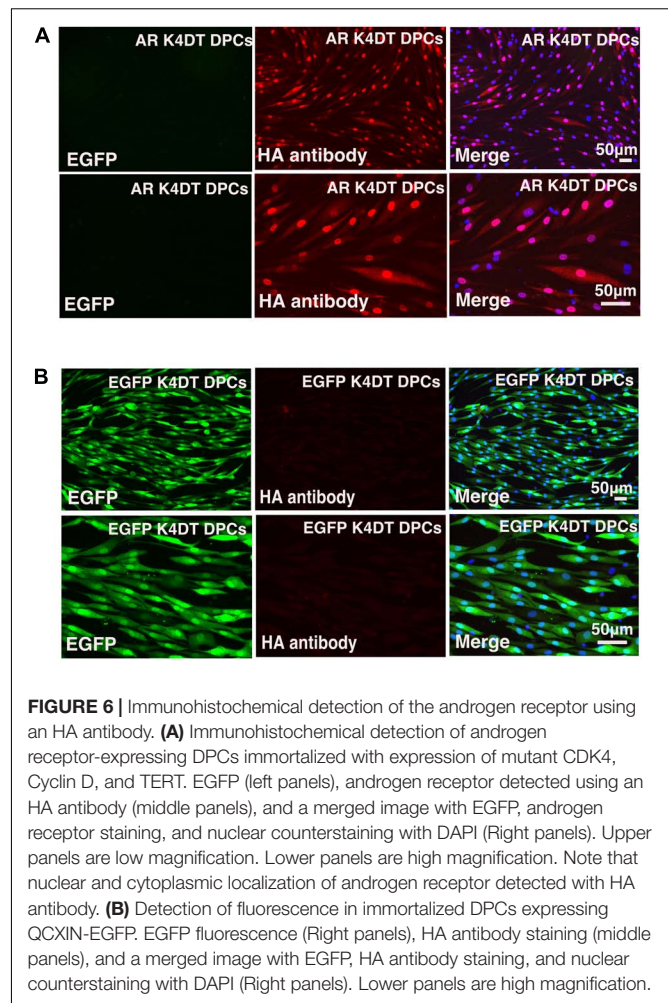
| Cell line | Cell cycle phase | | | |
|-----------|------------------|-------------|--------------|--------------|
| | G0/G1 | S | G2/M | Debris |
| Wild type | 70.7 ± 1.4 | 3.4 ± 0.1 | 15.5 ± 0.9 | 61.5 ± 4.0 |
| K4D | 48.8 ± 0.8** | 5.4 ± 0.2** | 19.7 ± 0.3** | 27.2 ± 1.4** |
| K4DT | 51.0 ± 0.5** | 6.3 ± 0.1** | 21.0 ± 0.2** | 26.1 ± 1.2** |

***p* < 0.01.

that we successfully established K4DT DPCs expressing the androgen receptor.

Visualization of Cellular Localization of the Androgen Receptor

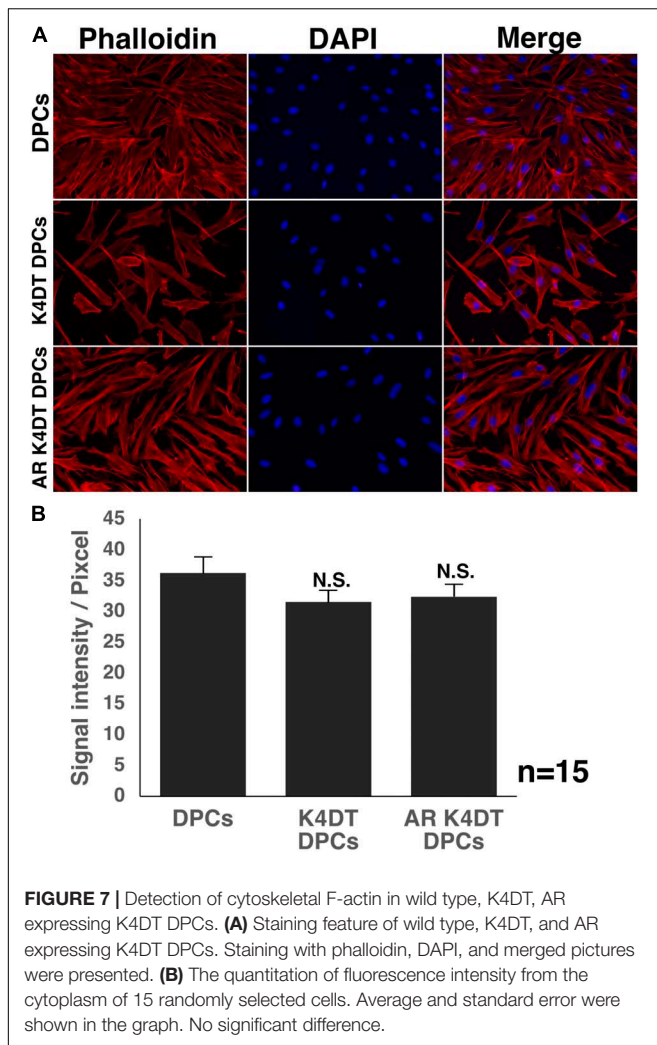
After stable introduction of the androgen receptor into K4DT DPCs, we detected the cellular localization of the androgen



receptor. As shown in **Figure 6B**, K4DT DPCs with QCXIN-EGFP (control) did not show any reactivity with the HA antibody (**Figure 6B**, Middle upper panel), indicating the specific binding of the antibodies. Interestingly, K4DT DPCs with QCXIN-AR showed positive staining in the cytoplasm and nuclear (**Figure 6A**, Upper middle panel). As shown in the merged picture with 4',6-diamidino-2-phenylindole (DAPI) (upper right panel of **Figure 6A**), staining for the androgen receptor via the HA tag revealed cytoplasmic and nuclear localization, in agreement with the previous manuscript (Fang et al., 1996). From these results, we concluded that we successfully established immortalized DPCs with constant expression of the androgen receptor.

Cellular Distribution of F-Actin

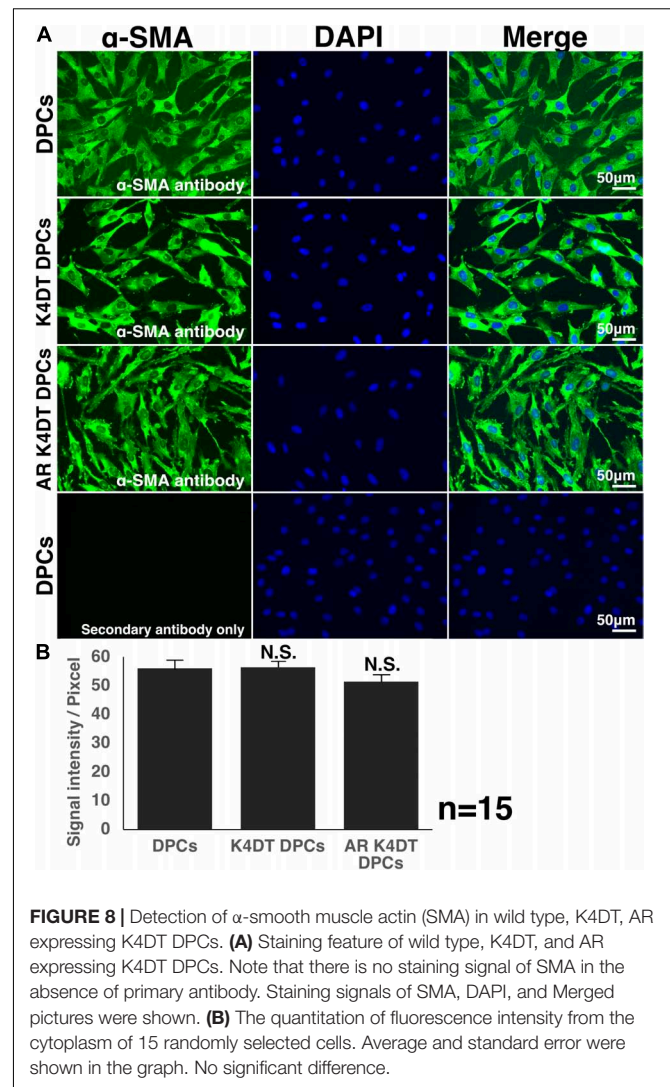
The cytoskeletal F-actin has critical role for the cell migration, and cell division and proliferation (Debacq-Chainiaux et al., 2009). We detected the cellular distribution of F-actin among wild type, K4DT, androgen receptor (AR) expressing K4DT DPCs. In the fluorescence images, we could not observe significant difference of F-actin in these three types of cells (**Figure 7A**). Furthermore, we measured the fluorescence



intensity of randomly selected 15 cytoplasm (Supplementary Figure S5). As shown in Figure 7B, we did not observe any statistical difference among wild type, K4DT, and AR expressing K4DT DPCs.

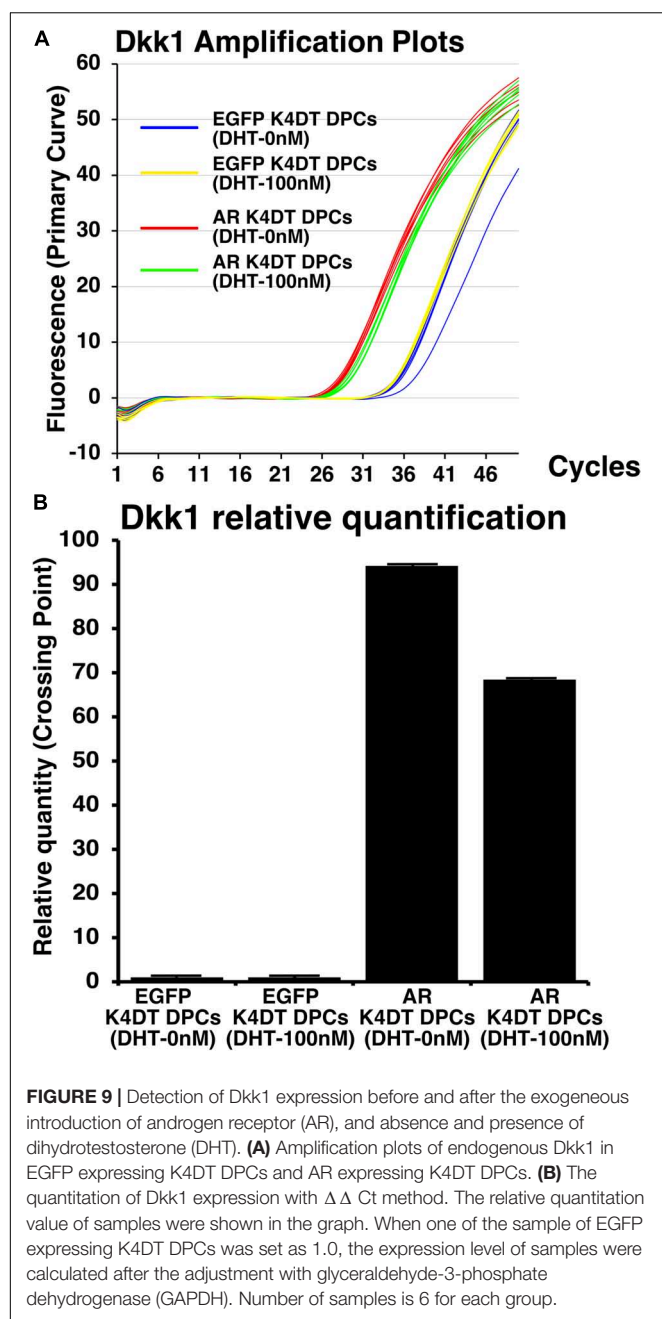
Expression of AR in K4DT DPCs Induces the Expression of Downstream Gene, Dkk1

Before and after the introduction of AR, we also exposed 100 nM of dihydrotestosterone to the cells. After the exposure, we detected the expression of Dkk1, which is known to locate the downstream of gene network of testosterone signaling. We used Taqman probe method for the accurate quantitation of Dkk1. In Figure 9A, we showed the amplification plots of Dkk1 mRNA in AR expressing DPCs and EGFP expressing DPCs with and without treatment of 100 nM of dihydrotestosterone. From the amplification curve, we showed the relative expression of Dkk1 has dramatically elevated after the exogenous introduction of AR (Figure 9B and Supplementary Figure S9). Interestingly,



expression level was around 70% after the treatment of dihydrotestosterone.

Furthermore, Inui et al. reported that TGF β 1 is upregulated by androgen in DPCs of AGA, suggesting that TGF β 1 is the potential downstream of testosterone signaling pathway (Inui et al., 2002). To evaluate this possibility, we detected the expression level of TGF β 1 in EGFP expressing DPCs, and AR expressing DPCs, under the absence and presence of DHT. As shown in Supplementary Figures S8A,B, although we observed marginal increase after the introduction of AR into K4DT DPCs, but its upregulation was not so evident. Furthermore, the expression difference of TGF β 1 was not apparent between absence and presence of AR, when it compared with that of Dkk1. Amplification plots of GAPDH for TGF β 1 showed almost no difference among the samples, indicating that slight increase of TGF β 1 expression is not due to the sample quality (Supplementary Figure S10). From this situation, we explained that TGF β 1 might be mainly regulated by various types of



signaling pathways, although testosterone signaling pathway would be one of the factors of them.

Nuclear Translocation Is Accelerated by the Treatment of Dihydrotestosterone

To detect the functionality of exogenous introduced AR, we detected localization of nuclear and cytoplasm localization of AR with HA tag antibody. As shown in **Figure 10A**, AR expressing K4DT DPCs showed pale positive staining in the cytoplasm and nuclear staining, before DHT treatment. However, to be noted, the pale positive staining in the cytoplasm has disappeared (**Figure 10A**, lower left), and the localization of AR becomes

only limited within the nuclear (**Figure 10A**, lower right). The incidence of the nuclear + cytoplasm cell becomes significantly lower after the DHT treatment (**Figure 10B**). Furthermore, the incidence of cells which showed the positive staining only within the nuclear significantly increased after the DHT treatment (**Figure 10B**). From these observations, we concluded that our introduced AR with HA tag works properly against DHT ligand treatment.

Anti-testosterone Reagent, MDV3100, Partially Inhibit the Nuclear Translocation of AR

In previous section, we showed that our established AR expressing K4DT DPCs detect the nuclear translocation of AR with HA antibody after the DHT treatment. These results guided us to build the hypothesis that our established cell might be useful to detect the anti-testosterone effect. We evaluated the effects of MDV3100, which is distributed as anti-testosterone compound, Enzalutamide in clinical stage of prostate cancer treatment. MDV3100 (Enzalutamide) is authorized as the anti-prostate cancer drug (Gibbons et al., 2015), and inhibits nuclear translocation of AR, and coactivator recruitment (Tran et al., 2009). Based on these clinical data, we exposed the 10 μ M of MDV3100 to the cell culture medium under the existence of 100 nM DHT. As shown in **Figure 11**, although treatment of DHT completely erased the positive signal of the cytoplasm as upper right panel of **Figure 11A**, addition of MDV3100 showed existence of pale positive cells for their cytoplasm (**Figure 11A**, lower right). For the accurate evaluation, we counted the cell count of cells, which both positive for cytoplasm and nuclear (blue bar in **Figure 11B**), or cells, which only positive within the nuclear (orange bar in **Figure 11B**). Based on the counting data, we summarized the percentage of cells, which both positive for cytoplasm and nuclear (blue bar) or cells, which only positive within the nuclear (orange bar), absence and presence of MDV3100, in **Figure 11C**. As the results of statistical difference, we concluded that the MDV3100 treatment significantly increases the cell incidence which positive both for nuclear and cytoplasm (**Figure 11C**, blue bar). Furthermore, MDV3100 treatment significantly decreased the incidence of cells, which only positive nuclear (**Figure 11C**, orange bar). From these data, we concluded that treatment of MDV3100 partially inhibit the translocation of AR from cytoplasm to nuclear.

DISCUSSION

In this study, we established the first immortalized human follicle dermal papilla cells expressing mutant CDK4, Cyclin D1, and TERT, and we showed that immortalized DPCs retained the characteristics of primary cells as well as an intact chromosomal karyotype. In the previous manuscript, DPCs with SV40 were reported (Kim et al., 2003). However, as shown in swine embryonic fibroblasts, even at passage 8 these cells already exhibited polyploid abnormalities at a rate of 16.4%, indicating

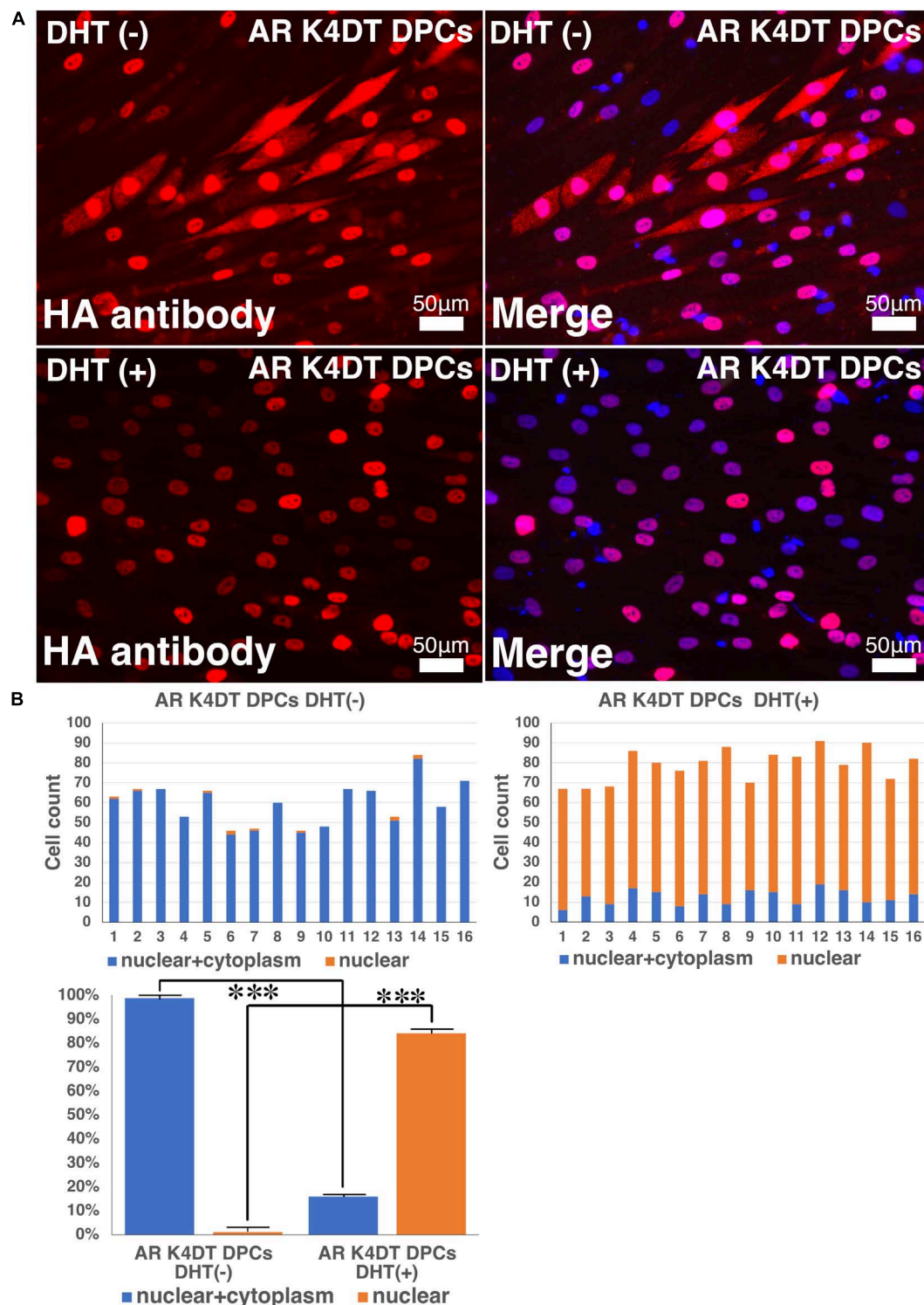


FIGURE 10 | Detection of nuclear translocation of androgen receptor (AR) under absence and presence of dihydrotestosterone (DHT). **(A)** Representative staining feature of AR K4DT DPCs with and without DHT. Note that under the presence of DHT, the localization of AR in the cytoplasm is almost negative, and AR localize within the nuclear. **(B)** Count of cells, which positive nuclear and cytoplasm (blue bar) and cells, which positive only within the nuclear (orange bar). Left side, results from 16 images before DHT treatment. Right side, results from 16 images after DHT treatment. Bottom panel, percentage of cells, which positive both nuclear and cytoplasm (blue bar) and percentage of cells, which positive only within the nuclear (orange bar). The statistical significance more than 0.1% were shown with three stars. $N = 16$ for each group.

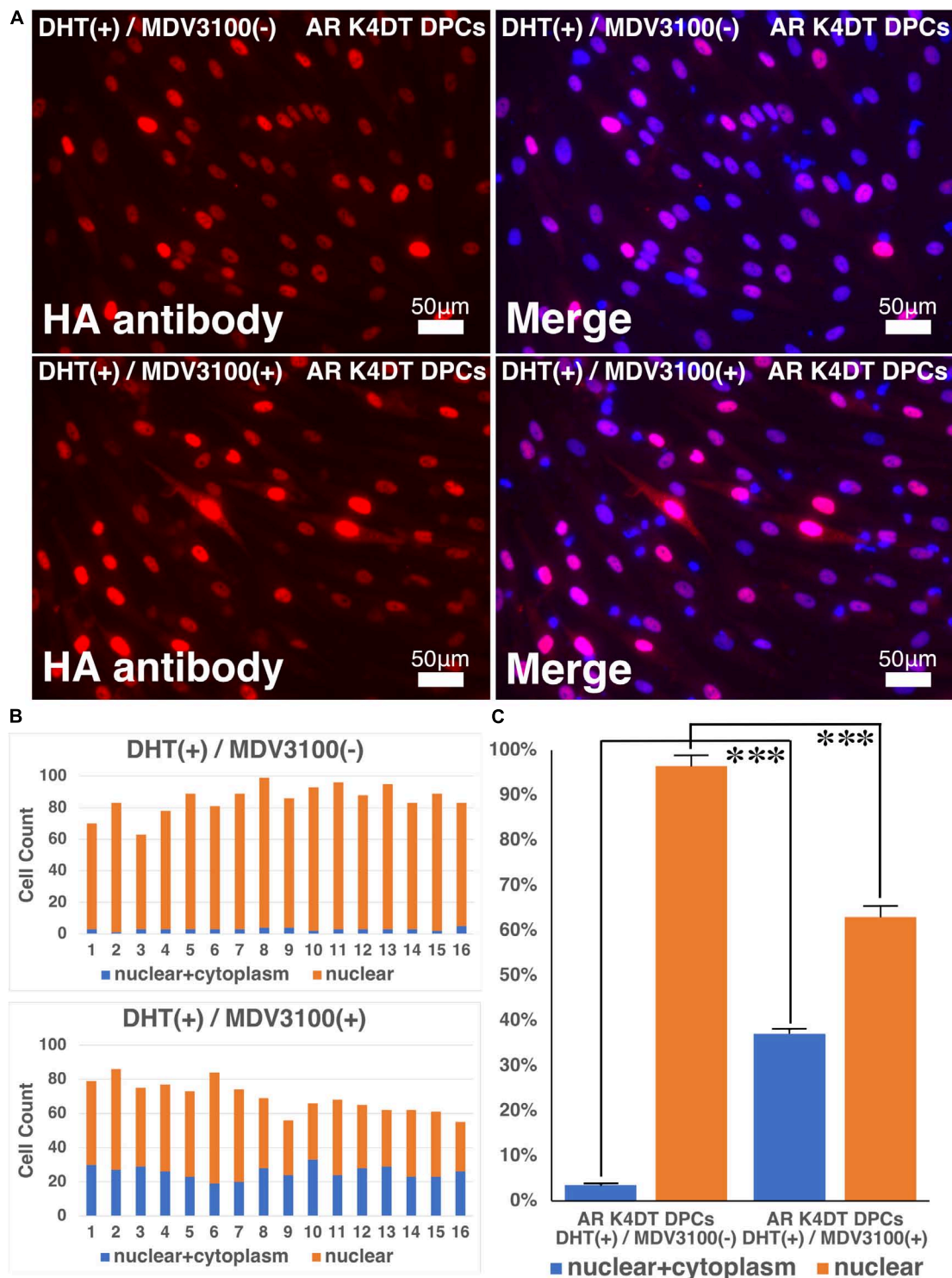


FIGURE 11 | Nuclear translocation of AR by DHT is partially inhibited by MVD3100 in AR expressing K4DT DPCs. **(A)** Representative staining feature of AR with HA tag antibody after the DHT treatment, under the absence and presence of MDV3100. **(B)** Upper panel, Count of cells, which positive nuclear and cytoplasm (blue bar) and cells, which positive only within the nuclear (orange bar) under the absence of MDV3100. Lower panel, Count of cells, which positive nuclear and cytoplasm (blue bar) and cells, which positive only within the nuclear (orange bar) under the existence of MDV3100. **(C)** Percentage of cells, which positive both nuclear and cytoplasm (blue bar) and percentage of cells, which positive only within the nuclear (orange bar). Comparison between absence of presence of MDV3100. The statistical significance more than 0.1% were shown with three stars. $N = 16$ for each group.

that SV40-expressing cells frequently experience chromosomal abnormalities (Fukuda et al., 2012a).

The combined expression of mutant CDK4, Cyclin D1, and TERT enables us to efficiently immortalize various cell types, as mentioned previously. The basic principle of this K4DT immortalization method is bypassing the negative feedback signal from the senescence protein p16 (Fukuda et al., 2018). Once cells reach the senescence phase, p16 accumulates in the cells (Shiomi et al., 2011). p16 proteins bind to CDK4 and negatively regulate the kinase activity of the CDK4-Cyclin D1 complex, resulting in a slowdown of cell cycle turnover. The R24C mutant of CDK4 is resistant to negative regulation via p16 due to an amino acid alteration at the p16 binding site. Co-expression of Cyclin D1 forms a functional enzymatic complex, resulting in continuous cell growth. However, expression of mutant CDK4 and Cyclin D1 is not enough, since these genes are not able to prevent shortening of the telomere sequence at the end of chromosomes. The addition of TERT expression allows for extension of the telomere sequence, resulting in immortalization. We previously reported that this K4DT method can be applied to various cell types, such as fibroblasts (Katayama et al., 2016) and intestinal epithelial cells (Kuroda et al., 2015b). In this study, we showed that expression of mutant CDK4, Cyclin D, and TERT allows us to efficiently establish immortalized cells from human DPCs.

We showed that immortalized K4DT cells retain the original nature of primary cells. We observed positive staining for alkaline phosphatase, a surrogate marker, suggesting that our established K4DT DPCs retained the original nature of the primary cells. In agreement with this result, a previous study showed that K4DT cells derived from the human skeletal muscle cells of patients with myotonic dystrophy type 1 (DM1) retained the original pathogenic condition, such as the abnormal splicing of exon 11 of BIN1 (bridging integrator-1) and exon 5 of MBNL1 (muscle-specific splicing factors muscle blind-like protein 1) (Pantic et al., 2016). However, for a more precise classification of the nature of the original cells, global transcriptome analysis would be necessary. As the supportive evidences of original nature, we detected the cellular distribution of F-actin and SMA (**Figure 8** and **Supplementary Figure S6**). We also detected the fluorescence intensity of F-actin and SMA in randomly selected area, we did not detect any difference among wild type, K4DT, and AR expressing K4DT DPCs. These data suggest that K4DT method would be more advantageous to keep the nature of the original cells.

Through chromosome analysis, we observed that 100% of cells exhibited perfect normal condition, 46 + XY. However, in the G-banding analysis, one sample out of 20 mitotic cells possessed an abnormality in chromosome 1. We previously showed that around 6.5% of cells exhibited abnormal chromosome patterns even in normal swine fibroblasts (Fukuda et al., 2012a). Therefore, approximately 5% of observed chromosome abnormalities can be attributed to an artifact caused by sample preparation for chromosome analysis.

Through senescence-associated β -gal staining, we observed that several K4D cells showed intense staining, but the majority

of cells did not. Though not confirmed, the estimated efficiency of gene introduction was around 80–85% based on the results from enhanced green fluorescence protein (EGFP)-expressing lentivirus (**Figure 1B**). Since efficient cell growth requires double infection with mutant CDK4 and Cyclin D1-expressing lentiviruses, an estimated 64% of cells would be doubly-infected, while the rest (~36%) would have a single transgene, mutant CDK4 or Cyclin D1. There is a possibility that the SA-positive cells described above are cells infected with a single transgene.

When considering the biology of DPCs and their relationship with AGA, we must note the importance of the androgen receptor, since DHT is classified as one of the major causes of the progression of AGA. Hormone dependency must be implemented when using cultured DPCs as a research tool for studying AGA (Kwack et al., 2008, 2010). Upon recognizing this issue, we determined the endogenous expression level of the androgen receptor in immortalized DPCs, as shown in **Figure 4D**. Based on the results in **Figure 4D**, we concluded that the endogenous expression level of the androgen receptor was already suppressed during the cell culture period of the provider, which is good agreement with the previous finding that expression level of androgen receptor was strongly suppressed in primary rat derived DPCs. In brief, Kwack et al. (2008) showed that the expression level of the androgen receptor gene dramatically decreased after passage 6. Although the detailed mechanism for the gene silencing of the androgen receptor is not understood, we decided to introduce the androgen receptor gene under an artificial promoter. Furthermore, we introduced an HA protein tag to facilitate detection of the introduced androgen receptor. Western blot analysis revealed high expression of the androgen receptor via its expression cassette in our established immortalized DPCs. Furthermore, we also detected beautiful localization of the androgen receptor in the nuclear and cytoplasm of our established cells. Furthermore, we showed that downstream gene, Dkk1, is highly activated after the introduction of AR. The elevated mRNA level of Dkk1 indicate that our established AR expressing K4DT DPCs involves the gene network related to testosterone. Interestingly, we detected the expression level of TGF β , which previously identified as elevated gene after the DHT treatment. However, we did not observe any significant change in the expression level of TGF β even after the expression of AR and existence of DHT. The biological significance of TGF β in DPCs would be necessary to be addressed in further investigation.

Furthermore, owing to the introduction of an HA protein tag, we successfully detected the translocation of introduced AR into the nucleus after the DHT treatment. The sensitivity of the high affinity HA antibody is so high that a cytoplasm-to-nucleus transition could be effectively detected by this system. Furthermore, we showed that MDV3100 (Enzalutamide) partially inhibits the nuclear translocation of AR. MDV3100 (Enzalutamide) is authorized drug for prostate cancer, and has anti-testosterone activity. To develop more specific and efficient anti-testosterone drugs, various types of compounds are under development. As one of the candidates, CH5137291 has reported to have more strong effect to inhibit the nuclear translocation of AR. Although CH513791 is not distributed yet in

the market, we are planning to test the effect of CH513791 to AR translocation as next study. The established immortalized DPC line with androgen receptor expression described in this study is a beneficial tool for the screening of anti-testosterone compounds, which would be useful for the prevention of AGA and other testosterone-related diseases, such as prostatic hypertrophy and prostate cancer. We plan to share our established DPCs with scientists worldwide to facilitate further research using this innovative cell line.

DATA AVAILABILITY STATEMENT

The data sets used and/or analyzed during the current study are available from the corresponding author on reasonable request.

AUTHOR CONTRIBUTIONS

TF, KT, ST, AO, and TE did the experiments. TF, KN, and TK contributed the design of the experiments. TF and KT wrote the manuscript. TK provided the experimental materials.

FUNDING

This work was supported in part by a research grant from the Hoyu Foundation.

ACKNOWLEDGMENTS

We are grateful to Dr. Hiroyuki Miyoshi (RIKEN BRC, Tsukuba, Japan) for providing the lentivirus-expressing system. We also thank Dr. Hiroshi Tomita, Dr. Eriko Sugano, and Dr. Taku Ozaki (Iwate University) for mentoring the graduate and undergraduate students of our laboratory.

REFERENCES

- Coskuner, E. R., Ozkan, B., and Culha, M. G. (2019). Sexual problems of men with androgenic alopecia treated with 5-Alpha reductase inhibitors. *Sex. Med. Rev.* 7, 277–282. doi: 10.1016/j.sxmr.2018.07.003
- Danilenko, D. M., Ring, B. D., and Pierce, G. F. (1996). Growth factors and cytokines in hair follicle development and cycling: recent insights from animal models and the potentials for clinical therapy. *Mol. Med. Today* 2, 460–467. doi: 10.1016/1357-4310(96)10045-9
- Davis, B. K. (1962). Phases of the hair-growth cycle. *Nature* 194, 694–694. doi: 10.1038/194694a0
- Debacq-Chainiaux, F., Eruslimsky, J. D., Campisi, J., and Toussaint, O. (2009). Protocols to detect senescence-associated beta-galactosidase (SA- β gal) activity, a biomarker of senescent cells in culture and *in vivo*. *Nat. Protoc.* 4, 1798–1806. doi: 10.1038/nprot.2009.191
- Detmar, M., Schaart, F. M., Blume, U., and Orfanos, C. E. (1993). Culture of hair matrix and follicular keratinocytes. *J. Invest. Dermatol.* 101, 130S–134S. doi: 10.1016/0022-202X(93)90513-H
- Donai, K., Kiyono, T., Eitsuka, T., Guo, Y., Kuroda, K., Sone, H., et al. (2014). Bovine and porcine fibroblasts can be immortalized with intact karyotype by

SUPPLEMENTARY MATERIAL

The Supplementary Material for this article can be found online at: <https://www.frontiersin.org/articles/10.3389/fcell.2020.00157/full#supplementary-material>

FIGURE S1 | Detection of potential cell morphological changes and fluorescence of immortalized DPCs expressing QCXIN-EGFP and QCXIN-AR before G418 selection. Immortalized DPCs infected with QCXIN-EGFP (upper panels). Immortalized DPCs infected with QCXIN-AR (lower panels).

FIGURE S2 | Full length gel photos for **Figure 2A**. Upper panel, detected gel image of CDK4 and Cyclin D. Lower panel, detected gel image of TERT and TSC2.

FIGURE S3 | Full length blot photo for **Figure 2B**. Upper panel, detected blot image of CDK4. Middle panel, detected blot image of Cyclin D. Lower panel, detected image of alpha-tubulin. The corresponding area of Figures are marked by the rectangles.

FIGURE S4 | Full length blot photo for **Figure 5B**. Upper panel, detected blot image of HA antibody. Lower panel, detected blot image of alpha-tubulin. The corresponding area of Figures are marked by the rectangles.

FIGURE S5 | F-actin staining of measurement of fluorescence intensity of the 15 area. The area of the measurement of fluorescence intensity in wild type DPCs, K4DT DPCs, AR expressing DPCs were shown with white rectangles.

FIGURE S6 | Immunostaining of α -smooth muscle actin (SMA) of wild type, K4DT, and AR expressing K4DT DPCs. The area of the measurement of fluorescence intensity in wild type DPCs, K4DT DPCs, AR expressing DPCs were shown with white rectangles.

FIGURE S7 | Amplification plots of androgen receptor (AR) with real time PCR analysis. Expression AR in wild type DPCs, K4DT DPCs, HE16, human normal prostate derived RNA were evaluated.

FIGURE S8 | Amplification plots of TGF β 1 with real time PCR analysis. **(A)** Amplification plots of TGF β 1 in K4DT DPCs and AR expressing K4DT AR DPCs with and without dihydrotestosterone. **(B)** The quantitation of TGF β 1 expression with $\Delta\Delta$ Ct method.

FIGURE S9 | Amplification plots of glyceraldehyde-3-phosphate dehydrogenase (GAPDH) with real time PCR method for the quantitation of Dkk1.

FIGURE S10 | Amplification plots of glyceraldehyde-3-phosphate dehydrogenase (GAPDH) with real time PCR method for the quantitation of TGF β 1.

- the expression of mutant cyclin dependent kinase 4, cyclin D, and telomerase. *J. Biotechnol.* 176, 50–57. doi: 10.1016/j.jbiotec.2014.02.017
- Donai, K., Kuroda, K., Guo, Y., So, K.-H., Sone, H., Kobayashi, M., et al. (2013). Establishment of a reporter system to monitor silencing status in induced pluripotent stem cell lines. *Anal. Biochem.* 443, 104–112. doi: 10.1016/j.ab.2013.08.014
- Driskell, R. R., Clavel, C., Rendl, M., and Watt, F. M. (2011). Hair follicle dermal papilla cells at a glance. *J. Cell Sci.* 124, 1179–1182. doi: 10.1242/jcs.082446
- Fang, Y., Fliss, A. E., Robins, D. M., and Caplan, A. J. (1996). Hsp90 regulates androgen receptor hormone binding affinity *in vivo*. *J. Biol. Chem.* 271, 28697–28702. doi: 10.1074/jbc.271.45.28697
- Fukuda, T., Eitsuka, T., Donai, K., Kurita, M., Saito, T., Okamoto, H., et al. (2018). Expression of human mutant cyclin dependent kinase 4, Cyclin D and telomerase extends the life span but does not immortalize fibroblasts derived from loggerhead sea turtle (*Caretta caretta*). *Sci. Rep.* 8:9229. doi: 10.1038/s41598-018-27271-x
- Fukuda, T., Iino, Y., Eitsuka, T., Onuma, M., Katayama, M., Murata, K., et al. (2016). Cellular conservation of endangered midget buffalo (Lowland Anoa, *Bubalus quarlesi*) by establishment of primary cultured cell, and its immortalization with expression of cell cycle regulators. *Cytotechnology* 68, 1937–1947. doi: 10.1007/s10616-016-0004-0

- Fukuda, T., Katayama, M., Yoshizawa, T., Eitsuka, T., Mizukami, H., Nakagawa, K., et al. (2012a). Efficient establishment of pig embryonic fibroblast cell lines with conditional expression of the simian vacuolating virus 40 large T fragment. *Biosci. Biotechnol. Biochem.* 76, 1372–1377. doi: 10.1271/bbb.120155
- Fukuda, T., Kurita, J., Saito, T., Yuasa, K., Kurita, M., Donai, K., et al. (2012b). Efficient establishment of primary fibroblast cultures from the hawksbill sea turtle (*Eretmochelys imbricata*). *Vitr. Cell. Dev. Biol. Anim.* 48, 660–665. doi: 10.1007/s11626-012-9565-1
- Fukuda, T., Tani, T., Haraguchi, S., Donai, K., Nakajima, N., Uenishi, H., et al. (2017). Expression of six proteins causes reprogramming of porcine fibroblasts into induced pluripotent stem cells with both active X chromosomes. *J. Cell. Biochem.* 118, 537–553. doi: 10.1002/jcb.25727
- Gibbons, J. A., Ouatas, T., Krauwinkel, W., Ohtsu, Y., van der Walt, J.-S., Beddo, V., et al. (2015). Clinical pharmacokinetic studies of enzalutamide. *Clin. Pharmacokinet.* 54, 1043–1055. doi: 10.1007/s40262-015-0271-5
- Gouko, R., Onuma, M., Eitsuka, T., Katayama, M., Takahashi, K., Nakagawa, K., et al. (2018). Efficient immortalization of cells derived from critically endangered Tsushima leopard cat (*Prionailurus bengalensis euptilurus*) with expression of mutant CDK4, Cyclin D1, and telomerase reverse transcriptase. *Cytotechnology* 70, 1619–1630. doi: 10.1007/s10616-018-0254-0
- Guo, L., Degenstein, L., and Fuchs, E. (1996). Keratinocyte growth factor is required for hair development but not for wound healing. *Genes Dev.* 10, 165–175. doi: 10.1101/gad.10.2.165
- Gupta, A. K., and Charrette, A. (2014). The efficacy and safety of 5 α -reductase inhibitors in androgenetic alopecia: a network meta-analysis and benefit–risk assessment of finasteride and dutasteride. *J. Dermatolog. Treat.* 25, 156–161. doi: 10.3109/09546634.2013.813011
- Hébert, J. M., Rosenquist, T., Götz, J., and Martin, G. R. (1994). FGF5 as a regulator of the hair growth cycle: evidence from targeted and spontaneous mutations. *Cell* 78, 1017–1025. doi: 10.1016/0092-8674(94)90276-3
- Inui, S., Fukuzato, Y., Nakajima, T., Yoshikawa, K., and Itami, S. (2002). Androgen-inducible TGF- β 1 from balding dermal papilla cells inhibits epithelial cell growth: a clue to understanding paradoxical effects of androgen on human hair growth. *FASEB J.* 16, 1967–1969. doi: 10.1096/fj.02-0043fj
- Katayama, M., Hirayama, T., Kiyono, T., Onuma, M., Tani, T., Takaeda, S., et al. (2017). Immortalized prairie vole-derived fibroblasts (VMF-K4DTs) can be transformed into pluripotent stem cells and provide a useful tool with which to determine optimal reprogramming conditions. *J. Reprod. Dev.* 63, 311–318. doi: 10.1262/jrd.2016-164
- Katayama, M., Kiyono, T., Horie, K., Hirayama, T., Eitsuka, T., Kuroda, K., et al. (2016). Establishment of an immortalized cell line derived from the prairie vole via lentivirus-mediated transduction of mutant cyclin-dependent kinase 4, cyclin D, and telomerase reverse transcriptase. *Exp. Anim.* 65, 87–96. doi: 10.1538/expanim.15-0061
- Katayama, M., Kiyono, T., Kuroda, K., Ueda, K., Onuma, M., Shirakawa, H., et al. (2019). Rat-derived feeder cells immortalized by expression of mutant CDK4, cyclin D, and telomerase can support stem cell growth. *Biochim. Biophys. Acta Mol. Cell Res.* 1866, 945–956. doi: 10.1016/j.bbamcr.2019.02.013
- Kaufman, K. D., and Dawber, R. P. (1999). Finasteride, a Type 2 5 α -reductase inhibitor, in the treatment of men with androgenetic alopecia. *Expert. Opin. Investig. Drugs* 8, 403–415. doi: 10.1517/13543784.8.4.403
- Kim, C. D., Lee, M. H., and Roh, S. S. (2003). Identification of androgen-regulated genes in SV40-transformed human hair dermal papilla cells. *J. Dermatol. Sci.* 32, 143–149. doi: 10.1016/s0923-1811(03)00093-8
- Kuroda, K., Kiyono, T., Eitsuka, T., Isogai, H., Takahashi, K., Donai, K., et al. (2015a). Establishment of cell lines derived from the genus macaca through controlled expression of cell cycle regulators. *J. Cell. Biochem.* 116, 205–211. doi: 10.1002/jcb.24963
- Kuroda, K., Kiyono, T., Isogai, E., Masuda, M., Narita, M., Okuno, K., et al. (2015b). Immortalization of fetal bovine colon epithelial cells by expression of human Cyclin D1, mutant cyclin dependent Kinase 4, and telomerase reverse transcriptase: an in vitro model for bacterial infection. *PLoS One* 10:e0143473. doi: 10.1371/journal.pone.0143473
- Kwack, M. H., Ahn, J. S., Kim, M. K., Kim, J. C., and Sung, Y. K. (2010). Preventable effect of L-threonate, an ascorbate metabolite, on androgen-driven balding via repression of dihydrotestosterone-induced dickkopf-1 expression in human hair dermal papilla cells. *BMB Rep.* 43, 688–692. doi: 10.3858/BMBRep.2010.43.10.688
- Kwack, M. H., Sung, Y. K., Chung, E. J., Im, S. U., Ahn, J. S., Kim, M. K., et al. (2008). Dihydrotestosterone-inducible dickkopf 1 from balding dermal papilla cells causes apoptosis in follicular keratinocytes. *J. Invest. Dermatol.* 128, 262–269. doi: 10.1038/SJ.JID.5700999
- Milner, Y., Kashgarian, M., Sudnik, J., Filippi, M., Kizoulis, M., and Stenn, K. (2002). Exogen, shedding phase of the hair growth cycle: characterization of a mouse model. *J. Invest. Dermatol.* 119, 639–644. doi: 10.1046/J.1523-1747.2002.01842.X
- Münster, U., Hammer, S., Blume-Peytavi, U., and Schäfer-Korting, M. (2003). Testosterone metabolism in human skin cells in vitro and its interaction with estradiol and dutasteride. *Skin Pharmacol. Physiol.* 16, 356–366. doi: 10.1159/000072930
- Pantic, B., Borgia, D., Giunco, S., Malena, A., Kiyono, T., Salvatori, S., et al. (2016). Reliable and versatile immortal muscle cell models from healthy and myotonic dystrophy type 1 primary human myoblasts. *Exp. Cell Res.* 342, 39–51. doi: 10.1016/j.yexcr.2016.02.013
- Qin, X.-Y., Fukuda, T., Yang, L., Zaha, H., Akanuma, H., Zeng, Q., et al. (2012). Effects of bisphenol A exposure on the proliferation and senescence of normal human mammary epithelial cells. *Cancer Biol. Ther.* 13, 296–306. doi: 10.4161/cbt.18942
- Shankar, K., Chakravarthi, M., and Shilpakar, R. (2009). Male androgenetic alopecia: population-based study in 1,005 subjects. *Int. J. Trichol.* 1:131. doi: 10.4103/0974-7753.58556
- Shiomi, K., Kiyono, T., Okamura, K., Uezumi, M., Goto, Y., Yasumoto, S., et al. (2011). CDK4 and cyclin D1 allow human myogenic cells to recapture growth property without compromising differentiation potential. *Gene Ther.* 18, 857–866. doi: 10.1038/gt.2011.44
- Tani, T., Eitsuka, T., Katayama, M., Nagamine, T., Nakaya, Y., Suzuki, H., et al. (2019). Establishment of immortalized primary cell from the critically endangered Bonin flying fox (*Pteropus pselaphon*). *PLoS One* 14:e0221364. doi: 10.1371/journal.pone.0221364
- Topouzi, H., Logan, N. J., Williams, G., and Higgins, C. A. (2017). Methods for the isolation and 3D culture of dermal papilla cells from human hair follicles. *Exp. Dermatol.* 26, 491–496. doi: 10.1111/exd.13368
- Tran, C., Ouk, S., Clegg, N. J., Chen, Y., Watson, P. A., Arora, V., et al. (2009). Development of a second-generation antiandrogen for treatment of advanced prostate cancer. *Science* 324, 787–790. doi: 10.1126/science.1168175

Conflict of Interest: The authors declare that the research was conducted in the absence of any commercial or financial relationships that could be construed as a potential conflict of interest.

Copyright © 2020 Fukuda, Takahashi, Takase, Orimoto, Eitsuka, Nakagawa and Kiyono. This is an open-access article distributed under the terms of the Creative Commons Attribution License (CC BY). The use, distribution or reproduction in other forums is permitted, provided the original author(s) and the copyright owner(s) are credited and that the original publication in this journal is cited, in accordance with accepted academic practice. No use, distribution or reproduction is permitted which does not comply with these terms.



STAT3 Regulates Mouse Neural Progenitor Proliferation and Differentiation by Promoting Mitochondrial Metabolism

Yixun Su^{1,2,3}, Wenjun Zhang⁴, C. Pawan K. Patro^{2,5}, Jing Zhao³, Tianhao Mu^{2,5}, Zhongnan Ma^{6,7,8}, Jianqiang Xu⁶, Kenneth Ban^{2*}, Chenju Yi^{1*} and Yi Zhou^{2,3,7*}

¹ The Seventh Affiliated Hospital, Sun Yat-sen University, Shenzhen, China, ² Department of Biochemistry, Yong Loo Lin School of Medicine, National University of Singapore, Singapore, Singapore, ³ Neurobiology Programme, Life Sciences Institute, National University of Singapore, Singapore, Singapore, ⁴ School of Medicine, Indiana University, Indianapolis, IN, United States, ⁵ Cancer Science Institute of Singapore, Singapore, Singapore, ⁶ Department of Biology, Southern University of Science and Technology, Shenzhen, China, ⁷ West China Hospital, Sichuan University, Chengdu, China, ⁸ Model Animal Research Center of Nanjing University, Nanjing, China

OPEN ACCESS

Edited by:

Massimo Mattia Santoro,
University of Padua, Italy

Reviewed by:

Alexandra Chittka,
Queen Mary University of London,
United Kingdom
Jormay Lim,
National Taiwan University, Taiwan

*Correspondence:

Kenneth Ban
bchbhkk@nus.edu.sg
Chenju Yi
yichj@mail.sysu.edu.cn
Yi Zhou
zhouyi@wchscu.cn

Specialty section:

This article was submitted to
Cell Growth and Division,
a section of the journal
Frontiers in Cell and Developmental
Biology

Received: 30 January 2020

Accepted: 22 April 2020

Published: 19 May 2020

Citation:

Su Y, Zhang W, Patro CPK, Zhao J, Mu T, Ma Z, Xu J, Ban K, Yi C and Zhou Y (2020) STAT3 Regulates Mouse Neural Progenitor Proliferation and Differentiation by Promoting Mitochondrial Metabolism. *Front. Cell Dev. Biol.* 8:362. doi: 10.3389/fcell.2020.00362

The proliferation and differentiation of neural progenitor lay the foundation for brain development. In neural progenitors, activation of Signal Transducer and Activator of Transcription 3 (STAT3) has been found to promote proliferation and astrocytogenesis while suppressing neurogenesis. However, our study found that *Stat3* conditional knockout in neural progenitors (*Stat3* cKO) also results in increased proliferation and suppressed neurogenesis. To investigate how STAT3 regulates these processes, we attempted to identify potential STAT3 target genes by RNA-seq profiling of the control (CTL) and *Stat3* cKO neural progenitors. We found that STAT3 promotes the expression of genes involved in the mitochondrial oxidative phosphorylation (OXPHOS), and thereby promotes mitochondrial respiration and negatively regulates reactive oxygen species (ROS) production. In addition, we demonstrated that *Stat3* loss-of-function promotes proliferation via regulation of mitochondrial metabolism and downstream signaling pathways. Our study provides novel insights into the relation between STAT3, mitochondrial metabolism and the process of embryonic neurogenesis.

Keywords: neural progenitor, neurogenesis, proliferation, STAT3, mitochondria, OXPHOS

INTRODUCTION

Neural development is a complex, orchestrated process consists of multiple elements, including the self-renewal and differentiation of neural progenitors. Neural progenitors divide to self-renew and give rise to neurons in the early embryonic stage, and they become gliogenic in the later stages (Bayer and Altman, 1991; Kriegstein and Alvarez-Buylla, 2009). The self-renewal and differentiation of neural progenitors are fine-tuned by transcriptional factors and other pathways (Martynoga et al., 2012). Dysregulation of these processes could lead to severe developmental defects such as microcephaly and lissencephaly (reduced neurogenesis), or megalencephaly and autism spectrum disorder (overproduction of neurons) (Mochida, 2009; Fang et al., 2014).

Signal transducer and activator of transcription 3 (STAT3) plays an important role in neural progenitor self-renewal and differentiation. As a member of the STAT family, STAT3 responds to

cytokines and growth factors, and is then phosphorylated at tyrosine 705 residue by gp130/LIFR-associated JAK kinase, translocates into the nucleus and activates transcription of its target genes (Fu et al., 1990, 1992; Schindler et al., 1992; Darnell et al., 1994; Levy and Darnell, 2002). In addition, STAT3 also promotes gene expression in a tyrosine-phosphorylation-independent manner (Yang et al., 2005, 2007).

In embryonic neural progenitors, STAT3 has been found to be sufficient and necessary for astrocytogenesis: activation of STAT3 by IL6 family cytokines promotes the astrocyte marker GFAP expression, which is diminished in the *Stat3* conditional knockout (Bonni et al., 1997; Nakashima et al., 1999; Hong and Song, 2014). Mechanistically, activated STAT3 form a complex with SMAD1 and p300 and bind to the GFAP promoter to induce its expression (Nakashima et al., 1999). During the neurogenesis phase, activation of STAT3 also promotes cell proliferation and negatively regulates neurogenesis (Gu et al., 2005; Yoshimatsu et al., 2006; Cao et al., 2010; Chen et al., 2013; Hong and Song, 2015). However, knockout of STAT3 in astrocytes also resulted in a decreased proliferation rate (de la Iglesia et al., 2008).

STAT3 has been shown to be involved in mitochondrial metabolism in the central nervous system, which might play an important role in cell survival and axon outgrowth (Guo et al., 2008; Sarafian et al., 2010; Luo et al., 2016), but the causal mechanism remained unclear. It has also been shown that STAT3 could be translocated into mitochondria, and then promotes respiration by binding to protein complexes such as Complex I, or by regulating mitochondrial transcription (Wegrzyn et al., 2009; Macias et al., 2014; Carbognin et al., 2016; Xu et al., 2016). However, whether mitochondrial STAT3 could regulate mitochondrial metabolism was still controversial (Phillips et al., 2010). Furthermore, our previous report found that STAT3 does not localize in mitochondria, but in the mitochondria associated membranes (Su et al., 2019). Thus, STAT3 might regulate mitochondrial metabolism via other pathways.

In this study, we found that conditional knockout of STAT3 in neural progenitors also leads to increased proliferation and deteriorated neurogenesis. In addition, we found that STAT3 is not necessary for astrocyte differentiation, but instead only required for the expression of GFAP. To investigate the role of STAT3 in neural progenitor, we used RNA-seq analysis to uncover STAT3-dependent genes. We demonstrated that STAT3 promotes expression of genes that involve in the oxidative phosphorylation pathway and thereby promotes mitochondrial respiration. We demonstrated that this regulation is critical for *Stat3*-mediated neurogenesis. Our findings provide novel insights into the link between mitochondrial metabolism and the process of neurogenesis in brain development.

MATERIALS AND METHODS

Animals

The generation of mice with a conditional KO of *Stat3* has been described (Welte et al., 2003; Moh et al., 2007). Exons 18–20, which contain the SH2 domain of STAT3, were flanked by two loxP sites. Nestin-Cre transgenic mice [The Jackson Laboratory mice

database: B6.Cg(SJL)-TgN(Nes-cre)1Kln] expressing Cre under the control of a rat Nestin promoter/enhancer were described (Tronche et al., 1999). The Nestin-Cre *Stat3-flox/flox* (*Stat3-f/f*) mutant mice, designated as *Stat3* cKO, were generated by mating Nestin-Cre *Stat3-f/+* mice with *Stat3-f/f* mice. The genotype was determined by PCR as described (Welte et al., 2003). The genotyping primers sequence is listed in **Supplementary Table S1**. The sample result of genotyping is shown in **Supplementary Figure S1**. As the transgenic Nestin-Cre expression has been reported to cause metabolic changes (Harno et al., 2013), here we use Nestin-cre; *Stat3-flox/+* embryos as control (C; F/+) to account for the possible confounding effects. In addition, the control (C; F/+) mice are born in Mendelian ratios without observable growth defects. All experiments were done in a C57BL6 background. All procedures were performed in accordance with the National Institutes of Health Guide for the Care and Use of Laboratory Animals and under the approval of the NUS Institutional Animal Care and Use Committee.

The Cell Culture of Primary Embryonic Neural Progenitors

The primary neural progenitor culture was achieved according to an established protocol (Pacey et al., 2006) with some adjustment. In brief, pregnant mice were sacrificed by CO₂ overdose at the designated pregnancy stage. Embryonic brains were dissected and subjected to digestion with Accutase (Thermo Fisher Scientific) to isolate neural progenitors. The cells were then subjected to suspension culture in serum-free medium (SFM) supplemented with EGF and FGF at the density of 2×10^5 cells/ml. Fresh medium was replenished every other day. Cells grown into neurospheres were collected on the 3rd day for RNA/protein sample preparation. For differentiation assay in attachment culture, neurospheres were dissociated and cells were seeded onto poly-D-lysine and laminin (Sigma-Aldrich) coated coverslip at the density of 1×10^5 cells/ml in SFM with EGF/FGF (Sigma-Aldrich) supplement. To differentiate neural progenitors into neurons and glial cells, EGF and FGF were withdrawn on the 1st day after attachment. Half of the SFM was changed every other day, and the cells were collected for immunostaining or RNA/protein sample preparation. The detailed components of SFM and their source can be found in **Supplementary Table S2**.

RNA-seq

Neural progenitors isolated at E11 and E14 wild-type or *Stat3* cKO embryos were collected after culture for 3 days and were lysed directly by Trizol (Thermo Fisher Scientific) and total RNA was isolated according to manufacturer's protocol. cDNA was obtained using the M-MLV Reverse Transcriptase kit from Promega according to the manufacturer's protocol. RNA-seq experiment was carried out using Illumina HiSeq 2000 Sequencing System. The sequence files obtained were then undergone a quality check by FastQC, then processed and analyzed using the Tuxedo pipeline (Trapnell et al., 2012). Differentially expressed genes were then clustered using Database

for Annotation, Visualization and Integrated Discovery (DAVID) analysis (Huang et al., 2009a,b) for data mining.

RNA-Extraction and RT-qPCR

Neural progenitors were lysed directly by RNazol (Sigma-Aldrich) and total RNA was isolated according to the manufacturer's protocol. Reverse transcription was carried out with the M-MLV Reverse Transcriptase kit from Promega according to the manufacturer's protocol. qPCR experiment was carried out using SYBR green qPCR kit from KAPA and Applied Biosystems 7500 Real PCR System. qPCR primers used in the experiment can be found in **Supplementary Table S3**. Samples were assayed in duplicate and normalized to endogenous *Gapdh*.

Neurosphere Assay

Neural progenitors isolated from embryonic brains were seeded in 24-well plate at 2×10^5 cells/ml in SFM with growth factors. After 5 days, the neurospheres were imaged using an inverted microscope. The neurosphere diameter was measured using ImageJ software.

CFSE Assay

CFSE assay was carried out using the CellTrace CFSE Cell Proliferation Kit according to the manufacturer's protocol (Thermo). Briefly, neural progenitors isolated from embryonic brains were stained with 5 μ M CFSE for 20 min, washed with SFM once, and cultured for 48 h. Subsequently, cells were digested with trypsin and fixed with 2% paraformaldehyde and subjected to flow cytometry analysis.

BrdU Incorporation Assay

BrdU was added to the primary neural progenitor cell culture at 10 μ g/ml. cells were cultured for another 2 h before collected for staining and flow cytometry analysis.

Intracellular Indirect Immunostaining for Flow Cytometry Analysis

Cells were collected by trypsinization and fixed with 2% paraformaldehyde at 4°C overnight and washed once with intracellular staining buffer (ICSB, 1% FBS in PBS with 0.01% sodium azide). Cells were then permeabilized by 90% ice-cold methanol and washed once with ICSB. (For staining of BrdU, cells were then treated with DNase for 1 h at 37°C to expose the antigen, and washed once with ICSB.) Subsequently, cells were incubated with primary antibody diluted in ICSB for 1 hr at room temperature, washed once, followed by fluorophore-conjugated secondary antibody incubation for 30 min. cells were then stained with DAPI or TO-PRO, washed once and subjected to flow cytometry analysis.

Chromatin Immunoprecipitation Assay

Wild-type neurospheres were crosslinked with formaldehyde at a final concentration of 1% for 10 min followed by quenching with Glycine. Chromatin extracts were fragmented by sonication and precleared with protein G Dynabeads, and subsequently precipitated with anti-STAT3 antibody (Santa Cruz, C20) or

normal rabbit IgG (Santa Cruz) overnight at 4°C. After washing and elution, crosslink reversal was done by incubating at 65°C for 8 h. The eluted DNA was purified and analyzed by qPCR with primers specific to the predicted STAT3 binding site. qPCR experiment was carried out using SYBR green qPCR kit from KAPA and Applied Biosystems 7500 Real PCR System. Primer sequences for Chip-qPCR could be found in **Supplementary Table S4**. Samples were assayed in duplicate.

Dual-Luciferase Reporter Assay

Promoters of genes of interest were cloned into pGL4.17 vector (Promega) and transfected into Neuro2A cells along with the pRL-TK vector (Promega). Sixteen hours after transfection, cells were treated with DMSO or STAT3 inhibitor STAT3i at 2 μ g/ml. After 48 h, cells were lysed with Passive lysis buffer (Promega) and subjected to luciferase assay in a 96-well format in plate readers according to the manufacturer's protocol. Primer sequences for the generation of reporter vector could be found in **Supplementary Table S5**.

Complex I Activity Assay

Complex I activity was measured using the Complex I activity kit from Cayman Chemistry, according to the manufacturer's protocol. In brief, neurospheres cultured for 4 days were homogenized in Mitochondrial Homogenization Buffer (Cayman) and were mixed with Complex I Activity Assay Buffer, NaN₃, FF-BSA reagent and loaded into the test 96-well plate. A mix containing NADH and Ubiquinone was added into each well. The plate was immediately placed in a plate reader to measure absorbance at the wavelength of 340 nm every 30 s for 15 min at 25°C. The decrease rate of absorbance, which reflects the decrease in NADH concentration, was determined to be the activity of Complex I. After the experiment, cells from different groups were lysed to analysis the protein level.

Mitochondrial Membrane Potential and ROS Measurement

Neurospheres cultured for 4 days were dissociated into single cells with Accutase (Thermo Fisher Scientific) and was resuspended in SFM containing 5 μ M Mitotracker CMXRed (Thermo Fisher Scientific), or 5 μ M Mitosox Red (Thermo Fisher Scientific) or 5 μ M CM-DCFDA (Thermo Fisher Scientific), respectively, and incubated in 37°C CO₂ incubator for 30 min. Cells were then stained with 1 μ g/ml Topro-3 as a live-dead indicator, followed by flow cytometry analysis. For microscopic imaging, neural progenitors cultured on poly-D-lysine and laminin coated coverslips were stained with Mitosox Red or DCFDA for 30 min, washed once with PBS, fixed with 4% PFA and mounted with Prolong Gold DAPI mounting media before subjecting to imaging.

Seahorse OCR/ECAR Assay

Neurospheres cultured for 4 days were dissociated into single cells and seeded into the Seahorse 24-well test plate coated with the cell-tak reagent at the density of 1×10^5 cells/well. Cells were then centrifuged at 200 g for 1 min to achieve cell

attachment. After equilibrated at 37°C incubator (no CO₂) for 1 h, oxygen consumption rate (OCR) and extracellular acidification rate (ECAR) of cells were analyzed using Seahorse XFe24 machine. The assay medium was SFM supplemented with sodium pyruvate. For Mito-stress assay, OCR and ECAR of cells were measured three times at basal state and after addition of 1 μ M oligomycin, 2 μ M of FCCP, and a mix of 1 μ M Rotenone and 1 μ M Antimycin A, respectively. After the experiment, cells from different groups were lysed and subjected to western blot experiment to confirm the same seeding density between groups. For glycolysis assay, the ECAR of cells were measured 3 times at basal level and after the addition of 20 mM of Glucose, 1 μ M oligomycin, and 50 mM 2DG, respectively.

ADP/ATP Ratio Assay

ADP/ATP ratio assay was conducted using the ADP/ATP ratio assay kit from Sigma Aldrich (MAK135) according to the manufacturer's protocol. Briefly, $\sim 10^4$ cells were seeded in each well of the 96-well plate. After culture for 1 day, the medium was removed and the ATP reagent containing substrate, co-substrate, and ATP enzymes was added to the plate, and luciferase activity was measured (RLU_A) after 1 min incubation. The luciferase activity was measured again (RLU_B) after another 10 min incubation to get the basal luminescence before adding the ADP enzymes. Therefore, the ADP enzymes were added to the plate, and the luciferase activity was measured (RLU_C) after 1 min incubation. The ADP/ATP ratio were determined as (RLU_C-RLU_B)/RLU_A.

Mitochondrial DNA Copy Number Measurement

Neurospheres cultured for 4 days were lysed with RIPA buffer. The lysate was then subjected to qPCR experiment using primer pairs targeted to mitochondrial DNA or genomic DNA. The experiment was carried out with SYBR Green qPCR kit from KAPA and Applied Biosystems 7500 Real PCR System. The mitochondrial DNA copy number was normalized to the genomic DNA copy number. Samples were assayed in duplicate.

Western Blot

Cells were lysed with RIPA buffer (50 mM Tris-HCl pH7.4, 150 mM NaCl, 1% NP-40, 0.25% Na-deoxycholate and 1 mM EDTA), centrifuged at 20000 g for 10 min and supernatant were collected. Protein concentrations were measured and 20 μ g of total protein were loaded into each well in SDS-PAGE. Samples were then transferred to PVDF membrane (Thermo) and immunoblotted with anti-NDUFS3 (Invitrogen), anti-NDUFA13 (Invitrogen), anti-SDHA (CST), anti-beta-actin (Santa Cruz), anti-GAPDH (Sigma), anti-STAT3 (CST), anti-pAMPK (CST), AMPK (CST), anti-pS-AKT (CST), anti-AKT (CST), anti-CASP3 (CST), anti-p-p38 (CST), anti-p38 (CST), anti-mTOR (CST), anti-pS-STAT3 (CST), anti-pY-STAT3 (CST), anti-LC3 (CST), anti-GFAP (SCBT), anti-ALDH1L1 (Abcam) followed by HRP-conjugated secondary antibody (Thermo) incubation and the SuperSignal West Femto Maximum Sensitivity Substrate (Thermo) was used to detect signal.

Immunofluorescence

Tissues were isolated and fixed in 4% paraformaldehyde (PFA) in PBS overnight at 4°C. Fixed tissues were dehydrated by incubation in a series ethanol gradient and Xylene, then embedded in paraffin wax for sectioning at the thickness of 5 μ m. Slices obtained were rehydrated and boiled in Sodium Citrate solution at 120°C for 20 min for antigen retrieval. Slices were washed in PBS once before the blocking step. Cells cultured on the coverslip were fixed in 4% paraformaldehyde (PFA) in PBS overnight at 4°C. Subsequently, coverslips were washed in PBS three times before blocking.

The brain slices or coverslips were incubated for 1 h in blocking solution containing 5% bovine serum albumin (BSA, Sigma) and 0.1% Triton X-100 (Sigma) in PBS. They were then incubated with primary antibody overnight at 4°C, followed by washing three times in PBS before incubation with fluorophore-conjugated secondary antibodies. After secondary antibody incubation, they were stained with DAPI, washed three times and mounted with Prolong Gold Mounting Medium (Thermo) for imaging. Images were captured using a Zeiss Axio Imager M2 fluorescence microscope. Image analysis was done using ImageJ. The mitochondria morphology was analyzed by ImageJ plugin MiNA (Valente et al., 2017).

Transfection

Overexpression or knockdown of STAT3 and the OXPHOS genes in cell lines were done by transfection using Lipofectamine 3000 (Thermo Fisher Scientific) according to the manufacturer's protocol. Briefly, 2.0 μ g of plasmid DNA were used for each well of a 6-well plate. DNA was mixed with 7.5 μ l of P3000 reagent and 5 μ l Lipofectamine 3000 in OptiMEM (Thermo Fisher Scientific), incubated for 5 min and added to the cells. The backbone of the overexpression vectors was pMX vector from Addgene, while the shRNA vectors were constructed from pLVX-shRNA2 (Clontech). The shRNA sequences were obtained from Sigma Aldrich database. The primers for shRNA vectors generation were listed in **Supplementary Table S6**.

Lentivirus Preparation and Neural Progenitor Infection

The lentivirus was produced using the 3rd generation system. The virus envelope plasmid and the packaging plasmids, as well as the pLVX-shRNA2 plasmids, were transfected into 293T cell lines. Six hours after transfection, media were changed to the fresh ones. The lentivirus containing media were collected after 24 h and then subjected to ultracentrifugation at 100,000 g for 1 h to concentrate the lentivirus particle. The lentivirus particles were then resuspended in SFM and stored at 4°C before used. To infect the neural progenitors, the primary neural progenitors were dissociated from neurospheres via multiple pipetting. Cells were then seeded in the lentivirus-containing SFM at 2×10^5 cells/ml.

Drug Treatment

For the STA-21 treatment of neural progenitors, STA-21 was added to cell culture at 2 μ g/ml. After 48 h, neural

progenitors were collected for RNA extraction or subjected to cell differentiation.

For the investigation of the effect of ROS on proliferation, neural progenitors were treated with 10 μ M H₂O₂, or 20 mM NAC or DMSO control. To investigate the effect of AMPK and autophagy pathway, neural progenitors were treated with 4 mM 2-deoxyglucose (2DG), 1 μ M Metformin, 2 mM 3 mA, or 2.5 μ M Compound C.

Statistics

Statistical significance was determined by Student's *t*-test or Mann–Whitney test using GraphPad Prism 6.01. The *p*-value < 0.05 was considered significant. Unless otherwise specified, data were presented as mean and the standard deviation (mean \pm SD).

RESULTS

Stat3 Deletion in Neural Progenitors Resulted in Faster Proliferation and Reduced Neurogenesis

In this study, we investigated the function of STAT3 in neural progenitors using the Nestin-cre; Stat3-flox mice, which achieves *Stat3* conditional KO in neural progenitors by E14 (Tronche et al., 1999; Moh et al., 2007) (Supplementary Figure S1). To determine the effect of STAT3 on neural progenitor proliferation, we carried out the primary neurosphere growth assay on neural progenitors isolated from E15.5 embryos. Intriguingly, we found that deletion of *Stat3* in neural progenitor cells leads to an increase of neurosphere size compared to the control (CTL), indicating a faster cell growth (Figure 1A). In addition, the CFSE proliferation assay further confirmed an accelerated mitosis pace in *Stat3* cKO neural progenitors (Figure 1B) compare to control neural progenitors, suggesting a potential role of STAT3 as a negative regulator of neural progenitor proliferation. Consistently, we found that the developing cortex of *Stat3* cKO contains higher numbers of Sox2+ and Ki-67+ cells compared to the CTL, indicating that *Stat3* deletion promotes self-renewal and proliferation *in vivo* (Figures 1E,I,J).

To examine how *Stat3* deletion affects the differentiation potential of neural progenitors, we quantified the MAP2⁺ neurons and the GFAP⁺ astrocytes in the differentiated CTL and *Stat3* cKO neural progenitors. We found that conditional deletion of *Stat3* resulted in fewer MAP2⁺ neuron generation and abolished astrocyte differentiation associated GFAP expression (Figures 1C,D). Immunostaining experiment of postnatal day 1 brain slices also demonstrated that *Stat3* cKO leads to decreased neuronal differentiation, as was shown by the decreased NeuN+ cell percentage (Figures 1G,K).

To examine if astrogenesis is indeed inhibited in *Stat3* cKO, we analyzed the expression of the pan-astrocyte marker ALDH1L1, along with GFAP, in differentiated neural progenitors. Interestingly, ALDH1L1 expression was not affected by *Stat3* cKO, while that of GFAP was

abolished (Figure 1E). Similarly, we found that *Stat3* cKO generated a higher percentage of ALDH1L1+ cells compared to the CTL (Figures 1H,L). This suggested that STAT3 is not necessary for astrogenesis but negatively regulates it instead.

Expression Profile Analysis of Stat3 cKO in Neural Progenitor Cells

To gain insight into the downstream pathway of STAT3 in neural progenitors, we performed RNA-Seq analysis on the CTL and *Stat3* cKO neural progenitors isolated from E11 or E14 embryos. For the expression analysis, the RNA-seq data were processed using the Tophat-Cufflinks workflow (Trapnell et al., 2012), then clustered according to their expression level differential in the CTL and *Stat3* cKO populations at the E11 and E14 stages. To filter for potential direct target genes of STAT3, the genes that were differentially expressed were cross-referenced with the DECODE database to identify those with the potential STAT3 binding sites (Figures 2A,B). Genes that were uniquely upregulated in control cells from E11 to E14 compare to that of *Stat3* cKO cells are potentially STAT3 target genes, which were further analyzed using the gene-set enrichment tool, DAVID, for gene annotation and pathway enrichment analysis (Huang da et al., 2009a,b) (Figure 2C).

Functional annotation of the potential STAT3 target genes by cellular compartment (GO_CC) localized a significant set of enriched genes to the mitochondria. Consistent with this finding, annotation with Kyoto Encyclopedia of Genes and Genomes (KEGG) pathway revealed that the putative STAT3 target genes are mainly enriched in the Oxidative phosphorylation (OXPHOS) pathway, and to a lesser extent in other pathways such as purine metabolism, pyrimidine metabolism, and one carbon pool by folate. These genes were also enriched in pathways associated with neurodegenerative diseases such as Huntington's disease, Parkinson's disease and Alzheimer's disease (Figure 2C).

Given our findings that STAT3 is required for the differentiation of neurons and astrocytes, we next examined the expression of marker genes of different cell types, such as radial glia, intermediate progenitor cells (IPCs), neurons and astrocytes. We found that compared to the CTL, *Stat3* cKO neural progenitors showed increased expression of radial glia markers such as *Sox2*, *Pax6*, and *Sfrp2*, and decreased expression of most IPC and neuronal markers (Supplementary Figures S2A–C). The majority of glial markers such as *Aqp4*, *Aldh1l1*, and *Mfge8* were upregulated in *Stat3* cKO progenitors, while *Gfap* expression was suppressed (Supplementary Figure S2D). These results support our *in vitro* findings that *Stat3* loss-of-function led to decreased neuron differentiation.

Interestingly, *Stat3* cKO also resulted in the increased expression of upper layer (layer II–III) neuron markers such as *Cux1*, *Cux2*, but decreased expression of deeper layer (layer IV–VII) markers such as *Ctip2* and *Tbr1*. This result is consistent with previous reports by Hong et al. that *Stat3* cKO resulted in a larger number of upper layer neuron generation, suggesting a possibility that STAT3 might function to regulate layer

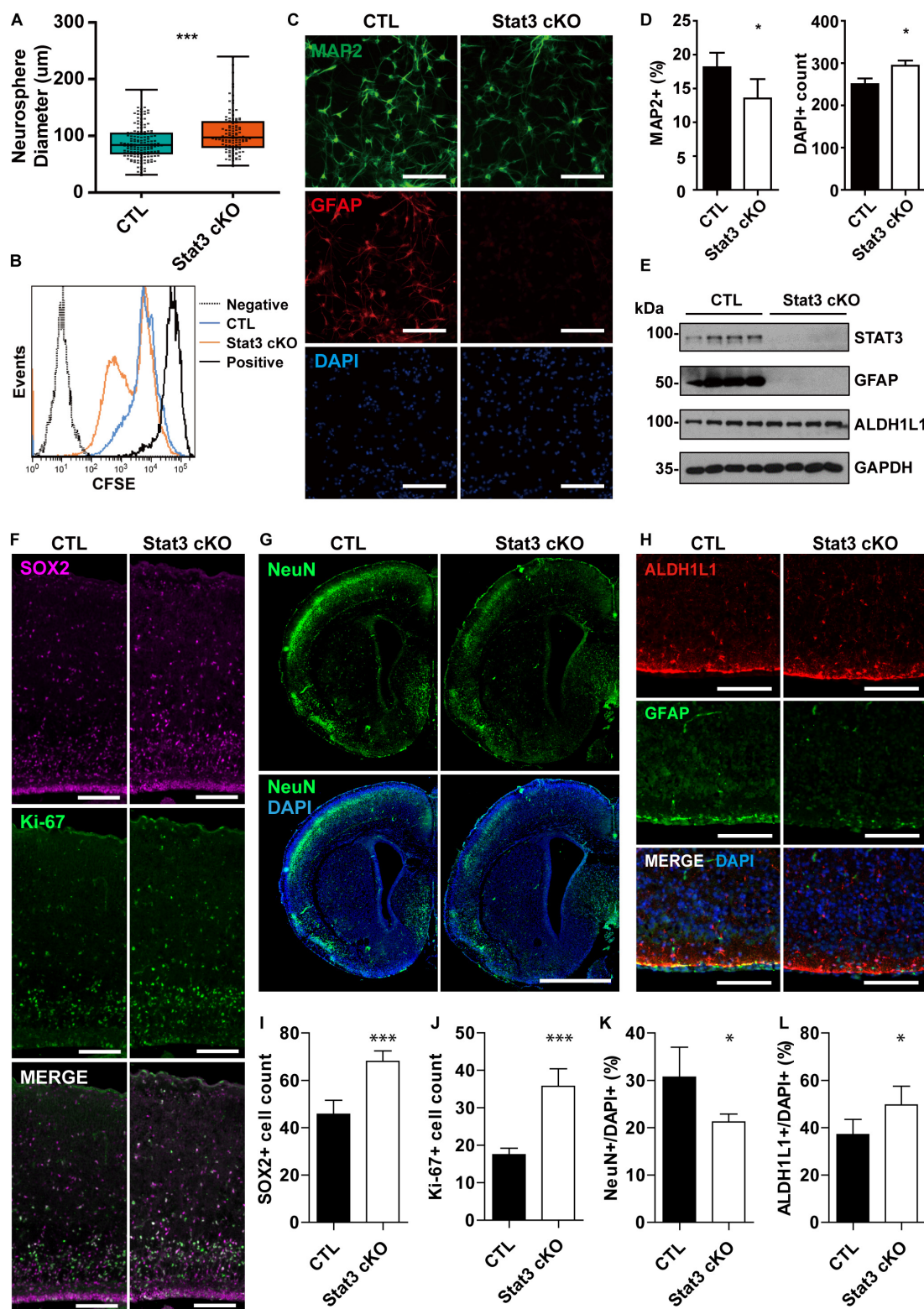


FIGURE 1 | *Stat3* cKO in neural progenitors leads to increased proliferation rate and decreased neuronal differentiation. **(A)** Neurosphere assay showed that *Stat3* cKO neural progenitor has a higher proliferation rate. Box plot represents the median, maximum and minimum value as well as the interquartile range. Mann-Whitney test was used to determine the statistical significance. **(B)** CFSE showed that *Stat3* cKO cells divided faster than control cells (C; F/+). **(C,D)** Immunofluorescence staining of MAP2 and GFAP in differentiated control and *Stat3* cKO neural progenitors. Statistical significance was determined using the student t-test. Error bars

(Continued)

FIGURE 1 | Continued

represent mean \pm standard deviations. **(E)** Western blot of differentiated neural progenitor samples showed that *Stat3* cKO led to the loss of GFAP expression, but the ALDH1L1 expression was not altered. **(F)** Immunostaining of radial glia marker SOX2 and proliferation marker Ki67 in E17 mouse brain. Scale Bar: 100 μ m. **(G)** Immunostaining of NeuN in P1 mouse brain. Scale bar: 250 μ m. **(H)** Immunostaining of GFAP and ALDH1L1, both astrocyte markers, in the P1 mouse brain. Scale bar: 20 μ m. **(I–L)** Cell counts and percentages obtained from **(F–H)**. The cell numbers were quantified from five images, respectively. Error bars represent mean \pm standard deviations. *** $p < 0.001$, * $p < 0.05$.

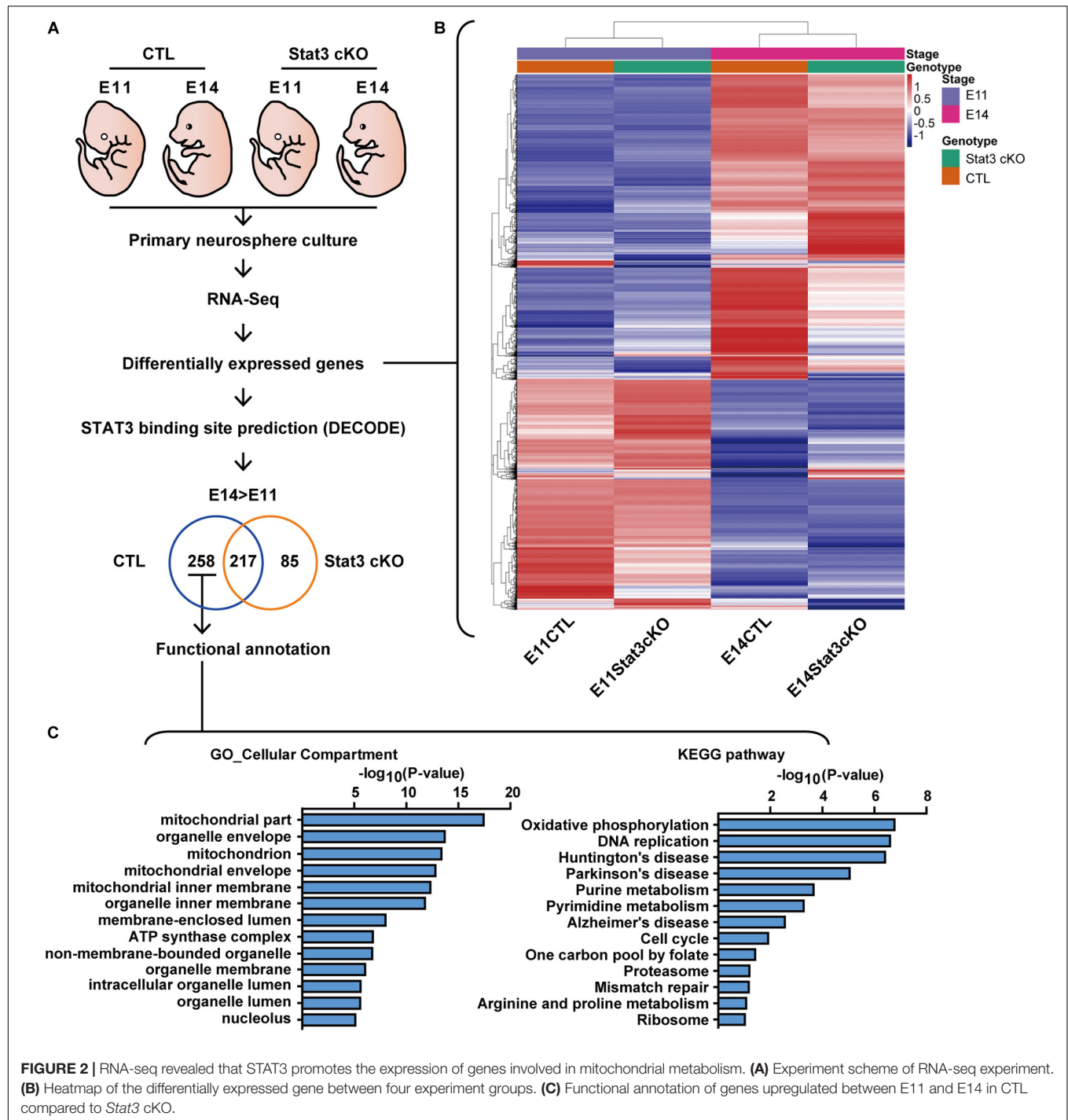


FIGURE 2 | RNA-seq revealed that STAT3 promotes the expression of genes involved in mitochondrial metabolism. **(A)** Experiment scheme of RNA-seq experiment. **(B)** Heatmap of the differentially expressed gene between four experiment groups. **(C)** Functional annotation of genes upregulated between E11 and E14 in CTL compared to *Stat3* cKO.

specification during cortical development (Hong and Song, 2015) (**Supplementary Figure S2E**).

STAT3 Promotes the Expression of Oxidative Phosphorylation (OXPHOS) Genes in Neural Progenitor Cells

RNA-seq analysis revealed a group of putative STAT3 targets that not only involves in the OXPHOS pathways, but is also implicated in neurodegenerative diseases (**Figures 2C, 3A**). Previous studies have demonstrated that OXPHOS genes are highly expressed in the VZ in E14.5 mouse brain (Visel et al., 2004), suggesting the governing of OXPHOS genes expression may be critical during brain development (**Supplementary Figure S3A**).

To validate our RNA-seq results showing differential expression of OXPHOS genes, we performed quantitative reverse-transcription PCR (RT-qPCR) to compare expression of selected genes, including complex I genes (*Ndufa1*, *Ndubf5*, *Ndubf7*, *Ndufc1* and *Ndufs1*), complex III genes (*Cyc1* and *Uqcrh*), as well as complex V genes (*Atp5b*, *Atp5g1*, *Atp5h*, and *Atp5o*), in CTL and *Stat3* cKO neural progenitors at E12 and E14. In agreement with the RNA-seq analysis, we found that the expression of these putative STAT3 target OXPHOS genes was significantly upregulated in E14 CTL neural progenitors, and significantly downregulated in E14 *Stat3* cKO neural progenitors (**Figure 3B**). However, the protein level of OXPHOS genes was not altered in *Stat3* cKO neural progenitors at E14. We speculated that the change in the protein level might become evident in the later stage due to delayed response of protein turnover. Indeed, the OXPHOS protein level was downregulated in *Stat3* cKO neural progenitors at E17 (**Figure 3C**).

To further confirm that STAT3 regulate the OXPHOS gene expression, we examined the expression of OXPHOS genes in neural cells with drug/genetic-modulated STAT3 activity. Expression of these OXPHOS genes was downregulated under treatment of STA-21 in E14 neural progenitors (**Supplementary Figure S3B**). In addition, the deletion of *Stat3* with CRISPR in ESC-derived mouse neural stem cells led to the downregulation of OXPHOS genes, while overexpression of STAT3 in Neuro2A cells upregulated OXPHOS gene expression (**Supplementary Figures S3C,D**). Taken together, these results strongly support that STAT3 is indispensable for the transcription regulation of OXPHOS genes during neurogenesis.

Next, we investigated whether STAT3 directly regulates the expression of the OXPHOS genes. By performing ChIP-qPCR assays using E14 WT neural progenitors, we found that STAT3 bound to the promoter or enhancer loci of a significant proportion of the target OXPHOS genes (**Figure 3D**). In addition, unphosphorylated STAT3 has a higher affinity to some of these loci and promotes gene expression, compared to the tyrosine-phosphorylated STAT3 (**Supplementary Figure S4**). Luciferase reporter assays with selected promoter/enhancer regions in Neuro2A cells further demonstrated that treatment of STAT3 inhibitor Static or mutation of the putative STAT3 binding sites in those regions significantly attenuates the reporter activity (**Figure 3E**). Taken together, these results support the hypothesis

that STAT3 promotes the expression of OXPHOS gene via direct transcriptional regulation.

STAT3 Promotes Mitochondria Respiration in Neural Progenitors

Given that OXPHOS genes are involved in mitochondrial respiration, we next examined whether *Stat3* loss-of-function would alter the oxygen consumption rate (OCR). We found that, at E14, the basal OCR of *Stat3* cKO and CTL neural progenitors remains indistinguishable. However, at E17, the increment of basal OCR, Maximum OCR and Proton Leak in *Stat3* cKO neural progenitors is significantly hindered when compare with that of the CTL cells (**Figures 4A–E**). These results suggest that there is a demand for energy metabolic increases in neural progenitors from E14 to E17, and STAT3 is a critical drive during this process.

As several of the candidate STAT3 target OXPHOS genes are components of complex I, we examined the complex I activity and found that *Stat3* loss-of-function decreased the activity of complex I at E17 (**Figure 4F**). In addition, we found that this impaired complex I activity was associated with a decrease in mitochondrial membrane potential (MMP) (**Figures 4G,H**). To exclude the possibility that the decrease of mitochondrial complex I activity was due to mitochondrial functional alternation, we examined the mitochondrial copy number by qPCR, and found that there were no significant differences between the CTL and *Stat3* cKO cells (**Figure 4I**).

As mitochondrial respiration is crucial for cellular energy balance, we next examined the ADP/ATP ratio and the related signaling pathways in *Stat3* cKO and control neural progenitors. We found that *Stat3* cKO cells had an elevated ADP/ATP ratio (**Figure 4J**), which correlated with increased activation of AMPK, the energy balance sensor (**Figure 4O**). Concomitantly, we found that the phosphorylation of mTOR was decreased in *Stat3* cKO cells. This suggested that the change in mitochondria energy production altered signaling pathways linked to energy and nutrient sensing.

Finally, we found that *Stat3* cKO neural progenitors showed decreased glycolytic flux, which is in line with the observation of the decrease expression of the majority of glycolytic genes (**Supplementary Figures S5A–D**). Accordingly, we noted a decrease in the expression of pentose phosphate pathway genes that are closely linked with glycolysis (**Supplementary Figure S5F**). Conversely, the expression of genes involved in fatty acid beta-oxidation was increased suggesting a possible remodeling of metabolic fluxes in *Stat3* cKO (**Supplementary Figure S5E**).

STAT3 Negatively Regulates Reactive Oxygen Species (ROS) Production in Neural Progenitors

Whereas abnormal OXPHOS complex activity and MMP can affect mitochondrial ROS production (Murphy, 2009), we next sought to investigate whether the deletion of *Stat3* affects ROS production. We found that the deletion of STAT3 promoted the production of mitochondrial superoxide and cellular ROS level (**Figures 4K–N** and **Supplementary Figures S6D,E**).

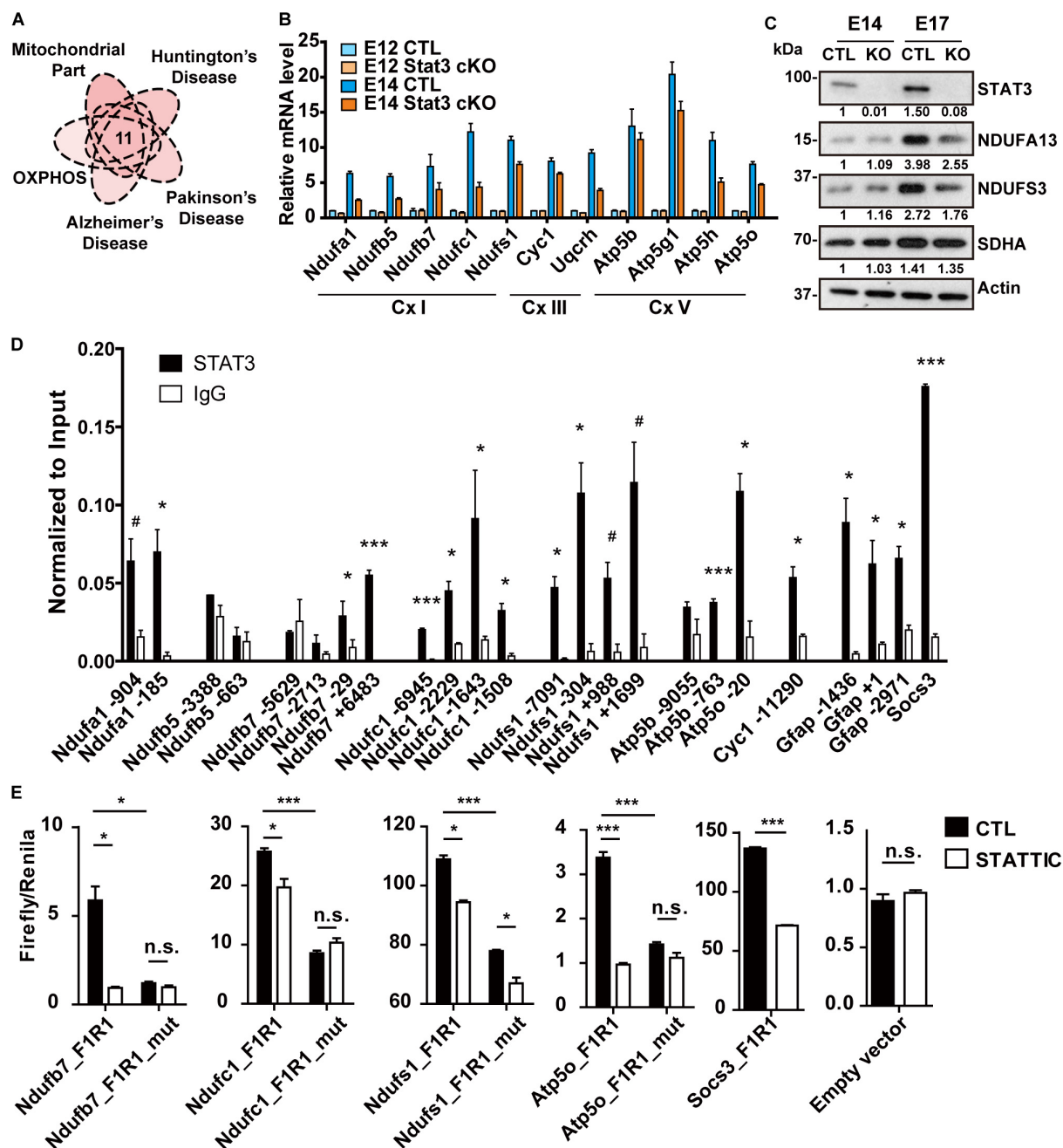
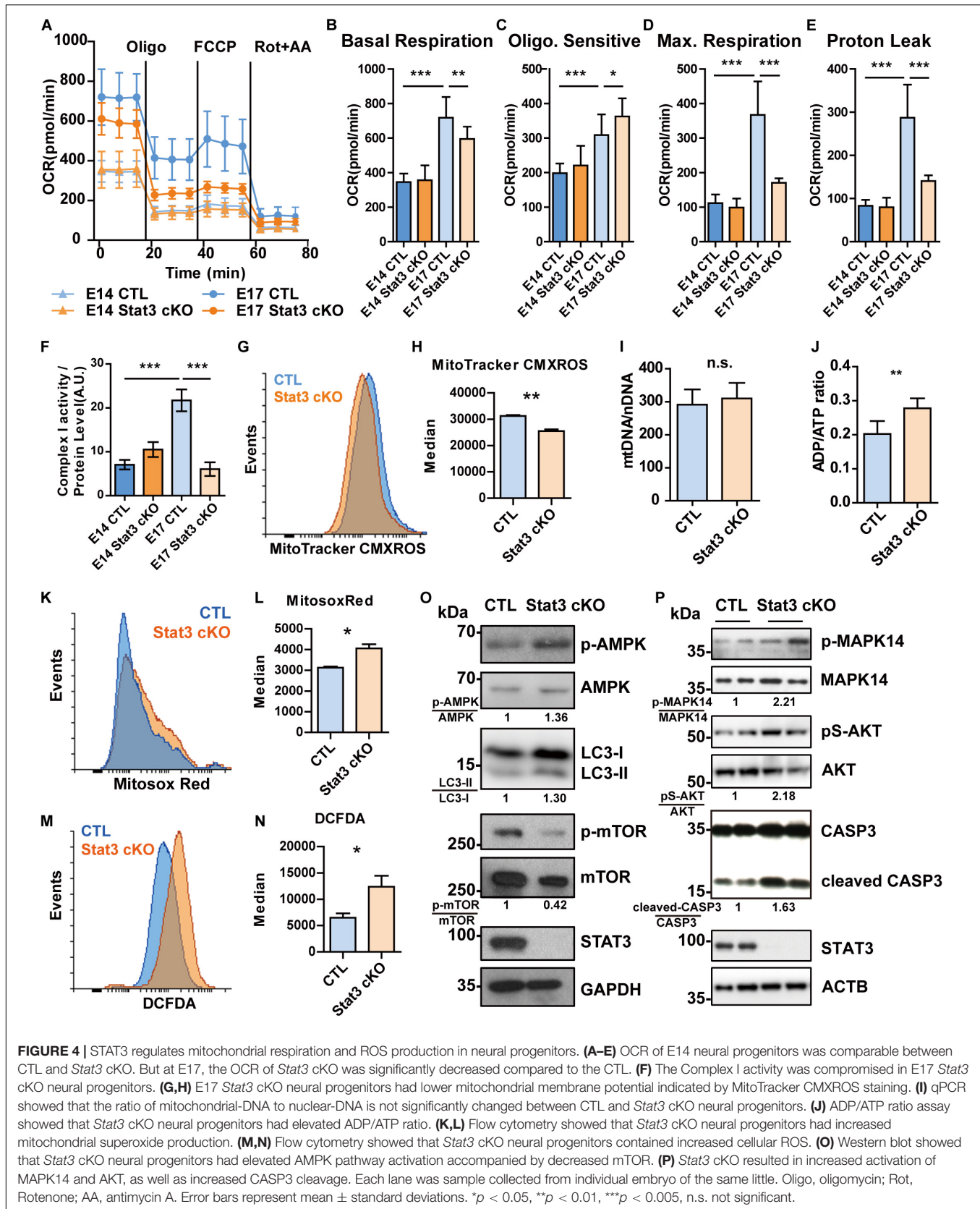


FIGURE 3 | STAT3 promotes the expression of OXPHOS genes in neural progenitors. **(A)** One group of potential STAT3 targets was involved in the mitochondrial oxidative phosphorylation as well as the neurodegenerative diseases. **(B)** RT-qPCR confirmed the expression of these genes was upregulated during neural progenitor development and downregulated in *Stat3* cKO. **(C)** Western blot showed that the expression of complex I proteins was downregulated in *Stat3* cKO neural progenitors isolated at E17. **(D)** ChIP-qPCR showed that STAT3 directed bind to the promoter or enhancer of the OXPHOS genes such as *Ndufa1*, *Ndufb7*, *Ndufc1*, *Ndufs1*, *Atp5b*, *Atp5o*. **(E)** Dual luciferase reporter assay showed that STAT3 binds to the promoter of OXPHOS genes and activate their transcription. Treatment of STAT3IC or mutation of the STAT3 binding site downregulated the reporter activity. *Socs3* promoter was used as the positive control, while the empty reporter vector was used as the negative control. #*p* < 0.08, **p* < 0.05, ***p* < 0.01, ****p* < 0.005, n.s. not significant. Error bars represent mean ± standard deviations.

Interestingly, Mitosox-Red-stained mitochondria were elongated in *Stat3* cKO cells, compared to the CTL cells, suggesting a fusion-fission defect in *Stat3* cKO neural progenitors (Supplementary Figures S6A–C).

As ROS signaling can activate different signaling pathways including PI3K/AKT (Lee et al., 2002; Leslie et al., 2003; Lim and Clement, 2007), we next sought to determine the activation status of key signaling pathways linked to ROS. We found that the AKT



pathway was activated in *Stat3* cKO neural progenitors, as well as the p38 MAPK (MAPK14) pathway (Figure 4P). Similarly, *Stat3* cKO led to a higher level of cleaved Caspase3 (Figure 4P). However, *Stat3* cKO did not result in increased apoptosis in neural progenitors (Supplementary Figure S7).

Knockdown of Putative STAT3-Target OXPHOS Genes Mimics the Phenotypes of *Stat3* cKO

We previously showed that *Stat3* loss-of-function can downregulate target OXPHOS genes and this correlated with a decrease in mitochondrial function. To determine whether the defects in mitochondrial respiration in *STAT3* cKO neural progenitors are mediated primarily by the downregulation of OXPHOS gene expression, we attempted to knockdown several of the target genes (including *Ndufc1*, *Ndufb5*, *Ndufb7*, *Ndufs1*, and *Atp5b*) in E15 neural progenitors using a lentiviral shRNA system. We found that knockdown of the selected target genes led to decreased mitochondrial OCR and increased mitochondrial ROS production, suggesting that downregulation of the target OXPHOS genes primarily mediates the mitochondrial metabolic change observed in *Stat3* loss-of-function (Figures 5A–C). Consistently, knockdown of the OXPHOS genes led to the activation of the AMPK pathway and increased autophagy (Figure 5D).

The results above demonstrate that *STAT3* is necessary to promote nuclear-encoded OXPHOS gene expression and thereby mitochondrial respiration in neural progenitors. To examine another possibility of whether *STAT3* regulates the OXPHOS genes expression via mitochondria metabolism, we used 2DG or H_2O_2 intervention to mimic the metabolic stress in *Stat3* cKO cells. We found that the OXPHOS genes expression was increased as a result of the drug treatment, in contrast to that in *Stat3* cKO (Supplementary Figure S9). This suggested that in *Stat3* cKO neural progenitors, downregulation of the OXPHOS genes expression leads to the disruption of mitochondrial metabolism, not *vice versa*.

We next sought to determine whether the downregulation of OXPHOS genes mediates the proliferation and differentiation phenotype of *Stat3* cKO neural progenitors. We found that knockdown of these OXPHOS genes led to increased cell proliferation, suggesting that the proliferative phenotype of *Stat3* cKO neural progenitors could be directly mediated by decreased expression of OXPHOS genes (Figures 5E,F). In addition, we found that knockdown of the OXPHOS genes in neural progenitor cells led to significantly lower neuronal differentiation, except that of *Atp5b* (Figures 5G,H). However, knockdown of the selected OXPHOS genes other than *Ndufs1* did not alter the astrogenesis of neural progenitors (Figures 5G,I).

In summary, knockdown of OXPHOS genes was able to reproduce several phenotypes of *Stat3* cKO neural progenitor cells, including reduced OCR, increased ROS production, and activation of the AMPK pathway. In addition, the knockdown of OXPHOS genes resulted in an increased proliferation rate and reduced neurogenesis, similar to the *Stat3* cKO neural progenitors. These findings support the hypothesis that the

regulation of OXPHOS genes mediates the phenotypic changes observed in *Stat3* loss-of-function neural progenitors.

Activation of AMPK and ROS Pathways Promotes Neural Progenitor Proliferation

As mitochondria dysfunction in *Stat3* cKO activated the AMPK and ROS pathway, we wondered if these pathways mediated the hyperproliferative phenotype of *Stat3* cKO neural progenitors.

To investigate the role of AMPK in neural progenitor proliferation, we treated E15 neural progenitors with AMPK agonists 2DG and Metformin as well as AMPK suppressors Compound C and inhibitor of downstream autophagy 3 mA. Treatment of 2-deoxyglucose (2DG) and Metformin in CTL neural progenitors induced a starvation state similar to that of *Stat3* cKO, as was dictated by the ADP/ATP ratio (Figure 6A). 2DG and Metformin treatment resulted in increased neurosphere size and BrdU incorporation in CTL neural progenitor, while treatment of Compound C and 3mA decreased the neurosphere size and BrdU incorporation (Figures 6B,C), suggesting that AMPK pathway activation is both sufficient and necessary for neural progenitor proliferation. To investigate whether ROS signaling regulates neural progenitor proliferation, H_2O_2 and ROS scavenger *N*-acetylcysteine (NAC) was added to the CTL neural progenitors. Treatment of H_2O_2 led to increased BrdU incorporation and neurosphere growth, while NAC treatment decreased them, suggesting that ROS signaling is also sufficient and necessary for neural progenitor proliferation (Figure 6D). Modulation of AMPK pathway and ROS downstream pathway AKT by drug treatment was verified by western blot analysis (Figures 6E,F).

DISCUSSION

STAT3 has been shown to play an important role in neural progenitor development, but its function and downstream pathways are not fully understood. Our study discovers a new role of *STAT3* and sheds light on the downstream regulatory network. We found that *STAT3* is necessary for controlling the proliferation rate and promoting neurogenesis via a mitochondria-dependent pathway.

Previous studies found activation of *STAT3* by cytokines promotes neural progenitor proliferation and negatively regulates neurogenesis (Hong and Song, 2015). However, the effect of cytokines could be independent of the JAK-*STAT3* pathway. For instance, CNTF treatment induced neural progenitor proliferation and suppressed neurogenesis in both CTL and *Stat3* cKO neural progenitors (data not shown). Our study showed that loss of *STAT3* also results in increased proliferation and reduced neurogenesis. This is consistent with previous report that *Stat3* cKO astrocytes resulted in increased proliferation (de la Iglesia et al., 2008).

Additionally, we found that *STAT3* is not necessary for astrocytogenesis. Previous studies showed that *STAT3* is necessary for astrocyte marker GFAP expression (Hong and Song, 2014; Kanski et al., 2014). Several *STAT3* binding sites were found in *Gfap* promoter (Bonni et al., 1997;

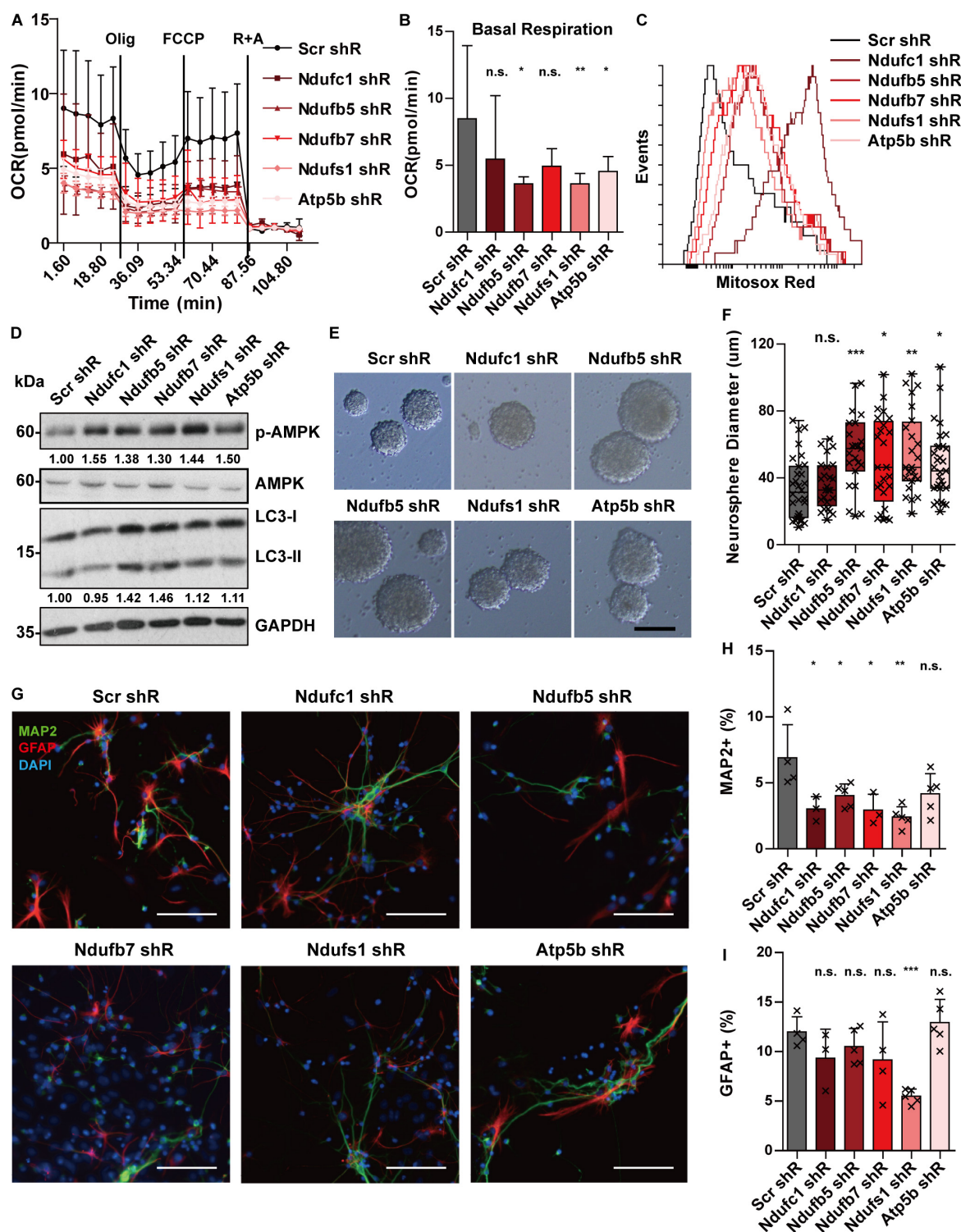
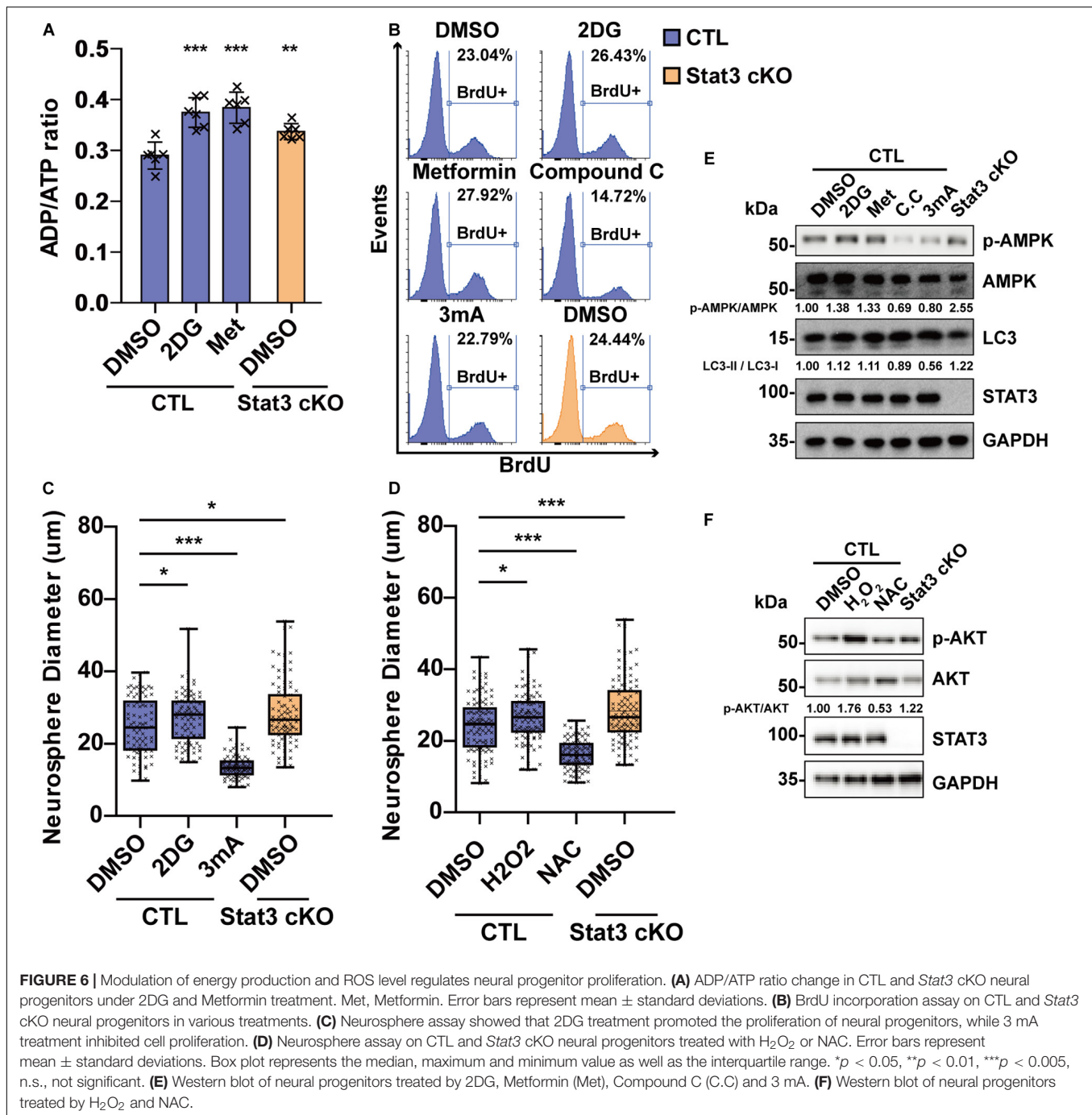


FIGURE 5 | Knockdown of OXPHOS genes mimics the phenotypes of Stat3 cKO. **(A,B)** Knockdown of OXPHOS genes downregulated OCR of neural progenitors. Error bars represent mean ± standard deviations. * $p < 0.05$, ** $p < 0.01$, *** $p < 0.005$, n.s. not significant. **(C)** Knockdown of OXPHOS genes promoted mitochondria superoxide production. **(D)** Knockdown of OXPHOS genes activated the AMPK pathway and the autophagy marker. **(E–H)** Knockdown of OXPHOS genes (except Ndufc1) led to a significantly higher proliferation rate of neural progenitors. Scale bar: 50 μm. Box plot represents the median, maximum and minimum value as well as the interquartile range. Mann–Whitney U test was used to determine the statistical significance of the neurosphere size difference. * $p < 0.05$, ** $p < 0.01$, *** $p < 0.005$, n.s. not significant. **(G–I)** Knockdown of OXPHOS genes resulted in decreased neurons and astrocytes generation. Error bars represent mean ± S.E.M. Knockdown efficiency was validated by RT-qPCR (**Supplementary Figure S8**).



Nakashima et al., 1999), and their interaction with STAT3 is critical for *Gfap* expression. However, GFAP is merely a marker of a subset of astrocytes (Zeisel et al., 2015). Lack of GFAP+ cells in *Stat3* cKO suggests that it leads to potentially functional tampered astrocytes, but not the reduction of the astrocyte cell number. On the contrary, expression of other astrocyte markers was even increased in *Stat3* cKO, which might due to increased proliferation of astrocyte precursors.

Our RNA-seq data showed that expression of upper layer neuronal marker was increased in *Stat3* cKO neural progenitors,

which was concomitant with the observation in previous study that *Stat3* cKO yielded significantly increased number of upper layer (layer II–III) neurons (Hong and Song, 2015). Upper layer neurons are generated after E14, when *Stat3* cKO neural progenitors start to show defect of mitochondrial respiration and increased proliferation rate (Gao et al., 2014). Therefore, increased upper layer neuron generation might result from the increased proliferation of neural progenitors. In addition, whether mitochondria respiration correlates with different layer neuron specification remains to be studied. Electron microscopic

study suggested that layer II–III neurons contain less volume of mitochondria compared to layer IV (Santuy et al., 2018), implying that neurons in different cortical layers might have different mitochondrial metabolism requirement.

In the canonical JAK-STAT pathway, STAT3 is tyrosine phosphorylated, undergoes nucleus import and activates gene expression (Fu et al., 1990, 1992; Schindler et al., 1992; Darnell et al., 1994; Levy and Darnell, 2002). However, STAT3 without tyrosine-phosphorylation (U-STAT3) could also promote gene expression. It has been reported that U-STAT3 could be imported into nucleus by Importin (Liu et al., 2005; Cimica et al., 2011). In addition, U-STAT3 could accumulate in the nucleus after prolonged IL6 treatment (Yang et al., 2005). U-STAT3 could interact with DNA and promote gene expression by forming homodimer, or in a complex with RELA (Yang et al., 2007; Timofeeva et al., 2012; Nkansah et al., 2013; Okada et al., 2018). Similarly, our data showed that overexpression of STAT3-CYE, a dominant negative mutant of STAT3 that mimic U-STAT3, could bind to the regulatory element of *Ndufc1* and promote its expression, while the overexpression of STAT3-CA, a constitutive active form of STAT3, could not. However, it remains unclear if other post-translational modifications of STAT3 regulate these genes expression. Furthermore, it was speculated that U-STAT3 might also function as a chromatin scaffold protein due to the long distance of their adjacent binding sites. Indeed, bisulfite sequencing revealed that the global DNA methylation level was decreased in *Stat3* cKO neural progenitors at E14. STAT3 activation could promote cell proliferation and suppress neurogenesis, while absence of STAT3 also leads to similar outcome, suggesting that the STAT3 activation or inactivation might be one of the molecular switch of neural progenitor fate.

It has been shown that STAT3 could be translocated into mitochondria, and that mitochondrial STAT3 promotes respiration by binding to protein complexes such as Complex I, or by regulating mitochondrial transcription (Wegrzyn et al., 2009; Macias et al., 2014; Carbognin et al., 2016; Xu et al., 2016). However, we have previously reported that STAT3 does not locate within mitochondria, but in mitochondria-associated ER membrane instead (Su et al., 2019), which is neglected by prior studies. Even if STAT3 is present in mitochondria, it is unlikely to directly regulate mitochondrial respiration, due to the stoichiometric difference between STAT3 and the OXPHOS complexes or the mitochondrial genome (the molecular ratio of Complex I and STAT3 is $\sim 10^5$ by estimation; and that of the mitochondrial genome and STAT3 is $\sim 10^2$) (Bogenhagen and Clayton, 1974; Shmookler Reis and Goldstein, 1983; Phillips et al., 2010). Thus, STAT3 might regulate mitochondrial respiration via other pathways. Our study showed STAT3 can promote mitochondrial respiration and limit ROS production by regulating the expression of nuclear-encoded OXPHOS genes during neural progenitor development. Similarly, it was shown that STAT3 regulates citrate synthase expression so as to promote mitochondrial metabolism in lymphocytes (MacPherson et al., 2017). Taken together, our results suggest a STAT3-regulated nuclear-transcription-dependent pathway that modulates mitochondrial metabolism.

Mitochondrial metabolism is closely associated with neural progenitor self-renewal and differentiation. Our data showed downregulation of OXPHOS genes in *Stat3* cKO leads to a disruption of mitochondrial metabolism, which promotes the proliferation of neural progenitors while negatively regulates neurogenesis, consistent with a previous study (Bartasaghi et al., 2015). In addition, mitochondrial metabolism could regulate neural progenitor proliferation and differentiation via activation of AMPK signaling or ROS-AKT signaling (Dasgupta and Milbrandt, 2009; Le Belle et al., 2011; Williams et al., 2011). Consistently, we found overactivation of both AMPK and AKT pathways in *Stat3* cKO neural progenitors. Though both are necessary for promoting neural progenitor proliferation, the AMPK and AKT signaling has an antagonistic effect on mTOR activation and the downstream response. (Gwinn et al., 2008; Zhao et al., 2017). The downregulated mTOR pathway in *Stat3* cKO neural progenitors we show here suggests the negative regulation by AMPK pathway might play a dominant role which is consistent with the proliferation phenotype, given that activation of mTOR complex 1 pathway negatively regulates neural progenitor self-renewal and promotes differentiation (Magri et al., 2011; Hartman et al., 2013). However, further study is required to understand how these metabolic-related pathways converge onto the neural progenitor cell fate.

In summary, we discovered a STAT3-mitochondria metabolism axis that regulates neural progenitor proliferation and differentiation.

DATA AVAILABILITY STATEMENT

The raw data generated for this study can be found in the GEO, accession number GSE148564.

ETHICS STATEMENT

The animal study was reviewed and approved by NUS Institutional Animal Care and Use Committee.

AUTHOR CONTRIBUTIONS

YS, KB, CY, and YZ conceived and designed the project. YS performed most of the experiments and analyzed the data. WZ established the mouse model. YZ and JZ performed the RNA-seq experiment. CP and TM analyzed the RNA-seq data. ZM and JX provided technical assistance. YS wrote the manuscript. WZ, KB, CY, and YZ revised the manuscript.

FUNDING

This work was supported by grants from the Singapore National Medical Research Council (R-713-000-181-511), the Ministry of Education (R-713-000-169-112), the National Nature Science Foundation of China (NSFC 81971309), Guangdong Basic

and Applied Basic Research Foundation (2019A1515011333), and Sun Yat-sen University Key Training Program for Youth Teachers (F7201931620002).

ACKNOWLEDGMENTS

We acknowledge Prof. Patrick Tan for his assistance in the RNA-seq experiments. Acknowledgments also go to Prof. Heng

Phon TOO, Prof Gavin Dawe, and Prof Marie Clement for their wonderful suggestions.

SUPPLEMENTARY MATERIAL

The Supplementary Material for this article can be found online at: <https://www.frontiersin.org/articles/10.3389/fcell.2020.00362/full#supplementary-material>

REFERENCES

- Bartessaghi, S., Graziano, V., Galavotti, S., Henriquez, N. V., Betts, J., Saxena, J., et al. (2015). Inhibition of oxidative metabolism leads to p53 genetic inactivation and transformation in neural stem cells. *Proc. Natl. Acad. Sci. U.S.A.* 112, 1059–1064.
- Bayer, S. A., and Altman, J. (1991). *Neocortical Development*. New York, NY: Raven Press, 255.
- Bogenhagen, D., and Clayton, D. A. (1974). The number of mitochondrial deoxyribonucleic acid genomes in mouse L and human HeLa cells. Quantitative isolation of mitochondrial deoxyribonucleic acid. *J. Biol. Chem.* 249, 7991–7995.
- Bonni, A., Sun, Y., Nadal-Vicens, M., Bhatt, A., Frank, D. A., Rozovsky, I., et al. (1997). Regulation of gliogenesis in the central nervous system by the JAK-STAT signaling pathway. *Science* 278, 477–483.
- Cao, F., Hata, R., Zhu, P., Nakashiro, K., and Sakanaka, M. (2010). Conditional deletion of Stat3 promotes neurogenesis and inhibits astroglialogenesis in neural stem cells. *Biochem. Biophys. Res. Commun.* 394, 843–847. doi: 10.1016/j.bbrc.2010.03.092
- Carbognin, E., Betto, R. M., Soriano, M. E., Smith, A. G., and Martello, G. (2016). Stat3 promotes mitochondrial transcription and oxidative respiration during maintenance and induction of naive pluripotency. *EMBO J.* 35, 618–634. doi: 10.15252/embj.201592629
- Chen, E., Xu, D., Lan, X., Jia, B., Sun, L., Zheng, J. C., et al. (2013). A novel role of the STAT3 pathway in brain inflammation-induced human neural progenitor cell differentiation. *Curr. Mol. Med.* 13, 1474–1484.
- Cimica, V., Chen, H. C., Iyer, J. K., and Reich, N. C. (2011). Dynamics of the STAT3 transcription factor: nuclear import dependent on Ran and importin-beta1. *PLoS One* 6:e20188. doi: 10.1371/journal.pone.0020188
- Darnell, J. E. Jr., Kerr, I. M., and Stark, G. R. (1994). Jak-STAT pathways and transcriptional activation in response to IFNs and other extracellular signaling proteins. *Science* 264, 1415–1421.
- Dasgupta, B., and Milbrandt, J. (2009). AMP-activated protein kinase phosphorylates retinoblastoma protein to control mammalian brain development. *Dev. Cell* 16, 256–270. doi: 10.1016/j.devcel.2009.01.005
- de la Iglesia, N., Konopka, G., Puram, S. V., Chan, J. A., Bachoo, R. M., You, M. J., et al. (2008). Identification of a PTEN-regulated STAT3 brain tumor suppressor pathway. *Genes Dev.* 22, 449–462. doi: 10.1101/gad.1606508
- Fang, W. Q., Chen, W. W., Jiang, L., Liu, K., Yung, W. H., Fu, A. K. Y., et al. (2014). Overproduction of upper-layer neurons in the neocortex leads to autism-like features in mice. *Cell Rep.* 9, 1635–1643. doi: 10.1016/j.celrep.2014.11.003
- Fu, X. Y., Kessler, D. S., Veals, S. A., Levy, D. E., and Darnell, J. E. Jr. (1990). ISGF3, the transcriptional activator induced by interferon alpha, consists of multiple interacting polypeptide chains. *Proc. Natl. Acad. Sci. U.S.A.* 87, 8555–8559.
- Fu, X. Y., Schindler, C., Improt, T., Aebersold, R., and Darnell, J. E. Jr. (1992). The proteins of ISGF-3, the interferon alpha-induced transcriptional activator, define a gene family involved in signal transduction. *Proc. Natl. Acad. Sci. U.S.A.* 89, 7840–7843.
- Gao, P., Postiglione, M. P., Krieger, T. G., Hernandez, L., Wang, C., Han, Z., et al. (2014). Deterministic progenitor behavior and unitary production of neurons in the neocortex. *Cell* 159, 775–788. doi: 10.1016/j.cell.2014.10.027
- Gu, F., Hata, R., Ma, Y. J., Tanaka, J., Mitsuda, N., Kumon, Y., et al. (2005). Suppression of Stat3 promotes neurogenesis in cultured neural stem cells. *J. Neurosci. Res.* 81, 163–171.
- Guo, Z., Jiang, H., Xu, X., Duan, W., and Mattson, M. P. (2008). Leptin-mediated cell survival signaling in hippocampal neurons mediated by JAK STAT3 and mitochondrial stabilization. *J. Biol. Chem.* 283, 1754–1763.
- Gwinn, D. M., Shackelford, D. B., Egan, D. F., Mihaylova, M. M., Mery, A., Vazquez, D. S., et al. (2008). AMPK phosphorylation of raptor mediates a metabolic checkpoint. *Mol. Cell* 30, 214–226. doi: 10.1016/j.molcel.2008.03.003
- Harno, E., Cottrell, E. C., and White, A. (2013). Metabolic pitfalls of CNS Cre-based technology. *Cell Metab.* 18, 21–28. doi: 10.1016/j.cmet.2013.05.019
- Hartman, N. W., Lin, T. V., Zhang, L., Paquet, G. E., Feliciano, D. M., and Bordey, A. (2013). mTORC1 targets the translational repressor 4E-BP2, but not S6 kinase 1/2, to regulate neural stem cell self-renewal in vivo. *Cell Rep.* 5, 433–444. doi: 10.1016/j.celrep.2013.09.017
- Hong, S., and Song, M. R. (2014). STAT3 but not STAT1 is required for astrocyte differentiation. *PLoS One* 9:e86851. doi: 10.1371/journal.pone.0086851
- Hong, S., and Song, M. R. (2015). Signal transducer and activator of transcription-3 maintains the stemness of radial glia at mid-neurogenesis. *J. Neurosci.* 35, 1011–1023. doi: 10.1523/JNEUROSCI.2119-14.2015
- Huang da, W., Sherman, B. T., and Lempicki, R. A. (2009a). Bioinformatics enrichment tools: paths toward the comprehensive functional analysis of large gene lists. *Nucleic Acids Res.* 37, 1–13. doi: 10.1093/nar/gkn923
- Huang da, W., Sherman, B. T., and Lempicki, R. A. (2009b). Systematic and integrative analysis of large gene lists using DAVID bioinformatics resources. *Nat. Protoc.* 4, 44–57. doi: 10.1038/nprot.2008.211
- Kanski, R., van Strien, M. E., van Tijn, P., and Hol, E. M. (2014). A star is born: new insights into the mechanism of astrogenesis. *Cell. Mol. Life Sci.* 71, 433–447. doi: 10.1007/s00018-013-1435-9
- Kriegstein, A., and Alvarez-Buylla, A. (2009). The glial nature of embryonic and adult neural stem cells. *Annu. Rev. Neurosci.* 32, 149–184. doi: 10.1146/annurev.neuro.051508.135600
- Le Belle, J. E., Orozco, N. M., Paucar, A. A., Saxe, J. P., Mottahedeh, J., Pyle, A. D., et al. (2011). Proliferative neural stem cells have high endogenous ROS levels that regulate self-renewal and neurogenesis in a PI3K/Akt-dependant manner. *Cell Stem Cell* 8, 59–71. doi: 10.1016/j.stem.2010.11.028
- Lee, S. R., Yang, K. S., Kwon, J., Lee, C., Jeong, W., and Rhee, S. G. (2002). Reversible inactivation of the tumor suppressor PTEN by H2O2. *J. Biol. Chem.* 277, 20336–20342.
- Leslie, N. R., Bennett, D., Lindsay, Y. E., Stewart, H., Gray, A., and Downes, C. P. (2003). Redox regulation of PI 3-kinase signalling via inactivation of PTEN. *EMBO J.* 22, 5501–5510.
- Levy, D. E., and Darnell, J. E. Jr. (2002). Stats: transcriptional control and biological impact. *Nat. Rev. Mol. Cell Biol.* 3, 651–662.
- Lim, S., and Clement, M. V. (2007). Phosphorylation of the survival kinase Akt by superoxide is dependent on an ascorbate-reversible oxidation of PTEN. *Free Radical Biol. Med.* 42, 1178–1192.
- Liu, L., McBride, K. M., and Reich, N. C. (2005). STAT3 nuclear import is independent of tyrosine phosphorylation and mediated by importin-alpha3. *Proc. Natl. Acad. Sci. U.S.A.* 102, 8150–8155.
- Luo, X., Ribeiro, M., Bray, E. R., Lee, D. H., Yungher, B. J., Mehta, S. T., et al. (2016). Enhanced transcriptional activity and mitochondrial localization of STAT3 co-induce axon regrowth in the adult central nervous system. *Cell Rep.* 15, 398–410. doi: 10.1016/j.celrep.2016.03.029
- Macias, E., Rao, D., Carbajal, S., Kiguchi, K., and DiGiovanni, J. (2014). Stat3 binds to mtDNA and regulates mitochondrial gene expression in keratinocytes. *J. Invest. Dermatol.* 134, 1971–1980. doi: 10.1038/jid.2014.68

- MacPherson, S., Horkoff, M., Gravel, C., Hoffmann, T., Zuber, J., and Lum, J. J. (2017). STAT3 regulation of citrate synthase is essential during the initiation of lymphocyte cell growth. *Cell Rep.* 19, 910–918. doi: 10.1016/j.celrep.2017.04.012
- Magri, L., Cambiaghi, M., Cominelli, M., Alfaro-Cervello, C., Cursi, M., Pala, M., et al. (2011). Sustained activation of mTOR pathway in embryonic neural stem cells leads to development of tuberous sclerosis complex-associated lesions. *Cell Stem Cell.* 9, 447–462. doi: 10.1016/j.stem.2011.09.008
- Martynoga, B., Drechsel, D., and Guillemot, F. (2012). Molecular control of neurogenesis: a view from the mammalian cerebral cortex. *Cold Spring Harb. Perspect. Biol.* 4:a008359.
- Mochida, G. H. (2009). Genetics and biology of microcephaly and lissencephaly. *Semin. Pediatr. Neurol.* 16, 120–126. doi: 10.1016/j.spen.2009.07.001
- Moh, A., Iwamoto, Y., Chai, G. X., Zhang, S. S., Kano, A., Yang, D. D., et al. (2007). Role of STAT3 in liver regeneration: survival, DNA synthesis, inflammatory reaction and liver mass recovery. *Lab. Invest.* 87, 1018–1028.
- Murphy, M. P. (2009). How mitochondria produce reactive oxygen species. *Biochem. J.* 417, 1–13. doi: 10.1042/BJ20081386
- Nakashima, K., Yanagisawa, M., Arakawa, H., Kimura, N., Hisatsune, T., Kawabata, M., et al. (1999). Synergistic signaling in fetal brain by STAT3-Smad1 complex bridged by p300. *Science* 284, 479–482.
- Nkansah, E., Shah, R., Collie, G. W., Parkinson, G. N., Palmer, J., Rahman, K. M., et al. (2013). Observation of unphosphorylated STAT3 core protein binding to target dsDNA by PEMSA and X-ray crystallography. *FEBS Lett.* 587, 833–839. doi: 10.1016/j.febslet.2013.01.065
- Okada, Y., Watanabe, T., Shoji, T., Taguchi, K., Ogo, N., and Asai, A. (2018). Visualization and quantification of dynamic STAT3 homodimerization in living cells using homoFluoppi. *Sci Rep.* 8:2385. doi: 10.1038/s41598-018-20234-2
- Pacey, L., Stead, S., Gleave, J., Tomczyk, K., and Doering, L. (2006). Neural stem cell culture: neurosphere generation, microscopical analysis and cryopreservation. *Nat. Protoc.* 1, 215–222.
- Phillips, D., Reilley, M. J., Aponte, A. M., Wang, G., Boja, E., Gucek, M., et al. (2010). Stoichiometry of STAT3 and mitochondrial proteins: implications for the regulation of oxidative phosphorylation by protein-protein interactions. *J. Biol. Chem.* 285, 23532–23536. doi: 10.1074/jbc.C110.152652
- Santuy, A., Turegano-Lopez, M., Rodriguez, J. R., Alonso-Nanclares, L., DeFelipe, J., and Merchán-Pérez, A. (2018). A quantitative study on the distribution of mitochondria in the neuropil of the juvenile rat somatosensory cortex. *Cereb. Cortex* 28, 3673–3684. doi: 10.1093/cercor/bhy159
- Sarafian, T. A., Montes, C., Imura, T., Qi, J., Coppola, G., Geschwind, D. H., et al. (2010). Disruption of astrocyte STAT3 signaling decreases mitochondrial function and increases oxidative stress in vitro. *PLoS One* 5:e9532. doi: 10.1371/journal.pone.0009532
- Schindler, C., Shuai, K., Prezioso, V. R., and Darnell, J. E. Jr. (1992). Interferon-dependent tyrosine phosphorylation of a latent cytoplasmic transcription factor. *Science* 257, 809–813.
- Shmookler Reis, R. J., and Goldstein, S. (1983). Mitochondrial DNA in mortal and immortal human cells. Genome number, integrity, and methylation. *J. Biol. Chem.* 258, 9078–9085.
- Su, Y., Huang, X., Huang, Z., Huang, T., Xu, Y., and Yi, C. (2019). STAT3 localizes in mitochondria-associated ER membranes instead of in mitochondria. *Front. Cell Dev. Biol.* 8:274. doi: 10.3389/fcell.2020.00274
- Timofeeva, O. A., Chasovskikh, S., Lonskaya, I., Tarasova, N. I., Khavrutskii, L., Tarasov, S. G., et al. (2012). Mechanisms of unphosphorylated STAT3 transcription factor binding to DNA. *J. Biol. Chem.* 287, 14192–14200. doi: 10.1074/jbc.M111.323899
- Trapnell, C., Roberts, A., Goff, L., Pertea, G., Kim, D., Kelley, D. R., et al. (2012). Differential gene and transcript expression analysis of RNA-seq experiments with TopHat and Cufflinks. *Nat. Protoc.* 7, 562–578. doi: 10.1038/nprot.2012.016
- Tronche, F., Kellendonk, C., Kretz, O., Gass, P., Anlag, K., Orban, P. C., et al. (1999). Disruption of the glucocorticoid receptor gene in the nervous system results in reduced anxiety. *Nat. Genet.* 23, 99–103.
- Valente, A. J., Maddalena, L. A., Robb, E. L., Moradi, F., and Stuart, J. A. (2017). A simple ImageJ macro tool for analyzing mitochondrial network morphology in mammalian cell culture. *Acta Histochem.* 119, 315–326. doi: 10.1016/j.acthis.2017.03.001
- Visel, A., Thaller, C., and Eichele, G. (2004). GenePaint.org: an atlas of gene expression patterns in the mouse embryo. *Nucleic Acids Res.* 32, D552–D556.
- Węgrzyn, J., Potla, R., Chwae, Y. J., Sepuri, N. B., Zhang, Q., Koeck, T., et al. (2009). Function of mitochondrial Stat3 in cellular respiration. *Science* 323, 793–797. doi: 10.1126/science.1164551
- Welte, T., Zhang, S. S., Wang, T., Zhang, Z., Hesslein, D. G., Yin, Z., et al. (2003). STAT3 deletion during hematopoiesis causes Crohn's disease-like pathogenesis and lethality: a critical role of STAT3 in innate immunity. *Proc. Natl. Acad. Sci. U.S.A.* 100, 1879–1884.
- Williams, T., Courchet, J., Viollet, B., Brenman, J. E., and Polleux, F. (2011). AMP-activated protein kinase (AMPK) activity is not required for neuronal development but regulates axogenesis during metabolic stress. *Proc. Natl. Acad. Sci. U.S.A.* 108, 5849–5854.
- Xu, Y. S., Liang, J. J., Wang, Y., Zhao, X. J., Xu, L., Xu, Y. Y., et al. (2016). STAT3 undergoes Acetylation-dependent mitochondrial translocation to regulate pyruvate metabolism. *Sci. Rep.* 6:39517. doi: 10.1038/srep39517
- Yang, J., Chatterjee-Kishore, M., Staugaitis, S. M., Nguyen, H., Schlessinger, K., Levy, D. E., et al. (2005). Novel roles of unphosphorylated STAT3 in oncogenesis and transcriptional regulation. *Cancer Res.* 65, 939–947.
- Yang, J., Liao, X., Agarwal, M. K., Barnes, L., Auron, P. E., and Stark, G. R. (2007). Unphosphorylated STAT3 accumulates in response to IL-6 and activates transcription by binding to NFκB. *Genes Dev.* 21, 1396–1408.
- Yoshimatsu, T., Kawaguchi, D., Oishi, K., Takeda, K., Akira, S., Masuyama, N., et al. (2006). Non-cell-autonomous action of STAT3 in maintenance of neural precursor cells in the mouse neocortex. *Development* 133, 2553–2563.
- Zeisel, A., Munoz-Manchado, A. B., Codeluppi, S., Lönnerberg, P., La Manno, G., Jureus, A., et al. (2015). Brain structure. Cell types in the mouse cortex and hippocampus revealed by single-cell RNA-seq. *Science* 347, 1138–1142.
- Zhao, Y., Hu, X., Liu, Y., Dong, S., Wen, Z., He, W., et al. (2017). ROS signaling under metabolic stress: cross-talk between AMPK and AKT pathway. *Mol. Cancer* 16:79. doi: 10.1186/s12943-017-0648-1

Conflict of Interest: The authors declare that the research was conducted in the absence of any commercial or financial relationships that could be construed as a potential conflict of interest.

Copyright © 2020 Su, Zhang, Patro, Zhao, Mu, Ma, Xu, Ban, Yi and Zhou. This is an open-access article distributed under the terms of the Creative Commons Attribution License (CC BY). The use, distribution or reproduction in other forums is permitted, provided the original author(s) and the copyright owner(s) are credited and that the original publication in this journal is cited, in accordance with accepted academic practice. No use, distribution or reproduction is permitted which does not comply with these terms.



An Engineered Mouse to Identify Proliferating Cells and Their Derivatives

Jihyun Jang^{1†}, Kurt A. Engleka^{2,3†}, Feiyan Liu^{2,3}, Li Li³, Guang Song¹, Jonathan A. Epstein^{2,3} and Deqiang Li^{1*}

¹ Department of Surgery, Center for Vascular and Inflammatory Diseases, University of Maryland School of Medicine, Baltimore, MD, United States, ² Department of Cell and Developmental Biology, Perelman School of Medicine, University of Pennsylvania, Philadelphia, PA, United States, ³ Penn Cardiovascular Institute, Perelman School of Medicine, University of Pennsylvania, Philadelphia, PA, United States

OPEN ACCESS

Edited by:

Alain De Bruin,
Utrecht University, Netherlands

Reviewed by:

Bin Zhou,
Shanghai Institute of Biochemistry
and Cell Biology (CAS), China
Marcos Malumbres,
Spanish National Cancer Research
Center, Spain

*Correspondence:

Deqiang Li
dqli@som.umaryland.edu

[†]These authors have contributed
equally to this work

Specialty section:

This article was submitted to
Cell Growth and Division,
a section of the journal
Frontiers in Cell and Developmental
Biology

Received: 14 February 2020

Accepted: 29 April 2020

Published: 25 May 2020

Citation:

Jang J, Engleka KA, Liu F, Li L,
Song G, Epstein JA and Li D (2020)
An Engineered Mouse to Identify
Proliferating Cells and Their
Derivatives.
Front. Cell Dev. Biol. 8:388.
doi: 10.3389/fcell.2020.00388

Background: Cell proliferation is a fundamental event during development, disease, and regeneration. Effectively tracking and quantifying proliferating cells and their derivatives is critical for addressing many research questions. Cell cycle expression such as for Ki67, proliferating cell nuclear antigen (PCNA), or aurora kinase B (Aurkb), or measurement of 5-bromo-2'-deoxyuridine (BrdU) or ³H-thymidine incorporation have been widely used to assess and quantify cell proliferation. These are powerful tools for detecting actively proliferating cells, but they do not identify cell populations derived from proliferating progenitors over time.

Aims: We developed a new mouse tool for lineage tracing of proliferating cells by targeting the *Aurkb* allele.

Results: In quiescent cells or cells arrested at G1/S, little or no *Aurkb* mRNA is detectable. In cycling cells, *Aurkb* transcripts are detectable at G2 and become undetectable by telophase. These findings suggest that *Aurkb* transcription is restricted to proliferating cells and is tightly coupled to cell proliferation. Accordingly, we generated an *Aurkb*^{ER Cre/+} mouse by targeting a tamoxifen inducible Cre cassette into the start codon of *Aurkb*. We find that the *Aurkb*^{ER Cre/+} mouse faithfully labels proliferating cells in developing embryos and regenerative adult tissues such as intestine but does not label quiescent cells such as post-mitotic neurons.

Conclusion: The *Aurkb*^{ER Cre/+} mouse faithfully labels proliferating cells and their derivatives in developing embryos and regenerative adult tissues. This new mouse tool provides a novel genetic tracing capability for studying tissue proliferation and regeneration.

Keywords: cell proliferation, aurora kinase B, mouse model, lineage tracing, regeneration, development

INTRODUCTION

Cell proliferation is a fundamental biological event in all multicellular organisms (Nasmyth, 2001). Identification or quantification of proliferating cells is essential to understanding organogenesis, morphogenesis, tumorigenesis, and regeneration. Replicating cells can be identified based on expression of cell-cycle markers, such as Ki67, proliferating cell nuclear antigen (PCNA), aurora

kinase B (Aurkb), or the incorporation of thymidine analogs, such as ³H-thymidine, 5-bromo-2'-deoxyuridine (BrdU), or 5-ethynyl-2'-deoxyuridine (EdU) (Mitchison and Salmon, 2001). Incorporation of 5-iodo-2'-deoxyuridine (IdU) has been used to analyze proliferation in human tissue (Pan et al., 2013). These assays are suitable for detecting actively proliferating or label-retaining cells. However, retrospective lineage tracing is often desired when proliferating cells must be tracked for their growth pattern or quantity under certain biological conditions such as tissue morphogenesis or regeneration.

Genetic engineering in the mouse allows lineage tracing mouse models to track the derivatives of proliferating cells. One model is the mosaic analysis with double markers (MADM) mouse model, which labels dividing cells through interchromosomal recombination (Zong et al., 2005), although its application is limited due to low labeling efficiency. More recently, a Ki67^{IRES-CreER/+} mouse was generated and used to track proliferating cells in brain or heart (Basak et al., 2018; Kretzschmar et al., 2018). However, Ki67 is expressed throughout the cell cycle including G1, and some non-proliferative cells such as adult cardiomyocytes can poise at G1 for an extended period of time without cell division (Alvarez et al., 2019).

Aurkb, a key component of the chromosomal passenger complex, localizes to the centromeres to ensure precise chromosome segregation during mitosis and to the midbody to assist cytoplasmic separation during cytokinesis (van der Waal et al., 2012). Knockdown or inhibition of Aurkb *in vitro* inhibits cell proliferation (Yu et al., 2015; Helfrich et al., 2016), while knockout of Aurkb in mice results in mitotic defects in the inner cell mass (Fernandez-Miranda et al., 2011). Increased expression of Aurkb is associated with tumorigenesis and inhibition of Aurkb may be an effective cancer therapeutic target (Tang et al., 2017; Tischer and Gergely, 2019). Aurkb has been widely used to identify mitotic cells using immunofluorescence or immunohistochemical methods with anti-Aurkb antibodies (Vader and Lens, 2008; Liu and Lampson, 2009; van der Waal et al., 2012; Tian et al., 2015; Nakada et al., 2017; Yu et al., 2019).

In order to track cell proliferation retrospectively, we have generated Aurkb^{ER Cre/+} mice by targeting a tamoxifen inducible Cre cassette into the start codon of Aurkb. By characterizing the Aurkb^{ER Cre} allele *in vitro* and *in vivo*, we show that Aurkb^{ER Cre/+} mice faithfully label proliferating cells and their derivatives during development and regeneration.

MATERIALS AND METHODS

Mice

Aurkb^{ER Cre/+} mice were generated by homologous recombination in embryonic stem cells targeting a Cre-Ert2-V2A-tdTomato-Frt-PGK-neo-Frt cassette into the start codon of the Aurkb locus. Thus, the insertion of this cassette will lead to the ablation of endogenous Aurkb expression in the target allele. The PGK-Neo cassette was removed by breeding the initial progeny to mice expressing ubiquitous

FlpE recombinase (Rodriguez et al., 2000). Southern blot confirmed the expected homologous recombination and germ line transmission of the targeted allele. The Aurkb^{ER Cre} allele is detected by PCR using the following primers: Forward: 5'-GTGGGCTCTATGGCTTCTGA-3', Reverse (common): 5'-CAAATTCTTGAGCCCCACAC-3'; product size: 501 bp. The wild-type allele is detected by using the following primers: Forward: 5'-ATGGACCTAGAGCGGGAGAT-3' and Reverse (common); product size: 264 bp. The V2A-tdTomato included in the targeting construct potentially provides a means to fluorescently label Aurkb-expressing cells without disrupting Cre-Ert2 function. However, although we were able to detect tdTomato protein expression by immunofluorescence using antibodies on fixed intestinal crypts (Supplementary Figure 1), the spontaneous tdTomato fluorescence was below levels of detection. B6.129 × 1-Gt (ROSA)^{TM1(EYFP)Cos/+} (abbreviated as R26R^{eYFP}) mice were purchased from The Jackson Laboratory (stock number: 006148). All mice were maintained on a mixed genetic background. All animal protocols were approved by the University of Pennsylvania Institutional Animal Care and Use Committee (IACUC #: 803396) and the University of Maryland Baltimore Institutional Animal Care and Use Committee (IACUC #: 0118005).

Administration of Tamoxifen and 5-Bromo-2'-Deoxyuridine (BrdU) *in vivo*

Tamoxifen (Sigma-Aldrich, St. Louis, MO, United States) (10 mg/ml) was dissolved in corn oil. Tamoxifen [2 or 100 or 150 mg/kg body weight (BW)] was given to Aurkb^{ER Cre/+}; R26R^{eYFP/+} mice by either intraperitoneal injection or gavage. BrdU (Sigma-Aldrich, St. Louis, MO, United States) (10 mg/ml) was dissolved in phosphate-buffered saline (PBS) and intraperitoneally delivered to Aurkb^{ER Cre/+}; R26R^{eYFP/+} mice (100 mg/kg BW).

Histology, Immunofluorescence and RNAscope

All specimens for paraffin sections were fixed in 4% (w/v) paraformaldehyde (PFA) overnight, dehydrated through an ethanol series, paraffin embedded, and sectioned (6–7 μm). Primary antibodies (Supplementary Table 1) were incubated at 4°C overnight and secondary antibodies (Alexa 488, 555, or 647, Life Technologies, Grand Island, NY, United States) were incubated at room temperature for 1 h. The Aurkb RNAscope probe (173–1483 bp of the *Mus musculus* Aurkb mRNA sequence) was designed and provided by Advanced Cell Diagnostics (Hayward, CA, United States). RNAscope *in situ* hybridizations (Ikpa et al., 2016) were performed according to the protocol provided by manufacturer.

Image Analysis and Quantification

ImageJ software was used for quantification of GFP+ and/or BrdU+ cells on histology slides. Samples from 3–6 mice each were counted at any given time point or condition. The reported values represent the mean score.

Live Cell Imaging

Time-lapse phase-contrast and GFP immunofluorescence images of mouse embryo fibroblasts (MEFs) were taken for 22 h after 4-OH tamoxifen induction (final concentration: 1 μ g/ml) by using the IncuCyte live-cell culture system (Essen Bioscience). The images were then analyzed and converted to movie format by using IncuCyte software.

Fluorescence-Activated Cell Sorting (FACS) Analyses

MEFs were isolated and cultured as previously described (Li et al., 2011). MEFs were treated with either control vehicles or designated cell cycle inhibitors, then digested and collected as single cell suspensions. The cell suspension was washed with PBS and then fixed with intracellular fixation buffer (eBiosciences). For intracellular FACS analyses, cells were permeabilized with permeabilization buffer (eBiosciences) and then incubated with GFP antibodies (see **Supplementary Table 1**) for 2 h at room temperature, followed by incubation with secondary antibodies (Alexa fluor, Life Technologies) for 1 h at room temperature. Samples were run and analyzed using a BD FACS Canto II instrument and software (BD Biosciences).

Quantitative Real-Time PCR (qRT-PCR)

Heart, brain, and embryonic tissues were microdissected in cold PBS and snap frozen in liquid nitrogen. TRIzol reagent (Life Technologies, Grand Island, NY, United States) was used to extract total RNA and complementary DNA (cDNA) was generated with the Superscript III kit (Life Technologies, Grand Island, NY, United States). SYBR Green quantitative RT-PCR was performed using the StepOne Plus Real-Time PCR System (Applied Biosystems, Foster City, CA, United States). Primers for *Aurkb*: P1F (forward): 5'-TCGCTGTTGTTCCCTCTCT-3', P1R (reverse): 5'-TTCAGGCCAGACTGAGACG-3'; P2F (forward): TCGCTGTTGTTCCCTCTCT, P2R (reverse): TTCAGGCCAGACTGAGACG. Primers for *Gapdh*: Forward: 5'-TCTTGCTCAGTGCTCTTGCTGG-3', Reverse: 5'-TCCTGGTATGACAATGAATAC GGC-3'.

Western Blotting

E12.5 embryos were minced in cold lysis buffer (50 mM Tris-HCl (pH 7.4), 150 mM NaCl, 1 mM EDTA- Na_2 , 1 mM EGTA, 1% Triton X-100, 0.5% Sodium Deoxycholate and 0.1% SDS with Protease inhibitor cocktail (Roche); 1 mM phenylmethylsulfonyl fluoride was added before use). Protein samples were resolved on 4–12% SDS-PAGE acrylamide gel before transferring to PVDF membranes. We used primary antibodies to Aurkb (1:1000), Cre (1:1000) and GAPDH (1:5000). Primary antibodies were visualized by chemiluminescence using HRP-conjugated secondary antibodies.

Statistical Analysis

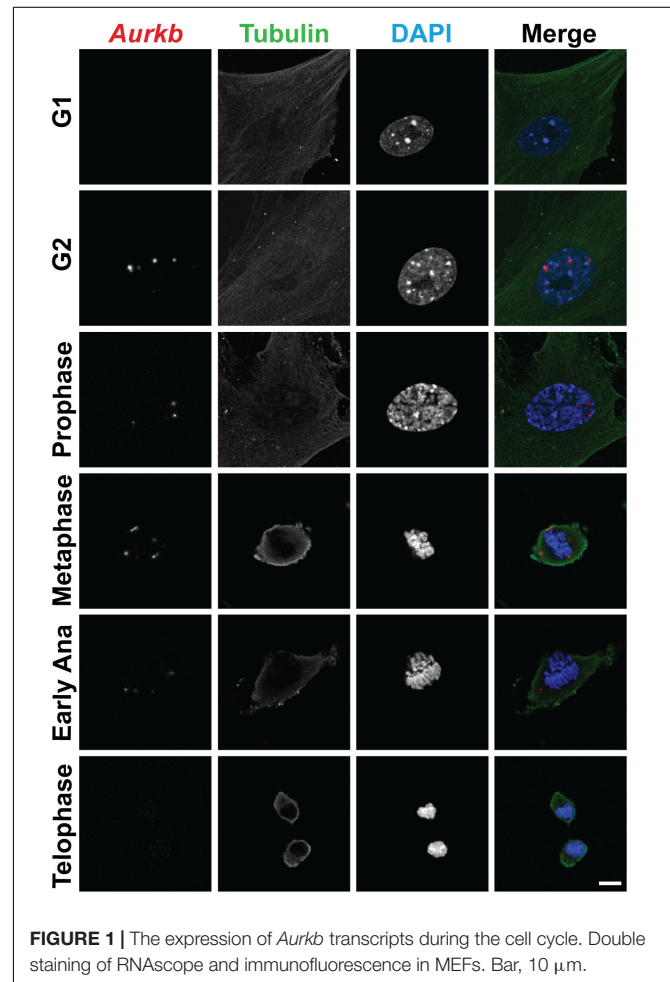
Data are presented as mean \pm SEM. Statistical significance between two groups was determined using two-tailed Student's *t*-test or chi square test. If significance is to be tested between

multiple groups, an analysis of variance is performed, followed by Bonferroni *post hoc* test. $P < 0.05$ was considered significant.

RESULTS

Aurkb Is Expressed in Proliferating but Not in Quiescent Cells

In cultured MEFs, *Aurkb* protein is undetectable at G1 phase, but expression becomes prominent at G2 and it is localized to the nucleus. *Aurkb* reaches and maintains a strong expression level throughout M phase. *Aurkb* re-localizes to the midbody at telophase (**Supplementary Figure 2**). These findings are consistent with previous observations (Crosio et al., 2002; Li et al., 2015). *Aurkb* mRNA is not detectable at G1 but is detectable by G2. Message is present through M phase but becomes undetectable at telophase (**Figure 1**). These results suggest that *Aurkb* transcript expression is correlated with the phase of the cell cycle and is largely restricted to mitotic cells. To further test this association, we forced MEFs to arrest at G1/S phase by exposure to hydroxyurea or mimosine (Park et al., 2012) and then assessed the presence of *Aurkb* transcripts.



Aurkb transcriptional levels were significantly decreased in hydroxyurea- and mimosine-treated groups as compared to the control group (Figure 2A). Both brain and heart experience a proliferation transition from being highly proliferative at embryonic stage to being mostly proliferatively inert in adulthood (Brooks et al., 1998). *Aurkb* transcription significantly declines from being high at embryonic day (E) 14.5 to being almost undetectable in adult heart and brain (Figure 2B). Altogether,

these data suggest that *Aurkb* transcription is coupled with cell proliferation *in vitro* and *in vivo*. Accordingly, we generated *Aurkb*^{ER Cre/+} mice by targeting a Cre-Ert2 cassette into the start codon of the *Aurkb* locus (Figure 3A). As expected, *Aurkb* mRNA was reduced to about 50% in *Aurkb*^{ER Cre/+} heterozygous mice as compared to their wildtype littermate controls (Figure 3C). In contrast, *Aurkb* protein expression was similar between *Aurkb*^{ER Cre/+} heterozygous mice and wildtype

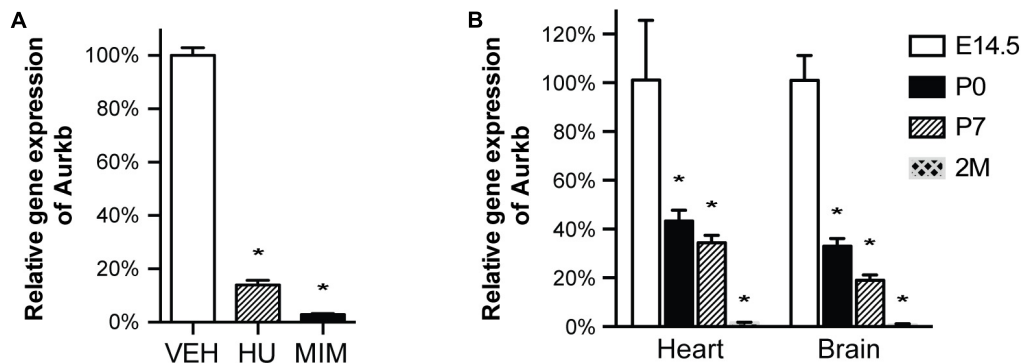


FIGURE 2 | *Aurkb* transcription is coupled with cell proliferation. (A) MEFs were cultured for 48 h with normal media (control), or treated with hydroxyurea (2 mM), or mimosine (1 mM). The transcriptional levels of *Aurkb* were quantified by qRT-PCR. *Gapdh* was used as a cDNA loading control. Three independent biological samples were used in each condition. * $P < 0.05$ when compared to the control condition analyzed by ANOVA followed by Bonferroni *post hoc* test; VEH, vehicle control; HU, hydroxyurea; MIM, mimosine; (B) The relative transcriptional levels of *Aurkb* in heart and brain at E14.5, postnatal day 0 (P0), postnatal day 7 (P7), and 2 months (2M). *Gapdh* was used as a cDNA loading control. $n = 3$ in each group. * $P < 0.05$ when compared to E14.5 analyzed by ANOVA followed by Bonferroni *post hoc* test.

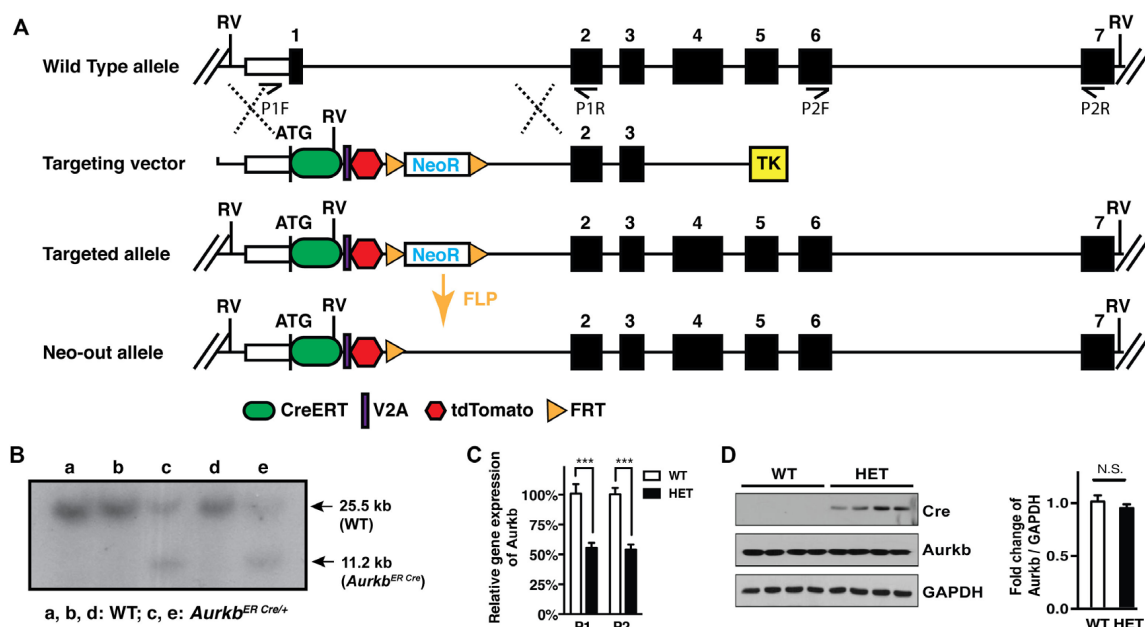


FIGURE 3 | *Aurkb* gene targeting. (A) Schematic of the generation of the *Aurkb*^{ER Cre} allele; (B) Southern blot of DNA extracted from *Aurkb*^{ER Cre/+} MEFs. DNAs were digested by *EcoRV* (RV). The ³²P-radiolabeled 5' DNA probe used (~500 bp) is located upstream of the 5' arm but downstream to the 5' RV enzyme site. P1F, P1R, P2F, and P2R are primer sets for detecting *Aurkb* transcripts; (C) *Aurkb* mRNA expression in wildtype (WT) and heterozygous (HET) E12.5 embryos. $n = 4$ in each group. *** $P < 0.001$ by a Student's *t*-test; (D) *Aurkb* protein expression in WT and HET E12.5 embryos. GAPDH was used as a protein loading control. Densitometric quantification of *Aurkb* was shown on the right. N.S., not significant.

controls (Figure 3D). *Aurkb*^{ER Cre/+} heterozygous mice are phenotypically normal and fertile. The total knockout of *Aurkb* resulted in early post-implantation lethality by E9.5 (Fernandez-Miranda et al., 2011). Consistently, we did not recover any *Aurkb*^{ER Cre/ER Cre} embryos at E10.5 (0/21).

Aurkb^{ER Cre} Labels Proliferating Cells *in vitro*

To characterize the labeling of *Aurkb*^{ER Cre} *in vitro* and test whether it is associated with cell proliferation, we generated *Aurkb*^{ER Cre/+}; *R26R^{eYFP/+}* MEFs and tracked *Aurkb*^{ER Cre} labeling by following the YFP reporter activities after 4-OH tamoxifen induction. YFP signal was detectable in proliferating MEFs about 16 h after 4-OH tamoxifen induction, became strong immediately prior to cell division, and maintained expression in daughter cells (Supplementary Video 1). In contrast, there was no YFP signal in non-dividing *Aurkb*^{ER Cre/+}; *R26R^{eYFP/+}* MEFs. Note that YFP signal is well recognized by GFP antibodies. Hereafter, we use GFP antibodies to measure YFP expression when referring to *Aurkb*^{ER Cre/+} fate-mapped cells. There was negligible *R26R^{eYFP/+}* reporter activity in *Aurkb*^{ER Cre/+}; *R26R^{eYFP/+}* MEFs without 4-OH tamoxifen induction (Figure 4A), indicating that there is little to no leakiness of the *Aurkb*^{ER Cre/+} allele. According to the expression profile of *Aurkb*, we expected to see *Aurkb*^{ER Cre/+} labeling cells as they enter G2 phase. To further analyze the association between *Aurkb*^{ER Cre/+} labeling and cell proliferation, we arrested MEFs at G1/S phase by either hydroxyurea or mimosine treatment, as evidenced by the absence of BrdU incorporation (Figure 4A). *R26R^{eYFP/+}* reporter activities were significantly lower for cell cycle inhibitor-treated *Aurkb*^{ER Cre/+}; *R26R^{eYFP/+}* MEFs compared to those under normal culture conditions (Figures 4A,B). This lineage tracing result mirrors the *Aurkb* transcription profile when wild-type MEFs are arrested at G1/S phase (Figure 2A). These results suggest that *Aurkb*^{ER Cre} labels proliferating but not non-dividing cells *in vitro*.

Aurkb^{ER Cre} Labels Proliferating Cells During Embryonic Development

Next we sought to determine whether *Aurkb*^{ER Cre} labels highly proliferative cells during embryonic development *in vivo*. We confirmed that *Aurkb* heterozygosity did not grossly affect embryonic morphogenesis or cellular growth (Supplementary Figure 3), validating the use of *Aurkb*^{ER Cre/+} as a lineage tracing tool during embryonic development. When E8.5 *Aurkb*^{ER Cre/+}; *R26R^{eYFP/+}* embryos were induced with tamoxifen, extensive labeling of the embryo was observed. Importantly, there was no leakiness of *Aurkb*^{ER Cre} labeling when corn oil but not tamoxifen was administered (Supplementary Figure 4). When we labeled developing embryos with both *Aurkb*^{ER Cre} and BrdU, we found that about 85% of embryonic cells are labeled by both systems (Figure 5). Further, we performed double immunofluorescence staining of GFP and PCNA on these embryos. We found that nearly 93% of embryonic cells are double positive (Supplementary Figure 5). Altogether, these data indicate that *Aurkb*^{ER Cre} is a sensitive

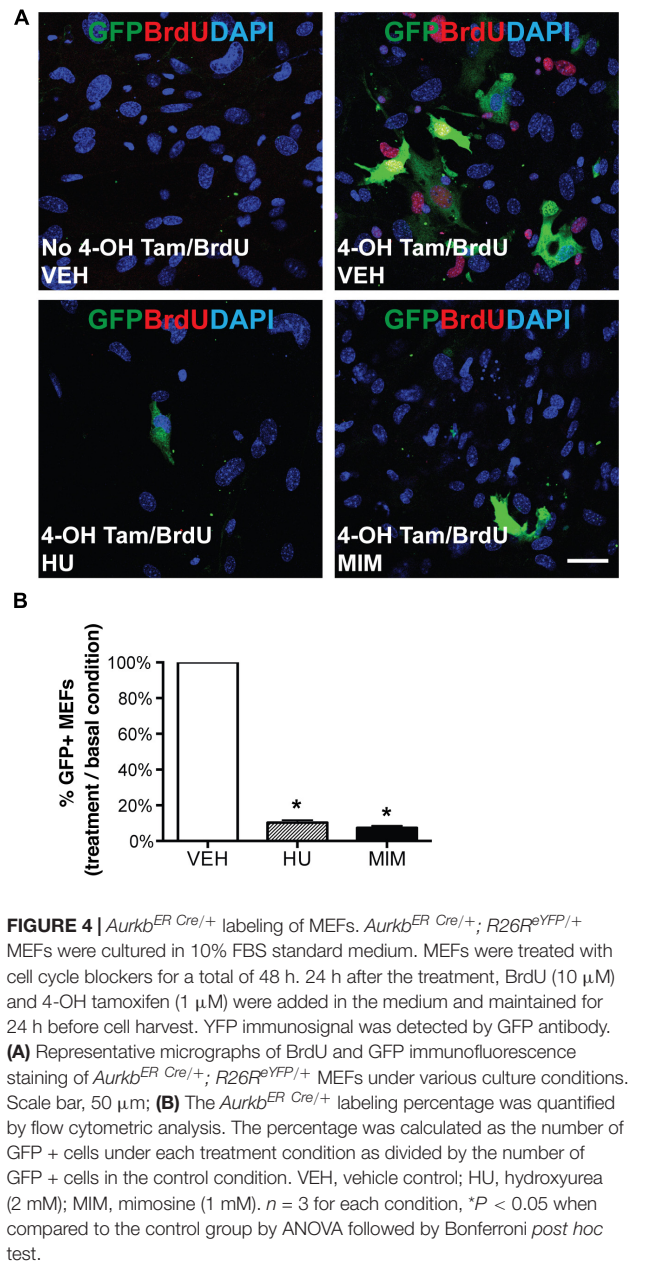


FIGURE 4 | *Aurkb*^{ER Cre/+} labeling of MEFs. *Aurkb*^{ER Cre/+}; *R26R^{eYFP/+}* MEFs were cultured in 10% FBS standard medium. MEFs were treated with cell cycle blockers for a total of 48 h. 24 h after the treatment, BrdU (10 μ M) and 4-OH tamoxifen (1 μ M) were added in the medium and maintained for 24 h before cell harvest. YFP immunosignal was detected by GFP antibody. **(A)** Representative micrographs of BrdU and GFP immunofluorescence staining of *Aurkb*^{ER Cre/+}; *R26R^{eYFP/+}* MEFs under various culture conditions. Scale bar, 50 μ m; **(B)** The *Aurkb*^{ER Cre/+} labeling percentage was quantified by flow cytometric analysis. The percentage was calculated as the number of GFP + cells under each treatment condition as divided by the number of GFP + cells in the control condition. VEH, vehicle control; HU, hydroxyurea (2 mM); MIM, mimosine (1 mM). $n = 3$ for each condition, * $P < 0.05$ when compared to the control group by ANOVA followed by Bonferroni *post hoc* test.

and reliable system for lineage tracking of proliferating embryonic cells.

Tamoxifen Activation of *Aurkb*^{ER Cre} Labels Proliferating Adult Stem/Progenitor Cells but Not Post-mitotic Cells *in vivo*

Next, we assessed *Aurkb*^{ER Cre} labeling in adult regenerative tissues. Two-month-old *Aurkb*^{ER Cre/+}; *R26R^{eYFP/+}* mice were given a single dose of tamoxifen (100 mg/kg BW) and we followed the labeling pattern of the YFP reporter over time in the intestine. The labeling displayed a dynamic expansion

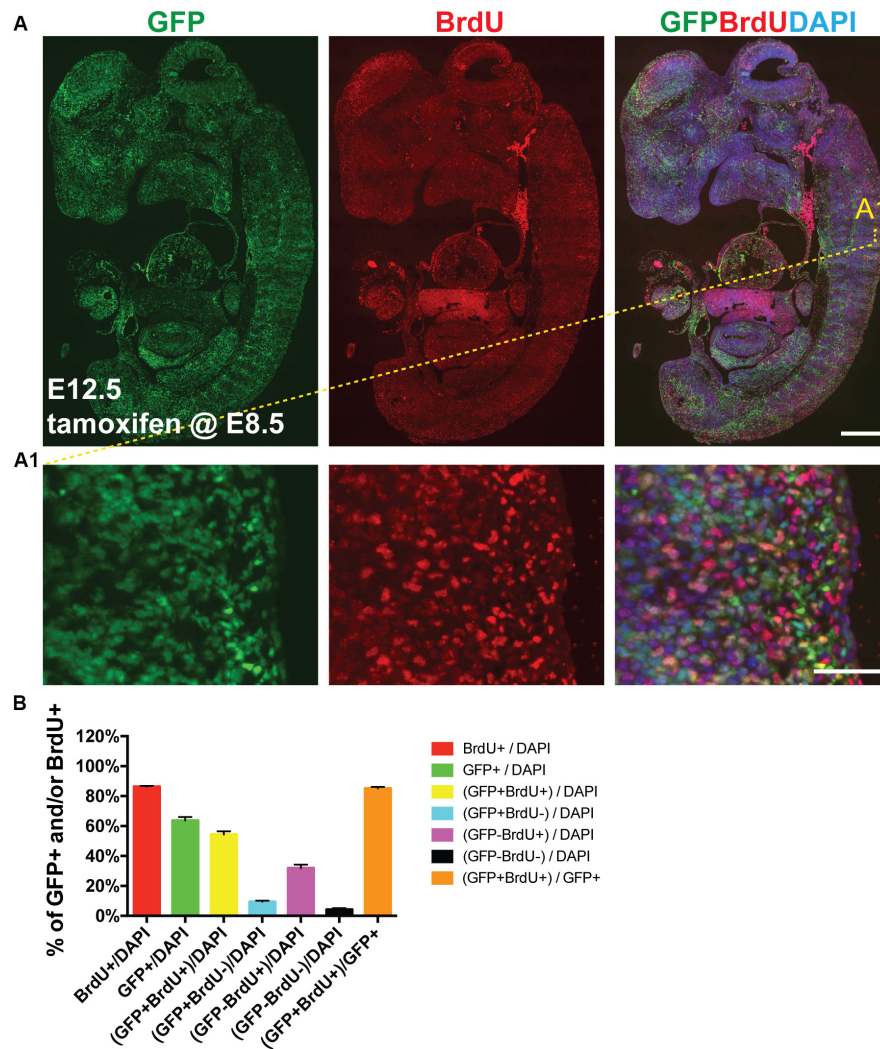


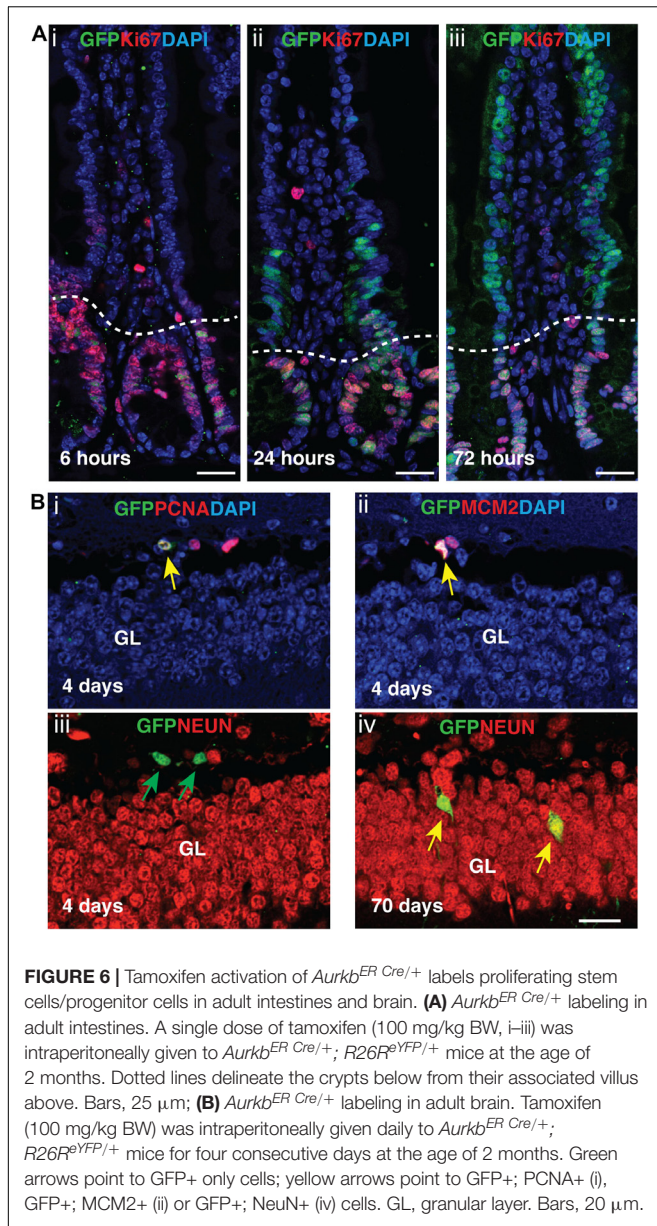
FIGURE 5 | *Aurkb^{ER Cre/+}* labels proliferating cells in developing embryos. Tamoxifen (150 mg/kg BW) was given to pregnant mice at E8.5 by gavage. BrdU (100 mg/kg BW) was intraperitoneally given to pregnant mice for four consecutive days (E8.5, E9.5, E10.5, and E11.5, one injection/day). **(A and A1)** Representative immunofluorescence micrographs of an E12.5 *Aurkb^{ER Cre/+}; R26R^{eYFP/+}* embryo (sagittal section). Scale bars, A, 500 μ m; A1, 50 μ m; **(B)** Labeling quantification of *Aurkb^{ER Cre/+}* and/or BrdU (n = 4).

from the initial crypt (6 h after tamoxifen administration) to the entire crypt-villus structure over a course of 3 days (**Figure 6A**), greatly resembling the lineage tracking pattern of intestinal stem cells (ISCs) and progenitors, which are known to be highly proliferative (Barker, 2014). In the crypt zone where Ki67-positive ISCs and progenitors reside, *Aurkb^{ER Cre/+}* labeling colocalizes with Ki67. In the villi where derivative, Ki67-negative intestinal epithelial cells reside, *Aurkb^{ER Cre/+}* labeling colocalizes with derivatives of the crypt ISCs that appear over time (**Figure 6A**). Further, administration of low doses of tamoxifen (2 mg/kg BW) in adult *Aurkb^{ER Cre/+}; R26R^{eYFP/+}* mice revealed that single earlier *Aurkb*-labeled intestinal progenitor cells (PCNA+) expanded to form clusters of enterocytes after 7 days (**Supplementary Figure 6**). Altogether, these data indicate that *Aurkb^{ER Cre/+}* labels proliferating progenitor cells in the intestine. In brain, neuronal nuclei

(NeuN)-positive post-mitotic neurons were not promptly labeled after tamoxifen exposure but eventually became labeled (70 days after the initial tamoxifen induction). This occurred presumably through transit amplifying mini-chromosome maintenance proteins (MCM2)-positive progenitors (**Figure 6B**). This is consistent with NeuN-positive neurons as terminally quiescent cells, renewing through neural stem cells and progenitors with prolonged kinetics.

DISCUSSION

Assessment of cell proliferation *in vivo* generally relies on the use of BrdU incorporation or “snapshots” of cell cycle marker expression such as PCNA or Ki67. Both approaches are important complementary methods for detecting actively proliferating



cells. However, increased focus on adult tissue regeneration calls for new tools to enable the detection of tissues and cell lineages derived from proliferating adult progenitor cells under various conditions. The MADM mouse can be used for tracking populations derived from proliferative progenitors. However, its application is limited due to its low detection sensitivity (Zong, 2014). A *Ki67^{IRESCreER}* mouse tracks proliferating cells based on Ki67 expression (Basak et al., 2018). However, Ki67 is transcribed broadly throughout the cell cycle, a feature that appears a critical factor in its reliability as a proliferation marker (Miller et al., 2018). In this report, we describe a new genetic mouse tool, *Aurkb*^{ER Cre/+}, which can label cells based on *Aurkb* transcription. We found that *Aurkb*^{ER Cre} labels proliferating cells *in vitro* and *in vivo*. In developing embryos, *Aurkb*^{ER Cre} labeling overlaps well with cell proliferation markers such as

BrdU and PCNA but it does not label quiescent cells. We notice that the overlap between *Aurkb*^{ER Cre} labeling and BrdU or PCNA seems quite high during development, even though *Aurkb*^{ER Cre} labeling was induced by a short pulse of tamoxifen. This is primarily due to the high proliferative characteristics of developing embryos: both earlier proliferating embryonic cells and their later derivatives are all mitotic.

Since *Aurkb*^{ER Cre} labeling is based on *Aurkb* transcription, which turns on at G2 phase, *Aurkb*^{ER Cre} labeling should not be interpreted as an absolute cell division or cytokinetic marker. For instance, certain cells such as bi- or multinucleated adult cardiomyocytes and hepatocytes can undergo karyokinesis without cytokinesis under physiological or pathological conditions (Gentric et al., 2012; Derks and Bergmann, 2020). These cells may be labeled by *Aurkb*^{ER Cre} in the absence of cell division. In these specific instances, *Aurkb* protein expression and other cytokinetic events should be analyzed instead.

Since *Aurkb*^{ER Cre/+} is built by a knock-in strategy, the *Aurkb* transcript is disrupted in the targeted allele. In contrast, *Aurkb* protein expression level in *Aurkb*^{ER Cre/+} heterozygous mice was quite similar to their wildtype controls (**Figure 3D**). This is consistent with other reports that heterozygous knockout mice can express similar or more than half of the proteins relative to wildtype control mice in the target genes (Gineste et al., 2013; Zhou et al., 2015; Arkhipov et al., 2019). It is reported that an *Aurkb* knockout mouse in which exons 2–6 were excised is embryonic lethal, older *Aurkb* heterozygous mice approximately 12–24 months of age show decreased survival due to susceptibility for tumorigenesis, and a fraction of *Aurkb* heterozygous males suffer from oligospermia by 12 months of age (Fernandez-Miranda et al., 2011). In our current study, we used much younger mice less than 3-months of age. We did not observe reproductive defects or spontaneous cancer development in young *Aurkb*^{ER Cre/+} mice. Nonetheless, it is possible that *Aurkb*^{ER Cre/+} mice may develop aforementioned pathologies over time, due to genome or chromosomal instability, even though we did not observe such problems in our colony. On the other hand, by intercrossing *Aurkb*^{ER Cre/+} heterozygous mice, the progeny with genotype of *Aurkb*^{ER Cre/ER Cre} can be used to study the phenotype of *Aurkb* depletion or requirement of *Aurkb* expression in cell division and cytokinesis.

The *Aurkb*^{ER Cre/+} mouse is an important new tool for lineage tracing proliferating cells during embryonic development and adult tissue regeneration. For instance, when crossed to multi-color reporters such as the confetti mouse strain (Snippert et al., 2010), the *Aurkb*^{ER Cre/+} mouse can be used to study the clonogenicity of neurons or other cell types in the developing embryos or tissue regeneration (e.g., whether cells are derived from multiple progenitor cells or from rare dominant clones). Similarly, the *Aurkb*^{ER Cre/+} mouse can be used to track tissue regeneration such as occurring from those rare stem cells whose derivatives forming over long periods of time will be more readily detected with this tool. The *Aurkb*^{ER Cre/+} mouse allows the ability to track how tissues with low rates of proliferation such as brain, lung and heart are regenerated over time in various physiological or pathological conditions. We anticipate the coupling of *Aurkb* knockout with inducible Cre-mediated

capability will be a powerful reagent for the investigation of cell proliferation in the context of *Aurkb* expression.

DATA AVAILABILITY STATEMENT

All datasets generated for this study are included in the article/**Supplementary Material**.

ETHICS STATEMENT

The animal studies were reviewed and approved by the University of Pennsylvania Institutional Animal Care and Use Committee and the University of Maryland Baltimore Institutional Animal Care and Use Committee.

AUTHOR CONTRIBUTIONS

JE and DL conceived and designed the study. JJ, KE, and DL analyzed the experiments and wrote the original draft. JJ, KE, JE, and DL edited and finalized the manuscript. JJ, KE, FL, LL, GS, and DL performed the experiments. All authors reviewed the results and approved the final version of the manuscript.

REFERENCES

- Alvarez, R. Jr., Wang, B. J., Quijada, P. J., Avitabile, D., and Ho, T. (2019). Cardiomyocyte cell cycle dynamics and proliferation revealed through cardiac-specific transgenesis of fluorescent ubiquitinated cell cycle indicator (FUCCI). *J. Mol. Cell Cardiol.* 127, 154–164. doi: 10.1016/j.yjmcc.2018.12.007
- Arkhipov, S. N., Potter, D. L., Geurts, A. M., and Pavlov, T. S. (2019). Knockout of P2rx7 purinergic receptor attenuates cyst growth in a rat model of ARPKD. *Am. J. Physiol. Renal Physiol.* 317, F1649–F1655. doi: 10.1152/ajprenal.00395.2019
- Barker, N. (2014). Adult intestinal stem cells: critical drivers of epithelial homeostasis and regeneration. *Nat. Rev. Mol. Cell Biol.* 15, 19–33. doi: 10.1038/nrm3721
- Basak, O., Krieger, T. G., Muraro, M. J., Wiebrands, K., Stange, D. E., Frias-Aldeguer, J., et al. (2018). Troy+ brain stem cells cycle through quiescence and regulate their number by sensing niche occupancy. *Proc. Natl. Acad. Sci. U.S.A.* 115, E610–E619. doi: 10.1073/pnas.1715911114
- Bond, A. M., Ming, G. L., and Song, H. (2015). Adult mammalian neural stem cells and neurogenesis: five decades later. *Cell Stem Cell* 17, 385–395. doi: 10.1016/j.stem.2015.09.003
- Brooks, G., Poolman, R. A., and Li, J. M. (1998). Arresting developments in the cardiac myocyte cell cycle: role of cyclin-dependent kinase inhibitors. *Cardiovasc. Res.* 39, 301–311. doi: 10.1016/s0008-6363(98)00125-4
- Crosio, C., Fimia, G. M., Loury, R., Kimura, M., Okano, Y., Zhou, H., et al. (2002). Mitotic phosphorylation of histone H3: spatio-temporal regulation by mammalian Aurora kinases. *Mol. Cell Biol.* 22, 874–885. doi: 10.1128/mcb.22.3.874-885.2002
- Derks, W., and Bergmann, O. (2020). Polyploidy in cardiomyocytes: roadblock to heart regeneration? *Circ. Res.* 126, 552–565. doi: 10.1161/CIRCRESAHA.119.315408
- Fernandez-Miranda, G., Trakala, M., Martin, J., Escobar, B., Gonzalez, A., Ghyselinck, N. B., et al. (2011). Genetic disruption of aurora B uncovers an essential role for aurora C during early mammalian development. *Development* 138, 2661–2672. doi: 10.1242/dev.066381
- Gentric, G., Celton-Morizur, S., and Desdouets, C. (2012). Polyploidy and liver proliferation. *Clin. Res. Hepatol. Gastroenterol.* 36, 29–34. doi: 10.1016/j.clinre.2011.05.011
- Gineste, C., De Winter, J. M., Kohl, C., Witt, C. C., Giannesini, B., Brohm, K., et al. (2013). In vivo and in vitro investigations of heterozygous nebulin knock-out mice disclose a mild skeletal muscle phenotype. *Neuromuscul. Disord.* 23, 357–369. doi: 10.1016/j.nmd.2012.12.011
- Helfrich, B. A., Kim, J., Gao, D., Chan, D. C., Zhang, Z., Tan, A. C., et al. (2016). Barasertib (AZD1152), a small molecule aurora b inhibitor, inhibits the growth of SCLC cell lines in vitro and in vivo. *Mol. Cancer Ther.* 15, 2314–2322. doi: 10.1158/1535-7163.MCT-16-0298
- Ikpa, P. T., Sladdens, H. F., Steinbrecher, K. A., Peppelenbosch, M. P., de Jonge, H. R., Smits, R., et al. (2016). Guanylin and uroguanylin are produced by mouse intestinal epithelial cells of columnar and secretory lineage. *Histochem. Cell. Biol.* 146, 445–455. doi: 10.1007/s00418-016-1453-4
- Kretschmar, K., Post, Y., Bannier-Helaoet, M., Mattiotti, A., Drost, J., Basak, O., et al. (2018). Profiling proliferative cells and their progeny in damaged murine hearts. *Proc. Natl. Acad. Sci. U.S.A.* 115, E12245–E12254. doi: 10.1073/pnas.1805829115
- Li, D., Hallett, M. A., Zhu, W., Rubart, M., Liu, Y., Yang, Z., et al. (2011). Dishevelled-associated activator of morphogenesis 1 (Daam1) is required for heart morphogenesis. *Development* 138, 303–315. doi: 10.1242/dev.055566
- Li, S., Deng, Z., Fu, J., Xu, C., Xin, G., Wu, Z., et al. (2015). Spatial Compartmentalization Specializes the Function of Aurora A and Aurora B. *J. Biol. Chem.* 290, 17546–17558. doi: 10.1074/jbc.M115.652453
- Liu, D., and Lampson, M. A. (2009). Regulation of kinetochore-microtubule attachments by Aurora B kinase. *Biochem. Soc. Trans.* 37(Pt 5), 976–980. doi: 10.1042/BST0370976
- Miller, I., Min, M., Yang, C., Tian, C., Gookin, S., Carter, D., et al. (2018). Ki67 is a graded rather than a binary marker of proliferation versus quiescence. *Cell Rep.* 24, 1105–1112. doi: 10.1016/j.celrep.2018.06.110
- Mitchison, T. J., and Salmon, E. D. (2001). Mitosis: a history of division. *Nat. Cell Biol.* 3, E17–E21. doi: 10.1038/35050656
- Nakada, Y., Canseco, D. C., Thet, S., Abdalsalam, S., Asaithamby, A., Santos, C. X., et al. (2017). Hypoxia induces heart regeneration in adult mice. *Nature* 541, 222–227. doi: 10.1038/nature20173
- Nasmyth, K. (2001). A prize for proliferation. *Cell* 107, 689–701. doi: 10.1016/s0092-8674(01)00604-3

FUNDING

This work was supported by the American Heart Association Scientist Development Grant (17SDG33650102) and department seed fund to DL; the Cotswold Foundation, the WW Smith Endowed Chair, and the National Institutes of Health (NIH) grant R35 HL140018 to JE.

ACKNOWLEDGMENTS

We thank the financial support from Department of Surgery, University of Maryland School of Medicine. We thank the Penn Cardiovascular Institute Histology Core for technical assistance, and the Penn CDB Microscopy Core for confocal imaging. We also thank Dr. Weinian Shou, Indiana University School of Medicine, for advice on the manuscript.

SUPPLEMENTARY MATERIAL

The Supplementary Material for this article can be found online at: <https://www.frontiersin.org/articles/10.3389/fcell.2020.00388/full#supplementary-material>

- Pan, Q., Nicholson, A. M., Barr, H., Harrison, L. A., Wilson, G. D., Burkert, J., et al. (2013). Identification of lineage-uncommitted, long-lived, label-retaining cells in healthy human esophagus and stomach, and in metaplastic esophagus. *Gastroenterology* 144, 761–770. doi: 10.1053/j.gastro.2012.12.022
- Park, S. Y., Im, J. S., Park, S. R., Kim, S. E., Wang, H. J., and Lee, J. K. (2012). Mimosine arrests the cell cycle prior to the onset of DNA replication by preventing the binding of human Ctf4/And-1 to chromatin via Hif-1 α activation in HeLa cells. *Cell Cycle* 11, 761–766. doi: 10.4161/cc.11.4.19209
- Rodriguez, C. I., Buchholz, F., Galloway, J., Sequerra, R., Kasper, J., Ayala, R., et al. (2000). High-efficiency deleter mice show that FLPe is an alternative to Cre-loxP. *Nat. Genet.* 25, 139–140. doi: 10.1038/75973
- Snippert, H. J., van der Flier, L. G., Sato, T., van Es, J. H., van den Born, M., Kroon-Veenboer, C., et al. (2010). Intestinal crypt homeostasis results from neutral competition between symmetrically dividing Lgr5 stem cells. *Cell* 143, 134–144. doi: 10.1016/j.cell.2010.09.016
- Tang, A., Gao, K., Chu, L., Zhang, R., Yang, J., and Zheng, J. (2017). Aurora kinases: novel therapy targets in cancers. *Oncotarget* 8, 23937–23954. doi: 10.18632/oncotarget.14893
- Tian, Y., Liu, Y., Wang, T., Zhou, N., Kong, J., Chen, L., et al. (2015). A microRNA-Hippo pathway that promotes cardiomyocyte proliferation and cardiac regeneration in mice. *Sci. Transl. Med.* 7:279ra238. doi: 10.1126/scitranslmed.3010841
- Tischer, J., and Gergely, F. (2019). Anti-mitotic therapies in cancer. *J. Cell Biol.* 218, 10–11. doi: 10.1083/jcb.201808077
- Vader, G., and Lens, S. M. (2008). The Aurora kinase family in cell division and cancer. *Biochim. Biophys. Acta* 1786, 60–72. doi: 10.1016/j.bbcan.2008.07.003
- van der Waal, M. S., Hengeveld, R. C., van der Horst, A., and Lens, S. M. (2012). Cell division control by the chromosomal passenger complex. *Exp. Cell Res.* 318, 1407–1420. doi: 10.1016/j.yexcr.2012.03.015
- Yu, J. J., Zhou, L. D., Zhao, T. T., Bai, W., Zhou, J., and Zhang, W. (2015). Knockdown of aurora-b inhibits the growth of non-small cell lung cancer A549 cells. *Oncol. Lett.* 10, 1642–1648. doi: 10.3892/ol.2015.3467
- Yu, K. W., Zhong, N., Xiao, Y., and She, Z. Y. (2019). Mechanisms of kinesin-7 CENP-E in kinetochore-microtubule capture and chromosome alignment during cell division. *Biol. Cell* 111, 143–160. doi: 10.1111/boc.201800082
- Zhou, C., Ding, L., Deel, M. E., Ferrick, E. A., Emeson, R. B., and Gallagher, M. J. (2015). Altered intrathalamic GABA neurotransmission in a mouse model of a human genetic absence epilepsy syndrome. *Neurobiol. Dis.* 73, 407–417. doi: 10.1016/j.nbd.2014.10.021
- Zong, H. (2014). Generation and applications of MADM-based mouse genetic mosaic system. *Methods Mol. Biol.* 1194, 187–201. doi: 10.1007/978-1-4939-1215-5_10
- Zong, H., Espinosa, J. S., Su, H. H., Muzumdar, M. D., and Luo, L. (2005). Mosaic analysis with double markers in mice. *Cell* 121, 479–492. doi: 10.1016/j.cell.2005.02.012

Conflict of Interest: The authors declare that the research was conducted in the absence of any commercial or financial relationships that could be construed as a potential conflict of interest.

Copyright © 2020 Jang, Engleka, Liu, Li, Song, Epstein and Li. This is an open-access article distributed under the terms of the Creative Commons Attribution License (CC BY). The use, distribution or reproduction in other forums is permitted, provided the original author(s) and the copyright owner(s) are credited and that the original publication in this journal is cited, in accordance with accepted academic practice. No use, distribution or reproduction is permitted which does not comply with these terms.



Dusp4 Contributes to Anesthesia Neurotoxicity via Mediated Neural Differentiation in Primates

Jia Yan^{1†}, Jingjie Li^{1†}, Yanyong Cheng^{1†}, Ying Zhang¹, Zhenning Zhou², Lei Zhang^{1*} and Hong Jiang^{1*}

¹ Department of Anesthesiology, Shanghai Ninth People's Hospital, Shanghai Jiao Tong University School of Medicine, Shanghai, China, ² Institute of Neuroscience, Chinese Academy of Sciences, Shanghai, China

OPEN ACCESS

Edited by:

Dominic C. Voon,
Kanazawa University, Japan

Reviewed by:

Yiyang Zhang,
Massachusetts General Hospital,
Harvard Medical School,
United States
Yuanlin Dong,
Massachusetts General Hospital,
Harvard Medical School,
United States

*Correspondence:

Lei Zhang
weiyimzhl@126.com
Hong Jiang
dr_hongjiang@163.com

[†] These authors have contributed
equally to this work

Specialty section:

This article was submitted to
Cell Growth and Division,
a section of the journal
Frontiers in Cell and Developmental
Biology

Received: 22 May 2020

Accepted: 27 July 2020

Published: 19 August 2020

Citation:

Yan J, Li J, Cheng Y, Zhang Y,
Zhou Z, Zhang L and Jiang H (2020)
Dusp4 Contributes to Anesthesia
Neurotoxicity via Mediated Neural
Differentiation in Primates.
Front. Cell Dev. Biol. 8:786.
doi: 10.3389/fcell.2020.00786

Background: Children who are exposed to anesthesia multiple times may undergo cognitive impairment during development. The underlying mechanism has been revealed as anesthesia-induced cognitive deficiency in young rodents and monkeys. However, the molecular mechanism of sevoflurane-induced neural development toxicity is unclear.

Methods: By combining RNA sequencing analysis of macaques' prefrontal cortex and human neural differentiation, this study investigates the mechanism of sevoflurane-induced neurotoxicity in primates.

Results: The level of dual specificity protein phosphatase 4 (Dusp4) was significantly downregulated in non-human primates after sevoflurane treatment. We further uncovered the dynamical expression of Dusp4 during the human neural differentiation of human embryonic stem cells and found that knockdown of Dusp4 could significantly inhibit human neural differentiation.

Conclusion: This study indicated that Dusp4 is critically involved in the sevoflurane-induced inhibition of neural differentiation in non-human primate and the regulation of human neural differentiation. It also suggested that Dusp4 is a potential therapeutic target for preventing the sevoflurane-induced neurotoxicity in primates.

Keywords: anesthesia, sevoflurane, DUSP4, neural differentiation, primate

INTRODUCTION

For young children, the safety of general anesthesia exposure is a critical health issue, which receives widespread attention (Rappaport et al., 2011; Vutskits and Xie, 2016). The U.S. Food and Drug Administration (FDA) issued an official warning that repeated or long-term management of general anesthetic may affect children's brains development (FDA Safety Announcement December 14, 2016). Until now, three well-known clinical studies evaluate the effects of general anesthesia on neurodevelopment, which are the General Anesthesia compared to Spinal anesthesia (GAS) trial, the Mayo Anesthesia Safety in Kids (MASK) study, and the Pediatric Anesthesia Neuro Development Assessment (PANDA). By using the Behavior Rating Inventory of Executive Function (BRIEF) and the Child Behavior Checklist (CBCL), the results indicate that anesthesia causes specific neurobehavioral changes in infants. What needs to be mentioned is that the MASK study

(Warner et al., 2018; Ing and Brambrink, 2019; Zaccariello et al., 2019) assesses the association between multiple general anesthetic exposures and neurodevelopmental deficit, which reveals that the processing speed, fine motor, motor coordination, and visual-motor integration capabilities dampen in multiple but single exposure.

Sevoflurane, the most commonly used anesthetic in children, is reported to induce neurotoxicity and cognitive impairment in non-human primates and rodents (Shen et al., 2013; Zhang et al., 2013; Yi et al., 2016). Aberrant neural differentiation is ascribed to cognitive impairment in young rodents (Cho et al., 2015). Recently, one study even demonstrated that sevoflurane inhibited neural differentiation (Zhang et al., 2019b). Nevertheless, the mechanism is still unknown (Zhang et al., 2015; Wang et al., 2016; Yi et al., 2016; Liu et al., 2020). In addition, in consideration of the different developmental specificity and timing between primates and rodents (Xue et al., 2013), the mechanism of the sevoflurane upon neural differentiation requires further elucidation in primates.

Dual specificity protein phosphatase 4 (Dusp4) is a key gene in neural differentiation (Kim et al., 2015), which is proved to regulate many genes involved in neural differentiation network, such as extracellular signal-regulated kinases (ERKs) (Guan and Butch, 1995; Chu et al., 1996; Ichimanda and Hijiya, 2018), c-Jun N-terminal kinases (JNKs) (Cadabert et al., 2005), and p38 (Engstrom et al., 2015; Kim et al., 2015; Odaka et al., 2016). Dusp4 is also critical for the endoderm specification (Brown et al., 2008) and cardiac specification (Liu et al., 2007). Irregular expression of Dusp4 might induce carcinoma (Sieben et al., 2005; Venter et al., 2005; Wang et al., 2007; Hasegawa et al., 2008). However, whether sevoflurane-induced neural development toxicity is mediated by dusp4 remains unclear. Thus, in the present study, we aim to explore the effects of sevoflurane on neural differentiation and the underlying mechanisms in primates. By combining the RNA sequencing analysis of macaque's prefrontal cortex and human neural differentiation, we found that Dusp4 was associated with sevoflurane-induced neurotoxicity. Moreover, sevoflurane treatment-caused Dusp4 downregulation was specifically in non-human primates but mice. Finally, our findings identified that Dusp4 was a target in terms of the prevention and treatment of postoperative cognitive decline in children.

MATERIALS AND METHODS

Rhesus Macaque and Mice Anesthesia

The animal studies were performed according to the guidelines of the Institute of Laboratory Animal Science, Peking Union Medical College, and Chinese Academy of Medical Sciences (Peking, China). The use of rhesus macaque in this research was approved by the Institutional Animal Care and Use Committee (protocol Number XC17001). The control group has three female rhesus macaques, and two female and one male rhesus macaques in the anesthesia group. In this study, the rhesus macaques received 6–8% anesthetic sevoflurane with 100% oxygen for the induction (2–4 min) of the

general anesthesia, and then received 2.5–3% sevoflurane and 100% oxygen with endotracheal intubation for 4 h for the maintenance of the general anesthesia. The rhesus macaques received the sevoflurane anesthesia on postnatal day 7 (P7) and then on P21 and P35 days. All the animals returned to their mothers in the cages after the anesthesia. The temperatures of the rhesus macaques were maintained by placing the rhesus macaques in a warm box (37°C). We harvested the prefrontal cortex immediately after the third time of sevoflurane treatment.

C57BL/6 mice at P6 (Shanghai SLAC Laboratory Animal, Zhangjiang, Shanghai, China) were used in the studies. The animal protocol was approved by the Standing Committee on Animals at Shanghai Ninth People's Hospital, Shanghai, China. The mice were housed in a temperature- and humidity-controlled environment (20–22°C; 12-h light/dark on a reversed light cycle) with free access to water and food. The mice received sevoflurane anesthesia as described in previous studies (Shen et al., 2013; Lu et al., 2017). The mice in the anesthesia group were exposed to 3% sevoflurane with 60% O₂ for 2 h daily with 3 days on P6, P7, and P8. The mice in the control group received 60% O₂. We use a warm box to maintain the rectal temperature of all the mice at 37°C. The prefrontal cortex tissues of mice were harvested at the end of the sevoflurane anesthesia administration.

Construction of Dusp4 Knockdown HESCs

To downregulate the Dusp4, three Dusp4 shRNA were constructed inside the pGMLV-SC5 vectors. The human embryonic stem cells (hESCs) were cultured in mTeSR 1 medium (EMCELL Technologies, Canada) and Y27632 (1:1000) on Matrigel-coated plates. Cells were digested by Accutase Cell Detachment Solution (Thermo, United States) for passage cultivation. Three shRNAs were mixed to infect the cells. After 48-h infection, mTeSR 1 and 1 µg/ml (final concentration) puromycin were used to screen the transfected hESCs.

The Dusp4-shRNA oligo sequences are as follows:

| shRNA | Oligomeric single-stranded DNA sequence 5' to 3' |
|-------------------|---|
| Control – forward | gataTGTTCTCCGAACGTGTACAGTTTCAAGAACGTGA CACGTTCCGAGAAATTTTTc |
| Control – reverse | aattgAAAAAATTCCTCGAACGTGTACAGTTCTCTTGAAC GTGACACGTTCCGAGAAcA |
| shRNA1 – forward | gatccGGAGGCTTCGAGTTCTGTTAATCAAGAGATTAAC GAACTCGAAGGCTCTCTTTTTg |
| shRNA1 – reverse | aattcAAAAAAGGAGGCTTCGAGTTCTGTTAATCTCTTGA TTAACGAACCTCGAAGGCTCCg |
| shRNA2 – forward | gatccGCATCACGGCTCTGTTGAATGTTCAAGAGACATTC AACAGAGCCGTGATGCTTTTTg |
| shRNA2 – reverse | aattcAAAAAAGCATCACGGCTCTGTTGAATGTCTCTTGA CATTCAACAGAGCCGTGATGCg |
| shRNA3 – forward | gatccGCCATAGAGTACATCGATGCCTTCAAGAGAGGCAT CGATGTACTCTATGGCTTTTTTg |
| shRNA3 – reverse | aattcAAAAAAGCCATAGAGTACATCGATGCCTCTCTTGA GGCATCGATGTACTCTATGGCg |

Quantitative RT-PCR (qPCR)

The whole RNA was extracted by using RNAiso Plus (TaKaRa, China). cDNA inverse transcription was performed by using cDNA Synthesis Kit (TaKaRa, China). GAPDH is used for reference gene for normalize q-PCR. Detailed qPCR primer information are placed after the references.

Primers for the qPCR detection are listed as follows:

| | |
|--------|--|
| Pax6 | PF: 5'-AACGATAACATACCAAGCGTGT-3' PR: 5'-GGTCTGCCCGTTCAACATC-3' |
| Oct4 | PF: 5'-CTTGAATCCCGAATGGAAGGG-3' PR: 5'-GTGTATATCCAGGGTGATCTC-3' |
| Sox2 | PF: 5'-TACAGCATGCTCTACTCGCAG-3' PR: 5'-GAGGAAGAGGTAACACAGGG-3' |
| Nestin | PF: 5'-CTGCTACCCCTTGAGACACCTG-3' PR: 5'-GGGCTCTGATCTCTGCATCTAC-3' |
| Tuj1 | PF: 5'-TTTGGACATCTCTTCAGGCC-3' PR: 5'-TTTCACACTCCTTCCGCAC-3' |
| Dusp4 | PF: 5'-GGCGTATGAGAGGTTTTCC-3' PR: 5'-TGGTCGTGTAGTGGGGTCC-3' |
| GAPDH | PF: 5'-GGAGCGAGATCCCTCCAAAT-3' PR: 5'-GGCTGTTGTCATCTCTCATGG-3' |

PF, primer forward; PR, primer reverse.

Neural Differentiation of hESCs *in vitro*

Neural differentiation analysis by using hESCs was performed as described in a previous study (Wattanapanitch et al., 2014). Briefly, the H9 cells were seeded in mTESR 1 medium on Matrigel-coated plates to obtain 80% confluency after seeding. Then the medium was changed to neural induction medium, which contains a 1:1 mixture of DMEM/F12 and neurobasal medium, 1 × N2 supplement, 1 × B27 supplement, 5 µg/ml insulin, 1 mM L-glutamine, 0.1 mM non-essential amino acids, 0.1 mM 2-mercaptoethanol, and supplemented with 1 µM dorsomorphin and 10 µM SB431542. The medium was changed every day for 9 days. Ten days post-differentiation, the NPCs were cultured in the neural maintenance medium, which contains a 1:1 mixture of DMEM/F12 and neurobasal medium, 1 × N2 supplement, 1 × B27 supplement, 5 µg/ml insulin, 1 mM L-glutamine, 0.1 mM non-essential amino acids, 0.1 mM 2-mercaptoethanol, and supplemented with 20 ng/ml bFGF. We also detected the expressions of neural progenitor marker Pax6 on day 12 and the expressions of neuron marker Tju1 on day 25.

Immunofluorescence Staining

Cells were fixed with 4% paraformaldehyde (Sigma-Aldrich, United States) for 18 min and washed with PBS solution. Then all the cells were treated with 0.2% Triton X-100 (Sigma-Aldrich, United States) for 8 min. Cells were then blocked with 3% bovine serum albumin (BSA) (Sigma-Aldrich, United States) in PBS solution for 1 h. Then incubated cells with primary antibodies, anti-Pax6 antibody (Abcam, ab5790, United States) or anti-TUJ1 antibody (Abcam, ab78078, United States), were diluted in 1% (w/v) BSA in PBS solution overnight at 4°C. After the

incubation, cells were washed with PBS three times and stained with secondary antibodies for 2 h at room temperature.

Western Blot

Every 50 mg tissues of mouse brain was lysed by the mixture of 0.5 ml RIPA plus 5 µl PMSF on ice. Then the samples were centrifuged at 12,000 rpm for 5 min at 4°C. Cells were lysed by using an SDS buffer (Beyotime, China) to obtain the protein for electrophoresis.

Then all the protein was transferred into PVDF membrane (Bio-Rad, United States). Primary antibodies were used in incubation, including anti-GAPDH (Abcam, ab9485, United States) antibody, anti-DUSP4 antibody (Abcam, ab216576, United States), anti-TUJ1 antibody (Abcam, ab78078, United States), anti-PAX6 antibody (Abcam, ab195045, United States), anti-p-ERK antibody (CST, #8544, United States), anti-ERK antibody (CST, #4695, United States), anti-p-p38 antibody (CST, #4511, United States), anti-p38 antibody (CST, #8690, United States), anti-p-JNK antibody (CST, #9251, United States), and anti-JNK antibody (CST, #9252, United States). Protein expression signaling was visualized through enhanced chemiluminescence (ECL) substrate (Thermo, United States).

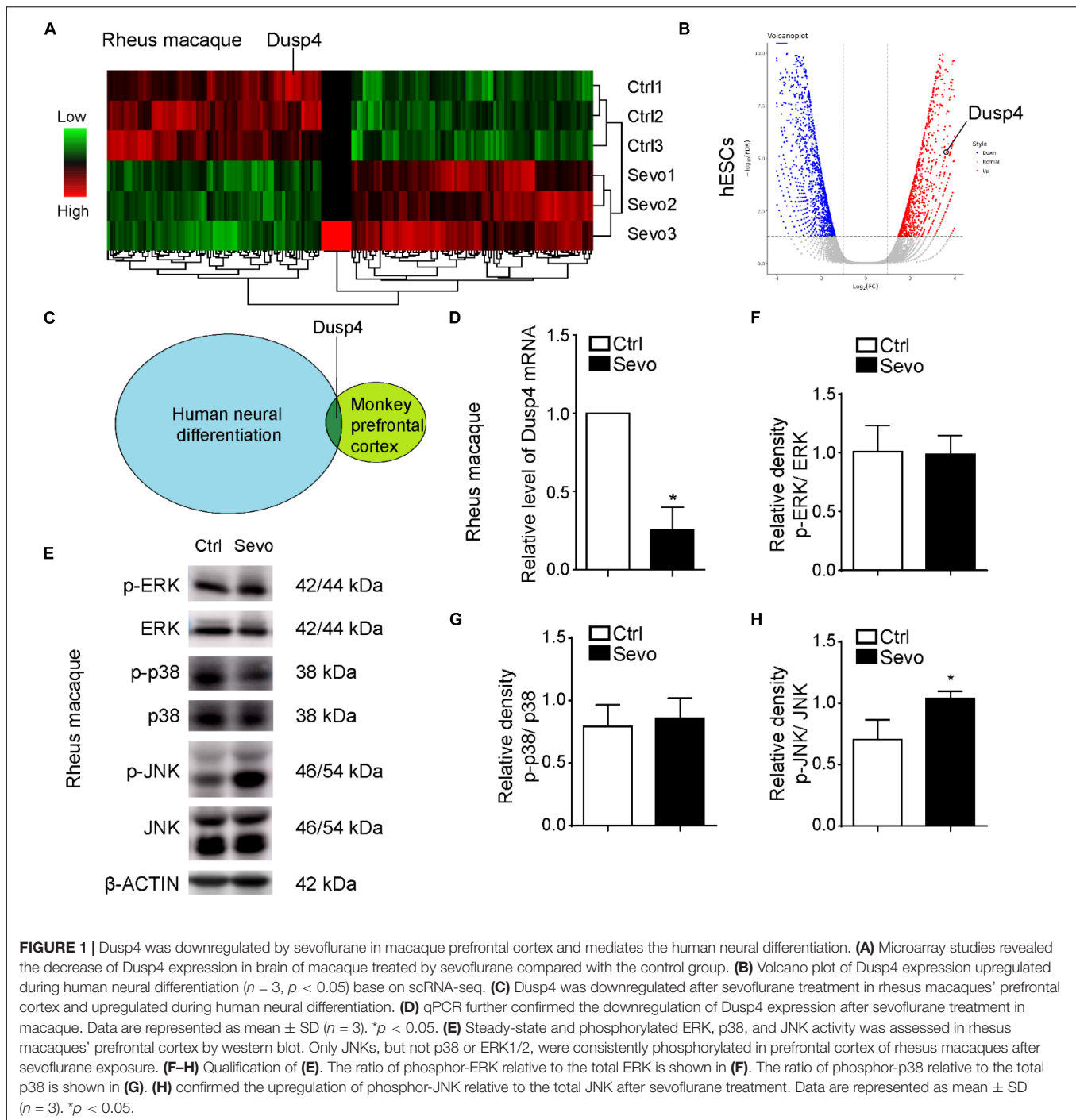
Statistics

The data were presented as mean ± standard deviation (SD). The significance of statistics was analyzed by Student's *t*-test, one-way ANOVA and two-way ANOVA (* and # *p* < 0.05, ** and ## *p* < 0.01, *** and ### *p* < 0.001). The study employed two-tailed hypothesis and statistically significant *p* values were < 0.05. Each experiment was repeated three times. We used GraphPad (GraphPad Software) to analyze all of the study data.

RESULTS

Sevoflurane Decreased the Expression of Dusp4 in Prefrontal Cortex of Rhesus Macaque

Alvarado et al. (2017) and us demonstrated that sevoflurane induced myelination damage of the central nervous system and caused behavior changes (e.g., anxiety and visual recognition memory) in infant rhesus macaques (Zhang et al., 2019a). Here, we performed multiple sevoflurane exposures in infant rhesus macaques on postnatal day 7 (P7), P14, and P28 repetitively, with each exposure lasting for 4 h per time as shown in a previous study (Alvarado et al., 2017). After the anesthesia, we collected brain tissues from prefrontal cortex and performed the RNA sequencing to examine the gene expression. As a result, there were 78 upregulated genes and 98 downregulated genes in sevoflurane exposure group (Figure 1A). Neural differentiation is involved in the early state in the infant's brain development and characterized by rapid structural and functional changes (Vasung et al., 2018). The influence of neural differentiation during early development could result in significant physiological and



cognitive impairment (Di Lullo and Kriegstein, 2017; Presumey et al., 2017). Sevoflurane inhibited neural differentiation of mouse embryonic stem cells (ESCs) into neural progenitor cells (NPCs) (Zhang et al., 2019b). To determine the effects of sevoflurane on neural differentiation in primate and clarify the underlying mechanisms, we performed the human neural differentiation with H9 hESCs and detected the whole genome expression by using bulk-RNA sequencing analysis. Interestingly, we combined the results of these two RNA

sequencing earlier and found that Dusp4 was downregulated after sevoflurane treatment in rhesus macaques' prefrontal cortex and upregulated during human neural differentiation (Figures 1B,C). Dusp4 could promote neural differentiation in mice, which is, however, unclear in human neural differentiation (Kim et al., 2015). So, our results indicated its possible function in sevoflurane-induced neurotoxicity. Then we confirmed the downregulation of Dusp4 in prefrontal cortex of rhesus macaques after sevoflurane treatment by qPCR

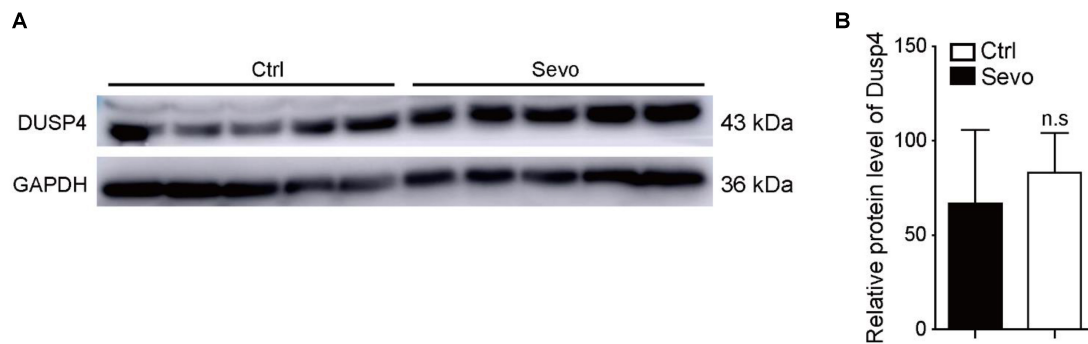


FIGURE 2 | Sevoflurane has no effect on the expression of Dusp4 in prefrontal cortex of mice. **(A)** Western blot indicated that the protein level of Dusp4 was not altered in prefrontal cortex of C57 after sevoflurane exposure. **(B)** Qualification of A showed there is no significant difference of the protein level of Dusp4 between sevoflurane group and control group ($n = 5$).

(Figure 1D). To explain the underlying molecular mechanisms, we tested the Dusp4-related classic downstream target genes or signal pathway by using rhesus macaque samples. As a result, we found that JNKs were consistently phosphorylated in prefrontal cortex of rhesus macaques after sevoflurane exposure (Figures 1E–H). Sevoflurane had only effects on JNK phosphorylation in primate (Figures 1E,H). It is consistent with a previous work where induced DUSP4 reduction enhanced c-Jun N-terminal kinase (JNK) activity (Denhez et al., 2019).

Sevoflurane Has No Effect on the Expression of Dusp4 in Prefrontal Cortex of Mice

Anesthetics can induce neuronal apoptosis which causes cognitive impairment in rodents and rhesus macaques (Vutskits and Xie, 2016). So, we exposed mice model to sevoflurane repeatedly, but failed to find similar results. In opposition, the protein level of Dusp4 was not altered in the prefrontal cortex of C57 after sevoflurane exposure (Figures 2A,B). This suggested that mice and rhesus macaques had different gene regulation manners when exposed to sevoflurane. The results indicated that Dusp4 could be the possible sevoflurane-related downstream. In terms of the proximity between human and rhesus macaque, Dusp4 might be still involved in the potential mechanism of sevoflurane-induced neurotoxicity in primates. In addition, it further hinted that the results in rodent model could not fully explain the phenotype in primate due to the differences in species.

Dusp4 Mediates Neural Differentiation of HESCs Into NPCs

A previous study showed that Dusp4 regulated retinoic acid-treated neural differentiation in mouse ESCs (Kim et al., 2015). However, whether Dusp4 was involved in the regulation of human neural differentiation remains unknown. Our results showed that Dusp4 was significantly upregulated during the human neural differentiation, especially on day 12 (Figure 3A). Vis-a-vis, sevoflurane downregulated the Dusp4 level which also

indicated its potential role in neurotoxicity. To explore the mechanisms further, we downregulated the Dusp4 expression by using three different shRNA mixed viruses (Figure 3B) in H9 hESCs. The results failed to show any influences upon the ability of self-renewal in hESCs (Figures 3C,D). However, the human neural differentiation in hESCs was significantly repressed after downregulation of Dusp4 (Figure 3E). The formation of rosette structure detected by Pax6 was interrupted after downregulating Dusp4, which indicated the repression of neural induction (Figure 3F). The reduction of neuronal class III β -tubulin (Tuj1) (Sullivan and Cleveland, 1986; Caccamo et al., 1989), a marker of mature neuron, further indicated the neurogenesis repression after the downregulation of Dusp4 (Figures 3G,I). In addition, we found that the expression of neural progenitor marker Nestin and Pax6 (Figure 3H) were descended by Dusp4 downregulation. In conclusion, Dusp4 plays an important role in the progress of human neural differentiation.

DISCUSSION

In the current study, we found that sevoflurane downregulated the Dusp4 expression in prefrontal cortex of rhesus macaque but not in mice. Also, Dusp4-mediated neural differentiation from hESCs into NPCs may be involved in sevoflurane-induced neurotoxicity.

Neural differentiation is ascribed to cognitive impairment in young rodents (Cho et al., 2015). Abnormal neural differentiation results in neurological and psychiatric disorders, serious behavior disorders, and some other nervous system diseases (Goncalves et al., 2016). Neural progenitor cells exist right after infants' birth for further brain neural development (Rolando and Taylor, 2014). In this study, by combining the RNA sequencing analysis of macaque's prefrontal cortex and human neural differentiation, we found that Dusp4 may work as a key gene in sevoflurane-induced neurotoxicity. By using the *in vitro* human neural differentiation system, we knocked down the Dusp4 to mimic the Dusp4 downregulation caused by sevoflurane exposure to check the inhibition of neural differentiation.

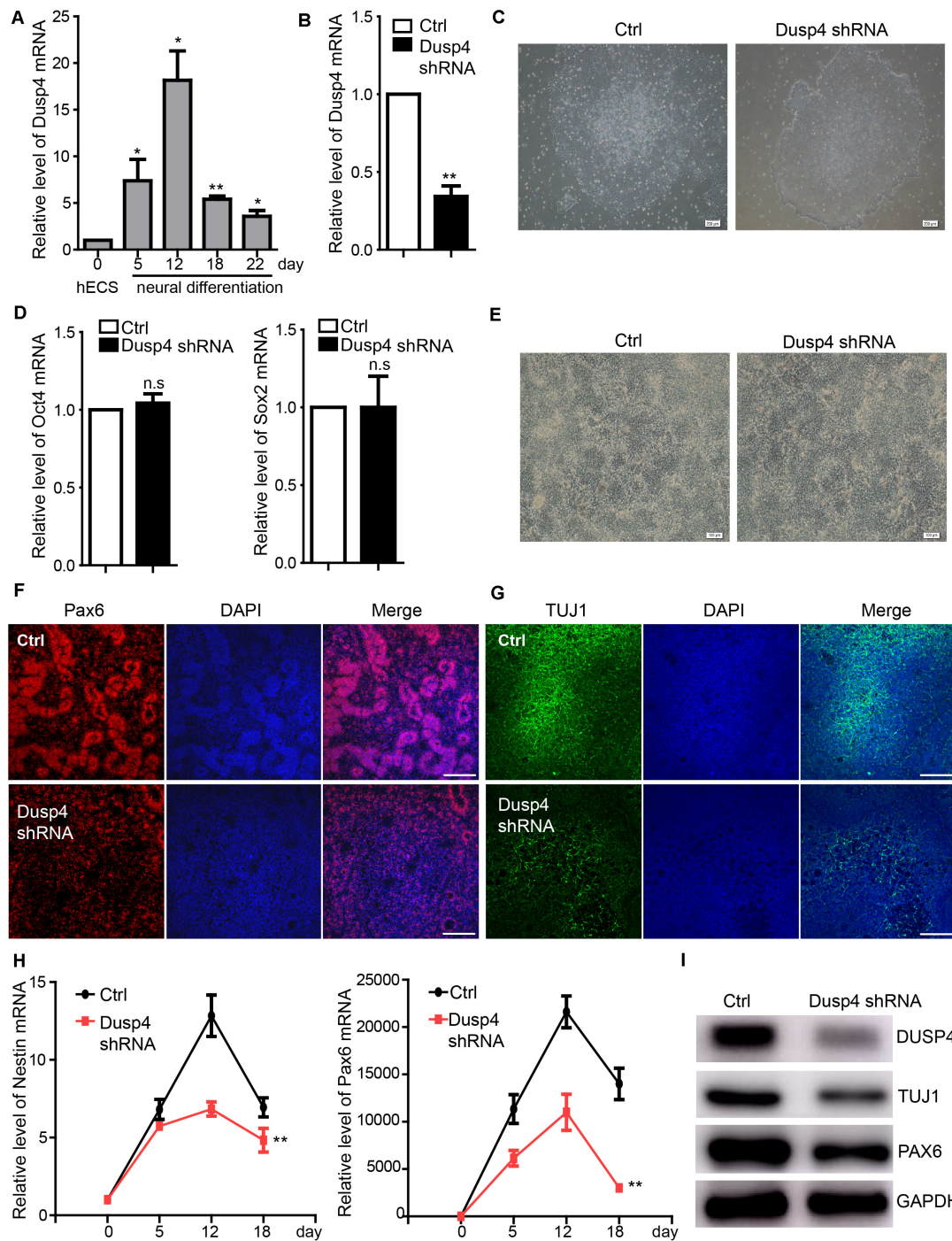


FIGURE 3 | Dusp4 mediates neural differentiation of hESCs. **(A)** qPCR detection of the Dusp4 expression trend during the neural differentiation of hESCs from 0 to 22 days. Data are represented as mean \pm SD ($n = 3$). * $p < 0.05$, ** $p < 0.01$. **(B)** Downregulation of Dusp4 expression by Dusp4 shRNA compared with the control group detected at day 5 during the neural differentiation of hESCs. Data are represented as mean \pm SD ($n = 3$). ** $p < 0.01$. **(C)** There was no significant difference in clone formation assay between the Dusp4 knockdown group and control group. Ctrl: hESCs with empty pGMLV-SC5 vector. Scale bar represents 200 μ m. **(D)** The results of qPCR showed that there is no significant difference of stemness markers (Oct4 and Sox2) expression between the Dusp4 knockdown group and control group. Data are represented as mean \pm SD ($n = 3$). **(E)** Morphology of neural differentiation of two different groups. Scale bar represents 100 μ m. **(F)** Immunofluorescence staining of Pax6 indicated that neural differentiation of hESCs was inhibited by Dusp4 knockdown at day 6. Scale bar represents 100 μ m. **(G)** Immunofluorescence staining of TUJ1 showed that neurogenesis was further repressed by Dusp4 knockdown at day 28. Scale bar represents 100 μ m. **(H)** qPCR analysis showed that dusp4 knockdown repressed the expression of neural progenitor genes (Nestin and Pax6) on days 5, 12, and 18 during the neural differentiation. Data are represented as mean \pm SD ($n = 3$). ** $p < 0.01$. **(I)** Results of western blot indicated that the expression of mature neuron gene TUJ1 was downregulated by dusp4 knockdown on day 28.

The level of Dusp4 was specifically downregulated after sevoflurane treatment in non-human primates. However, there was no statistical difference of Dusp4 expression in rodents. Our results demonstrated that the mechanisms of neurodevelopment toxicity caused by sevoflurane were different between primate and rodent due to various neurodevelopment. We further uncovered the dynamical expression of Dusp4 during the human neural differentiation by using hESCs. The human neural differentiation could be significantly inhibited after Dusp4 is knocked down.

There are several limitations in the present study. First, we did not monitor the hypoxia and hypotension during general anesthesia in rhesus macaque model. However, the protocol of anesthesia management was the same as in the previous study (Alvarado et al., 2017), which did not show hypoxia and hypotension. Second, the sample size of rhesus macaques (3:3) may not be sufficient enough in the current study; thus, adding the sample size should be performed in the future.

In conclusion, this study indicated that Dusp4 may be involved in the sevoflurane-induced neurotoxicity in non-human primates, which regulated the human neural differentiation in priority.

DATA AVAILABILITY STATEMENT

The datasets presented in this study can be found in online repositories. The names of the repository/repositories and accession number(s) can be found below: <https://www.ncbi.nlm.nih.gov/geo/>, GSE148436; <https://www.ncbi.nlm.nih.gov/geo/>, GSE148437; <https://www.ncbi.nlm.nih.gov/geo/>, GSE148438.

REFERENCES

- Alvarado, M. C., Murphy, K. L., and Baxter, M. G. (2017). Visual recognition memory is impaired in rhesus monkeys repeatedly exposed to sevoflurane in infancy. *Br. J. Anaesth.* 119, 517–523. doi: 10.1093/bja/aew473
- Brown, J. L., Snir, M., Noshmeh, H., Kirby, M., Hong, S. K., Elkahoul, A. G., et al. (2008). Transcriptional profiling of endogenous germ layer precursor cells identifies dusp4 as an essential gene in zebrafish endoderm specification. *Proc. Natl. Acad. Sci. U.S.A.* 105, 12337–12342. doi: 10.1073/pnas.0805589105
- Caccamo, D. V., Herman, M. M., Frankfurter, A., Katsetos, C. D., Collins, V. P., Rubinstein, L. J., et al. (1989). An immunohistochemical study of neuropeptides and neuronal cytoskeletal proteins in the neuroepithelial component of a spontaneous murine ovarian teratoma. Primitive neuroepithelium displays immunoreactivity for neuropeptides and neuron-associated beta-tubulin isotype. *Am. J. Pathol.* 135, 801–813.
- Cadalbert, L., Sloss, C. M., Cameron, P., and Pelvin, R. (2005). Conditional expression of MAP kinase phosphatase-2 protects against genotoxic stress-induced apoptosis by binding and selective dephosphorylation of nuclear activated c-jun N-terminal kinase. *Cell Signal* 17, 1254–1264. doi: 10.1016/j.cellsig.2005.01.003
- Cho, K. O., Lybrand, Z. R., Ito, N., Brulet, R., Tafacory, F., Zhang, L., et al. (2015). Aberrant hippocampal neurogenesis contributes to epilepsy and associated cognitive decline. *Nat. Commun.* 6:6606.
- Chu, Y., Solski, P. A., Khosravi-Far, R., Der, C. J., and Kelly, K. (1996). The mitogen-activated protein kinase phosphatases PAC1, MKP-1, and MKP-2 have unique substrate specificities and reduced activity in vivo toward the ERK2 sevenmaker mutation. *J. Biol. Chem.* 271, 6497–6501. doi: 10.1074/jbc.271.11.6497
- Denhez, B., Rousseau, M., Dancosst, D. A., Lizotte, F., Guay, A., Auger-Messier, M., et al. (2019). Diabetes-Induced DUSP4 reduction promotes podocyte dysfunction and progression of diabetic nephropathy. *Diabetes* 68, 1026–1039. doi: 10.2337/db18-0837
- Di Lullo, E., and Kriegstein, A. R. (2017). The use of brain organoids to investigate neural development and disease. *Nat. Rev. Neurosci.* 18, 573–584. doi: 10.1038/nrn.2017.107
- Engstrom, A., Wang, H., and Xia, Z. (2015). Lead decreases cell survival, proliferation, and neuronal differentiation of primary cultured adult neural precursor cells through activation of the JNK and p38 MAP kinases. *Toxicol. In Vitro* 29, 1146–1155. doi: 10.1016/j.tiv.2015.05.001
- Goncalves, J. T., Schafer, S. T., and Gage, F. H. (2016). Adult neurogenesis in the hippocampus: from stem cells to behavior. *Cell* 167, 897–914. doi: 10.1016/j.cell.2016.10.021
- Guan, K. L., and Butch, E. (1995). Isolation and characterization of a novel dual specific phosphatase, HVH2, which selectively dephosphorylates the mitogen-activated protein kinase. *J. Biol. Chem.* 270, 7197–7203. doi: 10.1074/jbc.270.13.7197
- Hasegawa, T., Enomoto, A., Kato, T., Kawai, K., Miyamoto, R., Jijiwa, M., et al. (2008). Roles of induced expression of MAPK phosphatase-2 in tumor development in RET-MEN2A transgenic mice. *Oncogene* 27, 5684–5695. doi: 10.1038/onc.2008.182
- Ichimanda, M., and Hijiya, N. (2018). Downregulation of dual-specificity phosphatase 4 enhances cell proliferation and invasiveness in colorectal carcinomas. *Cancer Sci.* 109, 250–258. doi: 10.1111/cas.13444
- Ing, C., and Brambrink, A. M. (2019). Mayo Anesthesia Safety in Kids continued: two new studies and a potential redirection of the field. *Br. J. Anaesth.* 122, 716–719. doi: 10.1016/j.bja.2019.03.011

ETHICS STATEMENT

The animal studies were performed according to the guidelines and regulations of the Institute of Laboratory Animal Science, Peking Union Medical College and Chinese Academy of Medical Science (Beijing, China). Efforts were made to minimize the number of animals in the studies. The use of rhesus macaque in research at the Institute of Laboratory Animal Science was approved by the Institutional Animal Care and Use Committee (Protocol number #XC17001).

AUTHOR CONTRIBUTIONS

HJ, LZ, and JY: study concept and design. JL, YC, YZ, and ZZ: acquisition of the data, analysis and interpretation of the data. LZ and JY: draft the manuscript, obtain funding, administrative, technical, and material support. All authors have read and approved the manuscript.

FUNDING

This research was supported by the National Natural Science Foundation of China (81870818, 81970990, 81771132, and 81801067), Shanghai Pujiang Program (2019PJD025), Two Hundred Talent of Shanghai Jiao Tong University School of Medicine (20191818), funding of Shanghai Ninth People's Hospital (JYZZ014), Foundation of Shanghai Municipal Health Commission (#21840052), and Wu Jieping Medical Foundation (320.6750.19089-74).

- Kim, S. Y., Han, Y. M., Oh, M., Kim, W. K., Oh, K. J., Lee, S. C., et al. (2015). DUSP4 regulates neuronal differentiation and calcium homeostasis by modulating ERK1/2 phosphorylation. *Stem Cells Dev.* 24, 686–700. doi: 10.1089/scd.2014.0434
- Liu, F., Liu, S., Patterson, T. A., Fogle, C., Hanig, J. P., Slikker, W. Jr., et al. (2020). Effects of Xenon-Based Anesthetic Exposure on the Expression Levels of Polysialic Acid Neural Cell Adhesion Molecule (PSA-NCAM) on Human Neural Stem Cell-Derived Neurons. *Mol. Neurobiol.* 57, 217–225. doi: 10.1007/s12035-019-01771-x
- Liu, Y., Asakura, M., Inoue, H., Nakamura, T., Sano, M., Niu, Z., et al. (2007). Sox17 is essential for the specification of cardiac mesoderm in embryonic stem cells. *Proc. Natl. Acad. Sci. U.S.A.* 104, 3859–3864. doi: 10.1073/pnas.0609100104
- Lu, H., Liufu, N., Dong, Y., Xu, G., Zhang, Y., Shu, L., et al. (2017). Sevoflurane acts on ubiquitination-proteasome pathway to reduce postsynaptic density 95 protein levels in young mice. *Anesthesiology* 127, 961–975. doi: 10.1097/aln.0000000000001889
- Odaka, H., Numakawa, T., Yoshimura, A., Nakajima, S., Adachi, N., Ooshima, Y., et al. (2016). Chronic glucocorticoid exposure suppressed the differentiation and survival of embryonic neural stem/progenitor cells: possible involvement of ERK and PI3K/Akt signaling in the neuronal differentiation. *Neurosci. Res.* 113, 28–36. doi: 10.1016/j.neures.2016.07.002
- Presumey, J., Bialas, A. R., and Carroll, M. C. (2017). Complement System in Neural Synapse Elimination in Development and Disease. *Adv. Immunol.* 135, 53–79. doi: 10.1016/bs.ai.2017.06.004
- Rappaport, B., Mellon, R. D., Simone, A., and Woodcock, J. (2011). Defining safe use of anesthesia in children. *N. Engl. J. Med.* 364, 1387–1390. doi: 10.1056/nejmp1102155
- Rolando, C., and Taylor, V. (2014). Neural stem cell of the hippocampus: development, physiology regulation, and dysfunction in disease. *Curr. Top. Dev. Biol.* 107, 183–206. doi: 10.1016/b978-0-12-416022-4.00007-x
- Shen, X., Dong, Y., Xu, Z., Wang, H., Miao, C., Soriano, S. G., et al. (2013). Selective anesthesia-induced neuroinflammation in developing mouse brain and cognitive impairment. *Anesthesiology* 118, 502–515. doi: 10.1097/aln.0b013e3182834d77
- Sieben, N. L., Oosting, J., Flanagan, A. M., Prat, J., Roemen, G. M., Kolkman-Uljee, S. M., et al. (2005). Differential gene expression in ovarian tumors reveals Dusp 4 and Serpina 5 as key regulators for benign behavior of serous borderline tumors. *J. Clin. Oncol.* 23, 7257–7264. doi: 10.1200/jco.2005.02.2541
- Sullivan, K. F., and Cleveland, D. W. (1986). Identification of conserved isotype-defining variable region sequences for four vertebrate beta tubulin polypeptide classes. *Proc. Natl. Acad. Sci. U.S.A.* 83, 4327–4331. doi: 10.1073/pnas.83.12.4327
- Vasung, L., Turk, E. A., Ferradal, S. L., Sutin, J., Stout, J. N., Ahtam, B., et al. (2018). Exploring early human brain development with structural and physiological neuroimaging. *Neuroimage* 187, 226–254. doi: 10.1016/j.neuroimage.2018.07.041
- Venter, D. J., Ramus, S. J., Hammet, F. M., de Silva, M., Hutchins, A. M., Petrovic, V., et al. (2005). Complex CGH alterations on chromosome arm 8p at candidate tumor suppressor gene loci in breast cancer cell lines. *Cancer Genet. Cytogenet.* 160, 134–140. doi: 10.1016/j.cancergencyto.2004.12.007
- Vutskits, L., and Xie, Z. (2016). Lasting impact of general anaesthesia on the brain: mechanisms and relevance. *Nat. Rev. Neurosci.* 17, 705–717. doi: 10.1038/nrn.2016.128
- Wang, H., Lu, Y., Huang, W., Papoutsakis, E. T., Fuhrken, P., Eklund, E. A., et al. (2007). HoxA10 activates transcription of the gene encoding mitogen-activated protein kinase phosphatase 2 (Mkp2) in myeloid cells. *J. Biol. Chem.* 282, 16164–16176. doi: 10.1074/jbc.m610556200
- Wang, Q., Li, G., Li, B., Chen, Q., Lv, D., Liu, J., et al. (2016). Sevoflurane represses the self-renewal ability by regulating miR-7a/b/Klf4 signalling pathway in mouse embryonic stem cells. *Cell Prolif.* 49, 609–617. doi: 10.1111/cpr.12283
- Warner, D. O., Zaccariello, M. J., Katusic, S. K., Schroeder, D. R., Hanson, A. C., Schulte, P. J., et al. (2018). Neuropsychological and behavioral outcomes after exposure of young children to procedures requiring general anesthesia: the Mayo Anesthesia Safety in Kids (MASK) Study. *Anesthesiology* 129, 89–105. doi: 10.1097/aln.0000000000002232
- Wattanapanitch, M., Klinkumhom, N., Potirat, P., Amornpisutt, R., Lorthongpanich, C., U-pratya, Y., et al. (2014). Dual small-molecule targeting of SMAD signaling stimulates human induced pluripotent stem cells toward neural lineages. *PLoS One* 9:e106952. doi: 10.1371/journal.pone.0106952
- Xue, Z., Huang, K., Cai, C., Cai, L., Jiang, C. Y., Feng, Y., et al. (2013). Genetic programs in human and mouse early embryos revealed by single-cell RNA sequencing. *Nature* 500, 593–597. doi: 10.1038/nature12364
- Yi, X., Cai, Y., Zhang, N., Wang, Q., and Li, W. (2016). Sevoflurane inhibits embryonic stem cell self-renewal and subsequent neural differentiation by modulating the let-7a-Lin28 signaling pathway. *Cell Tissue Res.* 365, 319–330. doi: 10.1007/s00441-016-2394-x
- Zaccariello, M. J., Frank, R. D., Lee, M., Kirsch, A. C., Schroeder, D. R., Hanson, A. C., et al. (2019). Patterns of neuropsychological changes after general anaesthesia in young children: secondary analysis of the Mayo Anesthesia Safety in Kids study. *Br. J. Anaesth.* 122, 671–681. doi: 10.1016/j.bja.2019.01.022
- Zhang, L., Xue, Z., Liu, Q., Liu, Y., Xi, S., Cheng, Y., et al. (2019a). Disrupted (folate) metabolism with anesthesia leads to myelination deficits mediated by epigenetic regulation of ERMN. *EBioMedicine* 43, 473–486. doi: 10.1016/j.ebiom.2019.04.048
- Zhang, L., Yan, J., Liu, Q., Xie, Z., and Jiang, H. (2019b). LncRNA Rik-. (203). contributes to anesthesia neurotoxicity via microRNA-101a-3p and GSK-3beta-mediated neural differentiation. *Sci. Rep.* 9:6822.
- Zhang, L., Zhang, Y., Hu, R., Yan, J., Huang, Y., Jiang, J., et al. (2015). Isoflurane Inhibits Embryonic Stem Cell Self-Renewal and Neural Differentiation Through miR-9/E-cadherin Signaling. *Stem Cells Dev.* 24, 1912–1922. doi: 10.1089/scd.2014.0397
- Zhang, Y., Dong, Y., Zheng, H., Shie, V., Wang, H., Busscher, J. J., et al. (2013). Sevoflurane inhibits neurogenesis and the Wnt-catenin signaling pathway in mouse neural progenitor cells. *Curr. Mol. Med.* 13, 1446–1454. doi: 10.2174/15665240113139990073

Conflict of Interest: The authors declare that the research was conducted in the absence of any commercial or financial relationships that could be construed as a potential conflict of interest.

Copyright © 2020 Yan, Li, Cheng, Zhang, Zhou, Zhang and Jiang. This is an open-access article distributed under the terms of the Creative Commons Attribution License (CC BY). The use, distribution or reproduction in other forums is permitted, provided the original author(s) and the copyright owner(s) are credited and that the original publication in this journal is cited, in accordance with accepted academic practice. No use, distribution or reproduction is permitted which does not comply with these terms.



Citicoline Protects Auditory Hair Cells Against Neomycin-Induced Damage

OPEN ACCESS

Edited by:

Eiman Aleem,

The University of Arizona College of Medicine - Phoenix, United States

Reviewed by:

Yibo Luo,

The University of Toledo, United States

Pietro Gareri,

Center for Cognitive Disorders and Dementia, Asp Catanzaro, Italy

Pawel Grieb,

Mossakowski Medical Research Centre, Polish Academy of Sciences, Poland

*Correspondence:

Yilai Shu

yilai_shu@fudan.edu.cn

Renjie Chai

renjiiec@seu.edu.cn

Xia Gao

xiagaogao@hotmail.com

† These authors have contributed equally to this work

Specialty section:

This article was submitted to

Cell Growth and Division,

a section of the journal

Frontiers in Cell and Developmental Biology

Received: 02 April 2020

Accepted: 13 July 2020

Published: 31 August 2020

Citation:

Zhong Z, Fu X, Li H, Chen J, Wang M, Gao S, Zhang L, Cheng C, Zhang Y, Li P, Zhang S, Qian X, Shu Y, Chai R and Gao X (2020) Citicoline Protects Auditory Hair Cells Against Neomycin-Induced Damage. *Front. Cell Dev. Biol.* 8:712. doi: 10.3389/fcell.2020.00712

Zhenhua Zhong^{1,2†}, Xiaolong Fu^{3†}, He Li^{4†}, Jie Chen^{1†}, Maohua Wang⁵, Song Gao⁶, Liyan Zhang³, Cheng Cheng¹, Yuan Zhang³, Peipei Li⁷, Shasha Zhang³, Xiaoyun Qian¹, Yilai Shu^{8*}, Renjie Chai^{3,9,10,11*} and Xia Gao^{1*}

¹ Jiangsu Provincial Key Medical Discipline (Laboratory), Department of Otolaryngology Head and Neck Surgery, Nanjing Drum Tower Hospital Clinical College of Nanjing Medical University, Nanjing, China, ² Department of Otolaryngology, Head and Neck Surgery, The Affiliated Hospital of Yangzhou University, Yangzhou University, Yangzhou, China, ³ MOE Key Laboratory for Developmental Genes and Human Disease, Jiangsu Province High-Tech Key Laboratory for Bio-Medical Research, Institute of Life Sciences, Southeast University, Nanjing, China, ⁴ Department of Otolaryngology-Head and Neck Surgery, First Affiliated Hospital of Wenzhou Medical University, Wenzhou, China, ⁵ Department of Otolaryngology, Head and Neck Surgery, Xiangya School of Medicine, Central South University, Changsha, China, ⁶ Department of Otolaryngology, Affiliated People's Hospital of Jiangsu University, Zhenjiang, China, ⁷ School of Life Sciences, Shandong University, Jinan, China, ⁸ ENT Institute and Department of Otorhinolaryngology, Eye & ENT Hospital, State Key Laboratory of Medical Neurobiology, Institute of Biomedical Sciences, NHC Key Laboratory of Hearing Medicine, Fudan University, Shanghai, China, ⁹ Co-innovation Center of Neuroregeneration, Nantong University, Nantong, China, ¹⁰ Institute for Stem Cell and Regeneration, Chinese Academy of Sciences, Beijing, China, ¹¹ Beijing Key Laboratory of Neural Regeneration and Repair, Capital Medical University, Beijing, China

Aminoglycoside-induced hair cell (HC) loss is one of the most important causes of hearing loss. After entering the inner ear, aminoglycosides induce the production of high levels of reactive oxygen species (ROS) that subsequently activate apoptosis in HCs. Citicoline, a nucleoside derivative, plays a therapeutic role in central nervous system injury and in neurodegenerative disease models, including addictive disorders, stroke, head trauma, and cognitive impairment in the elderly, and has been widely used in the clinic as an FDA approved drug. However, its effect on auditory HCs remains unknown. Here, we used HC-like HEI-OC-1 cells and whole organ explant cultured mouse cochleae to explore the effect of citicoline on aminoglycoside-induced HC damage. Consistent with previous reports, both ROS levels and apoptosis were significantly increased in neomycin-induced cochlear HCs and HEI-OC-1 cells compared to undamaged controls. Interestingly, we found that co-treatment with citicoline significantly protected against neomycin-induced HC loss in both HEI-OC-1 cells and whole organ explant cultured cochleae. Furthermore, we demonstrated that citicoline could significantly reduce neomycin-induced mitochondrial dysfunction and inhibit neomycin-induced ROS accumulation and subsequent apoptosis. Thus, we conclude that citicoline can protect against neomycin-induced HC loss by inhibiting ROS aggregation and thus preventing apoptosis in HCs, and this suggests that citicoline might serve as a potential therapeutic drug in the clinic to protect HCs.

Keywords: citicoline, hair cell, apoptosis, reactive oxygen species, aminoglycosides

INTRODUCTION

Sensorineural hearing loss remains a serious sensory disorder worldwide. Once the hair cells (HCs) of the inner ear are damaged, sensorineural hearing loss is permanent due to the inability of mammalian HCs to regenerate. The causes of hearing loss include many factors, such as noise, age, and ototoxic drugs, all of which can induce apoptosis in HCs (Prasad and Bondy, 2020). Damage caused by aminoglycosides, which are the most commonly used ototoxic drugs, is a major cause of HC death (Waguespack and Ricci, 2005). Therefore, it is important to investigate the molecular mechanism behind aminoglycoside-induced auditory sensory cell damage and to seek effective drugs for preventing and treating aminoglycoside-induced deafness. Several studies have suggested that aminoglycosides induce intrinsic apoptosis of HCs through oxidative stress (Mangiardi et al., 2004; Coffin et al., 2013; Sun et al., 2014, 2015; Liu et al., 2016), while others have reported that the accumulation of reactive oxygen species (ROS) plays an important role in the death of HCs (Clerici et al., 1996; Choung et al., 2009). ROS can be cleared by physiological cellular processes; however, they are harmful when their concentration exceeds the cell's capacity to remove them (He et al., 2020). Thus, the survival of HCs requires a balance between oxidative stress and anti-oxidation (Franco and Cidlowski, 2009; Filomeni et al., 2015), suggesting that preventing the accumulation of ROS might be a potential treatment for preventing ototoxicity.

Citicoline, a nucleoside derivative, is an essential endogenous intermediate in phosphatidylcholine biosynthetic pathways. Citicoline is widely distributed in the body, and it can easily cross the blood-brain barrier and penetrate brain cells to provide neural protection (Secades and Lorenzo, 2006). It has been widely demonstrated that citicoline can activate the biosynthesis of phospholipids in neuronal membranes, and this stimulates brain metabolism and the neurotransmitter system (Secades and Lorenzo, 2006). It also plays an important role in promoting the recovery of brain function and in awakening from sleep (Adibhatla et al., 2002). When used as a long-term medication, citicoline is a safe and well-tolerated drug without significant systemic side effects. Citicoline can be used to treat addictive disorders (Wignall and Brown, 2014), stroke, head trauma (Saver, 2008), and cognitive impairment in the elderly (Cotroneo et al., 2013), and it is also effective in the treatment of glaucoma (Parisi et al., 2008). In addition, citicoline has anti-apoptotic effects by disrupting mitochondria-dependent cell death mechanisms and promoting the regeneration of nerve axons, and it can protect retinal ganglion cells from damage (Oshitari et al., 2002).

There have been no reports on whether citicoline can protect auditory HCs from aminoglycoside-induced injury up to now. In our study, we used the HC-like House Ear Institute Organ of Corti 1 (HEI-OC-1) cell line along with explant cultured cochlear HCs to establish an *in vitro* neomycin-induced damage model in auditory HCs with the aim to investigate the potential protective effect of citicoline in auditory HCs.

MATERIALS AND METHODS

Animals

All animal procedures were performed according to protocols approved by the Animal Care and Use Committee of Southeast University, and all efforts were made to minimize the number of animals used and to prevent their suffering.

Cell Cultures and Tissue Cultures

Consistent with previous studies, we used HEI-OC1 (House Ear Institute-organ of Corti 1) cells derived from long-term cultures of Immortomouse cochleae. HEI-OC1 cells express *Atoh1*, *Prestin*, *Myo7a*, and other cellular markers specific for auditory sensory HCs when cultured either under permissive or non-permissive conditions. The cells were cultured in DMEM containing 10% fetal bovine serum and 100 IU/ml penicillin (A0166, Sigma-Aldrich, St. Louis, United States) at 37°C and 5% CO₂ (Kalinec et al., 2003; He et al., 2020) and sub-cultured at 80% confluency using 0.25% trypsin/EDTA (25200056, Life Technologies, Waltham, MA, United States). Neomycin (N6386, Sigma-Aldrich) was used at a final concentration of 10 mM to damage the HEI-OC-1 cells. Citicoline (C0256, Sigma-Aldrich) was used at a final concentration of 10 μM to treat the HEI-OC-1 cells.

Cochleae were dissected from postnatal day (P)3 mice and cultured as previously reported (Chen et al., 2013). The explant cultured tissue was pretreated with 10 μM citicoline for 12 h, then 0.5 mM neomycin was added for 12 h to damage the HCs. After removal of the neomycin, the tissues were recovered in serum-free medium for an additional 12 h together with 10 μM citicoline. Animal experiments were conducted in accordance with the guidelines of the Committee of Animal Protection and Utilization of Southeast University and were approved by the Animal Experimental Ethics Committee of Southeast University.

Real-Time PCR

Total RNA was extracted from HEI-OC-1 cells or whole cochleae with Trizol reagent (PR910, Protein Biotechnology, Beijing, China), and the integrity of the RNA samples was evaluated by OD260/280 measurements. cDNA was obtained using the Revertaid First Strand cDNA Synthesis Kit (K1622, Thermo Fisher Scientific) according to the manufacturer's protocol. Real-time PCR was performed on a Biosystems CFX96 real-time PCR system (Bio-Rad, Hercules, CA, United States) using SYBR Green qRT-PCR Master Mix (4913850001, Roche Life Science, Basel, Switzerland). The primer sequences are listed in **Table 1**. The qRT-PCR conditions were as follows: initial denaturing for 15 s at 95°C followed by 40 cycles of denaturation at 95°C for 15 s, annealing at 60°C for 60 s, and extension at 72°C for 20 s. The mRNA expression values of the genes of interest were normalized to the mRNA expression of *Gapdh*. The results were calculated using the comparative cycle threshold ($\Delta\Delta Ct$) method.

TABLE 1 | PCR sequences used in the experiments.

| Gene | Forward sequence | Reverse sequence |
|-----------|----------------------|----------------------|
| Caspase-3 | AATCATGCCATTTGCCAGC | CTCAAGTGTGTAGGGGAGG |
| Caspase-8 | AGCCTATGCCACCTAGTGAT | GGAGAGCTGTAACTGTGCG |
| Bcl-2 | GGTGAAGTGGGGGAGGATTG | AGAGCGATGTTGTCCACCAG |
| Caspase-9 | CCTAGTGAGCGAGCTGCAAG | ACCGCTTTGCAAGAGTGAAG |
| Bax | TGAAGACAGGGGCTTTTTG | AATTCGCGGAGACACTCG |
| Alox15 | TCGGGACTCGGAAGCAGAAT | CCCATCGGTAACAGGGGAAC |
| Gsr | TGCACTTCCCGGTAGGAAAC | GATCGCAACTGGGTGAGAA |
| Sod1 | GGAGCAAGGTGCTTACAGA | AGTGACAGCGTCCAAGCAAT |
| Glrx | AGTCTGGAAGGTGGTCTGTG | CCATTAGCATGGCTGACGA |
| GADPH | GCAAGAGAGAGGCCCTCAG | TGTGAGGAGATGCTCAGTG |

Cell Number Analysis

HEI-OC-1 cells were incubated in 96-well plates for 24 h at a concentration of 2,000 cells/well in three replicates, and different drugs were added (controls received a similar volume of DMEM). The Cell Counting Kit (CCK-8; CC201, Protein Biotechnology, Beijing, China) was used to determine the cell viability at different time points after incubation or at different concentrations. After exposing the cochleae to citicoline and/or neomycin, the immunostained cells were quantified per 100 μ m in all three turns of the cochlea. The numbers of positive cells were counted in equal lengths from the apical to the basal turns of the cochlea.

Western Blot

The HEI-OC-1 cell line and cochlear tissue were lysed with ice-cold RIPA lysis buffer (PP109, Protein Biotechnology) plus Phosphatase Inhibitor Cocktails (04693132001, Roche) for 30 min at 4°C. Protein concentrations were determined using a BCA Protein Quantification Kit (PP202, Protein Biotechnology) according to the manufacturer's instructions. Equal amounts of protein were loaded onto a 12% Tris-glycine SDS-PAGE gel, separated at 120 volts for 1.5 to 2 h, and then transferred to a nitrocellulose membrane and blocked with 5% milk in PBST [1 \times PBS with 0.1% Triton X-100 (Solarbio, 1109F0521)] buffer. Cleaved caspase 3 was evaluated using anti-cleaved caspase 3 rabbit monoclonal antibody (1:1,000 dilution, 9664S, Cell Signaling Technology), and β -actin was measured using a mouse monoclonal antibody (1:5,000 dilution, ab119716, Abcam, Cambridge, United Kingdom). Peroxidase-conjugated goat anti-rabbit or anti-mouse immunoglobulin G (ab6789 and ab6721, Abcam) was used as the secondary antibody. The proteins were detected using a SuperSignal West Dura chemiluminescent substrate kit (34075, Thermo Scientific) according to the manufacturer's instructions. Semi-quantification of the western blot results was done by measuring the intensities of the bands using ImageJ.

Immunofluorescence

Anti-cleaved caspase 3 antibody (1:400 dilution, 9664S, Cell Signaling Technology), MitoSOX Red (M36008, Life Technologies), tetramethylrhodamine ethyl ester perchlorate

(TMRE, Sigma-Aldrich), anti-Myo7A antibody (1:1,000 dilution, 25–6790, Proteus Bioscience), anti-voltage dependent anion channel1 (VDAC1) polyclonal antibody (1:200 dilution, 10866-1-AP, Proteintec), and DAPI (1:1,000 dilution, C0060, Solarbio) were used to analyze apoptotic cells, measure ROS, stain HCs, measure mitochondrial number, and stain nuclei, respectively. Briefly, cells and cochlear tissues were fixed in 4% paraformaldehyde (158127, Sigma-Aldrich) for 1 h then washed three times with PBST [1 \times PBS with 0.1% Triton X-100 (Solarbio, 1109F0521)] and incubated for 1 h in blocking medium (PBS with 10% heat-inactivated donkey serum, 1% Triton X-100, 1% BSA, and 0.02% sodium azide at pH 7.2) at room temperature. The samples were marked with primary antibody diluted in PBT-1 (PBS with 10% Triton X-100, 5% heat-inactivated donkey serum, 1% BSA, and 0.02% sodium azide at pH 7.2) for overnight at 4°C. After washing three times with PBST, the samples were marked with the secondary antibody diluted in PBT-2 (PBS with 1% BSA and 0.1% Triton X-100 at pH 7.2) for 1 h. The samples were washed again three times and were imaged by confocal fluorescence microscopy (Leica SP5, Heidelberg, Germany).

The TUNEL Kit (11684817910, Roche, Indianapolis, IN, United States) was used to detect apoptotic cells following the manufacturer's instructions. TMRE was used for measuring the mitochondrial membrane potential (MMP), and Mito-SOX Red was used to analyze ROS levels. Briefly, the culture medium was removed from the dish and the samples were washed with PBS. The samples were then cultured in DMEM containing Mito-SOX Red or TMRE at 37°C for 30 min. The samples were then washed in pre-warmed PBS and imaged with a confocal microscope (LSM700; Zeiss, Heidenheim, Germany).

Flow Cytometry

Annexin V-FITC and propidium iodide (C1062, Beyotime) were used for apoptosis analysis following the manufacturer's instructions. After treating the HEI-OC-1 cells with citicoline and/or drugs, the cells were trypsinized and collected and then washed twice with PBS and resuspended in binding buffer at a concentration of 1×10^6 cells/ml. Annexin V-FITC and propidium iodide were added and gently mixed with the cells and incubated at room temperature for 10–20 min in the dark. Cells were analyzed as quickly as possible by flow cytometry (FACSCanto, BD, San Jose, CA, United States).

Mito-SOX Red and TMRE were used to analyze ROS production and to measure the MMP, respectively. After treating the HEI-OC-1 cells with citicoline and/or neomycin, the cells were trypsinized, collected, and resuspended in pre-warmed solution containing Mito-SOX Red or TMRE for 10 min. Following this, the cells were washed with PBS and analyzed by flow cytometry. All experiments were repeated at least three times.

Statistical Analysis

All data are shown as mean \pm standard deviation (SD), and all experiments were repeated at least three times. Statistical analyses were performed using Microsoft Excel and GraphPad Prism 6 software (La Jolla, CA, United States). For the cochlear tissue

culture experiments, “n” represents the number of independent cochleae, and for all HEI-OC-1 cell culture experiments “n” represents the number of replicates. When comparing two groups, a two-tailed, unpaired Student’s *t*-test was used to determine statistical significance. When comparing more than two groups, one-way ANOVA was used followed by Dunnett’s multiple comparison test. A *p*-value < 0.05 was considered to be statistically significant.

RESULTS

The Survival of HEI-OC-1 Cells Is Affected by Neomycin and Citicoline Treatment

To select the proper conditions to induce cell death in HEI-OC-1 cells, we exposed HEI-OC-1 cells to different doses of neomycin (1–20 mM) for different times (0–24 h). We found that the viability of HEI-OC-1 cells decreased gradually with increasing neomycin doses and time, and 50–60% of the HEI-OC-1 cells were alive after being treated with 10 mM neomycin for 24 h. Thus we chose this condition to induce HEI-OC-1 cell damage (Supplementary Figures S1A,B). Because there are no reports of using citicoline to protect against ototoxic drug-induced HC loss, we first determined the appropriate dose and treatment time of citicoline in HEI-OC-1 cells before neomycin exposure. We pre-treated the HEI-OC-1 cells with different concentrations of citicoline (1, 10, 100 μ M, 1 mM, and 2 mM) for different times (6, 12, and 24 h, respectively) and then treated the cells with 10 mM neomycin together with citicoline (the same concentration as pre-treatment) for 24 h. The CCK8 results showed that there was no protective effect of citicoline when added 6 h in advance, but there was a clear protective effect when citicoline was added 12 or 24 h in advance. Additionally, the viability of HEI-OC-1 cells gradually increased with low concentrations of citicoline, but once the concentration of citicoline was higher than 10 μ M the viability of HEI-OC-1 cells began to decrease. We also found that there was no significant difference in cell viability with the different pretreatment times (12 and 24 h). Therefore, we chose 10 μ M citicoline pretreatment for 12 h as the optimal treatment condition in this study (Supplementary Figures S1C–F).

Citicoline Treatment Protects HCs in Whole Organ Cultured Cochleae Against Neomycin Injury

Cochleae from P3 mice were used to investigate the role of citicoline in cochlear HCs after neomycin treatment (Figure 1A). We first used Myo7A and DAPI staining to observe the changes in the numbers of HCs in the apical, middle, and basal turns of the cochlea after different treatments. We found that the number of Myo7A and DAPI double-positive cells per 100 μ m of cochlear length of the apical, middle, and basal turns was significantly lower in the neomycin-only group than in the undamaged controls (Figures 1B,C). In contrast, the number of double-positive cells was significantly increased in

the citicoline-treated group compared with the neomycin-only group (Figures 1B,C).

Citicoline Reduces Apoptosis in Cochlear HCs After Neomycin Exposure

Next, we explored the role of citicoline in neomycin-induced HC injury. Previous studies have shown that cleaved caspase 3 and TUNEL can be used as markers for apoptosis induced by aminoglycosides (Matsui et al., 2002; Coffin et al., 2013; He et al., 2014). Therefore, immunofluorescence staining was used to evaluate the expression of cleaved caspase 3 and TUNEL in cochlear HCs after citicoline pretreatment. The results showed that the numbers of cleaved caspase 3-positive cells and TUNEL-positive cells per 100 mm of the cochlea in the middle turn were significantly increased in the neomycin-treated group compared with the undamaged controls (Figures 2A–D). Moreover, the citicoline-pretreated cochleae showed significantly lower numbers of caspase 3-positive cells and TUNEL-positive cells than the neomycin-only group (Figures 2A–D). Western blot results also showed that the expression levels of cleaved caspase 3 in the neomycin-only group were higher than in the undamaged controls (Figures 2E,F), while they were significantly decreased in the citicoline-treated group compared with the neomycin-only group (Figures 2E,F).

We also performed quantitative real-time polymerase chain reaction (qRT-PCR) to investigate the expression of apoptosis-related genes in the cochlea after citicoline treatment. Compared with the undamaged controls, the expression of the intrinsic and extrinsic pro-apoptotic genes *Casp3*, *Casp8*, and *Casp9* was significantly increased in the neomycin-only group, while the expression of the anti-apoptotic gene *Bcl2* was significantly decreased and expression of the pro-apoptotic gene *Bax* was not significantly different (Figure 2G). Notably, citicoline treatment significantly downregulated the expression of the pro-apoptotic genes *Bax*, *Casp3*, *Casp8*, and *Casp9* after neomycin exposure (Figure 2G). Together, these results suggest that citicoline reduces apoptosis in cochlear HCs after neomycin exposure.

Citicoline Reduces Apoptosis in HEI-OC-1 Cells After Neomycin Exposure

To investigate the role of citicoline in neomycin-induced death in HEI-OC-1 cells, the cells were pretreated with 10 μ M citicoline for 12 h and then treated with 10 mM neomycin along with citicoline for 24 h and allowed to recover in culture medium for another 12 h together with citicoline (Figure 3A). We labeled the dead cells with propidium iodide and labeled the cells undergoing apoptosis with Annexin V. The percentage of apoptotic cells was significantly higher after neomycin treatment compared to the undamaged group, while the percentage was significantly reduced in the citicoline-treated group compared with the neomycin-only group (Figures 3B,C). To verify this result, we performed TUNEL staining to further detect apoptosis in HEI-OC-1 cells. TUNEL staining showed that the proportion of TUNEL-positive cells in the neomycin-induced group was significantly higher than in the undamaged group, while the citicoline-treated group showed significantly lower percentages of

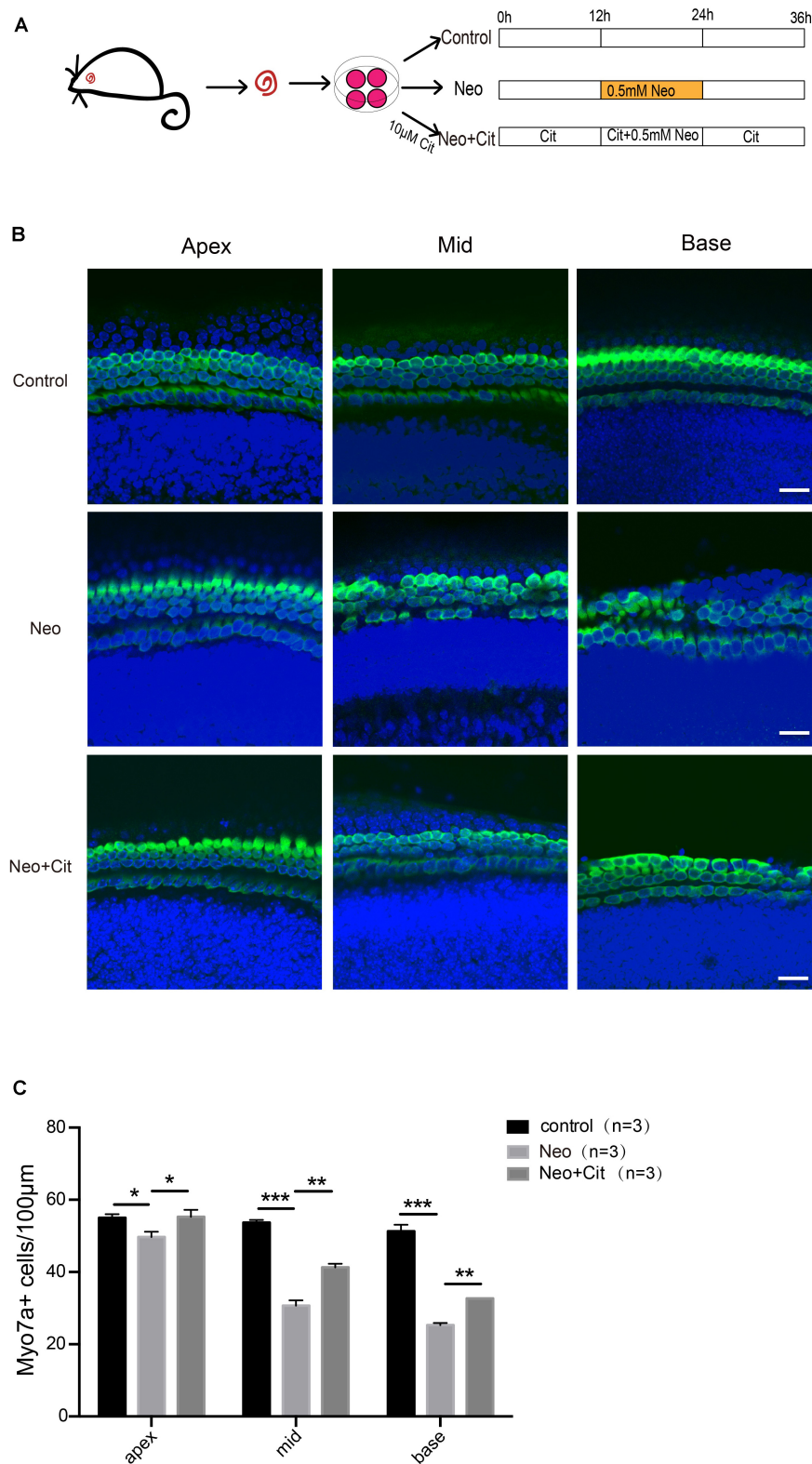
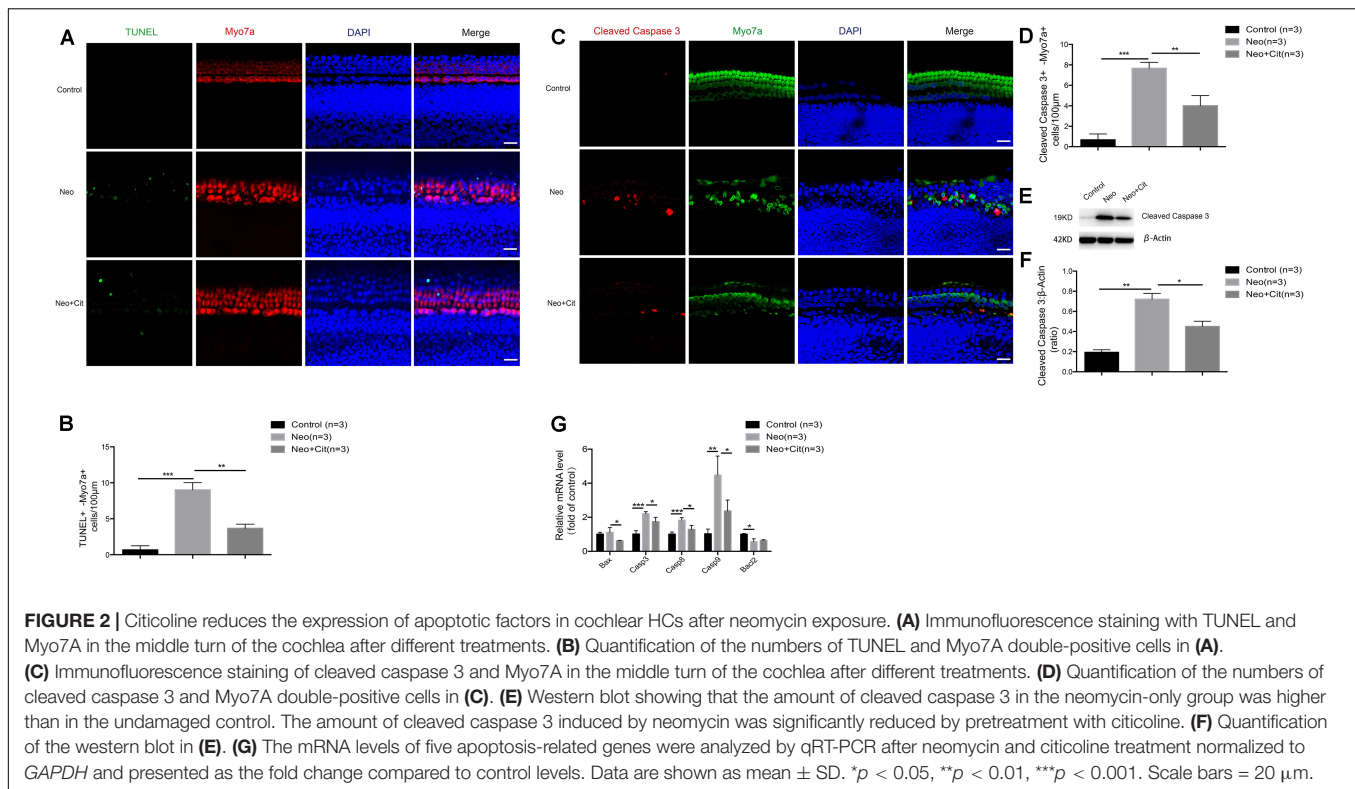


FIGURE 1 | Citicoline protects against apoptosis in cochlear HCs after neomycin injury. **(A)** Schematic diagram of drug addition in tissue culture.

(B) Immunofluorescence staining with Myo7A (green) and DAPI (blue) in the apical, middle, and basal turns of the cochlear explant cultures with different treatments.

(C) Quantification of the numbers of Myo7A and DAPI double-positive cells in **(B)**. Data are shown as mean \pm SD. * $p < 0.05$, ** $p < 0.01$, *** $p < 0.001$. Scale bars = 20 μ m.



TUNEL-positive cells compared with the neomycin-only group (Figures 3D,E). Together, these results show that citicoline decreases apoptosis in HEI-OC-1 cells after neomycin exposure.

Citicoline Reduces the Expression of Apoptotic Factors in HEI-OC-1 Cells After Neomycin Injury

We further studied the impact of citicoline on the expression of pro-apoptotic and anti-apoptotic factors in HEI-OC-1 cells after neomycin injury. Immunofluorescence staining indicated that the percentage of cleaved caspase 3-positive cells was significantly higher in the neomycin-only group compared with the undamaged controls (Figures 4A,B), but citicoline-treated cells showed a significantly reduced percentage of cleaved caspase 3-positive cells compared to the neomycin-only group (Figures 4A,B). Consistent with these results, we found that the protein levels of cleaved caspase 3 in HEI-OC-1 cells was significantly increased after neomycin treatment compared with the undamaged controls, and the protein levels were significantly reduced by citicoline pretreatment (Figures 4C,D). Furthermore, qRT-PCR analysis showed that the anti-apoptotic factor *Bcl-2* was significantly decreased in the neomycin-only group, while the expression of intrinsic and extrinsic pro-apoptotic marker genes, including *Bax*, *Casp3*, *Casp8*, and *Casp9*, was significantly higher compared to the undamaged controls (Figure 4E). In the citicoline-treated group, the expression levels of these intrinsic and extrinsic pro-apoptotic factors were significantly decreased, and expression of the anti-apoptotic factor *Bcl-2* was significantly higher compared to the neomycin-only group

(Figure 4E). Together, our results suggested that citicoline is involved in neomycin-induced HEI-OC-1 apoptosis by inhibiting the expression of both intrinsic and extrinsic apoptotic factors.

Citicoline Attenuates Oxidative Stress in Cochlear HCs After Neomycin Injury

In this experiment, we sought to determine the relationship between citicoline and oxidative stress in cochlear HCs. We dissected and cultured the basilar membranes from P3 mice and treated them with neomycin together with citicoline, and Mito-SOX Red was used to measure mitochondrial ROS levels in the cochlea. Quantification of Mito-SOX Red colocalization with Myo7A showed that the ROS levels were increased in the cochlea after neomycin treatment compared with the undamaged group, and the citicoline-treated cochlea showed significantly lower ROS levels compared to the neomycin-only group (Figures 5A,B).

We next performed qRT-PCR to measure the mRNA expression of redox-related genes in cochlear HCs after neomycin treatment. We found that the expression of the antioxidant genes *Gsr*, *Sod1*, and *Glrx* was significantly decreased in cochlear HCs after neomycin exposure compared with undamaged controls, and the pro-oxidant factor *Alox15* was significantly increased in the neomycin-only group (Figure 5C). We then measured the expression of these genes after treatment with citicoline. We found that the expression of the antioxidant genes *Gsr*, *Sod1*, and *Glrx* was significantly increased and the pro-oxidant factor *Alox15* was significantly reduced compared with the neomycin-only group (Figure 5C).

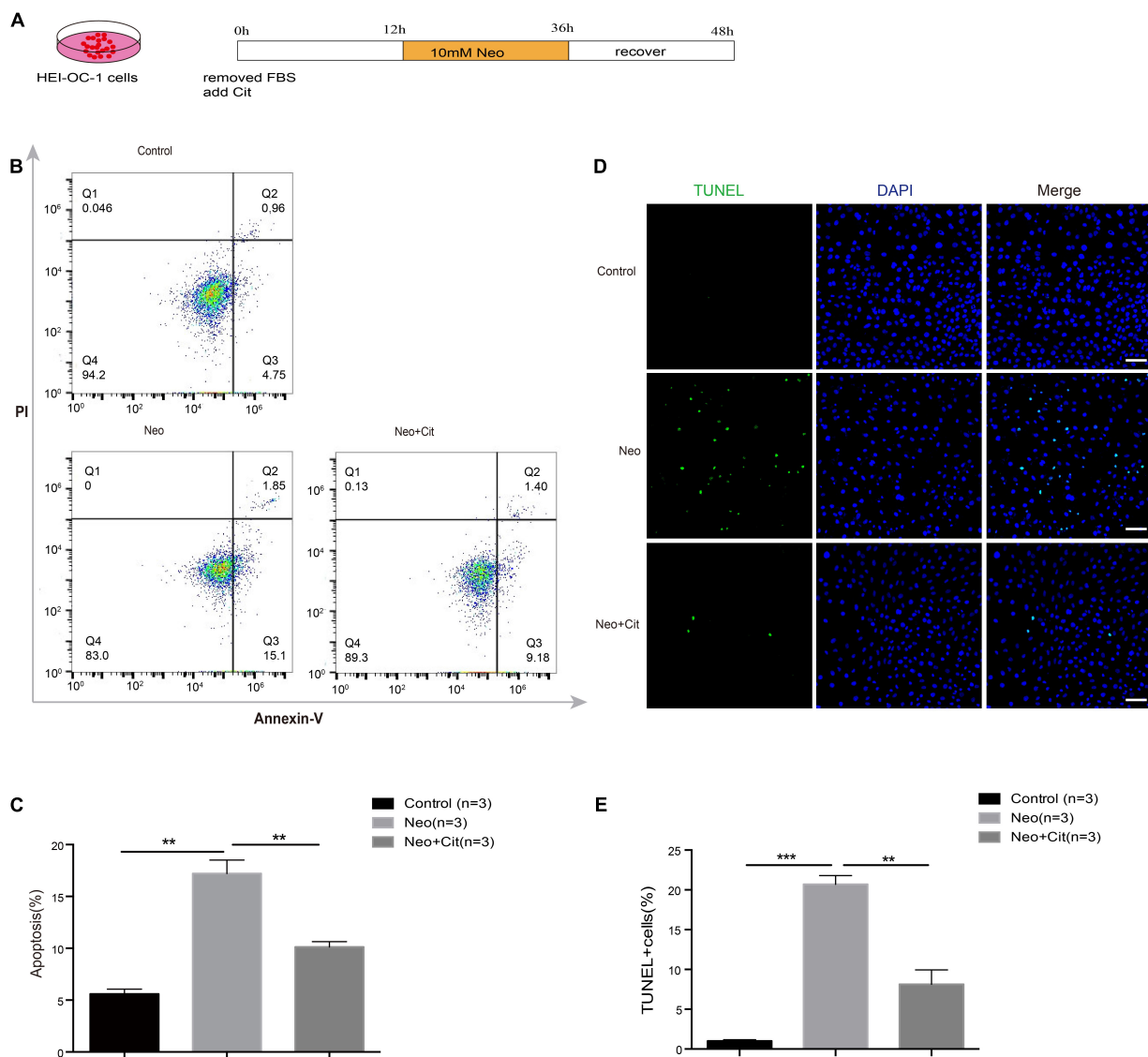


FIGURE 3 | Citicoline protects against apoptosis in HEI-OC-1 cells after neomycin exposure. **(A)** Schematic diagram of citicoline (Cit) and neomycin addition in cell culture. **(B)** Apoptosis analysis by flow cytometry after different treatments. The upper right quadrants, lower right quadrants, and lower left quadrants of the images represent late apoptotic cells, early apoptotic cells, and live cells, respectively. **(C)** Flow cytometry results showing that the percentages of apoptotic cells after neomycin treatment were significantly higher compared with the undamaged controls. The amount of apoptosis induced by neomycin was significantly reduced by pretreatment with citicoline. **(D)** TUNEL and DAPI double staining showing the apoptotic HEI-OC-1 cells after different treatments. **(E)** The number of TUNEL/DAPI double-positive cells after neomycin exposure was significantly reduced by treatment with citicoline. Data are shown as mean \pm SD. * $p < 0.05$, ** $p < 0.01$, *** $p < 0.001$. Scale bars = 20 μ m.

Citicoline Increases the Mitochondrial Membrane Potential of HEI-OC-1 Cells After Neomycin Exposure

To further explore the mechanism behind the role of citicoline in neomycin-induced apoptosis of HEI-OC-1 cells, we used TMRE kits to measure changes in the MMP in HEI-OC-1 cells using immunofluorescence staining and flow cytometry analysis. The TMRE intensity was significantly decreased after neomycin treatment compared to the undamaged control group (Figures 6A–C), and the citicoline-treated cells showed

a significantly greater TMRE intensity than the neomycin-only group (Figures 6A–C). These results demonstrated that citicoline protects HEI-OC-1 cells from apoptosis by inhibiting MMP dysfunction.

Citicoline Inhibits Neomycin-Induced Oxidative Stress in HEI-OC-1 Cells

We used Mito-SOX Red to evaluate mitochondrial ROS levels in HEI-OC-1 cells after neomycin treatment. Immunofluorescence and flow cytometry results showed that the ROS levels were

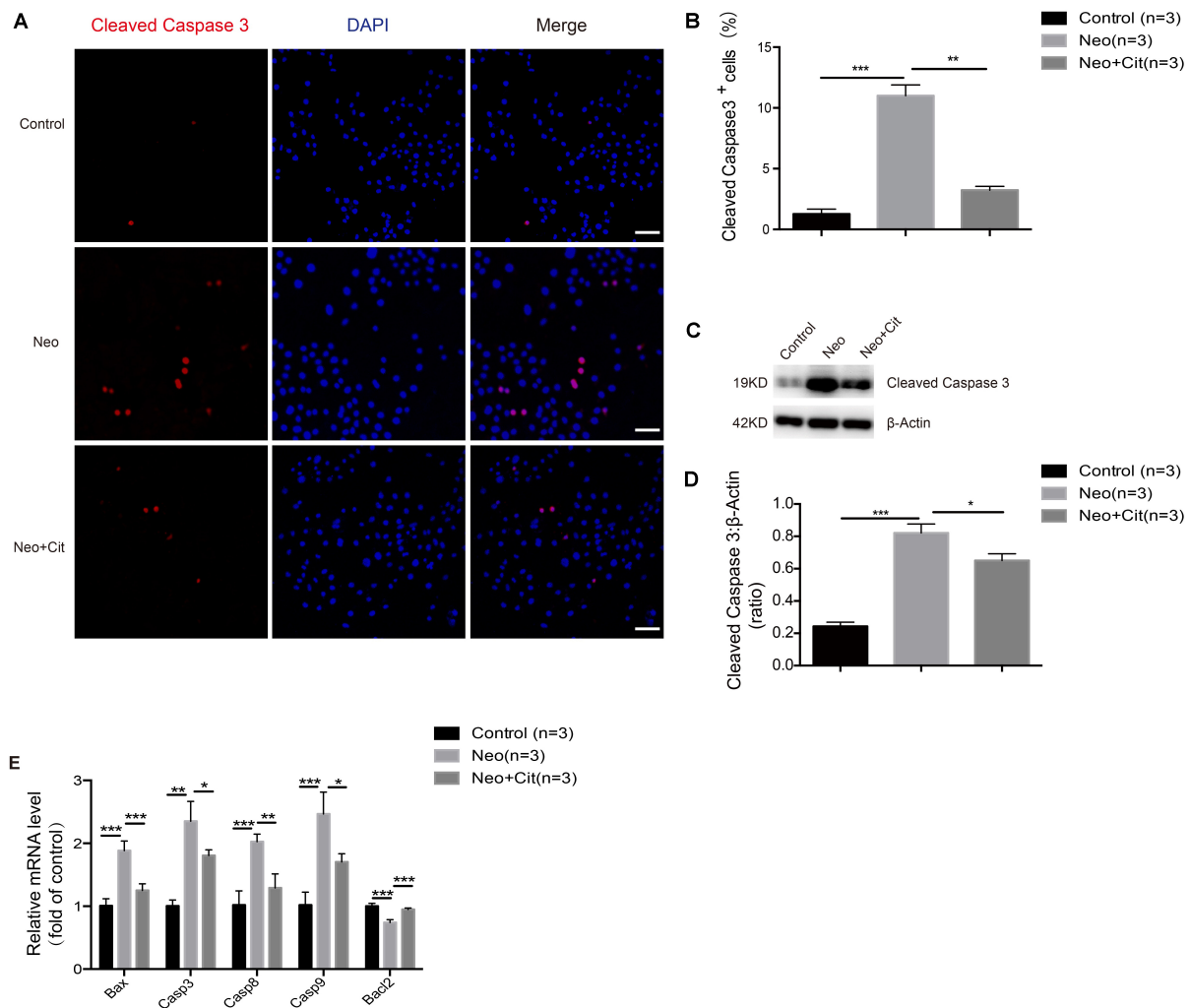


FIGURE 4 | Citicoline reduces the expression of apoptotic factors in HEI-OC-1 cells after neomycin exposure. **(A)** Cleaved caspase 3 and DAPI double staining confirmed the apoptotic cells after different treatments. **(B)** Quantification of the numbers of cleaved caspase 3 and DAPI double-positive cells in **(A)**. **(C)** Western blot showing that the amount of cleaved caspase 3 in the neomycin-only groups was higher than in the undamaged controls. The amount of cleaved caspase 3 induced by neomycin was significantly reduced by pretreatment with citicoline. **(D)** Quantification of the western blot in **(C)**. **(E)** The mRNA levels of five apoptosis-related genes were analyzed by qRT-PCR normalized to *GAPDH* and presented as the fold of control levels. Data are shown as mean \pm SD. * $p < 0.05$, ** $p < 0.01$, *** $p < 0.001$. Scale bars = 20 μ m.

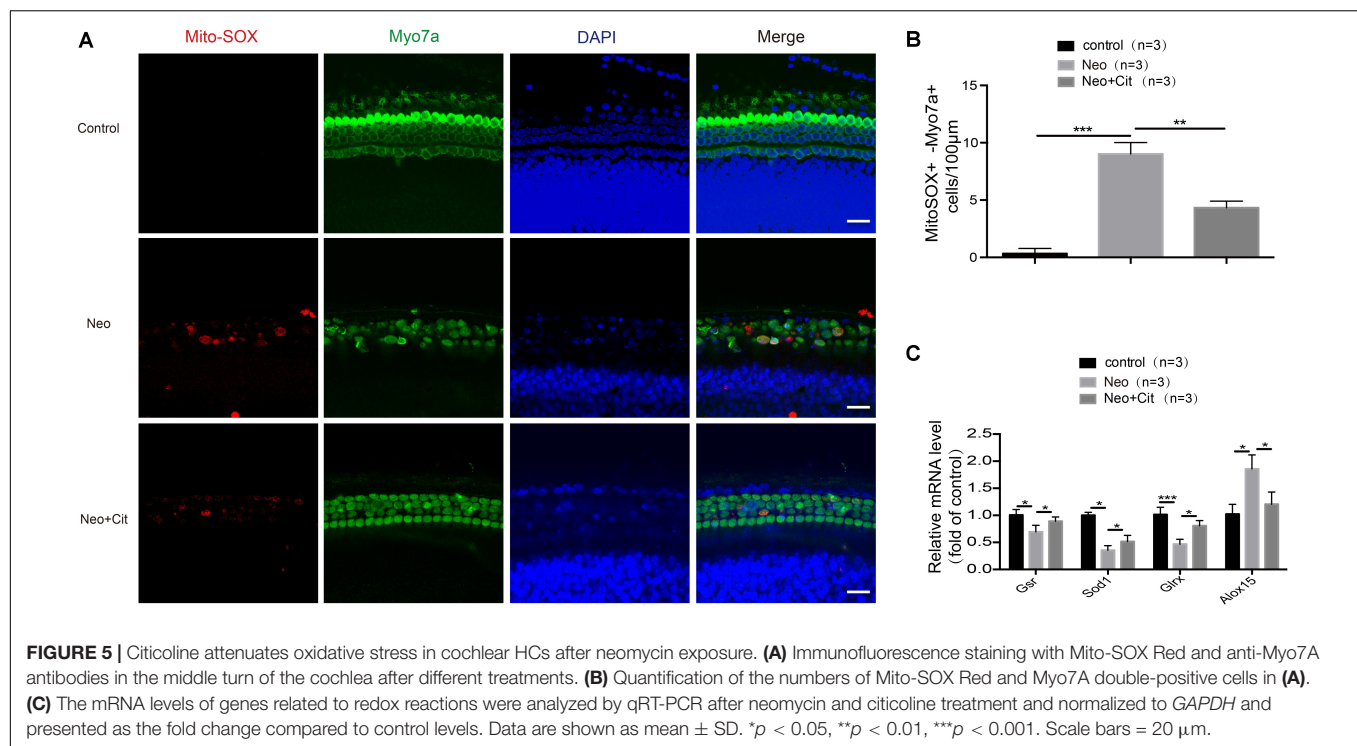
significantly increased after neomycin treatment compared with the undamaged group and were significantly reduced in the citicoline-treated group compared with the neomycin-only group (Figures 7A–C).

To further verify our findings, we analyzed the mRNA expression of four redox-related genes by qPCR. The expression of the pro-oxidant factor *Alox15* increased after neomycin treatment compared with the undamaged controls, while the antioxidant genes *Gsr*, *Sod1*, and *Glxr* were significantly decreased in the neomycin-only group (Figure 7D). In addition, treatment with citicoline significantly upregulated the expression of the antioxidant genes *Gsr*, *Sod1*, and *Glxr* and reduced the expression of the pro-oxidant factor *Alox15* compared with the neomycin-only group (Figure 7D). Our results indicated that citicoline increased the expression of antioxidant genes and

decreased the expression of pro-oxidant genes and thus reduced mitochondrial ROS levels in the cells and prevented apoptosis after neomycin injury.

Citicoline Downregulates the Expression of VDAC1 in HEI-OC-1 Cells After Neomycin Exposure

VDAC1 is a major channel protein located in the outer mitochondrial membrane, and it plays an important regulatory role in the communication between the mitochondria and other parts of the cell. Compared with the undamaged group, the neomycin-only group was characterized by the obviously enhanced VDAC1-positive staining; however, treatment with citicoline significantly downregulated the mitochondrial



fluorescence intensity (**Figures 8A,B**). The VDAC1 staining further confirmed that citicoline inhibits neomycin-induced oxidative stress by reducing mitochondrial ROS levels.

DISCUSSION

Ototoxic drugs are a common cause of sensorineural hearing loss, and aminoglycosides are the most commonly used ototoxic drugs. Cochlear HCs are susceptible to aminoglycoside-mediated cytotoxicity and cannot be regenerated once damaged, and thus aminoglycoside ototoxicity is usually associated with permanent sensorineural deafness (Nadol, 1993; Lazarou et al., 2015; Correia-Melo et al., 2017). Recent studies have reported that HCs in the mouse cochlea have a very limited ability to regenerate during the neonatal period, but this limited spontaneous HC regeneration is not sufficient to restore hearing ability once HCs are destroyed by aminoglycosides, and all regenerative ability is lost a few days after birth (Li et al., 2016; Ni et al., 2016; Waqas et al., 2016; Lu et al., 2017). To explore the mechanisms through which ototoxic drugs cause auditory sensory cell injury and to take appropriate control measures, it has become especially urgent to prevent and treat such diseases. Previous studies have shown that the toxic effects of aminoglycosides on auditory sensory cells are clearly associated with oxidative stress-induced cellular damage and the induction of apoptosis.

Citicoline, a nucleoside derivative, is an indispensable endogenous intermediate in the biosynthesis of phosphatidylcholine, which has been widely demonstrated to play a therapeutic role in the development of central nervous

system injury and neurodegenerative diseases, and citicoline has specific effects on promoting brain function recovery and in promoting wakefulness (Wignall and Brown, 2014). Citicoline is a safe and well-tolerated drug without significant systemic side effects, and it has been shown that 100 μ M of citicoline is not harmful to retinal cells (Davinelli et al., 2017), and even up to 1000 μ M citicoline is not harmful to retinal neuroglial cells *in vitro* (Matteucci et al., 2014). We found that the protective effect of citicoline is dose dependent, and the viability of HEI-OC-1 cells was highest when the concentration of citicoline was 10 μ M. We still observed the protective effect at a concentration of 100 μ M, but the protective effect began to decline significantly when the concentration of citicoline reached 1 mM. Taken together, these results confirm that citicoline is safe for HEI-OC1 cells *in vitro*, which is consistent with the good tolerability profile for citicoline in clinical studies (**Supplementary Figure S1**).

Citicoline is an old drug, and we often ignore its other functions, such as whether it also protects HCs. Previous studies focusing on nerve cells found that citicoline plays a protective role through anti-oxidation and anti-apoptosis activities (Barrachina et al., 2002; Park et al., 2006), and we hypothesized that citicoline might also have an important protective effect against aminoglycoside-induced HC injury. In this study, we investigated the role of citicoline in both neomycin-induced injury in HEI-OC-1 cells and in cochlear HCs, and we found that citicoline significantly decreased apoptosis after neomycin injury in both contexts (**Figures 1, 3**).

Apoptosis occurs via both intrinsic and extrinsic pathways (Rybak and Kelly, 2003). The aminoglycosides are believed to induce apoptosis by releasing the apoptotic enzyme activation

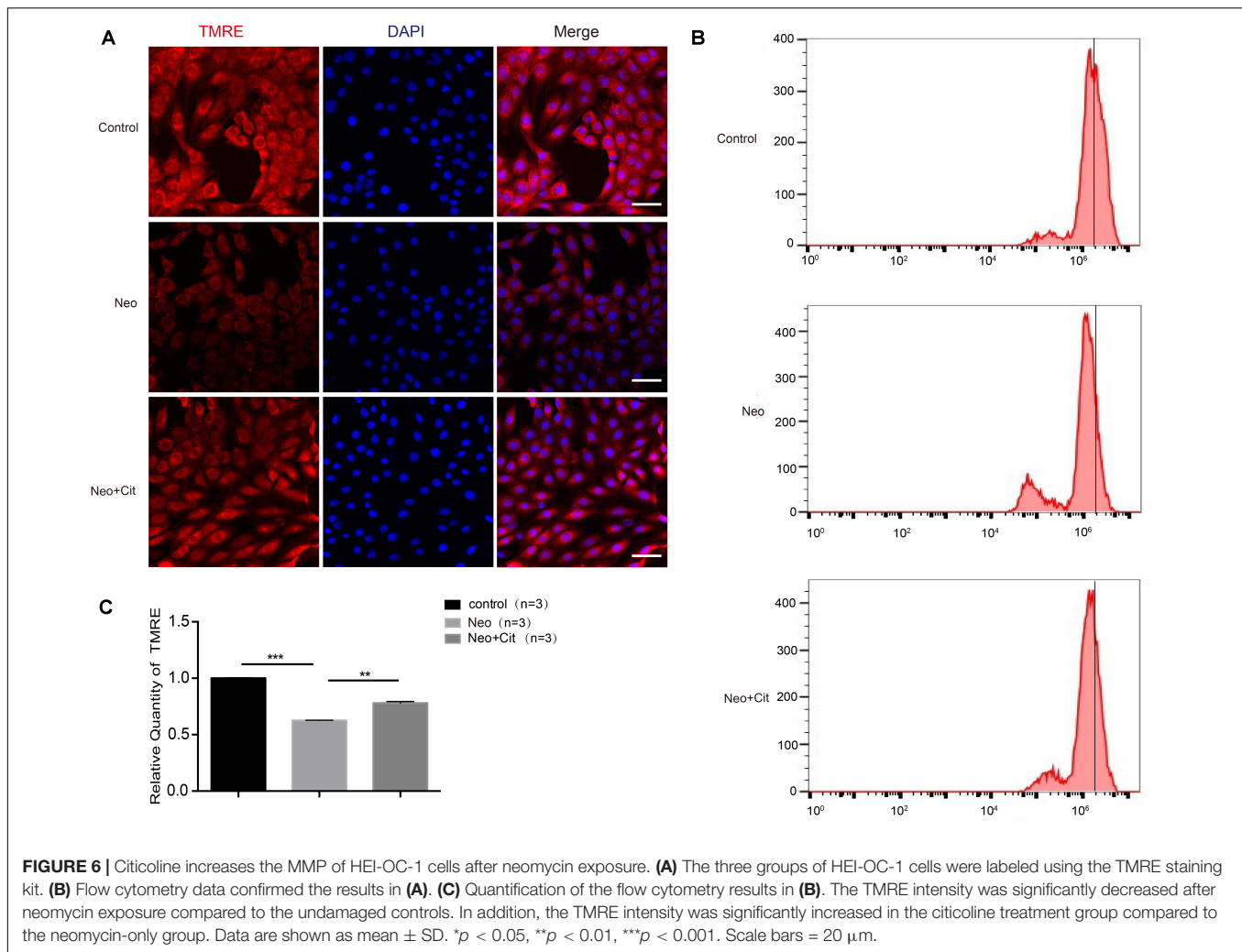


FIGURE 6 | Citicoline increases the MMP of HEI-OC-1 cells after neomycin exposure. **(A)** The three groups of HEI-OC-1 cells were labeled using the TMRE staining kit. **(B)** Flow cytometry data confirmed the results in **(A)**. **(C)** Quantification of the flow cytometry results in **(B)**. The TMRE intensity was significantly decreased after neomycin exposure compared to the undamaged controls. In addition, the TMRE intensity was significantly increased in the citicoline treatment group compared to the neomycin-only group. Data are shown as mean \pm SD. * p < 0.05, ** p < 0.01, *** p < 0.001. Scale bars = 20 μ m.

factor that subsequently activates caspases (Karasawa and Steyger, 2011). In this study, we found that cell death and apoptosis dramatically increased in both HEI-OC-1 cells and in cochlear HCs after neomycin injury, while citicoline significantly reduced the neomycin-induced cell death and apoptosis (Figures 2, 4). Furthermore, qRT-PCR analyses indicated that the expression of intrinsic and extrinsic pro-apoptotic genes (*Bax*, *Casp3*, *Casp8*, and *Casp9*) was significantly decreased in the citicoline-treated group after neomycin exposure, while the expression of the anti-apoptotic gene *Bcl-2* was significantly increased (Figures 2, 4). These results suggest that citicoline plays a critical anti-apoptotic role.

Bcl-2 family proteins regulate the integrity of the mitochondrial outer membrane and play an important role in determining mitochondria-mediated apoptosis. Pro-apoptotic proteins such as *Bax* translocate to the mitochondrial outer membrane to form oligomeric complexes when they encounter apoptotic signals, resulting in increased mitochondrial outer membrane permeabilization, Cytochrome-C release, and Caspase activation, while anti-apoptotic proteins such as *Bcl-2* prevent this process (Martinou and Youle, 2011). Citicoline

inhibits apoptosis in nerve cells by promoting the expression of anti-apoptotic factor *Bcl-2* and reducing the expression of the pro-apoptotic factor *Bax* (Levites et al., 2002). In addition, citicoline was also reported to protect the retina by increasing *Bcl-2* expression (Schuettauf et al., 2006). Our results show that the expression of the anti-apoptotic gene *Bcl-2* was significantly increased and the expression of the pro-apoptotic gene *Bax* was significantly decreased after citicoline treatment. This suggested that citicoline can inhibit neomycin-induced HC injury by affecting the expression of *Bax* and *Bcl-2*.

Ototoxic drugs cause hearing loss by inducing HC apoptosis, primarily by altering the MMP of the mitochondria (Huang et al., 2000; Wu et al., 2002; Sun et al., 2015; Guan et al., 2016; He et al., 2016; Yu et al., 2017). Mitochondria play an important role in cell metabolism, and aminoglycoside-induced apoptosis is closely related to mitochondrial dysfunction, which leads to decreased MMP and increased ROS (Joza et al., 2001; Chipuk et al., 2004; Coffin et al., 2013; Sun et al., 2014, 2015; Mei et al., 2015). The accumulation of ROS in the mitochondria is an important trigger of apoptosis, and it has been reported that ROS play an important role in noise-induced and ototoxic drug-induced HC

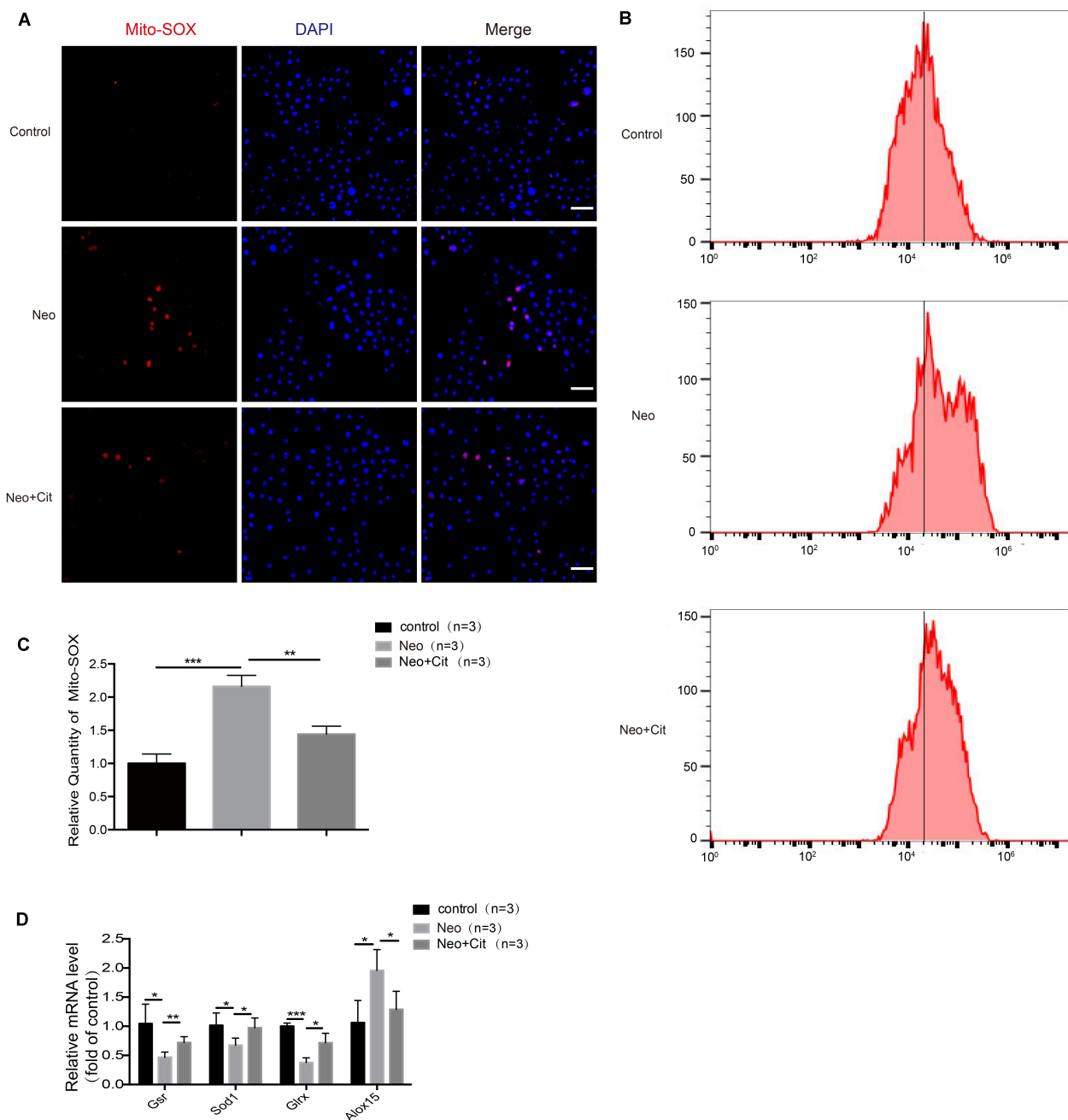


FIGURE 7 | Citicoline modulates neomycin-induced oxidative stress in HEI-OC-1 cells. **(A)** The three groups of HEI-OC-1 cells were labeled using the Mito-SOX Red staining kit. **(B)** Flow cytometry data confirmed the results in **(A)**. **(C)** Quantification of the flow cytometry results in **(B)**. The ROS levels were significantly increased after neomycin treatment compared to the undamaged group. The ROS levels induced by neomycin were significantly reduced by pretreatment with citicoline. **(D)** The mRNA levels of genes related to redox reactions were analyzed by qRT-PCR and normalized to *GAPDH* and presented as the fold change compared to control levels. Data are shown as mean \pm SD. * p < 0.05, ** p < 0.01, *** p < 0.001. Scale bars = 20 μ m.

damage and hearing loss (Sun et al., 2014, 2015; Chen et al., 2015). Previous studies have shown that ROS accumulation triggers mitochondrial depolarization, changes mitochondrial membrane permeability, and induces apoptosis (Rybak et al., 2007; Nemec and Khaled, 2008; Chen et al., 2015; Sun et al., 2015). In the present study, we demonstrated that citicoline significantly

increased the MMP of HEI-OC-1 cells and decreased ROS levels in HEI-OC-1 cells and in cochlear HCs after neomycin exposure (Figures 5–7), suggesting that citicoline alleviates mitochondrial dysfunction in both cell types after neomycin exposure.

In response to aminoglycoside-induced ROS accumulation, antioxidant genes are upregulated to counteract this

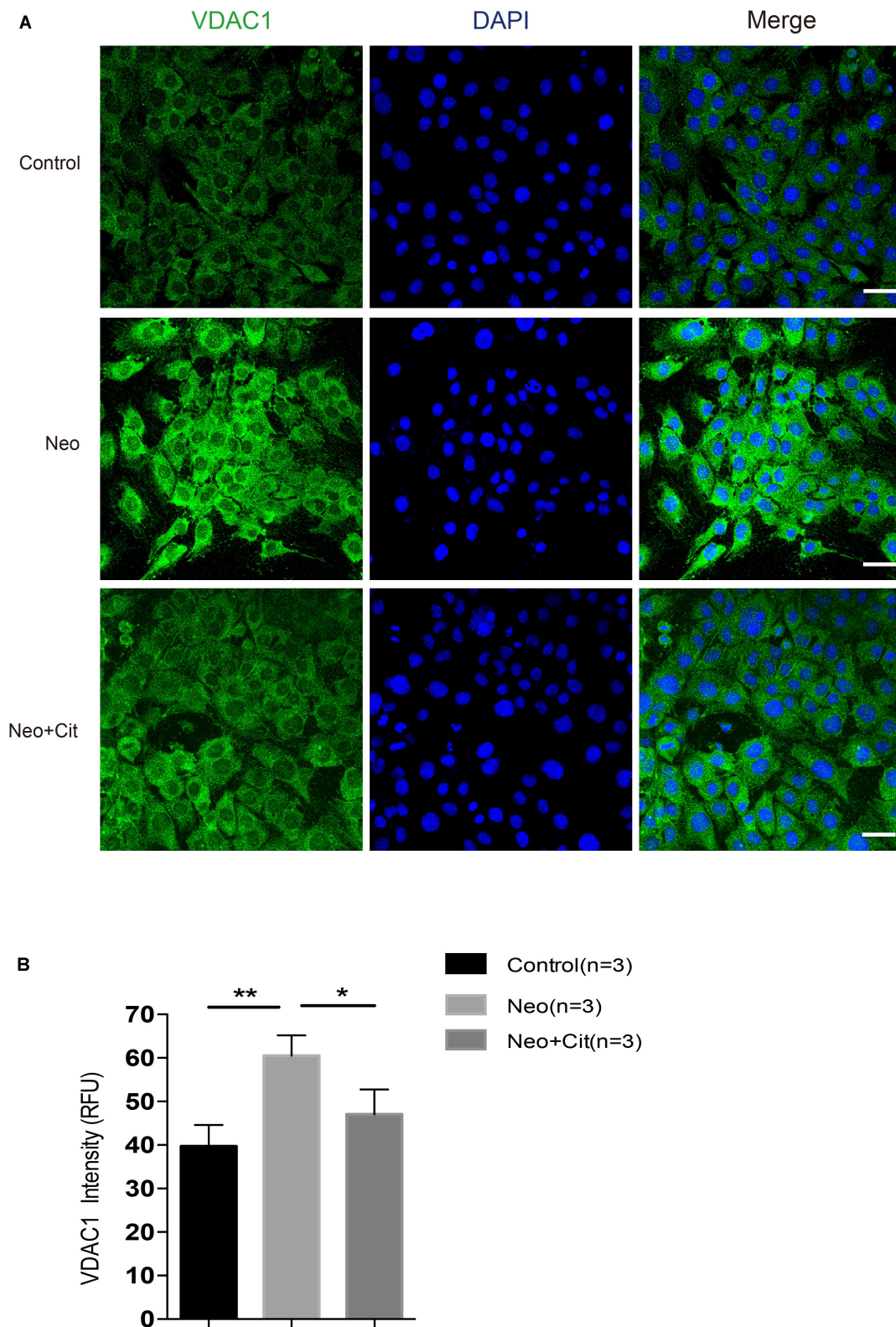


FIGURE 8 | Citicoline downregulates the expression of the VDAC1 of HEI-OC-1 cells after neomycin exposure. **(A)** The three groups of HEI-OC-1 cells were labeled using the mitochondrial marker VDAC1 and DAPI double staining. **(B)** Quantitative analysis histogram of VDAC-1 staining intensity scanning in **(A)**. Data are shown as mean \pm SD. * $p < 0.05$, ** $p < 0.01$, *** $p < 0.001$. Scale bars = 20 μ m.

accumulation. Therefore, the balance between oxidant and antioxidant gene expression is critical for the rate of ROS accumulation, and many genes coordinate with each other to regulate the balance between the production and scavenging of ROS. Administration of ROS-scavenging antioxidants (Sha and Schacht, 2000; Kawamoto et al., 2004; Kim et al., 2009; Ding et al., 2013), as well as inhibition of oxidase (Kim et al., 2010), can reduce the ROS production, thus attenuating the subsequent HC death in ototoxic drug-treated cochleae. In this study, the expression of antioxidant genes was significantly decreased and the expression of pro-oxidation factors was significantly increased after neomycin exposure compared with undamaged controls. We also found that citicoline significantly increased the expression of several key antioxidant genes such as *Gsr*, *Sod1*, and *Glrx* and decreased the expression of the pro-oxidation factor *Alox15* (Figures 5, 7). Overall, these results indicate that citicoline increases the expression of antioxidant genes, thus leading to decreased ROS levels and preventing neomycin-mediated mitochondrial dysfunction and apoptosis in HEI-OC-1 cells and cochlear HCs.

In our study, the expression of antioxidant genes was significantly downregulated after neomycin exposure. We consider that increased ROS activates the cell defense mechanism in the early stage of cell damage, thus activating the cell antioxidant mechanism and up-regulating antioxidant factors to clear the ROS. However, with the aggravation of cell damage, aminoglycoside exposure induces large increases of ROS in the cochlear HCs that overwhelm the cellular defense mechanisms (Jozza et al., 2001; Esterberg et al., 2016). This leads to the imbalance between intracellular oxidation and antioxidation resulting in a significant down-regulation of antioxidant factors and a significant increase in oxidant factors. Because we also previously found that the expression of antioxidant genes decreased after neomycin damaged hair cells (Chen et al., 2015; He et al., 2017), we hypothesize that the downregulation of antioxidant factors is related to the special sensitivity of HCs to aminoglycoside antibiotics, but this still needs further study.

VDAC is a major channel protein located in the outer mitochondrial membrane. It is well recognized that VDAC is involved in many physiological and pathophysiological processes, including Ca^{2+} homeostasis (Shoshan-Barmatz et al., 2006, 2010), energy metabolism (Shoshan-Barmatz et al., 2006; Saks et al., 2010), and cell apoptosis (Tsujimoto and Shimizu, 2002; Shoshan-Barmatz et al., 2010). VDAC has three isoforms (VDAC1-3), and VDAC1 is the main isoform mediating cell functions (De Stefani et al., 2012) and plays an important role in regulating intracellular ROS generation and subsequent apoptotic events (Chen et al., 2014). It is necessary for ROS to cross the outer mitochondrial membrane when released from the mitochondria to the cytoplasm, and this process is mediated by VDAC1. Increased intracellular ROS generation can be mostly suppressed by VDAC1 inhibitors, and thus VDAC1 appears to play a dominant role in regulating ROS generation (Chen et al., 2014). In our study, we demonstrated that citicoline significantly downregulated VDAC1 in HEI-OC-1 cells after neomycin exposure (Figure 8), thus leading to decreased ROS levels and inhibition of apoptosis.

Sirtuin 1 (SIRT1), the most conserved member of the NAD⁺-dependent protein deacetylase family, has been shown to have protective effects in various common neurodegenerative disorders (Herskovits and Guarente, 2014). Citicoline has been recently shown to increase SIRT1 protein expression, and this is strongly related to its neuroprotective activities (Hurtado et al., 2013). A previous study showed that increased SIRT1 protects against cisplatin-induced damage to HCs (Xiong et al., 2019). Therefore, we will further study whether the protective effect of citicoline on neomycin-induced HC damage works through SIRT1 activation.

In summary, we first used citicoline on hair cells and clarified the importance of the drug on ear hair cells for the first time. Our study provides the first report that citicoline protects auditory HCs against neomycin injury by preventing mitochondrial dysfunction and the upregulation of antioxidant genes, thus leading to decreased ROS levels and preventing apoptosis. This study therefore provides experimental evidence for the potential clinical application of citicoline to prevent aminoglycoside-induced auditory HC damage.

DATA AVAILABILITY STATEMENT

The original contributions presented in the study are included in the article/Supplementary Material, further inquiries can be directed to the corresponding author/s.

ETHICS STATEMENT

The animal study was reviewed and approved by the Animal Care and Use Committee of Southeast University. Written informed consent was obtained from the owners for the participation of their animals in this study.

AUTHOR CONTRIBUTIONS

ZZ, XF, HL, and JC contributed equally to this work. All the authors made substantial and direct intellectual contributions to the work and approved it for publication.

FUNDING

This work was supported by grants from the National Key R&D Program of China (No. 2017YFA0103903), the Strategic Priority Research Program of the Chinese Academy of Sciences (XDA16010303), the National Natural Science Foundation of China (Nos. 81970882, 81900937, 81970884, 81771019, 81822011, 81771013, and 81870721), the Natural Science Foundation from Jiangsu Province (BE2019711), Shenzhen Fundamental Research Program (JCYJ20190814093401920), the K. C. Wong Education Foundation, Boehringer Ingelheim Pharma GmbH, and the Science and Technology Commission of Shanghai Municipality (17ZR1448600 and 18410712400).

SUPPLEMENTARY MATERIAL

The Supplementary Material for this article can be found online at: <https://www.frontiersin.org/articles/10.3389/fcell.2020.00712/full#supplementary-material>

FIGURE S1 | Citicoline promotes HEI-OC1 cells survival after neomycin exposure. **(A)** The CCK-8 kit measured the cell viability after treatment with different neomycin concentrations (1–20 mM) for 24 h. **(B)** The cell viability was measured

by the CCK-8 kit after treatment with 10 mM neomycin for different times (0, 6, 12, 24, 48 h). **(C)** The cell viability after neomycin exposure was measured with the CCK-8 kit after pretreatment with different citicoline concentrations (1, 10, 100 μ M, 1 mM, 2 mM) for different times (6, 12, 24 h). **(D)** CCK-8 result of HEI-OC1 cells pre-treated with different citicoline concentrations for 6 h after neomycin exposure. **(E)** CCK-8 result of HEI-OC1 cells pre-treated with different citicoline concentrations for 12 h after neomycin exposure. **(F)** CCK-8 result of HEI-OC1 cells pre-treated with different citicoline concentrations for 24 h after neomycin exposure. Data are shown as mean \pm SD. * $p < 0.05$, ** $p < 0.01$, *** $p < 0.001$.

REFERENCES

- Adibhatla, R. M., Hatcher, J. F., and Dempsey, R. J. (2002). Citicoline: neuroprotective mechanisms in cerebral ischemia. *J. Neurochem.* 80, 12–23. doi: 10.1046/j.0022-3042.2001.00697.x
- Barrachina, M., Secades, J., Lozano, R., Gómez-Santos, C., Ambrosio, S., and Ferrer, I. (2002). Citicoline increases glutathione redox ratio and reduces caspase-3 activation and cell death in staurosporine-treated SH—SY5Y human neuroblastoma cells. *Brain Res.* 957, 184–190.
- Chen, H., Gao, W., Yang, Y., Guo, S., Wang, H., Wang, W., et al. (2014). Inhibition of Vdac1 Prevents Ca^{2+} -mediated oxidative stress and apoptosis induced by 5-aminolevulinic acid mediated sonodynamic therapy in Thp-1 macrophages. *Apoptosis* 19, 1712–1726. doi: 10.1007/s10495-014-1045-5
- Chen, Y., Li, L., Ni, W., Zhang, Y., Sun, S., Miao, D., et al. (2015). Bmi1 regulates auditory hair cell survival by maintaining redox balance. *Cell Death Dis.* 6:e1605. doi: 10.1038/cddis.2014.549
- Chen, Y., Yu, H., Zhang, Y., Li, W., Lu, N., Ni, W., et al. (2013). Cotransfection of Pax2 and Math1 promote in situ cochlear hair cell regeneration after neomycin insult. *Sci. Rep.* 3:2996.
- Chipuk, J. E., Kuwana, T., Bouchier-Hayes, L., Droin, N. M., Newmeyer, D. D., Schuler, M., et al. (2004). Direct activation of bax by p53 mediates mitochondrial membrane permeabilization and apoptosis. *Science* 303, 1010–1014. doi: 10.1126/science.1092734
- Choung, Y. H., Taura, A., Pak, K., Choi, S. J., Masuda, M., and Ryan, A. F. (2009). Generation of highly-reactive oxygen species is closely related to hair cell damage in rat organ of Corti treated with gentamicin. *Neuroscience* 161, 214–226. doi: 10.1016/j.neuroscience.2009.02.085
- Clerici, W. J., Hensley, K., DiMartino, D. L., Buttrfield, D. A. (1996). Direct detection of ototoxicant-induced reactive oxygen species generation in cochlear explants. *Hear. Res.* 98, 116–124. doi: 10.1016/0378-5955(96)00075-5
- Coffin, A. B., Rubel, E. W., and Raible, D. W. (2013). Bax, bcl2, and p53 differentially regulate neomycin- and gentamicin-induced hair cell death in the zebrafish lateral line. *J. Assoc. ResOtolaryngol.* 14, 645–659. doi: 10.1007/s10162-013-0404-1
- Correia-Melo, C., Ichim, G., Tait, S. W. G., and Passos, J. F. (2017). Depletion of mitochondria in mammalian cells through enforced mitophagy. *Nat. Protocols* 12, 183–194. doi: 10.1038/nprot.2016.159
- Cotroneo, A. M., Castagna, A., Putignano, S., Lacava, R., Fantò, F., Monteleone, F., et al. (2013). Effectiveness and safety of citicoline in mild vascular cognitive impairment: the IDEALE study. *Clin. Interv. Aging* 8, 131–137.
- Davinelli, S., Chiosi, F., Di Marco, R., Costagliola, C., and Scapagnini, G. (2017). Cytoprotective effects of citicoline and homotaurine against glutamate and high glucose neurotoxicity in primary cultured retinal cells. *Oxidat. Med. Cell. Longev.* 2017:2825703.
- De Stefani, D., Bononi, A., Romagnoli, A., Messina, A., De Pinto, V., Pinton, P., et al. (2012). VDAC1 selectively transfers apoptotic Ca^{2+} signals to mitochondria. *Cell Death Differ.* 19, 267–273. doi: 10.1038/cdd.2011.92
- Ding, D., Qi, W., Yu, D., Jiang, H., Han, C., Kim, M. J., et al. (2013). Addition of exogenous NAD^{+} prevents mefloquine-induced neuroaxonal and hair cell degeneration through reduction of caspase-3-mediated apoptosis in cochlear organotypic cultures. *PLoS One* 8:e79817. doi: 10.1371/journal.pone.0079817
- Esterberg, R., Linbo, T., Pickett, S. B., Wu, P., Ou, H. C., Rubel, E. W., et al. (2016). Mitochondrial calcium uptake underlies ROS generation during aminoglycoside-induced hair cell death. *J. Clin. Invest.* 126, 3556–3566. doi: 10.1172/jci84939
- Filomeni, G., De Zio, D., and Cecconi, F. (2015). Oxidative stress and autophagy: the clash between damage and metabolic needs. *Cell Death Differ.* 22, 377–388. doi: 10.1038/cdd.2014.150
- Franco, R., and Cidlowski, J. A. (2009). Apoptosis and glutathione: beyond an antioxidant. *Cell Death Differ.* 16, 1303–1314. doi: 10.1038/cdd.2009.107
- Guan, M., Fang, Q., He, Z., Li, Y., Qian, F., Qian, X., et al. (2016). Inhibition of ARC decreases the survival of HEI-OC-1 cells after neomycin damage in vitro. *Oncotarget* 7, 66647–66659. doi: 10.18632/oncotarget.11336
- He, Y., Yu, H., Cai, C., Shan, S., Chai, R., and Li, H. (2014). Inhibition of H3K4me2 methylation protects auditory hair cells from neomycin-induced apoptosis. *Mol. Neurobiol.* 52, 1–10.
- He, Z., Guo, L., Shu, Y., Fang, Q., Zhou, H., Liu, Y., et al. (2017). Autophagy protects auditory hair cells against neomycin-induced damage. *Autophagy* 13, 1884–1904. doi: 10.1080/15548627.2017.1359449
- He, Z., Sun, S., Waqas, M., Zhang, X., Qian, F., Cheng, C., et al. (2016). Reduced TRMU expression increases the sensitivity of hair-cell-like HEI-OC-1 cells to neomycin damage in vitro. *Sci. Rep.* 6:29621.
- He, Z. H., Zou, S. Y., Li, M., Liao, F. L., Wu, X., Sun, H. Y., et al. (2020). The nuclear transcription factor FoxG1 affects the sensitivity of mimetic aging hair cells to inflammation by regulating autophagy pathways. *Redox Biol.* 28:101364. doi: 10.1016/j.redox.2019.101364
- Herskovits, A. Z., and Guarente, L. (2014). SIRT1 in neurodevelopment and brain senescence. *Neuron* 81, 471–483. doi: 10.1016/j.neuron.2014.01.028
- Huang, T., Cheng, A. G., Stupak, H., Liu, W., Kim, A., Staecker, H., et al. (2000). Oxidative stress induced apoptosis of cochlear sensory cells: otoprotective strategies. *Int. J. Dev. Neurosci.* 18, 259–270. doi: 10.1016/s0736-5748(99)00094-5
- Hurtado, O., Hernández-Jiménez, M., Zarruk, J. G., Cuartero, M. I., Ballesteros, I., Camarero, G., et al. (2013). Citicoline (CDP-choline) increases Sirtuin1 expression concomitant to neuroprotection in experimental stroke. *J. Neurochem.* 126, 816–819.
- Joza, N., Susin, S. A., Daugas, E., Stanford, W. L., Cho, S. K., Li, C. Y., et al. (2001). Essential role of the mitochondrial apoptosis-inducing factor in programmed cell death. *Nature* 410, 549–554. doi: 10.1038/35069004
- Kalincic, G. M., Webster, P., Lim, D. J., and Kalincic, F. (2003). A cochlear cell line as an in vitro system for drug ototoxicity screening. *Audiol. Neurotol.* 8, 177–189. doi: 10.1159/000071059
- Karasawa, T., and Steyger, P. S. (2011). Intracellular mechanisms of aminoglycoside-induced cytotoxicity. *Integr. Biol. (Camb)* 3, 879–886.
- Kawamoto, K., Sha, S. H., Minoda, R., Izumikawa, M., Kuriyama, H., Schacht, J., et al. (2004). Antioxidant gene therapy can protect hearing and hair cells from ototoxicity. *Mol. Ther.* 9, 173–181. doi: 10.1016/j.ymthe.2003.11.020
- Kim, H. J., Lee, J. H., Kim, S. J., Oh, G. S., Moon, H. D., Kwon, K. B., et al. (2010). Roles of NADPH oxidases in cisplatin induced reactive oxygen species generation and ototoxicity. *J. Neurosci.* 30, 3933–3946. doi: 10.1523/jneurosci.6054-09.2010
- Kim, S. J., Park, C., Han, A. L., Youn, M. J., Lee, J. H., Kim, Y., et al. (2009). Ebselen attenuates cisplatin-induced ROS generation through Nrf2 activation in auditory cells. *Hear. Res.* 251, 70–82. doi: 10.1016/j.heares.2009.03.003
- Lazarou, M., Sliter, D. A., Kane, L. A., Sarraf, S. A., Wang, C., Burman, J. L., et al. (2015). The ubiquitin kinase PINK1 recruits autophagy receptors to induce mitophagy. *Nature* 524, 309–314. doi: 10.1038/nature14893
- Levites, Y., Amit, T., Youdim, M. B., and Mandel, S. (2002). Involvement of protein kinase C activation and cell survival/ cell cycle genes in green tea polyphenol (-)-Epigallocatechin 3-gallate neuroprotective action. *J. Biol. Chem.* 277, 30574–30580. doi: 10.1074/jbc.m202832200

- Li, W., You, D., Chen, Y., Chai, R., and Li, H. (2016). Regeneration of hair cells in the mammalian vestibular system. *Front. Med.* 10, 143–151. doi: 10.1007/s11684-016-0451-1
- Liu, L., Chen, Y., Qi, J., Zhang, Y., He, Y., Ni, W., et al. (2016). Wnt activation protects against neomycin-induced hair cell damage in the mouse cochlea. *Cell Death Dis.* 7:e2136. doi: 10.1038/cddis.2016.35
- Lu, X., Shan, S., Qi, J., Li, W., Liu, L., Zhang, Y., et al. (2017). Bmi1 regulates the proliferation of cochlear supporting cells via the canonical wnt signaling pathway. *Mol. Neurobiol.* 54, 1326–1339. doi: 10.1007/s12035-016-9686-8
- Mangiardi, D. A., Katherine, M. L. W., May, K. E., Messana, E. P., Mountain, D. C., and Cotanche, D. A. (2004). Progression of hair cell ejection and molecular markers of apoptosis in the avian cochlea following gentamicin treatment. *J. Comp. Neurol.* 475, 1–18. doi: 10.1002/cne.20129
- Martinou, J. C., and Youle, R. J. (2011). Mitochondria in apoptosis: Bcl-2 family members and mitochondrial dynamics. *Dev. Cell* 21, 92–101. doi: 10.1016/j.devcel.2011.06.017
- Matsui, J. I., Ogilvie, J. M., and Warchol, M. E. (2002). Inhibition of caspases prevents ototoxic and ongoing hair cell death. *J. Neurosci. Official J. Soc. Neurosci.* 22, 1218–1227. doi: 10.1523/jneurosci.22-04-01218.2002
- Matteucci, A., Varano, M., Gaddini, L., Mallozzi, C., Villa, M., Pricci, F., et al. (2014). Neuroprotective effects of citicoline in in vitro models of retinal neurodegeneration. *Int. J. Mol. Sci.* 15, 6286–6297. doi: 10.3390/ijms15046286
- Mei, H., Sun, S., Bai, Y., Chen, Y., Chai, R., and Li, H. (2015). Reduced mtdna copy number increases the sensitivity of tumor cells to chemotherapeutic drugs. *Cell Death Dis.* 6:e1710. doi: 10.1038/cddis.2015.78
- Nadol, J. B. (1993). Hearing loss. *N. Engl. J. Med.* 329, 1092–1102.
- Nemec, K. N., and Khaled, A. R. (2008). Therapeutic modulation of apoptosis: targeting the bcl-2 family at the interface of the mitochondrial membrane. *Yonsei Med. J.* 49, 689–697.
- Ni, W., Zeng, S., Li, W., Chen, Y., Zhang, S., Tang, M., et al. (2016). Wnt activation followed by Notch inhibition promotes mitotic hair cell regeneration in the postnatal mouse cochlea. *Oncotarget* 7, 66754–66768. doi: 10.18632/oncotarget.11479
- Oshitari, T., Fujimoto, N., and Adachi—Usami, E. (2002). Citicoline has a protective effect on damaged retinal ganglion cells in mouse culture retina. *Neuroreport* 13, 2109–2111. doi: 10.1097/00001756-200211150-00023
- Parisi, V., Coppola, G., Centofanti, M., Oddone, F., Angrisani, A. M., Ziccardi, L., et al. (2008). Evidence of the neuroprotective role of citicoline in glaucoma patients. *Prog. Brain Res.* 173, 541–554. doi: 10.1016/s0079-6123(08)01137-0
- Park, C. H., Kim, Y. S., Cheon, E. W., Noh, H. S., Cho, C. H., Chung, I. Y., et al. (2006). Action of citicoline on rat retinal expression of extracellular-signal-regulated kinase (ERK1/2). *Brain Res.* 1081, 203–210. doi: 10.1016/j.brainres.2005.12.128
- Prasad, K. N., and Bondy, S. C. (2020). Increased oxidative stress, inflammation, and glutamate: potential preventive and therapeutic targets for hearing disorders. *Mech. Ageing Dev.* 185:111191. doi: 10.1016/j.mad.2019.111191
- Rybak, L. P., and Kelly, T. (2003). Ototoxicity: bioprotective mechanisms. *Curr. Opin. Otolaryngol. Head Neck Surg.* 11, 328–333. doi: 10.1097/00020840-200310000-00004
- Rybak, L. P., Whitworth, C. A., Mukherjee, D., and Ramkumar, V. (2007). Mechanisms of cisplatin-induced ototoxicity and prevention. *Hear Res.* 226, 157–167. doi: 10.1016/j.heares.2006.09.015
- Saks, V., Guzun, R., Timohhina, N., Tepp, K., Varikmaa, M., Monge, C., et al. (2010). Structure-function relationships in feedback regulation of energy fluxes in vivo in health and disease: mitochondrial interactosome. *Biochim. Biophys. Acta* 1797, 678–697. doi: 10.1016/j.bbabi.2010.01.011
- Saver, J. L. (2008). Citicoline: update on a promising and widely available agent for neuroprotection and neurorepair. *Rev. Neurol. Dis.* 5, 167–177.
- Schuettauf, F., Rejdak, R., Thaler, S., Bolz, S., Lehaci, C., Mankowska, A., et al. (2006). Citicoline and lithium rescue retinal ganglion cells following partial optic nerve crush in the rat. *Exp. Eye Res.* 83, 1128–1134. doi: 10.1016/j.exer.2006.05.021
- Secades, J. J., and Lorenzo, J. L. (2006). Citicoline: pharmacological and clinical review. *Methods Find Exp. Clin. Pharmacol.* 28, 1–56.
- Sha, S. H., and Schacht, J. (2000). Antioxidants attenuate gentamicin-induced free radical formation in vitro and ototoxicity in vivo: D-methionine is a potential protectant. *Hear Res.* 142, 34–40. doi: 10.1016/s0378-5955(00)00003-4
- Shoshan-Barmatz, V., De Pinto, V., Zweckstetter, M., Raviv, Z., Keinan, N., and Arbel, N. N. (2010). VDAC, a multi-functional mitochondrial protein regulating cell life and death. *Mol. Aspects Med.* 31, 227–285. doi: 10.1016/j.mam.2010.03.002
- Shoshan-Barmatz, V., Israelson, A., Brdiczka, D., and Sheu, S. S. (2006). The voltage-dependent anion channel (VDAC): function in intracellular signalling, cell life and cell death. *Curr. Pharm. Des.* 12, 2249–2270. doi: 10.2174/13816120677585111
- Sun, S., Sun, M., Zhang, Y., Cheng, C., Waqas, M., Yu, H., et al. (2014). In vivo overexpression of x-linked inhibitor of apoptosis protein protects against neomycin-induced hair cell loss in the apical turn of the cochlea during the ototoxic-sensitive period. *Front. Cell. Neurosci.* 8:248. doi: 10.3389/fncel.2014.00248
- Sun, S., Yu, H., Honglin, M., Ni, W., Zhang, Y., Guo, L., et al. (2015). Inhibition of the activation and recruitment of microglia-like cells protects against neomycin-induced ototoxicity. *Mol. Neurobiol.* 51, 252–267. doi: 10.1007/s12035-014-8712-y
- Tsujimoto, Y., and Shimizu, S. (2002). The voltage-dependent anion channel: an essential player in apoptosis. *Biochimie* 84, 187–193. doi: 10.1016/s0300-9084(02)01370-6
- Waguespack, J. R., and Ricci, A. J. (2005). Aminoglycoside ototoxicity: permeant drugs cause permanent hair cell loss. *J. Physiol.* 567, 505–521.
- Waqas, M., Zhang, S., He, Z., Tang, M., and Chai, R. (2016). Role of Wnt and Notch signaling in regulating hair cell regeneration in the cochlea. *Front. Med.* 10, 237–249. doi: 10.1007/s11684-016-0464-9
- Wignall, N. D., and Brown, E. S. (2014). Citicoline in addictive disorders: a review of the literature. *Am. J. Drug Alcohol. Abuse* 40, 262–268. doi: 10.3109/00952990.2014.925467
- Wu, W. J., Sha, S. H., and Schacht, J. (2002). Recent advances in understanding aminoglycoside ototoxicity and its prevention. *Audiol. Neurotol.* 7, 171–174. doi: 10.1159/000058305
- Xiong, H., Chen, S., Lai, L., Yang, H., Xu, Y., Pang, J., et al. (2019). Modulation of miR-34a/SIRT1 signaling protects cochlear hair cells against oxidative stress and delays age-related hearing loss through coordinated regulation of mitophagy and mitochondrial biogenesis. *Neurobiol. Aging* 79, 30–42. doi: 10.1016/j.neurobiolaging.2019.03.013
- Yu, X., Liu, W., Fan, Z., Qian, F., Zhang, D., Han, Y., et al. (2017). c-Myb knockdown increases the neomycin-induced damage to hair-cell-like HEI-OC1 cells in vitro. *Sci. Rep.* 7:41094.

Conflict of Interest: The authors declare that the research was conducted in the absence of any commercial or financial relationships that could be construed as a potential conflict of interest.

Copyright © 2020 Zhong, Fu, Li, Chen, Wang, Gao, Zhang, Cheng, Zhang, Li, Zhang, Qian, Shu, Chai and Gao. This is an open-access article distributed under the terms of the Creative Commons Attribution License (CC BY). The use, distribution or reproduction in other forums is permitted, provided the original author(s) and the copyright owner(s) are credited and that the original publication in this journal is cited, in accordance with accepted academic practice. No use, distribution or reproduction is permitted which does not comply with these terms.



Functional Versatility of the CDK Inhibitor p57^{Kip2}

Justine Creff and Arnaud Besson*

Centre National de la Recherche Scientifique, Laboratoire de Biologie Cellulaire et Moléculaire du Contrôle de la Prolifération, Centre de Biologie Intégrative, Université de Toulouse, Toulouse, France

OPEN ACCESS

Edited by:

Lisa Porter,
University of Windsor, Canada

Reviewed by:

Philipp Kaldis,
Lund University, Sweden
Adriana Borriello,
University of Campania "Luigi
Vanvitelli", Italy

*Correspondence:

Arnaud Besson
arnaud.besson@univ-tlse3.fr

Specialty section:

This article was submitted to
Cell Growth and Division,
a section of the journal
Frontiers in Cell and Developmental
Biology

Received: 17 July 2020

Accepted: 17 September 2020

Published: 07 October 2020

Citation:

Creff J and Besson A (2020)
Functional Versatility of the CDK
Inhibitor p57^{Kip2}.
Front. Cell Dev. Biol. 8:584590.
doi: 10.3389/fcell.2020.584590

The cyclin/CDK inhibitor p57^{Kip2} belongs to the Cip/Kip family, with p21^{Cip1} and p27^{Kip1}, and is the least studied member of the family. Unlike the other family members, p57^{Kip2} has a unique role during embryogenesis and is the only CDK inhibitor required for embryonic development. p57^{Kip2} is encoded by the imprinted gene *CDKN1C*, which is the gene most frequently silenced or mutated in the genetic disorder Beckwith–Wiedemann syndrome (BWS), characterized by multiple developmental anomalies. Although initially identified as a cell cycle inhibitor based on its homology to other Cip/Kip family proteins, multiple novel functions have been ascribed to p57^{Kip2} in recent years that participate in the control of various cellular processes, including apoptosis, migration and transcription. Here, we will review our current knowledge on p57^{Kip2} structure, regulation, and its diverse functions during development and homeostasis, as well as its potential implication in the development of various pathologies, including cancer.

Keywords: p57^{Kip2}, CDK inhibitor, cell cycle, development, transcription, stem cells, *CDKN1C*

INTRODUCTION

The cell division cycle is the fundamental process by which a cell duplicates its cytoplasmic and nuclear contents and divides in two genetically identical daughter cells. Cell cycle progression is driven by specific combinations of heterodimeric cyclin/CDK (cyclin-dependent kinase) complexes that license progression from one cell cycle phase to the next. In these complexes, the CDK is the catalytic subunit that has serine/threonine kinase activity and the cyclin subunit allows CDK activation and determines substrate specificity (Malumbres and Barbacid, 2005; Suryadinata et al., 2010). These actors are finely regulated at the level of transcription, localization, post-translational modifications (mainly phosphorylation) and protein degradation. Another level of regulation is their association with inhibitory partners called CKIs (Cyclin-dependent Kinase Inhibitor). CKIs are divided in two families according to their structure, CDK binding specificity and evolutionary origin: the INK4 family and the Cip/Kip family (Sherr and Roberts, 1999; Besson et al., 2008; Suryadinata et al., 2010).

The INK4 family (Inhibitors of CDK4) is composed of four proteins, p16^{INK4A}, p15^{INK4B}, p18^{INK4C}, and p19^{INK4D} that specifically bind to CDK4 and CDK6 and inhibit their interaction with D-type cyclins, thus preventing their activation (Sherr and Roberts, 1999; Besson et al., 2008). In contrast, members of the Cip/Kip family, p21^{Cip1/Waf1} (p21) (Harper et al., 1993), p27^{Kip1} (p27) (Polyak et al., 1994; Toyoshima and Hunter, 1994) and p57^{Kip2} (p57) (Lee et al., 1995; Matsuoka et al., 1995) bind to both CDK and cyclin subunits and have the ability to inhibit all cyclin/CDK complexes (Sherr and Roberts, 1999; Besson et al., 2008). Cip/Kip proteins share a conserved

cyclin/CDK interaction domain in their N-terminal part, but diverge in their C-termini, suggesting that they play specific roles (Yoon et al., 2012). By inhibiting CDK activity, CKIs block proliferation and they are considered as tumor suppressor.

More recently, the characterization of the CKI interaction networks indicates that Cip/Kip family members plays multiple functions in the cell and that their roles are not restricted to cell cycle control but also extends to the regulation of other cellular processes (Besson et al., 2008).

In this review, we focus on the least studied Cip/Kip family member, p57, and give an overview of its regulation, multiple functions in physiology and implication in pathology.

THE *CDKN1C* GENE

p57 is encoded by *CDKN1C*, located in the telomeric region of chromosome 11 at 11p15.5 in human (Matsuoka et al., 1995), and in the distal region of chromosome 7 in mice (Hatada and Mukai, 1995). *CDKN1C* contains four exons and three introns and p57 is encoded only from exons 2 and 3 (Tokino et al., 1996).

CDKN1C is a paternally imprinted gene, with preferential expression from the maternal allele (Matsuoka et al., 1996). The 11p15.5 locus contains a cluster of genes submitted to genomic imprinting. Parental or genomic imprinting is a process required for normal embryonic development that involves epigenetic modifications of a gene causing its monoallelic expression in a parental-dependent manner (Monk et al., 2019). Imprinted genes are commonly found in clusters, which contain imprinting control regions (ICRs) that are enriched in CpG islands and are differentially methylated on each allele. These regions also often include non-coding antisense RNAs that are essential for maintaining imprinting (Reik and Walter, 2001). Interestingly, the region homologous to 11p15.5 on murine chromosome 7 has the same gene cluster arrangement, highlighting the importance of this organization for the regulation of these genes. This locus covers about 1 Mb and is organized in two domains controlled by two regulatory centers, ICR1 and ICR2 (Figure 1).

ICR1 in the telomeric domain controls the reciprocal expression of *H19* (maternal expression) and *IGF2* (paternal expression). The expression of these two genes depends on the same pair of enhancers whose access is regulated by ICR1 (Leighton et al., 1995). On the maternal allele, unmethylated ICR1 is bound by CTCF (CCCTC-binding factor), a zinc-finger protein with insulating activity, preventing the interaction of the enhancers with the *IGF2* promoter, but allowing activation of the *H19* promoter, which is expressed. Conversely, on the paternal allele, CTCF does not recognize the methylated ICR1, allowing the interaction of the enhancers with the *IGF2* promoter and its expression, while *H19* is repressed (Hark et al., 2000; Eggermann et al., 2014b).

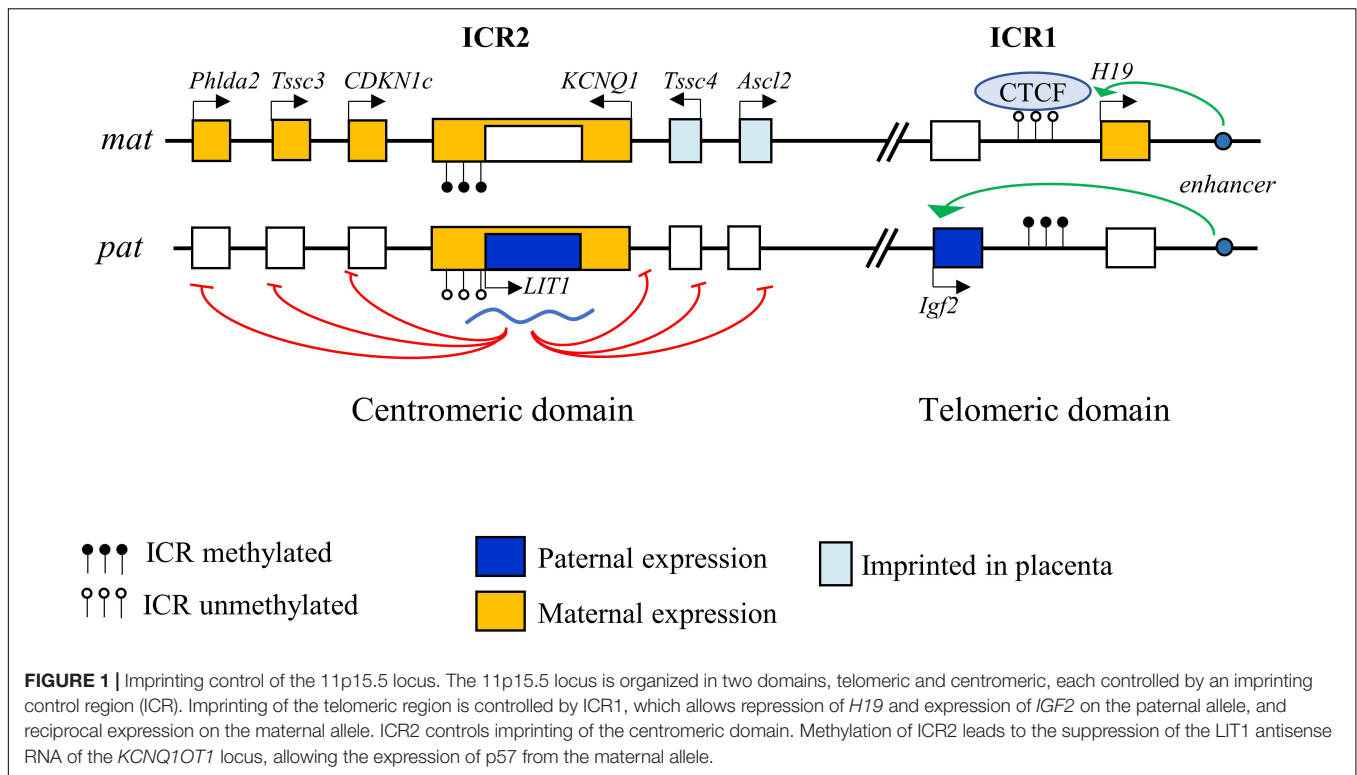
The centromeric domain is approximately 800 kb in size and contains several ubiquitously imprinted genes, including *KCNQ1*, *KCNQ1OT1* (*KCNQ1 Opposite strand/antisense transcript 1*, a.k.a. *LIT1* [Long QT intron transcript 1]), *CDKN1C*, *SLC22A18*, and *PHLDA2*, whose expression is regulated by ICR2. ICR2, located in intron 10 of *KCNQ1* corresponding to the *KCNQ1OT1* promoter,

is methylated on the maternal allele, which represses *KCNQ1OT1* expression and thereby allows maternal expression of all the other genes of the domain. Conversely, ICR2 is unmethylated on the paternal allele, allowing *KCNQ1OT1* expression. *KCNQ1OT1* is a non-coding antisense RNA that represses in cis the other genes of the domain (Fitzpatrick et al., 2002; Eggermann et al., 2014b) (Figure 1). *KCNQ1OT1* directly binds to chromatin at the promoters of the imprinted genes and recruits histone methyltransferase complexes such as EZH2 (Enhancer of Zeste 2 Polycomb Repressive Complex 2 Subunit) and EHMT2 (Euchromatic Histone Lysine Methyltransferase 2), resulting in a repressive chromatin state (Pandey et al., 2008). In addition, *KCNQ1OT1* recruits DNMT1 (DNA methyltransferase 1) to these promoters, causing their hypermethylation and reinforcing paternal repression (Mohammad et al., 2010). Imprinting defects in this locus are one of the most frequent cause of development of several syndromes (see below). Some genes in this locus are imprinted only in the placenta in mice (*Ascl2*, *CD81*, and *Tssc4*) (Shmela and Gicquel, 2013).

REGULATION OF *CDKN1C* EXPRESSION

p57 expression is finely regulated by many signals and transcription factors. *CDKN1C* promoter analysis revealed the presence of several consensus sites for various transcription factors, including several SP1 (Stimulatory protein-1) sites, a Glucocorticoid response element (GRE) site, and a TATA box. The transcription factors E47, E2F1 and EGR1 (Early growth response gene 1), Tcf4, Hif1- α , as well as MyoD, via a p73 dependent mechanism, all promote p57 expression (Samuelsson et al., 1999; Rothschild et al., 2006; Vaccarello et al., 2006; Ma and Cress, 2007; Roeb et al., 2007; Wierenga et al., 2014). Stimulation with glucocorticoids or BMPs also induce p57 expression (Samuelsson et al., 1999; Gosselet et al., 2007; Shi and Liu, 2011; Zhang et al., 2015). Conversely, p57 transcription is repressed by the Notch effectors Hes1 and Herp2, as well as Id2 and PAX3-FOXO1 (Rothschild et al., 2006; Jia et al., 2007; Roeb et al., 2007; Riccio et al., 2008). TGF- β signals have antagonistic roles depending on cell type. Indeed, the TGF- β /Smad pathway stimulates p57 expression in hematopoietic stem cells, whereas it induces its degradation in osteoblasts (Urano et al., 1999; Scandura et al., 2004). The *CDKN1C* promoter is strongly regulated by methylation on the numerous CpG islands located upstream and downstream of the transcription start site, which appears to play a critical role in mediating p57 silencing in cancers (see below).

In carcinomas, multiple micro-RNAs have been shown to repress p57 expression. For example, p57 is targeted by miR221/222 in gastric, lung and hepatocellular cancers, promoting cell proliferation and tumor growth (Fornari et al., 2008; Kim et al., 2009; Wang et al., 2013). Similarly, p57 expression is down-regulated by miR25 in glioma and gastric cancer (Kim et al., 2009; Zhang et al., 2015) and by miR21 in prostate cancer (Mishra et al., 2014). In the context of stem cells, p57 is regulated by miR92. In human embryonic stem cells, miR92-b targets p57, promoting G₁/S transition and



stem cell proliferation (Sengupta et al., 2009). Conversely, in pancreatic cancer p57 is targeted by miR92-a, and miR92-a is downregulated in chemoresistant cancer stem cells, leading to p57 upregulation, which promotes cancer stem cell quiescence and treatment resistance (Cioffi et al., 2015). Recently, Long Non-Coding RNAs (lncRNAs) other than *KCNQ1OT1* have also been identified as regulators of p57 expression. lncRNAs may regulate gene expression by several mechanisms, either acting as scaffolds, guides or by interacting with chromatin modifying proteins (Fatica and Bozzoni, 2014). Several lncRNAs overexpressed in cancer, notably *SNHG17* in colorectal and gastric cancer, *SH3PXD2A-AS1* in colorectal cancer, or *lncRNA00511* in non-small cell lung carcinoma, were shown to downregulate p57 via their interaction with EZH2, the catalytic subunit of the Polycomb Repressive Complex 2 (PRC2), a methyltransferase that causes chromatin condensation (Sun et al., 2016; Ma et al., 2017, 2018; Zhang et al., 2019a). Inversely, *LINC00628* is downregulated in colorectal cancer, which is associated with poor prognosis, and its interaction with EZH2 leads to p57 upregulation (Zhang et al., 2020). Other mechanisms have been identified, for instance in gastric cancer, the lncRNA *ARHGAP27P1* activates p57 expression through binding to JMJD3 (Jumonji-Domain containing 3), causing demethylation of the p57 promoter (Zhang et al., 2019b).

Over the past few years, RNA modifications were shown to play an important role in RNA stability and translation and it appears that aberrant modifications are involved in tumorigenesis (Chen et al., 2019). NSUN2 (NOP2/Sun RNA methyltransferase 2), the main enzyme catalyzing 5-methylcytosine (m⁵C) formation, is upregulated in gastric cancer

and promote cell proliferation and tumorigenesis via m⁵C methylation of the p57 mRNA, repressing p57 expression (Mei et al., 2020).

Unlike other Cip/Kip family members, p57 exhibits a tissue-specific expression pattern with marked variations of expression from embryogenesis to adulthood. During embryogenesis, p57 is strongly expressed from E9.5 to birth, with peak expression at key stages of differentiation in each organ. p57 is present in all three embryonic germ layers (endoderm, mesoderm, and ectoderm), and is found in the majority of organs: cartilage, skeletal muscle, heart, nervous system, and parenchymal organs (intestine, pancreas, lungs, adrenals, thymus, gonad, and kidney) as well as in extra-embryonic tissues. After E13.5, its expression strongly decreases in most tissues, but persists in skeletal muscle, kidney, intestine, palate, and lens (Nagahama et al., 2001; Westbury et al., 2001). In adults, p57 is expressed in post-mitotic cells of a limited number of tissues (heart, brain, lungs, skeletal muscle, placenta, kidney, gonads, intestine, and more weakly in the liver and spleen), which distinguishes it from the ubiquitous expression of p27 and p21 (Lee et al., 1995; Matsuoka et al., 1995).

p57 STRUCTURE AND REGULATION

p57^{Kip2} is a protein of 316 amino acids in human and 335 in mice, with an apparent molecular weight of 57 kDa. The murine p57 protein is organized into four domains (Figure 2): domain I comprises the cyclin/CDK binding domain and has high homology to p21 and p27. Domain II is a Proline-rich region of 82 amino acids, followed by domain III of 107 amino

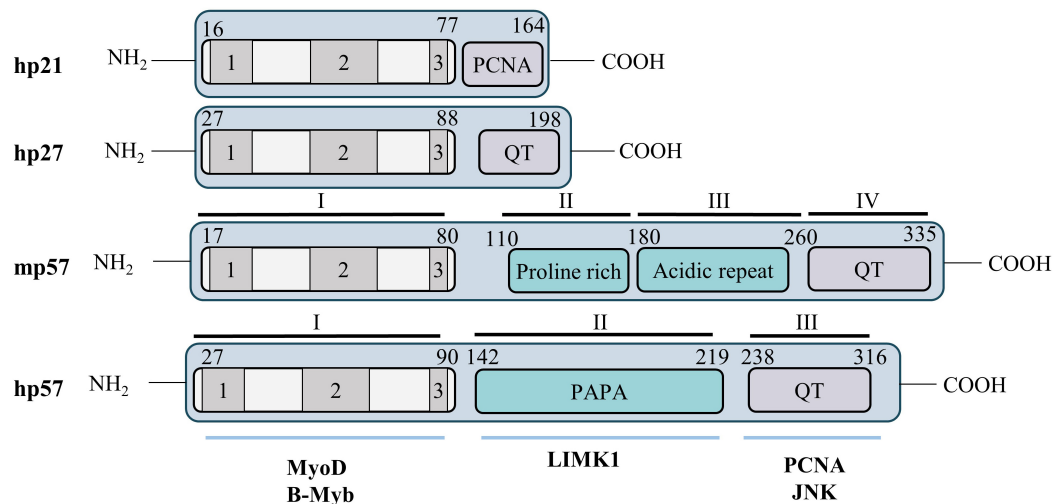


FIGURE 2 | Structure of the p57^{Kip2} protein. Cip/Kip proteins are highly conserved in their N-terminal domain that mediates binding to cyclins and CDKs, but diverge in their C-terminal part. Nevertheless, the C-terminus of p57 presents some homology with p21 (PCNA binding domain) and p27 (QT motif). Murine and human p57 are conserved in their N- and C-terminal domains but the central domains (II and III) in mice are substituted by a unique PAPA domain in human (II). The N-terminal CDK binding/inhibitory domain (KID) of p57 is subdivided in three domains: a cyclin binding domain (1), a CDK binding domain (2) and a 3₁₀ helix (3). The C-terminal QT domain (238–316) of p57 presents strong homology to the p27 QT motif at amino acids 302–316. It also contains three other conserved motifs: a PCNA binding domain (272–297) similar to p21, a nuclear localization signal (NLS, 278–281), and a CDK phosphorylation site (T310). Through its diverse domains p57 is able to interact with multiple partners involved in numerous cellular process, such as MyoD, b-Myb, LIMK1, PCNA, or JNK.

acids rich in acidic residues (glutamic and aspartic acids). Finally, domain IV comprises a conserved motif called the QT domain presenting homology with p27 (QT motif) and p21 (PCNA binding domain). Human p57 is conserved in the C- and N-terminal parts, however, the central domains II and III are replaced by a single distinct domain rich in Proline/Alanine repeats, the PAPA domain (**Figure 2**) (Lee et al., 1995; Matsuoka et al., 1995). It is important to note that, like other Cip/Kip family proteins, p57 is an intrinsically unstructured protein that adopts a tertiary conformation only after binding to its different partners (Adkins and Lumb, 2002; Lacy et al., 2004).

The N-terminal domain I is necessary and sufficient for cyclin/CDK complex inhibition. This domain is subdivided in three regions: a cyclin binding domain, a CDK binding site and a 3₁₀ helix. The 3₁₀ helix is not required for binding to cyclin/CDKs but allows inhibition of Cyclin A/CDK2 and Cyclin E/CDK2 activity by inserting into the catalytic pocket of CDK2, thus blocking ATP hydrolysis, as reported for p27 (Russo et al., 1996; Hashimoto et al., 1998). This N-terminal domain also mediates the interaction with transcription factors such as b-Myb and MyoD (Reynaud et al., 2000; Joaquin and Watson, 2003). The PAPA domain is unique to p57 and may confer to p57 distinct functionalities from p21 and p27 via the interaction with different proteins. For example, this central region of p57 interacts with the kinase LIMK1, a Rho effector involved in regulation of actin polymerization (Yokoo et al., 2003). Finally, the C-terminal QT domain of p57 shares homology with the C-termini of both p27 (QT motif) and p21 (PCNA binding site). Importantly, the PCNA binding site of p57 was found to participate in mediating growth inhibition (Watanabe et al., 1998) and gain-of-function mutations in this domain were later discovered to cause the development of growth-restriction syndromes such as IMaGe

(intrauterine growth restriction, metaphyseal dysplasia, adrenal hypoplasia congenita, and genital anomalies) and Silver Russell (see below) (Arboleda et al., 2012; Brioude et al., 2013b). The QT domain of p57 also mediates interaction with the stress-activated protein kinase JNK1 (Chang et al., 2003). A putative Nuclear Localization Sequence (NLS) consensus site has been identified, at the C-terminus of p57 by homology with p27 (Lee et al., 1995). Finally, the C-terminus of p57 contains a consensus site for CDK2 phosphorylation on Thr310 in human (Thr329 in mice) that allows degradation of p57, similarly to Thr187 on p27 (Kamura et al., 2003).

The degradation of p57 is mediated by the proteasome. Phosphorylation of Thr310 by cyclin E/CDK2 complexes creates a binding site for the F-box protein Skp2, leading to p57 ubiquitination by the Skp2-SCF (Skp1, Cullin, F-box) complex and to its degradation by the proteasome (Kamura et al., 2003). A second F-box protein, FBL12, has been involved in p57 degradation. In osteoblasts, TGFβ1 stimulates FBL12 expression that interacts with p57 phosphorylated on Thr310 and causes its proteasomal degradation independently of Skp2 (Kim et al., 2008).

ANIMAL MODELS OF p57

Knockout of *Cdkn1c* in mice (p57^{KO}) causes embryonic (approximately 10% of mutant embryos die between E13 and E16) and perinatal lethality, with less than 10% of animals surviving to adulthood (Yan et al., 1997; Zhang et al., 1997). p57^{KO} embryos display numerous developmental abnormalities that are mainly caused by defects in differentiation and increased apoptosis. For example, p57^{KO} mice frequently

exhibit cleft palate, abdominal wall closure defects (umbilical hernia and omphalocele) associated with defective abdominal muscle development, truncation or shortening of the intestine, bone shortening and ossification delay due to defective chondrocyte differentiation, adrenal hyperplasia, renal dysplasia, and increased apoptosis in the lens (**Table 1**) (Yan et al., 1997; Zhang et al., 1997; Susaki et al., 2009). Consistent with *Cdkn1c* imprinting, animals inheriting a null allele from their mother ($p57^{+/-m}$) exhibit a phenotype similar to homozygous $p57^{-/-}$ animals. Importantly, a transgenic approach to insert a second *Cdkn1c* allele outside of the imprinted locus (i.e., two expressed copies of *Cdkn1c*) caused intrauterine growth restriction and embryonic lethality (Andrews et al., 2007). Thus, these studies have shown that unlike other CDK inhibitors, p57 is required for embryonic development and that expression of a single *Cdkn1c* allele is required.

Indeed, mice lacking p21 develop normally and are tumor free for the first 7 months (Deng et al., 1995), however aging mice (~16 months) spontaneously develop tumors of hematopoietic, endothelial or epithelial origin (Martin-Caballero et al., 2001). Consistent with its CDK inhibitory function, p21 loss accelerates the development of Ras-induced mammary and salivary tumors (Adnane et al., 2000). Similarly, p27 loss does not cause overt developmental defects, however $p27^{KO}$ mice are significantly larger and present multiple organ hyperplasia due to increased cell proliferation, and display retinal dysplasia and female sterility (Fero et al., 1996; Nakayama et al., 1996). p27 deficient animals spontaneously develop pituitary tumors within a few months and are dramatically more susceptible to carcinogenesis induced by genotoxic agents or oncogene activation (Fero et al., 1996, 1998; Nakayama et al., 1996). Moreover, p27 acts as a haploinsufficient tumor suppressor, as p27 heterozygote mice also display a predisposition to tumor development induced by carcinogens or irradiation (Fero et al., 1998) or in conjunction with inactivation of another tumor suppressor such as PTEN (Di Cristofano et al., 2001). Finally, an inactivating mutation in p27 was discovered in rats as the cause of MENX (Multiple Endocrine Neoplasia X) syndrome. This mutation is a tandem duplication of eight

nucleotides causing a frameshift leading to rapid degradation of p27 and decreased p27 protein level (Pellegata et al., 2006). Subsequently, six germline mutations of p27 have been identified as the origin of a rare MEN syndrome in humans called MEN4 (Pellegata et al., 2006; Marinoni and Pellegata, 2011).

A number of functional redundancies and compensatory mechanisms between CKIs have been highlighted by the generation of double or triple mutants, as well as knock-in mutants (**Tables 1, 2**). Interestingly, double $p27^{-/-}/p57^{KO}$ or $p21^{-/-}/p57^{KO}$ knockout in mice exacerbate certain phenotypes of $p57^{KO}$ mice. There is worsening of placental and lens defects, and increased embryonic lethality in $p27^{-/-}/p57^{KO}$ animals (Zhang et al., 1998). On the other hand, $p21^{-/-}/p57^{KO}$ double mutation aggravates skeletal defects, and causes the appearance of phenotypes not observed in the single mutants, such as impaired lung and skeletal muscle development (Zhang et al., 1999). Triple $p21^{-/-}/p27^{-/-}/p57^{KO}$ knockout animals exhibit phenotypes similar to $p27^{-/-}/p57^{KO}$ mice and die between E11.5 and E15.5 (Tateishi et al., 2012) (**Table 2**) (for detailed review see, Ciernerych and Sicinski, 2005).

In addition, a $p57^{p27KI}$ knock-in mouse model, where the coding sequence of p27 was inserted in the p57 locus, revealed significant functional redundancy between p27 and p57 when compared with $p57^{KO}$ mice, as p27 corrects certain phenotypes caused by the absence of p57, highlighting the importance of CDK inhibition by p57 during development (**Table 1**) (Susaki et al., 2009). Nevertheless, several phenotypes of $p57^{KO}$ mice, such as kidney dysplasia, abdominal wall defects or adrenal hyperplasia, are not restored in $p57^{p27KI}$ mutants, indicating that p57 plays specific functions during development (**Table 1**) (Susaki et al., 2009). Generation of another knock-in mutant, $p57^{CK-}$, in which p57 no longer binds to cyclin/CDK complexes due to four point mutations, provided genetic evidence of

TABLE 1 | Summary of phenotypes observed in $p57^{KO}$, $p57^{p27KI}$, and $p57^{CK-}$ mice.

| $p57^{KO}$ | $p57^{p27KI}$ | $p57^{CK-}$ | Interpretation |
|-------------------------------|---------------|----------------|---------------------------------------|
| • Neonatal death (90%) | Rescue | Phenocopy | CDK dependent |
| • Lens defect (60%) | Rescue | Phenocopy | CDK dependent |
| • Bone shortening (100%) | Rescue | Phenocopy | CDK dependent |
| • Bone shortening (100%) | Rescue | Phenocopy | CDK dependent |
| • Abdominal wall defect (95%) | Phenocopy | Phenocopy | CDK dependent, but p27 cannot rescue? |
| • Intestine shortening (30%) | Rescue | Rescue | CDK independent, common with p27? |
| • Kidney dysplasia (80%) | Phenocopy | Rescue | CDK independent |
| • Cleft palate (50%) | Rescue | Increase (76%) | CDK dependent and independent |
| • Adrenal hyperplasia (70%) | Rescue 50% | Increase | CDK dependent and independent |

TABLE 2 | Phenotypes associated with loss of Cip/Kip proteins in mice.

| Genotypes | Phenotypes | References |
|--------------------------------|---|--|
| $p21^{-/-}$ | Viable No major developmental anomalies | Deng et al., 1995 |
| $p27^{-/-}$ | Viable Organomegaly, female sterility, increase body size | Nakayama et al., 1996 Fero et al., 1996 |
| $p57^{-/-}$ | Lethal at birth Multiple developmental anomalies | Yan et al., 1997 Zhang et al., 1997 |
| $p21^{-/-} p27^{-/-}$ | Viable, similar to $p27^{-/-}$ with more pronounced ovarian hyperplasia | Tateishi et al., 2012 Jirawatnotai et al., 2003 |
| $p21^{-/-} p57^{KO}$ | Lethal at birth, similar to $p57^{-/-}$ with new phenotypes (impaired lung and skeletal muscle development) | Zhang et al., 1999 |
| $p27^{-/-} p57^{KO}$ | Embryonic lethal (E12–E16.5), similar to $p57^{KO}$ with more pronounced phenotypes (placenta, lens) | Zhang et al., 1998 |
| $p21^{-/-} p27^{-/-} p57^{KO}$ | Embryonic lethal (E11.5–E15.5), similar to $p27^{-/-} p57^{KO}$ | Tateishi et al., 2012 |

cyclin/CDK independent functions of p57 during development (Duquesnes et al., 2016). Indeed, some phenotypes of p57^{KO} mice are completely absent in p57^{CK−} mice, such as kidney dysplasia and intestinal shortening (Table 1). Surprisingly, others phenotypes, including adrenal hyperplasia and cleft palate, were aggravated or more frequent in p57^{CK−} mice compared to p57^{KO}, suggesting that in these tissues p57 plays both CDK dependent and independent roles (Table 1). A possible explanation for these phenotypes is that CDK-dependent degradation of the p57^{CK−} protein is partly defective, leading to increased levels of the mutant protein, which could potentially exert a dominant negative effect (Duquesnes et al., 2016).

FUNCTIONS OF p57

Canonical Function in Cell Cycle Regulation

The role of Cip/Kip family proteins as CDK inhibitor is well-established, and like p21 and p27, p57 causes a cell cycle arrest in G₁ (Sherr and Roberts, 1999; Besson et al., 2008). p57 is able to bind and inhibit all cyclin/CDK complexes, however, with a lower affinity for cyclin B/CDK1 and cyclin D2/CDK6 complexes (Matsuoka et al., 1995). p57 mediates cyclin/CDK complex inhibition by blocking the substrate interaction domain on cyclins and by insertion into the catalytic pocket of the CDKs, thus preventing binding of ATP and catalytic activity (Russo et al., 1996). Like other Cip/Kip proteins, p57 promotes the assembly of Cyclin D1-CDK4/6 complexes, which may remain active (Labaer et al., 1997). Indeed, the CDK inhibitory activity of p27 and p21 is regulated by phosphorylation on Tyr88 and Tyr77, respectively, which relaxes the inhibitory conformation of the CKI, allowing partial CDK activation (Chu et al., 2007; Grimmmler et al., 2007; James et al., 2008; Huang et al., 2015). This tyrosine is conserved in p57 (Tyr91), thus, a similar regulation of its CDK inhibitory activity by tyrosine kinases appears likely, although there is no direct evidence for this yet.

p57 can also inhibit the cell cycle via binding and inhibition of PCNA. Indeed, individual mutation of the CDK or PCNA binding site only results in partial loss of the growth inhibitory activity of p57 *in vitro*, whereas simultaneous loss of these two interactions completely abolishes the cell cycle inhibitory activity of p57 (Watanabe et al., 1998).

Finally, p57 also plays a role in trophoblast endoreplication. Endoreplication is a succession of G₁ and S phases without intervening mitosis, leading to formation of giant polyploid cells. This phenomenon is observed during trophoblast differentiation to allow placenta implantation. p57 levels oscillate during endoreplication, decreasing before S phase entry and accumulating after S phase and in G₁ (Hattori et al., 2000). p57^{KO} mice exhibit placental defects and it was shown *in vitro* that p57 is required to trigger mouse trophoblast endoreplication by inhibiting CDK1 activity (Ullah et al., 2008; Susaki et al., 2009).

Non-canonical Functions of p57

In addition to cell cycle control, an increasing number of studies have described non-canonical functions of p57. The ability of

p57 to regulate various cellular processes probably stems from its multi-domain structure and ability to interact with many protein partners. Indeed, a protein interactome has identified 183 direct potential partners of p57 involved in various cellular functions, including regulation of transcription, cytoskeleton and apoptosis (Duquesnes et al., 2016).

Cytoskeleton Regulation

All Cip/Kip family members have been shown to regulate cytoskeleton organization and cell migration by acting at different levels of the Rho/ROCK/LIMK/Cofilin pathway (Besson et al., 2004, 2008). *In vivo*, shRNA-mediated silencing of p57 delays neuronal migration in the cortex during development (Itoh et al., 2007) and p57 overexpression promotes radial migration of neural precursors (Tury et al., 2011). p57 is able to interact with LIMK1 via its unique central domain (Yokoo et al., 2003). LIMK1 is a serine/threonine kinase that promotes actin stress fiber assembly via phosphorylation of Cofilin, which inhibits its actin severing activity. LIMK1 is activated by the effectors of RhoA, ROCK1/2 (Rho-kinases) (Bernard, 2007). Binding of p57 to LIMK1 results in nuclear translocation and sequestration of LIMK1, which prevents Cofilin inhibition, resulting in decreased actin stress fiber formation (Yokoo et al., 2003). In agreement with these observations, p57 transfection into Schwann cells results in nuclear sequestration and inhibition of LIMK1, and a lack of Schwann cell differentiation (Heinen et al., 2008b). However, in HeLa cells the p57/LIMK1 interaction did not induce LIMK1 relocation in the nucleus, but increased its kinase activity, resulting in an increased number of stress fibers and decreased cell migration (Vlachos and Joseph, 2009). Similar findings were reported in hepatocellular carcinoma cells and decreased p57 levels in hepatocellular carcinoma samples correlated with the presence of metastases (Guo et al., 2015). In glioblastoma cells, p57 expression was also reported to inhibit cell migration and invasion (Sakai et al., 2004). Therefore, the role of p57 on cytoskeleton remodeling and migration appears to be mediated via its interaction with LIMK1 and to be dependent of the cellular context and subcellular location.

p57 and Apoptosis

Several phenotypes observed in p57^{KO} mice can be attributed to an increase of apoptosis caused by hyperproliferation and/or differentiation defects. Interestingly, p57 has the ability to modulate apoptosis by different mechanisms, and both pro and anti-apoptotic roles have been reported depending on the cellular context, the signaling pathway involved and the stress to which cells are submitted (Rossi and Antonangeli, 2015).

p57 protects against apoptosis indirectly by inhibiting CDKs. In response to stress, p38 phosphorylates p57 on Thr143, which increases its affinity for CDK2 and results in G₁ cell cycle arrest (Joaquin et al., 2012). p38 or p57 deficient MEFs (Mouse Embryonic Fibroblasts) exhibit decreased viability in response to osmotic or oxidative stress and UV exposure (Joaquin et al., 2012). Overexpression of p57 in HEK293 or HeLa cells can also protect against apoptosis independently of CDK inhibition by regulating the JNK/SAPK signaling pathway. In this model,

p57 interacts with JNK1 via its QT domain, preventing its interaction with c-Jun and thus inhibiting its kinase activity. Expression of the QT domain is sufficient to block JNK/SAPK mediated apoptosis in response to UVs or MEKK overexpression (Chang et al., 2003).

Conversely, in a HeLa Tet-On derived cell line that overexpresses p57 after induction, p57 potentiates apoptosis in response to different stresses. p57 sensitized cells to apoptosis induced by genotoxic agents such as staurosporine, cisplatin or etoposide, but had no effect on Fas-mediated apoptosis (Samuelsson et al., 2002; Vlachos et al., 2007). The pro-apoptotic effect of p57 in response to these drugs is CDK-independent and involves activation of the mitochondrial apoptosis pathway. In response to staurosporine, p57 relocates to mitochondrial membranes and promotes Bax activation and a decrease of mitochondrial membrane potential, resulting in cytochrome-c release in the cytosol and activation of caspases 9 and 3 (Vlachos et al., 2007). The specificity of the mitochondrial pathway was confirmed by overexpression of Bcl-2, which prevented the pro-apoptotic effect of p57 (Vlachos et al., 2007). The mechanism by which p57 activates the mitochondrial pathway is dependent on its ability to interact and stimulate LIMK1 activity. LIMK1-induced stabilization of actin fibers causes the displacement of hexokinase 1 (HK-1), a regulatory enzyme of the VDAC (Voltage-dependent Anion Channel) mitochondrial channel, allowing mitochondrial membrane depolarization and thus activation of the mitochondrial apoptotic pathway (Kavanagh et al., 2012). Finally, in H1299 non-small cell lung carcinoma cells, p57 transfection promoted p73 β -mediated apoptosis in response to cisplatin, although the mechanism was not investigated (Gonzalez et al., 2005).

Regulation of Transcription by p57

Like other Cip/Kip family members, p57 can repress transcription indirectly via the inhibition of cyclin/CDK complexes, which prevents phosphorylation of Rb proteins and E2F transcription factors activation (Sherr and Roberts, 1999; Besson et al., 2008). p57 also negatively regulates the activity of RNA polymerase II via its interaction with E2F1. The interaction with E2F1 allows the recruitment of p57 to DNA, where it inhibits CDK7 and CDK9, resulting in decreased phosphorylation of the C-terminal domain (CTD) of RNA polymerase II and leading to a decrease of global transcription (Ma et al., 2010). In addition to this CDK-dependent regulation, p57 may also directly regulate the activity of transcription factors.

Indeed, p57 binds directly to b-Myb and inhibits its transcriptional activity independently of CDKs (Joaquin and Watson, 2003). p57 is also involved in regulating the stability of the bHLH transcription factor MyoD. p57 promotes MyoD stability and muscle differentiation by inhibiting CDK2, preventing MyoD phosphorylation by CDK2 on Ser200, which destabilizes the protein (Reynaud et al., 1999). p57 also stabilizes MyoD in a CDK-independent manner by interacting directly with MyoD via its N-terminal 3₁₀ Helix region, protecting MyoD from degradation and promoting transactivation of muscle genes (Reynaud et al., 2000).

Similarly, p57 can interact directly with other bHLH transcription factors, including Ascl1 (Achaete-scute-like 1), NeuroD1 and Math2/NeuroD6 in neural progenitors. p57 then acts as a transcriptional repressor by directly inhibiting Ascl1 activity at target promoters, independently of CDKs (Joseph et al., 2009). Similarly, p57 can inhibit the transcriptional activity of Nurr1 independently of CDKs *in vitro*, and thus regulates dopaminergic neuron maturation (Joseph et al., 2003).

Finally, it was shown recently that p57 may also positively regulate transcription (Kullmann et al., 2020). p57 binds to and activates FHL2 (four-and-a-half LIM only protein 2), a multifunctional LIM domain only protein, which binds to and modulates the activity of several transcription factors, such as AP-1, β -catenin or the androgen receptor, by acting as a coactivator (Muller et al., 2000; Tran et al., 2016). FHL2 is inhibited by HDACs, and by binding to FHL2, p57 competes with HDAC1 and HDAC3 for FHL2 binding and prevents its inhibition (Kullmann et al., 2020).

Moreover, an interactome revealed that p57 has multiple partners involved in transcriptional regulation, including many transcription factors and HDAC7 (histone deacetylase 7), suggesting that p57 plays a major role in the regulation of transcription (Duquesnes et al., 2016).

p57 and Differentiation

p57 plays a key role in the differentiation of many cell types by inhibiting CDKs, promoting cell cycle exit, or via CDK-independent mechanisms. Several phenotypes observed in p57^{KO} mice are caused by a delay or defect of differentiation (Yan et al., 1997; Zhang et al., 1997).

Several studies have shown that p57 regulates various aspects of neurogenesis, notably by controlling cell differentiation in the central and peripheral nervous system. p57 is present in neural stem cells and controls their fate by promoting differentiation into astrocytes at the expense of the oligodendrocyte lineage (Jadasz et al., 2012). In the peripheral nervous system, p57 inhibits Schwann cell differentiation and its silencing by shRNA results in cell cycle exit, cell growth and differentiation, as well as an increase of myelin production (Heinen et al., 2008a). Similarly, in the central nervous system, p57 inhibits oligodendrocyte differentiation (Kremer et al., 2009). However, other reports found that p57 promotes differentiation of oligodendrocyte progenitors in rat primary cells *in vitro*, as well as *in vivo* in zebrafish (Park et al., 2005; Dugas et al., 2007). In the nucleus, p57 interacts and inhibits Ascl1, a transcription factor promoting oligodendrocyte differentiation (Nakatani et al., 2013; Gottle et al., 2015). During oligodendrocyte differentiation, p57 relocates to the cytoplasm, promoting the export and inhibition of the transcriptional repressor Hes5 and relieving Ascl1 inhibition, enhancing differentiation (Gottle et al., 2015). In this study, p57 regulated the localization of LIMK1 and CDK2, which contributed to oligodendrocyte differentiation (Gottle et al., 2015). Thus, the effect of p57 on oligodendrocyte differentiation appears dependent on its subcellular localization. In addition to these cell types, p57 is involved in cell cycle exit of neural progenitors and in the specification of amacrine retinal

interneurons (Dyer and Cepko, 2000), as well as in the differentiation of dopaminergic neurons (Joseph et al., 2003). In the latter, the transcription factor Nurr1 up-regulates p57 expression, and in turn, p57 binds to and inhibits Nurr1 transcriptional activity, promoting differentiation (Joseph et al., 2003).

p21 and p57 cooperate and are required *in vivo* for terminal differentiation of skeletal muscle cells. p21^{-/-}/p57^{KO} mice exhibit altered skeletal muscle differentiation due to increased proliferation, myoblast apoptosis, causing defects in myotube formation (Zhang et al., 1999). Expression of p57 increases during muscle differentiation and is induced indirectly by MyoD, via p73. In turn, p57 stabilizes MyoD in a positive feedback loop, promoting myogenesis (Vaccarello et al., 2006). MyoD can also directly stimulates p57 expression epigenetically by binding a negative regulatory *cis*-element, causing chromatin remodeling and lifting the inhibition of p57 expression (Busanello et al., 2012). The transcription factors Sp1 and Egr1 also participate in induction of p57 during myogenic differentiation (Figliola et al., 2008). In rhabdomyosarcomas, the chimeric protein PAX3-FOXO1 indirectly inhibits p57 transcription via destabilization of Egr1, which prevents myoblasts differentiation. Re-expressing p57 in these cells is sufficient to restore myogenic differentiation (Roeb et al., 2007).

p57 also participates in chondrocyte differentiation. Chondrocytes hypertrophic differentiation is required for ossification. Differentiated chondrocytes are characterized by high collagen X expression, strong alkaline phosphatase activity, and increased cell volume (Stewart et al., 2004). p57^{KO} mice exhibit bone shortening and an ossification delay caused by delayed chondrocyte differentiation associated with increased proliferation and decreased collagen X expression (Yan et al., 1997; Zhang et al., 1997). In chondrocytes, p57 expression is stimulated by C/EBP β during differentiation, leading to cell cycle arrest (Hirata et al., 2009) and p57 also potentiates the induction of collagen X expression mediated by BMP2 (Stewart et al., 2004).

Finally, in several tissues, the Notch/Hes1 signaling pathway inhibits p57 expression to promote proliferation of progenitors and prevent cell cycle exit and thus precocious differentiation, notably in the intestine (Riccio et al., 2008), lens (Jia et al., 2007), and pancreas (Georgia et al., 2006). Indeed, loss of p57 expression in human is associated with hyperinsulinism during infancy due to increased production of β -islet cells (Kassem et al., 2001; Avrahami et al., 2014). Conversely, bi-allelic expression of p57 or gain-of-function mutations associated with the IMAGE syndrome lead to reduced β -islet cell number and predisposition to diabetes (Kerns et al., 2014; Asahara et al., 2015). In fact, p57 appears to be a target of choice to promote the regeneration of pancreatic β -islets (Avrahami et al., 2014; Ou et al., 2019).

p57 in the Regulation of Stem Cell Fate and Maintenance

Several studies have revealed a crucial role of p57 in maintaining quiescence of resident adult stem cells in multiple tissues.

p57 is required for hematopoietic stem cell quiescence and their maintenance. Indeed, in a conditional knockout model, p57 ablation in adult mice results in a decreased

hematopoietic stem cell pool caused by an exit of quiescence state (G₀) and induction of apoptosis (Matsumoto et al., 2011b). Reconstitution of the hematopoietic system after transplantation is also reduced in absence of p57 (Matsumoto et al., 2011b). These hematopoiesis defects are corrected by expression of p27 in the p57 locus (p57^{p27KI} knock-in mice) (Matsumoto et al., 2011b). In hematopoietic stem cells of the fetal liver, p57 loss is accompanied by an increase of p27 expression, nevertheless neither p21 nor p27 knockout causes any defect, confirming that p57 is the primary CKI required for hematopoietic stem cell maintenance (Zou et al., 2011). Consistently, TGF- β 1 induces quiescence of hematopoietic stem cells and increases p57 levels (Yamazaki et al., 2009). Conversely, increased Skp2 expression, which induces p57 degradation, is necessary for cell cycle reentry of hematopoietic stem cells (Rodriguez et al., 2011). The role of p57 in controlling hematopoietic stem cell quiescence involves its interaction with the chaperone Hsc70, which results in cytoplasmic sequestration of Hsc70/Cyclin D1 complexes, inhibiting cell cycle entry. Similarly, p27 may also interact with Hsc70 to compensate for the loss of p57 (Zou et al., 2011).

In the lung, homeostasis and tissue regeneration are supported by resident pulmonary stem cells called BASCs (Bronchioalveolar Stem Cells) (Kim et al., 2005; Liu et al., 2019; Salwig et al., 2019). The self-renewal of these stem cells requires a precise regulation of p57 expression levels. Indeed, either loss or increase of p57 expression in BASCs causes a lack of self-renewal, leading to defective tissue regeneration (Zacharek et al., 2011). These results highlight the importance of p57 imprinting and monoallelic expression. In the lung, Bmi1 controls the expression of p57 and other imprinted genes, however, no overt methylation changes at individual promoters or ICRs were observed in absence of Bmi1, suggesting that Bmi1 regulates imprinted gene expression by another mechanism (Zacharek et al., 2011). How p57 controls BASC maintenance has not yet been investigated.

In the adult hippocampus, p57 is expressed in quiescent neural stem cells and absent in proliferative progenitors. The presence of p57 is critical for maintaining neural stem cell quiescence and while p57 ablation initially leads to an increase in stem cell proliferation and stimulates neurogenesis, it results over time in the exhaustion of the neural stem cell population and impairs neurogenesis in aged mice (Furutachi et al., 2013). Similarly, Nestin^{Cre}-driven deletion of p57 in the developing brain causes a decrease of Pax2⁺ interneuron progenitor number due to massive p53-dependent apoptosis, resulting in hydrocephalus (Matsumoto et al., 2011a). In contrast, during cortical development, p57^{KO} embryos exhibit macrocephaly caused by an increased proliferation of neural progenitors and stem cells (Mairet-Coello et al., 2012). p57 appears to play a key role in timing cell cycle exit of specific neural progenitor populations, and p57 deregulation leads to abnormal development of specific neuron layers, especially during late neurogenesis (Mairet-Coello et al., 2012). A recent study using the MADM (mosaic analysis with double markers) system revealed that p57 regulates cortical neurogenesis by distinct mechanisms (Laukoter et al., 2020). p57 controls neural stem cell proliferation in a non-cell autonomous manner, with a complete knockout causing macrocephaly (Laukoter et al., 2020).

However, conditional deletion of p57 in radial precursor (*Emx1*⁺ cells) causes microcephaly due to p53-mediated apoptosis, in this case p57 exerts a cell-autonomous growth-promoting function by promoting survival of maturing cortical projection neurons (Laukoter et al., 2020), consistent with the *Nestin*^{Cre}-driven phenotype previously observed (Matsumoto et al., 2011a). Interestingly, there is some contribution of the paternal allele during mouse brain development since *Nestin*^{Cre}-driven deletion of the paternal allele results in reduced adult brain size due to increased apoptosis of neural progenitors and a slight reduction of proliferation (Imaizumi et al., 2020). These findings are consistent with earlier observations that p57 exhibits biallelic expression in the developing brain (Matsuoka et al., 1996). Finally, p57 was recently involved in neural stem cell fate determination. In *Drosophila*, neural stem cells can enter a quiescence state either in G₀ or G₂ (25 and 75%, respectively) that determines their fate, as G₂ blocked cells can be rapidly activated to divide in response to nutritional stimuli, while G₀ cells respond more slowly (Otsuki and Brand, 2018). The choice between these two types of quiescence is determined at the embryonic stage and depends on the presence of the p57 homolog, Dacapo, which favors entry in the G₀ quiescent state at the expense of the G₂ one (Otsuki and Brand, 2019). Dacapo deletion leads to a change in the fate of the neural stem cells, which are then preferentially oriented toward a G₂ quiescence state (Otsuki and Brand, 2019).

In the developing skeletal muscle, p57 inhibition is required for maintenance of certain stem/progenitor cells. Notch inhibits p57 expression in Pax3^{+/7+} muscle progenitors via Hes1, allowing amplification of the progenitor pool (Zalc et al., 2014). Loss of Notch signaling leads to an increase of p57 expression in muscle progenitors, which is associated with precocious differentiation and progenitor depletion (Zalc et al., 2014). In adult muscle, satellite cells, the resident stem cells, derive from Pax3^{+/7+} progenitors and are mobilized in case of damage to regenerate muscle fibers. Surprisingly, p57 is not expressed in quiescent satellite cells but is induced during their mobilization (Mademtzoglou et al., 2018). In addition, loss of p57 *in vivo* increases proliferation and self-renewal of progenitors and myoblasts at the expense of their differentiation, and in case of damage, p57 absence causes satellite cell depletion and delays muscle regeneration (Mademtzoglou et al., 2018).

Finally, the presence of p57 was reported in other quiescent adult tissue stem cells, such as hair follicle stem cells (Leishman et al., 2013) as well as in Mex3a^{High} quiescent intestinal stem cells (Barriga et al., 2017), suggesting that p57 plays a general role in the maintenance of resident stem cells.

p57 IN HUMAN PATHOLOGIES

Deregulation of imprinting of the 11p15.5 locus, as well as loss of heterozygosity (LOH) or point mutations of *CDKN1C* are responsible for the development of several hereditary pathologies and may contribute to cancer development and progression. Alterations that cause loss of p57 function lead to the development of the Beckwith–Wiedemann syndrome, while

p57 gain of function leads to the development of Silver–Russell and IMaGe syndromes.

Beckwith–Wiedemann Syndrome

Beckwith–Wiedemann syndrome (BWS) (OMIM # 130650) is a rare genetic disorder with a prevalence of 1/13700 births, characterized by excessive growth, developmental anomalies and tumor predisposition during childhood. BWS has a highly variable presentation and patients usually display only a subset of phenotypes. Diagnosis is based on the presence of at least three major criteria (macrosomia, macroglossia, abdominal wall defects, hemihyperplasia, embryonal tumors, renal abnormalities, anterior ear lobe creases) or the association of two major criteria with at least one minor phenotype (neonatal hypoglycemia, characteristic facies, diastasis recti, cardiomegaly/structural cardiac anomalies...) (Weksberg et al., 2010). A molecular anomaly, of epigenetic or genetic origin, in the 11p15.5 region is identified in approximately 80% of BWS patients. Most epigenetic abnormalities are mosaic, meaning that only a fraction of the cells carry the molecular defect. The severity and penetrance of the phenotypes therefore depends on the underlying molecular mechanism and the percentage of mosaicism (Brioude et al., 2013a).

The majority of BWS patients present epigenetic abnormalities. Loss of ICR2 methylation on the maternal allele is the most common form and is observed in 50% of patients (Eggermann et al., 2014b). This anomaly results in biallelic expression of *KCNQ1OT1* and thus in loss of *CDKN1C* expression (**Figure 1**) (Eggermann et al., 2014b). Patients with anomalies of this centromeric region have a more severe phenotype and exhibit macroglossia and abdominal wall defects. Gain of methylation on ICR1 is observed in 5% of cases, resulting in biallelic expression of *IGF2*. Patients with this defect display a higher risk of developing tumors and organomegaly (Weksberg et al., 2010; Brioude et al., 2013a). Several genetic alterations are also responsible for BWS development. Among genetic anomalies, paternal isodisomies (UPD = Uniparental Disomy) are found in approximately 20% of patients. UPDs correspond to the duplication of the paternal 11p15.5 locus, with no maternal contribution for this region, thus leading to biallelic *IGF2* expression and loss of *CDKN1C* expression (Weksberg et al., 2010). Patients with UPDs have an increased risk of hemihyperplasia (Brioude et al., 2013a). Other chromosomal rearrangements have also been reported in rare (2–3%) cases, including extensive paternal duplications, carrying both ICR1 and ICR2 regions (1%), translocations/inversion (1%), which are usually transmitted by the mother, as well as ICR microdeletions (<1%) (Weksberg et al., 2010; Eggermann et al., 2014a). Finally, maternally inherited point mutations in *CDKN1C* are observed in 5% of sporadic cases and are responsible for the majority of familial cases (50%) of BWS (Eggermann et al., 2014b). Patients with *CDKN1C* mutations have particular phenotypes: almost all of them display abdominal wall defects (umbilical hernia or omphalocele) and have an increased incidence of cleft palate, genital anomalies and polydactyly (Romanelli et al., 2010). Mutations of *CDKN1C* described in BWS cover the entire coding region. They are mostly nonsense

mutations leading to truncation of the protein or mutations causing a frameshift, which strongly alters the structure of the protein. Some missense mutations have also been described in the cyclin/CDK binding domain (Eggermann et al., 2014b; Brioude et al., 2015).

Silver Russell and IMAGe Syndromes

In opposition to BWS, p57 gain of function mutations are associated with two very rare disorders, Silver-Russell syndrome (SRS) (OMIM # 180860) (1/100,000 birth) (Brioude et al., 2013b) and IMAGe syndrome (Intrauterine Growth Retardation, Metaphyseal dysplasia, Adrenal insufficiency, Genital abnormalities) (OMIM # 614732) (only a few dozen cases reported worldwide) (Arboleda et al., 2012). These pathologies cause opposite phenotypes to BWS and share a number of features, notably intrauterine growth retardation (Eggermann et al., 2014b).

The study of a familial form of IMAGe syndrome led to the identification of five missense mutations located in the PCNA binding domain of p57 (Arboleda et al., 2012). Expression of a transgene carrying these mutations in *Drosophila* caused decreased eye, wing and vascular network size, consistent with a gain of function in p57 (Arboleda et al., 2012). *In vitro*, these mutations were found to decrease binding to PCNA and to impair p57 ubiquitination, leading to p57 stabilization and inhibition of proliferation (Arboleda et al., 2012; Borges et al., 2015). Interestingly, mutation in DNA polymerase ϵ were recently identified in 15 cases of IMAGe syndrome (Logan et al., 2018). Given the impact of p57 mutations found in IMAGe on its interaction with PCNA, it would be interesting to investigate further their effect on PCNA function, DNA replication and S phase progression.

The most frequent molecular anomalies in SRS patients are loss of ICR1 methylation (60% of cases), which result in biallelic expression of *H19* and thus loss of *IGF2* expression. Chromosomal rearrangements with maternal duplications of the centromeric domain, containing ICR2, or of both domains have also been observed (Wakeling et al., 2017). Nevertheless, point mutations in *CDKN1C* causing a gain of function in p57 were recently found to cause SRS. Indeed, a gain of function mutation in the PCNA binding domain of p57 was identified in a familial form of SRS (Brioude et al., 2013b). Interestingly, the residue mutated (Arg279Leu) is also mutated in IMAGe syndrome (Arg279Pro). Tissue culture experiments suggest that this mutation in p57 does not affect the cell cycle but leads to stabilization of the protein, consistent with the ubiquitination defect previously observed in IMAGe syndrome (Brioude et al., 2013b).

p57 and Cancer

Like other CKIs, p57 is a putative tumor suppressor. However, the lethality of p57^{KO} mice has so far prevented to test this formally *in vivo* and the involvement of p57 in cancers remains to be addressed in animal models. Nevertheless, several lines of evidence indicate that p57 plays a role in carcinogenesis. For instance, BWS patients are predisposed to tumor development (Weksberg et al., 2010) and decreased p57 expression is observed

in many types of tumors, including in gastric, colorectal, pancreatic, pulmonary, and mammary carcinomas, as well as in leukemia (Li et al., 2003; Pateras et al., 2009; Borriello et al., 2011; Kavanagh and Joseph, 2011; Weis et al., 2015). Moreover, decreased p57 expression correlates with aggressiveness in several types of tumors and is associated with poor prognosis (Kavanagh and Joseph, 2011; Qiu et al., 2018). Interestingly, *CDKN1C* mutations are not frequently observed in cancers (Pateras et al., 2009). Loss of p57 expression in human carcinomas is caused predominantly by loss of heterozygosity of the 11p15.5 locus, methylation of the *CDKN1C* promoter, and histone methylations (Kikuchi et al., 2002; Pateras et al., 2006; Weis et al., 2015). In fact, loss of imprinting of *KCNQ1OT1* has been observed in colorectal cancer samples, but did not necessarily correlated with p57 expression (Nakano et al., 2006). However, loss of p57 expression has been observed in colorectal cancer, mainly due to promoter hypermethylation (Kikuchi et al., 2002) and it was shown that the expression of the methyltransferase DNMT3a is strongly increased in colorectal tumors (Weis et al., 2015). Consistently, DNMT3a deletion inhibits tumor formation *in vivo* at least in part by increasing p57 expression (Weis et al., 2015). Moreover, several miRNAs and lncRNAs have also been shown to repress p57 in various cancers, as described earlier (Kavanagh and Joseph, 2011; Stampone et al., 2018). Finally, loss of p57 may also be due to increased degradation caused by Skp2 overexpression (Pateras et al., 2006).

CONCLUSION

p57^{Kip2} has the particularity of being the only CDK inhibitor required for embryonic development. Since its discovery as a cyclin/CDK inhibitor, a growing number of studies have shown that p57 is a multifunctional protein involved in the regulation of other cellular processes such as cell migration, differentiation, apoptosis, transcriptional regulation or stem cell specification and fate. The generation of a p57^{CK-} knock-in mouse model has provided genetic evidence that some of its functions are independent of cyclins/CDKs during development, yet the underlying mechanisms remain largely unknown. How p57 is regulated also remains largely unclear. In view of its multiple functions, a better understanding of p57's functions and regulation would improve our comprehension of normal development and of the etiology of several genetic disorders and cancers. The fact that p57 is subjected to paternal imprinting makes it particularly vulnerable to genetic alterations leading to loss (BWS, cancer) or gain (IMAGe and SRS) of function of the only active allele. In addition to complex developmental growth disorders, p57 down-regulation is associated with the development of cancers and its decreased expression is correlated with aggressiveness in several tumor types. For example, decreased p57 expression correlates with poor clinical outcome in breast cancer (Yang et al., 2009). Similarly, p57 levels are inversely related to tumor growth and cancer stage in non-small cell lung cancer, hepatocellular and pancreatic carcinomas and others (Ito et al., 2001a,b; Pateras et al., 2006). Interestingly, in colorectal cancer, p57 levels are increased in low grade adenomas and

finally decrease in primary carcinomas (Li et al., 2003), perhaps reflecting a mechanism to initially limit tumor progression. Similarly, in Wilm's tumor, loss of heterozygosity of the 11p15.5 locus is associated with the reactivation of the paternal allele of p57, possibly to limit cell proliferation and cancer progression (Overall et al., 1996; Taniguchi et al., 1997). To conclude, several lines of evidence indicate a prominent role for p57 during tumorigenesis and stem cell regulation, and a significant number of studies suggest that p57 is a pertinent prognostic marker and that it may hold therapeutic potential both for anticancer treatment and to manipulate tissue progenitor/stem cells for regenerative medicine.

REFERENCES

- Adkins, J. N., and Lumb, K. J. (2002). Intrinsic structural disorder and sequence features of the cell cycle inhibitor p57Kip2. *Proteins* 46, 1–7. doi: 10.1002/prot.10018
- Adnane, J., Jackson, R. J., Nicosia, S. V., Cantor, A. B., Pledger, W. J., and Sebt, S. M. (2000). Loss of p21WAF1/CIP1 accelerates Ras oncogenesis in a transgenic/knockout mammary cancer model. *Oncogene* 19, 5338–5347. doi: 10.1038/sj.onc.1203956
- Andrews, S. C., Wood, M. D., Tunster, S. J., Barton, S. C., Surani, M. A., and John, R. M. (2007). Cdkn1c (p57Kip2) is the major regulator of embryonic growth within its imprinted domain on mouse distal chromosome 7. *BMC Dev. Biol.* 7:53. doi: 10.1186/1471-213X-7-53
- Arboleda, V. A., Lee, H., Parnai, R., Fleming, A., Banerjee, A., Ferraz-De-Souza, B., et al. (2012). Mutations in the PCNA-binding domain of CDKN1C cause image syndrome. *Nat. Genet.* 44, 788–792. doi: 10.1038/ng.2275
- Asahara, S., Etoh, H., Inoue, H., Teruyama, K., Shibutani, Y., Ihara, Y., et al. (2015). Paternal allelic mutation at the Kcnq1 locus reduces pancreatic beta-cell mass by epigenetic modification of Cdkn1c. *Proc. Natl. Acad. Sci. U.S.A.* 112, 8332–8337. doi: 10.1073/pnas.1422104112
- Avrahami, D., Li, C., Yu, M., Jiao, Y., Zhang, J., Naji, A., et al. (2014). Targeting the cell cycle inhibitor p57Kip2 promotes adult human beta cell replication. *J. Clin. Invest.* 124, 670–674. doi: 10.1172/jci69519
- Barriga, F. M., Montagni, E., Mana, M., Mendez-Lago, M., Hernando-Momblona, X., Sevillano, M., et al. (2017). Mex3a marks a slowly dividing subpopulation of Lgr5+ intestinal stem cells. *Cell Stem Cell* 20, 801.e7–816.e7. doi: 10.1016/j.stem.2017.02.007
- Bernard, O. (2007). Lim kinases, regulators of actin dynamics. *Int. J. Biochem. Cell Biol.* 39, 1071–1076. doi: 10.1016/j.biocel.2006.11.011
- Besson, A., Assoian, R. K., and Roberts, J. M. (2004). Regulation of the cytoskeleton: an oncogenic function for CDK inhibitors? *Nat. Rev. Cancer* 4, 948–955. doi: 10.1038/nrc1501
- Besson, A., Dowdy, S. F., and Roberts, J. M. (2008). CDK inhibitors: cell cycle regulators and beyond. *Dev. Cell* 14, 159–169. doi: 10.1016/j.devcel.2008.01.013
- Borges, K. S., Arboleda, V. A., and Vilain, E. (2015). Mutations in the PCNA-binding site of CDKN1C inhibit cell proliferation by impairing the entry into S phase. *Cell Div.* 10:2. doi: 10.1186/s13008-015-0008-8
- Borriello, A., Caldarelli, I., Bencivenga, D., Criscuolo, M., Cucciolla, V., Tramontano, A., et al. (2011). p57(Kip2) and cancer: time for a critical appraisal. *Mol. Cancer Res.* 9, 1269–1284. doi: 10.1158/1541-7786.MCR-11-0220
- Brioude, F., Lacoste, A., Netchine, I., Vazquez, M. P., Auber, F., Audry, G., et al. (2013a). Beckwith-Wiedemann syndrome: growth pattern and tumor risk according to molecular mechanism, and guidelines for tumor surveillance. *Horm. Res. Paediatr.* 80, 457–465. doi: 10.1159/000355544
- Brioude, F., Oliver-Petit, I., Blaise, A., Praz, F., Rossignol, S., Le Jule, M., et al. (2013b). Cdkn1C mutation affecting the PcnA-binding domain as a cause of familial Russell Silver syndrome. *J. Med. Genet.* 50, 823–830. doi: 10.1136/jmedgenet-2013-101691
- Brioude, F., Netchine, I., Praz, F., Le Jule, M., Calmel, C., Lacombe, D., et al. (2015). Mutations of the imprinted CDKN1C gene as a cause of the overgrowth beckwith-wiedemann syndrome: clinical spectrum and functional characterization. *Hum. Mutat.* 36, 894–902. doi: 10.1002/humu.22824
- Busanello, A., Battistelli, C., Carbone, M., Mostocotto, C., and Maione, R. (2012). MyoD regulates p57kip2 expression by interacting with a distant cis-element and modifying a higher order chromatin structure. *Nucleic Acids Res.* 40, 8266–8275. doi: 10.1093/nar/gks619
- Chang, T. S., Kim, M. J., Ryoo, K., Park, J., Eom, S. J., Shim, J., et al. (2003). p57KIP2 modulates stress-activated signaling by inhibiting c-Jun N-terminal kinase/stress-activated protein Kinase. *J. Biol. Chem.* 278, 48092–48098. doi: 10.1074/jbc.m309421200
- Chen, X. Y., Zhang, J., and Zhu, J. S. (2019). The role of m(6)A RNA methylation in human cancer. *Mol. Cancer* 18:103. doi: 10.1186/s12943-019-1033-z
- Chu, I., Sun, J., Arnaout, A., Kahn, H., Hanna, W., Narod, S., et al. (2007). p27 phosphorylation by Src regulates inhibition of cyclin E-Cdk2. *Cell* 128, 281–294. doi: 10.1016/j.cell.2006.11.049
- Ciemerych, M. A., and Sicinski, P. (2005). Cell cycle in mouse development. *Oncogene* 24, 2877–2898. doi: 10.1038/sj.onc.1208608
- Cioffi, M., Trabulo, S. M., Sanchez-Ripoll, Y., Miranda-Lorenzo, I., Lonardo, E., Dorado, J., et al. (2015). The miR-17-92 cluster counteracts quiescence and chemoresistance in a distinct subpopulation of pancreatic cancer stem cells. *Gut* 64, 1936–1948. doi: 10.1136/gutjnl-2014-308470
- Deng, C., Zhang, P., Harper, J. W., Elledge, S. J., and Leder, P. (1995). Mice lacking p21CIP1/WAF1 undergo normal development, but are defective in G1 checkpoint control. *Cell* 82, 675–684. doi: 10.1016/0092-8674(95)90039-x
- Di Cristofano, A., De Acetis, M., Koff, A., Cordon-Cardo, C., and Pandolfi, P. P. (2001). Pten and p27KIP1 cooperate in prostate cancer tumor suppression in the mouse. *Nat. Genet.* 27, 222–224. doi: 10.1038/84879
- Dugas, J. C., Ibrahim, A., and Barres, B. A. (2007). A crucial role for p57(Kip2) in the intracellular timer that controls oligodendrocyte differentiation. *J. Neurosci.* 27, 6185–6196. doi: 10.1523/jneurosci.0628-07.2007
- Duquesnes, N., Callot, C., Jeannot, P., Daburon, V., Nakayama, K. I., Manenti, S., et al. (2016). p57(Kip2) knock-in mouse reveals CDK-independent contribution in the development of Beckwith-Wiedemann syndrome. *J. Pathol.* 239, 250–261. doi: 10.1002/path.4721
- Dyer, M. A., and Cepko, C. L. (2000). p57(Kip2) regulates progenitor cell proliferation and amacrine interneuron development in the mouse retina. *Development* 127, 3593–3605.
- Eggermann, T., Algar, E., Lapunzina, P., Mackay, D., Maher, E. R., Mannens, M., et al. (2014a). Clinical utility gene card for: Beckwith-Wiedemann Syndrome. *Eur. J. Hum. Genet.* 22. doi: 10.1038/ejhg.2013.132
- Eggermann, T., Binder, G., Brioude, F., Maher, E. R., Lapunzina, P., Cubellis, M. V., et al. (2014b). CDKN1C mutations: two sides of the same coin. *Trends Mol. Med.* 20, 614–622. doi: 10.1016/j.molmed.2014.09.001
- Fatica, A., and Bozzoni, I. (2014). Long non-coding RNAs: new players in cell differentiation and development. *Nat. Rev. Genet.* 15, 7–21. doi: 10.1038/nrg3606
- Fero, M. L., Randel, E., Gurley, K. E., Roberts, J. M., and Kemp, C. J. (1998). The murine gene p27Kip1 is haplo-insufficient for tumour suppression. *Nature* 396, 177–180. doi: 10.1038/24179
- Fero, M. L., Rivkin, M., Tasch, M., Porter, P., Carow, C. E., Firpo, E., et al. (1996). A syndrome of multiorgan hyperplasia with features of gigantism, tumorigenesis,

AUTHOR CONTRIBUTIONS

All authors listed have made a substantial, direct and intellectual contribution to the work, and approved it for publication.

FUNDING

AB was supported by funds from the Ligue Nationale Contre le Cancer and Fondation ARC pour la Recherche sur le Cancer and by an “FRM Equipes” grant (DEQ20170336707) from the Fondation pour la Recherche Médicale.

- and female sterility in p27(Kip1)-deficient mice. *Cell* 85, 733–744. doi: 10.1016/s0092-8674(00)81239-8
- Figliola, R., Busanello, A., Vaccarello, G., and Maione, R. (2008). Regulation of p57(KIP2) during muscle differentiation: role of Egr1, Sp1 and DNA hypomethylation. *J. Mol. Biol.* 380, 265–277. doi: 10.1016/j.jmb.2008.05.004
- Fitzpatrick, G. V., Soloway, P. D., and Higgins, M. J. (2002). Regional loss of imprinting and growth deficiency in mice with a targeted deletion of KvDMR1. *Nat. Genet.* 32, 426–431. doi: 10.1038/ng988
- Fornari, F., Gramantieri, L., Ferracin, M., Veronese, A., Sabbioni, S., Calin, G. A., et al. (2008). MiR-221 controls CDKN1C/p57 and Cdkn1B/p27 expression in human hepatocellular carcinoma. *Oncogene* 27, 5651–5661. doi: 10.1038/onc.2008.178
- Furutachi, S., Matsumoto, A., Nakayama, K. I., and Gotoh, Y. (2013). p57 controls adult neural stem cell quiescence and modulates the pace of lifelong neurogenesis. *Embo J.* 32, 970–981. doi: 10.1038/emboj.2013.50
- Georgia, S., Soliz, R., Li, M., Zhang, P., and Bhushan, A. (2006). p57 and Hes1 coordinate cell cycle exit with self-renewal of pancreatic progenitors. *Dev. Biol.* 298, 22–31. doi: 10.1016/j.ydbio.2006.05.036
- Gonzalez, S., Perez-Perez, M. M., Hernando, E., Serrano, M., and Cordon-Cardo, C. (2005). p73beta-Mediated apoptosis requires p57kip2 induction and IEX-1 inhibition. *Cancer Res.* 65, 2186–2192. doi: 10.1158/0008-5472.can-04-3047
- Gosselet, F. P., Magnaldo, T., Culerrier, R. M., Sarasin, A., and Ehrhart, J. C. (2007). BMP2 and BMP6 control p57(Kip2) expression and cell growth arrest/terminal differentiation in normal primary human epidermal keratinocytes. *Cell Signal.* 19, 731–739. doi: 10.1016/j.cellsig.2006.09.006
- Gottle, P., Sabo, J. K., Heinen, A., Venables, G., Torres, K., Tzekova, N., et al. (2015). Oligodendroglial maturation is dependent on intracellular protein shuttling. *J. Neurosci.* 35, 906–919. doi: 10.1523/jneurosci.1423-14.2015
- Grimmler, M., Wang, Y., Mund, T., Cilensek, Z., Keidel, E. M., Waddell, M. B., et al. (2007). Cdk-inhibitory activity and stability of p27Kip1 are directly regulated by oncogenic tyrosine kinases. *Cell* 128, 269–280. doi: 10.1016/j.cell.2006.11.047
- Guo, H., Li, Y., Tian, T., Han, L., Ruan, Z., Liang, X., et al. (2015). The role of cytoplasmic p57 in invasion of hepatocellular carcinoma. *BMC Gastroenterol.* 15:104. doi: 10.1186/s12876-015-0319-x
- Hark, A. T., Schoenherr, C. J., Katz, D. J., Ingram, R. S., Levorse, J. M., and Tilghman, S. M. (2000). CTCF mediates methylation-sensitive enhancer-blocking activity at the H19/Igf2 locus. *Nature* 405, 486–489. doi: 10.1038/35013106
- Harper, J. W., Adami, G. R., Wei, N., Keyomarsi, K., and Elledge, S. J. (1993). The p21 Cdk-interacting protein Cip1 is a potent inhibitor of G1 cyclin-dependent kinases. *Cell* 75, 805–816. doi: 10.1016/0092-8674(93)90499-g
- Hashimoto, Y., Kohri, K., Kaneko, Y., Morisaki, H., Kato, T., Ikeda, K., et al. (1998). Critical role for the 310 helix region of p57(Kip2) in cyclin-dependent kinase 2 inhibition and growth suppression. *J. Biol. Chem.* 273, 16544–16550. doi: 10.1074/jbc.273.26.16544
- Hatada, I., and Mukai, T. (1995). Genomic imprinting of p57KIP2, a cyclin-dependent kinase inhibitor, in mouse. *Nat. Genet.* 11, 204–206. doi: 10.1038/ng1095-204
- Hattori, N., Davies, T. C., Anson-Cartwright, L., and Cross, J. C. (2000). Periodic expression of the cyclin-dependent kinase inhibitor p57(Kip2) in trophoblast giant cells defines a G2-like gap phase of the endocycle. *Mol. Biol. Cell* 11, 1037–1045. doi: 10.1091/mbc.11.3.1037
- Heinen, A., Kremer, D., Gottle, P., Kruse, F., Hasse, B., Lehmann, H., et al. (2008a). The cyclin-dependent kinase inhibitor p57kip2 is a negative regulator of Schwann cell differentiation and in vitro myelination. *Proc. Natl. Acad. Sci. U.S.A.* 105, 8748–8753. doi: 10.1073/pnas.0802659105
- Heinen, A., Kremer, D., Hartung, H. P., and Kury, P. (2008b). p57 kip2's role beyond Schwann cell cycle control. *Cell Cycle* 7, 2781–2786. doi: 10.4161/cc.7.18.6629
- Hirata, M., Kugimiya, F., Fukai, A., Ohba, S., Kawamura, N., Ogasawara, T., et al. (2009). C/EBpbeta Promotes transition from proliferation to hypertrophic differentiation of chondrocytes through transactivation of p57. *PLoS One* 4:e4543. doi: 10.1371/journal.pone.0004543
- Huang, Y., Yoon, M. K., Otieno, S., Lelli, M., and Kriwacki, R. W. (2015). The activity and stability of the intrinsically disordered Cip/Kip protein family are regulated by non-receptor tyrosine kinases. *J. Mol. Biol.* 427, 371–386. doi: 10.1016/j.jmb.2014.11.011
- Imaizumi, Y., Furutachi, S., Watanabe, T., Miya, H., Kawaguchi, D., and Gotoh, Y. (2020). Role of the imprinted allele of the Cdkn1c gene in mouse neocortical development. *Sci. Rep.* 10:1884. doi: 10.1038/s41598-020-58629-9
- Ito, Y., Takeda, T., Sakon, M., Tsujimoto, M., Monden, M., and Matsuura, N. (2001a). Expression of p57/Kip2 protein in hepatocellular carcinoma. *Oncology* 61, 221–225. doi: 10.1159/000055378
- Ito, Y., Takeda, T., Wakasa, K., Tsujimoto, M., and Matsuura, N. (2001b). Expression of p57/Kip2 protein in pancreatic adenocarcinoma. *Pancreas* 23, 246–250. doi: 10.1097/00006676-200110000-00004
- Itoh, Y., Masuyama, N., Nakayama, K., Nakayama, K. I., and Gotoh, Y. (2007). The cyclin-dependent kinase inhibitors p57 and p27 regulate neuronal migration in the developing mouse neocortex. *J. Biol. Chem.* 282, 390–396. doi: 10.1074/jbc.m609944200
- Jadasz, J. J., Rivera, F. J., Taubert, A., Kandasamy, M., Sandner, B., Weidner, N., et al. (2012). p57kip2 regulates glial fate decision in adult neural stem cells. *Development* 139, 3306–3315. doi: 10.1242/dev.074518
- James, M. K., Ray, A., Leznova, D., and Blain, S. W. (2008). Differential modification of p27Kip1 controls its cyclin D-cdk4 inhibitory activity. *Mol. Cell Biol.* 28, 498–510. doi: 10.1128/mcb.02171-06
- Jia, J., Lin, M., Zhang, L., York, J. P., and Zhang, P. (2007). The Notch signaling pathway controls the size of the ocular lens by directly suppressing p57Kip2 expression. *Mol. Cell Biol.* 27, 7236–7247. doi: 10.1128/mcb.00780-07
- Jirawatnotai, S., Moons, D. S., Stocco, C. O., Franks, R., Hales, D. B., Gibori, G., et al. (2003). The cyclin-dependent kinase inhibitors p27^{Kip1} and p21^{Cip1} cooperate to restrict proliferative life span in differentiating ovarian cells. *J. Biol. Chem.* 278, 17021–17027. doi: 10.1074/jbc.M301206200
- Joaquin, M., Gubern, A., Gonzalez-Nunez, D., Josue Ruiz, E., Ferreira, I., De Nadal, E., et al. (2012). The p57 Cdk1 integrates stress signals into cell-cycle progression to promote cell survival upon stress. *Embo J.* 31, 2952–2964. doi: 10.1038/emboj.2012.122
- Joaquin, M., and Watson, R. J. (2003). The cell cycle-regulated B-Myb transcription factor overcomes cyclin-dependent kinase inhibitory activity of p57(KIP2) by interacting with its cyclin-binding domain. *J. Biol. Chem.* 278, 44255–44264. doi: 10.1074/jbc.m308953200
- Joseph, B., Andersson, E. R., Vlachos, P., Sodersten, E., Liu, L., Teixeira, A. I., et al. (2009). p57Kip2 is a repressor of Mash1 activity and neuronal differentiation in neural stem cells. *Cell Death Differ.* 16, 1256–1265. doi: 10.1038/cdd.2009.72
- Joseph, B., Wallen-Mackenzie, A., Benoit, G., Murata, T., Joodmardi, E., Okret, S., et al. (2003). p57(Kip2) cooperates with Nurr1 in developing dopamine cells. *Proc. Natl. Acad. Sci. U.S.A.* 100, 15619–15624. doi: 10.1073/pnas.2635658100
- Kamura, T., Hara, T., Kotoshiba, S., Yada, M., Ishida, N., Imaki, H., et al. (2003). Degradation of p57Kip2 mediated by SCFSkp2-dependent ubiquitylation. *Proc. Natl. Acad. Sci. U.S.A.* 100, 10231–10236. doi: 10.1073/pnas.1831009100
- Kassem, S. A., Ariel, I., Thornton, P. S., Hussain, K., Smith, V., Lindley, K. J., et al. (2001). p57(KIP2) expression in normal islet cells and in hyperinsulinism of infancy. *Diabetes* 50, 2763–2769. doi: 10.2337/diabetes.50.12.2763
- Kavanagh, E., and Joseph, B. (2011). The hallmarks of CDKN1C (p57. KIP2) in cancer. *Biochim. Biophys. Acta* 1816, 50–56. doi: 10.1016/j.bbcan.2011.03.002
- Kavanagh, E., Vlachos, P., Emourgeon, V., Rodhe, J., and Joseph, B. (2012). p57(KIP2) control of actin cytoskeleton dynamics is responsible for its mitochondrial pro-apoptotic effect. *Cell Death Dis.* 3:e311. doi: 10.1038/cddis.2012.51
- Kerns, S. L., Guevara-Aguirre, J., Andrew, S., Geng, J., Guevara, C., Guevara-Aguirre, M., et al. (2014). A novel variant in Cdkn1C is associated with intrauterine growth restriction, short stature, and early-adulthood-onset diabetes. *J. Clin. Endocrinol. Metab.* 99, E2117–E2122. doi: 10.1210/jc.2014-1949
- Kikuchi, T., Toyota, M., Itoh, F., Suzuki, H., Obata, T., Yamamoto, H., et al. (2002). Inactivation of p57kip2 by regional promoter hypermethylation and histone deacetylation in human tumors. *Oncogene* 21, 2741–2749. doi: 10.1038/sj.onc.1205376
- Kim, C. F., Jackson, E. L., Woolfenden, A. E., Lawrence, S., Babar, I., Vogel, S., et al. (2005). Identification of bronchioalveolar stem cells in normal lung and lung cancer. *Cell* 121, 823–835. doi: 10.1016/j.cell.2005.03.032
- Kim, M., Nakamoto, T., Nishimori, S., Tanaka, K., and Chiba, T. (2008). A new ubiquitin ligase involved in p57kip2 proteolysis regulates osteoblast cell differentiation. *Embo Rep.* 9, 878–884. doi: 10.1038/embo.2008.125

- Kim, Y. K., Yu, J., Han, T. S., Park, S. Y., Namkoong, B., Kim, D. H., et al. (2009). Functional links between clustered microRNAs: suppression of cell-cycle inhibitors by microRNA clusters in gastric cancer. *Nucleic Acids Res.* 37, 1672–1681. doi: 10.1093/nar/gkp002
- Kremer, D., Heinen, A., Jadasz, J., Gottle, P., Zimmermann, K., Zickler, P., et al. (2009). p57kip2 is dynamically regulated in experimental autoimmune encephalomyelitis and interferes with oligodendroglial maturation. *Proc. Natl. Acad. Sci. U.S.A.* 106, 9087–9092. doi: 10.1073/pnas.0900204106
- Kullmann, M. K., Podmirsej, S. R., Roilo, M., and Hengst, L. (2020). The Cdk inhibitor p57(Kip2) enhances the activity of the transcriptional coactivator FHL2. *Sci. Rep.* 10:7140. doi: 10.1038/s41598-020-62641-4
- Labauer, J., Garrett, M. D., Stevenson, L. F., Slingerland, J. M., Sandhu, C., Chou, H. S., et al. (1997). New functional activities for the p21 family of CDK inhibitors. *Genes Dev.* 11, 847–862. doi: 10.1101/gad.11.7.847
- Lacy, E. R., Filippov, I., Lewis, W. S., Otieno, S., Xiao, L., Weiss, S., et al. (2004). p27 binds cyclin-CDK complexes through a sequential mechanism involving binding-induced protein folding. *Nat. Struct. Mol. Biol.* 11, 358–364. doi: 10.1038/nsmb746
- Laukoter, S., Beattie, R., Pauler, F. M., Amberg, N., Nakayama, K. I., and Hippenmeyer, S. (2020). Imprinted Cdkn1c genomic locus cell-autonomously promotes cell survival in cerebral cortex development. *Nat. Commun.* 11:195. doi: 10.1038/s41467-019-14077-2
- Lee, M. H., Reynisdottir, I., and Massague, J. (1995). Cloning of p57kip2, a cyclin-dependent kinase inhibitor with unique domain structure and tissue distribution. *Genes Dev.* 9, 639–649. doi: 10.1101/gad.9.6.639
- Leighton, P. A., Saam, J. R., Ingram, R. S., Stewart, C. L., and Tilghman, S. M. (1995). An enhancer deletion affects both H19 and Igf2 expression. *Genes Dev.* 9, 2079–2089. doi: 10.1101/gad.9.17.2079
- Leishman, E., Howard, J. M., Garcia, G. E., Miao, Q., Ku, A. T., Dekker, J. D., et al. (2013). Foxp1 maintains hair follicle stem cell quiescence through regulation of Fgf18. *Development* 140, 3809–3818. doi: 10.1242/dev.097477
- Li, J. Q., Wu, F., Usuki, H., Kubo, A., Masaki, T., Fujita, J., et al. (2003). Loss of p57kip2 is associated with colorectal carcinogenesis. *Int. J. Oncol.* 23, 1537–1543. doi: 10.3892/ijo.23.6.1537
- Liu, Q., Liu, K., Cui, G., Huang, X., Yao, S., Guo, W., et al. (2019). Lung regeneration by multipotent stem cells residing at the bronchioalveolar-duct junction. *Nat. Genet.* 51, 728–738. doi: 10.1038/s41588-019-0346-6
- Logan, C. V., Murray, J. E., Parry, D. A., Robertson, A., Bellelli, R., Tarnauskaite, Z., et al. (2018). DNA polymerase epsilon deficiency causes image syndrome with variable immunodeficiency. *Am. J. Hum. Genet.* 103, 1038–1044. doi: 10.1016/j.ajhg.2018.10.024
- Ma, Y., Chen, L., Wright, G. M., Pillai, S. R., Chellappan, S. P., and Cress, W. D. (2010). Cdkn1C negatively regulates RNA polymerase II C-terminal domain phosphorylation in an E2F1-dependent manner. *J. Biol. Chem.* 285, 9813–9822. doi: 10.1074/jbc.M109.091496
- Ma, Y., and Cress, W. D. (2007). Transcriptional upregulation of p57 (Kip2) by the cyclin-dependent kinase inhibitor BMS-387032 is E2F dependent and serves as a negative feedback loop limiting cytotoxicity. *Oncogene* 26, 3532–3540. doi: 10.1038/sj.onc.1210143
- Ma, Z., Gu, S., Song, M., Yan, C., Hui, B., Ji, H., et al. (2017). Long non-coding RNA SNHG17 is an unfavourable prognostic factor and promotes cell proliferation by epigenetically silencing P57 in colorectal cancer. *Mol. Biosyst.* 13, 2350–2361. doi: 10.1039/c7mb00280g
- Ma, Z., Peng, P., Zhou, J., Hui, B., Ji, H., Wang, J., et al. (2018). Long non-coding RNA Sh3pxd2A-As1 promotes cell progression partly through epigenetic silencing P57 and KLF2 in colorectal cancer. *Cell Physiol. Biochem.* 46, 2197–2214. doi: 10.1159/000489589
- Mademtoglou, D., Asakura, Y., Borok, M. J., Alonso-Martin, S., Mourikis, P., Kodaka, Y., et al. (2018). Cellular localization of the cell cycle inhibitor Cdkn1c controls growth arrest of adult skeletal muscle stem cells. *eLife* 7:e33337. doi: 10.7554/eLife.33337.021
- Mairet-Coello, G., Turly, A., Van Buskirk, E., Robinson, K., Genestine, M., and Dicicco-Bloom, E. (2012). p57(KIP2) regulates radial glia and intermediate precursor cell cycle dynamics and lower layer neurogenesis in developing cerebral cortex. *Development* 139, 475–487. doi: 10.1242/dev.067314
- Malumbres, M., and Barbacid, M. (2005). Mammalian cyclin-dependent kinases. *Trends Biochem. Sci.* 30, 630–641. doi: 10.1016/j.tibs.2005.09.005
- Marinoni, I., and Pellegata, N. S. (2011). p27kip1: a new multiple endocrine neoplasia gene? *Neuroendocrinology* 93, 19–28. doi: 10.1159/000320366
- Martin-Caballero, J., Flores, J. M., Garcia-Palencia, P., and Serrano, M. (2001). Tumor susceptibility of p21(Waf1/Cip1)-deficient mice. *Cancer Res* 61, 6234–6238.
- Matsumoto, A., Susaki, E., Onoyama, I., Nakayama, K., Hoshino, M., and Nakayama, K. I. (2011a). Deregulation of the p57-E2F1-p53 axis results in nonobstructive hydrocephalus and cerebellar malformation in mice. *Mol. Cell Biol.* 31, 4176–4192. doi: 10.1128/mcb.05370-11
- Matsumoto, A., Takeishi, S., Kanie, T., Susaki, E., Onoyama, I., Tateishi, Y., et al. (2011b). p57 is required for quiescence and maintenance of adult hematopoietic stem cells. *Cell Stem Cell* 9, 262–271. doi: 10.1016/j.stem.2011.06.014
- Matsuoka, S., Edwards, M. C., Bai, C., Parker, S., Zhang, P., Baldini, A., et al. (1995). p57kip2, a structurally distinct member of the p21CIP1 Cdk inhibitor family, is a candidate tumor suppressor gene. *Genes Dev.* 9, 650–662. doi: 10.1101/gad.9.6.650
- Matsuoka, S., Thompson, J. S., Edwards, M. C., Bartletta, J. M., Grundy, P., Kalikin, L. M., et al. (1996). Imprinting of the gene encoding a human cyclin-dependent kinase inhibitor, p57kip2, on chromosome 11p15. *Proc. Natl. Acad. Sci. U.S.A.* 93, 3026–3030. doi: 10.1073/pnas.93.7.3026
- Mei, L., Shen, C., Miao, R., Wang, J. Z., Cao, M. D., Zhang, Y. S., et al. (2020). RNA methyltransferase NSUN2 promotes gastric cancer cell proliferation by repressing p57(Kip2) by an m(5)C-dependent manner. *Cell Death Dis.* 11:270. doi: 10.1038/s41419-020-2487-z
- Mishra, S., Lin, C. L., Huang, T. H., Bouamar, H., and Sun, L. Z. (2014). MicroRNA-21 inhibits p57Kip2 expression in prostate cancer. *Mol. Cancer* 13:212. doi: 10.1186/1476-4598-13-212
- Mohammad, F., Mondal, T., Guseva, N., Pandey, G. K., and Kanduri, C. (2010). Kcnq1ot1 noncoding RNA mediates transcriptional gene silencing by interacting with Dnmt1. *Development* 137, 2493–2499. doi: 10.1242/dev.048181
- Monk, D., Mackay, D. J. G., Eggermann, T., Maher, E. R., and Riccio, A. (2019). Genomic imprinting disorders: lessons on how genome, epigenome and environment interact. *Nat. Rev. Genet.* 20, 235–248. doi: 10.1038/s41576-018-0092-0
- Muller, J. M., Isle, U., Metzger, E., Rempel, A., Moser, M., Pscherer, A., et al. (2000). FHL2, a novel tissue-specific coactivator of the androgen receptor. *Embo J.* 19, 359–369. doi: 10.1093/emboj/19.3.359
- Nagahama, H., Hatakeyama, S., Nakayama, K., Nagata, M., Tomita, K., and Nakayama, K. (2001). Spatial and temporal expression patterns of the cyclin-dependent kinase (CDK) inhibitors p27Kip1 and p57Kip2 during mouse development. *Anat. Embryol.* 203, 77–87. doi: 10.1007/s004290000146
- Nakano, S., Murakami, K., Meguro, M., Soejima, H., Higashimoto, K., Urano, T., et al. (2006). Expression profile of LIT1/KCNQ1OT1 and epigenetic status at the KVDNR1 in colorectal cancers. *Cancer Sci.* 97, 1147–1154. doi: 10.1111/j.1349-7006.2006.00305.x
- Nakatani, H., Martin, E., Hassani, H., Clavairoly, A., Maire, C. L., Viadieu, A., et al. (2013). Ascl1/Mash1 promotes brain oligodendrogenesis during myelination and remyelination. *J. Neurosci.* 33, 9752–9768. doi: 10.1523/jneurosci.0805-13.2013
- Nakayama, K., Ishida, N., Shirane, M., Inomata, A., Inoue, T., Shishido, N., et al. (1996). Mice lacking p27(Kip1) display increased body size, multiple organ hyperplasia, retinal dysplasia, and pituitary tumors. *Cell* 85, 707–720. doi: 10.1016/s0092-8674(00)81237-4
- Otsuki, L., and Brand, A. H. (2018). Cell cycle heterogeneity directs the timing of neural stem cell activation from quiescence. *Science* 360, 99–102. doi: 10.1126/science.aan8795
- Otsuki, L., and Brand, A. H. (2019). Dorsal-ventral differences in neural stem cell quiescence are induced by p57(KIP2)/Dacapo. *Dev. Cell* 49, 293–300e3. doi: 10.1016/j.devcel.2019.02.015
- Ou, K., Yu, M., Moss, N. G., Wang, Y. J., Wang, A. W., Nguyen, S. C., et al. (2019). Targeted demethylation at the Cdkn1C/p57 locus induces human beta cell replication. *J. Clin. Invest.* 129, 209–214. doi: 10.1172/jci99170
- Overall, M. L., Spencer, J., Bakker, M., Dziadek, M., and Smith, P. J. (1996). p57KIP2 is expressed in Wilms' tumor with LOH of 11p15.5. *Genes Chromosomes Cancer* 17, 56–59. doi: 10.1002/(sici)1098-2264(199609)17:1<56::aid-gcc8>3.0.co;2-1

- Pandey, R. R., Mondal, T., Mohammad, F., Enroth, S., Redrup, L., Komorowski, J., et al. (2008). Kcnq1ot1 antisense noncoding RNA mediates lineage-specific transcriptional silencing through chromatin-level regulation. *Mol. Cell* 32, 232–246. doi: 10.1016/j.molcel.2008.08.022
- Park, H. C., Boyce, J., Shin, J., and Appel, B. (2005). Oligodendrocyte specification in zebrafish requires notch-regulated cyclin-dependent kinase inhibitor function. *J. Neurosci.* 25, 6836–6844. doi: 10.1523/jneurosci.0981-05.2005
- Pateras, I. S., Apostolopoulou, K., Koutsami, M., Evangelou, K., Tsantoulis, P., Liloglou, T., et al. (2006). Downregulation of the Kip family members p27(KIP1) and p57(KIP2) by SKP2 and the role of methylation in p57(KIP2) inactivation in non-small cell lung cancer. *Int. J. Cancer* 119, 2546–2556. doi: 10.1002/ijc.22214
- Pateras, I. S., Apostolopoulou, K., Niforou, K., Kotsinas, A., and Gorgoulis, V. G. (2009). p57kip2: "Kip"ing the cell under control. *Mol. Cancer Res.* 7, 1902–1919. doi: 10.1158/1541-7786.mcr-09-0317
- Pellegata, N. S., Quintanilla-Martinez, L., Siggelkow, H., Samson, E., Bink, K., Hofler, H., et al. (2006). Germ-line mutations in p27Kip1 cause a multiple endocrine neoplasia syndrome in rats and humans. *Proc. Natl. Acad. Sci. U.S.A.* 103, 15558–15563. doi: 10.1073/pnas.0603877103
- Polyak, K., Lee, M. H., Erdjument-Bromage, H., Koff, A., Roberts, J. M., Tempst, P., et al. (1994). Cloning of p27Kip1, a cyclin-dependent kinase inhibitor and a potential mediator of extracellular antimitogenic signals. *Cell* 78, 59–66. doi: 10.1016/0092-8674(94)90572-x
- Qiu, Z., Li, Y., Zeng, B., Guan, X., and Li, H. (2018). Downregulated CDKN1C/p57(kip2) drives tumorigenesis and associates with poor overall survival in breast cancer. *Biochem. Biophys. Res. Commun.* 497, 187–193. doi: 10.1016/j.bbrc.2018.02.052
- Reik, W., and Walter, J. (2001). Genomic imprinting: parental influence on the genome. *Nat. Rev. Genet.* 2, 21–32. doi: 10.1038/35047554
- Reynaud, E. G., Leibovitch, M. P., Tintignac, L. A., Pelpel, K., Guillier, M., and Leibovitch, S. A. (2000). Stabilization of MyoD by direct binding to p57(Kip2). *J. Biol. Chem.* 275, 18767–18776. doi: 10.1074/jbc.M907412199
- Reynaud, E. G., Pelpel, K., Guillier, M., Leibovitch, M. P., and Leibovitch, S. A. (1999). p57(Kip2) stabilizes the MyoD protein by inhibiting cyclin E-Cdk2 kinase activity in growing myoblasts. *Mol. Cell Biol.* 19, 7621–7629. doi: 10.1128/mcb.19.11.7621
- Riccio, O., Van Gijn, M. E., Bezdek, A. C., Pellegrinet, L., Van Es, J. H., Zimmer-Strobl, U., et al. (2008). Loss of intestinal crypt progenitor cells owing to inactivation of both Notch1 and Notch2 is accompanied by derepression of CDK inhibitors p27Kip1 and p57Kip2. *Embo Rep.* 9, 377–383. doi: 10.1038/embor.2008.7
- Rodriguez, S., Wang, L., Mumaw, C., Srour, E. F., Lo Celso, C., Nakayama, K., et al. (2011). The SKP2 E3 ligase regulates basal homeostasis and stress-induced regeneration of HSCs. *Blood* 117, 6509–6519. doi: 10.1182/blood-2010-11-321521
- Roeb, W., Boyer, A., Cavenue, W. K., and Arden, K. C. (2007). Pax3-Foxo1 controls expression of the p57Kip2 cell-cycle regulator through degradation of EGR1. *Proc. Natl. Acad. Sci. U.S.A.* 104, 18085–18090. doi: 10.1073/pnas.0708910104
- Romanelli, V., Belinchon, A., Benito-Sanz, S., Martinez-Glez, V., Gracia-Bouthelier, R., Heath, K. E., et al. (2010). CDKN1C (p57(Kip2)) analysis in Beckwith-Wiedemann syndrome (BWS) patients: genotype-phenotype correlations, novel mutations, and polymorphisms. *Am. J. Med. Genet. A* 152A, 1390–1397. doi: 10.1002/ajmg.a.33453
- Rossi, M. N., and Antonangeli, F. (2015). Cellular response upon stress: p57 contribution to the final outcome. *Mediat. Inflamm.* 2015, 259325. doi: 10.1155/2015/259325
- Rothschild, G., Zhao, X., Iavarone, A., and Lasorella, A. (2006). E Proteins and Id2 converge on p57Kip2 to regulate cell cycle in neural cells. *Mol. Cell Biol.* 26, 4351–4361. doi: 10.1128/mcb.01743-05
- Russo, A. A., Jeffrey, P. D., Patten, A. K., Massague, J., and Pavletich, N. P. (1996). Crystal structure of the p27Kip1 cyclin-dependent-kinase inhibitor bound to the cyclin A-Cdk2 complex. *Nature* 382, 325–331. doi: 10.1038/382325a0
- Sakai, K., Peraud, A., Mainprize, T., Nakayama, J., Tsugu, A., Hongo, K., et al. (2004). Inducible expression of p57KIP2 inhibits glioma cell motility and invasion. *J. Neurooncol.* 68, 217–223. doi: 10.1023/b:neon.0000033380.08940.c8
- Salwig, I., Spitznagel, B., Vazquez-Armendariz, A. I., Khalooghi, K., Guenther, S., Herold, S., et al. (2019). Bronchioalveolar stem cells are a main source for regeneration of distal lung epithelia in vivo. *Embo J.* 38:e102099. doi: 10.15252/embj.2019102099
- Samuelsson, M. K., Pazirandeh, A., Davani, B., and Okret, S. (1999). p57Kip2, a glucocorticoid-induced inhibitor of cell cycle progression in HeLa cells. *Mol. Endocrinol.* 13, 1811–1822. doi: 10.1210/mend.13.11.0379
- Samuelsson, M. K., Pazirandeh, A., and Okret, S. (2002). A pro-apoptotic effect of the CDK inhibitor p57(Kip2) on staurosporine-induced apoptosis in HeLa cells. *Biochem. Biophys. Res. Commun.* 296, 702–709. doi: 10.1016/s0006-291x(02)00912-9
- Scandura, J. M., Bocconi, P., Massague, J., and Nimer, S. D. (2004). Transforming growth factor beta-induced cell cycle arrest of human hematopoietic cells requires p57KIP2 up-regulation. *Proc. Natl. Acad. Sci. U.S.A.* 101, 15231–15236. doi: 10.1073/pnas.0406771101
- Sengupta, S., Nie, J., Wagner, R. J., Yang, C., Stewart, R., and Thomson, J. A. (2009). MicroRNA 92b controls the G1/S checkpoint gene p57 in human embryonic stem cells. *Stem Cells* 27, 1524–1528. doi: 10.1002/stem.84
- Sherr, C. J., and Roberts, J. M. (1999). CDK inhibitors: positive and negative regulators of G1-phase progression. *Genes Dev.* 13, 1501–1512. doi: 10.1101/gad.13.12.1501
- Shi, Y., and Liu, J. P. (2011). Gdf11 facilitates temporal progression of neurogenesis in the developing spinal cord. *J. Neurosci.* 31, 883–893. doi: 10.1523/jneurosci.2394-10.2011
- Shmela, M. E., and Gicquel, C. F. (2013). Human diseases versus mouse models: insights into the regulation of genomic imprinting at the human 11p15/mouse distal chromosome 7 region. *J. Med. Genet.* 50, 11–20. doi: 10.1136/jmedgenet-2012-101321
- Stampone, E., Caldarelli, I., Zullo, A., Bencivenga, D., Mancini, F. P., Della Ragione, F., et al. (2018). Genetic and epigenetic control of CDKN1C expression: importance in cell commitment and differentiation. *Tissue Homeost. Hum. Dis. Int. J. Mol. Sci.* 19:1055. doi: 10.3390/ijms19041055
- Stewart, M. C., Kadlcek, R. M., Robbins, P. D., Macleod, J. N., and Ballock, R. T. (2004). Expression and activity of the CDK inhibitor p57Kip2 in chondrocytes undergoing hypertrophic differentiation. *J. Bone Miner. Res.* 19, 123–132. doi: 10.1359/jbmr.0301209
- Sun, C. C., Li, S. J., Li, G., Hua, R. X., Zhou, X. H., and Li, D. J. (2016). Long intergenic noncoding RNA 00511 acts as an oncogene in non-small-cell lung cancer by binding to EZH2 and suppressing p57. *Mol. Ther. Nucleic Acids* 5:e385. doi: 10.1038/mtna.2016.94
- Suryadinata, R., Sadowski, M., and Sarcevic, B. (2010). Control of cell cycle progression by phosphorylation of cyclin-dependent kinase (CDK) substrates. *Biosci. Rep.* 30, 243–255. doi: 10.1042/bsr20090171
- Susaki, E., Nakayama, K., Yamasaki, L., and Nakayama, K. I. (2009). Common and specific roles of the related CDK inhibitors p27 and p57 revealed by a knock-in mouse model. *Proc. Natl. Acad. Sci. U.S.A.* 106, 5192–5197. doi: 10.1073/pnas.0811712106
- Taniguchi, T., Okamoto, K., and Reeve, A. E. (1997). Human p57(KIP2) defines a new imprinted domain on chromosome 11p but is not a tumour suppressor gene in Wilms tumour. *Oncogene* 14, 1201–1206. doi: 10.1038/sj.onc.1200934
- Tateishi, Y., Matsumoto, A., Kanie, T., Hara, E., Nakayama, K., and Nakayama, K. I. (2012). Development of mice without Cip/Kip CDK inhibitors. *Biochem. Biophys. Res. Commun.* 427, 285–292. doi: 10.1016/j.bbrc.2012.09.041
- Tokino, T., Urano, T., Furuhashi, T., Matsushima, M., Miyatsu, T., Sasaki, S., et al. (1996). Characterization of the human p57KIP2 gene: alternative splicing, insertion/deletion polymorphisms in VNTR sequences in the coding region, and mutational analysis. *Hum. Genet.* 97, 625–631. doi: 10.1007/bf02281873
- Toyoshima, H., and Hunter, T. (1994). p27, a novel inhibitor of G1 cyclin-Cdk protein kinase activity, is related to p21. *Cell* 78, 67–74. doi: 10.1016/0092-8674(94)90573-8
- Tran, M. K., Kurakula, K., Koenis, D. S., and De Vries, C. J. (2016). Protein-protein interactions of the Lim-only protein FHL2 and functional implication of the interactions relevant in cardiovascular disease. *Biochim. Biophys. Acta* 1863, 219–228. doi: 10.1016/j.bbamcr.2015.11.002
- Tury, A., Mairret-Coello, G., and Dicicco-Bloom, E. (2011). The cyclin-dependent kinase inhibitor p57Kip2 regulates cell cycle exit, differentiation, and migration of embryonic cerebral cortical precursors. *Cereb. Cortex* 21, 1840–1856. doi: 10.1093/cercor/bhq254
- Ullah, Z., Kohn, M. J., Yagi, R., Vassilev, L. T., and Depamphilis, M. L. (2008). Differentiation of trophoblast stem cells into giant cells is triggered by p57/Kip2

- inhibition of CDK1 activity. *Genes Dev.* 22, 3024–3036. doi: 10.1101/gad.1718108
- Urano, T., Yashiroda, H., Muraoka, M., Tanaka, K., Hosoi, T., Inoue, S., et al. (1999). p57(Kip2) is degraded through the proteasome in osteoblasts stimulated to proliferation by transforming growth factor beta1. *J. Biol. Chem.* 274, 12197–12200. doi: 10.1074/jbc.274.18.12197
- Vaccarello, G., Figliola, R., Cramerotti, S., Novelli, F., and Maione, R. (2006). p57Kip2 is induced by MyoD through a p73-dependent pathway. *J. Mol. Biol.* 356, 578–588. doi: 10.1016/j.jmb.2005.12.024
- Vlachos, P., and Joseph, B. (2009). The Cdk inhibitor p57(Kip2) controls LIM-kinase 1 activity and regulates actin cytoskeleton dynamics. *Oncogene* 28, 4175–4188. doi: 10.1038/onc.2009.269
- Vlachos, P., Nyman, U., Hajji, N., and Joseph, B. (2007). The cell cycle inhibitor p57(Kip2) promotes cell death via the mitochondrial apoptotic pathway. *Cell Death Differ.* 14, 1497–1507. doi: 10.1038/sj.cdd.4402158
- Wakeling, E. L., Brioude, F., Lokulo-Sodipe, O., O'connell, S. M., Salem, J., Blik, J., et al. (2017). Diagnosis and management of Silver-Russell syndrome: first international consensus statement. *Nat. Rev. Endocrinol.* 13, 105–124. doi: 10.1038/nrendo.2016.138
- Wang, Y., Dai, W., Chu, X., Yang, B., Zhao, M., and Sun, Y. (2013). Metformin inhibits lung cancer cells proliferation through repressing microRNA-222. *Biotechnol. Lett.* 35, 2013–2019. doi: 10.1007/s10529-013-1309-0
- Watanabe, H., Pan, Z. Q., Schreiber-Agus, N., Depinho, R. A., Hurwitz, J., and Xiong, Y. (1998). Suppression of cell transformation by the cyclin-dependent kinase inhibitor p57KIP2 requires binding to proliferating cell nuclear antigen. *Proc. Natl. Acad. Sci. U.S.A.* 95, 1392–1397. doi: 10.1073/pnas.95.4.1392
- Weis, B., Schmidt, J., Maamar, H., Raj, A., Lin, H., Toth, C., et al. (2015). Inhibition of intestinal tumor formation by deletion of the DNA methyltransferase 3a. *Oncogene* 34, 1822–1830. doi: 10.1038/onc.2014.114
- Weksberg, R., Shuman, C., and Beckwith, J. B. (2010). Beckwith-Wiedemann syndrome. *Eur. J. Hum. Genet.* 18, 8–14. doi: 10.1038/ejhg.2009.106
- Westbury, J., Watkins, M., Ferguson-Smith, A. C., and Smith, J. (2001). Dynamic temporal and spatial regulation of the cdk inhibitor p57(kip2) during embryo morphogenesis. *Mech. Dev.* 109, 83–89. doi: 10.1016/s0925-4773(01)00512-3
- Wierenga, A. T., Vellenga, E., and Schuringa, J. J. (2014). Convergence of hypoxia and TGFbeta pathways on cell cycle regulation in human hematopoietic stem/progenitor cells. *PLoS One* 9:e93494. doi: 10.1371/journal.pone.0093494
- Yamazaki, S., Iwama, A., Takayanagi, S., Eto, K., Ema, H., and Nakauchi, H. (2009). TGF-beta as a candidate bone marrow niche signal to induce hematopoietic stem cell hibernation. *Blood* 113, 1250–1256. doi: 10.1182/blood-2008-04-146480
- Yan, Y., Frisen, J., Lee, M. H., Massague, J., and Barbacid, M. (1997). Ablation of the CDK inhibitor p57Kip2 results in increased apoptosis and delayed differentiation during mouse development. *Genes Dev.* 11, 973–983. doi: 10.1101/gad.11.8.973
- Yang, X., Karuturi, R. K., Sun, F., Aau, M., Yu, K., Shao, R., et al. (2009). Cdkn1C (p57) is a direct target of Ezh2 and suppressed by multiple epigenetic mechanisms in breast cancer cells. *PLoS One* 4:e5011. doi: 10.1371/journal.pone.0005011
- Yokoo, T., Toyoshima, H., Miura, M., Wang, Y., Iida, K. T., Suzuki, H., et al. (2003). p57Kip2 regulates actin dynamics by binding and translocating LIM-kinase 1 to the nucleus. *J. Biol. Chem.* 278, 52919–52923. doi: 10.1074/jbc.m309334200
- Yoon, M. K., Mitrea, D. M., Ou, L., and Kriwacki, R. W. (2012). Cell cycle regulation by the intrinsically disordered proteins p21 and p27. *Biochem. Soc. Trans.* 40, 981–988. doi: 10.1042/bst20120092
- Zacharek, S. J., Fillmore, C. M., Lau, A. N., Gludish, D. W., Chou, A., Ho, J. W., et al. (2011). Lung stem cell self-renewal relies on BMI1-dependent control of expression at imprinted loci. *Cell Stem Cell* 9, 272–281. doi: 10.1016/j.stem.2011.07.007
- Zalc, A., Hayashi, S., Aurade, F., Brohl, D., Chang, T., Mademtoglou, D., et al. (2014). Antagonistic regulation of p57kip2 by Hes/Hey downstream of Notch signaling and muscle regulatory factors regulates skeletal muscle growth arrest. *Development* 141, 2780–2790. doi: 10.1242/dev.110155
- Zhang, G., Xu, Y., Wang, S., Gong, Z., Zou, C., Zhang, H., et al. (2019a). LncRNA SNHG17 promotes gastric cancer progression by epigenetically silencing of p15 and p57. *J. Cell Physiol.* 234, 5163–5174. doi: 10.1002/jcp.27320
- Zhang, G., Xu, Y., Zou, C., Tang, Y., Lu, J., Gong, Z., et al. (2019b). Long noncoding RNA ARHGAP27P1 inhibits gastric cancer cell proliferation and cell cycle progression through epigenetically regulating p15 and p16. *Aging* 11, 9090–9110. doi: 10.18632/aging.102377
- Zhang, J., Gong, X., Tian, K., Chen, D., Sun, J., Wang, G., et al. (2015). miR-25 promotes glioma cell proliferation by targeting CDKN1C. *Biomed. Pharmacother.* 71, 7–14. doi: 10.1016/j.biopha.2015.02.005
- Zhang, M. C., Zhang, L., Zhang, M. Q., Yang, G. X., Wang, F. Z., and Ding, P. (2020). Downregulated LINC00628 aggravates the progression of colorectal cancer via inhibiting p57 level. *Eur. Rev. Med. Pharmacol. Sci.* 24, 1763–1770.
- Zhang, P., Liegeois, N. J., Wong, C., Finegold, M., Hou, H., Thompson, J. C., et al. (1997). Altered cell differentiation and proliferation in mice lacking p57KIP2 indicates a role in Beckwith-Wiedemann syndrome. *Nature* 387, 151–158. doi: 10.1038/387151a0
- Zhang, P., Wong, C., Depinho, R. A., Harper, J. W., and Elledge, S. J. (1998). Cooperation between the Cdk inhibitors p27(KIP1) and p57(KIP2) in the control of tissue growth and development. *Genes Dev.* 12, 3162–3167. doi: 10.1101/gad.12.20.3162
- Zhang, P., Wong, C., Liu, D., Finegold, M., Harper, J. W., and Elledge, S. J. (1999). p21(CIP1) and p57(KIP2) control muscle differentiation at the myogenin step. *Genes Dev.* 13, 213–224. doi: 10.1101/gad.13.2.213
- Zou, P., Yoshihara, H., Hosokawa, K., Tai, I., Shinmyozu, K., Tsukahara, F., et al. (2011). p57(Kip2) and p27(Kip1) cooperate to maintain hematopoietic stem cell quiescence through interactions with Hsc70. *Cell Stem Cell* 9, 247–261. doi: 10.1016/j.stem.2011.07.003

Conflict of Interest: The authors declare that the research was conducted in the absence of any commercial or financial relationships that could be construed as a potential conflict of interest.

Copyright © 2020 Creff and Besson. This is an open-access article distributed under the terms of the Creative Commons Attribution License (CC BY). The use, distribution or reproduction in other forums is permitted, provided the original author(s) and the copyright owner(s) are credited and that the original publication in this journal is cited, in accordance with accepted academic practice. No use, distribution or reproduction is permitted which does not comply with these terms.



The Origins and Roles of Methylthiolated Cytokinins: Evidence From Among Life Kingdoms

Maya Gibb, Anna B. Kisiala*, Erin N. Morrison and R. J. Neil Emery

Department of Biology, Trent University, Peterborough, ON, Canada

OPEN ACCESS

Edited by:

Andrew Burgess,
Anzac Research Institute, Australia

Reviewed by:

Wendy A. Stirk,
University of KwaZulu-Natal,
South Africa
Klára Hoyerová,
Institute of Experimental Botany,
Academy of Sciences of the Czech
Republic, Czechia

*Correspondence:

Anna B. Kisiala
annakisiala@trentu.ca

Specialty section:

This article was submitted to
Cell Growth and Division,
a section of the journal
Frontiers in Cell and Developmental
Biology

Received: 12 September 2020

Accepted: 19 October 2020

Published: 09 November 2020

Citation:

Gibb M, Kisiala AB, Morrison EN
and Emery RJN (2020) The Origins
and Roles of Methylthiolated
Cytokinins: Evidence From Among
Life Kingdoms.
Front. Cell Dev. Biol. 8:605672.
doi: 10.3389/fcell.2020.605672

Cytokinins (CKs) are a group of adenine-derived, small signaling molecules of crucial importance for growth and multiple developmental processes in plants. Biological roles of classical CKs: isopentenyladenine (iP), *trans* and *cis* isomers of zeatin (*tZ*, *cZ*), and dihydrozeatin, have been studied extensively and their functions are well defined in many aspects of plant physiology. In parallel, extensive knowledge exists for genes involved in tRNA modifications that lead to the production of tRNA-bound methylthiolated CKs, especially in bacterial and mammalian systems. However, not much is known about the origins, fates, and possible functions of the unbound methylthiolated CKs (2MeS-CKs) in biological systems. 2MeS-CKs are the free base or riboside derivatives of iP or Z-type CKs, modified by the addition of a thiol group (–SH) at position 2 of the adenine ring that is subsequently methylated. Based on the evidence to date, these distinctive CK conjugates are derived exclusively via the tRNA degradation pathway. This review summarizes the knowledge on the probable steps involved in the biosynthesis of unbound 2MeS-CKs across diverse kingdoms of life. Furthermore, it provides examples of CK profiles of organisms from which the presence of 2MeS-CKs have been detected and confirms a close association and balance between the production of classical CKs and 2MeS-CKs. Finally, it discusses available reports regarding the possible physiological functions of 2MeS-CKs in different biological systems.

Keywords: 2MeSZ, 2MeSiP, methylthiolated cytokinins, methylthiotransferase, tRNA degradation pathway

INTRODUCTION

Cytokinins (CKs) are a group of adenine-derived, small signaling molecules, that comprise a class of phytohormones that are of crucial importance for multiple growth and developmental processes in plants (Spíchal, 2012; Kieber and Schaller, 2018). Plant CKs play a significant role in regulating cell proliferation and differentiation, control of shoot/root balance, transduction of nutritional signals (source/sink distribution), delaying senescence, and increasing crop productivity (Sakakibara, 2006). Cytokinins exist in two main structural forms, depending on the chemistry of the side chain attached at N⁶ position to the adenine ring – isoprenoid or aromatic. Regarding the structure of their side chain, classical, isoprenoid CKs include isopentenyladenine (iP), zeatin (*trans* and *cis* isomers; *tZ*, *cZ*), dihydrozeatin (DZ), and their various derivatives and conjugates (Kisiala et al., 2019) that often strongly differ in their biological activity (Spíchal, 2012).

In plants, isoprenoid CKs can be synthesized via two metabolic pathways, the *de novo* pathway, and the tRNA degradation pathway. In *de novo* CK biosynthesis, specific isopentenyltransferase

(IPT) enzymes (adenylate IPTs) add the isopentenyl sidechains (originating mainly from the methylerythritol phosphate pathway; MEP) to adenosine tri- di- or monophosphates (ATP, ADP, AMP). The *de novo* pathway, that is often a main source of plant CKs, is localized mainly in cell plastids and results predominantly in the production of iP- and tZ-type CKs that typically demonstrate high biological activity (Sakakibara, 2006).

The other known CK production pathway involves a modification of the adenine base at position 37 of tRNA molecules with the isopentenyl sidechain obtained primarily via the mevalonate pathway (MVA). Production of CKs through tRNA degradation is localized mainly in the cytosol. Generally, tRNA modifications contribute to an increased adaptation to environmental conditions through the control of translational efficiency and fidelity, in addition to reading frame maintenance (Dabravolski, 2020; Liaqat et al., 2020). Following the degradation of the modified tRNA molecules, cZ-type CKs are produced. Although the tRNA degradation pathway is thought to play only a minor role in overall CK production, it contributes significantly to the levels of cZ-CKs in certain plant species (Emery et al., 1998; Frébort et al., 2011; Gajdošová et al., 2011).

The presence of CK metabolites, or the genetic mechanisms required for CK production, have been reported in all kingdoms of life (Björk, 1995; Mayaka et al., 2019). Cytokinin biosynthesis involves conserved mechanisms even among evolutionary distant organisms, and the formation of CKs in bacteria, fungi, plants, or mammals all involve specific gene homologs and their corresponding enzymes, including IPT, adenosine kinase (AK), LONELY GUY (LOG) and a CK-degradation enzyme, cytokinin oxidase/dehydrogenase (CKX; Sakakibara, 2006; Chanclud et al., 2016; Trdá et al., 2017; Daudu et al., 2019). Genes encoding enzymes responsible for subsequent steps of CK metabolism exist in a variety of different organisms, although not all genes have been fully characterized or discovered.

Since the end of the 20th century, significant discoveries in plants have been made; from not even knowing if plants synthesized their own CKs (Holland, 1997), to having nearly comprehensively defined CK pathways, leading to identification of the active CKs and their corresponding conjugates (e.g., *cis* and *trans*-zeatin, iP, DZ and nucleotide, riboside, glucoside conjugates) (Kieber and Schaller, 2018). Unknown CK pathways are now rare and include those that may produce aromatic side chain CKs (Frébort et al., 2011) and the seldomly observed conjugates such as lupinic acid, a zeatin metabolite isolated from *Lupinus angustifolius* seedlings (Guern and Peaud-Lenoel, 2012), mono- and dimethylated isopentenyladenine CKs found in virulent *Rhodococcus fascians* strains (Jameson, 2019) or discadenine, iP derivative unique for slime mold *Dictyostelium discoideum* (Aoki et al., 2020). Another curious case is that of the hydrophobic, methylthiolated CKs (2MeS-CKs) (Figure 1). 2MeS-CKs are iP- or Z-type CKs modified by addition of a thiol group (–SH) at the position 2 of the adenine ring and its subsequent methylation (Tarkowski et al., 2010). Based on the evidence to date, these unique CK conjugates are derived exclusively via the tRNA degradation pathway (Koenig et al., 2002; Morrison et al., 2015a, 2017). 2MeS-CKs are commonly observed, yet they are poorly understood in terms of their origins,

biological activity and functions. Due to their low quantities in plant tissues, the development of analytical methods with adequate sensitivity to detect these compounds is essential in order to elucidate their biological function (Tarkowski et al., 2010). A survey of CK review literature has yet to offer a place for 2MeS-CK production in the overall CK pathway schemes (Spíchal, 2012; Morrison et al., 2015a, 2017).

This review will summarize the knowledge on the probable steps involved in biosynthesis of the unbound 2MeS-CKs. Furthermore, it will provide examples of CK profiles for organisms from which 2MeS-CKs were previously detected and confirm a close association and balance between production of classical CKs and 2MeS-CKs. Finally, it will discuss available reports regarding any possible physiological functions of 2MeS-CKs in different biological systems.

THE STEPS OF 2MeS-CK PRODUCTION VIA THE tRNA DEGRADATION PATHWAY

The Biosynthesis of the Initial CKs via tRNA Modification: tRNA Dimethylallyltransferase (EC 2.5.1.75): MiaA/MOD5/AtIPT2 and 9/TRIT1

The first step toward 2MeS-CK production involves the initial formation of a CK in the tRNA degradation pathway. It involves the addition of an isopentenyl group to an adenine at position 37 of tRNA molecules, which is known to read codons beginning with uridine (Figure 2). This isopentenyl addition occurs via the tRNA-isopentenyltransferase enzyme (tRNA-IPT) and it creates a tRNA-bound N⁶-isopentenyladenosine phosphate (iPRP). It also represents the rate limiting step of CK biosynthesis. To date, tRNA-IPT homologs have been identified in bacteria, fungi, plants, insects, and mammals (Pertry et al., 2009; Dabravolski, 2020).

In bacteria, the enzyme responsible for tRNA isopentenylation is MiaA (Buck and Ames, 1984; Gray et al., 1996; Koenig et al., 2002). A deletion of the *miaA* gene in *Salmonella typhimurium*, a pathogenic, Gram-negative bacterium, caused extensive pleiotropic effects, including a temperature-sensitive growth phenotype (Blum, 1988). *miaA* mutant strain of *Bradorhizobium* spp. displayed a significant reduction in CK production but was also characterized by more intense growth in CK-free media (Podlešáková et al., 2013). The isopentenyl side chain of the tRNA-bound iP can be further modified via *cis*-hydroxylase, forming a tRNA-bound *cis* isomer of Zeatin (tRNA-cZ) and, upon tRNA degradation, iP- or cZ-type CKs are released (Cherayil and Lipsett, 1977; Morris et al., 1981; McGaw and Burch, 1995). tRNA-derived cZ-CKs are often thought to have significantly reduced biological activity, compared to the *de novo* synthesized, highly active tZ-type CKs (Sakakibara, 2006; Wang et al., 2020); however, recent studies suggested cZ is strongly involved in plant stress alleviation (Gajdošová et al., 2011; Schäfer et al., 2015; Silva-Navas et al., 2019). *trans*-zeatin secretion in plant symbiotic *Methylobacterium* was previously linked to a tRNA source since the presence of Z

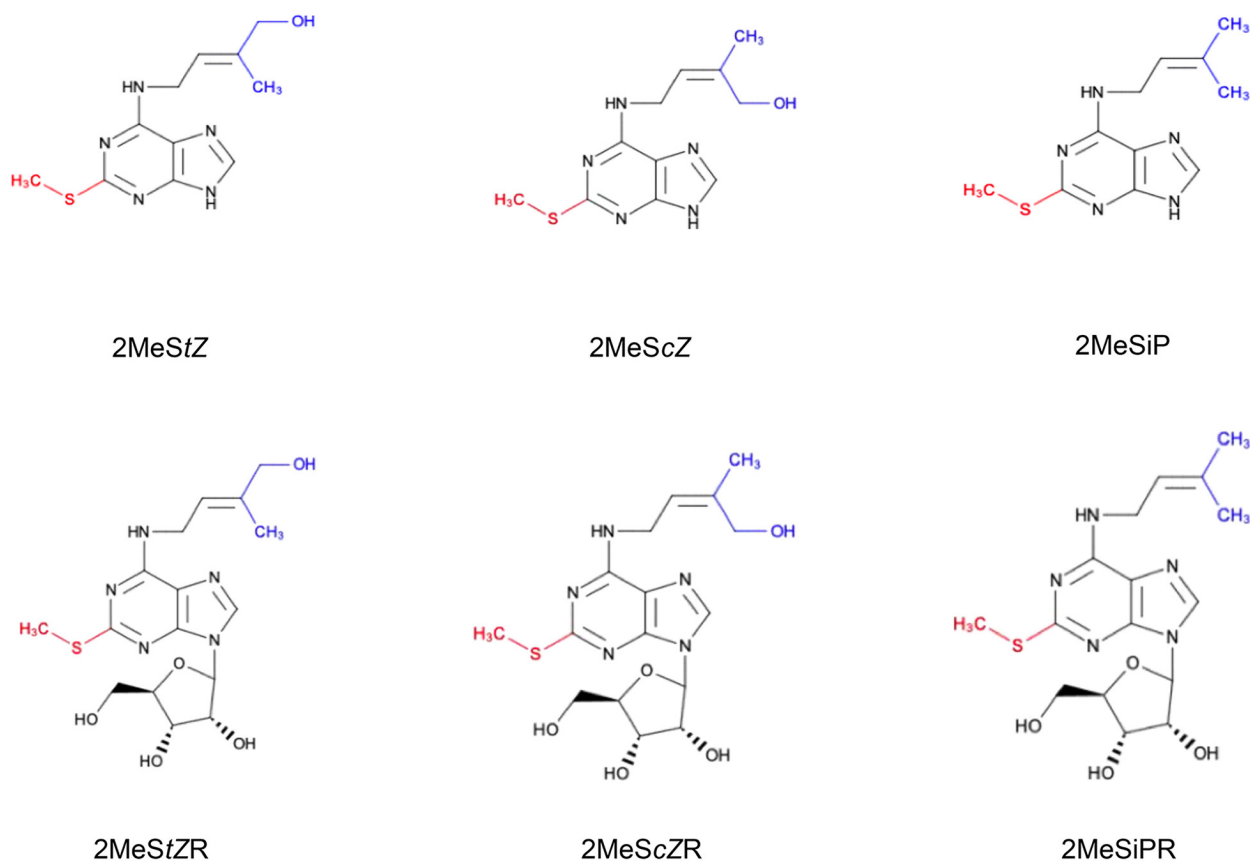


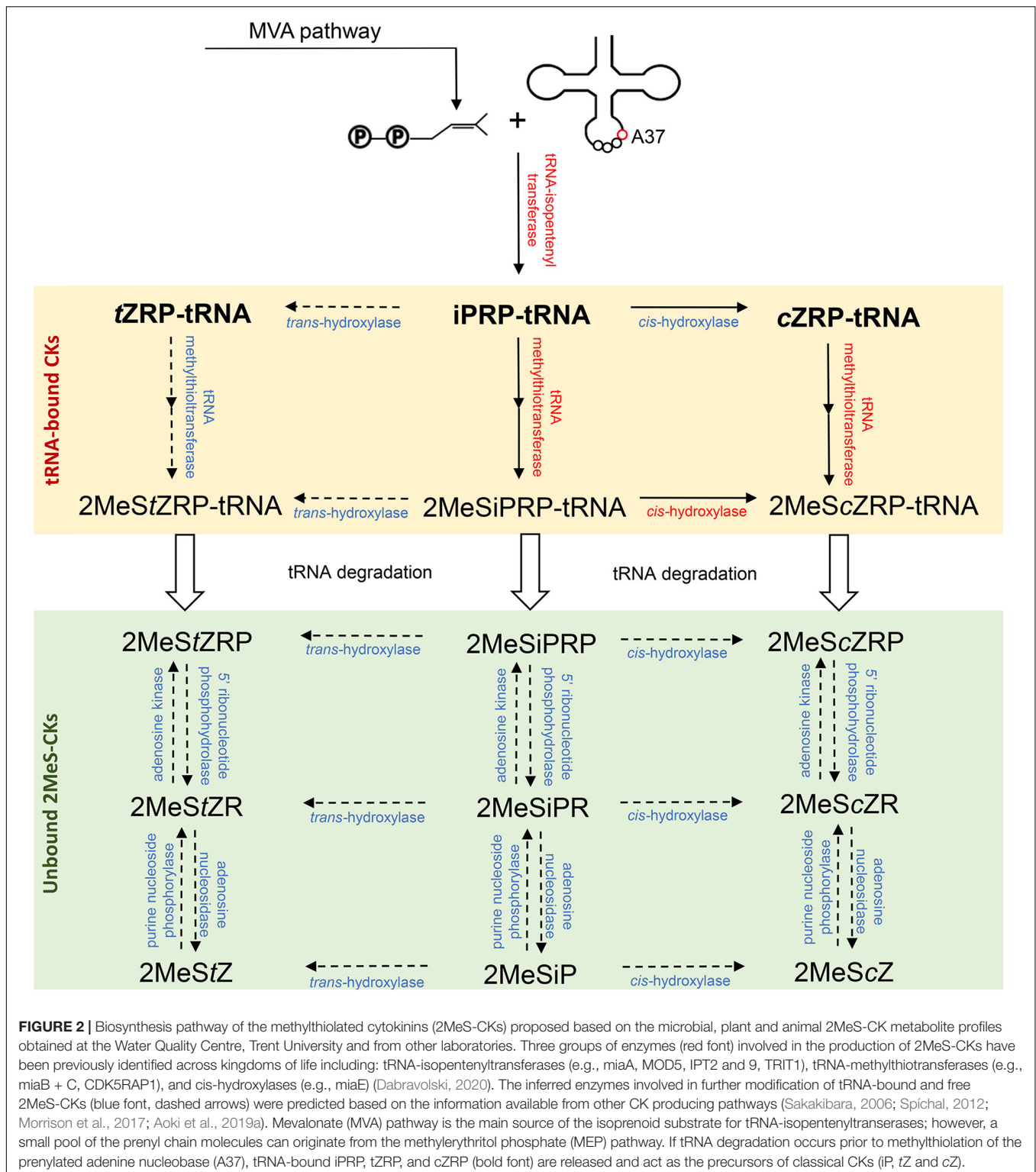
FIGURE 1 | Chemical structures of methylthiolated cytokinins (2MeS-CKs). The attachment of the $-S-CH_3$ group (red) at C_2 position of the adenine ring of tRNA-bound CKs is regulated by methylthiotransferase-like enzymes. 2MeS-CK forms differ based on the modifications to their isoprenoid side chain (blue) and include: 2-methylthio-*trans*Zeatin (2MeStZ), 2-methylthio-*cis*Zeatin (2MeScZ), and 2-methylthio-isopentenyladenine (2MeSiP), and their riboside derivatives: 2MeStZR, 2MeScZR and 2MeSiPR, respectively.

trans-isomers was detected even in the absence of the genetic machinery for *de novo* pathway synthesis. The tRNA hydrolysate of the *Methylobacterium extorquens miaA* mutant also lacked the precursor riboside forms, *trans*-zeatin riboside (*tZR*) and isopentenyladenosine (*iPR*) (Koenig et al., 2002). The presence of significant levels of *tZ* and its derivatives have since been reported from a wide selection of plant-associated *Methylobacterium* strains (Jorge et al., 2019), additionally supporting the claim that, unlike plants, some bacteria can derive *tZ*-type CKs via a tRNA source. The possibility of obtaining *tZ*-type CKs via the tRNA-IPT activity was also proposed for a phytopathogenic fungi-plant interaction system (Morrison et al., 2017) while production of *tZ*-type CK via *de novo* biosynthesis pathway has been previously identified in a fungal rye pathogen, ergot (*Claviceps purpurea*) (Hinsch et al., 2015).

The dominance of *cZ*- and *iP*-type CKs in the hormone profiles of saprophytic and biotrophic fungal species suggests that the tRNA degradation is the predominant CK pathway in that kingdom (Morrison et al., 2015b; Moffatt et al., 2018). A fungal tRNA-isopentenyltransferase gene homolog (*MOD5*) was first identified in yeast (*Saccharomyces cerevisiae*) (Laten et al., 1978; Dihanich et al., 1987). Evidence to support its

function in CK production was demonstrated via a *Mod5-1* mutation in *S. cerevisiae* that caused a significant reduction in biosynthesis of *iPR* from cytoplasmic and mitochondrial tRNA (Laten et al., 1978). *Mod5*, a yeast tRNA-isopentenyltransferase, is also involved in protein synthesis and sporulation (Laten et al., 1978) and *Mod5* mutants displayed reduced resistance to antifungal agents (Suzuki et al., 2012). More recently, a survey confirmed production of zeatin-type CKs in a wide range of yeast species (Streletsii et al., 2019); however, the authors did not resolve their data between the *trans*- and *cis*-isomers.

tRNA-IPT genes responsible for CK biosynthesis have been identified in pathogenic fungi and fungal CK production is a crucial factor in strain virulence (Chanclud et al., 2016; Morrison et al., 2017; Trdá et al., 2017). Cytokinin Synthesis 1 (*CKS1*), a gene encoding a tRNA-IPT was identified in the rice pathogen, *Magnaporthe oryzae* (Chanclud et al., 2016). *cks1* mutants showed normal *in vitro* growth; however, the deletion resulted in impaired CK production preventing the mutants from maintaining nutrient levels at the site of infection. This in turn, led to the induction of early and strong plant defenses suggesting that fungal CKs contribute to metabolite mobilization and to rice defense inhibition (Chanclud et al., 2016). In *Ustilago*



maydis, a biotrophic fungal pathogen that causes corn smut disease, the tRNA-IPT homolog was designated as *UMAG_10043* (Morrison et al., 2017). Deletion of *UMAG_10043* resulted in a loss of CK production and significantly reduced virulence of the fungus during infection of maize seedlings and cobs

but it also affected fungus filamentous growth and its ability to modify CKs taken up from the media (Morrison et al., 2017). The analysis of *LmIPT* (XP_003842057) silenced lines of *Leptosphaeria maculans*, a hemibiotrophic fungal pathogen of oilseed rape, demonstrated a significant reduction in *cZ* levels

(Trdá et al., 2017). However, no other phenotypic effects were observed in the mutants, and total CK levels were not altered, suggesting that another, alternative CK biosynthesis pathway might be active in *L. maculans* (Trdá et al., 2017).

Another microbial CK producer, slime mold (*Dictyostelium discoideum*) is a member of the *Amoebozoa* phylum and possesses three IPT genes, two of which are putative tRNA-IPT genes (*iptB* and *iptC*) (Anjard and Loomis, 2008; Nishii et al., 2018). These tRNA-IPT gene candidates are thought to be distantly related to plant IPTs and they were acquired in *Dictyostelium* by horizontal gene transfer (Eichinger et al., 2005; Nishii et al., 2018). Although the biological role of the two putative tRNA-IPTs in *D. discoideum* have not been confirmed, the available CK profiles suggest they might be involved in the production of *cZ*-type and 2Me-S-type CKs by slime mold (Aoki et al., 2019a).

In plants, CKs contribute an important role in inducing plant cell division, differentiation and regulation of various aspects of plant development and interaction with the biotic and abiotic environment (Sakakibara, 2006; Kieber and Schaller, 2018). tRNA-IPT homologs were identified in *Physcomitrella patens*, a moss species that belongs to the early divergent clade of land plants utilizing CKs for growth control (Lindner et al., 2014). In *Arabidopsis thaliana*, 9 isopentenyltransferase genes have been identified (*AtIPT1-9*), although only two; *AtIPT2* (AT2G27760) and *AtIPT9* (AT5G20040) are known to be responsible for modifying tRNA and production of *cZ* type CKs (Miyawaki et al., 2006). Although *cZ* activity is greatly limited in comparison with *tZ* or *iP* type CKs, the evidence supports the importance of plant tRNA-IPTs. For example, the *atipt2 9* double mutants demonstrate reduced *cZ* CK levels, but their *iP* and *tZ*-type CKs are not affected, and yet they often have a chlorotic phenotype (Miyawaki et al., 2006).

The available studies of CKs in the kingdom of Animalia indicate the existence of an active tRNA pathway in insects and mammals. Cytokinin metabolites have been found in insects (e.g., Straka et al., 2010; Andreas et al., 2020); although, it has been postulated that CK presence in insects might be a result of the activity of bacterial symbionts (Giron et al., 2013). In silkworm (*Bombyx mori*), a candidate tRNA-IPT gene with three alternative splicing isoforms (*BmIPT1-BmITP3*) was recently identified (Chen et al., 2019). A recombinant vector containing *BmIPT1* could restore isopentenylolation of tRNA in the IPT-deficient yeast strain MT-8 suggesting *BmIPT1* is a functional tRNA-IPT enzyme in *B. mori*. Although no CK data are available for silkworm to date, the importance of *BmIPT1* was demonstrated following the *i*⁶A (*iPR*) modification at position A37 in tRNA, which resulted in severe abnormalities in silk spinning and metamorphosis (Chen et al., 2019).

Cytokinin presence and metabolism has been reported in canine tissues (Seegobin et al., 2018) and human cell cultures (Aoki et al., 2019b), and the CK profiles indicate that tRNA degradation is the only source of unbound mammalian CKs. tRNA-isopentenyltransferase 1 (*TRIT1*), a homolog of the prokaryotic *miaA*, facilitates production of tRNA-bound *iP*-type CKs in human cytosol and mitochondria (Lamichhane et al., 2013; Smaldino et al., 2015). *TRIT1* was previously suggested to play a role as a tumor suppressor (Spinola et al., 2005), in

selenoprotein regulation (Fradejas et al., 2013) in gene-mediated transcriptional silencing (Smaldino et al., 2015) and amyloid fiber folding (Waller et al., 2017). The product of the *TRIT1* gene, *iPR*, has long been the lone CK type detected as tRNA-bound or as a free mononucleotide in mammals (Persson et al., 1994; Golovko et al., 2000). Since then, more recent studies on CK profiling by High Performance Liquid Chromatography Tandem Mass Spectrometry (HPLC-MS/MS) revealed a presence of seven types of CKs in a range of canine tissues (Seegobin et al., 2018). The presence of unbound CK derivatives in HeLa cell cultures were detected, strengthening the evidence of *TRIT1* activity in CK biosynthesis in mammalian cells (Aoki et al., 2019b).

The First Step of Methylthiolation of tRNA-Bound CKs: tRNA-2-Methylthio-N(6)-Dimethylallyladenosine Synthase (EC 2.8.4.3):

MiaB + MiaC/AT4G36390/CDK5RAP1

Following isopentenylolation, methylthiolation of the adenine ring at the C₂ position is the next step of the tRNA degradation pathway that leads to the production of 2MeS-CKs (**Figure 2**). In bacteria, the gene responsible for methylthiolation is *miaB* which modifies tRNA-bound *i*⁶A (*iPR*) or *io*⁶A (*cis*Zeatin riboside; *cZR*) to *ms*²*i*⁶A (2-methylthio-isopentenyladenine riboside; 2MeSi*iPR*) and *ms*²*io*⁶A (2-methylthio-*cis*Zeatin riboside; 2MeSc*ZR*), respectively (Esberg et al., 1999; more details on hydroxylation of the isoprenoid chain of tRNA-bound CKs will be provided in the section “Hydroxylation of the Isopentenyl Chain of tRNA-Bound 2MeSi*P*-CKs: tRNA-*ms*2*io*6A37-Hydroxylase: MiaE/CYP450”). Methylthiolation requires iron (Fe), cysteine (Cys), S-adenosylmethionine (SAM) and is thought to occur in two steps, initially as thiolation of *i*⁶A37 (tRNA-bound *iPR*) to *s*²*i*⁶A37, and a subsequent methyl transfer gives *ms*²*i*⁶A37 (tRNA-bound 2MeSi*P*) (Esberg et al., 1999). It remains unknown whether each reaction is catalyzed by a single enzyme (*MiaB* + *MiaC*) or both steps are facilitated by the same enzyme, *MiaB* (Pierrel et al., 2003). However, *Escherichia coli* mutant strains that lacked a functional *miaB* gene were shown to contain only the product of the first step in the tRNA pathway, *i*⁶A37; thus it is suggested that the *MiaB* protein is involved in formation of the C-S bond that can be further methylated via *MiaC* activity (Esberg et al., 1999). A conserved canonical Cys triad is found both in the N-terminal half of *miaB* genes and in enzymes such as biotin and lipoate synthases, which are involved in catalyzing C-H to C-S bond conversion reactions. The motif provides Cys ligands for a [4Fe-4S]^{+2/+1} cluster. The Cys triad and iron cluster are essential for thiolation activity which indicates that *MiaB*, biotin synthase, and lipoate synthase all utilize similar radical mechanisms to activate sulfur (S) and insert it into the respective substrates (Pierrel et al., 2002). Additionally, *MiaB* enzymes contain a sequence of 60–80 residues in the C-terminal region that is similar to the β-barrel RNA-binding domains (Anantharaman et al., 2001). This domain, known as TRAM, was identified as the site likely involved in binding the tRNA substrate (Pierrel et al., 2003). The level of synthesis of the 2-methylthiol group of *ms*²*io*⁶A (2MeSc*ZR*) is sensitive to the presence of S or

Fe and may function as a signal device for the availability of these elements (Buck and Griffiths, 1982; Buck and Ames, 1984).

The role of the *miaC* gene has been postulated to exist but never identified (Pierrel et al., 2004). *MiaC* is thought to function during the methylthiolation reaction as a methyltransferase following the S transfer performed by *MiaB*. Examples of methyltransferase genes in plant pathogenic bacteria can be found in *Streptomyces turgidiscabies* and *R. fascians* which both carry a *fas* operon (Joshi and Loria, 2007; Pertry et al., 2009). The *fas* operon contains two open reading frames (ORFs) that code for methyltransferases (*mtr-1* and *mtr-2*) which may be involved in the methylthiolation of bacterial CKs (Frébert et al., 2011).

Unlike bacteria, there are no *miaB* homologs yet identified from fungi. Correspondingly, 2MeS-CKs have not been found in axenic fungal cultures (Table 1; Hinsch et al., 2015; Chanclud et al., 2016; Morrison et al., 2017; Vedenicheva et al., 2018). Previously, 2MeS-CKs were detected from temperate forest fungi collected *in situ* (Morrison et al., 2015b); however, these samples were not grown aseptically and would have had an associated microbiome, including bacteria capable of producing 2MeS-CKs.

2-Methylthio-Zeatin riboside (2MeSZR) and 2-methylthio-Zeatin (2MeSZ) accumulated in the infected cobs during the later stages of maize infection by *U. maydis* but were not present in aseptic fungal cultures or in control plant tissue. This finding suggests there is a fungal-stimulated, plant-origin of 2MeS-CKs that may be involved in promoting tissue proliferation around the site of infection (Morrison et al., 2015a).

Apart from fungi, *miaB* homolog genes can be found across all kingdoms of life, indicating their evolutionarily conserved character and universal roles in posttranscriptional

and posttranslational RNA modifications (Anantharaman et al., 2002). Figure 3 presents a MAFFT alignment (Geneious Prime 2020.2.3) of the characterized and predicted *miaB*-like proteins in model and non-model species from *Archaea*, *Bacteria*, *Protista*, *Planta*, and *Animalia*. The top candidates were selected based on the highest sequence similarity with *E. coli* *miaB* protein sequence (accession no. WP_000162747.1) using non-redundant BLASTp searches on 59 selected taxids. Searches were done using the BLOSUM62 matrix and default parameters.¹ A signature *miaB* motif that has three cysteine residues spaced by 3 and 2 amino acids (CxxxCxxC; Figure 3), and that is responsible for iron binding in the process of thiolation (Esberg et al., 1999), was present in all the analyzed sequences. Another highly conserved *miaB* motif (IVGFPGET; Figure 3; Esberg et al., 1999) was found in 18 species including representatives of *Archaea*, *Bacteria* and *Protists*. The presence of the TRAM domain (PF01938) responsible for nucleic acid binding, has been identified in 54 of the 59 aligned sequences²; however, the remaining five accessions revealed similar sequence structure to those of TRAM domains from the other analyzed taxons (Figure 3).

The *A. thaliana* homolog of bacterial *miaB* gene is known as AT4G36390. Structurally, AT4G36390 resembles *miaB* as it contains a C terminal RNA-binding TRAM domain and functions similarly to bacterial tRNA methylthiotransferases (Dabravolski, 2020). AT4G36390 is predicted to localize mainly to the mitochondria and carry an [Fe-S]; however, much of its role remains unknown (Dabravolski, 2020).

¹<https://www.ncbi.nlm.nih.gov/protein/accessed August 2020>

²<https://pfam.xfam.org/and NCBI Batch CD-Search Tool accessed August 2020>

TABLE 1 | Profiles of methylthiolated cytokinins (2MeS-CKs) among representatives of different life kingdoms.

| Kingdom | Species | 2MeS-CKs detected | 2MeS-CK level | Total CK level | References |
|----------|--|--------------------------------|--------------------------------|--------------------------------|--------------------------|
| Bacteria | <i>Erwinia amylovora</i> CFBP1430 | 2MeSZ, 2MeSiP, 2MeSiPR | 1–5 pmol/mL | 10–20 pmol/mL | Daudu et al., 2019 |
| | <i>Methylobacterium jeotgali</i> LMG23639(T) | 2MeSZ, 2MeSZR | 5–10 pmol/mL | 10–20 pmol/mL | Jorge et al., 2019 |
| Protists | Slime mold (<i>Dictyostelium discoideum</i>) (aggregation) | 2MeSiP | 1–5 pmol/10 ⁶ cells | 1–5 pmol/10 ⁶ cells | Aoki et al., 2019a |
| | <i>Euglena gracilis</i> (cell pellet) | MeSiP | 1–5 pmol/gFW | 20–50 pmol/gFW | Noble et al., 2014 |
| Fungi | <i>Magnaporthe oryzae</i> (mycelia) | n.d. | n.d. | 150–200 pmol/gFW | Chanclud et al., 2016 |
| | <i>Ustilago maydis</i> (mycelia) | n.d. | n.d. | 20–50 pmol/gFW | Morrison et al., 2017 |
| Plants | Soybean (<i>Glycine max</i>) (seed; R6) | 2MeSZ, 2MeSZR | 1–15 ng/gFW | 5–30 ng/gFW | Kambhampati et al., 2017 |
| | <i>Arabidopsis thaliana</i> Col (seed) | 2MeSZ, 2MeSiP, 2MeSZR | 100–150 pmol/gFW | 10,000–15,000 pmol/gFW | Butler, 2019 |
| Animals | <i>Rhinusa pilosa</i> (adult) | 2MeSZ, 2MeSZR | 1,500–2,000 pmol/gFW | 2,000–2,500 pmol/gFW | Andreas et al., 2020 |
| | Dog (<i>Canis familiaris</i>) (stomach) | 2MeSiP, 2MeSZR, 2MeSiPR | 15–20 pmol/gFW | 50–100 pmol/gFW | Seegobin et al., 2018 |
| | HeLa cells (<i>Homo sapiens</i>) | 2MeSZ, 2MeSiP, 2MeSZR, 2MeSiPR | 1,000–5,000 pmol/mL | 5,000–10,000 pmol/mL | Aoki et al., 2019b |

Using HPLC-MS/MS analysis at the Water Quality Centre, Trent University, example organisms of the Prokaryotae (bacteria) and the Eukaryotae (protists, fungi, plants, and animals) were scanned for presence of 2MeSZ, 2MeSZR, 2MeSiP, and 2MeSiPR. 2MeS-CKs were detected in the representatives of all the analyzed kingdoms except for fungi. n.d., not detected.



FIGURE 3 | MAFFT alignment of 59 miaB-like protein sequences including representatives of Archaea, Bacteria, Protista, Planta, and Animalia kingdoms. All amino acid sequences were trimmed to the length of *E. coli* miaB (WP_000162747.1; 1–474 aa). WP_000162747.1 accession was set as reference sequence and all aligned sequences were sorted by the number of differences to reference sequence. Black color indicates regions identical to those of *E. coli* miaB, gray color indicates differences in the aligned sequences from miaB protein. The locations of three highly conserved miaB regions are highlighted by the purple arrows: Cys motif (CxxxCxxC) – involved in methylthiolation of the prenylated adenine in tRNA 37 position, was identified in all the analyzed sequences; IVGFPGET motif was found in 18 accessions, including representatives of Archaea, Bacteria and Protista; TRAM domain, responsible for nucleic acid binding, was present in 54 out of the 59 aligned sequences. The alignment, motif search and visualization were performed using Align/Assemble function in Geneious Prime 2020.2.3.

In mammals, cyclin dependent kinase 5 regulatory subunit-associated protein 1 (CDK5RAP1) is a type of radical SAM enzyme that reductively cleaves S-adenosyl-L-methionine (Atta et al., 2010), with homology to *miaB* (Kaminska et al., 2008; Reiter et al., 2012). CDK5RAP1 is responsible for methylthiolation of tRNA-bound CKs and has roles in altering stability of tRNA molecules, interactions with ribosomes and translation (Jenner et al., 2010; Horvath and Chinnery, 2015). The presence of unbound 2MeS-CK metabolites was recently reported from the surveyed canine tissues and human cell cultures (Seegobin et al., 2018; Aoki et al., 2019b).

Hydroxylation of the Isopentenyl Chain of tRNA-Bound 2MeSiP-CKs: tRNA-ms²io⁶A37-Hydroxylase: MiaE/CYP450

A further step of the 2MeS-CK production via tRNA degradation pathway involves hydroxylation of the isopentenyl side chain which can occur before or after methylthiolation (Dabravolski, 2020) (Figure 2). The biosynthesis of tRNA-bound ms²io⁶A (2MeScZR) in *S. typhimurium* involves multiple enzymatic activities and their corresponding genetic loci of which *miaE* is responsible for the hydroxylation step (Persson and Björk, 1993). The tRNA-(ms²io⁶A37)-hydroxylase is present in *Salmonella* under anaerobic conditions; but the hydroxylation reaction does not occur in the absence of oxygen, indicating that it depends on the presence of molecular oxygen (Buck and Ames, 1984).

Bacterial MiaE hydroxylates a terminal methyl group of ms²i⁶A (2MeSiPR) to form ms²io⁶A (2MeScZR). Cloning the *miaE* gene that encodes the tRNA hydroxylase from *S. typhimurium* and complementing the *E. coli* strain that is naturally deficient in ms²io⁶A hydroxylation gene increased the rate of ms²i⁶A37 (2MeSiPR) hydroxylation by approximately 250-fold (Persson and Björk, 1993). It has been suggested that the *miaE* gene may encode either the tRNA-(ms²io⁶A37)-hydroxylase or a cofactor necessary for the hydroxylation reaction. However, it is unlikely that *miaE* encodes a cofactor needed for only one reaction, and even less likely that *E. coli* would have kept the hydroxylating enzyme through evolution despite the absence of the necessary cofactor; therefore, it seems more probable that the *miaE* gene encodes the tRNA-(ms²io⁶A37)-hydroxylase itself (Persson and Björk, 1993).

Fungi lack the *miaE* gene as it is not found in eukaryotes (Persson and Björk, 1993; Frébort et al., 2011). In plants, conversion of iPR and 2MeSiPR to cZ and 2MeScZR, respectively, occurs through hydroxylases, which function similarly to bacterial MiaE enzymes (Takei et al., 2004). BLASTp searches could not identify corresponding hydroxylase homologs in mammalian candidates (Seegobin et al., 2018). However, CYP450 enzymes that are involved in hormone metabolism in mammals (Nebert and Russell, 2002; Schmidt et al., 2008) remain to be investigated for their potential role as *cis*-hydroxylating agents, especially regarding the previously detected 2MeSZR metabolites in both canine tissues and human cells (Seegobin et al., 2018; Aoki et al., 2019b).

2MeS-CK METABOLITES ASSOCIATE WITH THE PROFILES OF MORE COMMONLY STUDIED CKs ACROSS THE KINGDOMS OF LIFE

Unbound 2MeS-CKs are present in biological systems as a result of degradation of the tRNA molecules modified by the set of genes described in the previous sections. The genes responsible for subsequent steps of 2MeS-CK biosynthesis and the effects of tRNA modifications leading to the formation of bound 2MeS-CKs in microbes and mammals have been known for decades; but the highly sensitive methods of HPLC-MS/MS that enable the precise detection and quantification of unbound, hydrophobic 2MeS-CK metabolites from biological samples have only been available for the last 10 years (Tarkowski et al., 2010; Šimura et al., 2018; Kisiala et al., 2019). Table 1 is a summary of the previously published HPLC-MS/MS results which confirm a recurring presence of 2MeS-CKs among species from various kingdoms of life including microbes, plants, and animals.

To date, most research on CK molecules have investigated plant classical CKs (unmodified iP-, tZ-, cZ-, and DZ-types) while not much interest has been put into explaining the presence of unbound 2MeS-CKs in biological systems (Großkinsky et al., 2016). This, in consequence, resulted in a general lack of studies involving mutants impaired in the function of 2MeS-CK biosynthetic genes, as compared to *IPT*, *LOG*, or *CKX* modifications, creating additional challenges for understanding the methylthiolated CK compounds. Nevertheless, the available CK profiling data on *miaB* knock-out mutant of *E. coli* (JW0658-1) revealed a lack of 2MeS-CKs while, simultaneously, the levels of iPRP were considerably increased in the culture lysate (Daudu et al., 2019). These findings support other evidence from genetic studies that the pool of available prenyl-tRNA – the precursor molecule of the classical CKs originated via tRNA degradation pathway – is also the source of unbound 2MeS-CKs (Esberg et al., 1999; Morrison et al., 2017; Figure 2). The metabolite profiles reported for microbial, plant and animal-derived 2MeS-CKs often reflect the close association between this group of compounds and select, classical CK types (particularly, iP and its precursor forms), which implies that they originate from a common precursor in the tRNA degradation pathway.

Methylobacterium strains are plant-associated bacteria well known for their plant growth promoting characteristics and unique capabilities to synthesize high levels of biologically active tZ-type CKs. The study of CK profiles of eight *Methylobacterium* isolates revealed that strains secreting the highest levels of 2MeS-CKs (specifically 2MeSZ) simultaneously had low tZ production (i.e., *M. organophillum* NBRC103119: tZ – 12.4 pmol/10 mL, 2MeSZ – 119.6 pmol/10 mL, and *M. oryzae* LMG23582(T): tZ – 212.9 pmol/10 mL, 2MeSZ – 39.9 pmol/10 mL) (Jorge et al., 2019).

In plants, the analysis of CK profiles during the reproductive development of 27 field grown soybean cultivars revealed an association between the levels of 2MeS-CKs and CK nucleotides. Namely, the cultivars characterized by the higher 2MeSZ levels in their pods at R4 growth stage contained lower concentrations

of iPRP while high iPRP production was associated with the lower 2MeSZ levels in the developing pods (Pearson's $r = -0.467$) (Kambhampati et al., 2017). A clear, offsetting balance between the levels of CK nucleotides and 2MeSCKs occurs during the reproductive growth stages of *A. thaliana* WT as well as its two tRNA-IPT mutants, *ipt2* and *ipt9* (Butler, 2019). In detail, in immature siliques, *Arabidopsis* plants contained prominent levels of iPRP and a relatively low concentrations of a single 2MeS-CK form (2MeSZ). On the other hand, CK profiles of maturing seeds lacked any nucleotide CK precursors while considerable increases in the concentrations of 2MeS-CK derivatives [2MeSZ, 2MeSZR and 2-methylthio-isopentenyladenine (2MeSiP)] were observed (Butler, 2019).

These types of inverse associations were also characteristic for the HPLC-MS/MS profiles of CKs reported from representatives of six orders of Insecta (Andreas et al., 2020). For example, larvae of two stem-boring beetle species, *Mecinus janthinus* and *Mecinus janthiniformis*, demonstrated highly elevated concentrations of nucleotide precursors of the classical CKs and only trace levels of 2MeS-CK derivatives. The adult forms of these two weevils had unusually high levels of 2MeS-CKs (2MeSZ and 2MeSiP), and minimal concentrations of the classical CKs (*tZ*- and *iP*-type) suggesting there were different activities of the genes in the tRNA modification pathway during subsequent stages of insect development. Similar associations were observed among other insect forms and species (Andreas et al., 2020).

A negative association between the levels of 2MeS-CKs and classical CKs was reported from analyses of mammalian samples (Seegobin et al., 2018). The presence of 2MeS-CKs was identified in 8 out of 21 tested canine organs and tissues, which included: the inner and outer kidney medulla, stomach, appendix, small and large intestine, bile and thyroid. In most of the analyzed organs, *iP*-type CKs were the predominant CK forms while 2MeS-CKs were generally found at much lower levels. However, in bile, considerably higher concentration of 2MeS-CKs were detected, which was accompanied by lower levels of *iP*-type CKs (i.e., thyroid: 2MeS-type CKs – 3.82 pmol/gFW, *iP*-type CKs – 1392.75 pmol/gFW; bile: 2MeS-type CKs – 229.96 pmol/gFW, *iP*-type CKs – 114.68 pmol/gFW) (Seegobin et al., 2018).

EVIDENCE OF THE POTENTIAL PHYSIOLOGICAL ROLES OF 2MeS-CKs

Despite the availability of mass spectrometry methods for the analysis of 2MeS-CKs (Tarkowski et al., 2010; Kisiala et al., 2019) and emerging number of reports of their presence in different biological systems (including mammals, plants, pathogen-host associations, bacteria, and algae), the functional significance of 2MeS-CKs continues to remain poorly understood (Esberg et al., 1999; Morrison et al., 2015a; Kambhampati et al., 2017; Daudu et al., 2019; Koshla et al., 2019). Most knowledge about the role of 2MeS-CKs stems from their occurrence in post translational tRNA modifications which have a role in translational efficiency, fidelity, and specificity of codon/anticodon interactions (Persson and Björk, 1993; Golovko et al., 2000; Koshla et al., 2020). Deletion of key genes in

the methylthiolation pathway can result in aberrant phenotypes most often related to impacts on translation (Koshla et al., 2019). However, the impact of the released, methylthiolated CK compounds on the physiology of organisms has yet to be fully understood.

Koshla et al. (2019, 2020) examined the impact of *miaA*, *B* and *AB* null mutants in *Streptomyces albus* showing that *miaA* and *B* deficiency caused significant changes in morphology of *Streptomyces* and its secondary metabolome profile. Likely caused by less efficient translation, the *miaAB* mutant was devoid of endogenous antibacterial activity while the parent *miaA* mutant still displayed some antibacterial activity (Koshla et al., 2019). *miaB* mutants had delayed biomass production and *miaAB* mutants produced sparse aerial hyphae without spore chains compared to the parental mutant *miaA* (Koshla et al., 2020), suggesting that, even in the absence of *miaA*, *miaB* functions to maintain cell cycle and morphology. Phenotypic discrimination between the mutated bacterial lines was highly conditional and only possible on specific media during early stages of their lifecycle; indicating that the impact of methylthiolation may be specific to certain stages of the growth cycle under defined nutrient conditions (Koshla et al., 2020). Although the levels of unbound 2MeS-CKs were not analyzed, this study suggests that the removal of genes responsible for thiolation impacts total free 2MeS-CKs and thereby also has an impact on the overall development of the bacteria (Koshla et al., 2020).

Similar to bacteria, knockdown mutations of enzymes responsible for the methylthiolation of tRNA in mammals resulted in changes to cell cycle. Mammalian CDK5RAP1 is related to the regulation and progression of the M phase of the cell cycle (Wang et al., 2015). Deficiency of the CDK5RAP1 enzyme (a homolog of bacterial *miaB*) in the knockdown mutation of human breast cancer cell line MCF-7 suppressed tumor growth through cell arrest at the G2/M phase and induced cell apoptosis (Wang et al., 2015). Cytokinins have antitumor effects, with exogenous *iPR* treatment causing autophagic cell death; however, CDK5RAP1 reduced the antitumor effect of endogenous *iPR* by converting it to 2MeSiPR and protecting glioma initiating cells (GICs) from autophagy triggered by *iPR* toxicity. Isopentenyladenosine was not converted directly to 2MeSiPR when it was exogenously applied to GICs (Yamamoto et al., 2019).

The hypermodifications of tRNA not only aid in translation and cell cycle functioning, but after degradation of the modified tRNAs, they act as small molecules able to trigger physiological effects and activate CK receptors (Daudu et al., 2017, 2019). The role of histidine kinase (HK) CK receptors from *Malus domestica* (apple tree) in the perception of classical and methylthiolated CKs were examined utilizing a histidine kinase deletion mutant in yeast (*sln1* deletion) (Daudu et al., 2017). Complementation assays and examining yeast cell growth in response to CK addition revealed that MdCHK2 have higher sensitivity to *iP* and 2MeSiP (1 nM) relative to other CKs tested. Other examined MdCHKs also responded to 2MeS-CKs (5 nM–5 μ M depending on receptor) indicating that 2MeS-CKs can be perceived by CK receptors and trigger growth responses (Daudu et al., 2017).

The yeast mutant strain *sln1Δ*-MdCHK was further utilized as a CK biosensor and was exposed to extracts from a variety of organisms to detect their production of CKs (Daudu et al., 2019). When exposed to supernatant extracts from *E. coli miaB* deletion mutant, yeast growth was triggered but was considered to be less than the wildtype. Yeast growth was not decreased due to changes in total level of CKs as these were similar between the wildtype (16.6 pmol/mL) and *miaB* mutant (17.9 pmol/mL). The *E. coli miaB* deletion strain had higher levels of iPRP and iP relative to the WT strain while it was suggested that the limited yeast growth was due to reduction in 2MeSiP which was not detected in the *miaB* deletion mutant (Daudu et al., 2019).

The ability of receptors to respond to 2MeS-CKs suggests these unique CKs can trigger downstream impacts such as growth changes. Correlations between 2MeS-CK levels and observed phenotypes can indicate a potential role or influence that 2MeS-CKs may have on a system. In a field trial sampling of twenty-seven soybean cultivars high quantities of 2MeSZR and 2MeSZ were detected at all three stages of seed filling (R4,5,6) of high yielding varieties. There was also a positive correlation of 2MeSZ with all yield components measured suggesting 2MeS-CKs may play a role in seed filling and subsequent yield formation in soybean (Kambhampati et al., 2017).

In plant-microbe interaction systems, 2MeS-type CKs are often suggested to be of microbial origin. Cytokinins, including bacterially produced 2MeS-CKs play a role in the dormancy of annual ryegrass (*Lolium rigidum*) seeds (Goggin et al., 2015). Removal of the bacterial symbiont resulted in seeds being unable to break dormancy in the dark, suggesting that a complex integration between plant hormones and those produced by bacterial microflora, including 2MeS-CKs, play an important role in controlling seed maturation in *L. rigidum* (Goggin et al., 2015).

Spikes in 2MeS-CKs have been detected during host-pathogen relations where increased plant growth is a disease symptom. *A. thaliana* infection by a bacterial phytopathogenic strain of *R. fascians* had the same spectrum of CKs as the non-pathogenic counterpart; yet the former had higher levels of 2MeScZ, iP and cZ (Pertry et al., 2009). The authors suggested that 2MeS-CKs may be less cytotoxic than classical CKs which could account for their accumulation during infection (Pertry et al., 2009). The low but consistent presence of 2MeS-CKs may be important in eliciting plant responses during disease development (Giron and Glevarec, 2014). The accumulation of cZ and 2MeS-CKs in infected plant tissues and the transient peak in the levels of iP, 2MeSiP, and 2-methylthio-*trans*Zeatin (2MeStZ) in the early interaction phase hinted at the biological significance of the identified bacterial 2MeS-CKs (Pertry et al., 2009). These characteristics also suggest that 2MeS-CKs may be more resistant to CK degrading enzymes (CKX) and are capable of escaping attempts by the host to balance CKs (Morrison et al., 2015a). Therefore, 2MeS-CKs are thought to help hijack the plant machinery while avoiding deleterious effects on plant development and activation of CK mediated plant defenses (Giron and Glevarec, 2014). Overall, 2MeS-CKs may be responsible for continuous tissue proliferation and symptom maintenance during plant-pathogen interaction (Pertry et al., 2009). Observations of the *Zea mays* – *U. maydis* plant-pathogen

system led to the similar conclusion as previously suggested for the 2MeS-CK effect in *Arabidopsis* – *R. fascians* interaction. Although the fungus *U. maydis* does not produce 2MeS-CKs separate from the plant, during the *Zea mays* – *U. maydis* relation an accumulation of 2MeS-CKs (specifically 2MeSZR and 2MeSZ) occurred in the infected plant tissue during the later stages of cob infection (days 20–28) while these CKs were not detected in the control cobs (Morrison et al., 2015a, 2017).

The contribution of CK interplay was examined in the human pathogen, *Mycobacterium tuberculosis*, the causative agent of tuberculosis. This bacterium secretes several iP- and tZ-type CKs including 2MeSiP, 2MeSiPR and 2MeStZR (Samanovic et al., 2015). A higher activity of *M. tuberculosis* LOG-like enzyme, Rv105, results in CK accumulation including 2MeSiP. That, in turn, increases sensitivity of bacterial strains to nitric oxide, a defense response from the host cells, detrimental to pathogen survival. These results suggest that among other CKs, 2MeS-CKs play a role in sensitizing the pathogen to the activation of host defense mechanisms (Samanovic et al., 2015).

While most studies focus on the impact of gene deletion and the resulting effects which might then be rescued through gene complementation (Koshla et al., 2020), few have added exogenous 2MeS-CKs to rescue deletion phenotypes or applied exogenous methylthiol CK derivatives to examine their impact on a biological system.

The HPLC-MS/MS analysis of CK profiles in microalgae *Chlorella vulgaris* revealed that 2MeS-CKs were the prevalent CKs in both culture supernatant and cell pellet, with 2MeSZ being the most abundant in the pellet (4.7 pmol/g) and at high concentrations in the supernatant (220.7 pmol/g) followed by other methylthiol conjugates (Ramphal, 2016). To understand the role of 2MeS-CKs in *C. vulgaris* cell cycle, the effect of exogenous 2MeSZ treatment on the cell growth and select metabolite production were examined. Culture supplementation with 2MeSZ resulted in growth stimulation and had an impact on the microalgae fatty acid profiles in a manner comparable to those of the other active CKs that were tested (tZ, benzyladenine). In particular, significant increases in linolenic acid (18-carbon chain with three double bonds; 18:3) occurred at 10^{-7} and 10^{-6} M 2MeSZ concentrations; 204 and 457% increase relative to the control, respectively (Ramphal, 2016). It indicates that the addition of exogenous methylthiol CKs can impact growth as well as fatty acid metabolism in algae. Modified secondary metabolite production was also a result of the deletion of *miaB* in the bacterium, *S. albus* (Koshla et al., 2020). These studies suggest that the methylthiolated CK compounds are not only necessary for efficient translation but likely are also involved in activating downstream metabolic pathways.

CONCLUSION

Physiological roles of classical CKs (unmodified iP, tZ, cZ, and DZ and their derivatives) have been studied extensively to help uncover the functions of these signaling molecules in different aspects of plant physiology. In parallel, extensive knowledge exists for genes involved in tRNA modifications that lead to the

production of tRNA-bound 2MeS-CKs, especially in bacterial and mammalian systems. However, not much is known about the fate and possible function of the unbound 2MeS-CKs, derived via degradation of the modified tRNA molecules in biological systems.

There is a compelling need to further study this most elusive group of CKs as evidenced by their frequent detection, which is often at high concentrations when found in different plant organs and at different developmental stages; moreover, there is an increasing number of reports on 2MeS-CK presence in other, non-plant organisms. Suggestions of the potential metabolic activities of unbound 2MeS-CKs have been made previously. The limited physiological data available indicate that 2MeS-CKs may play a role that is similar to classical CKs; whereby, 2MeS-CKs impact cell division as they are often detected in systems where active proliferation occurs, like plant-pathogen disease development and mammalian cancer cells. In addition, 2MeS-CKs may be able to reduce the pool of more active iP-type CKs resulting in production of less cytotoxic forms of CKs. As discussed above, conversion of iPR in mammals to 2MeSiPR reduced the anticancer effect of iPR on cells thus decreasing the potency of the CK application. Likewise, production of 2MeS-CKs during plant-pathogen disease development may allow for persistent accumulation of forms that are more resistant to degradation and, therefore, can act over a longer period of time. Finally, exogenous application of 2MeS-CKs can impact cell metabolism and growth as seen in *C. vulgaris*.

The potential impact of 2MeS-CKs should no longer be overlooked. Their functional role needs to be better understood and further investigation into the deletion of key genes in the

methylthiolation pathways as well as the exogenous applications of 2MeS-CKs should be continued to determine the physiological roles of these compounds. However, parsing out the translation-efficiency effects of bound 2MeS-CKs and physiological effects of unbound 2MeS-CKs may prove to be quite difficult. With this in mind, the development of CK mutants impaired in functioning of 2MeS-CK biosynthesis genes might create significant challenges and the possible, strong pleiotropic effects of the mutations targeting the genes involved in tRNA modifications have to be considered. tRNA-bound 2MeS-CKs play critical roles in diverse aspects of RNA metabolism and the effect of their disturbance might be difficult to separate from the potential physiological roles of unbound 2MeS-CKs obtained via tRNA degradation. New approaches that separate effects of tRNA-bound and unbound-2MeS-CKs will have to be developed to overcome that challenge, of fully understanding the often-prevalent and enigmatic 2MeS-CKs.

AUTHOR CONTRIBUTIONS

MG and AK wrote the first draft of the manuscript. EM and RE wrote sections of the manuscript. All authors contributed to manuscript revision, read and approved the submitted version.

FUNDING

RE was supported by Discovery Grant from the Natural Sciences and Engineering Research Council of Canada (RGPIN-05436).

REFERENCES

- Anantharaman, V., Koonin, E. V., and Aravind, L. (2001). TRAM, a predicted RNA-binding domain, common to tRNA uracil methylation and adenine thiolation enzymes. *FEMS Microbiol. Lett.* 197, 215–221. doi: 10.1111/j.1574-6968.2001.tb10606.x
- Anantharaman, V., Koonin, E. V., and Aravind, L. (2002). Comparative genomics and evolution of proteins involved in RNA metabolism. *Nucleic Acid Res.* 30, 1427–1464. doi: 10.1093/nar/30.7.1427
- Andreas, P., Kisiala, A., Emery, R. J. N., Clerck-Floate, D., Tooker, J., Price, M. III, et al. (2020). Cytokinins are abundant and widespread among insect species. *Plants* 9:208. doi: 10.3390/plants9020208
- Anjard, C., and Loomis, W. F. (2008). Cytokinins induce sporulation in *Dictyostelium*. *Development* 135, 819–827. doi: 10.1242/dev.018051
- Aoki, M. M., Emery, R. J. N., Anjard, C., Brunetti, C. R., and Huber, R. J. (2020). Cytokinins in *Dictyostelia* – A unique model for studying the functions of signaling agents from species to kingdoms. *Front. Cell Dev. Biol.* 8:511. doi: 10.3389/fcell.2020.00511
- Aoki, M. M., Kisiala, A. B., Li, S., Stock, N. L., Brunetti, C. R., Huber, R. J., et al. (2019a). Cytokinin detection during the *Dictyostelium discoideum* life cycle: profiles are dynamic and affect cell growth and spore germination. *Biomolecules* 9:702. doi: 10.3390/biom9110702
- Aoki, M. M., Seegobin, M., Kisiala, A., Noble, A., Brunetti, C., and Emery, R. J. N. (2019b). Phytohormone metabolism in human cells: cytokinins are taken up and interconverted in HeLa cell culture. *FASEB BioAdv.* 1, 320–331. doi: 10.1096/fba.2018-00032
- Atta, M., Mulliez, E., Arragain, S., Forouhar, F., Hunt, J. F., and Fontecave, M. (2010). S-Adenosylmethionine-dependent radical-based modification of biological macromolecules. *Curr. Opin. Struc. Biol.* 20, 684–692. doi: 10.1016/j.sbi.2010.09.009
- Björk, G. R. (1995). Genetic dissection of synthesis and function of modified nucleosides in bacterial transfer RNA. *Prog. Nucleic Acid Res. Mol. Biol.* 50, 263–338. doi: 10.1016/s0079-6603(08)60817-x
- Blum, P. H. (1988). Reduced leu operon expression in a miaA mutant of *Salmonella typhimurium*. *J. Bacteriol.* 170, 5125–5133. doi: 10.1128/jb.170.11.5125-5133.1988
- Buck, M., and Ames, B. N. (1984). A modified nucleotide in tRNA as a possible regulator of aerobiosis: synthesis of cis-2-methyl-thioribosylzeatin in the tRNA of *Salmonella*. *Cell* 36, 523–531. doi: 10.1016/0092-8674(84)90245-9
- Buck, M., and Griffiths, E. (1982). Iron mediated methylthiolation of tRNA as a regulator of operon expression in *Escherichia coli*. *Nucleic Acids Res.* 10, 2609–2624. doi: 10.1093/nar/10.8.2609
- Butler, C. (2019). *cis-Cytokinins from the tRNA-Degradation Pathway Impact the Phenotype and Metabolome of Arabidopsis thaliana: Evidence from AtIPT2 and AtIPT9 Null Mutants*. master's thesis, Trent University, Peterborough, ON.
- Chanclud, E., Kisiala, A., Emery, R. J., Chalvon, V., Ducasse, A., Romiti-Michel, C., et al. (2016). Cytokinin production by the rice blast fungus is a pivotal requirement for full virulence. *PLoS Pathog.* 12:e1005457. doi: 10.1371/journal.ppat.1005457
- Chen, Y., Bai, B., Yan, H., Wen, F., Qin, D., Jander, G., et al. (2019). Systemic disruption of the homeostasis of transfer RNA isopentenyltransferase causes growth and development abnormalities in *Bombyx mori*. *Insect Mol. Biol.* 28, 380–391. doi: 10.1111/imb.12561
- Cherayil, J. D., and Lipsett, M. N. (1977). Zeatin ribonucleosides in the transfer ribonucleic acid of *Rhizobium leguminosarum*, *Agrobacterium tumefaciens*, *Corynebacterium fascians*, and *Erwinia amylovora*. *J. Bacteriol.* 131, 741–744. doi: 10.1128/jb.131.3.741-744.1977
- Dabravolski, S. (2020). Multi-faceted nature of the tRNA isopentenyltransferase. *Funct. Plant Biol.* 47, 475–485. doi: 10.1071/FP19255

- Daudu, D., Allion, E., Liesecke, F., Papon, N., Courdavault, V., Dugé de Bernonville, T., et al. (2017). CHASE-containing histidine kinase receptors in apple tree: from a common receptor structure to divergent cytokinin binding properties and specific functions. *Front. Plant Sci.* 8:1614. doi: 10.3389/fpls.2017.01614
- Daudu, D., Kisiala, A., Ribeiro, C. W., Mélin, C., Perrot, L., Clastre, M., et al. (2019). Setting-up a fast and reliable cytokinin biosensor based on a plant histidine kinase receptor expressed in *Saccharomyces cerevisiae*. *J. Biotechnol.* 289, 103–111. doi: 10.1016/j.jbiotec.2018.11.013
- Dihanih, M. E., Najarian, D., Clark, R., Gillman, E. C., Martin, N. C., and Hopper, A. K. (1987). Isolation and characterization of MOD5, a gene required for isopentenylolation of cytoplasmic and mitochondrial tRNAs of *Saccharomyces cerevisiae*. *Mol. Cell. Biol.* 7, 177–184. doi: 10.1128/mcb.7.1.177
- Eichinger, L., Pachebat, J. A., Glöckner, G., Rajandream, M. A., Sugang, R., Berriman, M., et al. (2005). The genome of the social amoeba *Dictyostelium discoideum*. *Nature* 435, 43–57. doi: 10.1038/nature03481
- Emery, R. J. N., Lepoint, L., Barton, J. E., Turner, N. C., and Atkins, C. A. (1998). Cis-isomers of cytokinins predominate in chickpea seeds throughout their development. *Plant Physiol.* 117, 1515–1523. doi: 10.1104/pp.117.4.1515
- Esberg, B., Leung, H.-C. E., Tsui, H.-C. T., Björk, G. R., and Winkler, M. E. (1999). Identification of the miaB gene, involved in methylthiolation of isopentenylated A37 derivatives in the tRNA of *Salmonella typhimurium* and *Escherichia coli*. *J. Bacteriol.* 181, 7256–7265. doi: 10.1128/jb.181.23.7256-7265.1999
- Fradejas, N., Carlson, B. A., Rijntjes, E., Becker, N.-P., Tobe, R., and Schweizer, U. (2013). Mammalian Trt1 is a tRNA([Ser]Sec)-isopentenyl transferase required for full selenoprotein expression. *Biochem. J.* 450, 427–432. doi: 10.1042/BJ20121713
- Frébort, I., Kowalska, M., Hluska, T., Frébortová, J., and Galuszka, P. (2011). Evolution of cytokinin biosynthesis and degradation. *J. Exp. Bot.* 62, 2431–2452. doi: 10.1093/jxb/err004
- Gajdošová, S., Spíchal, R., Kaminek, M., Hoyerová, K., Novák, O., Dobrev, P. I., et al. (2011). Distribution, biological activities, metabolism, and the conceivable function of cis-zeatin-type cytokinins in plants. *J. Exp. Bot.* 62, 2827–2840. doi: 10.1093/jxb/erq457
- Giron, D., Frago, E., Glevarec, G., Pieterse, C. M. J., and Dicke, M. (2013). Cytokinins as key regulators in plant–microbe–insect interactions: connecting plant growth and defence. *Funct. Ecol.* 27, 599–609. doi: 10.1111/1365-2435.12042
- Giron, D., and Glevarec, G. (2014). Cytokinin-induced phenotypes in plant–insect interactions: learning from the bacterial world. *J. Chem. Ecol.* 40, 826–835. doi: 10.1007/s10886-014-0466-5
- Goggin, D. E., Emery, R. N., Kurepin, L. V., and Powles, S. B. (2015). A potential role for endogenous microflora in dormancy release, cytokinin metabolism and the response to fluridone in *Lolium rigidum* seeds. *Ann. Bot.* 115, 293–301. doi: 10.1093/aob/mcu231
- Golovko, A., Hjälm, G., Htjbon, F., and Nicander, B. (2000). Cloning of a human tRNA isopentenyl transferase. *Gene* 258, 85–93. doi: 10.1016/S0378-1119(00)00421-2
- Gray, J., Gelvin, S. B., Meilan, R., and Morris, R. O. (1996). Transfer RNA is the source of extracellular isopentenyladenine in a Ti-plasmidless strain of *Agrobacterium tumefaciens*. *Plant Physiol.* 110, 431–438. doi: 10.1104/pp.110.2.431
- Großskinsky, D. K., Tafner, R., Moreno, M. V., Stenglein, S. A., García de Salamone, I. E., Nelson, L. M., et al. (2016). Cytokinin production by *Pseudomonas fluorescens* G20-18 determines biocontrol activity against *Pseudomonas syringae* in Arabidopsis. *Sci. Rep.* 6, 23310. doi: 10.1038/srep23310
- Guern, J., and Peaud-Lenoel, C. (2012). *Metabolism and Molecular Activities of Cytokinins: Proceedings of the International Colloquium of the Centre National de la Recherche Scientifique held at Gif-sur-Yvette (France) 2–6 September 1980*. Cham: Springer Science and Business Media.
- Hinsch, J., Vrabka, J., Oeser, B., Novák, O., Galuszka, P., and Tudzynski, P. (2015). De novo biosynthesis of cytokinins in the biotrophic fungus *Claviceps purpurea*. *Environ. Microbiol.* 17, 2935–2951. doi: 10.1111/1462-2920.12838
- Holland, M. A. (1997). Occam's razor applied to hormonology (Are cytokinins produced by plants?). *Plant Physiol.* 115, 865–868. doi: 10.1104/pp.115.3.865
- Horvath, R., and Chinnery, P. F. (2015). Modifying mitochondrial tRNAs: delivering what the cell needs. *Cell Metab.* 21, 351–352. doi: 10.1016/j.cmet.2015.02.012
- Jameson, P. E. (2019). Virulent *Rhodococcus fascians* produce unique methylated cytokinins. *Plants* 8:582. doi: 10.3390/plants8120582
- Jenner, L. B., Demeshkina, N., Yusupova, G., and Yusupov, M. (2010). Structural aspects of messenger RNA reading frame maintenance by the ribosome. *Nat. Struct. Mol. Biol.* 17, 555–560. doi: 10.1038/nsmb.1790
- Jorge, G. L., Kisiala, A., Morrison, E., Aoki, M., Nogueira, A. P. O., and Emery, R. J. N. (2019). Endosymbiotic *Methylobacterium oryzae* mitigates the impact of limited water availability in lentil (*Lens culinaris* Medik.) by increasing plant cytokinin levels. *Environ. Exp. Bot.* 162, 525–540. doi: 10.1016/j.envexpbot.2019.03.028
- Joshi, M. V., and Loria, R. (2007). *Streptomyces turgidiscabies* possesses a functional cytokinin biosynthetic pathway and produces leafy galls. *MPMI* 20, 751–758. doi: 10.1094/MPMI-20-7-0751
- Kambhampati, S., Kurepin, L., Kisiala, A., Bruce, K., Cober, E., Morrison, M., et al. (2017). Yield associated traits correlate with cytokinin profiles in developing pods and seeds of field-grown soybean cultivars. *Field Crops Res.* 214, 175–184. doi: 10.1016/j.fcr.2017.09.009
- Kaminska, K. H., Baraniak, U., Boniecki, M., Nowaczyk, K., Czerwoniec, A., and Bujnicki, J. M. (2008). Structural bioinformatics analysis of enzymes involved in the biosynthesis pathway of the hypermodified nucleoside ms(2)io(6)A37 in tRNA. *Proteins* 70, 1–18. doi: 10.1002/prot.21640
- Kieber, J. J., and Schaller, G. E. (2018). Cytokinin signaling in plant development. *Development* 145:dev149344. doi: 10.1242/dev.149344
- Kisiala, A., Kambhampati, S., Stock, N. L., Aoki, M., and Emery, R. J. N. (2019). Quantification of cytokinins using high-resolution accurate-mass orbitrap mass spectrometry and parallel reaction monitoring (PRM). *Anal. Chem.* 91, 15049–15056. doi: 10.1021/acs.analchem.9b03728
- Koenig, R. L., Morris, R. O., and Polacco, J. C. (2002). tRNA is the source of low-level trans-Zeatin production in *Methylobacterium* spp. *J. Bacteriol.* 184, 1832–1842. doi: 10.1128/JB.184.7.1832-1842.2002
- Koshla, O., Kravets, V., Dacyuk, Y., Ostash, I., Süßmuth, R., and Ostash, B. (2020). Genetic analysis of *Streptomyces albus* J1074 mia mutants suggests complex relationships between post-transcriptional tRNA^X modifications and physiological traits. [published online ahead of print, 2020 Jul 17]. *Folia Microbiol.* [Epub ahead of print]. doi: 10.1007/s12223-020-00811-7
- Koshla, O., Yushchuk, O., Ostash, I., Dacyuk, Y., Myronovskiy, M., Jäger, G., et al. (2019). Gene miaA for post-transcriptional modification of tRNA^X is important for morphological and metabolic differentiation in *Streptomyces*. *Mol. Microbiol.* 112, 249–265. doi: 10.1111/mmi.14266
- Lamichane, T. N., Mattijssen, S., and Maraia, R. J. (2013). Human cells have a limited set of tRNA anticodon loop substrates of the tRNA isopentenyltransferase TRIT1 tumor suppressor. *Mol. Cell Biol.* 33, 4900–4908. doi: 10.1128/MCB.01041-13
- Laten, H., Gorman, J., and Bock, R. M. (1978). Isopentenyladenosine deficient tRNA from an antisuppressor mutant of *Saccharomyces cerevisiae*. *Nucleic Acids Res.* 5, 4329–4342. doi: 10.1093/nar/5.11.4329
- Liaquat, A., Stiller, C., Michel, M., Sednev, M. V., and Höbartner, C. (2020). N6-isopentenyladenosine in RNA determines the cleavage site of endonuclease deoxyribozymes. *Angew. Chem.* 132, 18786–18790. doi: 10.1002/ange.202006218
- Lindner, A.-C., Lang, D., Seifert, M., Podlešáková, K., Novák, O., Strnad, M., et al. (2014). Isopentenyltransferase-1 (IPT1) knockout in *Physcomitrella* together with phylogenetic analyses of IPTs provide insights into evolution of plant cytokinin biosynthesis. *J. Exp. Bot.* 65, 2533–2543. doi: 10.1093/jxb/eru142
- Mayaka, J. B., Huang, Q., Xiao, Y., Zhong, Q., Ni, J., and Shen, Y. (2019). The Lonely Guy (LOG) homologue SiRe_0427 from the thermophilic Archaeon *Sulfolobus islandicus* REY15A is a phosphoribohydrolase representing a novel group. *Appl. Environ. Microbiol.* 85:e01739-19. doi: 10.1128/AEM.01739-19
- McGaw, B. A., and Burch, L. R. (1995). “Cytokinin biosynthesis and metabolism,” in *Plant Hormones: Physiology, Biochemistry, and Molecular Biology*, 2nd Edn, ed. P. J. Davies (Dodrecht: Kluwer Academic Publishers), 98–117. doi: 10.1007/978-94-011-0473-9_5

- Miyawaki, K., Tarkowski, P., Matsumoto-Kitano, M., Kato, T., Sato, S., Tarkowska, D., et al. (2006). Roles of Arabidopsis ATP/ADP isopentenyltransferases and tRNA isopentenyltransferases in cytokinin biosynthesis. *PNAS* 103, 16598–16603. doi: 10.1073/pnas.0603522103
- Moffatt, K., Monroy Flores, C., Andreas, P., Kisiala, A., and Emery, R. J. N. (2018). Phytohormone profiling reveals fungal signatures and strong manipulation of infection cycle in the *Gymnosporangium juniper-virginianae* dual-host plant system. *Botany* 96, 57–65. doi: 10.1139/cjb-2017-0178
- Morris, R. O., Regier, D. A., Olson, R. M., Struxness, L. A., and Armstrong, D. J. (1981). Distribution of cytokinin-active nucleosides in isoaccepting transfer ribonucleic acids from *Agrobacterium tumefaciens*. *Biochemistry* 20, 6012–6017. doi: 10.1021/bi00524a014
- Morrison, E. N., Emery, R. J., and Saville, B. (2015a). Phytohormone involvement in the *Ustilago maydis* – *Zea mays* pathosystem: relationships between abscisic acid and cytokinin levels and strain virulence in infected cob tissue. *PLoS One* 10:e0130945. doi: 10.1371/journal.pone.0130945
- Morrison, E. N., Knowles, S., Hayward, A., Thorn, R. G., Saville, B. J., and Emery, R. J. N. (2015b). Detection of phytohormones in temperate forest fungi predicts consistent abscisic acid production and a common pathway for cytokinin biosynthesis. *Mycologia* 107, 245–257. doi: 10.3852/14-157
- Morrison, E. N., Emery, R. J. N., and Saville, B. J. (2017). Fungal derived cytokinins are necessary for normal *Ustilago maydis* infection of maize. *Plant Pathol.* 66, 726–742. doi: 10.1111/ppa.12629
- Nebert, D. W., and Russell, D. W. (2002). Clinical importance of the cytochromes P450. *Lancet* 360, 1155–1162. doi: 10.1016/S0140-6736(02)11203-7
- Nishii, K., Wright, F., Chen, Y.-Y., and Möller, M. (2018). Tangled history of a multigene family: the evolution of ISOPENTENYLTRANSFERASE genes. *PLoS One* 13:e0201198. doi: 10.1371/journal.pone.0201198
- Noble, A., Kisiala, A., Galer, A., Clysdale, D., and Emery, R. J. N. (2014). *Euglena gracilis* (Euglenophyceae) produces abscisic acid and cytokinins and responds to their exogenous application singly and in combination with other growth regulators. *Eur. J. Phycol.* 49, 244–254. doi: 10.1080/09670262.2014.911353
- Persson, B. C., and Björk, G. R. (1993). Isolation of the gene (*miaE*) encoding the hydroxylase involved in the synthesis of 2-methylthio-cis-ribozeatin in tRNA of *Salmonella typhimurium* and characterization of mutants. *J. Bacteriol.* 175, 7776–7785. doi: 10.1128/jb.175.24.7776-7785.1993
- Persson, B. C., Esberg, B., Olafsson, O., and Björk, G. R. (1994). Synthesis and function of isopentenyl adenosine derivatives in tRNA. *Biochimie* 76, 1152–1160. doi: 10.1016/0300-9084(94)90044-2
- Pertry, I., Václavíková, K., Depuydt, S., Galuszka, P., Spíchal, L., Temmerman, W., et al. (2009). Identification of *Rhodococcus fascians* cytokinins and their *modus operandi* to reshape the plant. *PNAS* 106, 929–934. doi: 10.1073/pnas.0811683106
- Pierrel, F., Björk, G. R., Fontecave, M., and Atta, M. (2002). Enzymatic modification of tRNAs: *MiaB* is an iron-sulfur protein. *J. Biol. Chem.* 277, 13367–13370. doi: 10.1074/jbc.C100609200
- Pierrel, F., Douki, T., Fontecave, M., and Atta, M. (2004). *MiaB* protein is a bifunctional radical-S-adenosylmethionine enzyme involved in thiolation and methylation of tRNA. *J. Biol. Chem.* 279, 47555–47563. doi: 10.1074/jbc.M408562200
- Pierrel, F., Hernandez, H. L., Johnson, M. K., Fontecave, M., and Atta, M. (2003). *MiaB* protein from *Thermotoga maritima*. Characterization of an extremely thermophilic tRNA-methylthiotransferase. *J. Biol. Chem.* 278, 29515–29524. doi: 10.1074/jbc.M301518200
- Podlešáková, K., Fardoux, J., Patrel, D., Bonaldi, K., Novák, O., Strnad, M., et al. (2013). Rhizobial synthesized cytokinins contribute to but are not essential for the symbiotic interaction between photosynthetic *Bradyrhizobia* and *Aeschynomene legumes*. *MPMI* 26, 1232–1238. doi: 10.1094/MPMI-03-13-0076-R
- Ramphal, K. (2016). *Hormonal algae: A Source of Functional Fatty Acids*. master's thesis, Trent University, Peterborough, ON.
- Reiter, V., Matschkal, D. M., Wagner, M., Globisch, D., Kneutinger, A. C., Müller, M., et al. (2012). The CDK5 repressor CDK5RAP1 is a methylthiotransferase acting on nuclear and mitochondrial RNA. *Nucleic Acids Res.* 40, 6235–6240. doi: 10.1093/nar/gks240
- Sakakibara, H. (2006). Cytokinins: activity, biosynthesis, and translocation. *Ann. Rev. Plant Biol.* 57, 431–449. doi: 10.1146/annurev.arplant.57.032905.105231
- Samanovic, M. I., Tu, S., Novák, O., Iyer, L. M., McAllister, F. E., Aravind, L., et al. (2015). Proteasomal control of cytokinin synthesis protects *Mycobacterium tuberculosis* against nitric oxide. *Mol. Cell.* 57, 984–994. doi: 10.1016/j.molcel.2015.01.024
- Schäfer, M., Brütting, C., Canales, I. M., Großkinsky, D. K., Vankova, R., Baldwin, I. T., et al. (2015). The role of cis-zeatin-type cytokinins in plant growth regulation and mediating responses to environmental interactions. *J. Exp. Bot.* 66, 4873–4884. doi: 10.1093/jxb/erv214
- Schmidt, U., Ahmed, J., Michalsky, E., Hoepfner, M., and Preissner, R. (2008). Comparative Vegf receptor tyrosine kinase modeling for the development of highly specific inhibitors of tumor angiogenesis. *Genome Inform.* 20, 243–251. doi: 10.11234/gi1990.20.243
- Seegobin, M., Kisiala, A., Noble, A., Kaplan, D., Brunetti, C., and Emery, R. J. N. (2018). *Canis familiaris* tissues are characterized by different profiles of cytokinins typical of the tRNA degradation pathway. *FASEB J.* [Epub ahead of print]. doi: 10.1096/fj.201800347
- Silva-Navas, J., Conesa, C. M., Saez, A., Navarro-Neila, S., Garcia-Mina, J. M., Zamarreño, A. M., et al. (2019). Role of cis-zeatin in root responses to phosphate starvation. *New Phytol.* 224, 242–257. doi: 10.1111/nph.16020
- Šimura, J., Antoniadis, I., Široká, J., Tarkowská, D., Strnad, M., Ljung, K., et al. (2018). Plant hormonomics: multiple phytohormone profiling by targeted metabolomics. *Plant Physiol.* 177, 476–489. doi: 10.1104/pp.18.00293
- Smaldino, P. J., Read, D. F., Pratt-Hyatt, M., Hopper, A. K., and Engelke, D. R. (2015). The cytoplasmic and nuclear populations of the eukaryote tRNA-isopentenyl transferase have distinct functions with implications in human cancer. *Gene* 556, 13–18. doi: 10.1016/j.gene.2014.09.049
- Spíchal, L. (2012). Cytokinins – recent news and views of evolutionarily old molecules. *Funct. Plant Biol.* 39, 267–284. doi: 10.1071/fp11276
- Spinola, M., Galvan, A., Pignatiello, C., Conti, B., Pastorino, U., Nicander, B., et al. (2005). Identification and functional characterization of the candidate tumor suppressor gene TRIT1 in human lung cancer. *Oncogene* 24, 5502–5509. doi: 10.1038/sj.onc.1208687
- Straka, J., Hayward, A., and Emery, R. J. (2010). Gall-inducing *Pachypsylla celtidis* (Psyllidae) infiltrate hackberry trees with high concentrations of phytohormones. *J. Plant Interact.* 5, 197–203. doi: 10.1080/17429145.2010.484552
- Streletskaia, R. A., Kachalkin, A. V., Glushakova, A. M., Yurkov, A. M., and Demin, V. V. (2019). Yeasts producing zeatin. *PeerJ* 7:e6474. doi: 10.7717/peerj.6474
- Suzuki, G., Shimazu, N., and Tanaka, M. (2012). A yeast prion, Mod5, promotes acquired drug resistance and cell survival under environmental stress. *Science* 336, 355–359. doi: 10.1126/science.1219491
- Takei, K., Yamaya, T., and Sakakibara, H. (2004). Arabidopsis CYP735A1 and CYP735A2 encode cytokinin hydroxylases that catalyze the biosynthesis of trans-Zeatin. *J. Biol. Chem.* 279, 41866–41872. doi: 10.1074/jbc.M406337200
- Tarkowski, P., Václavíková, K., Novák, O., Pertry, I., Hanuš, J., Whenham, R., et al. (2010). Analysis of 2-methylthio-derivatives of isoprenoid cytokinins by liquid chromatography-tandem mass spectrometry. *Anal. Chim. Acta* 680, 86–91. doi: 10.1016/j.aca.2010.09.020
- Trdák, L., Barešová, M., Šásek, V., Nováková, M., Zahajská, L., Dobrev, P. I., et al. (2017). Cytokinin metabolism of pathogenic fungus *Leptosphaeria maculans* involves isopentenyltransferase, adenosine kinase and cytokinin oxidase/dehydrogenase. *Front. Microbiol.* 8:1374. doi: 10.3389/fmicb.2017.01374
- Vedenicheva, N. P., Al-Maali, G. A., Bisko, N. A., Shcherbatiuk, M. M., Lomberg, M. L., Mytropolska, N. Y., et al. (2018). Comparative analysis of cytokinins in mycelial biomass of medicinal mushrooms. *Int. J. Med. Mushrooms* 20, 837–847. doi: 10.1615/IntJMedMushrooms.2018027797
- Waller, T. J., Read, D. F., Engelke, D. R., and Smaldino, P. J. (2017). The human tRNA-modifying protein, TRIT1, forms amyloid fibers *in vitro*. *Gene* 612, 19–24. doi: 10.1016/j.gene.2016.10.041
- Wang, H., Wei, L., Li, C., Zhou, J., and Li, Z. (2015). CDK5RAP1 deficiency induces cell cycle arrest and apoptosis in human breast cancer cell line by the

- ROS/JNK signaling pathway. *Oncol. Rep.* 33, 1089–1096. doi: 10.3892/or.2015.3736
- Wang, X., Lin, S., Liu, D., Gan, L., McAvoy, R., Ding, J., et al. (2020). Evolution and roles of cytokinin genes in angiosperms 1: do ancient IPTs play housekeeping while non-ancient IPTs play regulatory roles? *Hortic. Res.* 7:28. doi: 10.1038/s41438-019-0211-x
- Yamamoto, T., Fujimura, A., Wei, F. Y., Shinojima, N., Kuroda, J. I., Mukasa, A., et al. (2019). 2-Methylthio conversion of N6-Isopentenyladenosine in mitochondrial tRNAs by CDK5RAP1 promotes the maintenance of glioma-initiating cells. *iScience* 21, 42–56. doi: 10.1016/j.isci.2019.10.012

Conflict of Interest: The authors declare that the research was conducted in the absence of any commercial or financial relationships that could be construed as a potential conflict of interest.

Copyright © 2020 Gibb, Kisiala, Morrison and Emery. This is an open-access article distributed under the terms of the Creative Commons Attribution License (CC BY). The use, distribution or reproduction in other forums is permitted, provided the original author(s) and the copyright owner(s) are credited and that the original publication in this journal is cited, in accordance with accepted academic practice. No use, distribution or reproduction is permitted which does not comply with these terms.



TULP2, a New RNA-Binding Protein, Is Required for Mouse Spermatid Differentiation and Male Fertility

Meimei Zheng^{1,2†}, Xu Chen^{1†}, Yiqiang Cui^{1†}, Wen Li¹, Haiqian Dai¹, Qiuling Yue¹, Hao Zhang¹, Ying Zheng³, Xuejiang Guo^{1*} and Hui Zhu^{1*}

¹ State Key Laboratory of Reproductive Medicine, Department of Histology and Embryology, Nanjing Medical University, Nanjing, China, ² Reproductive Medicine Center of No. 960 Hospital of PLA, Jinan, China, ³ Department of Histology and Embryology, School of Medicine, Yangzhou University, Yangzhou, China

OPEN ACCESS

Edited by:

Dominic C. Voon,
Kanazawa University, Japan

Reviewed by:

Mahboobeh Amoushahi,
Aarhus University, Denmark
Kaio Cesar Chaboli Alevi,
São Paulo State University, Brazil

*Correspondence:

Hui Zhu
njzhuhui@njmu.edu.cn
Xuejiang Guo
guo_xuejiang@njmu.edu.cn

[†] These authors have contributed
equally to this work

Specialty section:

This article was submitted to
Cell Growth and Division,
a section of the journal
Frontiers in Cell and Developmental
Biology

Received: 30 October 2020

Accepted: 27 January 2021

Published: 18 February 2021

Citation:

Zheng M, Chen X, Cui Y, Li W,
Dai H, Yue Q, Zhang H, Zheng Y,
Guo X and Zhu H (2021) TULP2,
a New RNA-Binding Protein, Is
Required for Mouse Spermatid
Differentiation and Male Fertility.
Front. Cell Dev. Biol. 9:623738.
doi: 10.3389/fcell.2021.623738

Spermatogenesis requires a large number of proteins to be properly expressed at certain stages, during which post-transcriptional regulation plays an important role. RNA-binding proteins (RBPs) are key players in post-transcriptional regulation, but only a few RBPs have been recognized and preliminary explored their function in spermatogenesis at present. Here we identified a new RBP tubby-like protein 2 (TULP2) and found three potential deleterious missense mutations of *Tulp2* gene in dyszoospermia patients. Therefore, we explored the function and mechanism of TULP2 in male reproduction. TULP2 was specifically expressed in the testis and localized to spermatids. Studies on *Tulp2* knockout mice demonstrated that the loss of TULP2 led to male sterility; on the one hand, increases in elongated spermatid apoptosis and restricted spermatid release resulted in a decreased sperm count; on the other hand, the abnormal differentiation of spermatids induced defective sperm tail structures and reduced ATP contents, influencing sperm motility. Transcriptome sequencing of mouse testis revealed the potential target molecular network of TULP2, which played its role in spermatogenesis by regulating specific transcripts related to the cytoskeleton, apoptosis, RNA metabolism and biosynthesis, and energy metabolism. We also explored the potential regulator of TULP2 protein function by using immunoprecipitation and mass spectrometry analysis, indicating that TULP2 might be recognized by CCT8 and correctly folded by the CCT complex to play a role in spermiogenesis. Our results demonstrated the important role of TULP2 in spermatid differentiation and male fertility, which could provide an effective target for the clinical diagnosis and treatment of patients with oligo-astheno-teratozoospermia, and enrich the biological theory of the role of RBPs in male reproduction.

Keywords: spermatid differentiation, RNA binding protein, male infertility, oligo-astheno-teratozoospermia, TULP2

INTRODUCTION

Approximately half of infertility is associated with the male partner (Salas-Huetos et al., 2017; Cao et al., 2018; Vander Borgh and Wyns, 2018). Clinically, male infertility often manifests as azoospermia, oligozoospermia, teratozoospermia, and/or asthenozoospermia, resulting from underlying spermatogenesis disorders (Bracke et al., 2018). Therefore, research on the process

and mechanism of spermatogenesis has been a hot spot in the field of reproductive medicine to reveal the pathogenesis of spermatogenic disorders and improve the diagnosis and treatment of male infertility.

Spermatogenesis is a complex process of cell division and differentiation, in which a large number of proteins expressed in a certain time sequence and a specific way participate or play a regulatory role (Chalmel and Rolland, 2015; Ozturk and Uysal, 2018). However, gene transcription is not continuous during spermatogenesis, and the differentiation of male germ cells involves long periods of transcriptional inactivation (one during the homologous recombination of spermatocytes entering early meiosis and another in late elongating spermatids at the time of chromatin condensation in spermiogenesis). Many mRNAs need to be synthesized in advance and stored at the ribonucleoprotein (RNP) granules called chromatoid bodies (Kotaja and Sassone-Corsi, 2007), then translated according to a certain time sequence (Paronetto and Sette, 2010). Thus, post-transcriptional regulation is particularly important for gene expression during spermatogenesis. Studies have shown that variable gene splicing occurs frequently in testicles, and at least 700 mRNAs are regulated at the translation level (Iguchi et al., 2006; Meijer et al., 2007; Grosso et al., 2008).

RNA-binding proteins (RBPs) are defined by their ability to recognize and bind to specific sequences of RNA, then regulate the fate of RNA, including the regulation of RNA surveillance, capping, splicing, nucleocytoplasmic transport to subcellular locations, translation and RNA degradation (Vanderweyde et al., 2013). Therefore, RBPs play a key role in the post-transcriptional regulation of gene expression. The role of RBPs in male reproduction has a few been reported. For example, DAZL can promote spermatogonia differentiation (Schrans-Stassen et al., 2001). The deficiency of PTBP2 results in increased spermatocyte apoptosis and stagnant differentiation of round spermatids (Zagore et al., 2015). Losing of TENR affects the count, morphology and motility of sperm (Connolly et al., 2005). All these indicate that RBPs play an important role in various stages of spermatogenesis and are key regulatory factors that ensure male fertility.

However, compared with the recognition of the importance of RBPs, there have been relatively few reports of the functions and mechanisms of RBPs. Only a small number of RBPs have been identified, and moreover, the biological functions and RNA targets of most known RBPs are still unclear. Therefore, screening RBPs during spermatogenesis and studying their functions and the molecular mechanism of their gene expression regulation after transcription will help to elucidate the molecular mechanism of spermatogenesis and provide valuable information related to the etiology, diagnosis and treatment of male infertility.

For this purpose, a mouse spermatogenic cell-specific RBP profile was generated in our laboratory with reference to the Kwon et al. (2013) method, and obtained many novel candidate RBPs (unpublished data). Among these, tubby-like protein 2 (TULP2) firstly attracted our attention. Mouse *Tulp2* has homologous genes in human that encode proteins belonging to the TULP family (North et al., 1997). Sequence analysis showed that both human and mouse TULP2 contained two

conserved domains [Tub (Tubby) and DUF1168] but did not possess the canonical RBP domain (Albihlal and Gerber, 2018; Wang et al., 2018). However, with the discovery of new RBPs in recent years, it has been realized that the domains of RBPs may differ considerably from the original defined range, and a considerable number of RBPs without canonical RNA-binding domains (RBDs) are found *in vivo* (Ray et al., 2017). Mining and functional studies of these unconventional RBPs have become a focus of life science research (Beckmann et al., 2015). Similarly, this kind of RBPs may be more worthy of exploration in spermatogenesis.

Interestingly, there were the study examining the mRNA level of *Tulp2* in adult human multiple tissues and found it was only expressed in the testes, suggesting TULP2 might play an important role in male reproduction (North et al., 1997). Furthermore, by the analysis of *Tulp2* gene sequence on blood samples that we collected from 300 unrelated infertile men with dyszoospermia, we identified 13 cases of heterozygote (c.832C > T [p.Arg278Trp]) mutations, 2 cases of heterozygote (c.871A > G [p.Thr291Ala]) mutations, and 2 cases of heterozygote (c.829C > A [p.Leu277Met]) mutations. For these mutation sites, we searched Polyphen2 and SIFT databases and they were predicted to be potentially deleterious (Supplementary Figure 1). This result again indicated the potential relationship between *Tulp2* and male reproduction.

Therefore, we hypothesize that TULP2 is a new type of RBP in spermatogenic cells and play a role in male fertility. Further elucidation of its function may provide novel perspectives for the study of spermatogenesis mechanisms. In this study, a *Tulp2* knockout mouse model was constructed for the first time to explore the role and mechanism of TULP2. Based on the expression and localization characteristics, we focused on revealing the role of TULP2 in spermatid differentiation and its effect on sperm function, and initially elucidated the regulatory molecular network of TULP2. The results provide an effective target for the pathogenesis studies and the diagnosis and treatment of male infertility.

MATERIALS AND METHODS

Animals

This study was approved by the ethics committees of Nanjing Medical University. *Tulp2* knockout mice were generated on the C57BL6 background via Cas9/RNA-mediated gene targeting as described previously (Shen et al., 2013) and bred at the animal center of Nanjing Medical University (Nanjing, China). The mice were kept under environmentally controlled conditions with unlimited access to food and water (Zhu et al., 2019). *Tulp2*^{-/-} mice were designed as the experimental group and littermate wild type (WT) mice as the control group.

RNA Isolation, cDNA Synthesized, PCR and qPCR Analyses

Total RNA was extracted from tissues and using the TRIzol reagent (Invitrogen, 15596-026) according to the manufacturer's instructions. cDNA was synthesized with PrimeScript RT reagent

Kit (TaKaRa, RR037A). cDNA from multiple tissues of three adult WT mice and testes of 1–7 week-old WT mice (three mice of each age) were amplified by polymerase chain reaction (PCR) using random primers and Premix Taq (Takara, RR901). The PCR products were analyzed by 1.5% w/v agarose gel electrophoresis using mouse β -actin as the control gene. Quantitative real-time PCR of cDNA from testes of adult *Tulp2*^{-/-} mice and WT mice (three mice of each group) was performed using AceQ qPCR SYBR Green Master Mix (Vazyme, Q141-02) according to the manufacturer's instructions with an ABI Q5 real-time PCR System (Applied Biosystems, Thermo Fisher Scientific). The primer sequences used for these experiments are listed in **Supplementary Table 1**.

Western Blot Analysis

Protein samples were prepared from testes of *Tulp2*^{-/-} mice and WT mice (three mice of each group) or from 293T cells (three times cultured independently) using RIPA lysis buffer (Beyotime, P0013C) containing a protease inhibitor cocktail (Bimake, B14001). The samples were subjected to electrophoresis and transferred to nitrocellulose membranes (Bio-Rad, 1620177). The membranes were blocked and then incubated overnight with the following antibodies: anti-TULP2 (Abclonal produced the TULP2 antibody by the injection of rabbits with a peptide corresponding to amino acids 78–305 of the mouse protein; 1:5000), anti-CCT8 (Abclonal, A4449; 1:1000), anti-Flag (Proteintech, 20543-1-AP; 1:1000), and anti-ACTIN (Millipore, MAB1501; 1:8000). The membranes were then washed and incubated for 1 h with a horseradish peroxidase-conjugated anti-rabbit IgG secondary antibody (Thermo, 31460; 1:3000) or an anti-mouse IgG secondary antibody (Proteintech, SA00001-1; 1:1000). The proteins bands were detected using an ECL kit (Thermo, 32109) and Bio-Rad gel imaging system.

Histological Analysis and Immunofluorescence

Histological analysis was performed by using standard procedures. Testes and epididymides from three *Tulp2*^{-/-} mice and three WT mice were fixed using modified Davidson's fluid (Latendresse et al., 2002), and embedded in paraffin. The whole tissue was sectioned consecutively (5 μ m thick) and collected on the slide. For the testis tissue, one section at an interval of 50 sections was taken for staining (total approximately 30 sections of each testis). Periodic acid-Schiff (PAS) staining was performed for testis sections according to the manufacturer's protocol (Thermo, 87007) to determine the stage of spermatogenesis. Each stage showing a distinct ordering of cell associations along the length of the seminiferous tubules was designated with Roman numerals, and approximately 200 tubules from each section were analyzed under microscopy (Ahmed and de Rooij, 2009). According to our previously published protocols, epididymis sections (approximately four sections selected at intervals from each epididymis tissue) were stained with hematoxylin-eosin (HE) (Beyotime, C0105S) to observe sperm density (Zhu et al., 2019). Sperm

from testis suspensions, the caput epididymis, the corpus epididymis, and the cauda epididymis of three *Tulp2*^{-/-} mice and three WT mice were transferred to slides (two sperm slides prepared from each tissue of each mouse) and naturally dried. After immobilization with 4% PFA, sperm morphology was observed by HE staining. The sections were viewed with an optical microscope (Zeiss, Germany). For ultrastructural examination, 2.5% glutaraldehyde-fixed sperm from cauda epididymis of three *Tulp2*^{-/-} mice and three WT mice were post-fixed with 2% (wt/vol) OsO₄ and embedded in Araldite. Ultrathin sections were stained with uranyl acetate and lead citrate and analyzed using electron microscopy (JEOL, Japan).

For immunofluorescence analysis, the testicular section from each mouse was blocked in 1% bovine serum albumin and then incubated overnight at 4°C with primary antibodies against TULP2 and rabbit control IgG (Abclonal, AC005) at a dilution of 1:100. The sections were then incubated with a 488-conjugated secondary antibody (Proteintech, SA00013-2) at a 1:500 dilution for 1 h at room temperature. The slides were viewed with a LSM700 confocal microscope (Zeiss, Germany).

Fertility Tests

Five adult *Tulp2*^{-/-} mice and WT mice (aged 2–3 months) were used for fertility study. Each male was mated with two females, and vaginal plugs were checked every morning. The number of offspring produced per female was recorded for 5 months.

Computer-Assisted Sperm Analysis

Mature sperm from *Tulp2*^{-/-} and WT mice were obtained by making small incisions throughout the cauda epididymis, followed by extrusion and suspension in 200 μ l of human tubal fluid (HTF) culture medium (EasyCheck, M1130). The sperm samples (10 μ l) were subjected to Computer Assisted Sperm Analyzer (CASA) detection with the IVOS II™ system (Hamilton Thorne, United States). Motility parameters for three couple mice (the experimental and control groups) were measured and analyzed.

Terminal Deoxynucleotidyl Transferase dUTP Nick End Labeling Assays

DNA fragmentation was determined as an index of apoptosis in paraffin-embedded mouse testis sections from three *Tulp2*^{-/-} mice and three WT mice via the terminal deoxynucleotidyl transferase dUTP nick end labeling (TUNEL) assay (Vazyme, A113-01) according to the manufacturer's specifications. Briefly, the testis sections were washed in PBS and equilibrated with TdT buffer for 20 min at room temperature. TdT buffer was removed and terminal transferase reaction mix was added. The reaction was performed for 1 h at 37°C. Sections were washed with PBS and counterstained with Hoechst. All spermatogenesis tubules (approximately 200 tubules) from each section from each mouse were analyzed using a LSM700 confocal microscope (Zeiss, Germany). The nuclei of TUNEL-positive cells show red fluorescence. According to the stage of spermatogenesis and the

nuclear morphology of spermatogenic cells, apoptotic cells were classified and counted by two researchers using double-blind.

Measurement of Sperm ATP *in vitro*

Sperm samples from three *Tulp2*^{-/-} mice and three WT mice were washed twice and resuspended in lysis buffer, then vortexed and placed on ice. An average of 5×10^7 sperm were used for ATP analysis. ATP was measured by luminometric methods using commercially available luciferin/luciferase reagents as per the manufacturer's instructions (Beyotime, S0027) in a luminometer (TD-20/20, Turner Designs).

Immunoprecipitation and Mass Spectrometry

HEK293T cells were transfected with the Flag-TULP2 overexpression plasmid using Lipofectamine 3000 (Thermo Fisher Scientific), and empty vector plasmid was used as control. 48 h after transfection, cells were collected for immunoprecipitation via a protocol that was described previously (Zhu et al., 2019). Cell transfection and immunoprecipitation experiments were performed three times. Then the immunoprecipitates were analyzed by mass spectrometry as described previously (Zhu et al., 2019). In brief, elution was first performed in protein extraction buffer by ultrafiltration using a 10-kDa filter membrane. Cysteine residues were reduced with dithiothreitol (DTT) at a final concentration of 5 mmol/L at 56°C for 25 min and then alkylated in iodoacetamide at 14 mmol/L for 30 min at room temperature. Unreacted iodoacetamide was quenched with DTT for 15 min. The lysates were then diluted to 1.6 mol/L urea with 25 mmol/L Tris at pH 8.2. CaCl₂ was added to a final concentration of 1 mmol/L, followed by overnight digestion with trypsin at a concentration of 5 ng/μL at 37°C. Finally, 0.4% trifluoroacetic acid was added to stop digestion. We used an OASIS HLB extraction box (Waters, Milford, MA, United States) to desalinate the peptides, followed by mass spectrometry analysis. All raw files were searched using MaxQuant software (version 1.3.0.5, Martinsried, Germany) against the UniProt human proteome database.

Co-immunoprecipitation

Co-immunoprecipitation was performed as described previously (Zhu et al., 2010). Testes from three WT mice were lysed using RIPA buffer supplemented with a 1% (v/v) protease inhibitor cocktail instead of lysis buffer. The lysate was incubated on ice for 40 min, followed by centrifugation at $12000 \times g$ for 20 min at 4°C. The supernatant was pre-cleared with 50 μL of Protein A/G magnetic beads (Bimake, B23202) and then incubated with the target antibody at 4°C overnight. A normal IgG antibody was used as a control. The next day, the co-immunoprecipitated proteins were eluted with Pierce IgG Elution Buffer (Thermo, 21004), followed by western blotting.

Transcriptome Sequencing Analysis

Total testis RNA was extracted respectively from three wild-type and three *Tulp2*^{-/-} mice using TRIzol reagent (Invitrogen),

followed by clean up with an RNeasy mini kit (QIAGEN, 74104), and RNA quality was examined. A total amount of 1 μg of qualified RNA per sample was used as the input material for library preparation. The libraries were generated using the VAHTS mRNA-seq v2 Library Prep Kit for Illumina (Vazyme, NR601) following the manufacturer's recommendations. The library concentration was measured using a Qubit RNA Assay Kit on a Qubit 3.0 fluorometer for preliminary quantification. After it was verified that the insert size was consistent with expectations, the qualified insert size was accurately quantified using qPCR with a Step One Plus Real-Time PCR system (ABI, United States). The clustering of the index-coded samples was performed on a cBot Cluster Generation System (Illumina, United States) according to the manufacturer's instructions. After cluster generation, the library preparations were sequenced on the Illumina HiSeq × Ten platform and 150 bp paired-end module. The uniquely mapped reads of genes were counted using DESeq2, and the presence of transcripts abundances were expressed as fragments per kilobase of exon per million fragments mapped (FPKM). Based on the FPKM values of WT mice, the transcripts were normalized to evaluate the differences in gene expression of *Tulp2*^{-/-} mice. Significant differentially expressed genes were screened according to a fold change > 1.5, and the DAVID database was used to analyze Gene Ontology (GO) annotations.

Statistical Analysis

All experiments were repeated at least three times. The differences between the treatment and control groups were analyzed using a *t*-test. Values of *P* < 0.05 were considered to be statistically significant. All data represent the mean ± the standard deviation of the mean (SD).

RESULTS

TULP2 Is Specifically Expressed in the Testis and Localized to Spermatids

Reverse transcription polymerase chain reaction (RT-PCR) was used to evaluate the distribution of *Tulp2* mRNA in various tissues of mice, including the heart, liver, spleen, lung, kidney, brain, ovary, testis, and epididymis. As shown in **Figure 1A**, *Tulp2* was only expressed in the testis. Testis maturation is age dependent, and the first wave of spermatogenesis takes place within 35 days postnatal in mice (Griswold, 2016). Analysis using testis mRNA obtained from mice of different ages in the weeks after birth showed that *Tulp2* was first detected in the testes of 3-week-old mice, when round spermatids had appeared, after which its expression remained constant (**Figure 1B**). We further detected the expression characteristics of TULP2 in the testis by immunofluorescence (IF) analysis. The results demonstrated TULP2 expression in germ cells within the seminiferous tubules (**Figure 1C**); its expression was initiated in round spermatids and remained until step 12 elongated spermatids (**Figure 1D**). The above results suggested a potential important role of TULP2 in male reproductive function, very likely influencing spermiogenesis in the testis.

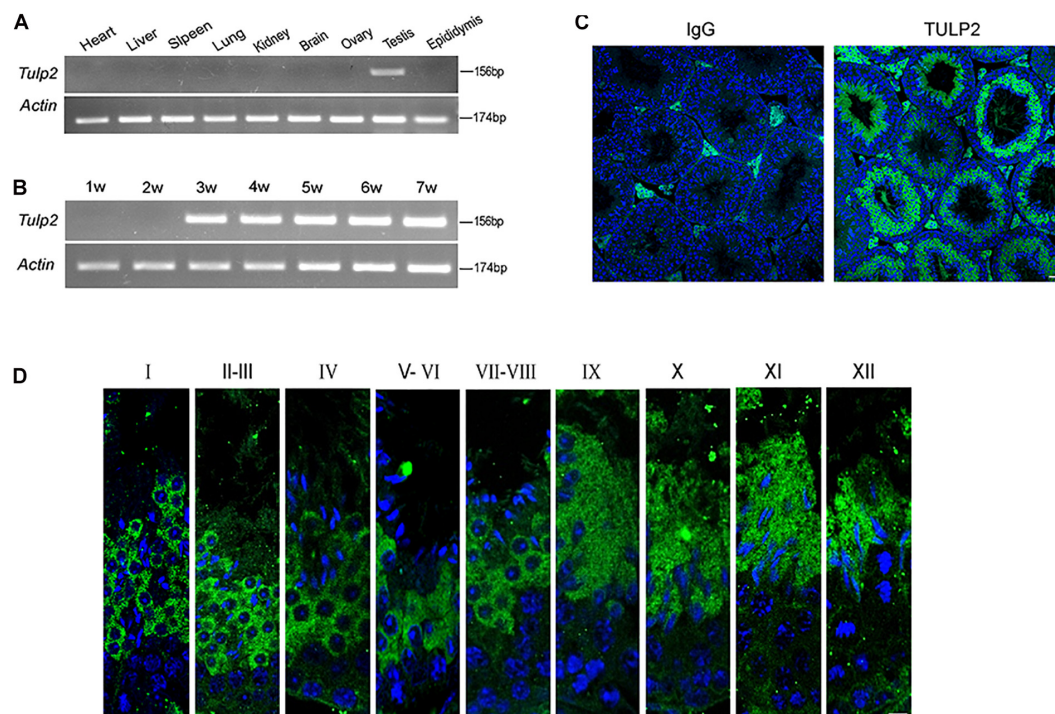


FIGURE 1 | Distribution of TULP2 in mouse tissues. **(A)** The presence of *Tulp2* mRNA was evaluated in various tissues from adult mice using RT-PCR. *Tulp2* mRNA was only detected in the testis. *Actin* was amplified as an internal control. **(B)** The testicular *Tulp2* mRNA expression profile was tested at the indicated time points after birth using RT-PCR. *Actin* was amplified as an internal control. *Tulp2* expression was first observed in 3-week-old mice and continued until adulthood. **(C)** Immunofluorescence localization of the TULP2 protein in adult mouse testes. TULP2 expression in germ cells within the seminiferous tubules. **(D)** Each image shows a stage of the seminiferous epithelial cycle, denoted by Roman numerals at the top of each image. Anti-TULP2 antibody (green) and Hoechst staining (blue). TULP2 was expressed in the cytoplasm of step 1–12 spermatids in spermiogenesis. Scale bars: 20 μ m.

Targeted Disruption of TULP2 Results in Male Infertility

To investigate whether TULP2 is required for male fertility, *Tulp2* knockout mice were produced using the CRISPR/Cas9 system. The injection of a single guide RNA targeting *Tulp2* exon 2 produced knockout mice harboring a 49-bp deletion (Figure 2A). A representative image of Sanger sequence results for the verification of the *Tulp2*^{-/-} mouse is shown in Figure 2A. We confirmed the lack of TULP2 in the testes of *Tulp2*^{-/-} mice by western blot and immunofluorescence assays (Figures 2B,C).

Mating tests were performed, and continuous monitoring was conducted for 5 months to analyze the fertility of the mice. As a result, we found that the female *Tulp2*^{-/-} mice were fertile and exhibited litter sizes comparable to those of WT females. In contrast, *Tulp2*^{-/-} males were infertile and produced no litters (Figure 2D). These results suggest that TULP2 is required for male reproduction.

Decreases in the Sperm Count and Motility Are the Potential Cause of Infertility in *Tulp2*^{-/-} Male Mice

To determine the cause of infertility in male *Tulp2*^{-/-} mice, we examined the physiological parameters of sperm

collected from cauda epididymis of the mice. CASA showed that the sperm count, motility and progressive motility were significantly decreased in *Tulp2*^{-/-} mice compared with WT mice (Figure 3A, ***P* < 0.01, ****P* < 0.001). The decreased sperm number was verified by the assessment of the histological structure of the epididymis. As shown in Figure 3B, sperm quantities in the lumen of the epididymis duct were obviously reduced in *Tulp2*^{-/-} mice compared with WT mice.

Increased Apoptosis and Limited Release of Elongated Spermatids Reduce the Epididymis Sperm Count in *Tulp2*^{-/-} Mice

Sperm are produced in the seminiferous tubules of the testis. To determine the cause of the observed decrease in sperm output, we first observed the histological structure of the testis by morphological staining. Intact spermatogenic tubules and spermatogenic cells at all stages could be seen in the testes of WT and *Tulp2*^{-/-} mice. However, retained elongated spermatids were frequently observed in the middle and base of stage VII–X seminiferous tubules of *Tulp2*^{-/-} mice, which should have been released into the lumen at stage VIII (Figure 3C, black arrow). This may be responsible for the decreased number of epididymal sperm in *Tulp2*^{-/-} mice.

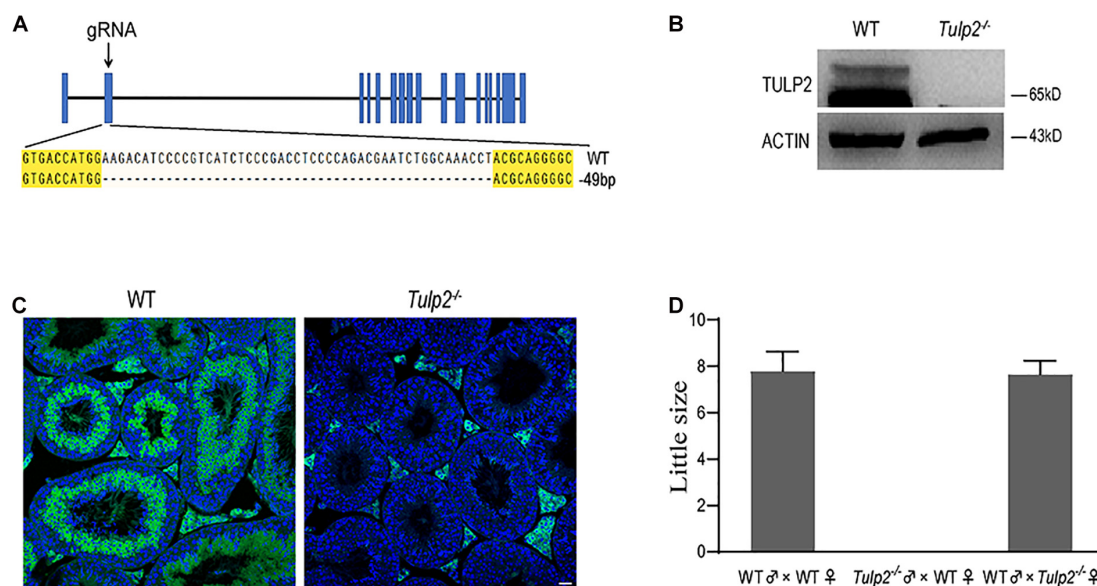


FIGURE 2 | Generation of *Tulp2* knockout mice and assessment of male fertility. **(A)** Image of Sanger sequencing results showing a 49-bp deletion in the targeted region. **(B)** Western blot analysis of testicular TULP2 expression. ACTIN was used as an internal control. TULP2 was detected in WT mice, whereas it was absent in *Tulp2*^{-/-} mice. **(C)** TULP2 levels in the testes of *Tulp2*^{-/-} and WT mice were evaluated via immunofluorescence analysis. No TULP2 signal was detected in *Tulp2*^{-/-} mice. Scale bars: 20 μ m. **(D)** Average litter size of pups produced by *Tulp2*^{-/-} mice mated with WT mice. *Tulp2*^{-/-} male mice are infertile ($n = 5$).

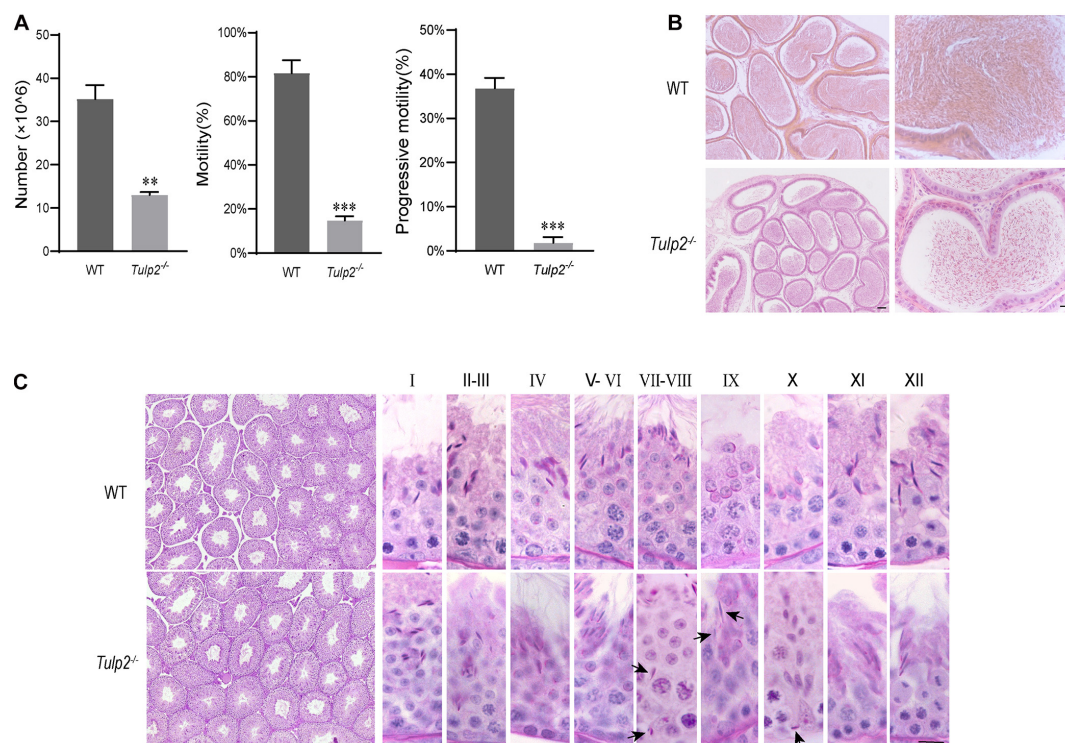


FIGURE 3 | Analysis of basic factors related to male fertility. **(A)** Computer-assisted sperm analysis. The sperm number was reduced, and motility and progressive motility were decreased in *Tulp2*^{-/-} mice ($n = 3$, ** $P < 0.01$, *** $P < 0.001$). **(B)** HE-stained sections show the histological structure of the epididymis from WT and *Tulp2*^{-/-} mice. The number of sperm in the *Tulp2*^{-/-} mouse epididymis was decreased compared with that in WT mice. **(C)** Periodic acid-Schiff-stained sections show the histological structure of the testes from WT and *Tulp2*^{-/-} mice. Each image shows a stage of the seminiferous epithelial cycle, which is denoted by Roman numerals at the top of the image. The spermatogenic lumen is complete, and the spermatogenic cells are arranged neatly. There are residual elongated spermatids in the lumen of stage VII–X (black arrow). Scale bars: 50 μ m.

To reveal the reason for limited elongated spermatid release, we evaluated the state of spermatogenic cells in *Tulp2*^{-/-} and WT mice. TUNEL analysis was performed in the testes of these two groups, and the results showed that the average number of apoptotic cells per tubule was significantly increased in *Tulp2*^{-/-} mice (Figure 4B, **P* < 0.05). According to the classified statistics, the apoptosis of elongated spermatids in *Tulp2*^{-/-} mice was significantly increased compared with that in WT mice (Figure 4C, **P* < 0.05), and these apoptotic cells were mainly elongated spermatids deposited in the base of the lumen (Figure 4A).

Abnormal Differentiation of Spermatids Results in a Defective Sperm Tail, Which Decreases Sperm Motility in *Tulp2*^{-/-} Mice

We observed the morphology and structure of spermatozoa from the cauda epididymis. Under light microscopy, the spermatozoa

from WT mice showed a normal morphology, including well-shaped heads and long, smooth tails. However, obvious tail abnormalities were found in the sperm of *Tulp2*^{-/-} mice, mainly exhibiting tail folding and curling (Figure 5A). According to the statistics, the deformity rate of the sperm tail in *Tulp2*^{-/-} mice was significantly higher than that in WT mice (Figure 5B, ****P* < 0.001). By observing the spermatozoa in testicular suspensions, the caput epididymis and the corpus epididymis from *Tulp2*^{-/-} mice, we found that they showed deformities consistent with the sperm in the cauda epididymis (Figure 5C). The above results indicated that sperm deformity originated from the abnormal differentiation of spermatids and that the loss of TULP2 affected spermiogenesis in the testes.

The ultrastructure of sperm from the two groups was further observed under a transmission electron microscope. As expected, sperm from the WT mice showed normally developed flagella. However, an obviously increase in structural abnormalities of the sperm tail was found in *Tulp2*^{-/-} mice. In these mice, two or more cross-sections of the same sperm flagellum were frequently found enclosed in one cell membrane; in the flagellum,

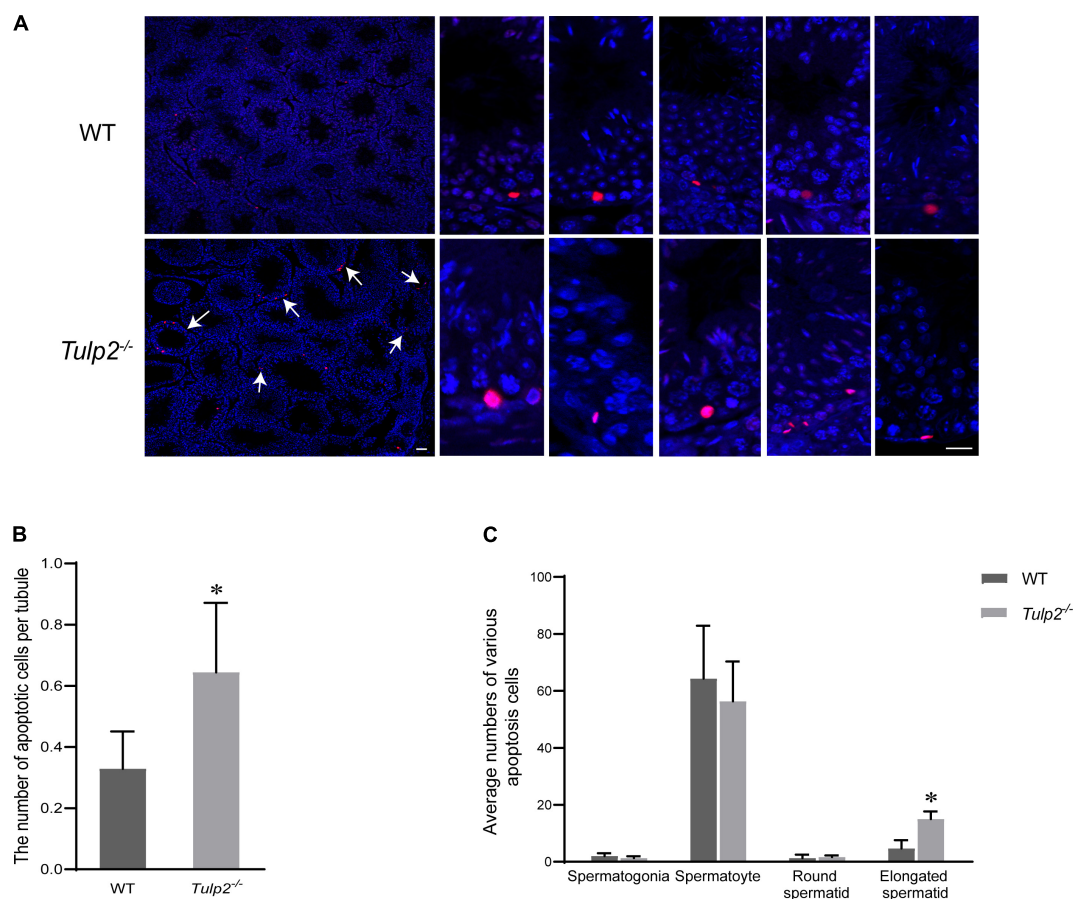


FIGURE 4 | Analysis of the causes of spermatozoa loss. **(A)** Statistics of testicular apoptosis. Terminal deoxynucleotidyl transferase nick-end-labeling (TUNEL) staining in testes. The apoptotic cells in *Tulp2*^{-/-} mice were significantly increased (as shown by white arrow). The TUNEL-positive cells show red fluorescence localization in the nucleus. Scale bars: 50 μ m. **(B)** Analysis of the number of apoptotic cells per tubule. The number of cells was increased in *Tulp2*^{-/-} mice (*n* = 3, **P* < 0.05). **(C)** Average numbers of various apoptotic cells were classified and counted. The number of elongated spermatids showing apoptosis increased significantly (*n* = 3, **P* < 0.05).

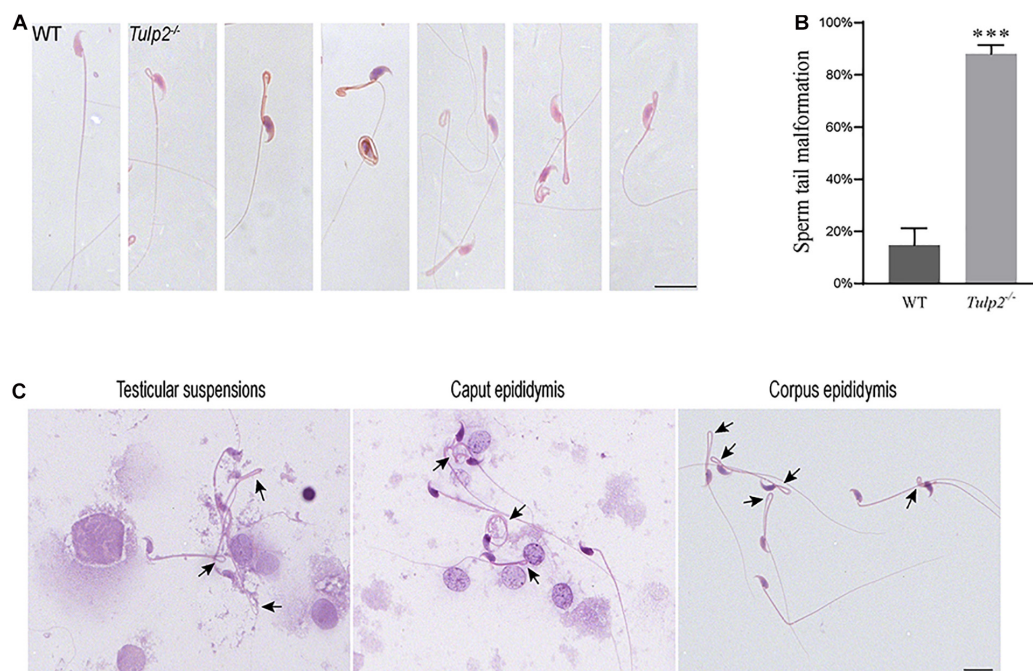


FIGURE 5 | Analysis of sperm malformation. **(A)** The morphology of spermatozoa in WT and *Tulp2*^{-/-} mice. The sperm of *Tulp2*^{-/-} mice showed tail folding and curling. **(B)** Statistics tail malformation rates. Tail malformation was significantly increased in *Tulp2*^{-/-} mice ($n = 3$, *** $P < 0.001$). **(C)** Spermatozoon morphology was observed in testis suspensions, the caput epididymis and the corpus epididymis. The black arrow showed sperm tail malformation. Scale bars: 20 μm.

mitochondria, microtubules and peripheral dense fibers were all structurally abnormal, which mainly manifested as a lack of inner mitochondrial membrane (IMM) cristae (as shown by “↑”), partial absence of “9 + 2” microtubules (as shown “Δ”), and incomplete peripheral dense fibers (as shown “☆”) (Figure 6A).

Mitochondria, peripheral dense fibers and microtubules are the structural basis of sperm motility, and abnormalities of these structures inevitably affect sperm motility. Among these structures, the mitochondrial sheath is the center of the sperm energy supply. We detected the ATP content of the sperm and found that it was significantly lower in *Tulp2*^{-/-} mice than in wild-type mice (Figure 6B, *** $P < 0.001$). All of the above results suggest that TULP2 deletion may affect the process of spermiogenesis and result in damage to mitochondria, microtubules, and peripheral dense fibers, which are responsible for decreased sperm motility.

The Absence of TULP2 Affects the Expression of a Number of Genes in Mouse Testes

As an RBP, TULP2 should play its role in spermatogenesis by regulating specific target RNAs. To further analyze and clarify the mechanism by which TULP2 affects spermatogenesis, the differential expression profiles of testicular transcripts in *Tulp2*^{-/-} and WT mice were established by transcriptome sequencing. As a result, 1446 genes with an expression difference of 1.5 fold or more were identified between the two groups (Supplementary Table 2), among which 638 presented GO

annotations. The GO annotations were classified into three major categories: cellular components, biological processes and molecular functions (Figure 7A). In the category of cellular components, most of the differentially expressed genes were most strongly associated with the cytoplasm, followed by the plasma membrane, cytoskeleton or mitochondrion, and a few were related to components such as cilia or projections. The classification according to biological processes indicated that the differentially expressed genes were mostly related to the regulation of RNA metabolism and biosynthesis, followed by cell events (apoptosis and differentiation), while others were involved in energy metabolism, spermatogenesis, etc. When we analyzed molecular functions, we found that these genes mainly showed binding activity, including the binding of proteins, cytoskeletal, enzymes, RNA, ATP, ions, etc.

According to the results of GO annotation, we selected genes related to key events to test their expression levels to verify the sequencing results. The apoptosis-related genes included *Pycard* (PYD and CARD domain containing) and *Ltbr* (lymphotoxin B receptor). The energy metabolism-related genes included *Ccl1* [chemokine (C-C motif) ligand 1], *Camk2d* (calcium/calmodulin-dependent protein kinase type II, delta), and *Acvr1c* (activin A receptor, type 1C). The spermatogenesis-related genes included *Inpp5b* (inositol polyphosphate-5-phosphatase B) and *Ggt1* (gamma-glutamyl transferase 1). The RNA metabolism-related gene *Klf8* (kruppel-like factor 8) was also included. The real-time PCR results were consistent with the sequencing data (Figure 7B, * $P < 0.05$, ** $P < 0.01$).

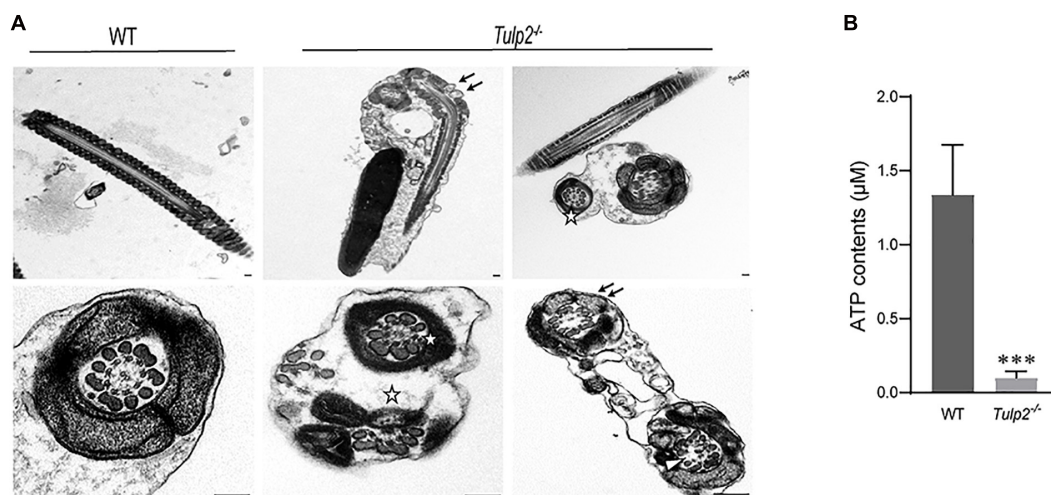


FIGURE 6 | Assessment of sperm ultrastructure and ATP levels. **(A)** Transmission electron microscopy (TEM) images of sperm ultrastructures are shown, revealing a lack of inner mitochondrial membrane (IMM) cristae (as shown by “↑”), partial absence of “9 + 2” microtubules (as shown by “Δ”), and incomplete peripheral dense fibers (as shown by “☆”) ($n = 3$). Scale bars: 1 μm . **(B)** Tested ATP contents of sperm between WT and *Tulp2*^{-/-} mice. The ATP level was significantly lower in *Tulp2*^{-/-} mice ($n = 3$, *** $P < 0.001$).

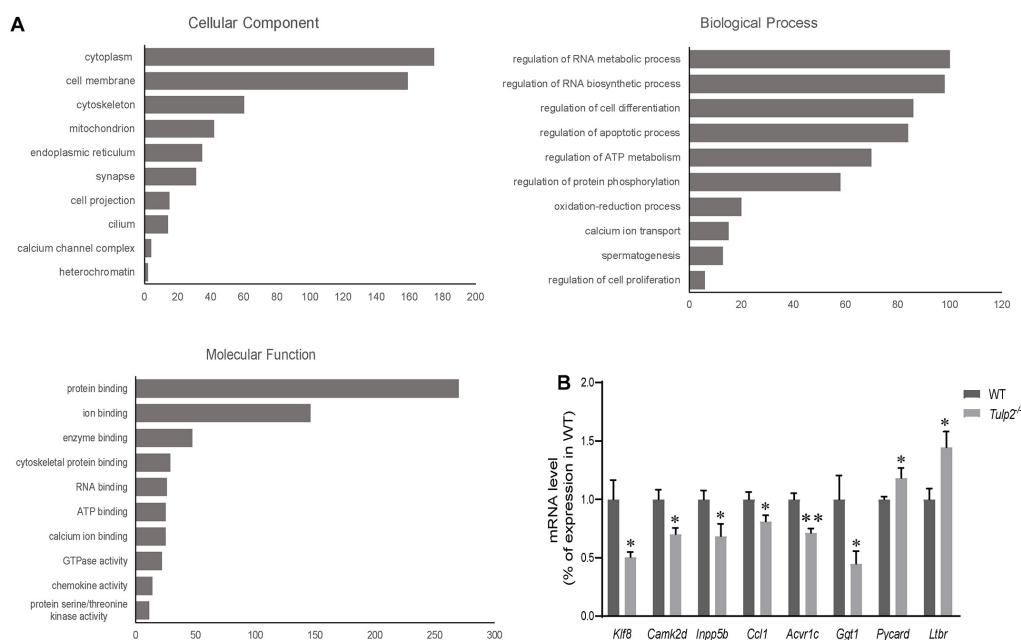
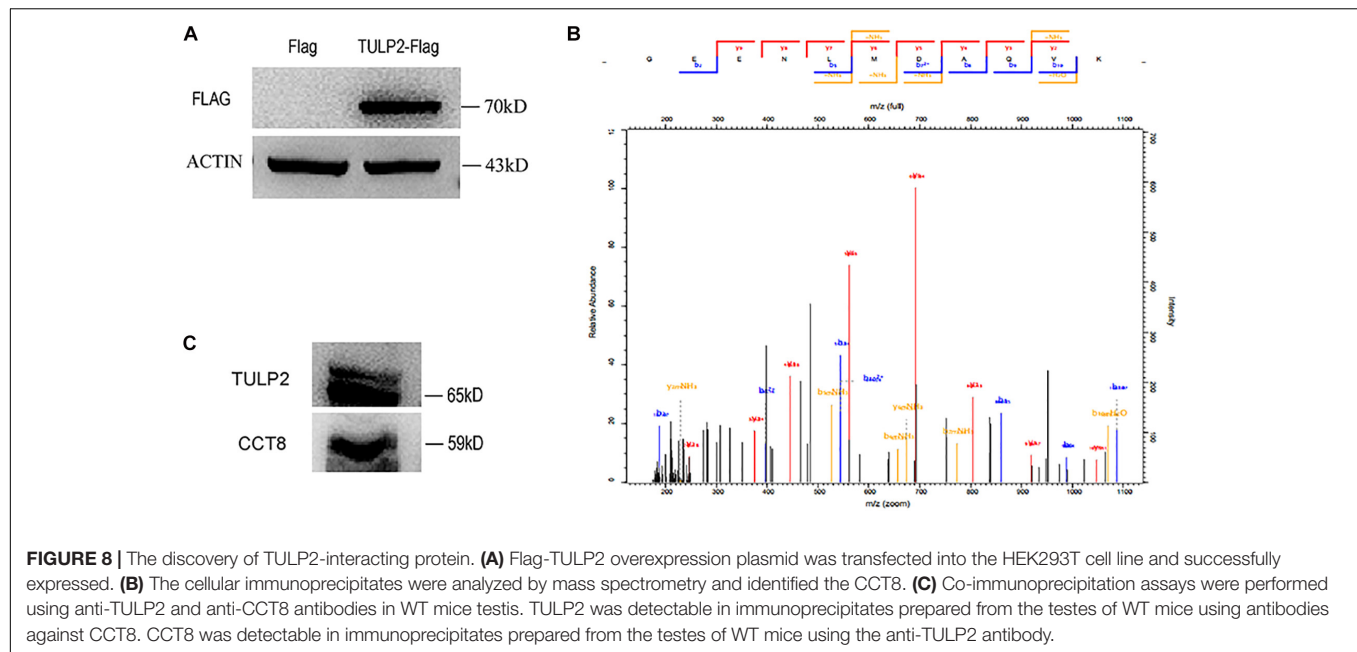


FIGURE 7 | Analysis of mRNA transcriptome sequencing data. **(A)** Genes showing a difference of more than 1.5 fold were analyzed according to GO annotations and classified into three major categories: cellular component, biological process, and molecular function. **(B)** The genes in each pathway were verified using real-time PCR. The results were consistent with the sequencing data ($n = 3$, * $P < 0.05$, ** $P < 0.01$).

TULP2 Interacts With CCT8, Participating in the Regulation of Spermatogenesis

To further investigate the molecular function of TULP2, we constructed a TULP2 overexpression plasmid with Flag label and transfected it into the HEK293T cell line. After the transfection of the TULP2 plasmid, the cellular proteins

were extracted, and the transfection efficiency was detected by western blotting with an anti-Flag antibody. The results showed that the TULP2 protein was successfully expressed in HEK293T cells (Figure 8A). HEK293T cell proteins were extracted after transfection with the TULP2 plasmid, and an immunoprecipitation experiment was carried out. Then, the samples were identified using mass spectrometry, which detected CCT8 (T-complex protein 1 subunit theta) (Figure 8B).



Co-immunoprecipitation and western blot analysis using anti-TULP2 and anti-CCT8 antibodies were performed to examine the interaction between TULP2 and CCT8. TULP2 was detectable in immunoprecipitates prepared from the testes of WT mice using antibodies against CCT8. Similarly, CCT8 was detectable in immunoprecipitates prepared from the testes of WT mice using the anti-TULP2 antibody (Figure 8C).

DISCUSSION

Spermatogenesis takes place in the testis and is one of the most complex differentiation events that occur within developmental biology, necessitating the controlled regulation of gene expression (Sutherland et al., 2015). Post-transcriptional regulation of gene expression is essential for the progression of spermatogenesis (Idler and Yan, 2012). Thus, the study of RBPs, which is the core factors in post-transcriptional regulation, has become a key focus in the field of male reproductive biology.

Based on our previous study, we focused on a new candidate RNA binding protein, TULP2, and through cross-linking immunoprecipitation (CLIP) confirming that TULP2 could indeed bind RNAs (Supplementary Figure 2). The exact role of TULP2 in spermatogenesis and male reproduction is still unknown. In this study, we constructed *Tulp2* gene knockout mice to study the effect of the absence of the product of this gene. The results confirmed that TULP2 is necessary for maintaining male fertility and *Tulp2*^{-/-} mice showed the phenotype of oligo-astheno-teratozoospermia. In these mice, abnormal deposition of apoptotic elongated spermatids in testis was observed (resulting the decreased sperm count in epididymis); the sperm showed reduced motility and tail deformity, in which the structures of microtubule, mitochondria and peripheral dense fibers were all damaged.

The sufficient quantity and quality of sperm is the guarantee of male fertility, which depends on the orderly completion of spermatogenesis (Neto et al., 2016). We confirm the specific expression of TULP2 in testicular spermatid, which suggests that TULP2 is involved in spermatid differentiation during spermatogenesis. In the process of spermatid differentiation, round spermatids undergo dramatic morphological, molecular and cellular alterations, laying a foundation for the generation of functional sperm (Ozturk et al., 2017; Zakrzewski et al., 2021). Fully developed elongated spermatids ultimate release from the seminiferous epithelium into the tubule lumen to ensure an adequate sperm count (Wen et al., 2016). Defects at various structure of spermatid during spermiogenesis may cause elongated spermatid to be retained within the epithelium and apoptosis (O'Donnell, 2015). In addition, abnormal differentiation of spermatid may result in structural defects of sperm, decreased motility, and impaired fertilization (Ray et al., 2017). Therefore, our results confirmed that TULP2 is a key factor in regulating spermatid differentiation and ensuring sperm quality.

As an RBP, TULP2 theoretically plays a role in post-transcriptional regulation and affects the expression of a series of genes, resulting in various phenotypes (Idler and Yan, 2012; Kang et al., 2020). The analysis of these downstream genes could furtherly elucidate the molecular mechanism of TULP2 regulating spermatogenesis. We established the differential expression profiles of testicular transcripts between *Tulp2*^{-/-} and WT mice by transcriptome sequencing, and 1446 genes exhibiting an expression difference of more than 1.5 fold were identified. These differentially expressed transcripts should be direct or indirect targets of TULP2, and also the molecules that TULP2 affects when it plays the role. By using the bioinformatics analysis (GO annotation), we furtherly elucidate

the association between the exertion of TULP2 function and these molecular changes.

According to the analysis of cellular components, these differentially expressed genes were mainly related to the cytoplasm, especially structures such as the cytoskeleton, mitochondria, and cilia. This characteristic was consistent with the function that TULP2 participates in the differentiation of spermatids. During spermiogenesis, the structures and components of the cytoplasm of spermatids undergo major alterations and transformations (Ozturk et al., 2017; Zakrzewski et al., 2021). Structural differentiation in the cytoplasm includes processes such as the development of the Golgi apparatus into the acrosome and the extension and assembly of the flagellum (Lehti and Sironen, 2016; Touré et al., 2020). The key structures in the sperm flagellum related to motility include the cytoskeleton, mitochondria, etc. (Pleuger et al., 2020), which were the categories showing the highest abundance of differentially expressed genes.

Based on the analysis of biological processes, most of the differentially expressed genes were associated with the regulation of RNA metabolism and biosynthesis; a further literature review indicated that these genes mainly consisted of transcription factors and that some were RBPs (Xing et al., 2019; Hardison et al., 2020) (**Supplementary Figure 3A**). Both of transcription factors and RBPs regulate the downstream target molecular network to control a plethora of developmental and physiological processes (Hentze et al., 2018; Auer et al., 2020). Therefore, we think that TULP2 is a relatively upstream regulatory factor, which indirectly confirms the important role of TULP2 in spermatogenesis. In addition, many differentially expressed genes were associated with biological processes such as apoptosis, energy metabolism and spermatogenesis. Such molecular changes correspond to the results of our phenotype research, which confirm that TULP2 uses these molecules to perform its function.

From the perspective of molecular functions, the differentially expressed genes were mainly related to binding activity, particularly protein binding (including cytoskeletal proteins and enzymes) (**Supplementary Figure 3B**), and the literature review showed these enzymes are mainly related to energy metabolism (Matsumoto et al., 2012; Cuvelier et al., 2018). We think this should be related to the role of TULP2 in the differentiation of the sperm tail. The most important components of the sperm flagellum are cytoskeletal proteins (Lehti and Sironen, 2017), while enzyme activity is the molecular basis for ATP generation and sperm motility (Moraes and Meyers, 2018). Thus, TULP2 regulates the expression of these genes to participate in the assembly of the sperm tail and energy metabolism. On the other hand, “protein binding” activity may be due to the considerable number of transcription factors among the potential targets that are regulated by TULP2, which usually bind related co-transcription factors when performing their functions (Herzel et al., 2017). In addition, some potential targets of TULP2 showed RNA-binding activity, which are assumed to be the RBPs that we have analyzed in the “biological process” section.

Therefore, the GO analysis verified the role of TULP2 in spermatid differentiation from different perspectives, and the

results of the biological process and molecular function analyses also confirmed each other. To gain a deeper understanding of the molecular function of TULP2 in spermiogenesis, we showed that TULP2 interacts with CCT8 by mass spectrometry and co-immunoprecipitation. CCT8 is a subunit of the CCT complex (also known as the TCP1 complex) (Brackley and Grantham, 2009). As a cytosolic chaperonin, the CCT complex assists in the folding of approximately 10% of cytosolic proteins to achieve their native structure (Jin et al., 2019; Vallin and Grantham, 2019). Studies in planarian flatworms suggest that each CCT subunit may play important roles in spermiogenesis (Counts et al., 2017). Therefore, we speculate that TULP2 might be the substrate of CCT8 and be correctly folded by the CCT complex, which requires further verification in the future.

In summary, TULP2 is a new RBP that we identified for the first time that is specifically expressed in the testes and localized to spermatids. We demonstrated that TULP2 participates in the normal differentiation of spermatids by regulating a series of transcripts related to the cytoskeleton, mitochondria and apoptosis and thereby affects sperm counts and tail assembly. In this process, CCT8 may bind to TULP2, which is correctly folded by the CCT complex and plays a role in spermiogenesis (schematic diagram for the role of TULP2 in spermiogenesis was shown in **Supplementary Figure 4**). Due to the typical oligo-astheno-teratozoospermia and infertility phenotype exhibited by mice after the loss of TULP2, and three potential deleterious missense mutations of this gene had been found in dyszoospermia patients, *Tulp2* is likely to be a potential pathogenic gene in patients with these conditions. TULP2 and its downstream molecules become the potential targets for the clinical diagnosis and treatment of these patients. In the future, further research is required to confirm if potential deleterious mutations affect TULP2 protein function.

DATA AVAILABILITY STATEMENT

The datasets presented in this study can be found in online repositories. The names of the repository/repositories and accession number(s) can be found in the article/**Supplementary Material**.

ETHICS STATEMENT

The animal study was reviewed and approved by Ethics Committee of Experimental Animal Welfare, Nanjing Medical University.

AUTHOR CONTRIBUTIONS

HuZ and XG conceived and designed the project. YC, MZ, and QY performed the experiments. MZ, XC, and YC collected the data. MZ, XC, WL, HD, HaZ, HuZ, and YZ analyzed the data. MZ and XC created the figures and tables and drafted the manuscript. HuZ critically revised the manuscript. All authors read and approved the final version of the manuscript.

FUNDING

This work was supported by grants from the National Natural Science Foundation of China (grant number: 31871164, 82071702); Natural Science Foundation of Jiangsu Province (grant number: BK20181370); National Key R&D Program (grant number: 2016YFA0503300); Natural Science Foundation of Jiangsu Province (grant number: BK20180673).

SUPPLEMENTARY MATERIAL

The Supplementary Material for this article can be found online at: <https://www.frontiersin.org/articles/10.3389/fcell.2021.623738/full#supplementary-material>

Supplementary Figure 1 | Identification of three potential deleterious missense mutations of *Tulp2* gene in dyszoospermia patients.

Supplementary Figure 2 | TULP2 binds RNAs through cross-linking immunoprecipitation. **(A)** TULP2 plasmid with Flag label was transfected

into HEK293T cells. The HEK293T cell proteins were extracted after transfection, and an immunoprecipitation experiment was carried out. **(B)** The autoradiograph of a CLIP experiment revealed TULP2 can bind RNA (black arrow).

Supplementary Figure 3 | The classification and proportions of differentially expressed genes were summarized according to the results of GO analysis. **(A)** The classification and proportions of differentially expressed genes related to the regulation of RNA metabolism and biosynthesis, and mainly were transcription factors and some were RBPs. **(B)** The classification and proportions of differentially expressed genes related to the protein binding, mainly were transcription factors, enzymes and cytoskeletal proteins.

Supplementary Figure 4 | Schematic diagram for the role of TULP2 in spermiogenesis. TULP2 interact with CCT8 and regulate a series of transcripts to play a role in normal spermatid differentiation. The loss of TULP2 leads to abnormal spermatids differentiation, increased spermatids apoptosis and abnormal spermatids deposition, resulting in reduced sperm count, decreased motility and sperm malformation.

Supplementary Table 1 | Primer sequences and target fragment size of each gene.

Supplementary Table 2 | 1446 genes showing an expression difference of 1.5 fold or more.

REFERENCES

- Ahmed, E. A., and de Rooij, D. G. (2009). Staging of mouse seminiferous tubule cross-sections. *Methods Mol. Biol.* 558, 263–277. doi: 10.1007/978-1-60761-103-5_16
- Albahlal, W. S., and Gerber, A. P. (2018). Unconventional RNA-binding proteins: an uncharted zone in RNA biology. *FEBS Lett.* 592, 2917–2931. doi: 10.1002/1873-3468.13161
- Auer, J., Stoddart, J. J., Christodoulou, I., Lima, A., Skouloudaki, K., Hall, H. N., et al. (2020). Of numbers and movement - understanding transcription factor pathogenesis by advanced microscopy. *Dis. Model. Mech.* 13:dmm046516. doi: 10.1242/dmm.046516
- Beckmann, B. M., Horos, R., Fischer, B., Castello, A., Eichelbaum, K., Alleaume, A. M., et al. (2015). The RNA-binding proteomes from yeast to man harbour conserved enigmRBPs. *Nat. Commun.* 6:10127. doi: 10.1038/ncomms10127
- Bracke, A., Peeters, K., Punjabi, U., Hoogewijs, D., and Dewilde, S. (2018). A search for molecular mechanisms underlying male idiopathic infertility. *Reprod. Biomed. Online.* 36, 327–339. doi: 10.1016/j.rbmo.2017.12.005
- Brackley, K. I., and Grantham, J. (2009). Activities of the chaperonin containing TCP-1 (CCT): implications for cell cycle progression and cytoskeletal organisation. *Cell Stress Chaperones* 14, 23–31. doi: 10.1007/s12192-008-0057-x
- Cao, X., Cui, Y., Zhang, X., Lou, J., Zhou, J., Bei, H., et al. (2018). Proteomic profile of human spermatozoa in healthy and asthenozoospermic individuals. *Reprod. Biol. Endocrinol.* 16:16. doi: 10.1186/s12958-018-0334-1
- Chalmel, F., and Rolland, A. D. (2015). Linking transcriptomics and proteomics in spermatogenesis. *Reproduction* 150, R149–R157. doi: 10.1530/REP-15-0073
- Connolly, C. M., Dearth, A. T., and Braun, R. E. (2005). Disruption of murine Tenr results in teratospermia and male infertility. *Dev. Biol.* 278, 13–21. doi: 10.1016/j.ydbio.2004.10.009
- Counts, J. T., Hester, T. M., and Rouhana, L. (2017). Genetic expansion of chaperonin-containing TCP-1 (CCT/TRiC) complex subunits yields testis-specific isoforms required for spermatogenesis in planarian flatworms. *Mol. Reprod. Dev.* 84, 1271–1284. doi: 10.1002/mrd.22925
- Cuvelier, E., Méquinion, M., Leghay, C., Sibrant, W., Stevenard, A., Sarchione, A., et al. (2018). Overexpression of wild-type human alpha-synuclein causes metabolism abnormalities in Thy1-aSYN transgenic mice. *Front. Mol. Neurosci.* 11:321. doi: 10.3389/fnmol.2018.00321
- Griswold, M. D. (2016). Spermatogenesis: the commitment to meiosis. *Physiol. Rev.* 96, 1–17. doi: 10.1152/physrev.00013.2015
- Grosso, A. R., Gomes, A. Q., Barbosa-Morais, N. L., Caldeira, S., Thorne, N. P., Grech, G., et al. (2008). Tissue-specific splicing factor gene expression signatures. *Nucleic Acids Res.* 36, 4823–4832. doi: 10.1093/nar/gkn463
- Hardison, R. C., Zhang, Y., Keller, C. A., Xiang, G., Heuston, E. F., An, L., et al. (2020). Systematic integration of GATA transcription factors and epigenomes via IDEAS paints the regulatory landscape of hematopoietic cells. *IUBMB Life* 72, 27–38. doi: 10.1002/iub.2195
- Hentze, M. W., Castello, A., Schwarzl, T., and Preiss, T. (2018). A brave new world of RNA-binding proteins. *Nat. Rev. Mol. Cell Biol.* 19, 327–341. doi: 10.1038/nrm.2017.130
- Herzel, L., Otzto, D., Alpert, T., and Neugebauer, K. M. (2017). Splicing and transcription touch base: co-transcriptional spliceosome assembly and function. *Nat. Rev. Mol. Cell Biol.* 18, 637–650. doi: 10.1038/nrm.2017.63
- Idler, R. K., and Yan, W. (2012). Control of messenger RNA fate by RNA-binding proteins: an emphasis on mammalian spermatogenesis. *J. Androl.* 33, 309–337. doi: 10.2164/jandrol.111.014167
- Iguchi, N., Tobias, J. W., and Hecht, N. B. (2006). Expression profiling reveals meiotic male germ cell mRNAs that are translationally up- and down-regulated. *Proc. Natl. Acad. Sci. U.S.A.* 103, 7712–7717. doi: 10.1073/pnas.0510999103
- Jin, M., Liu, C., Han, W., and Cong, Y. (2019). TRiC/CCT chaperonin: structure and function. *Subcell Biochem.* 93, 625–654. doi: 10.1007/978-3-030-28151-9_19
- Kang, D., Lee, Y., and Lee, J. S. (2020). RNA-Binding proteins in cancer: functional and therapeutic perspectives. *Cancers* 12:2699. doi: 10.3390/cancers12092699
- Kotaja, N., and Sassone-Corsi, P. (2007). The chromatoid body: a germ-cell-specific RNA-processing centre. *Nat. Rev. Mol. Cell Biol.* 8, 85–90. doi: 10.1038/nrm2081
- Kwon, S. C., Yi, H., Eichelbaum, K., Föhr, S., Fischer, B., You, K. T., et al. (2013). The RNA-binding protein repertoire of embryonic stem cells. *Nat. Struct. Mol. Biol.* 20, 1122–1130. doi: 10.1038/nsmb.2638
- Latendresse, J. R., Warbritton, A. R., Jonassen, H., and Creasy, D. M. (2002). Fixation of testes and eyes using a modified Davidson's fluid: comparison with Bouin's fluid and conventional Davidson's fluid. *Toxicol. Pathol.* 30, 524–533. doi: 10.1080/01926230290105721
- Lehti, M. S., and Sironen, A. (2016). Formation and function of the manchette and flagellum during spermatogenesis. *Reproduction* 151, R43–R54. doi: 10.1530/REP-15-0310
- Lehti, M. S., and Sironen, A. (2017). Formation and function of sperm tail structures in association with sperm motility defects. *Biol. Reprod.* 97, 522–536. doi: 10.1093/biolre/i0x096

- Matsumoto, T., Kinoshita, T., Matsuzaka, H., Nakai, R., Kirii, Y., Yokota, K., et al. (2012). Crystal structure of non-phosphorylated MAP2K6 in a putative auto-inhibition state. *J. Biochem.* 151, 541–549. doi: 10.1093/jb/mvs023
- Meijer, H. A., Bushell, M., Hill, K., Gant, T. W., Willis, A. E., Jones, P., et al. (2007). A novel method for poly(A) fractionation reveals a large population of mRNAs with a short poly(A) tail in mammalian cells. *Nucleic Acids Res.* 35, e132. doi: 10.1093/nar/gkm830
- Moraes, C. R., and Meyers, S. (2018). The sperm mitochondrion: organelle of many functions. *Anim. Reprod. Sci.* 194, 71–80. doi: 10.1016/j.anireprosci.2018.03.024
- Neto, F. T., Bach, P. V., Najari, B. B., Li, P. S., and Goldstein, M. (2016). Spermatogenesis in humans and its affecting factors. *Semin. cell Dev. Biol.* 59, 10–26. doi: 10.1016/j.semcdb.2016.04.009
- North, M. A., Naggert, J. K., Yan, Y., Noben-Trauth, K., and Nishina, P. M. (1997). Molecular characterization of TUB, TULP1, and TULP2, members of the novel tubby gene family and their possible relation to ocular diseases. *Proc. Natl. Acad. Sci. U.S.A.* 94, 3128–3133. doi: 10.1073/pnas.94.7.3128
- O'Donnell, L. (2015). Mechanisms of spermiogenesis and spermiation and how they are disturbed. *Spermatogenesis* 4:e979623. doi: 10.4161/21565562.2014.979623
- Ozturk, N., Steger, K., and Schagdarsurengin, U. (2017). The impact of autophagy in spermiogenesis. *Asian. J. Androl.* 19, 617–618. doi: 10.4103/1008-682X.190324
- Ozturk, S., and Uysal, F. (2018). Potential roles of the poly(A)-binding proteins in translational regulation during spermatogenesis. *J. Reprod. Dev.* 64, 289–296. doi: 10.1262/jrd.2018-026
- Paronetto, M. P., and Sette, C. (2010). Role of RNA-binding proteins in mammalian spermatogenesis. *Int. J. Androl.* 33, 2–12. doi: 10.1111/j.1365-2605.2009.00959.x
- Pleuger, C., Lehti, M. S., Dunleavy, J. E., Fietz, D., and O'Bryan, M. K. (2020). Haploid male germ cells—the grand central station of protein transport. *Hum. Reprod. Update* 26, 474–500. doi: 10.1093/humupd/dmaa004
- Ray, D., Ha, K., Nie, K., Zheng, H., Hughes, T. R., and Morris, Q. D. (2017). RNAcompete methodology and application to determine sequence preferences of unconventional RNA-binding proteins. *Methods* 11, 3–15. doi: 10.1016/j.ymeth.2016.12.003
- Ray, P. F., Toure, A., Metzler-Guillemain, C., Mitchell, M. J., Arnoult, C., and Coutton, C. (2017). Genetic abnormalities leading to qualitative defects of sperm morphology or function. *Clin. Genet.* 91, 217–232. doi: 10.1111/cge.12905
- Salas-Huetos, A., Bulló, M., and Salas-Salvadó, J. (2017). Dietary patterns, foods and nutrients in male fertility parameters and fecundability: a systematic review of observational studies. *Hum. Reprod. Update* 23, 371–389. doi: 10.1093/humupd/dmx006
- Schrans-Stassen, B. H., Saunders, P. T., Cooke, H. J., and de Rooij, D. G. (2001). Nature of the spermatogenic arrest in Dazl^{-/-} mice. *Biol. Reprod.* 65, 771–776. doi: 10.1095/biolreprod65.3.771
- Shen, B., Zhang, J., Wu, H., Wang, J., Ma, K., Li, Z., et al. (2013). Generation of gene-modified mice via Cas9/RNA-mediated gene targeting. *Cell Res.* 23, 720–723. doi: 10.1038/cr.2013.46
- Sutherland, J. M., Siddall, N. A., Hime, G. R., and McLaughlin, E. A. (2015). RNA binding proteins in spermatogenesis: an in depth focus on the Musashi family. *Asian. J. Androl.* 17, 529–536. doi: 10.4103/1008-682X.151397
- Touré, A., Martinez, G., Kherraf, Z. E., Cazin, C., Beurois, J., Arnoult, C., et al. (2020). The genetic architecture of morphological abnormalities of the sperm tail. *Hum. Genet.* [Epub ahead of print]. doi: 10.1007/s00439-020-02113-x
- Vallin, J., and Grantham, J. (2019). The role of the molecular chaperone CCT in protein folding and mediation of cytoskeleton-associated processes: implications for cancer cell biology. *Cell Stress Chaperones* 24, 17–27. doi: 10.1007/s12192-018-0949-3
- Vander Borgh, M., and Wyns, C. (2018). Fertility and infertility: definition and epidemiology. *Clin. Biochem.* 62, 2–10. doi: 10.1016/j.clinbiochem.2018.03.012
- Vanderweyde, T., Youmans, K., Liu-Yesucevitz, L., and Wolozin, B. (2013). Role of stress granules and RNA-binding proteins in neurodegeneration: a mini-review. *Gerontology* 59, 524–533. doi: 10.1159/000354170
- Wang, M., Xu, Z., and Kong, Y. (2018). The tubby-like proteins kingdom in animals and plants. *Gene* 642, 16–25. doi: 10.1016/j.gene.2017.10.077
- Wen, Q., Tang, E. I., Xiao, X., Gao, Y., Chu, D. S., Mruk, D. D., et al. (2016). Transport of germ cells across the seminiferous epithelium during spermatogenesis—the involvement of both actin- and microtubule-based cytoskeletons. *Tissue Barriers* 4:e1265042. doi: 10.1080/21688370.2016.1265042
- Xing, S., Gai, K., Li, X., Shao, P., Zeng, Z., Zhao, X., et al. (2019). Tcf1 and Lef1 are required for the immunosuppressive function of regulatory T cells. *J. Exp. Med.* 216, 847–866. doi: 10.1084/jem.20182010
- Zagore, L. L., Grabinski, S. E., Sweet, T. J., Hannigan, M. M., Sramkoski, R. M., Li, Q., et al. (2015). RNA binding protein Ptbp2 is essential for male germ cell development. *Mol. Cell Biol.* 35, 4030–4042. doi: 10.1128/MCB.00676-15
- Zakrzewski, P., Lenartowska, M., and Buss, F. (2021). Diverse functions of myosin VI in spermiogenesis. *Histochem. Cell Biol.* [Epub ahead of print]. doi: 10.1007/s00418-020-01954-x
- Zhu, F., Yan, P., Zhang, J., Cui, Y., Zheng, M., Cheng, Y., et al. (2019). Deficiency of TPPP2, a factor linked to oligoasthenozoospermia, causes subfertility in male mice. *J. Cell Mol. Med.* 23, 2583–2594. doi: 10.1111/jcmm.14149
- Zhu, H., Cui, Y., Xie, J., Chen, L., Chen, X., Guo, X., et al. (2010). Proteomic analysis of testis biopsies in men treated with transient scrotal hyperthermia reveals the potential targets for contraceptive development. *Proteomics* 10, 3480–3493. doi: 10.1002/pmic.201000281

Conflict of Interest: The authors declare that the research was conducted in the absence of any commercial or financial relationships that could be construed as a potential conflict of interest.

Copyright © 2021 Zheng, Chen, Cui, Li, Dai, Yue, Zhang, Zheng, Guo and Zhu. This is an open-access article distributed under the terms of the Creative Commons Attribution License (CC BY). The use, distribution or reproduction in other forums is permitted, provided the original author(s) and the copyright owner(s) are credited and that the original publication in this journal is cited, in accordance with accepted academic practice. No use, distribution or reproduction is permitted which does not comply with these terms.



The Regulatory Role of Oxygen Metabolism in Exercise-Induced Cardiomyocyte Regeneration

Bing Bo^{1,2}, Shuangshuang Li¹, Ke Zhou^{1,2*} and Jianshe Wei^{3*}

¹ Kinesiology Department, School of Physical Education, Henan University, Kaifeng, China, ² Sports Reform and Development Research Center, School of Physical Education, Henan University, Kaifeng, China, ³ Institute for Brain Sciences Research, School of Life Sciences, Henan University, Kaifeng, China

OPEN ACCESS

Edited by:

Eiman Aleem,
The University of Arizona,
United States

Reviewed by:

Hideko Sone,
Yokohama College of Pharmacy,
Japan
Zhongzhou Yang,
Nanjing University, China

*Correspondence:

Jianshe Wei
jswei@henu.edu.cn
Ke Zhou
10180055@vip.henu.edu.cn

Specialty section:

This article was submitted to
Cell Growth and Division,
a section of the journal
Frontiers in Cell and Developmental
Biology

Received: 05 February 2021

Accepted: 29 March 2021

Published: 15 April 2021

Citation:

Bo B, Li S, Zhou K and Wei J
(2021) The Regulatory Role of Oxygen
Metabolism in Exercise-Induced
Cardiomyocyte Regeneration.
Front. Cell Dev. Biol. 9:664527.
doi: 10.3389/fcell.2021.664527

During heart failure, the heart is unable to regenerate lost or damaged cardiomyocytes and is therefore unable to generate adequate cardiac output. Previous research has demonstrated that cardiac regeneration can be promoted by a hypoxia-related oxygen metabolic mechanism. Numerous studies have indicated that exercise plays a regulatory role in the activation of regeneration capacity in both healthy and injured adult cardiomyocytes. However, the role of oxygen metabolism in regulating exercise-induced cardiomyocyte regeneration is unclear. This review focuses on the alteration of the oxygen environment and metabolism in the myocardium induced by exercise, including the effects of mild hypoxia, changes in energy metabolism, enhanced elimination of reactive oxygen species, augmentation of antioxidative capacity, and regulation of the oxygen-related metabolic and molecular pathway in the heart. Deciphering the regulatory role of oxygen metabolism and related factors during and after exercise in cardiomyocyte regeneration will provide biological insight into endogenous cardiac repair mechanisms. Furthermore, this work provides strong evidence for exercise as a cost-effective intervention to improve cardiomyocyte regeneration and restore cardiac function in this patient population.

Keywords: cardiomyocyte regeneration, exercise, oxygen metabolism, hypoxia, molecular pathway

INTRODUCTION

Heart failure (HF) is the primary cause of morbidity and mortality worldwide (Benjamin et al., 2019) and encompasses a variety of diseases impacting the heart and vasculature, leading to often fatal events, such as stroke, myocardial infarction (MI), and cardiac arrest (Benjamin et al., 2019; Pinckard et al., 2019). The adult mammalian heart is unable to regenerate lost or damaged cardiomyocytes at appropriate rates, and increasing evidence suggests that the mammalian heart is a postmitotic organ. Conversely, the neonatal heart has shown the ability to regenerate lost cardiomyocytes (Porrello et al., 2011). The adult heart has also demonstrated the ability to self-renew but at a much lower rate (Puente et al., 2014; Bergmann et al., 2015). The low rate of myocyte turnover that occurs in the adult heart is insufficient for the reconstitution of cardiac function in injured hearts (Nadal-Ginard, 2001; Bergmann et al., 2009). Cardiomyocyte regenerative capacity differs among species and life stages, closely related to the oxygen environment (Puente et al., 2014; Nakada et al., 2017). While oxygen-rich environments tend to induce cardiomyocytes to exit the cell cycle and lose regenerative ability after birth (Puente et al., 2014), hypoxia has been shown to

activate cardiomyocyte mitosis through inhibited aerobic respiration and oxidative DNA damage in adult mice (Nakada et al., 2017). These studies suggest that alterations of the oxygen environment and metabolism play a vital role in cardiomyocyte regeneration.

For decades, the benefits of regular exercise for the therapy of heart disease have been widely recognized (Sanchis-Gomar et al., 2015; Verdoorn et al., 2017). The fundamental basis for the positive impacts of exercise on the heart is the increase in cardiac size and output (Pluim et al., 1998; Pluim et al., 2000). In elite athletes, the 10–20% greater cardiac dimension observed vs. healthy individuals has been attributed to cardiac hypertrophy (Maillet et al., 2013). In addition to our understanding that exercise causes cardiomyocyte hypertrophy, a growing body of research suggests that running or swimming may be able to activate the proliferation and regeneration capacity of cardiomyocytes (Waring et al., 2014; Vujic et al., 2018). Although the exact mechanism of exercise-induced cardiomyocyte regeneration is unclear, alteration of the oxygen environment and oxygen metabolism in the myocardium has been highlighted. This brief review will focus on exercise and oxidative metabolic control, concluding with evidence of how changes in oxygen metabolism may be involved in exercise-induced cardiomyocyte regeneration.

CHARACTERISTICS OF CARDIOMYOCYTE REGENERATION

Cardiomyocyte Regeneration Is Primarily Triggered by Cardiomyocyte Proliferation

Unlike lower vertebrates (e.g., zebrafish and newts) that maintain cardiac proliferation and differentiation ability for the entire lifespan (Poss et al., 2002; Porrello and Olson, 2014), the adult mammalian heart has been considered to have no capacity for proliferation. However, this traditional view has been challenged. It shows that the cardiomyocyte turnover rate is approximately 0.5–1% per year and almost 45% of cardiomyocytes are renewed throughout the human lifetime (Bergmann et al., 2009). Thus, it would appear that cardiomyocytes do have the ability to regenerate at low rates under typical physiological conditions. Previous studies have shown that endogenous cardiac precursor cells, including Sca-1⁺ cells (Wang et al., 2006; Uchida et al., 2013) and Isl-1⁺ cells (Moretti et al., 2006; Weinberger et al., 2012) play a limited role in cardiac regeneration during physiological and pathological conditions. In particular, Li Y. et al. (2018) used four different mouse transgenic models to demonstrate that non-cardiomyocytes do not contribute to new cardiomyocyte production during homeostasis or after injury in the adult heart. To date, the replacement rate of cardiomyocytes from preexisting cardiomyocytes is approximate 0.76% annually in younger adult rodent under physiological conditions. This rate decreases with age but increases by up to 4 times in post-MI regions (Senyo et al., 2013). Together, these studies suggest that the renewal of cardiomyocytes in newborn (Porrello et al., 2011; Li Y. et al., 2018), aging, and pathological conditions (Li

Y. et al., 2018; Vagnozzi et al., 2018) is primarily derived from the proliferation of “preexisting” cardiomyocytes (Senyo et al., 2013). However, the reactivation and regulatory mechanisms of endogenous cardiomyocyte proliferation in adult hearts remain to be elucidated.

Cardiomyocyte Regenerative Capacity Differs Among Species and Life Stages

During embryonic heart development, cardiac growth is primarily attributed to the division of existing cardiomyocytes (Galdos et al., 2017). After birth, the ability of cardiac regeneration differs among species and life stages. Adult non-mammalian animals (e.g., zebrafish, axolotls, and newts) are capable of regenerating the myocardium tissue throughout the lifespan (Poss et al., 2002; Jopling et al., 2010; Vagnozzi et al., 2018). For zebrafish, surgical amputation of up to 20% of the ventricle causes a remarkable increase of 5-Bromo-2'-deoxyuridine (BrdU)-labeled cycling myocytes (Poss et al., 2002). Similar regenerative phenomena have been reported in axolotls (Flink, 2002) and newts (Laube et al., 2006). After 60% ablation of zebrafish cardiomyocytes via genetic technology, all cardiomyocytes were replaced within 30 days (Chablais and Jazwinska, 2012). Moreover, the expansion of newborn cardiomyocytes can almost completely restore the structure and function of the ventricle. However, some studies also questioned whether this extent of regeneration is sufficient for more serious myocardial injuries or not (Figure 1) (Gonzalez-Rosa et al., 2017).

In contrast, the ability of cardiomyocyte regeneration is finite in adult mammalian hearts (Bergmann et al., 2009). However, the newborn mammalian heart preserves excellent regenerative ability during a short period following birth. Porrello et al. (2013) found that 1-day-old neonatal mice display sufficient regenerative capacity from preexisting cardiomyocytes after resection of ventricular apex (Porrello et al., 2011) and MI surgery. Accordingly, echocardiography in these studies has revealed that regenerated ventricular tissue is fully functional within 2 months (Porrello et al., 2011) and 3 weeks (Porrello et al., 2013), respectively. However, the mice's heart has been shown to be incapable of regeneration 7 days after birth (Porrello et al., 2011, 2013), which is consistent with binucleation and arrest of the cardiomyocyte cell cycle (Soonpaa et al., 1996). Other studies have indicated that cardiomyogenic ability is limited in neonatal mice, which showed irreversible fibrosis, dilated cardiomyopathy (Andersen et al., 2016), and persistent scarring (Zebrowski et al., 2017) following apex resection. In neonatal porcine that undergo MI surgery, cardiomyocyte proliferation only lasts 2 days after birth, after which cardiomyocytes exit from the cell cycle, and contractile functions of the ventricle are damaged (Ye et al., 2018; Zhu et al., 2018). In a newborn child who suffers from severe MI due to coronary artery occlusion, clinicians have observed cardiac functional recovery within weeks after the initial ischemic insult. This phenomenon suggests that newborn human cardiomyocytes may preserve the intrinsic ability to replace injury cardiomyocyte and restore cardiac function entirely (Haubner et al., 2016). Moreover, cardiomyocyte proliferation is remarkable in newborn





| | Adult Zebrafish | Adult Newt | Neonatal Mouse | Adult Mouse |
|----------------------------------|---|---|---|---|
| Cardiomyocytes Morphology |  |  |  |  |
| Cardiomyocytes Nucleation | Mononucleated | Mononucleated | Mononucleated | Bi-or Multi-Regeneration |
| Cardiomyocytes Growth | Hyperplastic | Hyperplastic | Hyperplastic | Hypertrophic |
| Injury Response | Regeneration | Regeneration | Regeneration | Non-Regeneration |
| Oxygenation State | Low | Low | Low | High |
| Mitochondrial Respiration | Low | Low | Low | High |
| Oxidative Stress | Low | ? | Low | High |
| ROS Production | Low | ? | Low | High |

FIGURE 1 | The characteristics of cardiomyocyte regeneration in different species and life stages.

human hearts under pathological conditions (Farooqi et al., 2012; Nakagama et al., 2018).

Compared with adult mammalian cardiomyocytes, the heart of neonatal mammals and low vertebrates share reparative capabilities through cardiomyocyte proliferation in the myocardium (Gomes et al., 2016). Therefore, whether postmitotic stimulation that drives cardiomyocyte regeneration in zebrafish and neonatal mammals can induce similar responses in adult mammalian hearts, is a meaningful question (Foglia and Poss, 2016).

ROLE OF OXYGEN METABOLIC MECHANISM IN CARDIOMYOCYTE REGENERATION

Oxygen Environment of Cardiomyocytes Differ Among Species and Life Stages

Among the numerous regulators of cardiomyocyte regeneration, the oxygen environment has received increased attention (Puente et al., 2014; Kimura et al., 2015; Nakada et al., 2017; Sakaguchi et al., 2020). In different species and life stages, oxygen supply and metabolism are distinct. Compared to the air, the oxygen capacitance of the aquatic environment where zebrafish live is only 1/30th that of the air, which can be considered a reduced level of oxygenation. This extremely hypoxic context might explain the prominent tolerance of zebrafish to hypoxia (Rees et al., 2001; Roesner et al., 2006). The typical PaO_2 of oxygen-saturated water is 146 mmHg. Zebrafish can tolerate a PaO_2 of 15 mmHg (10% oxygen-saturation) for 48 h and even 8 mmHg (5% air-saturation) under hypoxic pretreatment (Rees et al., 2001). Moreover, the zebrafish heart is a primitive two-chamber organ, with a single atrium and single ventricle, which leads to the mixing

of arterial and venous blood. Similarly, the mammalian fetal circulation carries hypoxic blood with an arterial PaO_2 of 25–35 mmHg, mainly due to a large amount of arteriovenous mixing in the fetal circulation. After the newborn's first breath, the transition from embryonic to postnatal circulation significantly changes the oxygenation of cardiomyocytes. Meanwhile, the mammalian heart is characterized by four chambers, with an arteriovenous shunt in the neonatal heart. Thus, arterial PaO_2 immediately increases from 30 mmHg (Lawrence et al., 2008) to 100 mmHg (Webster and Abela, 2007). Compared to the relatively small regenerative capacity in the adult mammalian heart, the prominent cardiomyogenic capacity of zebrafish is very likely due to the “oxygen poor” environment. Therefore, the oxygen environment of cardiomyocytes plays a critical role in the maintenance and regulation of cardiomyocyte regeneration.

Increased Oxygen Supply After Birth Induces a Metabolic Switch and Cessation of Cardiomyocyte Proliferation

During the embryonic period, anaerobic glycolysis is the essential energy supply for the hypoxic heart. Soon after birth, with enhanced oxygen capacitance (20% oxygen in the air), the mammalian heart experiences a rapid shift in energy utilization. In the early newborn period, glycolysis and lactate oxidation are still the central metabolic process that supply energy. Simultaneously, fatty acid β -oxidation provides less than 15% of the heart's total adenosine triphosphate (ATP) requirements. The small amount of energy supplied by fatty acid β -oxidation is partly due to an inhibition of mitochondrial fatty acid uptake. However, within a few days following birth, a sharp increase in fatty acid β -oxidation coincides with a decrease in glycolytic rates. By 7 days postpartum, glycolysis is further reduced, and provides less than 10% of total ATP

produced by cardiomyocyte metabolism, whereas fatty acid β -oxidation increase progressively to produce 60–80% of ATP in the adult heart under standard physiological contexts (Lopaschuk et al., 1992, 2010). A recent study indicates that inhibition of fatty-acid utilization improves cardiomyocyte proliferation through DNA damage reduction and DNA-damage response (DDR) pathway in the postnatal heart (Cardoso et al., 2020). Proliferator-activated receptor α (PPAR α) regulates several genes that control mitochondrial import and oxidation of fatty acid in heart (Djouadi et al., 1999). Further study found that pharmacologic and genetic activation of PPAR α -mediated fatty acid β -oxidation promoted hypertrophic cardiomyocyte growth and maturation, which induced cytokinesis failure and cell cycle exit. The etomoxir (ETO)-mediates inhibition of myocardium fatty acid β -oxidation metabolism enhanced glycolysis and maintained cardiac proliferation in newborn mouse hearts at postnatal days 5 and 7 (Cao et al., 2019). Another study detected enzyme activity related to glycolytic and mitochondrial metabolism in the early postpartum period. For example, enzymes of Krebs cycle and fatty acid oxidation increase within 7 days of birth, with a simultaneous reduction of anaerobic glycolysis (Puente et al., 2014). These observations suggest that oxygen-dependent mitochondrial oxidative phosphorylation is the primary energy supply in adult cardiomyocytes. Interestingly, the mammalian heart's adaptability to high-concentration oxygen supply is synchronized with the stagnation of cardiomyocyte proliferation. However, the relationship between time window of metabolic shifts and cardiomyocyte regeneration in normal developmental and physiological settings remain unanswered.

The shift from anaerobic to aerobic metabolism is closely related to mitochondrial expansion in the myocardium, increase in reactive oxygen species (ROS) production, cardiomyocyte terminal differentiation, and cell cycle exit (Carley et al., 2014). Through comparison of the mitochondrial characteristics of zebrafish and newborn mouse hearts, it can be found that the mitochondrial expansion and cristae formation in mouse myocardial mitochondria is consistent with the time window in which cardiomyocyte regenerative ability is lost (Puente et al., 2014). Meanwhile, oxidative metabolism generates ROS through the mitochondria respiratory chain. ROS are produced by the secretion of the superoxide ion ($O_2^{\cdot -}$) due to electron leakage. This oxide can quickly transform into H_2O_2 and then into OH free radicals. A low concentration of ROS is harmless to cells and can be scavenged by antioxidants or the endogenous antioxidant pathway (Liaudet et al., 2009). However, the accumulation of ROS generates oxidative stress (Sarangarajan et al., 2017), inducing detrimental effects, such as oxidative nuclear DNA damage, proliferation, or inactivation of differentiation signaling pathways (Puente et al., 2014). It has been confirmed that some antioxidants (Pitx2 and TT-10) are able to enhance neonatal cardiomyocyte proliferation by activating the YAP signaling pathway (Puente et al., 2014; Tao et al., 2016; Hara et al., 2018). Previous studies have indicated that the process of proliferation in cardiomyocytes is associated with oxygen and aerobic respiration-mediated oxidative DNA damage (Puente et al., 2014; Kimura et al., 2015;

Liu et al., 2015; Bon-Mathier et al., 2019). The primary source of oxidative stress in postnatal cardiomyocytes is mitochondrial-derived ROS (Adam-Vizi and Chinopoulos, 2006). The shift from the hypoxic uterine environment to the postpartum environment causes a mitochondrial ROS-induced oxidative DNA damage response (DDR), which results in the arrest of the cardiomyocyte cell cycle. Puente et al. (2014) also indicated that activation of ATM kinase in response to DNA damage, in turn, activates Wee1 kinase, a repressor of cyclin-dependent kinase 1 (CDK1)-dependent G2-M transition. Wee1 did not immediately express in the nuclei of cardiomyocytes after birth, but was strongly upregulated at postnatal days 7 and 14 (Puente et al., 2014). Therefore, inhibition of Wee1 could induce greater activity of endogenous CDK1 and cyclin B1 (CCNB) complex to facilitate the G2/M phase and cardiomyocyte mitosis (Bicknell et al., 2004; Harvey et al., 2005; Mohamed et al., 2018). Moreover, the elimination of ROS can downregulate Wee1 expression to extend the postnatal cardiomyocyte proliferation window (Puente et al., 2014). Low concentrations of ROS may be able to regulate the protective pathways of ischemic preconditions (Zhou et al., 2018). Furthermore, cardiomyocyte adaptation to progressively higher oxygen supply after birth coincides with proliferation stagnation in the adult heart. The main reason for this phenomenon is oxygen-dependent mitochondrial metabolism (Nakada et al., 2017) and ROS production upregulation (Bon-Mathier et al., 2019).

Hypoxia and Cardiac Regeneration

The state of decreased oxygen availability is termed hypoxia and affects energy metabolism and contractile function of the myocardium (Essop, 2007; Cole et al., 2016). Chronic hypoxia can reduce mitochondrial fatty acid uptake and oxidation (Cole et al., 2016; Mansor et al., 2016), accompanied by decreased activity of fatty acid oxidation enzymes (Daneshrad et al., 2000; Kennedy et al., 2001; Heather et al., 2012), while glucose uptake (Hurford et al., 1990) and the activities glycolytic enzymes (Waskova-Arnostova et al., 2014; Cole et al., 2016; Mansor et al., 2016) increase after exposure to chronic hypoxia in the heart. Similarly, hypoxia reduces the mitochondrial respiration of fatty acid and pyruvate substrates, enzymatic activities of electron transport chain complexes I, II, and IV in subsarcolemmal mitochondria, and ROS generation (Heather et al., 2012). Metabolic alteration of the heart is primarily due to the shift from oxygen-fastidious fuels to oxygen-efficient substrates. One study group that exposed adult mice to a systemic gradual hypoxic environment (decreasing progressively in oxygen concentration by 1% per day from 20.9% ambient oxygen to 7% for 2 weeks) found that mitochondrial metabolism, ROS production, and oxidative DNA damage were reduced, all of which may be able to promote cell cycle reentry in differentiated cardiomyocytes at baseline or after injury (Nakada et al., 2017). A hypoxic environment may protect cardiomyocytes from ROS upregulation-induced oxidative DNA damage (Kikuchi et al., 2010). Additionally, hypoxia-induced metabolic reprogramming, cell cycle reentry, and regeneration in adult cardiomyocytes have been confirmed.

Hypoxia not only promotes cardiomyocyte proliferation at the cellular level, but also plays an important role in heart regeneration. For example, exposure to hypoxia (7% inspired oxygen concentration) for 7 days could remarkably increase the BrdU-positive cardiomyocyte and capillary collaterals, which provides supports for the improvement of left ventricular systolic function following myocardial infarction in mice heart (Nakada et al., 2017).

During the adaptation of cells to hypoxia, hypoxia-inducible factors (HIFs) are the most critical regulatory factors. HIFs are a family of obligate heterodimers composed of unstable α -subunits (HIF- α) (Wang et al., 1995; Kallio et al., 1997). Three HIF- α isoforms exist in humans: hypoxia-inducible factor 1 α (HIF-1 α), HIF-2 α , and HIF-3 α (Hu et al., 2003). HIF-1 α protein is stable under hypoxia, leading to transcriptional activation of multiple target genes involved in glycolytic, fatty acid, and mitochondrial metabolisms, as well as cell cycle regulators (Kaelin, 2005; Prabhakar and Semenza, 2015). HIF-1 participates in hypoxia-induced inhibition of fatty acid metabolism by reducing the DNA binding activity of PPAR α in rat cardiomyocytes (Belanger et al., 2007).

Additionally, the HIF-1 α protein is necessary for cardiomyocyte regeneration in injured hearts of zebrafish (Jopling et al., 2012) and hypoxic cardiomyocytes of fetuses (Dunwoodie, 2009) by regulating the cell cycle and cellular metabolism (Breckenridge et al., 2013; Guimaraes-Camboa et al., 2015; Hubbi and Semenza, 2015; Menendez-Montes et al., 2016). In HIF-1 α overexpressing transgenic mice, Kimura et al. (2015) used fate mapping to identify a few cardiomyocytes that preserved embryonic characteristics, including mononucleates, smaller cell size, lower levels of oxidative DNA damage, and contribution to cardiomyocyte regeneration. RNA sequencing analysis of isolated hypoxic proliferative cardiomyocytes indicated that an increase of HIF-1 α and a decrease of prolyl hydroxylases protected hypoxic proliferative cardiomyocytes from oxidative stress (Kimura et al., 2015). In MI rats, the upregulation of HIF-1 α protein and HIF-1 targets in mRNA have been detected within the first week after infarction (Hu et al., 2003). In pathological hearts, the ischemic tissue no longer receives oxygen or nutrients due to MI (Russell et al., 2004; Thygesen et al., 2018), resulting in the generation of free radicals and mitochondrial dysfunction by decreased utilization of fatty acid and increased employment of glycolysis and glucose oxidation (Sack et al., 1996; Davila-Roman et al., 2002). Therefore, ischemia inevitably induces local hypoxia in the affected tissue (Sousa Fialho et al., 2019).

These studies suggest that modulating oxygen levels or myocardial metabolism could be a novel method to induce new cardiomyocyte formation. This increase in cardiomyocyte renewal is likely due to decreased mitochondrial respiration, mitochondrial ROS production, and oxidative DNA damage under a systemic hypoxic microenvironment, thereby promoting cell cycle reentry. However, the risks associated with a hypoxic state of tissue need to be considered when transferring basic research results from small creatures to large animal models or human subjects.

POSSIBLE CHANGES OF EXERCISE-INDUCED PHYSIOLOGICAL EFFECTS ON HEART

Classification of Exercise

During exercise, the energetic source of skeletal muscle is mainly from carbohydrates, fatty acids and amino acids. Based on differences in mechanical action and energy metabolism of muscles, exercise is classified into dynamic and static exercise (Levine et al., 2015). Dynamic and static exercises differ in their mode, intensity, frequency, and volume (Patel et al., 2017).

Dynamic exercise mainly utilizes large skeletal muscle groups that can be continuously maintained and have rhythmic physical activity (Wahid et al., 2016). Moderate to high-intensity dynamic exercise is performed aerobically. Aerobic capacity is the ability of cardiopulmonary system supplying oxygen to tissue and skeletal muscle utilizing oxygen (Thompson et al., 2013). Cardiac output can maintain exercise for approximately 20 min during dynamic exercise and starts to decline thereafter due, at least in part, to cardiac drift (Coyle and Gonzalez-Alonso, 2001). With the extension of exercise time and the accumulation of cardiopulmonary system fatigue, insufficient oxygen supply cannot meet tissue demands for oxygen, causing relative hypoxia of tissues (such as muscles and myocardial tissues) (Michailidis et al., 2007; Powers and Jackson, 2008; Cimen et al., 2017). Whether this hypoxic environment can initiate the cardiomyocyte regeneration signaling pathway through the oxygen metabolic mechanism remains unclear.

Static exercise is a kind of strenuous physical activity with a short time. It is performed anaerobically that is maintained by energy in the contracted skeletal muscles and does not use oxygen to participate in energy production (Thompson et al., 2013). In the absence of oxygen, our cells produce ATP through the phosphate and glycolysis pathways. This method produces much less ATP than the aerobic oxidation pathway and causes accumulation of lactic acid. Static exercise is generally considered to consist of fast-twitch muscles and includes sprinting, powerlifting, and high-intensity interval training (HIIT). Static exercise leads to a continuous increase in lactic acid, and a turning point called the lactate threshold (LT). The definition of the LT is the point where the metabolic energy supply mode shifts from aerobic metabolism to anaerobic metabolism, leading to a continued increase in lactic acid and metabolic acidosis (Wasserman, 1986; Floria and Mareev, 1993).

Different types of exercise can induce a variety of different types of oxygen supplementation and consumption in cardiomyocytes. However, the relationship between exercise program and oxygen metabolism (e.g., intensity, frequency, and volume) needs to be further evaluated according to the physiological and pathological conditions of the individual (Merghani et al., 2016).

Potential Detrimental Effects of Exercise on the Heart

Although regular and appropriate exercise has been shown to affect cardiovascular function positively, strenuous acute

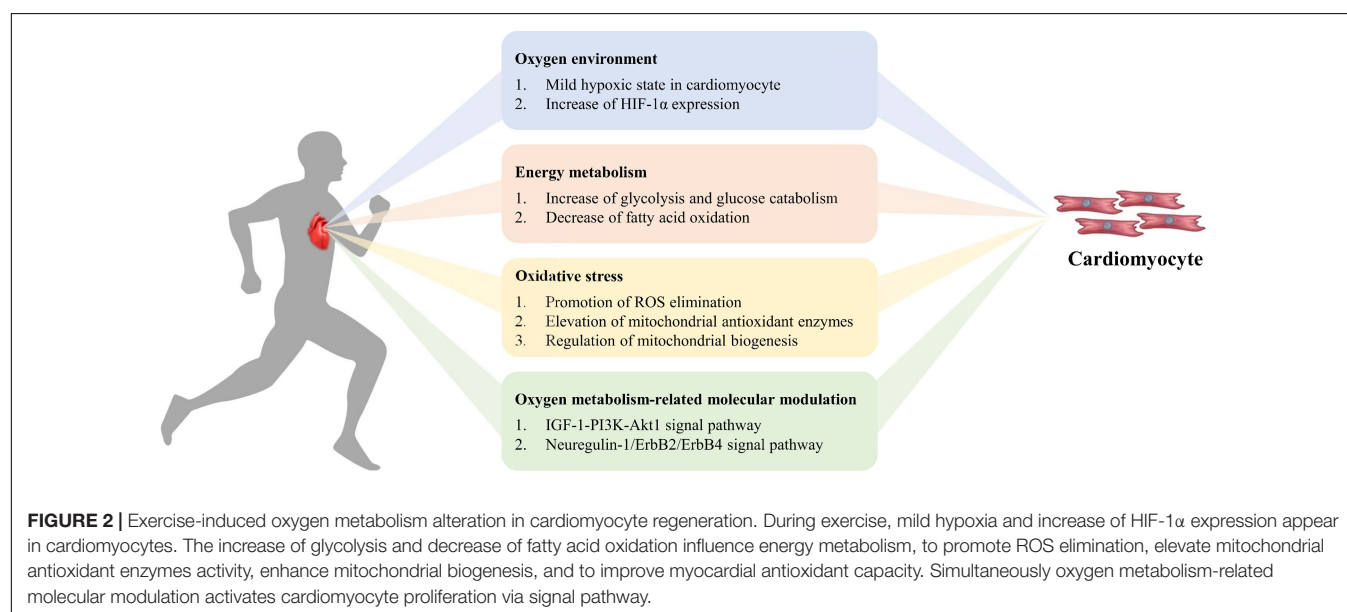
exercise or chronic excessive exercise training resulting in excessive cardiac stimulation may be harmful. Animal and human studies have confirmed that excessive acute and chronic exercise can increase cardiovascular pressure, leading to an alteration in the pathological structure of main arteries and remodeling of myocardial electrophysiology. Simultaneously, the atrium and right ventricle (RV) can experience transient acute volume overload, which leads to RV hypokinesia and diastolic dysfunction due to a sharp increase in returning blood volume caused by exercise (Parry-Williams and Sharma, 2020). Moreover, inflammation and fibrosis of the atria, ventricular septum, and RV of repeated overstimulation and injury induced by excessive exercise might be the essential reason of atrial and ventricular arrhythmias (O'Keefe et al., 2012). Therefore, the effect of exercise on heart structure and function is directly related to the type, intensity, and duration of the exercise program.

EXERCISE-INDUCED OXYGEN METABOLISM CHANGES IN CARDIOMYOCYTE REGENERATION

Regular exercise can result in changes in the cardiovascular and respiratory systems, through an increase in the provision of oxygen to working skeletal muscles and other tissues. Cardiac growth induced by exercise could improve myocardial contractility, arterial blood flow, and reduce myocardial ischemia in the mammalian heart (Duncker and Bache, 2008; Lavie et al., 2015; Platt et al., 2015; Vujic et al., 2018). However, the complex molecular and cellular mechanisms of exercise-induced cardiomyocyte renewal are ambiguous. In the following section, we will focus on the oxidative mechanisms involved in cardiomyocyte regeneration during and after exercise (Figure 2). Whether there is a dose-response effect due to exercise duration and intensity is debatable (Patel et al., 2017).

Exercise-Induced Oxygen Environment Variation in Cardiomyocytes

At rest, the total volume of ejected blood is $\sim 7,200$ L per day, which requires the heart to pump $\sim 100,000$ times and consume ~ 10 – 20% of the body's oxygen. To maintain this amount of work, the heart depends on high capillary density ($\sim 3,500$ capillaries per mm^2), continuous blood flow (~ 250 mL min^{-1}), and fatty acid oxidation (supplying 40–70% of cardiac ATP) (Laughlin and Tomanek, 1987; Duncker and Bache, 2008). As the most essential physiological stimulus, exercise increases myocardial contractility and oxygen consumption 3– $10 \times$ that of resting rates (Lopaschuk et al., 2010; Olver et al., 2015). To meet the elevated oxygen demand during exercise, myocardial blood perfusion increases from 0.8 $\text{mL/g} \cdot \text{min}$ at rest to 3.2 $\text{mL/g} \cdot \text{min}$ at peak exercise, improving overall oxygen supply (Gielen and Hambrecht, 2001; Duncker and Bache, 2008). Compared to untrained individuals, exercise leads to an approximate 20–100% increase in left ventricle mass (Kozakova et al., 2000; Zandrin et al., 2000). As exercise-induced cardiac mass increases, matched angiogenesis should occur so that capillary density is maintained in an effort to satisfy the new cardiomyocyte oxygen and nutrient demands. The capillary-myocyte ratio is used to determine capillary density in the heart. It has been demonstrated that the capillary density in dogs (Wyatt and Mitchell, 1978; Laughlin and Tomanek, 1987) and swine (Breisch et al., 1986) does not show an upward trend after exercise. In swine, although the division of coronary artery endothelial cells and the sprouting of capillaries increases at 1, 3, and 8 weeks, this alteration disappears after long-term exercise intervention (i.e., 16 weeks) and displays no difference from a sedentary group (White et al., 1998). This could mean that ventricle and capillary growth occur at different rates. Nevertheless, this mismatch between cardiomyocyte growth and capillary density increase may induce a mild hypoxic state in myocytes during and after exercise.



As the mediator of physiological and pathophysiological responses to hypoxia, HIF-1 α might be an essential indicator of the exercise-induced oxygen environment in the myocardium (Table 1). After 8 weeks of treadmill running, HIF-1 α mRNA expression increases in adult mice. Moreover, the upregulation of HIF-1 α also increases glucose transporter 1 (GLUT1) and lactate dehydrogenase A (LDHA) expression, which are related to significant metabolic adjustment in the myocardium (Vujic et al., 2018). A recent study indicated that mild-intensity exercise has a more significant effect on the increase of HIF-1 α upregulation than moderate- and high-intensity exercise (Bellafiore et al., 2019). Both dynamic and static exercise can increase the expression of HIF-1 α in cardiac tissue. Static exercise has a more substantial effect on upregulating HIF-1 α expression, as glycolysis is its primary energy supply (Flora et al., 2012). Under pathological conditions, 8 weeks of treadmill running could significantly increase the expression of HIF-1 α and vascular endothelial growth factor (VEGF) in transverse aortic constriction mice (Tian et al., 2020). Additionally, 4 weeks of HIIT consisting of running exercise also increased HIF-1 α content in the cardiac tissue of hypertensive rats (Holloway et al., 2015). However, other studies have suggested that HIF-1 α content decreases in response to exercise training (Pinho et al., 2012), or remains unchanged (Sylviana et al., 2018). These discrepancies might be due to model-specific factors, such as the program of exercise and animal strain. Taken together, these findings suggest that the relationship between HIF-1 α and cardiomyocyte regeneration within the exercise context is ambiguous. Further studies are needed to probe the specific effects of HIF-1 α under exercise-induced alteration of the oxygen environment.

Exercise-Induced Cardiac Energy Metabolism Changes in Cardiomyocytes

During exercise, more factors regulate cardiac energy metabolism. First, the increased local and circulating catecholamines (i.e., epinephrine and norepinephrine) elevate heart rate and myocardial contractility. Meanwhile, alterations in cardiac workload (specifically preload and afterload) augment changes to substrate metabolism in the heart, increasing energy demand (Taegtmeyer et al., 2016a; Gibb and Hill, 2018). Studies utilizing *in vitro* perfused hearts have reported that enhancement in workload is enough to increase cardiac carbohydrate and fatty acid catabolism (Goodwin et al., 1998; Goodwin and Taegtmeyer, 2000; Zhou et al., 2008). Additionally, Riehle et al. (2014) have suggested that 5 weeks of swim training significantly increases glycolysis, glucose oxidation, and fatty acid oxidation in isolated mice heart perfusions. Utilizing *in vivo* experiments, Bergman et al. (2009a,b) found that atrial pacing-induced the myocardium to utilize more fatty acids, glucose, and lactate to meet energy demand without affecting circulating substrates during increased heart workload. Epinephrine increases glucose catabolism partly through the activation of phosphofructokinase in hearts experiencing an elevated workload (Clark and Patten, 1981).

One more thing, oxidation of fatty acids is the main source of ATP production in the heart (Taegtmeyer et al., 2016a,b;

Gibb and Hill, 2018). During exercise, catecholamine-activated lipolysis in adipose tissue elevates circulating free fatty acid (FFA) levels to 2.4 mmol/L. Fat oxidation then increases FFA uptake and utilization efficiency. The effects of exercise on fatty acid oxidation are inconsistent, including reports that it is increased (Burelle et al., 2004; Riehle et al., 2014), decreased (Hafstad et al., 2011), or unaffected (Gibb et al., 2017). After 10 weeks of HIIT, fatty acid oxidation decreased, while glucose oxidation increased in the myocardium of mice, which contributed to a maximal 12% decrease in myocardial oxygen consumption (Hafstad et al., 2011). The dissipation of myocardial oxygen is primarily due to increased mitochondrial uncoupling, induced by either fatty acid oxidation (Himms-Hagen and Harper, 2001) or ROS (Echtay et al., 2002).

Interestingly, the heart can also easily consume excess circulating lactate (up to 10 mmol/L) that is produced by muscular glycolytic activity during intense exercise (Lassers et al., 1972; Brooks, 2009). Lactate use is nearly 40% of ATP production during exercise (Schonekess, 1997). Even relatively low-intensity exercise can elevate lactate oxidation (Gertz et al., 1988), which may also promote fat oxidation to produce ATP under high workloads in the heart (Goodwin and Taegtmeyer, 2000).

Likewise, the specific type of strenuous exercise (like resistance exercise and long-term endurance exercise) lowers blood glucose levels (Coyle, 2000), while high-intensity aerobic exercise may increase blood glucose levels (Kemppainen et al., 2002). Similarly, myocardial glucose uptake and oxidation display the same trend as detected in human studies during exercise (Gertz et al., 1988; Kemppainen et al., 2002). These findings revealed that exercise displayed diverse effects on circulating glucose levels, and myocardial glucose utilization relied on the type, intensity, and duration of exercise. Epinephrine increases glucose catabolism partly through the activation of phosphofructokinase (Clark and Patten, 1981). Gibb et al. (2017) indicated that 4 weeks of treadmill running decreased glucose utilization via glycolysis during exercise and the early recovery period after exercise in mice. However, upon adaptation and full recovery, steady-state glycolysis rates appear to be increased in the heart (Gibb et al., 2017). This study also indicated that kinase-deficient 6-phosphofructokinase/fructose-2,6-bisphosphatase transgenic (Glyco^{Lo}) mice appear to regulate genes sufficiently (e.g., C/EBP β and CITED4) (Bostrom et al., 2010; Bezzerides et al., 2016) partially related to exercise-induced cardiac growth (Gibb et al., 2017). The above results show that alterations in glycolysis caused by exercise are essential regulators of the cardiac growth process.

Furthermore, the adaptation to exercise is also regulated by hormones, like insulin-like growth factor 1 (IGF-1) (Kim et al., 2008) and neuregulin 1 (Waring et al., 2014; Cai et al., 2016), which are increased during exercise adaptation and likely promote glucose uptake and utilization. Metabolic alteration induced by these hormones is partially mediated by Akt (Pozuelo Rubio et al., 2003), which may increase glycolysis by activation of the myocardial form of 6-phosphofructokinase/fructose-2,6-bisphosphatase (PFK2) (Deprez et al., 1997; Mouton et al., 2010). Akt is an essential regulator of exercise-induced cardiomyocyte regeneration and plays a cardioprotective role through the

TABLE 1 | Factors related to oxygen mechanisms involved in exercise-induced cardiomyocyte regeneration.

| Classification | Factor | Species | Exercise model | Duration | Observation | References |
|--------------------------|----------------------------|---------|--|---------------------------------|--|------------------------|
| Oxygen environment | HIF-1 α | Mice | Running exercise: voluntarily running. | 8 weeks 5 days/week | HIF-1 α \uparrow ; New cardiomyocytes in adult mice \uparrow | Vujic et al., 2018 |
| | HIF-1 α | Mice | Running exercise: rotating treadmill, training intensity performed by 15, 30, and 45 days corresponded to a mild, moderate, and high intensity, respectively. | 15, 30, and 45 days 5 days/week | HIF-1 α \uparrow | Bellafore et al., 2019 |
| | HIF-1 α | Mice | Running exercise: ramp protocol increased from 11 m/min for 30 min/day to 13 m/min for 60 min/day. | 8 weeks 5 days/week | HIF-1 α and VEGF \uparrow | Tian et al., 2020 |
| | HIF-1 α | Rat | Running exercise: 20 m/min at a 10° incline, the session lasted 8 min in week1, 15 min in week 2, and 23 min in weeks 3 and 4. | 4 weeks 5 days/week | HIF-1 α \uparrow | Holloway et al., 2015 |
| | HIF-1 α | Rat | Running exercise: aerobic exercise protocol is 20 m/min for 30 min/day, anaerobic exercise protocol is 35 m/min for 20 min/day. | 1, 3, 7, and 10 days | HIF-1 α and VEGF \uparrow ; | Flora et al., 2012 |
| Energy metabolism | Glycolysis | Mice | Swimming exercise: ramp protocol increased from 10 min/day to two 90-min sessions, twice/day, the sessions were separated by at least a 4-h interval | 4 weeks 5 days/week | Glycolysis rate \uparrow | Riehle et al., 2014 |
| | Glycolysis | Mice | Running exercise: 22.3 m/min at a 10° incline, the session lasted 40 min in week 1, 50 min in week 2, and 60 min in weeks 3 and 4. | 4 weeks 5 days/week | Glycolysis decreased during exercise, but steady-state rates of glycolysis increased in the early and full recovery period after exercise. | Gibb et al., 2017 |
| | Fatty acid oxidation | Mice | Running exercise: consisted of 10 bouts of 4 min high intensity training, corresponding to 85–90% VO_{2max} , interspersed by 2 min active rest, speed gradually from 16 to 26 m/min | 10 weeks 5 days/week | Fatty acid oxidation \downarrow | Hafstad et al., 2011 |
| Mitochondrial biogenesis | ROS | Rat | Running exercise: 25 m/min at a 6° incline, the session lasted 40 min in week 1, 50 min in week 2, and 60 min in weeks 3 and 4. | 16 weeks 5 days/week | ROS production \downarrow | Starnes et al., 2007 |
| | ROS | Rat | Running exercise: endurance training ramp protocol increased from 10 m/min for 30 min/day up to 15 m/min for 60 min/day | 5 weeks 6 days/week | ROS production \downarrow ; ROS elimination \uparrow | Bo et al., 2008 |
| | AMPK/PGC-1 α | Mice | Running exercise: endurance training 1.0 km/h for 60 min/day | 16 weeks 5 days/week | AMPK/PGC-1 α signal transduction \uparrow | Wang et al., 2020 |
| | Sirt1/PGC-1 α | Rat | Running exercise: endurance training ramp protocol increased from 4.2 m/min up to 12 m/min for 30 min/day | 36 weeks 4-5 days/week | Sirt1 and PGC-1 α \uparrow | Bayod et al., 2012 |
| | Sirt1/PGC-1 α /PI3K | Rat | Running exercise: ramp protocol increased from 10 m/min for 30 min/day increased to 16 m/min and 60 min/day | 4 weeks 7 days/week | Sirt 1/PGC-1 α /PI3K signaling transduction \uparrow ; oxidative stress \downarrow | Jia et al., 2019 |
| | PGC-1 α | Mice | Swimming exercise: moderate intensity lasted 30 min/day. | 4 weeks 5 days/week | PGC-1 α \uparrow | Sylviana et al., 2018 |

AMPK, adenosine monophosphate-activated protein kinase; HIF-1 α , hypoxia-inducible factor 1 α ; PGC-1 α , peroxisome proliferator-activated receptor- γ coactivator 1 α ; PI3K, phosphoinositide 3-kinase; ROS, reactive oxygen species; Sirt1, NAD-dependent deacetylase sirtuin1; VEGF, vascular endothelial growth factor; VO_{2max} , maximum volume of oxygen consumption. \uparrow , upregulation; \downarrow , downregulation.

up-regulation of the glucose transporter 4 (GLUT4) during ischemia-reperfusion (IR) injury (Wang et al., 2015).

Collectively, the metabolic adaptations that occur in the heart in response to exercise have yet to be elucidated. Research on the effects of exercise-induced myocardial energy metabolism primarily depends on data acquired from gene expression analysis or enzymatic activity assays. Moreover, discrepancies in different studies may be due to different exercise models, animal strains, or tissue acquisition protocols. There is still a lack of research on the relationship between the metabolic changes caused by exercise and the activation of adaptive programs in the regeneration of cardiomyocytes. Additionally, the importance of substrate metabolism, intermediates, or final products for exercise-induced heart regeneration remains unclear. Therefore, careful design of exercise training plans is required.

Exercise Modulates Oxidative Stress in Cardiomyocytes

The mechanisms of exercise-induced oxygen reduction and oxygen metabolism alteration also include increased myocardial antioxidant capacity, decreased ROS accumulation, and thus, diminished ROS-induced mitochondrial uncoupling (Starnes et al., 2007; Bo et al., 2008). Starnes et al. (2007) found that ROS production decreased in rat myocardial mitochondria after 16 weeks of treadmill running. Bo et al. (2008) found that 6 weeks treadmill running could promote mitochondrial efficiency of oxidative phosphorylation through a decrease in ROS production and an increase in ROS elimination in rat hearts. Both short-term (10 days of treadmill training) (Hyatt et al., 2016) and long-term regular exercise (Radak et al., 2013; Ghiasi et al., 2015) can increase antioxidant enzymes and enhance oxidative stress resistance in the heart. Even 6 weeks of voluntary running with uneven exercise intensity can reduce oxidative stress in diabetic rats (Naderi et al., 2015; Chodari et al., 2019).

Further, decreases in oxidative stress and ROS production have also been detected in mice with diabetic cardiomyopathy following 16 weeks of running exercise (Wang et al., 2020). Moreover, 8 weeks of resistance exercise (Effting et al., 2019) or swim training (de Farias et al., 2013) can modulate redox imbalance and reduce oxidative damage in the myocardium in mice with diet-induced obesity. Exercise elevates the protein expression of several mitochondrial antioxidant enzymes, including superoxide dismutase 1 (SOD1) and superoxide dismutase 2 (SOD2), as well as the H_2O_2 removing enzymes glutathione peroxidase-1 and catalase. Thus, the exercise-induced reinforcement of antioxidant enzymes has a positive effect on the promotion of ROS elimination in myocardial mitochondria (Judge et al., 2005). However, whether the enhancement of ROS elimination and increased antioxidant levels induced by exercise in the myocardium can facilitate a reduction of oxidative DNA damage and activation of cardiomyocyte regeneration require further confirmation.

Numerous studies reveal that exercise training protects cardiac function through induced alterations in mitochondrial phenotype and biogenesis (Lee et al., 2012; Powers et al., 2014; Tao et al., 2015; Trewin et al., 2018; Boulghobra et al.,

2020), which is beneficial to exercise-induced cardiomyocyte regeneration. Exercise-associated changes in the redox milieu regulate several factors of mitochondrial biogenesis, such as adenosine monophosphate-activated protein kinase (AMPK), Sirtuins 1 (Sirt1), peroxisome proliferator-activated receptor- γ coactivator 1 α (PGC-1 α), and mitogen-activated protein kinase (MAPK). In hearts undergoing exercise training, ATP is consumed rapidly to upregulate the AMP/ATP ratio and increase the activity of AMPK, which induces a series of phosphorylation-dependent modification cascades of factors like PGC-1 α (Hardie et al., 2006). The activity of cardiac AMPK increases progressively with exercise intensity during treadmill running (Coven et al., 2003). Additionally, AMPK promotes translocation of GLUT4 to the cardiomyocyte membrane, which induces the upregulation of PFK2 and downstream fructose 2,6-bisphosphate to increase glycolysis (Marsin et al., 2000). After swim training, decreases in ROS production and an increase in antioxidative enzyme expression can be detected through the activation of AMPK in rat hearts (Ma et al., 2015; Wang et al., 2016). Sirt1 is a NAD^+ -dependent enzyme that regulates cardiomyocyte energy and functions through enhancing deacetylase activity (Bugger et al., 2016). Since Sirt1 relies on the NAD^+ /NADH ratio, it is sensitive to alterations induced by exercise in cardiomyocytes, such as cellular energy metabolism and redox status. The overexpression of Sirt1 can promote cardiomyocyte proliferation, with cardiac regeneration being demonstrated in both *in vivo* and *in vitro* studies (Li B. et al., 2018; Li et al., 2019). HIIT has been shown to upregulate the Sirt1 mRNA expression in diabetic rats and has been found to be more effective than continuous exercise training (Khakdan et al., 2018). Long-term running dramatically increases Sirt1 and PGC-1 α protein expression in the rat heart (Bayod et al., 2012). PGC-1 α is essential for mitochondrial density increment to ameliorate the efficiency of ATP production by reducing mitochondrial respiration in cardiomyocyte after exercise training (Watson et al., 2007; Wang et al., 2020). The concentration of PGC-1 α is upregulated in the myocardium of mice by swimming (Sylviana et al., 2018) and running (Li et al., 2011) exercises. The promotion of AMPK/PGC-1 α signal transduction induced by treadmill running is related to decreased ROS accumulation in the rat myocardium (Wang et al., 2020). The interconnecting role of AMPK-Sirt1 and PGC-1 α plays a regulatory role in cardiomyocyte mitochondria metabolism. For instance, 4 weeks of running training has been shown to promote the activity of the Sirt1/PGC-1 α /phosphatidylinositol three phosphate kinase (PI3K)/Akt signaling pathway in MI rat cardiomyocytes (Jia et al., 2019). Moreover, exercise can improve mitochondrial biogenesis, prevent diabetic cardiomyopathy-associated inhibition of PGC-1 α , and activate Akt signaling in mice with diabetic cardiomyopathy (Wang et al., 2015).

Although the positive role of exercise in regulating decreases in ROS accumulation, increases in antioxidative capacity, and promotion of mitochondrial biogenesis in cardiomyocytes is definite, possible molecular mechanisms remain controversial. However, clarifying the specific relationship between modulation of exercise in oxidative stress and regeneration in cardiomyocytes

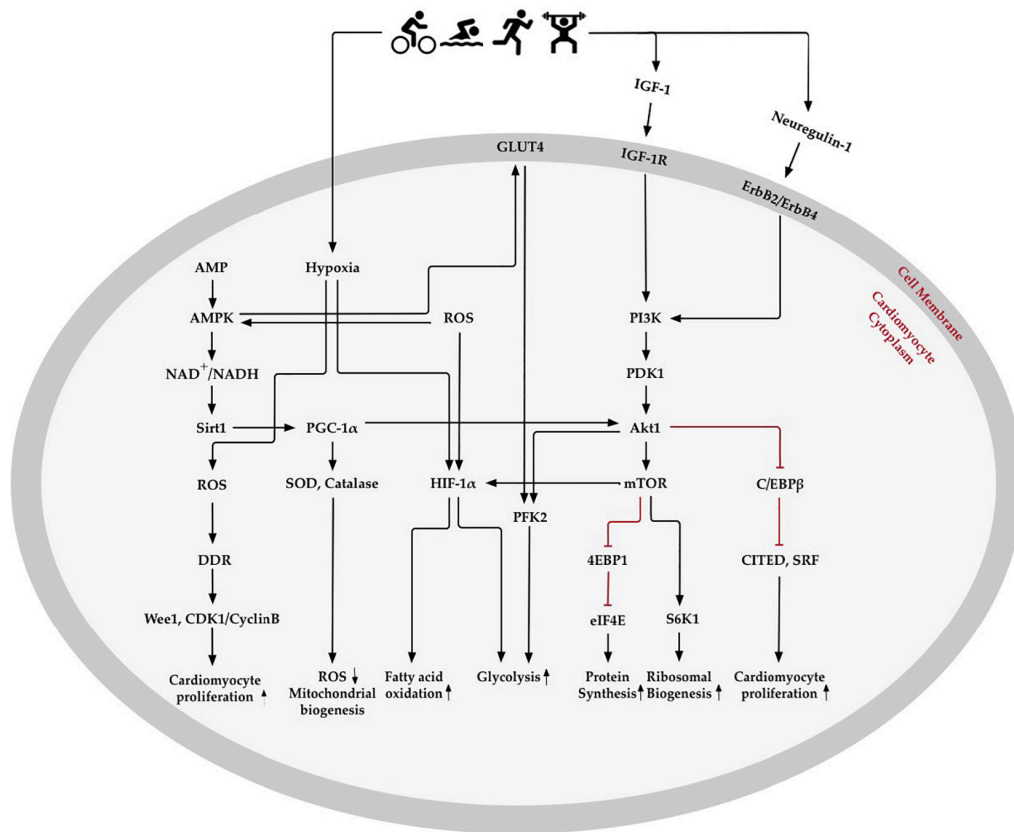


FIGURE 3 | Oxygen metabolism-related pathways in exercise-induced cardiomyocyte regeneration. Exercise stimulates physiological signaling pathways, such as those involved in creating mild hypoxia, changes in fatty acid and glycolysis metabolism, elimination of reactive oxygen species (ROS), enhancement of antioxidative capacity, and regulation of the oxygen metabolic molecular pathway in the heart. AMP-activated protein kinase (AMPK) enhances mitochondrial biogenesis and energy metabolism through Sirtuin1 (Sirt1) and peroxisome proliferator-activated receptor- γ coactivator 1 α (PGC-1 α), which increase antioxidative enzymes to promote ROS elimination and mitochondrial biogenesis. Exercise-induced hypoxia and increase in ROS content promotes hypoxia-inducible factors 1 α (HIF-1 α) expression, which decreases fatty acid oxidation and increases glycolysis. Insulin-like growth factor 1 (IGF-1) and neuregulin-1 activate phosphoinositide 3-kinase (PI3K) and downstream Akt signaling pathways. Akt activates 4EBP1 and S6K1, downstream of the mechanistic target of rapamycin (mTOR), which may promote protein and ribosomal synthesis. Akt, RAC- α serine/threonine-protein kinase; CDK1, cyclin dependent kinase 1; C/EBP β , CCAAT/enhancer binding protein- β ; CITED4, CBP/p300-interacting transactivator 4; DDR, DNA damage response; eIF4E, translation initiation factor eIF4E; GLUT4, glucose transporter 4; IGF-1R, IGF-1 receptor; PDK1, phosphoinositide-dependent protein kinase-1; PFK2, 6-phosphofructokinase/fructose-2,6-bisphosphatase; S6K1, ribosomal protein S6 kinase- β ; SOD, superoxide dismutase; SRF, serum response factor.

is complicated, due to the variety of exercise models and physiological conditions.

OXYGEN METABOLISM RELATED MOLECULAR CHANGES IN EXERCISE-INDUCED CARDIOMYOCYTE REGENERATION

The changes of oxygen metabolism might activate and interact with extracellular and intracellular signaling pathways to promote cardiomyocyte regeneration (**Figure 3**) (Bo et al., 2020). Exercise-induced cardiac growth is mediated mostly through increased insulin growth factor-1 (IGF-1) signaling in the hearts of athletes (Sereneri et al., 1999). The beneficial paracrine effect of IGF-1 in the heart acts via a downstream signaling

pathway by reducing ROS generation and oxidative DNA damage (Kajstura et al., 2001; Yang et al., 2005). Results from transgenic mice models show that the IGF-1-PI3K-Akt1 axis is critical to mediate exercise-induced cardiomyocyte regeneration (DeBosch et al., 2006; Medeiros et al., 2011; Ma et al., 2013; Palabiyik et al., 2019). For example, improved physiological growth of the heart can be induced by overexpression of the PI3K (p110 α) in mice (McMullen et al., 2004), while the physiological hypertrophy of heart is unable to be detected in dominant-negative PI3K (p110 α) transgenic mice (McMullen et al., 2003). Akt1 is a serine/threonine-protein kinase to regulate cell cycle through extending the half-life of cyclin D (Jia et al., 2008; Parekh et al., 2011). The activation of Akt1 and downstream effectors of mTOR, including S6K 1 and 4EBP1, are considered to be essential for modulating cardiac growth by regulating protein biosynthesis (Shiojima and Walsh, 2006). Moreover, swimming exercise increased the

activity of the PIK3/Akt1/mTOR signaling pathway in rats after 8 weeks of training (Ma et al., 2013; Palabiyik et al., 2019). Endurance exercise reduced C/EBP β expression, which was activated by upstream of Akt1 and PGC-1. The downregulation of C/EBP β promoted cardiomyocyte proliferation through negative regulation of CITED4 (Bostrom et al., 2010).

The neuregulin-1/ErbB2/ErbB4 pathway is another critical signaling pathway that changes in response to physical exercise and can stimulate the intracellular Akt signaling pathway by binding to the receptor on the cardiomyocyte membrane. The specific function of neuregulin-1 is to induce differentiated cardiomyocytes to reenter the cell cycle from S phase and experience both karyokinesis and cytokinesis, leading to cardiomyocyte proliferation in adult cardiomyocytes (D'Uva et al., 2015). Both low (55–60% of individual VO_{2max}) or high (85–90% of individual VO_{2max}) intensity of running can increase the number of newly formed cardiomyocytes through upregulated neuregulin-1 expression on rat hearts (Waring et al., 2014). It has been further demonstrated that 5 weeks of running exercise can increase neuregulin-1 expression and stimulate the downstream ErbB2, ErbB4, and PI3K/Akt signaling pathways to activate endogenous cardiac regeneration in MI rats (Cai et al., 2016).

CAN EXERCISE INDUCE CARDIAC REGENERATION THROUGH OXYGEN METABOLISM IN HUMANS?

Notably, alteration of oxygen environment and oxygen metabolism in the myocardium can trigger cardiomyocyte regeneration in the adult heart, especially when the environment becomes hypoxic (Puente et al., 2014; Nakada et al., 2017). Despite the lack of evidence that hypoxia induces cardiac regeneration in humans, hypoxic treatment may provide an entirely new therapeutic direction. For example, 3 weeks of passive intermittent short-term (3–5 min) hypoxia exposure (fraction of oxygen 10–21%) increased aerobic capacity and exercise tolerance in older men with and without coronary artery disease (Burtcher et al., 2004). Hypoxic therapy (inhaled oxygen concentration fraction 10–21%) will also lead to lower surgical risks compared with tissue regeneration *in vitro* and putative cardiac transplantation. Data suggests that the oxygen concentration that can activate cardiomyocyte regeneration is extremely low (7% air-saturation) (Kimura et al., 2017). This degree of hypoxia is equivalent to the oxygen concentration at the summit of Mount Everest (8,848 m). However, before the administration of hypoxic therapy, the “scean” effect of extreme hypoxia, which might bring fatal complications to organs like the brain and kidneys, should be considered. Under the regulation of neurohumoral factors, exercise can redistribute blood and oxygen throughout the body. As elucidated above, a mildly hypoxic environment and the reduction of oxidative damage induced by exercise in the myocardium can safely activate and promote cardiomyocyte regeneration.

SUMMARY AND FUTURE PERSPECTIVE

Collectively, exercise, as an intensity stimulation, can alter the oxygen environment and oxygen metabolism in the myocardium, including creating a mildly hypoxic environment, changing energy metabolism, promoting ROS elimination, enhancing antioxidative capacity, and regulating oxygen metabolic molecular pathway in the heart. According to the studies discussed above, these exercise-induced alterations have a significant positive effect on the activation and promotion of cardiomyocyte regeneration. A full determination of the regulatory role of oxygen metabolism and related factors during and after exercise in cardiomyocyte regeneration will provide biological insight into endogenous cardiac repair mechanisms.

However, the potential molecular mechanisms are not so much clear regarding the interactions between environmental oxygen-dependent metabolic switch in cardiomyocytes and exercise training. The future studies in the oxygen metabolism of exercise-induced cardiomyocyte regeneration require systematic and specific exercise models in extensive animal studies to clarify the molecular pathway, and to evaluate the efficacy of exercise. In particular, upstream signaling pathways, transcription factors, epigenetic modifiers, and mitochondrial function of cardiomyocyte involved in regulating the metabolic shift from a non-proliferative state to a regenerative state in the context of exercise, are essential research directions. Moreover, the effects of exercise depend on the type (aerobic/resistance), intensity (mild/moderate/intense/exhaustive), frequency (sessions per day/week/month), and subject characteristics (age, sex, endurance capacity, and health condition). Further work needs to address all these issues, providing a foundation for exercise as a cost-effective intervention to promote cardiomyocyte regeneration and restore cardiac function in clinical treatment.

AUTHOR CONTRIBUTIONS

BB conceived of the study, collected the data and material, and wrote the manuscript. SL helped collect and analyze the data and draft the manuscript. KZ helped draft the manuscript. JW helped conceive of the study, and revise the manuscript. All authors gave final approval for publication.

FUNDING

This study was supported by the National Natural Science Foundation of China grant 81271410 (JW), the Henan Science and Technology Development Project grants 182300410313 and 192102310023 (JW and BB), and the Science and Technology Key Project, Department of Education of Henan grant 19A890001 (BB).

REFERENCES

- Adam-Vizi, V., and Chinopoulos, C. (2006). Bioenergetics and the formation of mitochondrial reactive oxygen species. *Trends Pharmacol. Sci.* 27, 639–645. doi: 10.1016/j.tips.2006.10.005
- Andersen, D. C., Jensen, C. H., Baun, C., Hvidsten, S., Zebrowski, D. C., Engel, F. B., et al. (2016). Persistent scarring and dilated cardiomyopathy suggest incomplete regeneration of the apex resected neonatal mouse myocardium—A 180 days follow up study. *J. Mol. Cell. Cardiol.* 90, 47–52. doi: 10.1016/j.jmcc.2015.11.031
- Bayod, S., Del Valle, J., Lalanza, J. F., Sanchez-Roige, S., de Luxan-Delgado, B., Coto-Montes, A., et al. (2012). Long-term physical exercise induces changes in sirtuin 1 pathway and oxidative parameters in adult rat tissues. *Exp. Gerontol.* 47, 925–935. doi: 10.1016/j.exger.2012.08.004
- Belanger, A. J., Luo, Z., Vincent, K. A., Akita, G. Y., Cheng, S. H., Gregory, R. J., et al. (2007). Hypoxia-inducible factor 1 mediates hypoxia-induced cardiomyocyte lipid accumulation by reducing the DNA binding activity of peroxisome proliferator-activated receptor alpha/retinoid X receptor. *Biochem. Biophys. Res. Commun.* 364, 567–572. doi: 10.1016/j.bbrc.2007.10.062
- Bellafiore, M., Battaglia, G., Bianco, A., and Palma, A. (2019). Expression pattern of angiogenic factors in healthy heart in response to physical exercise intensity. *Front. Physiol.* 10:238. doi: 10.3389/fphys.2019.00238
- Benjamin, E. J., Muntner, P., Alonso, A., Bittencourt, M. S., Callaway, C. W., Carson, A. P., et al. (2019). Heart disease and stroke statistics-2019 update: a report from the American heart association. *Circulation* 139, e56–e528. doi: 10.1161/CIR.0000000000000659
- Bergman, B. C., Tsvetkova, T., Lowes, B., and Wolfel, E. E. (2009a). Myocardial FFA metabolism during rest and atrial pacing in humans. *Am. J. Physiol. Endocrinol. Metab.* 296, E358–E366. doi: 10.1152/ajpendo.90747.2008
- Bergman, B. C., Tsvetkova, T., Lowes, B., and Wolfel, E. E. (2009b). Myocardial glucose and lactate metabolism during rest and atrial pacing in humans. *J. Physiol.* 587(Pt 9), 2087–2099. doi: 10.1113/jphysiol.2008.168286
- Bergmann, O., Bhardwaj, R. D., Bernard, S., Zdunek, S., Barnabe-Heider, F., Walsh, S., et al. (2009). Evidence for cardiomyocyte renewal in humans. *Science* 324, 98–102. doi: 10.1126/science.1164680
- Bergmann, O., Zdunek, S., Felker, A., Salehpour, M., Alkass, K., Bernard, S., et al. (2015). Dynamics of cell generation and turnover in the human heart. *Cell* 161, 1566–1575. doi: 10.1016/j.cell.2015.05.026
- Bezzarides, V. J., Platt, C., Lerchenmuller, C., Paruchuri, K., Oh, N. L., Xiao, C., et al. (2016). CITED4 induces physiologic hypertrophy and promotes functional recovery after ischemic injury. *JCI Insight* 1:e85904. doi: 10.1172/jci.insight.85904
- Bicknell, K. A., Coxon, C. H., and Brooks, G. (2004). Forced expression of the cyclin B1-CDC2 complex induces proliferation in adult rat cardiomyocytes. *Biochem. J.* 382(Pt 2), 411–416. doi: 10.1042/BJ20031481
- Bo, B., Zhou, Y., Zheng, Q., Wang, G., Zhou, K., and Wei, J. (2020). The molecular mechanisms associated with aerobic exercise-induced cardiac regeneration. *Biomolecules* 11:19. doi: 10.3390/biom11010019
- Bo, H., Jiang, N., Ma, G., Qu, J., Zhang, G., Cao, D., et al. (2008). Regulation of mitochondrial uncoupling respiration during exercise in rat heart: role of reactive oxygen species (ROS) and uncoupling protein 2. *Free Radic. Biol. Med.* 44, 1373–1381. doi: 10.1016/j.freeradbiomed.2007.12.033
- Bon-Mathier, A.-C., Rignault-Clerc, S., Biellmann, C., and Rosenblatt-Velin, N. (2019). Oxygen as a key regulator of cardiomyocyte proliferation: new results about cell culture conditions! *Biochim. Biophys. Acta Mol. Cell Res.* 1867:118460. doi: 10.1016/j.bbamcr.2019.03.007
- Bostrom, P., Mann, N., Wu, J., Quintero, P. A., Plovie, E. R., Panakova, D., et al. (2010). C/EBPbeta controls exercise-induced cardiac growth and protects against pathological cardiac remodeling. *Cell* 143, 1072–1083. doi: 10.1016/j.cell.2010.11.036
- Boulghobra, D., Coste, F., Geny, B., and Reboul, C. (2020). Exercise training protects the heart against ischemia-reperfusion injury: a central role for mitochondria? *Free Radic. Biol. Med.* 152, 395–410. doi: 10.1016/j.freeradbiomed.2020.04.005
- Breckenridge, R. A., Piotrowska, I., Ng, K. E., Ragan, T. J., West, J. A., Kotecha, S., et al. (2013). Hypoxic regulation of hand1 controls the fetal-neonatal switch in cardiac metabolism. *PLoS Biol.* 11:e1001666. doi: 10.1371/journal.pbio.1001666
- Breisch, E. A., White, F. C., Nimmo, L. E., McKirnan, M. D., and Bloor, C. M. (1986). Exercise-induced cardiac hypertrophy: a correlation of blood flow and microvasculature. *J. Appl. Physiol.* (1985) 60, 1259–1267. doi: 10.1152/jappl.1986.60.4.1259
- Brooks, G. A. (2009). Cell-cell and intracellular lactate shuttles. *J. Physiol.* 587(Pt 23), 5591–5600. doi: 10.1113/jphysiol.2009.178350
- Bugger, H., Witt, C. N., and Bode, C. (2016). Mitochondrial sirtuins in the heart. *Heart Fail. Rev.* 21, 519–528. doi: 10.1007/s10741-016-9570-7
- Burelle, Y., Wambolt, R. B., Grist, M., Parsons, H. L., Chow, J. C., Antler, C., et al. (2004). Regular exercise is associated with a protective metabolic phenotype in the rat heart. *Am. J. Physiol. Heart Circ. Physiol.* 287, H1055–H1063. doi: 10.1152/ajpheart.00925.2003
- Burtscher, M., Pachinger, O., Ehrenbourg, I., Mitterbauer, G., Faulhaber, M., Puhlinger, R., et al. (2004). Intermittent hypoxia increases exercise tolerance in elderly men with and without coronary artery disease. *Int. J. Cardiol.* 96, 247–254. doi: 10.1016/j.ijcard.2003.07.021
- Cai, M. X., Shi, X. C., Chen, T., Tan, Z. N., Lin, Q. Q., Du, S. J., et al. (2016). Exercise training activates neuregulin 1/ErbB signaling and promotes cardiac repair in a rat myocardial infarction model. *Life Sci.* 149, 1–9. doi: 10.1016/j.lfs.2016.02.055
- Cao, T., Liccardo, D., LaCanna, R., Zhang, X., Lu, R., Finck, B. N., et al. (2019). Fatty acid oxidation promotes cardiomyocyte proliferation rate but does not change cardiomyocyte number in infant mice. *Front. Cell Dev. Biol.* 7:42. doi: 10.3389/fcell.2019.00042
- Cardoso, A. C., Lam, N. T., Savla, J. J., Nakada, Y., Pereira, A. H. M., Elnwasany, A., et al. (2020). Mitochondrial substrate utilization regulates cardiomyocyte cell cycle progression. *Nat. Metab.* 2, 167–178.
- Carley, A. N., Taegtmeier, H., and Lewandowski, E. D. (2014). Matrix revisited: mechanisms linking energy substrate metabolism to the function of the heart. *Circ. Res.* 114, 717–729. doi: 10.1161/CIRCRESAHA.114.301863
- Chablais, F., and Jazwinska, A. (2012). The regenerative capacity of the zebrafish heart is dependent on TGFbeta signaling. *Development* 139, 1921–1930. doi: 10.1242/dev.078543
- Chodari, L., Smailnejad, S., Fallahi, M., Khalaji, N., and Ghorbanzadeh, V. (2019). Oxidative stress is markedly reduced by combined voluntary exercise and testosterone in the heart of diabetic rats. *Acta Endocrinol. (Buchar)* 15, 173–181. doi: 10.4183/aeb.2019.173
- Cimen, B., Uz, A., Cetin, I., Cimen, L., and Cetin, A. (2017). Melatonin supplementation ameliorates energy charge and oxidative stress induced by acute exercise in rat heart tissue. *Acta Cardiol. Sin.* 33, 530–538. doi: 10.6515/acs20170331a
- Clark, M. G., and Patten, G. S. (1981). Epinephrine activation of phosphofructokinase in perfused rat heart independent of changes in effector concentrations. *J. Biol. Chem.* 256, 27–30.
- Cole, M. A., Abd Jamil, A. H., Heather, L. C., Murray, A. J., Sutton, E. R., Slingo, M., et al. (2016). On the pivotal role of PPARalpha in adaptation of the heart to hypoxia and why fat in the diet increases hypoxic injury. *FASEB J.* 30, 2684–2697. doi: 10.1096/fj.201500094R
- Coven, D. L., Hu, X., Cong, L., Bergeron, R., Shulman, G. I., Hardie, D. G., et al. (2003). Physiological role of AMP-activated protein kinase in the heart: graded activation during exercise. *Am. J. Physiol. Endocrinol. Metab.* 285, E629–E636. doi: 10.1152/ajpendo.00171.2003
- Coyle, E. F. (2000). Physical activity as a metabolic stressor. *Am. J. Clin. Nutr.* 72(2 Suppl.), 512S–520S. doi: 10.1093/ajcn/72.2.512S
- Coyle, E. F., and Gonzalez-Alonso, J. (2001). Cardiovascular drift during prolonged exercise: new perspectives. *Exerc. Sport Sci. Rev.* 29, 88–92. doi: 10.1097/00003677-200104000-00009
- D'Uva, G., Aharonov, A., Lauriola, M., Kain, D., Yahalom-Ronen, Y., Carvalho, S., et al. (2015). ERBB2 triggers mammalian heart regeneration by promoting cardiomyocyte dedifferentiation and proliferation. *Nat. Cell Biol.* 17, 627–638. doi: 10.1038/ncb3149
- Daneshmand, Z., Garcia-Riera, M. P., Verdys, M., and Rossi, A. (2000). Differential responses to chronic hypoxia and dietary restriction of aerobic capacity and enzyme levels in the rat myocardium. *Mol. Cell Biochem.* 210, 159–166. doi: 10.1023/a:1007137909171
- Davila-Roman, V. G., Vedala, G., Herrero, P., de las Fuentes, L., Rogers, J. G., Kelly, D. P., et al. (2002). Altered myocardial fatty acid and glucose metabolism

- in idiopathic dilated cardiomyopathy. *J. Am. Coll. Cardiol.* 40, 271–277. doi: 10.1016/s0735-1097(02)01967-8
- de Farias, J. M., Bom, K. F., Tromm, C. B., Luciano, T. F., Marques, S. O., Tuon, T., et al. (2013). Effect of physical training on the adipose tissue of diet-induced obesity mice: interaction between reactive oxygen species and lipolysis. *Horm. Metab. Res.* 45, 190–196. doi: 10.1055/s-0032-1323740
- DeBosch, B., Treskov, I., Lupu, T. S., Weinheimer, C., Kovacs, A., Courtois, M., et al. (2006). Akt1 is required for physiological cardiac growth. *Circulation* 113, 2097–2104. doi: 10.1161/CIRCULATIONAHA.105.595231
- Deprez, J., Vertommen, D., Alessi, D. R., Hue, L., and Rider, M. H. (1997). Phosphorylation and activation of heart 6-phosphofructo-2-kinase by protein kinase B and other protein kinases of the insulin signaling cascades. *J. Biol. Chem.* 272, 17269–17275. doi: 10.1074/jbc.272.28.17269
- Djouadi, F., Brandt, J. M., Weinheimer, C. J., Leone, T. C., Gonzalez, F. J., and Kelly, D. P. (1999). The role of the peroxisome proliferator-activated receptor alpha (PPAR alpha) in the control of cardiac lipid metabolism. *Prostaglandins Leukot. Essent. Fatty Acids* 60, 339–343. doi: 10.1016/s0952-3278(99)80009-x
- Duncker, D. J., and Bache, R. J. (2008). Regulation of coronary blood flow during exercise. *Physiol. Rev.* 88, 1009–1086. doi: 10.1152/physrev.00045.2006
- Dunwoodie, S. L. (2009). The role of hypoxia in development of the Mammalian embryo. *Dev. Cell* 17, 755–773. doi: 10.1016/j.devcel.2009.11.008
- Echtay, K. S., Roussel, D., St-Pierre, J., Jekabsons, M. B., Cadenas, S., Stuart, J. A., et al. (2002). Superoxide activates mitochondrial uncoupling proteins. *Nature* 415, 96–99. doi: 10.1038/415096a
- Effting, P. S., Bresciani, S. M. S., Sorato, H. R., Fernandes, B. B., Fidelis, G., Silva, P., et al. (2019). Resistance exercise modulates oxidative stress parameters and TNF-alpha content in the heart of mice with diet-induced obesity. *Arq. Bras. Cardiol.* 112, 545–552. doi: 10.5935/abc.20190072
- Essop, M. F. (2007). Cardiac metabolic adaptations in response to chronic hypoxia. *J. Physiol.* 584(Pt 3), 715–726. doi: 10.1113/jphysiol.2007.143511
- Farooqi, K. M., Sutton, N., Weinstein, S., Menegus, M., Spindola-Franco, H., and Pass, R. H. (2012). Neonatal myocardial infarction: case report and review of the literature. *Congenit. Heart Dis.* 7, E97–E102. doi: 10.1111/j.1747-0803.2012.00660.x
- Flink, I. L. (2002). Cell cycle reentry of ventricular and atrial cardiomyocytes and cells within the epicardium following amputation of the ventricular apex in the axolotl, *Amblystoma mexicanum*: confocal microscopic immunofluorescent image analysis of bromodeoxyuridine-labeled nuclei. *Anat. Embryol. (Berl.)* 205, 235–244. doi: 10.1007/s00429-002-0249-6
- Flora, R., Freisleben, H.-J., Ferdinal, F., Wanandi, S. I., and Sadikin, M. (2012). Correlation of hypoxia inducible factor-1 α and vascular endothelium growth factor in rat myocardium during aerobic and anaerobic exercise. *Med. J. Indones.* 21, 133–140. doi: 10.13181/mji.v21i3.493
- Floria, V. G., and Mareev, V. (1993). [Anaerobic threshold: definition, physiology and methods of determination]. *Kardiologiia* 33, 40–46.
- Foglia, M. J., and Poss, K. D. (2016). Building and re-building the heart by cardiomyocyte proliferation. *Development* 143, 729–740. doi: 10.1242/dev.132910
- Galdos, F. X., Guo, Y., Paige, S. L., VanDusen, N. J., Wu, S. M., and Pu, W. T. (2017). Cardiac regeneration: lessons from development. *Circ. Res.* 120, 941–959. doi: 10.1161/CIRCRESAHA.116.309040
- Gertz, E. W., Wisneski, J. A., Stanley, W. C., and Neese, R. A. (1988). Myocardial substrate utilization during exercise in humans. Dual carbon-labeled carbohydrate isotope experiments. *J. Clin. Invest.* 82, 2017–2025. doi: 10.1172/JCI113822
- Ghiasi, R., Mohammadi, M., Ashrafi Helan, J., Jafari Jozani, S. R., Mohammadi, S., Ghiasi, A., et al. (2015). Influence of two various durations of resistance exercise on oxidative stress in the male Rat's hearts. *J. Cardiovasc. Thorac. Res.* 7, 149–153. doi: 10.15171/jcvtr.2015.32
- Gibb, A. A., Epstein, P. N., Uchida, S., Zheng, Y., McNally, L. A., Obal, D., et al. (2017). Exercise-induced changes in glucose metabolism promote physiological cardiac growth. *Circulation* 136, 2144–2157. doi: 10.1161/CIRCULATIONAHA.117.028274
- Gibb, A. A., and Hill, B. G. (2018). Metabolic coordination of physiological and pathological cardiac remodeling. *Circ. Res.* 123, 107–128. doi: 10.1161/CIRCRESAHA.118.312017
- Gielen, S., and Hambrecht, R. (2001). Effects of exercise training on vascular function and myocardial perfusion. *Cardiol. Clin.* 19, 357–368. doi: 10.1016/s0733-8651(05)70222-8
- Gomes, R. S., Skroblin, P., Munster, A. B., Tomlins, H., Langley, S. R., Zampetaki, A., et al. (2016). “Young at Heart”: regenerative potential linked to immature cardiac phenotypes. *J. Mol. Cell. Cardiol.* 92, 105–108. doi: 10.1016/j.yjmcc.2016.01.026
- Gonzalez-Rosa, J. M., Burns, C. E., and Burns, C. G. (2017). Zebrafish heart regeneration: 15 years of discoveries. *Regeneration (Oxf.)* 4, 105–123. doi: 10.1002/reg2.83
- Goodwin, G. W., and Taegtmeyer, H. (2000). Improved energy homeostasis of the heart in the metabolic state of exercise. *Am. J. Physiol. Heart Circ. Physiol.* 279, H1490–H1501. doi: 10.1152/ajpheart.2000.279.4.H1490
- Goodwin, G. W., Taylor, C. S., and Taegtmeyer, H. (1998). Regulation of energy metabolism of the heart during acute increase in heart work. *J. Biol. Chem.* 273, 29530–29539. doi: 10.1074/jbc.273.45.29530
- Guimaraes-Camboa, N., Stowe, J., Aneas, I., Sakabe, N., Cattaneo, P., Henderson, L., et al. (2015). HIF1 α represses cell stress pathways to allow proliferation of hypoxic fetal cardiomyocytes. *Dev. Cell* 33, 507–521. doi: 10.1016/j.devcel.2015.04.021
- Hafstad, A. D., Boardman, N. T., Lund, J., Hagve, M., Khalid, A. M., Wisloff, U., et al. (2011). High intensity interval training alters substrate utilization and reduces oxygen consumption in the heart. *J. Appl. Physiol.* (1985) 111, 1235–1241. doi: 10.1152/japplphysiol.00594.2011
- Hara, H., Takeda, N., Kondo, M., Kubota, M., Saito, T., Maruyama, J., et al. (2018). Discovery of a small molecule to increase cardiomyocytes and protect the heart after ischemic injury. *JACC Basic Transl. Sci.* 3, 639–653. doi: 10.1016/j.jacpts.2018.07.005
- Hardie, D. G., Hawley, S. A., and Scott, J. W. (2006). AMP-activated protein kinase—development of the energy sensor concept. *J. Physiol.* 574(Pt 1), 7–15. doi: 10.1113/jphysiol.2006.108944
- Harvey, S. L., Charlet, A., Haas, W., Gygi, S. P., and Kellogg, D. R. (2005). Cdk1-dependent regulation of the mitotic inhibitor Wee1. *Cell* 122, 407–420. doi: 10.1016/j.cell.2005.05.029
- Haubner, B. J., Schneider, J., Schweigmann, U., Schuetz, T., Dichtl, W., Velik-Salchner, C., et al. (2016). Functional recovery of a human neonatal heart after severe myocardial infarction. *Circ. Res.* 118, 216–221. doi: 10.1161/CIRCRESAHA.115.307017
- Heather, L. C., Cole, M. A., Tan, J. J., Ambrose, L. J., Pope, S., Abd-Jamil, A. H., et al. (2012). Metabolic adaptation to chronic hypoxia in cardiac mitochondria. *Basic Res. Cardiol.* 107:268. doi: 10.1007/s00395-012-0268-2
- Himms-Hagen, J., and Harper, M. E. (2001). Physiological role of UCP3 may be export of fatty acids from mitochondria when fatty acid oxidation predominates: an hypothesis. *Exp. Biol. Med. (Maywood)* 226, 78–84. doi: 10.1177/153537020122600204
- Holloway, T. M., Bloemberg, D., da Silva, M. L., Simpson, J. A., Quadrilatero, J., and Spriet, L. L. (2015). High intensity interval and endurance training have opposing effects on markers of heart failure and cardiac remodeling in hypertensive rats. *PLoS One* 10:e0121138. doi: 10.1371/journal.pone.0121138
- Hu, C. J., Wang, L. Y., Chodosh, L. A., Keith, B., and Simon, M. C. (2003). Differential roles of hypoxia-inducible factor 1 α (HIF-1 α) and HIF-2 α in hypoxic gene regulation. *Mol. Cell. Biol.* 23, 9361–9374. doi: 10.1128/mcb.23.24.9361-9374.2003
- Hubbi, M. E., and Semenza, G. L. (2015). Regulation of cell proliferation by hypoxia-inducible factors. *Am. J. Physiol. Cell Physiol.* 309, C775–C782. doi: 10.1152/ajpcell.00279.2015
- Hurford, W. E., Crosby, G., Strauss, H. W., Jones, R., and Lowenstein, E. (1990). Ventricular performance and glucose uptake in rats during chronic hypobaric hypoxia. *J. Nucl. Med.* 31, 1344–1351.
- Hyatt, H. W., Smuder, A. J., Sollanek, K. J., Morton, A. B., Roberts, M. D., and Kavazis, A. N. (2016). Comparative changes in antioxidant enzymes and oxidative stress in cardiac, fast twitch and slow twitch skeletal muscles following endurance exercise training. *Int. J. Physiol. Pathophysiol. Pharmacol.* 8, 160–168.
- Jia, D., Hou, L., Lv, Y., Xi, L., and Tian, Z. (2019). Postinfarction exercise training alleviates cardiac dysfunction and adverse remodeling via mitochondrial biogenesis and SIRT1/PGC-1 α /PI3K/Akt signaling. *J. Cell. Physiol.* 234, 23705–23718. doi: 10.1002/jcp.28939

- Jia, S., Liu, Z., Zhang, S., Liu, P., Zhang, L., Lee, S. H., et al. (2008). Essential roles of PI(3)K-p110beta in cell growth, metabolism and tumorigenesis. *Nature* 454, 776–779. doi: 10.1038/nature07091
- Jopling, C., Sleep, E., Raya, M., Marti, M., Raya, A., and Izpisua Belmonte, J. C. (2010). Zebrafish heart regeneration occurs by cardiomyocyte dedifferentiation and proliferation. *Nature* 464, 606–609. doi: 10.1038/nature08899
- Jopling, C., Sune, G., Faucher, A., Fabregat, C., and Izpisua Belmonte, J. C. (2012). Hypoxia induces myocardial regeneration in zebrafish. *Circulation* 126, 3017–3027. doi: 10.1161/CIRCULATIONAHA.112.107888
- Judge, S., Jang, Y. M., Smith, A., Selman, C., Phillips, T., Speakman, J. R., et al. (2005). Exercise by lifelong voluntary wheel running reduces subsarcolemmal and interfibrillar mitochondrial hydrogen peroxide production in the heart. *Am. J. Physiol. Regul. Integr. Comp. Physiol.* 289, R1564–R1572. doi: 10.1152/ajpregu.00396.2005
- Kaelin, W. G. Jr. (2005). The von Hippel-Lindau protein, HIF hydroxylation, and oxygen sensing. *Biochem. Biophys. Res. Commun.* 338, 627–638. doi: 10.1016/j.bbrc.2005.08.165
- Kajstura, J., Fiordaliso, F., Andreoli, A. M., Li, B., Chimenti, S., Medow, M. S., et al. (2001). IGF-1 overexpression inhibits the development of diabetic cardiomyopathy and angiotensin II-mediated oxidative stress. *Diabetes* 50, 1414–1424. doi: 10.2337/diabetes.50.6.1414
- Kallio, P. J., Pongratz, I., Gradin, K., McGuire, J., and Poellinger, L. (1997). Activation of hypoxia-inducible factor 1alpha: posttranscriptional regulation and conformational change by recruitment of the Arnt transcription factor. *Proc. Natl. Acad. Sci. U.S.A.* 94, 5667–5672. doi: 10.1073/pnas.94.11.5667
- Kemppainen, J., Fujimoto, T., Kalliokoski, K. K., Viljanen, T., Nuutila, P., and Knuuti, J. (2002). Myocardial and skeletal muscle glucose uptake during exercise in humans. *J. Physiol.* 542(Pt 2), 403–412. doi: 10.1113/jphysiol.2002.018135
- Kennedy, S. L., Stanley, W. C., Panchal, A. R., and Mazzeo, R. S. (2001). Alterations in enzymes involved in fat metabolism after acute and chronic altitude exposure. *J. Appl. Physiol.* (1985) 90, 17–22. doi: 10.1152/jappl.2001.90.1.17
- Khakdan, S., Delfan, M., Heydarpour Meymeh, M., Kazerouni, F., Ghaedi, H., Shanaki, M., et al. (2018). High-intensity interval training (HIIT) effectively enhances heart function via miR-195 dependent cardiomyopathy reduction in high-fat high-fructose diet-induced diabetic rats. *Arch. Physiol. Biochem.* 126, 1–8. doi: 10.1080/13813455.2018.1511599
- Kikuchi, K., Holdway, J. E., Werdich, A. A., Anderson, R. M., Fang, Y., Egnaczyk, G. F., et al. (2010). Primary contribution to zebrafish heart regeneration by gata4(+) cardiomyocytes. *Nature* 464, 601–605. doi: 10.1038/nature08804
- Kim, J., Wende, A. R., Sena, S., Theobald, H. A., Soto, J., Sloan, C., et al. (2008). Insulin-like growth factor I receptor signaling is required for exercise-induced cardiac hypertrophy. *Mol. Endocrinol.* 22, 2531–2543. doi: 10.1210/me.2008-0265
- Kimura, W., Nakada, Y., and Sadek, H. A. (2017). Hypoxia-induced myocardial regeneration. *J. Appl. Physiol.* (1985) 123, 1676–1681. doi: 10.1152/japplphysiol.00328.2017
- Kimura, W., Xiao, F., Canseco, D. C., Muralidhar, S., Thet, S., Zhang, H. M., et al. (2015). Hypoxia fate mapping identifies cycling cardiomyocytes in the adult heart. *Nature* 523, 226–230. doi: 10.1038/nature14582
- Kozakova, M., Galetta, F., Gregorini, L., Bigalli, G., Franzoni, F., Giusti, C., et al. (2000). Coronary vasodilator capacity and epicardial vessel remodeling in physiological and hypertensive hypertrophy. *Hypertension* 36, 343–349. doi: 10.1161/01.hyp.36.3.343
- Lassers, B. W., Wahlqvist, M. L., Kaijser, L., and Carlson, L. A. (1972). Effect of nicotinic acid on myocardial metabolism in man at rest and during exercise. *J. Appl. Physiol.* 33, 72–80. doi: 10.1152/jappl.1972.33.1.72
- Laube, F., Heister, M., Scholz, C., Borchardt, T., and Braun, T. (2006). Re-programming of new cardiomyocytes is induced by tissue regeneration. *J. Cell Sci.* 119(Pt 22), 4719–4729. doi: 10.1242/jcs.03252
- Laughlin, M. H., and Tomanek, R. J. (1987). Myocardial capillarity and maximal capillary diffusion capacity in exercise-trained dogs. *J. Appl. Physiol.* (1985) 63, 1481–1486. doi: 10.1152/jappl.1987.63.4.1481
- Lavie, C. J., Arena, R., Swift, D. L., Johannsen, N. M., Sui, X., Lee, D. C., et al. (2015). Exercise and the cardiovascular system: clinical science and cardiovascular outcomes. *Circ. Res.* 117, 207–219. doi: 10.1161/CIRCRESAHA.117.305205
- Lawrence, J., Xiao, D., Xue, Q., Rejali, M., Yang, S., and Zhang, L. (2008). Prenatal nicotine exposure increases heart susceptibility to ischemia/reperfusion injury in adult offspring. *J. Pharmacol. Exp. Ther.* 324, 331–341. doi: 10.1124/jpet.107.132175
- Lee, Y., Min, K., Talbert, E. E., Kavazis, A. N., Smuder, A. J., Willis, W. T., et al. (2012). Exercise protects cardiac mitochondria against ischemia-reperfusion injury. *Med. Sci. Sports Exerc.* 44, 397–405. doi: 10.1249/MSS.0b013e318231c037
- Levine, B. D., Baggish, A. L., Kovacs, R. J., Link, M. S., Maron, M. S., Mitchell, J. H., et al. (2015). Eligibility and disqualification recommendations for competitive athletes with cardiovascular abnormalities: task force 1: classification of sports: dynamic, static, and impact: a scientific statement from the American heart association and American college of cardiology. *Circulation* 132, e262–e266. doi: 10.1161/CIR.0000000000000237
- Li, B., Hu, Y., Li, X., Jin, G., Chen, X., Chen, G., et al. (2018). Sirt1 antisense long noncoding RNA promotes cardiomyocyte proliferation by enhancing the stability of Sirt1. *J. Am. Heart Assoc.* 7:e009700. doi: 10.1161/JAHA.118.009700
- Li, B., Li, M., Li, X., Li, H., Lai, Y., Huang, S., et al. (2019). Sirt1-inducible deacetylation of p21 promotes cardiomyocyte proliferation. *Aging (Albany NY)* 11, 12546–12567. doi: 10.18632/aging.102587
- Li, L., Muhlfeld, C., Niemann, B., Pan, R., Li, R., Hilfiker-Kleiner, D., et al. (2011). Mitochondrial biogenesis and PGC-1alpha deacetylation by chronic treadmill exercise: differential response in cardiac and skeletal muscle. *Basic Res. Cardiol.* 106, 1221–1234. doi: 10.1007/s00395-011-0213-9
- Li, Y., He, L., Huang, X., Bhaloo, S. I., Zhao, H., Zhang, S., et al. (2018). Genetic lineage tracing of nonmyocyte population by dual recombinases. *Circulation* 138, 793–805. doi: 10.1161/CIRCULATIONAHA.118.034250
- Liaudet, L., Vassalli, G., and Pacher, P. (2009). Role of peroxynitrite in the redox regulation of cell signal transduction pathways. *Front. Biosci. (Landmark Ed)* 14:4809–4814. doi: 10.2741/3569
- Liu, Z., Li, T., Li, P., Wei, N., Zhao, Z., Liang, H., et al. (2015). The ambiguous relationship of oxidative stress, tau hyperphosphorylation, and autophagy dysfunction in Alzheimer's disease. *Oxid. Med. Cell. Longev.* 2015:352723. doi: 10.1155/2015/352723
- Lopaschuk, G. D., Collins-Nakai, R. L., and Itoi, T. (1992). Developmental changes in energy substrate use by the heart. *Cardiovasc. Res.* 26, 1172–1180. doi: 10.1093/cvr/26.12.1172
- Lopaschuk, G. D., Ussher, J. R., Folmes, C. D., Jaswal, J. S., and Stanley, W. C. (2010). Myocardial fatty acid metabolism in health and disease. *Physiol. Rev.* 90, 207–258. doi: 10.1152/physrev.00015.2009
- Ma, X., Fu, Y., Xiao, H., Song, Y., Chen, R., Shen, J., et al. (2015). Cardiac fibrosis alleviated by exercise training is AMPK-dependent. *PLoS One* 10:e0129971. doi: 10.1371/journal.pone.0129971
- Ma, Z., Qi, J., Meng, S., Wen, B., and Zhang, J. (2013). Swimming exercise training-induced left ventricular hypertrophy involves microRNAs and synergistic regulation of the PI3K/AKT/mTOR signaling pathway. *Eur. J. Appl. Physiol.* 113, 2473–2486. doi: 10.1007/s00421-013-2685-9
- Maillet, M., van Berlo, J. H., and Molkentin, J. D. (2013). Molecular basis of physiological heart growth: fundamental concepts and new players. *Nat. Rev. Mol. Cell Biol.* 14, 38–48. doi: 10.1038/nrm3495
- Mansor, L. S., Mehta, K., Aksentijevic, D., Carr, C. A., Lund, T., Cole, M. A., et al. (2016). Increased oxidative metabolism following hypoxia in the type 2 diabetic heart, despite normal hypoxia signalling and metabolic adaptation. *J. Physiol.* 594, 307–320. doi: 10.1113/JP271242
- Marsin, A. S., Bertrand, L., Rider, M. H., Deprez, J., Beauloye, C., Vincent, M. F., et al. (2000). Phosphorylation and activation of heart PFK-2 by AMPK has a role in the stimulation of glycolysis during ischaemia. *Curr. Biol.* 10, 1247–1255. doi: 10.1016/S0960-9822(00)00742-9
- McMullen, J. R., Shioi, T., Huang, W. Y., Zhang, L., Tarnavski, O., Bisping, E., et al. (2004). The insulin-like growth factor 1 receptor induces physiological heart growth via the phosphoinositide 3-kinase(p110alpha) pathway. *J. Biol. Chem.* 279, 4782–4793. doi: 10.1074/jbc.M310405200
- McMullen, J. R., Shioi, T., Zhang, L., Tarnavski, O., Sherwood, M. C., Kang, P. M., et al. (2003). Phosphoinositide 3-kinase(p110alpha) plays a critical role for the induction of physiological, but not pathological, cardiac hypertrophy. *Proc. Natl. Acad. Sci. U.S.A.* 100, 12355–12360. doi: 10.1073/pnas.1934654100
- Medeiros, C., Frederico, M. J., da Luz, G., Pauli, J. R., Silva, A. S., Pinho, R. A., et al. (2011). Exercise training reduces insulin resistance and upregulates the mTOR/p70S6k pathway in cardiac muscle of diet-induced obesity rats. *J. Cell. Physiol.* 226, 666–674. doi: 10.1002/jcp.22387

- Menendez-Montes, I., Escobar, B., Palacios, B., Gomez, M. J., Izquierdo-Garcia, J. L., Flores, L., et al. (2016). Myocardial VHL-HIF signaling controls an embryonic metabolic switch essential for cardiac maturation. *Dev. Cell* 39, 724–739. doi: 10.1016/j.devcel.2016.11.012
- Merghani, A., Malhotra, A., and Sharma, S. (2016). The U-shaped relationship between exercise and cardiac morbidity. *Trends Cardiovasc. Med.* 26, 232–240. doi: 10.1016/j.tcm.2015.06.005
- Michailidis, Y., Jamurtas, A. Z., Nikolaidis, M. G., Fatouros, I. G., Koutedakis, Y., Papassotiropoulos, I., et al. (2007). Sampling time is crucial for measurement of aerobic exercise-induced oxidative stress. *Med. Sci. Sports Exerc.* 39, 1107–1113. doi: 10.1249/01.mss.0b013e318053e7ba
- Mohamed, T. M. A., Ang, Y. S., Radzinsky, E., Zhou, P., Huang, Y., Elfenbein, A., et al. (2018). Regulation of cell cycle to stimulate adult cardiomyocyte proliferation and cardiac regeneration. *Cell* 173, 104–116.e12. doi: 10.1016/j.cell.2018.02.014
- Moretti, A., Caron, L., Nakano, A., Lam, J. T., Bernshausen, A., Chen, Y., et al. (2006). Multipotent embryonic isl1+ progenitor cells lead to cardiac, smooth muscle, and endothelial cell diversification. *Cell* 127, 1151–1165. doi: 10.1016/j.cell.2006.10.029
- Mouton, V., Toussaint, L., Vertommen, D., Gueuning, M. A., Maisin, L., Havaux, X., et al. (2010). Heart 6-phosphofructo-2-kinase activation by insulin requires PKB (protein kinase B), but not SGK3 (serum- and glucocorticoid-induced protein kinase 3). *Biochem. J.* 431, 267–275. doi: 10.1042/BJ20101089
- Nadal-Ginard, B. (2001). [Generation of new cardiomyocytes in the adult heart: Prospects of myocardial regeneration as an alternative to cardiac transplantation]. *Rev. Esp. Cardiol.* 54, 543–550. doi: 10.1016/s0300-8932(01)76354-3
- Naderi, R., Mohaddes, G., Mohammadi, M., Ghaznavi, R., Ghyasi, R., and Vatankehah, A. M. (2015). Voluntary exercise protects heart from oxidative stress in diabetic rats. *Adv. Pharm. Bull.* 5, 231–236. doi: 10.15171/apb.2015.032
- Nakada, Y., Canseco, D. C., Thet, S., Abdilsalam, S., Asaithamby, A., Santos, C. X., et al. (2017). Hypoxia induces heart regeneration in adult mice. *Nature* 541, 222–227. doi: 10.1038/nature20173
- Nakagama, Y., Inuzuka, R., Ichimura, K., Hinata, M., Takehara, H., Takeda, N., et al. (2018). Accelerated cardiomyocyte proliferation in the heart of a neonate With LEOPARD syndrome-associated fatal cardiomyopathy. *Circ. Heart Fail.* 11:e004660. doi: 10.1161/CIRCHEARTFAILURE.117.004660
- O'Keefe, J. H., Patil, H. R., Lavie, C. J., Magalski, A., Vogel, R. A., and McCullough, P. A. (2012). Potential adverse cardiovascular effects from excessive endurance exercise. *Mayo Clin. Proc.* 87, 587–595. doi: 10.1016/j.mayocp.2012.04.005
- Olver, T. D., Ferguson, B. S., and Laughlin, M. H. (2015). Molecular mechanisms for exercise training-induced changes in vascular structure and function: skeletal muscle, cardiac muscle, and the brain. *Prog. Mol. Biol. Transl. Sci.* 135, 227–257. doi: 10.1016/bs.pmbts.2015.07.017
- Palabiyik, O., Tastekin, E., Doganlar, Z. B., Tayfur, P., Dogan, A., and Vardar, S. A. (2019). Alteration in cardiac PI3K/Akt/mTOR and ERK signaling pathways with the use of growth hormone and swimming, and the roles of miR21 and miR133. *Biomed. Rep.* 0, 1–10. doi: 10.3892/br.2018.1179
- Parekh, P., Motiwale, L., Naik, N., and Rao, K. V. (2011). Downregulation of cyclin D1 is associated with decreased levels of p38 MAP kinases, Akt/PKB and Pak1 during chemopreventive effects of resveratrol in liver cancer cells. *Exp. Toxicol. Pathol.* 63, 167–173. doi: 10.1016/j.etp.2009.11.005
- Parry-Williams, G., and Sharma, S. (2020). The effects of endurance exercise on the heart: panacea or poison? *Nat. Rev. Cardiol.* 17, 402–412. doi: 10.1038/s41569-020-0354-3
- Patel, H., Alkhawam, H., Madanieh, R., Shah, N., Kosmas, C. E., and Vittorio, T. J. (2017). Aerobic vs anaerobic exercise training effects on the cardiovascular system. *World J. Cardiol.* 9, 134–138. doi: 10.4330/wjc.v9.i2.134
- Pinckard, K., Baskin, K. K., and Stanford, K. I. (2019). Effects of exercise to improve cardiovascular health. *Front. Cardiovasc. Med.* 6:69. doi: 10.3389/fcvm.2019.00069
- Pinho, C. A., Tromm, C. B., Tavares, A. M., Silva, L. A., Silveira, P. C., Souza, C. T., et al. (2012). Effects of different physical training protocols on ventricular oxidative stress parameters in infarction-induced rats. *Life Sci.* 90, 553–559. doi: 10.1016/j.lfs.2012.01.018
- Platt, C., Houstis, N., and Rosenzweig, A. (2015). Using exercise to measure and modify cardiac function. *Cell Metab.* 21, 227–236. doi: 10.1016/j.cmet.2015.01.014
- Pluim, B. M., Lamb, H. J., Kayser, H. W., Leijes, F., Beyerbach, H. P., Zwinderman, A. H., et al. (1998). Functional and metabolic evaluation of the athlete's heart by magnetic resonance imaging and dobutamine stress magnetic resonance spectroscopy. *Circulation* 97, 666–672. doi: 10.1161/01.cir.97.7.666
- Pluim, B. M., Zwinderman, A. H., van der Laarse, A., and van der Wall, E. E. (2000). The athlete's heart. A meta-analysis of cardiac structure and function. *Circulation* 101, 336–344. doi: 10.1161/01.cir.101.3.336
- Porrello, E. R., Mahmoud, A. I., Simpson, E., Hill, J. A., Richardson, J. A., Olson, E. N., et al. (2011). Transient regenerative potential of the neonatal mouse heart. *Science* 331, 1078–1080. doi: 10.1126/science.1200708
- Porrello, E. R., Mahmoud, A. I., Simpson, E., Johnson, B. A., Grinsfelder, D., Canseco, D., et al. (2013). Regulation of neonatal and adult mammalian heart regeneration by the miR-15 family. *Proc. Natl. Acad. Sci. U.S.A.* 110, 187–192. doi: 10.1073/pnas.1208863110
- Porrello, E. R., and Olson, E. N. (2014). A neonatal blueprint for cardiac regeneration. *Stem Cell Res* 13(3 Pt B), 556–570. doi: 10.1016/j.scr.2014.06.003
- Poss, K. D., Wilson, L. G., and Keating, M. T. (2002). Heart regeneration in zebrafish. *Science* 298, 2188–2190. doi: 10.1126/science.1077857
- Powers, S. K., and Jackson, M. J. (2008). Exercise-induced oxidative stress: cellular mechanisms and impact on muscle force production. *Physiol. Rev.* 88, 1243–1276. doi: 10.1152/physrev.00031.2007
- Powers, S. K., Smuder, A. J., Kavazis, A. N., and Quindry, J. C. (2014). Mechanisms of exercise-induced cardioprotection. *Physiology (Bethesda)* 29, 27–38. doi: 10.1152/physiol.00030.2013
- Pozuelo Rubio, M., Pegg, M., Wong, B. H., Morrice, N., and MacKintosh, C. (2003). 14-3-3s regulate fructose-2,6-bisphosphate levels by binding to PKB-phosphorylated cardiac fructose-2,6-bisphosphate kinase/phosphatase. *EMBO J.* 22, 3514–3523. doi: 10.1093/emboj/cdg363
- Prabhakar, N. R., and Semenza, G. L. (2015). Oxygen sensing and homeostasis. *Physiology (Bethesda)* 30, 340–348. doi: 10.1152/physiol.00022.2015
- Puente, B. N., Kimura, W., Muralidhar, S. A., Moon, J., Amatrua, J. F., Phelps, K. L., et al. (2014). The oxygen-rich postnatal environment induces cardiomyocyte cell-cycle arrest through DNA damage response. *Cell* 157, 565–579. doi: 10.1016/j.cell.2014.03.032
- Radak, Z., Zhao, Z., Koltai, E., Ohno, H., and Atalay, M. (2013). Oxygen consumption and usage during physical exercise: the balance between oxidative stress and ROS-dependent adaptive signaling. *Antioxid. Redox Signal.* 18, 1208–1246. doi: 10.1089/ars.2011.4498
- Rees, B. B., Sudradjat, F. A., and Love, J. W. (2001). Acclimation to hypoxia increases survival time of zebrafish, *Danio rerio*, during lethal hypoxia. *J. Exp. Zool.* 289, 266–272. doi: 10.1002/1097-010x(20010401/30)289:4<266::aid-jez7<3.0.co;2-5
- Riehle, C., Wende, A. R., Zhu, Y., Oliveira, K. J., Pereira, R. O., Jaishy, B. P., et al. (2014). Insulin receptor substrates are essential for the bioenergetic and hypertrophic response of the heart to exercise training. *Mol. Cell. Biol.* 34, 3450–3460. doi: 10.1128/MCB.00426-14
- Roesner, A., Hankel, T., and Burmester, T. (2006). Hypoxia induces a complex response of globin expression in zebrafish (*Danio rerio*). *J. Exp. Biol.* 209(Pt 11), 2129–2137. doi: 10.1242/jeb.02243
- Russell, R. R. III, Li, J., Coven, D. L., Pypaert, M., Zechner, C., Palmeri, M., et al. (2004). AMP-activated protein kinase mediates ischemic glucose uptake and prevents postischemic cardiac dysfunction, apoptosis, and injury. *J. Clin. Invest.* 114, 495–503. doi: 10.1172/JCI19297
- Sack, M. N., Rader, T. A., Park, S., Bastin, J., McCune, S. A., and Kelly, D. P. (1996). Fatty acid oxidation enzyme gene expression is downregulated in the failing heart. *Circulation* 94, 2837–2842. doi: 10.1161/01.cir.94.11.2837
- Sakaguchi, A., Nishiyama, C., and Kimura, W. (2020). Cardiac regeneration as an environmental adaptation. *Biochim. Biophys. Acta Mol. Cell Res.* 1867, 118623. doi: 10.1016/j.bbamcr.2019.118623
- Sanchis-Gomar, F., Fiuza-Luces, C., and Lucia, A. (2015). Exercise as the master polypill of the 21st century for the prevention of cardiovascular disease. *Int. J. Cardiol.* 181, 360–361. doi: 10.1016/j.ijcard.2014.12.048
- Sarangarajan, R., Meera, S., Rukkumani, R., Sankar, P., and Anuradha, G. (2017). Antioxidants: friend or foe? *Asian Pac. J. Trop. Med.* 10, 1111–1116. doi: 10.1016/j.apjtm.2017.10.017
- Schonekess, B. O. (1997). Competition between lactate and fatty acids as sources of ATP in the isolated working rat heart. *J. Mol. Cell. Cardiol.* 29, 2725–2733. doi: 10.1006/jmcc.1997.0504

- Senyo, S. E., Steinhauser, M. L., Pizzimenti, C. L., Yang, V. K., Cai, L., Wang, M., et al. (2013). Mammalian heart renewal by pre-existing cardiomyocytes. *Nature* 493, 433–436. doi: 10.1038/nature11682
- Serteri, G. G., Modesti, P. A., Boddi, M., Cecioni, I., Panizza, R., Coppo, M., et al. (1999). Cardiac growth factors in human hypertrophy. Relations with myocardial contractility and wall stress. *Circ. Res.* 85, 57–67. doi: 10.1161/01.res.85.1.57
- Shiojima, I., and Walsh, K. (2006). Regulation of cardiac growth and coronary angiogenesis by the Akt/PKB signaling pathway. *Genes Dev.* 20, 3347–3365. doi: 10.1101/gad.1492806
- Soonpaa, M. H., Kim, K. K., Pajak, L., Franklin, M., and Field, L. J. (1996). Cardiomyocyte DNA synthesis and binucleation during murine development. *Am. J. Physiol.* 271(5 Pt 2), H2183–H2189. doi: 10.1152/ajpheart.1996.271.5.H2183
- Sousa Fialho, M. D. L., Abd Jamil, A. H., Stannard, G. A., and Heather, L. C. (2019). Hypoxia-inducible factor 1 signalling, metabolism and its therapeutic potential in cardiovascular disease. *Biochim. Biophys. Acta Mol. Basis Dis.* 1865, 831–843. doi: 10.1016/j.bbdis.2018.09.024
- Starnes, J. W., Barnes, B. D., and Olsen, M. E. (2007). Exercise training decreases rat heart mitochondria free radical generation but does not prevent Ca²⁺-induced dysfunction. *J. Appl. Physiol.* (1985) 102, 1793–1798. doi: 10.1152/japplphysiol.00849.2006
- Sylviana, N., Helja, N., Qolbi, H. H., Goenawan, H., Lesmana, R., Syamsunarno, M. R. A., et al. (2018). Effect of swimming exercise to cardiac PGC-1 α and HIF-1 α gene expression in mice. *Asian J. Sports Med.* 9:e65079.
- Taegtmeier, H., Lam, T., and Davogustto, G. (2016a). Cardiac metabolism in perspective. *Compr. Physiol.* 6, 1675–1699. doi: 10.1002/cphy.c150056
- Taegtmeier, H., Young, M. E., Lopaschuk, G. D., Abel, E. D., Brunengraber, H., Darley-Usmar, V., et al. (2016b). Assessing cardiac metabolism: a scientific statement from the American heart association. *Circ Res* 118, 1659–1701. doi: 10.1161/RES.0000000000000097
- Tao, G., Kahr, P. C., Morikawa, Y., Zhang, M., Rahmani, M., Heallen, T. R., et al. (2016). Ptx2 promotes heart repair by activating the antioxidant response after cardiac injury. *Nature* 534, 119–123. doi: 10.1038/nature17959
- Tao, L., Bei, Y., Lin, S., Zhang, H., Zhou, Y., Jiang, J., et al. (2015). Exercise training protects against acute myocardial infarction via improving myocardial energy metabolism and mitochondrial biogenesis. *Cell. Physiol. Biochem.* 37, 162–175. doi: 10.1159/000430342
- Thompson, P. D., Arena, R., Riebe, D., Pescatello, L. S., and American College of Sports Medicine. (2013). ACSM's new preparticipation health screening recommendations from ACSM's guidelines for exercise testing and prescription, ninth edition. *Curr. Sports Med. Rep.* 12, 215–217. doi: 10.1249/JSR.0b013e31829a68cf
- Thygesen, K., Alpert, J. S., Jaffe, A. S., Chaitman, B. R., Bax, J. J., Morrow, D. A., et al. (2018). Fourth Universal definition of myocardial infarction (2018). *Circulation* 138, e618–e651. doi: 10.1161/CIR.0000000000000617
- Tian, X., Zhou, N., Yuan, J., Lu, L., Zhang, Q., Wei, M., et al. (2020). Heat shock transcription factor 1 regulates exercise-induced myocardial angiogenesis after pressure overload via HIF-1 α /VEGF pathway. *J. Cell. Mol. Med.* 24, 2178–2188. doi: 10.1111/jcmm.14872
- Trewin, A. J., Berry, B. J., and Wojtovich, A. P. (2018). Exercise and mitochondrial dynamics: keeping in shape with ROS and AMPK. *Antioxidants (Basel)* 7:7. doi: 10.3390/antiox7010007
- Uchida, S., De Gaspari, P., Kostin, S., Jenniches, K., Kilic, A., Izumiya, Y., et al. (2013). Sca1-derived cells are a source of myocardial renewal in the murine adult heart. *Stem Cell Rep.* 1, 397–410. doi: 10.1016/j.stemcr.2013.09.004
- Vagnozzi, R. J., Molkentin, J. D., and Houser, S. R. (2018). New myocyte formation in the adult heart: endogenous sources and therapeutic implications. *Circ. Res.* 123, 159–176. doi: 10.1161/CIRCRESAHA.118.311208
- Verdoorn, K. S., Matsuura, C., and Borges, J. P. (2017). Exercise for cardiac health and regeneration: killing two birds with one stone. *Ann. Transl. Med.* 5(Suppl. 1):S13. doi: 10.21037/atm.2017.03.10
- Vujic, A., Lerchenmuller, C., Wu, T. D., Guillermer, C., Rabolli, C. P., Gonzalez, E., et al. (2018). Exercise induces new cardiomyocyte generation in the adult mammalian heart. *Nat. Commun.* 9:1659. doi: 10.1038/s41467-018-04083-1
- Wahid, A., Manek, N., Nichols, M., Kelly, P., Foster, C., Webster, P., et al. (2016). Quantifying the association between physical activity and cardiovascular disease and diabetes: a systematic review and meta-analysis. *J. Am. Heart Assoc.* 5:e002495. doi: 10.1161/JAHA.115.002495
- Wang, G. L., Jiang, B. H., Rue, E. A., and Semenza, G. L. (1995). Hypoxia-inducible factor 1 is a basic-helix-loop-helix-PAS heterodimer regulated by cellular O₂ tension. *Proc. Natl. Acad. Sci. U.S.A.* 92, 5510–5514. doi: 10.1073/pnas.92.12.5510
- Wang, H., Bei, Y., Lu, Y., Sun, W., Liu, Q., Wang, Y., et al. (2015). Exercise prevents cardiac injury and improves mitochondrial biogenesis in advanced diabetic cardiomyopathy with PGC-1 α and Akt activation. *Cell. Physiol. Biochem.* 35, 2159–2168. doi: 10.1159/000374021
- Wang, J., Song, Y., Li, H., Shen, Q., Shen, J., An, X., et al. (2016). Exacerbated cardiac fibrosis induced by beta-adrenergic activation in old mice due to decreased AMPK activity. *Clin. Exp. Pharmacol. Physiol.* 43, 1029–1037. doi: 10.1111/1440-1681.12622
- Wang, S. Y., Zhu, S., Wu, J., Zhang, M., Xu, Y., Xu, W., et al. (2020). Exercise enhances cardiac function by improving mitochondrial dysfunction and maintaining energy homeostasis in the development of diabetic cardiomyopathy. *J. Mol. Med. (Berl.)* 98, 245–261. doi: 10.1007/s00109-019-01861-2
- Wang, X., Hu, Q., Nakamura, Y., Lee, J., Zhang, G., From, A. H., et al. (2006). The role of the sca-1+/CD31- cardiac progenitor cell population in postinfarction left ventricular remodeling. *Stem Cells* 24, 1779–1788. doi: 10.1634/stemcells.2005-0386
- Waring, C. D., Vicinanza, C., Papalamprou, A., Smith, A. J., Purushothaman, S., Goldspink, D. F., et al. (2014). The adult heart responds to increased workload with physiologic hypertrophy, cardiac stem cell activation, and new myocyte formation. *Eur. Heart J.* 35, 2722–2731. doi: 10.1093/eurheartj/ehs338
- Waskova-Arnostova, P., Kasparova, D., Elsnicova, B., Novotny, J., Neckar, J., Kolar, F., et al. (2014). Chronic hypoxia enhances expression and activity of mitochondrial creatine kinase and hexokinase in the rat ventricular myocardium. *Cell. Physiol. Biochem.* 33, 310–320. doi: 10.1159/000356671
- Wasserman, K. (1986). The anaerobic threshold: definition, physiological significance and identification. *Adv. Cardiol.* 35, 1–23.
- Watson, P. A., Reusch, J. E., McCune, S. A., Leinwand, L. A., Luckey, S. W., Konhilas, J. P., et al. (2007). Restoration of CREB function is linked to completion and stabilization of adaptive cardiac hypertrophy in response to exercise. *Am. J. Physiol. Heart Circ. Physiol.* 293, H246–H259. doi: 10.1152/ajpheart.00734.2006
- Webster, W. S., and Abela, D. (2007). The effect of hypoxia in development. *Birth Defects Res. C Embryo Today* 81, 215–228. doi: 10.1002/bdrc.20102
- Weinberger, F., Mehrkens, D., Friedrich, F. W., Stubbendorff, M., Hua, X., Muller, J. C., et al. (2012). Localization of Islet-1-positive cells in the healthy and infarcted adult murine heart. *Circ. Res.* 110, 1303–1310. doi: 10.1161/CIRCRESAHA.111.259630
- White, F. C., Bloor, C. M., McKirnan, M. D., and Carroll, S. M. (1998). Exercise training in swine promotes growth of arteriolar bed and capillary angiogenesis in heart. *J. Appl. Physiol.* (1985) 85, 1160–1168. doi: 10.1152/jappl.1998.85.3.1160
- Wyatt, H. L., and Mitchell, J. (1978). Influences of physical conditioning and deconditioning on coronary vasculature of dogs. *J. Appl. Physiol. Respir. Environ. Exerc. Physiol.* 45, 619–625. doi: 10.1152/jappl.1978.45.4.619
- Yang, S., Chintapalli, J., Sodagum, L., Baskin, S., Malhotra, A., Reiss, K., et al. (2005). Activated IGF-1R inhibits hyperglycemia-induced DNA damage and promotes DNA repair by homologous recombination. *Am. J. Physiol. Renal. Physiol.* 289, F1144–F1152. doi: 10.1152/ajprenal.00094.2005
- Ye, L., D'Agostino, G., Loo, S. J., Wang, C. X., Su, L. P., Tan, S. H., et al. (2018). Early regenerative capacity in the porcine heart. *Circulation* 138, 2798–2808. doi: 10.1161/CIRCULATIONAHA.117.031542
- Zandrino, F., Molinari, G., Smeraldi, A., Odaglia, G., Masperone, M. A., and Sardaneli, F. (2000). Magnetic resonance imaging of athlete's heart: myocardial mass, left ventricular function, and cross-sectional area of the coronary arteries. *Eur. Radiol.* 10, 319–325. doi: 10.1007/s003300050051
- Zebrowski, D. C., Jensen, C. H., Becker, R., Ferrazzi, F., Baun, C., Hvidsten, S., et al. (2017). Cardiac injury of the newborn mammalian heart accelerates cardiomyocyte terminal differentiation. *Sci. Rep.* 7:8362. doi: 10.1038/s41598-017-08947-2

- Zhou, L., Huang, H., Yuan, C. L., Keung, W., Lopaschuk, G. D., and Stanley, W. C. (2008). Metabolic response to an acute jump in cardiac workload: effects on malonyl-CoA, mechanical efficiency, and fatty acid oxidation. *Am. J. Physiol. Heart Circ. Physiol.* 294, H954–H960. doi: 10.1152/ajpheart.00557.2007
- Zhou, T., Prather, E. R., Garrison, D. E., and Zuo, L. (2018). Interplay between ROS and antioxidants during ischemia-reperfusion injuries in cardiac and skeletal muscle. *Int. J. Mol. Sci.* 19:417. doi: 10.3390/ijms19020417
- Zhu, W., Zhang, E., Zhao, M., Chong, Z., Fan, C., Tang, Y., et al. (2018). Regenerative potential of neonatal porcine hearts. *Circulation* 138, 2809–2816. doi: 10.1161/CIRCULATIONAHA.118.034886

Conflict of Interest: The authors declare that the research was conducted in the absence of any commercial or financial relationships that could be construed as a potential conflict of interest.

Copyright © 2021 Bo, Li, Zhou and Wei. This is an open-access article distributed under the terms of the Creative Commons Attribution License (CC BY). The use, distribution or reproduction in other forums is permitted, provided the original author(s) and the copyright owner(s) are credited and that the original publication in this journal is cited, in accordance with accepted academic practice. No use, distribution or reproduction is permitted which does not comply with these terms.



FOXC1 Negatively Regulates DKK1 Expression to Promote Gastric Cancer Cell Proliferation Through Activation of Wnt Signaling Pathway

Jiang Jiang^{1†}, Jianfang Li^{2†}, Weiwu Yao^{3†}, Wenfang Wang¹, Bowen Shi¹, Fei Yuan^{4*}, Jingyan Dong^{5*} and Huan Zhang^{1*}

¹ Department of Radiology, Ruijin Hospital, Shanghai Jiao Tong University School of Medicine, Shanghai, China,

² Department of General Surgery, Shanghai Key Laboratory of Gastric Neoplasms, Shanghai Institute of Digestive Surgery, Ruijin Hospital, Shanghai Jiao Tong University School of Medicine, Shanghai, China, ³ Department of Radiology, Tongren Hospital, Shanghai Jiao Tong University School of Medicine, Shanghai, China, ⁴ Department of Pathology, Ruijin Hospital, Shanghai Jiao Tong University School of Medicine, Shanghai, China, ⁵ Department of Ocular Fundus Diseases, Shanxi Eye Hospital, Shanxi, China

OPEN ACCESS

Edited by:

Elizabeth Lara Ostler,
University of Brighton,
United Kingdom

Reviewed by:

Toby Pheese,
Cardiff University, United Kingdom
YangXin Fu,
University of Alberta, Canada

*Correspondence:

Fei Yuan
daphny2014@163.com
Jingyan Dong
dongjingyan114@163.com
Huan Zhang
huanzhangy@126.com

[†]These authors have contributed
equally to this work and share first
authorship

Specialty section:

This article was submitted to
Cell Growth and Division,
a section of the journal
Frontiers in Cell and Developmental
Biology

Received: 01 February 2021

Accepted: 29 March 2021

Published: 27 April 2021

Citation:

Jiang J, Li J, Yao W, Wang W,
Shi B, Yuan F, Dong J and Zhang H
(2021) FOXC1 Negatively Regulates
DKK1 Expression to Promote Gastric
Cancer Cell Proliferation Through
Activation of Wnt Signaling Pathway.
Front. Cell Dev. Biol. 9:662624.
doi: 10.3389/fcell.2021.662624

Gastric cancer (GC), characterized by uncontrolled growth, is a common malignant tumor of the digestive system. The Wnt signaling pathway plays an important role in the tumorigenesis and proliferation of GC. Many studies on this signaling pathway have focused on its intracellular regulatory mechanism, whereas little attention has been given to extracellular regulatory factors. Dickkopf-1 (Dkk1) is a secretory glycoprotein, and it can bind inhibit activation of the Wnt pathway. However, the regulation and mechanism of DKK1 in the proliferation of GC remain unclear. FOXC1 plays an important role in organ development and tumor growth, but its role in GC tumor growth remains unknown. In this study, we found that the FOXC1 is highly expressed in patients with GC and high expression of FOXC1 correlates to poor prognosis. In addition, we found that the Wnt signaling pathway in GC cells with high FOXC1 expression was strongly activated. FOXC1 negatively regulates DKK1 expression by binding to its promoter region, thereby promoting the activation of Wnt pathway. FOXC1 can also form a complex with unphosphorylated β -catenin protein in the cytoplasm and then dissociates from β -catenin in the nucleus, thereby promoting the entry of β -catenin into the nucleus and regulating expression of c-MYC, which promotes the proliferation of GC cells. Our study not only reveals the function and mechanism of FOXC1 in GC, but also provides a potential target for clinic GC treatment.

Keywords: gastric cancer, FOXC1, DKK1, c-MYC, proliferation

INTRODUCTION

Gastric cancer (GC) is one of the most common malignant tumors in the digestive system, especially in East Asia. In 2013, approximately 984,000 people were diagnosed with GC, and nearly 841,000 died of GC (Fitzmaurice et al., 2015). Due to the lack of specific tumor biomarkers, many tumors were at an advanced stage when diagnosed and patients have lost the opportunity for

radical surgical treatment, for those patients, their 5-year survival rate is less than 10% (Shimada et al., 2014). Thus, identifying the underlying mechanisms and specific biomarkers is a pivotal project to treat GC.

Forkhead box (FOX) proteins are characterized by a winged helix DNA-binding domain (Erickson, 2001). These proteins have been shown to regulate diverse biological processes, including development, differentiation, proliferation, apoptosis, migration, invasion, and tumorigenesis (Jin et al., 2014). Forkhead box C1 (FOXCI), a member of the FOX protein family, is a key regulator of the development of the anterior chamber angle, and its abnormal expression correlates highly with the incidence of congenital glaucoma (Chen et al., 2016; Golson and Kaestner, 2016; Deng et al., 2017; Ramezani et al., 2019). Recent studies have shown that FOXCI dysregulation is strongly related to the occurrence and development of breast cancer, colon cancer, cervical cancer, Hodgkin's lymphoma, and prostate cancer (Ito et al., 2014; Jin et al., 2014; Hopkins et al., 2016; Gilding and Somervaille, 2019; Hsu et al., 2019). In 2014, Yuan et al. reported that FOXCI was associated with tumor size, the number of lymph node metastases, and prognosis, which indicated that FOXCI might play an important role in GC growth and metastasis (Xu et al., 2014). Zhong et al. reported that LINC00242 interacts with miR-141 and positively regulates FOXCI to contribute to HGC27 cell viability, migration, and invasion (Zhong et al., 2020). Moreover, previous studies have indicated that FOXCI promotes tumor proliferation through the PI3K-AKT, NF-KB and Wnt signaling pathways (Huang et al., 2017; Liu et al., 2018; Yu et al., 2018). However, its specific role in proliferation of GC remains to be studied.

Wnt signaling pathway play an important role in embryonic development, cell migration, and organogenesis (Chae and Bothwell, 2018). Its aberrant activation could contribute GC growth and metastasis (Zhan et al., 2017). In the classical Wnt signaling pathway, Wnt protein binds to cell surface receptors, including Frizzled (Fz) and low-density lipoprotein receptor-related protein 5/6 (LRP5/6), thereby transducing extracellular signal stimuli into cells (Reya and Clevers, 2005). Wnt proteins formed a complex with Fzd and LRP5/6, Which led to the level of phosphorylation β -catenin reduced and excessive accumulation of β -catenin in the cytoplasm; it then enters into the nucleus and forms a transcriptional complex with TCF or LEF, activating expression of target genes, such as c-MYC and cyclin D1 (Clevers and Nusse, 2012). Among them, the transcription factor c-Myc is one of the most widely investigated cancer-causing genes, being implicated in the formation, maintenance, and progression of several different cancer types (Duffy et al., 2021). Previous study has indicated that c-Myc is well-characterized β -catenin/TCF target gene (Sansom et al., 2007). And overexpression of MYC can rescue the growth-suppressive effects of FZD7 knockdown in gastric cancer cells (Flanagan et al., 2019). Previous study reported that FOXCI knockdown could inhibit the expression of MYC, however, the precise role and underlying signaling cascades in GC proliferation remain unclear.

Dickkopf-1 (Dkk1) is a secretory antagonist, which binds to the Wnt coreceptor LRP5/6 to desensitize cells to canonical Wnt ligands (Chae and Bothwell, 2018). DKK-1 is reported to be

over expressed in GC patients and recently, it was reported to play different roles in the tumor growth due to different tumor environment (Gomceli et al., 2012; Zhu et al., 2021). In 2018, Hong et al. reported that high DKK1 expression is a crucial prognostic factor for predicting tumor recurrence and survival in patients with resected advanced GC, which indicated DKK1 contributed GC recurrence (Hong et al., 2018). Meanwhile, in terms of tumor growth, DKK-1 inhibits the activation of Wnt signaling to influence GC growth by suppressing cancer stem cells (Wang et al., 2013). Therefore, it is particularly important to clearly explain the specific mechanism of DKK1 in the proliferation of GC. However, there are few studies to explore transcription factors that regulate DKK1 in GC.

In this study, we will explore the specific mechanisms that FOXCI promoted proliferation GC by inhibiting DKK1 expression.

MATERIALS AND METHODS

Patients and Human Tissue Information

Tumor tissue samples were obtained from Ruijin Hospital, Shanghai Jiao Tong University. Patients underwent curative GC resection between 2018 and 2019, and samples from these patients were used for immunohistochemistry (IHC). The Ethics Committee of Ruijin Hospital, Shanghai Jiao Tong University approved this project. All samples were anonymously coded in accordance with local ethical guidelines (as stipulated by the Declaration of Helsinki), and written informed consent was obtained.

Cell Culture and Reagents

Normal gastric cell (GES-1) and GC cell lines (AGS, SGC-7901, MGC-803, MKN-45, HGC-27) were stored at Shanghai Institute of Digestive Surgery, Ruijin Hospital. Cell lines were cultured in RPMI-1640 medium or Dulbecco's modified Eagle's medium (DMEM) with 10% fetal bovine serum (Gibco, United States) and 5 μ g/ml penicillin-streptomycin in a humidified incubator at 37°C with 5% CO₂.

Quantitative Real-Time PCR

Total cellular RNA was isolated from GC cells according to the EZB RNA reagent kit protocol, and 200 ng of total RNA was reverse transcribed to cDNA using a PrimeScript RT Master Mix Kit (Takara Bio). mRNA levels were measured by quantitative real-time PCR using SYBR Premix Ex Taq, and human GAPDH was used as an internal control.

Western Blot Analysis of Gene Expression

Western blotting was performed as described previously (Jiang et al., 2018). Antibodies against FOXCI, DKK1, c-MYC, and β -catenin were purchased from Abcam, and the secondary antibody (anti-rabbit IgG or anti-mouse IgG) was purchased from Proteintech. An anti-GAPDH antibody was used as an internal control. Detail information could be obtained in the **Supplementary Material 2**.

Expression Vectors and Gene Transfection

Plasmid transfection process was performed using Lipofectamine 2000 Reagent (Life Technology, Thermo Fisher Scientific, DE, United States). Full-length FOXC1 cDNAs were cloned into the pLVXyu-2Flag-3C-2 vector for FOXC1 expression. The c-MYC plasmid and DKK1 plasmid were gifts from Professor Guohong Hu at The Key Laboratory of Stem Cell Biology, Institute of Health Sciences, Shanghai Institutes for Biological Sciences. Stably transfected GC cells were established using puromycin selection after transfection with the expression vector or control plasmid. CRISPR/Cas9 vector plasmid was obtained from the Molecular and Cell Biology Laboratory, Fudan University. The sgRNA target sequence for FOXC1 was 5'-GGGTGCGAGTACACGCTCAT-3', and CRISPR/Cas9 vector plasmid was used as a control. Stably transfected GC cells for 24 h were established using puromycin selection for 2 weeks after transfection. Knockout efficiency were validated by Western blot with FOXC1 antibody.

Luciferase Assay

The pGL3-Basic Luciferase Reporter vector was a gift from Fudan University Shanghai Cancer Center. The 2.1-kb DKK1 and c-MYC promoter was cloned into the pGL3-Basic Luciferase Reporter vector. Activity of the DKK1 and c-MYC promoters was normalized by co-transfection with the Renilla luciferase reporter plasmid, which was a gift from Fudan University. Firefly and Renilla luciferase activities were measured at 48 h after transfection using a Dual-Luciferase Reporter Assay System (Promega).

TOP-Flash/FOP-Flash Reporter Assay

A TOP-flash/FOP-flash-dependent luciferase reporter assay was used to evaluate Wnt/LEF/TCF activity. TOP-flash/FOP flash and Renilla plasmids to demonstrate transfection efficiency were incubated for 24 h. Relative luciferase activity was determined using a dual-luciferase assay (Promega). Transfection efficiency was normalized according to Renilla luciferase activity. The cells were lysed at 16 h after transfection, and luciferase activities were determined.

Chromatin Immunoprecipitation Assay

GC cells (2×10^7) were used for chromatin immunoprecipitation assays, and an anti-FOXC1 antibody was used to pull down DKK1 and c-MYC promoter-protein complexes. This assay was performed using CST Chromatin Immunoprecipitation Kit (CST9002) according to the manufacturer's instructions. The DNA samples were analyzed by PCR for potential binding sites. The PCR products were separated and visualized on a 2.5% agarose gel. The primers used for PCR are listed in Table 1.

Immunofluorescence (IF) Staining and Confocal Microscopy

AGS and MKN-45 cells were seeded onto coverslips before they reached 80% confluence. The cells were fixed with 4% paraformaldehyde for 15 min, and the samples were kept in

phosphate-buffered saline (PBS) containing 0.1% Triton X-100 (PBS-T), quenched with 50 mM NH₄Cl in PBS-T, and blocked with 1% BSA in PBS-T. Immunostaining was performed using the appropriate primary and secondary antibodies, and images were acquired using a confocal microscope (Zeiss, LSM510).

Apoptosis Analysis and Cell Cycle Analysis by Flow Cytometry

Apoptosis was evaluated by flow cytometry. Briefly, cells were stained with Annexin V-FITC conjugate and propidium iodide solution. A FACSCalibur system (BD Biosciences, United States) was used to analyze apoptosis.

The cells were fixed in 75% ethanol and stained with PI/RNase Staining Buffer (BD Biosciences). The cell cycle was analyzed by flow cytometry using the FACSCalibur system (BD Biosciences, United States).

Cell Proliferation and Colony Formation Assay

GC cell proliferation was evaluated by the CCK-8 assay. For the colony formation assay, cells were seeded into six-well culture

TABLE 1 | Quantitative real time polymerase chain reaction assay (Q-PCR) primer.

| Gene name | Sequence detail information |
|----------------------------|-----------------------------|
| GAPDH-Forward | GCACCGTCAAGGCTGAGAAC |
| GAPDH-Reverse | TGGTGAAGACGCCAGTGGGA |
| FOXC1 -Forward | AACAGCATCCGCCACAACCTC |
| FOXC1-Reverse | TCCTTCTCCTCCTGTCTTCAC |
| YAP-Forward | TGTCCAGATGA ACGTCACAGC |
| YAP-Reverse | TGGTGGCTGTTT CACTGGAGCA |
| TAZ -Forward | CACCGTGTCCAATCACCAGTC |
| TAZ -Reverse | TCCAACGCATCAACTTCAGGT |
| β -catenin -Forward | CATCTACACAGTTTGATGCTGCT |
| β -catenin - Reverse | GCAGTTTTGTCTCAGTTCAGGGA |
| AXIN1 -Forward | GGTTTCCCTTGGACCTCG |
| AXIN1 -Reverse | CCGTGCAAGTCTCACCTTTAATG |
| NOTCH1 -Forward | GAGGCGTGGCAGACTATGC |
| NOTCH1 -Reverse | CTTGACTCCGTCAGCGTGA |
| BIRC5 -Forward | AGGACCACCGCATCTCTACAT |
| BIRC5 -Reverse | AAGTCTGGCTCGTTCTCAGTG |
| CCND1-Forward | GCTGCGAAGTGGAAACCATC |
| CCND1-Reverse | CCTCCTTCTGCACACATTTGAA |
| c-MYC -Forward | GTCAAGAGGCGAACACACAAC |
| c-MYC -Reverse | TTGGACGGACAGGATGTATGC |
| SPP1 -Forward | GAAGTTTCGCAGACCTGACAT |
| SPP1 -Reverse | GTATGCACCAATTCAACTCCTCG |
| GPC3 -Forward | ATTGGCAAGTTATGTGCCCAT |
| GPC3 -Reverse | TTCGGCTGGATAAGGTTTCTTC |
| BAX -Forward | CCCAGAGGCTCTTTTCCGAG |
| BAX -Reverse | CCAGCCCATGATGGTTCTGAT |
| PUMA-Forward | GCCAGATTTGTGAGACAAGAGG |
| PUMA-Reverse | CAGGCACCTAATTGGGCTC |
| DKK1 -Forward | CTCGGTTCTCAATTCACACG |
| DKK1 -Reverse | GCACTCCTCGTCTCTCTG |

plates at a density of 1,000–2,000 cells/well and grown for 10–14 days. The cells were fixed with methanol and stained with 0.1% crystal violet.

Mouse Models of GC Tumorigenesis

Ten nude mice were sorted into two groups, and GC cells (5×10^6 per mouse) were subcutaneously injected. The mice were sacrificed 5 weeks later. The tumors were removed and weighed, processed and embedded in paraffin for further study.

Statistical Analysis

All experiments that were presented in this work were repeated more than three times. Data was presented as mean \pm standard error of the mean. For statistical analysis, two-tailed independent Student's t-test was applied to a demonstration of homogeneity of variance with the F test or one-way or two-way ANOVA for more than two groups. Statistical significance was set as $P < 0.05$.

RESULTS

FOXC1 Expression Is Upregulated in Human Gastric Cancer Tissues and Cell Lines

To investigate the role of FOXC1 in human gastric cancer, the mRNA level data of FOXC1 in GC and adjacent normal tissues were obtained from GEPIA and analyzed. And the result indicated that the expression level of FOXC1 was increased in GC tissues compared with normal tissues (**Figure 1A**). To confirm the expression level of FOXC1 in GC, IHC staining was applied to detect the protein level of FOXC1. As shown in **Figure 1B**, compared to normal tissues, the protein level of FOXC1 was higher in 85.7% (18/21) of the GC tissues. qPCR and western blot were applied to evaluate mRNA and protein levels of FOXC1 in non-malignant (GES-1) and gastric cancer cell lines (AGS, SGC-7901, MGC-803, MKN-45, HGC-27). The results demonstrated that both mRNA and protein levels were significantly upregulated in GC cell lines (**Figures 1C,D**). The data was obtained from Kaplan-Meier Plotter and affy ID of FOXC1(213260_at) dataset used for the analysis¹. A total of 422 patients were concluded in our analysis and cut-off value for the high and low expression is 141. And number of patients in high and low expression groups are 300 and 122, respectively. The median survival time for high and low expression groups are 89.43 and 34.3 months respectively ($p = 0.0038$). In general, high expression of FOXC1 indicated a poor prognosis in GC (**Figure 1E**). These results indicate that FOXC1 might be an important oncogene in GC.

FOXC1 Contributes to Gastric Cancer Growth *in vitro* and *in vivo*

To investigate the role of FOXC1 in the tumorigenesis and progression of GC, we applied CRISPR-Cas9-mediated gene-editing system to knock out FOXC1 expression in AGS and MKN-45 cells. Meanwhile, FOXC1 sequence was cloned into

pCDNA plasmids overexpressed FOXC1 in AGS and MKN-45 cells. The efficiencies were confirmed by western blot and qPCR assays (**Figure 2A**). We observed that FOXC1 knockout (KO) significantly suppressed colony formation and cell proliferation, while FOXC1 overexpression dramatically enhanced cell viability and proliferation ($p < 0.05$) (**Figures 2B,C**). To study the oncogenic functions of FOXC1 in GC, we checked the effect of FOXC1 knockout on tumor growth and found that FOXC1 KO significantly decreased the tumor growth of MKN-45 cells ($p < 0.05$) (**Figures 2D–G**). FOXC1 expression level in xenografts was determined by IHC (**Figure 2H**).

Altered Expression of FOXC1 Affects the Cell Cycle in GC

Apoptosis and cell cycle are two main factors that affect tumor growth. To investigate the role of FOXC1, we applied flow cytometry for verification. The results demonstrated that FOXC1 KO in GC cells didn't affect apoptosis (**Figure 3A**), but decreased cell cycle progression ($p < 0.05$) (**Figure 3B**), indicating FOXC1 regulates the proliferation of GC cells through cell cycle. To search for downstream effectors of FOXC1-induced GC proliferation, we examined the expression levels of several signaling molecules (e.g., Wnt/ β -catenin, Notch, and Hippo) implicated in the regulation of cell proliferation during gastric carcinogenesis. qPCR and western blotting analyses revealed unchanged expression of the core components of those signaling pathways with FOXC1 KO (**Figures 3C,D**). To better understand the role of FOXC1 in the cell cycle of GC, we further measured mRNA levels of other target genes, such as baculoviral IAP repeat-containing protein 5 (BIRC5), cyclin D1 (CCND1), c-MYC, secreted phosphoprotein 1 (SPP1), and glypican 3 (GPC3) BAX and PUMA and found that CCND1 and c-MYC gene expression was downregulated in FOXC1 KO AGS cells (**Figure 3C**), demonstrating that FOXC1 promotes cell cycle via regulation of cyclin D1 and c-MYC.

FOXC1 Expression Enhances c-MYC Expression to Promote Gastric Cancer Cell Proliferation

Due to c-MYC is a critical transcription factor in regulating cell proliferation and development, we focused on c-Myc in regulating GC proliferation. To investigate the role of c-MYC in FOXC1-mediated GC proliferation, we next analyzed whether c-MYC expression is changed in AGS and MKN-45 cells with KO and overexpression of FOXC1, respectively. The results of qPCR and western blotting indicated that FOXC1 KO in AGS and MKN-45 cells decreased c-MYC expression, and consistently, FOXC1 overexpression dramatically enhanced c-MYC expression (**Figures 4A,B**). Furthermore, direct overexpression of c-MYC restore the FOXC1-deficient phenotype on cell proliferation in AGS and MKN-45 cells (**Figures 4C,D**). The results of luciferase activity assays indicated that FOXC1 could regulate c-MYC expression at the transcriptional level (**Figures 4E,F**). Given that FOXC1 is an important transcription factor, we next examined whether FOXC1 acts as a transcription factor to activate c-Myc expression in AGS and MKN-45 cells. We

¹<http://kmplot.com/analysis/index.php?p=service>

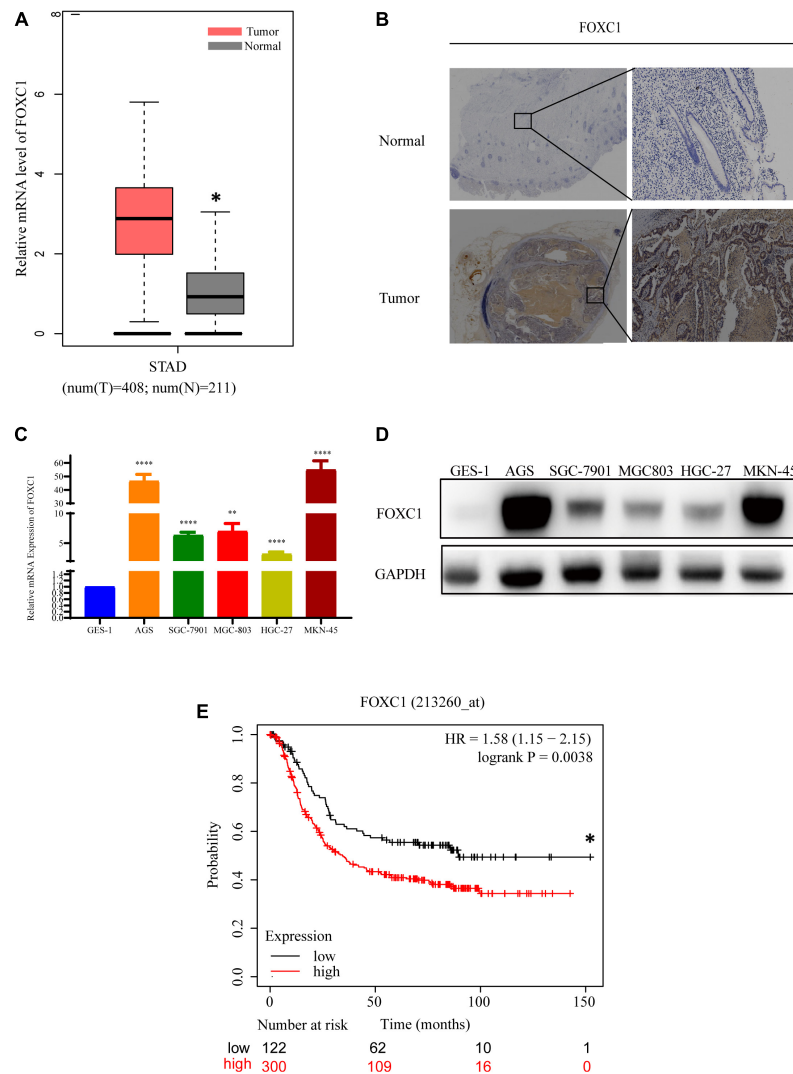


FIGURE 1 | FOXC1 expression is upregulated in human gastric cancer tissues and cell lines. **(A)** Comparison of relative mRNA levels of FOXC1 in gastric cancer and normal tissues. The data were downloaded from GEPIA (<http://gepia.cancer-pku.cn/detail.php?gene=FOXC1>). **(B)** IHC staining was applied to detect FOXC1 protein levels in gastric cancer and normal tissue. FOXC1 expression level was higher in 85.7% (18/21) of the GC tissues and representative images show increased FOXC1 expression in GC tissue (below panel) compared with adjacent normal gastric tissues (upper panel). **(C,D)** mRNA and protein levels of FOXC1 in the gastric cancer cell lines AGS, SGC-7901, MGC-803, MKN-45, HGC-27, and the GES-1 cell line. The expression levels of FOXC1 were normalized to GAPDH. (* $P < 0.05$, ** $P < 0.01$, **** $P < 0.001$). **(E)** Kaplan-Meier curves for the survival time of patients with gastric cancer. The data was obtained from Kaplan-Meier Plotter and affy ID of FOXC1(213260_at) dataset used for the analysis (<http://kmplot.com/analysis/index.php?p=service>). High and low expression groups are 300 and 122, respectively. The median survival time for high and low expression groups are 89.43 and 34.3 months respectively ($p = 0.0038$). Log-rank tests were used to determine statistical significance (* $P < 0.05$).

employed ChIP assay to confirmed whether there was a potential binding site in the c-MYC promoter. However, the results showed no direct binding of FOXC1 to the c-MYC promoter (**Figure 4G**).

FOXC1 Expression Enhances c-MYC Expression to Promote Gastric Cancer Cell Proliferation Through Activation of the Wnt Signaling Pathway

Considering c-MYC is an important target gene of the Wnt pathway, we hypothesized that FOXC1 may activate Wnt

signaling to enhance c-MYC expression. Given that AGS and MKN-45 cells expressed higher levels of FOXC1 than SGC-7901, MGC-803, HGC-27 cells. Further, Wnt activity was aberrant higher in AGS and MKN-45 cells than in SGC-7901, MGC-803, HGC-27 cells, as determined by TOP-Flash reporter assay (**Figure 1A**), indicating that Wnt activity is regulated and correlated with the FOXC1 levels in the cells (**Figure 5A**). β -Catenin aberrant cumulation in the cytoplasm is an important part for Wnt activation. We conducted qPCR and WB assay to explore the potential correlation of FOXC1 and β -Catenin, and the results indicated that FOXC1

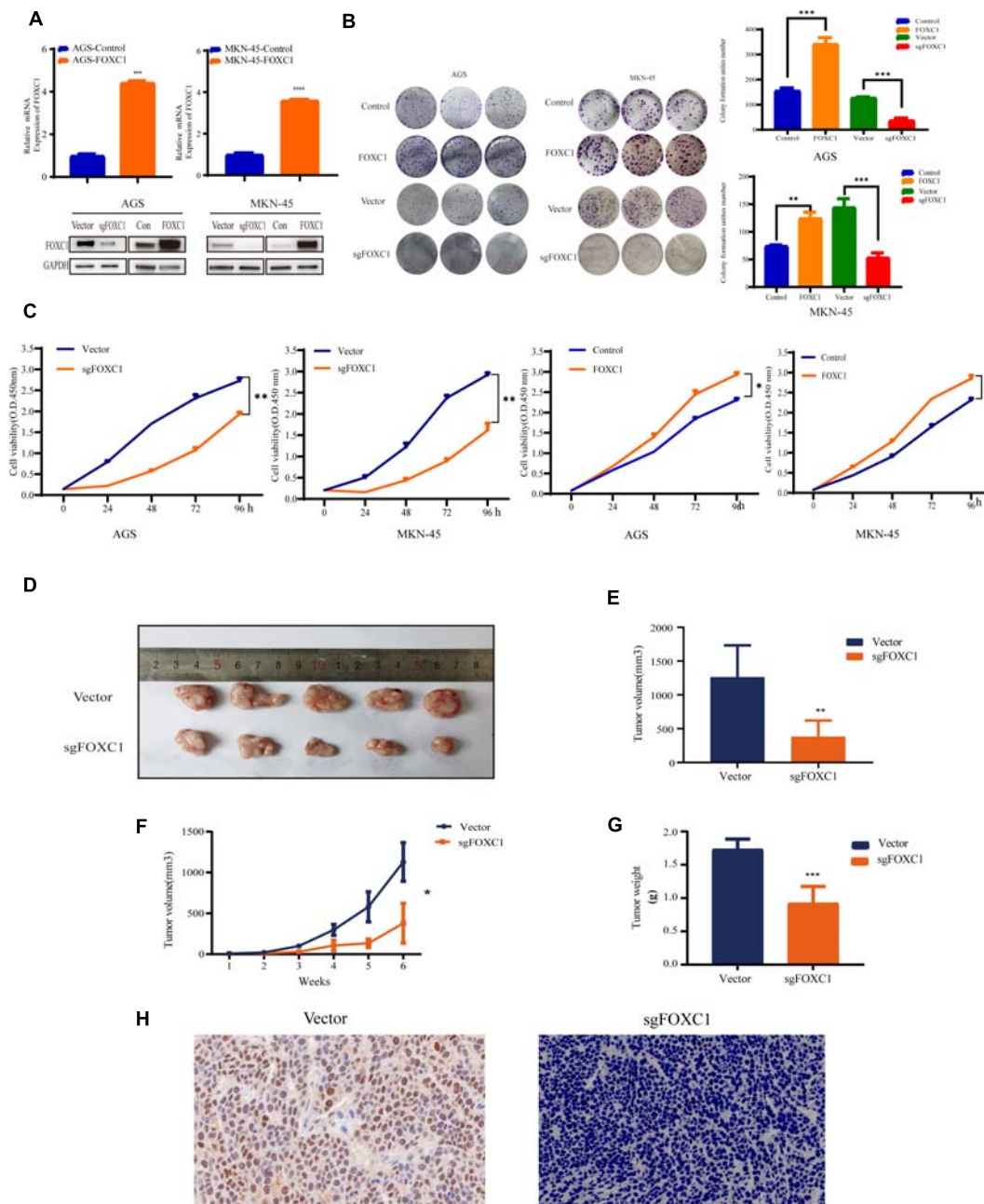


FIGURE 2 | FOXC1 contributes to gastric cancer growth *in vitro* and *in vivo*. **(A)** Verification of overexpression in AGS and MKN-45 cells using qPCR. FOXC1 knockout and overexpress efficiency was confirmed using western blotting, and GAPDH was used as an internal control. **(B,C)** The impact of FOXC1 expression *in vitro* on GC cell proliferation, as assessed using colony formation assays **(B)**. **(C)** CCK-8 proliferation assays in FOXC1 KO and overexpress AGS and MKN-45 cells, respectively. All CCK-8 assays were performed three times and showed the same trend and representative results were shown in panel **(C)**. **(D–G)** MKN-45-Vector and MKN-45-sgFOXC1 cells were injected subcutaneously into right forelimb five nude mice, respectively (5×10^6 cells for each mouse). Tumor size **(D)**, tumor volume **(E)**, tumor growth curves **(F)**, tumor weights **(G)** and IHC **(H)** are shown (* $P < 0.05$, ** $P < 0.01$, *** $P < 0.001$, **** $P < 0.0001$).

did not have a significant influence on β -catenin expression at transcription or translation level (**Figures 5B,C**). At the same time, we learned that the activity of the wnt signaling pathway is related to β -Catenin in the nucleus (Zhang et al., 2011). Thus, we further explore the distribution of β -catenin in cytoplasm and nucleus. Interestingly, the results showed

that β -catenin distribution in the nucleus increased with upregulation of FOXC1, while decreased with FOXC1 knockout, supporting the role of FOXC1 in activation of classic Wnt pathway (**Figures 5D,E**). In addition, β -Catenin will be labeled with E3 ubiquitin ligase after β -Catenin phosphorylation at Ser33/37/Thr41 in the cytoplasm (Reya and Clevers, 2005;

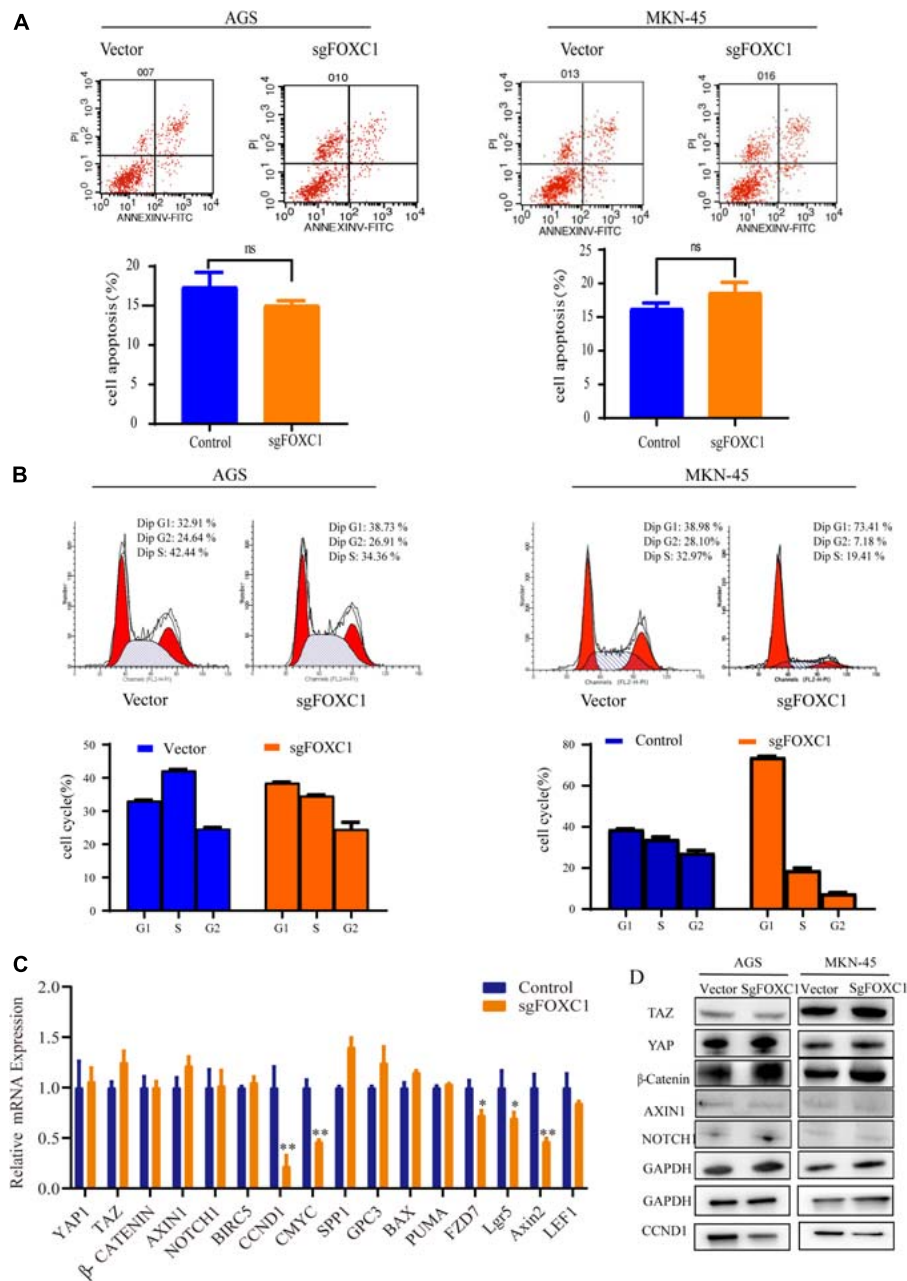


FIGURE 3 | Altered expression of FOXC1 affects the cell cycle in GC. **(A)** Annexin-V & Dead Cell (7-AAD) flow cytometry analysis to evaluate cell apoptosis. In the right-down panel in each plot was considered as early meaningful apoptosis. Representative figure of the three replicates of each proportion of early apoptosis was shown in panel **(A)**. The results flow cytometry assay on cell apoptosis in FOXC1 KO cell lines (AGS cells and MKN-45 cells) had no significant influence on cell apoptosis. Values are presented as the mean \pm standard deviation of three independent experiments ($P > 0.05$). **(B)** The results flow cytometry assay on cell cycle in FOXC1 KO cells lines (AGS cells and MKN-45 cells) showed that FOXC1 had a significant role in cell cycle regulation. Representative figure of the three replicates of each proportion of cell cycle was shown in panel **(B)**. Values are presented as the mean \pm standard deviation of three independent experiments ($*P < 0.05$, $**P < 0.01$). **(C,D)** Expression of core components of the Hippo, Wnt and Notch signaling pathways was determined by qPCR in FOXC1 KO AGS cells **(C)** and western blot **(D)** analyses in FOXC1 KO AGS and MKN-45 cells. ns, no significant difference and $P > 0.05$.

Clevers and Nusse, 2012; Zhan et al., 2017). We also found β -Catenin phosphorylation at Ser33/37/Thr41 increased with FOXC1 KO and decreased with FOXC1 overexpression (Figure 5F), supporting the conclusion that WNT signaling pathway is activated under the condition of high FOXC1 expression. Previous studies indicated FOXM1 could directly

bound to β -catenin *in vivo* and *in vitro* and Promoted β -catenin nuclear localization and controls Wnt target-gene expression (Zhang et al., 2011). Considering FOXC1 and FOXM1 belong to forkhead box family, thus we further explore the potential role of FOXC1 in nuclear localization of β -catenin. Our results showed that FOXC1 bound to β -catenin to form a complex

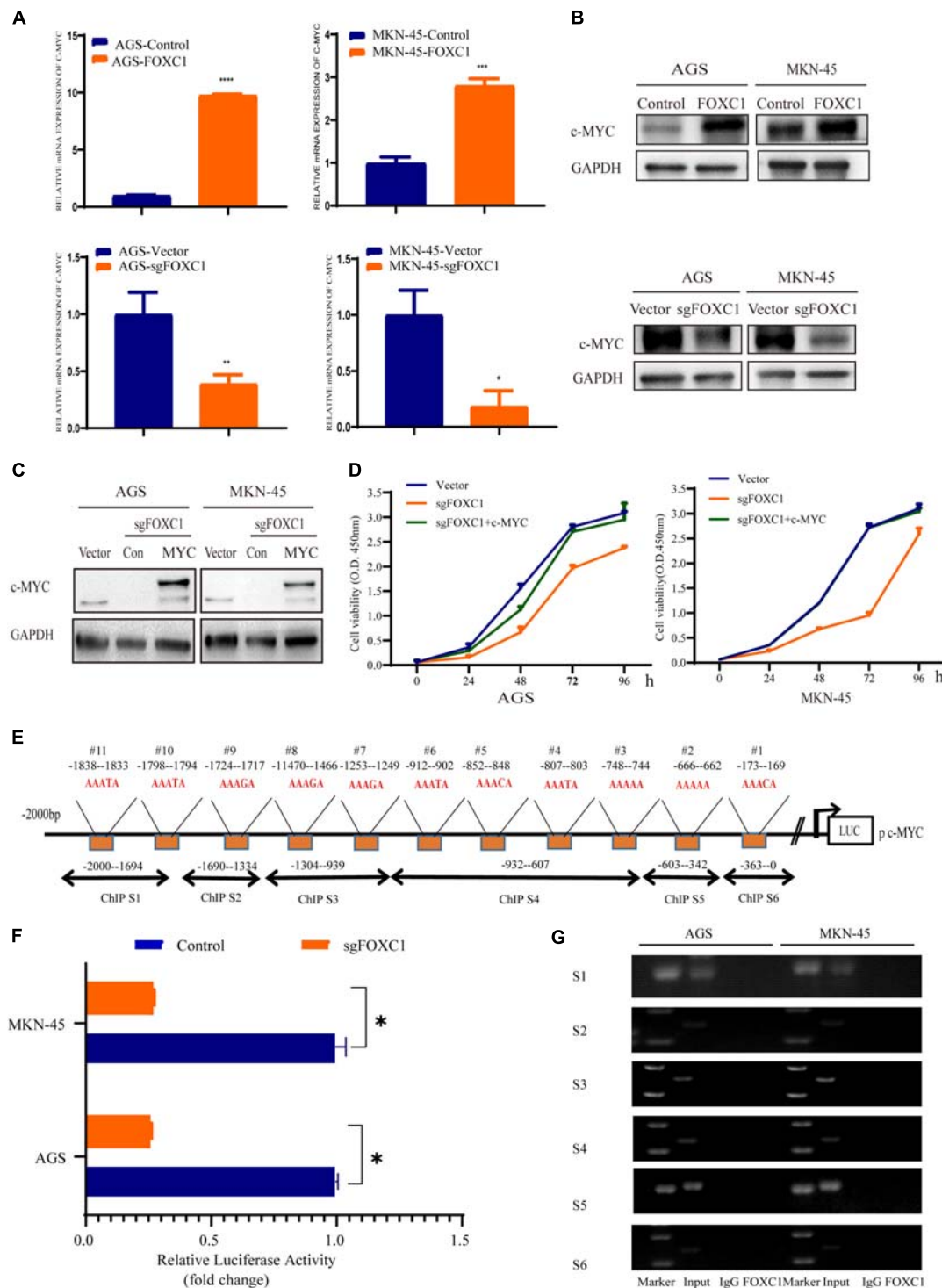


FIGURE 4 | FOXCI enhances c-MYC expression to regulate gastric cancer cell proliferation. **(A,B)** The results of qPCR **(A)** and western blot **(B)** assays indicated that knockout of FOXCI in AGS and MKN-45 cells dramatically decreased c-MYC expression but that forced FOXCI expression in AGS and MKN-45 cells dramatically enhanced c-MYC expression at transcriptional and translational level. Representative figure of the three replicates was shown. **(C)** Validation of ectopic expression of c-MYC in FOXCI KO AGS and MKN-45 cells using Western blotting. **(D)** Ectopic overexpression c-MYC in FOXCI KO AGS and MKN-45 cells could restore the FOXCI deficiency-induced phenotype of cell proliferation. All CCK-8 assays were performed three times and showed the same trend and representative results were shown in panel **(D)**. **(E)** The putative binding site of FOXCI in the 5' untranslated regions of c-MYC promoter. **(F)** A double luciferase activity assay in AGS and MKN-45 cells indicated that FOXCI regulates c-MYC expression at the transcriptional level. **(G)** ChIP assay results showed that there was no potential direct binding site of FOXCI in c-MYC promoter. * $P < 0.05$, ** $P < 0.01$, *** $P < 0.001$, **** $P < 0.0001$.

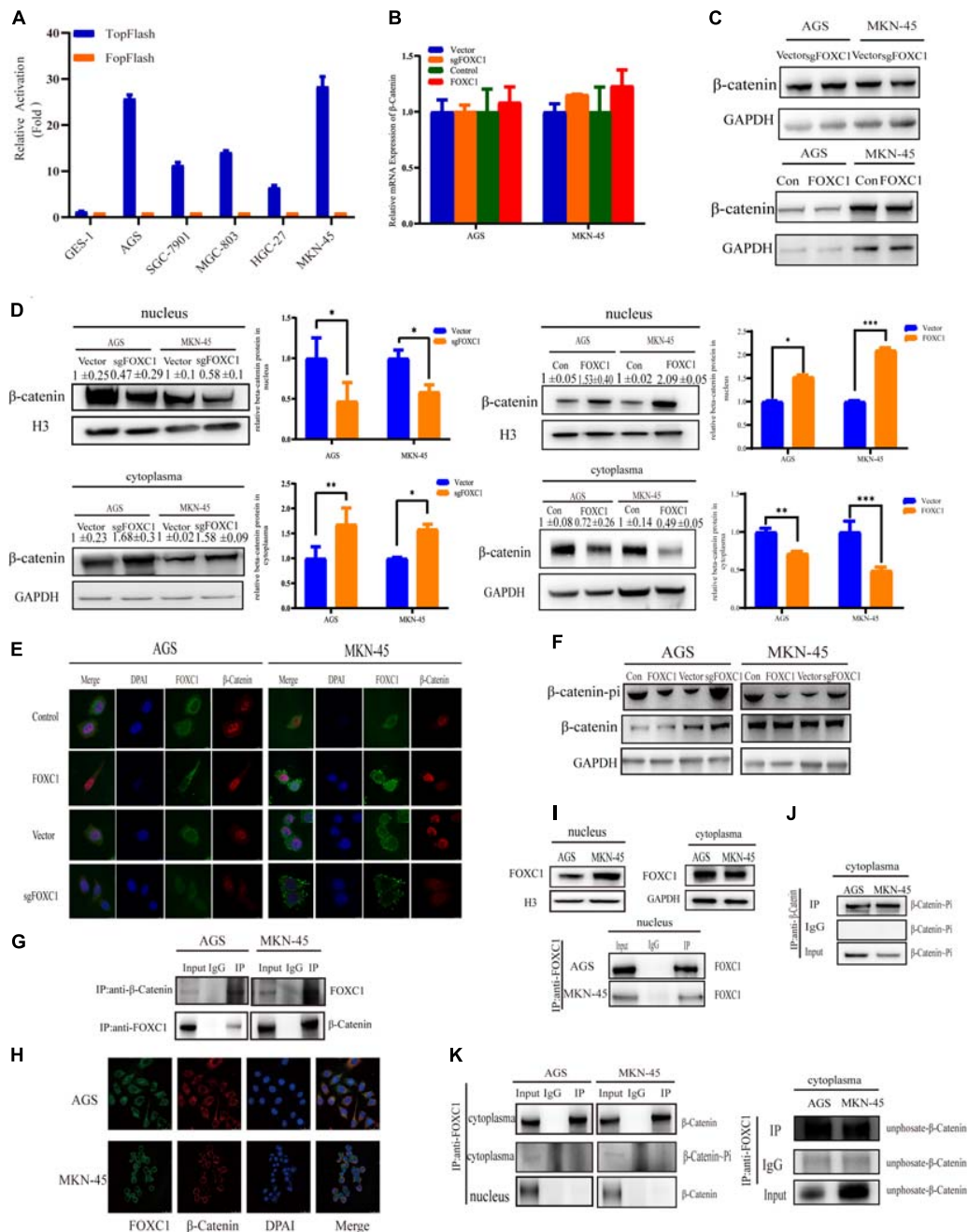


FIGURE 5 | FOXC1 enhances c-MYC expression to promote gastric cancer cell proliferation through activation of the Wnt signaling pathway. **(A)** TopFlash/FopFlash assays using normal gastric cells (GES-1) and gastric cancer cells (AGS, SGC-7901, MGC-803, MKN-45, HGC-27). **(B)** qPCR results in FOXC1 KO and FOXC1-overexpressing AGS and MKN-45 cells indicated that mRNA levels of β -catenin remained unchanged. **(C)** The results of western blot assays in FOXC1 KO and FOXC1-overexpressing AGS and MKN-45 cells indicated that protein levels of β -catenin remained unchanged (β -catenin Antibody: CST #8480S). **(D)** FOXC1 KO increased β -catenin levels in the cytoplasm but decreased them in the nucleus (β -catenin Antibody: CST #8480S). **(E)** Immunofluorescence assay in FOXC1 KO and FOXC1-overexpressing AGS and MKN-45 cells showed that the level of β -catenin translocation into nucleus changed with knockout and overexpression FOXC1 (β -catenin Antibody: CST #8480S). **(F)** FOXC1 overexpression inhibit the phospho- β -Catenin (Ser33/37/Thr41) in AGS and MKN-45 cells (phospho- β -Catenin (Ser33/37/Thr41) Antibody: CST #9561T). **(G,H)** co-IP assays and immunofluorescence assay indicated that FOXC1 binds to the β -catenin protein in the cytoplasm (β -catenin Antibody: CST #8084S; FOXC1 Antibody: Abcam #ab227977). **(I)** Western blot assays and immunoprecipitation assay were applied to confirmed the distribution of FOXC1 in the nucleus. **(J)** co-IP assay was applied to confirmed the distribution of phospho- β -Catenin (Ser33/37/Thr41) in the nucleus (phospho- β -Catenin (Ser33/37/Thr41) Antibody: CST #9561T). **(K)** co-IP assay was applied to confirmed whether FOXC1 bound to the β -catenin protein in the cytoplasm and nucleus. Immunoprecipitation assay results showed that FOXC1 bound to non-phospho- β -Catenin in the cytoplasm (β -catenin Antibody: CST #8084S; phospho- β -Catenin (Ser33/37/Thr41) Antibody: CST #9561T; Non-phospho- β -Catenin (Ser33/37/Thr41) Antibody: CST #8814T), and FOXC1 did not bound to β -Catenin in the nucleus (β -catenin Antibody: CST #8084S). * $P < 0.05$, ** $P < 0.01$, *** $P < 0.001$.

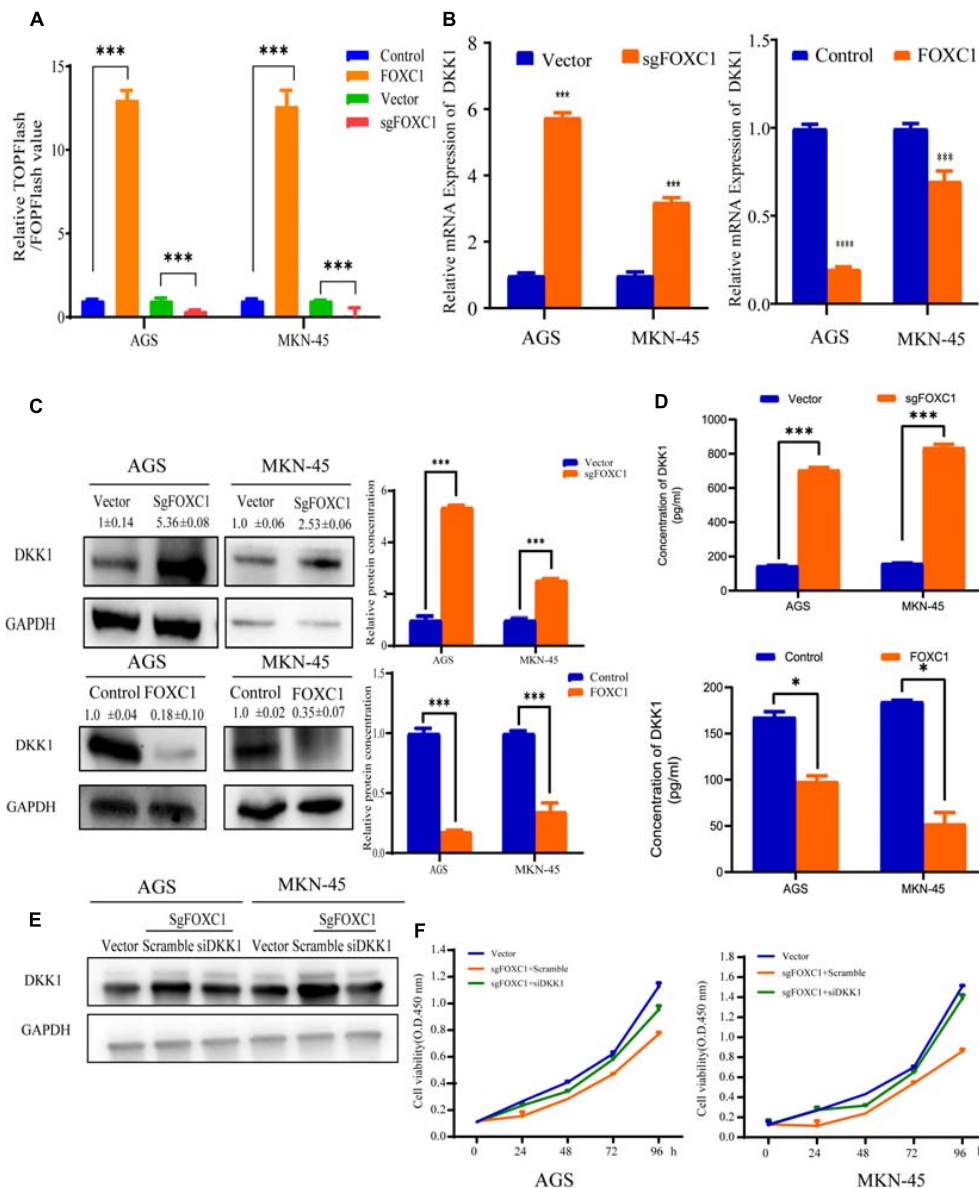


FIGURE 6 | FOXC1 promotes GC cell proliferation via downregulation of DKK1. (A) TopFlash/FopFlash assays were used to investigate activity of the Wnt signaling pathway in FOXC1 KO and FOXC1 overexpression AGS and MKN-45 cells. The results demonstrated that FOXC1 KO decreased activity of the Wnt signaling pathway and forced FOXC1 expression could increase activity of the Wnt signaling pathway. (B–D) qPCR (B), western blot (C) and ELISA (D) assays in FOXC1 knockout GC cells were used to analyze the mRNA and protein levels of DKK1. (E) Western blot assay was applied to confirmed the knockdown efficiency of DKK1 in FOXC1 KO AGS and MKN-45 cells. (F) DKK1 knockdown could restore FOXC1 KO-induced suppression of AGS and MKN-45 cell proliferation. All CCK-8 assays were performed three times and showed the same trend and representative results were shown in panel (F). * $P < 0.05$, *** $P < 0.001$.

in AGS and MKN-45 cells (Figures 5G,H). However, we also found a contradiction, that is, in Figure 4G, the ChIP experiment showed that there was no potential FOXC1 binding site in c-MYC promoter. Thus, we conducted COIP assays in the cytoplasm and nucleus, and the results showed FOXC1 bound to β -catenin in cytoplasm, but not in nucleus (Figures 5I–K). These results were consistent with previous result demonstrating that FOXC1 does not directly bind to the c-MYC promoter.

FOXC1 Promotes GC Cell Proliferation via Downregulation of DKK1

To find out the mechanism by which FOXC1 activates the Wnt signaling pathway, we first applied the TopFlash/FopFlash assay to determine the activity of Wnt pathway in FOXC1 KO GC cells. The results indicated that the activity of the Wnt signaling pathway was decreased in FOXC1 KO and increased in FOXC1 overexpression AGS and MKN-45 cells (Figure 6A). Considering the role of DKK1 in classic Wnt

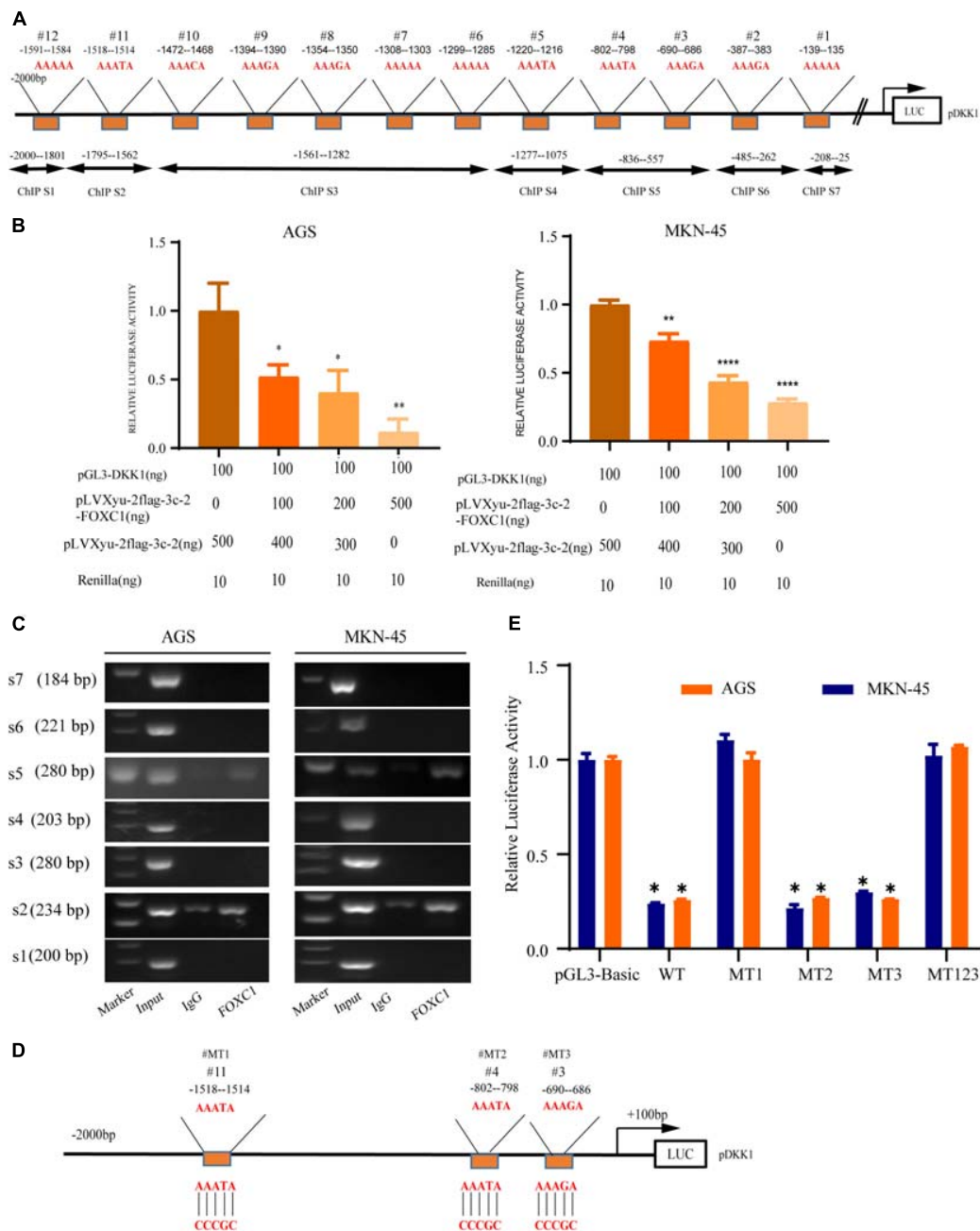


FIGURE 7 | DKK1 is downstream of FOXC1 in GC. **(A)** Considering the specific DNA sequence for FOX transcription factor (AAATA), A total of 12 putative FOXC1 binding sites in the 5' untranslated region of DKK1 promoter. **(B)** Double luciferase activity assay in AGS and MKN-45 cells to confirm the influence of FOXC1 on the transcription of DKK1. The results of Luciferase activity were dose-dependently decreased after co-transfection with FOXC1 (* $P < 0.05$), which is also indicated that FOXC1 negatively regulated DKK1 expression at transcriptional level. **(C)** Chromatin immunoprecipitation assay (ChIP) results demonstrated that FOXC1 binds directly to the DKK1 promoter at ChIP S2 and ChIP S5 in the **(A)**, which were consisted by three putative binding sites (site3#, site4# and site 11#). **(D,E)** Schematic diagram of mutation strategies in the DKK1 promoter. The results indicated that FOXC1 decreased the luciferase activity of the WT DKK1 promoter to approximately 75% of the corresponding control but did not affect the activity of MT123 or MT1 (* $P < 0.05$, ** $P > 0.05$, **** $P < 0.0001$).

signaling. We next examined the level of DKK1 expression, which is the antagonist of Wnt signaling, and found that the DKK1 mRNA level increased in FOXC1 KO GC cells and decreased in FOXC1-overexpressing GC cells (Figure 6B; Zhu et al., 2021). At the same time, we applied western

blot and EILSA assays were to confirm the correlation of DKK1 protein and FOXC1, and results indicated that FOXC1 negatively regulated DKK1 expression at translational level (Figures 6C,D). In addition, siDKK1 restored the cell proliferation repressed by FOXC1 KO in AGS and MKN-45 cells

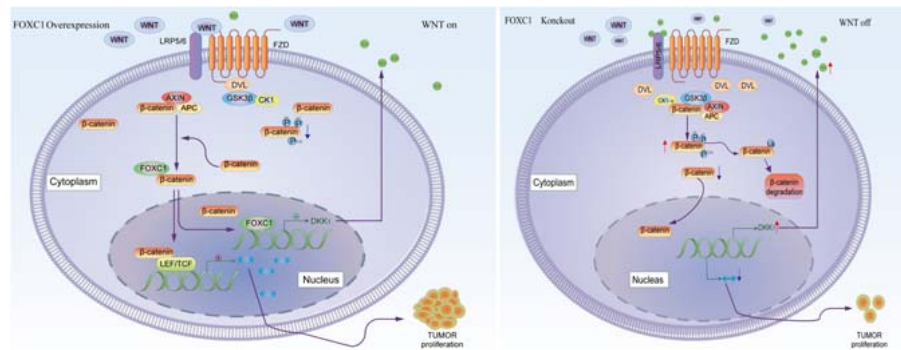


FIGURE 8 | Schematic depicting the role of FOXC1 and DKK1 in the regulation of gastric cancer proliferation. FOXC1 is overexpressed in gastric cancer cells and acts as a transcription factor that negatively regulates DKK1 expression by binding to its promoter region, thereby modulating the activation state of the Wnt signaling pathway and upregulating expression of c-MYC, promoting the proliferation of GC cells. At the same time, FOXC1 also forms a complex with the unphosphorylated β -catenin (Ser33/37/Thr41) protein in the cytoplasm but dissociates in the nucleus.

(Figures 6E,F). Those results indicated FOXC1 regulated GC cells proliferation through DKK1.

DKK1 Is a Downstream Target of FOXC1 in GC

A previous study indicated that AAAYA-rich sequences are the main DNA-binding sequence of FOX transcription factors (Berry et al., 2002), and we found 12 potential binding sites (AAAYAs) in the DKK1 promoter (Figure 7A). To evaluate possible interaction between DKK1 and FOXC1, the sequence from +100bp to -2000bp of the human DKK1 promoter was cloned into a luciferase reporter plasmid (pGL3-DKK1-Luc), and pGL3-DKK1-Luc plasmids with FOXC1 plasmids or control vectors were transiently transfected into AGS and MKN-45 cells. Luciferase assays indicated that FOXC1 significantly decreased the luciferase activity of DKK1 in both cell lines (Figure 7B). According to ChIP analysis, FOXC1 directly binds to the DKK1 promoter (sites #2 and #5) (Figure 7C). To further validate whether DKK1 is regulated directly by FOXC1, we used the wildtype (WT) or mutant (MT) promoter of DKK1 in the luciferase assay (Figure 7D). We found that FOXC1 reduced the luciferase activity of the WT DKK1 promoter to approximately 75% of the corresponding control but did not affect the activity of MT1 or MT123, suggesting that FOXC1 binds to the site #1 (-1514–1518 bp) in the DKK1 promoter (Figure 7E).

DISCUSSION

Wnt signaling pathway is highly activated in gastric cancer (GC) and can contribute growth and metastasis of GC (Zhao et al., 2014). Many studies explored the function of Wnt signaling pathway in tumor progression, however, the reason why it is highly activated in GC remains to be studied. Research to date on this pathway has mostly focused on positive regulatory factors, whereas its antagonist proteins have attracted little attention (Santos et al., 2016; Gao et al., 2018; Nanki et al., 2018; Yang et al., 2018). In this study, we found that FOXC1 was elevated in GC tissue and its level was associated with patients, poor

prognosis. Furthermore, the results showed that FOXC1 can promote growth of GC by modulating the tumor cell cycle, as mediated by c-MYC and cyclin D1, further supporting the role of FOXC1 in GC progression (Wang et al., 2018, 2020).

c-Myc is a critical transcription factor, and its aberrant expression of c-Myc can promote tumorigenesis and development (Sansom et al., 2007). For many years, c-Myc has been considered as a potential drug target for suppressing tumors, however, drug development for the c-Myc target itself has always been a difficult point due to the absence of a suitable pocket for high-affinity binding by low molecular weight inhibitors (Duffy et al., 2021). Recent studies have also shown that c-Myc is an important target gene of the wnt signaling pathway, and pharmacologic targeting of Fzd could effectively inhibited the growth of gastric adenomas by influence the expression of c-Myc (Flanagan et al., 2019; Ashrafizadeh et al., 2020). Therefore, inhibiting the activity of the Wnt pathway can significantly reduce the expression of c-Myc and inhibit the proliferation of tumor cells. In this study, we focused on c-Myc in regulating GC proliferation. While restore c-Myc expression could reverse the inhibition effect of FOXC1 knockout. And the results in this study indicated that, c-Myc is positively correlated with FOXC1 expression. Due to FOXC1 is a transcription factor, we explore whether c-Myc is a direct target gene of FOXC1. However, the result of ChIP assay showed that there were no potential binding sites in c-Myc promoter. Thus, we turned to focus on the activity of Wnt pathway in GC cells. Interestingly, the activity of Wnt pathway increased with FOXC1 overexpression and increased with FOXC1 knockout. Besides, the transcription of c-Myc also changes with Wnt signal pathway, which is consistent with the results of previous studies (Ramezani et al., 2019).

In further research, we interfere the expression of FOXC1 in AGS and MKN-45 cells. Expression of DKK1 was changed with knockout and overexpression of FOXC1 at transcriptional and translational level. These results indicate that FOXC1 might negatively regulate expression of DKK1. Considering the role of DKK1 in classic Wnt signaling, we sought to clarify the function of FOXC1 in GC proliferation by regulating DKK1 expression

(Zhu et al., 2021). Our study indicated that DKK1 expression negatively correlated with proliferative ability in GC cells, which is consistent with the results of a previous study of DKK1 in GC proliferation (Wang et al., 2013; Hong et al., 2018). These results suggested that FOXC1 regulated GC cell proliferation by regulating the expression of DKK1. Considering the role of FOXC1 and DKK1 expression in GC cells proliferation, we want to classify the specific mechanisms of FOXC1 and DKK1 expression in GC cells. Due to FOXC1 is a transcription factor, we further investigated whether DKK1 is a direct transcription target of FOXC1. Through a dual luciferase reporter assay and ChIP assay, we found that FOXC1 act as a transcription factor and directly bound to the DKK1 promoter region (-1518–1514) to negatively regulate transcription of this gene. Although there were three direct binding sites in the result of ChIP assay, the result of luciferase verified that there was only one site that were confirmed had a significant influence on DKK1 transcription due to the help of specific transcription cofactors, which is crucial to perform transcription activation functions. As for which transcriptional cofactors are, it remains to be further explored. At the same time, knockdown DKK1 expression in FOXC1 knockout cells could restore the effect of FOXC1 in promoting proliferation, which indicated the importance of FOXC1/DKK1 axis in GC proliferation.

β -Catenin aberrant cumulation in the cytoplasm is an important part for Wnt activation. In gastric cancer cells, the level expression of FOXC1 is associated with aberrant activation of Wnt pathway due to FOXC1 binding to DKK1 promoter to negatively regulated its transcription, which could affect the level of phosphate- β -Catenin at Ser33/37/Thr41 in the cytoplasm and contributed β -catenin aberrant cumulation in the cytoplasm. It is reported that FOXM1 could directly bound to β -catenin and Promoted β -catenin nuclear localization and controls Wnt target-gene expression (Zhang et al., 2011). Considering FOXC1 and FOXM1 belong to forkhead box family, thus we further explore the potential role of FOXC1 in nuclear localization of β -catenin. Our results showed that FOXC1 did not have a significant influence on β -Catenin at transcriptional level or translational level, it affected the level of phosphate- β -Catenin at Ser33/37/Thr41 in the cytoplasm and nuclear entrance process of β -Catenin. In addition, FOXC1 bound to unphosphorylated β -catenin to form a complex in the cytoplasm, and FOXC1 did not bind to β -catenin after the complex enters the nucleus (Figure 8). However, we did not clarify the specific mechanism of FOXC1 promotes β -catenin translocation into the nucleus. Therefore, we will further study the underlying mechanism by which FOXC1 regulates the function of β -catenin in future research.

In conclusion, our study revealed the function of FOXC1/DKK1 in GC cell proliferation, which provided a potential biomarker and target therapy for GC.

DATA AVAILABILITY STATEMENT

Publicly available datasets were analyzed in this study. This data can be found here: <http://gepia.cancer-pku.cn/detail.php?gene=FOXC1>; <http://kmplot.com/analysis/index.php?p=service&cancer=gastric>.

ETHICS STATEMENT

The studies involving human participants were reviewed and approved by The human sample study was reviewed and approved by Shanghai Jiao Tong University School of Medicine. The patients/participants provided their written informed consent to participate in this study. The animal study was reviewed and approved by the animal study was reviewed and approved by Shanghai Jiao Tong University School of Medicine.

AUTHOR CONTRIBUTIONS

HZ, JD, and FY conceived and designed the studies. JJ and HZ conducted most of the experiments and analyzed the data. JJ, BS, and WW conducted all animal studies. FY performed immunohistochemical technology and data analysis. JL provided technical support for some cell experiments. JJ and WY wrote this manuscript. All authors contributed to the article and approved the submitted version.

FUNDING

This study was supported by grants from National Natural Sciences Foundation of China (No. 81771789) and Medical Engineering Cross Research Foundation of Shanghai Jiao Tong University (No. ZH2018QNA52).

SUPPLEMENTARY MATERIAL

The Supplementary Material for this article can be found online at: <https://www.frontiersin.org/articles/10.3389/fcell.2021.662624/full#supplementary-material>

REFERENCES

- Ashrafizadeh, M., Ahmadi, Z., Mohamamdinejad, R., Yaribeygi, H., Serban, M. C., Orafi, H. M., et al. (2020). Curcumin therapeutic modulation of the wnt signaling pathway. *Curr. Pharm. Biotechnol.* 21, 1006–1015. doi: 10.2174/1389201021666200305115101
- Berry, F. B., Saleem, R. A., and Walter, M. A. (2002). FOXC1 transcriptional regulation is mediated by N- and C-terminal activation domains and contains a phosphorylated transcriptional inhibitory domain. *J. Biol. Chem.* 277, 10292–10297. doi: 10.1074/jbc.M110266200
- Chae, W. J., and Bothwell, A. L. M. (2018). Canonical and non-canonical wnt signaling in immune cells. *Trends Immunol.* 39, 830–847. doi: 10.1016/j.it.2018.08.006
- Chen, S., Jiao, S., Jia, Y., and Li, Y. (2016). Effects of targeted silencing of FOXC1 gene on proliferation and in vitro migration of human non-small-cell lung carcinoma cells. *Am. J. Transl. Res.* 8, 3309–3318.
- Clevers, H., and Nusse, R. (2012). Wnt/ β -catenin signaling and disease. *Cell* 149, 1192–1205. doi: 10.1016/j.cell.2012.05.012
- Deng, L., Liu, T., Zhang, B., Wu, H., Zhao, J., and Chen, J. (2017). Forkhead box C1 is targeted by microRNA-133b and promotes cell proliferation and migration

- in osteosarcoma. *Exp. Ther. Med.* 14, 2823–2830. doi: 10.3892/etm.2017.4870
- Duffy, M. J., O'Grady, S., Tang, M., and Crown, J. (2021). MYC as a target for cancer treatment. *Cancer Treat. Rev.* 94:102154. doi: 10.1016/j.ctrv.2021.102154
- Erickson, R. P. (2001). Forkhead genes and human disease. *J. Appl. Genet.* 42, 211–221.
- Fitzmaurice, C., Dicker, D., Pain, A., Hamavid, H., Moradi-Lakeh, M., MacIntyre, M. F., et al. (2015). The global burden of cancer 2013. *JAMA Oncol.* 1, 505–527. doi: 10.1001/jamaoncol.2015.0735
- Flanagan, D. J., Barker, N., Costanzo, N. S. D., Mason, E. A., Gurney, A., Meniel, V. S., et al. (2019). *Frizzled-7* is required for Wnt signaling in gastric tumors with and without *Apc* mutations. *Cancer Res.* 79, 970–981. doi: 10.1158/0008-5472.Can-18-2095
- Gao, J., Zhao, C., Liu, Q., Hou, X., Li, S., Xing, X., et al. (2018). Cyclin G2 suppresses Wnt/ β -catenin signaling and inhibits gastric cancer cell growth and migration through Dapper1. *J. Exp. Clin. Cancer Res.* 37:317. doi: 10.1186/s13046-018-0973-2
- Gilding, L. N., and Somerville, T. C. P. (2019). The diverse consequences of FOXC1 deregulation in cancer. *Cancers (Basel)* 11:184. doi: 10.3390/cancers11020184
- Golson, M. L., and Kaestner, K. H. (2016). Fox transcription factors: from development to disease. *Development* 143, 4558–4570. doi: 10.1242/dev.112672
- Gomceli, I., Bostanci, E. B., Ozer, I., Kemik, A. S., Turhan, N., Tez, M., et al. (2012). A novel screening biomarker in gastric cancer: serum Dickkopf-1. *Hepatogastroenterology* 59, 1661–1664. doi: 10.5754/hge11516
- Hong, S. A., Yoo, S. H., Lee, H. H., Sun, S., Won, H. S., Kim, O., et al. (2018). Prognostic value of Dickkopf-1 and β -catenin expression in advanced gastric cancer. *BMC Cancer* 18:506. doi: 10.1186/s12885-018-4420-8
- Hopkins, A., Mirzayans, F., and Berry, F. (2016). Foxc1 expression in early osteogenic differentiation is regulated by BMP4-SMAD activity. *J. Cell. Biochem.* 117, 1707–1717. doi: 10.1002/jcb.25464
- Hsu, H. H., Kuo, W. W., Shih, H. N., Cheng, S. F., Yang, C. K., Chen, M. C., et al. (2019). FOXC1 regulation of miR-31-5p confers oxaliplatin resistance by targeting LATS2 in colorectal cancer. *Cancers (Basel)* 11:1576. doi: 10.3390/cancers1101576
- Huang, L., Huang, Z., Fan, Y., He, L., Ye, M., Shi, K., et al. (2017). FOXC1 promotes proliferation and epithelial-mesenchymal transition in cervical carcinoma through the PI3K-AKT signal pathway. *Am. J. Transl. Res.* 9, 1297–1306.
- Ito, Y. A., Goping, I. S., Berry, F., and Walter, M. A. (2014). Dysfunction of the stress-responsive FOXC1 transcription factor contributes to the earlier-onset glaucoma observed in Axenfeld-Rieger syndrome patients. *Cell Death Dis.* 5:e1069. doi: 10.1038/cddis.2014.8
- Jiang, J., Wang, G. Z., Wang, Y., Huang, H. Z., Li, W. T., and Qu, X. D. (2018). Hypoxia-induced HMGB1 expression of HCC promotes tumor invasiveness and metastasis via regulating macrophage-derived IL-6. *Exp. Cell Res.* 367, 81–88. doi: 10.1016/j.yexcr.2018.03.025
- Jin, Y., Han, B., Chen, J., Wiedemeyer, R., Orsulic, S., Bose, S., et al. (2014). FOXC1 is a critical mediator of EGFR function in human basal-like breast cancer. *Ann. Surg. Oncol.* 21(Suppl. 4), S758–S766. doi: 10.1245/s10434-014-3980-3
- Liu, Y., Miao, Y., Gao, X., Wang, Y. Y., Wang, H., Zheng, Y. W., et al. (2018). MicroRNA-200a affects the proliferation of airway smooth muscle cells and airway remodeling by targeting FOXC1 via the PI3K/AKT signaling pathway in ovalbumin-induced asthmatic mice. *Cell. Physiol. Biochem.* 50, 2365–2389. doi: 10.1159/000495097
- Nanki, K., Toshimitsu, K., Takano, A., Fujii, M., Shimokawa, M., Ohta, Y., et al. (2018). Divergent routes toward Wnt and R-spondin niche independency during human gastric carcinogenesis. *Cell* 174, 856–869.e17. doi: 10.1016/j.cell.2018.07.027
- Ramezani, A., Nikraves, H., and Faghihloo, E. (2019). The roles of FOX proteins in virus-associated cancers. *J. Cell. Physiol.* 234, 3347–3361. doi: 10.1002/jcp.27295
- Reya, T., and Clevers, H. (2005). Wnt signalling in stem cells and cancer. *Nature* 434, 843–850. doi: 10.1038/nature03319
- Sansom, O. J., Meniel, V. S., Muncan, V., Phesse, T. J., Wilkins, J. A., Reed, K. R., et al. (2007). Myc deletion rescues Apc deficiency in the small intestine. *Nature* 446, 676–679. doi: 10.1038/nature05674
- Santos, J. C., Carrasco-Garcia, E., Garcia-Puga, M., Aldaz, P., Montes, M., Fernandez-Reyes, M., et al. (2016). SOX9 elevation acts with canonical WNT signaling to drive gastric cancer progression. *Cancer Res.* 76, 6735–6746. doi: 10.1158/0008-5472.Can-16-1120
- Shimada, H., Noie, T., Ohashi, M., Oba, K., and Takahashi, Y. (2014). Clinical significance of serum tumor markers for gastric cancer: a systematic review of literature by the task force of the Japanese gastric cancer association. *Gastric Cancer* 17, 26–33. doi: 10.1007/s10120-013-0259-5
- Wang, B., Liu, J., Ma, L. N., Xiao, H. L., Wang, Y. Z., Li, Y., et al. (2013). Chimeric 5/35 adenovirus-mediated Dickkopf-1 overexpression suppressed tumorigenicity of CD44⁺ gastric cancer cells via attenuating Wnt signaling. *J. Gastroenterol.* 48, 798–808. doi: 10.1007/s00535-012-0711-z
- Wang, J., Wang, Y., Zhang, H., Chang, J., Lu, M., Gao, W., et al. (2020). Identification of a novel microRNA-141-3p/Forkhead box C1/ β -catenin axis associated with rheumatoid arthritis synovial fibroblast function in vivo and in vitro. *Theranostics* 10, 5412–5434. doi: 10.7150/thno.45214
- Wang, L., Chai, L., Ji, Q., Cheng, R., Wang, J., and Han, S. (2018). Forkhead box protein C1 promotes cell proliferation and invasion in human cervical cancer. *Mol. Med. Rep.* 17, 4392–4398. doi: 10.3892/mmr.2018.8423
- Xu, Y., Shao, Q. S., Yao, H. B., Jin, Y., Ma, Y. Y., and Jia, L. H. (2014). Overexpression of FOXC1 correlates with poor prognosis in gastric cancer patients. *Histopathology* 64, 963–970. doi: 10.1111/his.12347
- Yang, X. Z., Cheng, T. T., He, Q. J., Lei, Z. Y., Chi, J., Tang, Z., et al. (2018). LINC01133 as ceRNA inhibits gastric cancer progression by sponging miR-106a-3p to regulate APC expression and the Wnt/ β -catenin pathway. *Mol. Cancer* 17:126. doi: 10.1186/s12943-018-0874-1
- Yu, Z., Xu, H., Wang, H., and Wang, Y. (2018). Foxc1 promotes the proliferation of fibroblast-like synoviocytes in rheumatoid arthritis via PI3K/AKT signalling pathway. *Tissue Cell* 53, 15–22. doi: 10.1016/j.tice.2018.05.011
- Zhan, T., Rindtorff, N., and Boutros, M. (2017). Wnt signaling in cancer. *Oncogene* 36, 1461–1473. doi: 10.1038/onc.2016.304
- Zhang, N., Wei, P., Gong, A., Chiu, W. T., Lee, H. T., Colman, H., et al. (2011). FoxM1 promotes β -catenin nuclear localization and controls Wnt target-gene expression and glioma tumorigenesis. *Cancer Cell* 20, 427–442. doi: 10.1016/j.ccr.2011.08.016
- Zhao, C. M., Hayakawa, Y., Kodama, Y., Muthupalani, S., Westphalen, C. B., Andersen, G. T., et al. (2014). Denervation suppresses gastric tumorigenesis. *Sci. Transl. Med.* 6:250ra115. doi: 10.1126/scitranslmed.3009569
- Zhong, X., Yu, X., Wen, X., Chen, L., and Gu, N. (2020). Activation of the LINC00242/miR-141/FOXC1 axis underpins the development of gastric cancer. *Cancer Cell Int.* 20:272. doi: 10.1186/s12935-020-01369-7
- Zhu, G., Song, J., Chen, W., Yuan, D., Wang, W., Chen, X., et al. (2021). Expression and role of Dickkopf-1 (Dkk1) in tumors: from the cells to the patients. *Cancer Manag. Res.* 13, 659–675. doi: 10.2147/cmar.S275172

Conflict of Interest: The authors declare that the research was conducted in the absence of any commercial or financial relationships that could be construed as a potential conflict of interest.

Copyright © 2021 Jiang, Li, Yao, Wang, Shi, Yuan, Dong and Zhang. This is an open-access article distributed under the terms of the Creative Commons Attribution License (CC BY). The use, distribution or reproduction in other forums is permitted, provided the original author(s) and the copyright owner(s) are credited and that the original publication in this journal is cited, in accordance with accepted academic practice. No use, distribution or reproduction is permitted which does not comply with these terms.



Stepwise Induction of Inner Ear Hair Cells From Mouse Embryonic Fibroblasts via Mesenchymal-to-Epithelial Transition and Formation of Otic Epithelial Cells

Qiong Yang^{1†}, Haosong Shi^{2†}, Yizhou Quan³, Qianqian Chen³, Wang Li¹, Li Wang¹, Yonghui Wang¹, Zhongzhong Ji³, Shan-Kai Yin², Hai-Bo Shi^{2*}, Huiming Xu^{1*} and Wei-Qiang Gao^{1,3*}

OPEN ACCESS

Edited by:

Zuoren Yu,
Tongji University, China

Reviewed by:

Yaobo Liu,
Soochow University, China
Guangshuo Ou,
Tsinghua University, China

*Correspondence:

Wei-Qiang Gao
gao.weiqiang@sjtu.edu.cn
Hai-Bo Shi
hbshi@sjtu.edu.cn
Huiming Xu
quxuhm123@163.com

[†] These authors have contributed
equally to this work

Specialty section:

This article was submitted to
Cell Growth and Division,
a section of the journal
Frontiers in Cell and Developmental
Biology

Received: 25 February 2021

Accepted: 17 March 2021

Published: 17 June 2021

Citation:

Yang Q, Shi H, Quan Y, Chen Q,
Li W, Wang L, Wang Y, Ji Z, Yin S-K,
Shi H-B, Xu H and Gao W-Q (2021)
Stepwise Induction of Inner Ear Hair
Cells From Mouse Embryonic
Fibroblasts via Mesenchymal-
to-Epithelial Transition and Formation
of Otic Epithelial Cells.
Front. Cell Dev. Biol. 9:672406.
doi: 10.3389/fcell.2021.672406

¹ State Key Laboratory of Oncogenes and Related Genes, Renji-Med X Stem Cell Research Center, Ren Ji Hospital, School of Medicine, Shanghai Jiao Tong University, Shanghai, China, ² Department of Otorhinolaryngology, The Sixth People's Hospital of Shanghai, Shanghai Jiao Tong University, Shanghai, China, ³ School of Biomedical Engineering and Med-X Research Institute, Shanghai Jiao Tong University, Shanghai, China

Although embryonic stem cells or induced pluripotent stem cells are able to differentiate into inner ear hair cells (HCs), they have drawbacks limiting their clinical application, including a potential risk of tumorigenicity. Direct reprogramming of fibroblasts to inner ear HCs could offer an alternative solution to this problem. Here, we present a stepwise guidance protocol to induce mouse embryonic fibroblasts to differentiate into inner ear HC-like cells (HCLs) via mesenchymal-to-epithelial transition and then acquisition of otic sensory epithelial cell traits by overexpression of three key transcription factors. These induced HCLs express multiple HC-specific proteins, display protrusions reminiscent of ciliary bundle structures, respond to voltage stimulation, form functional mechanotransduction channels, and exhibit a transcriptional profile of HC signature. Together, our work provides a new method to produce functional HCLs *in vitro*, which may have important implications for studies of HC development, drug discovery, and cell replacement therapy for hearing loss.

Keywords: hair cell regeneration, mesenchymal-to-epithelial transition (MET), hearing loss, mouse embryonic fibroblasts, transdifferentiation

INTRODUCTION

Inner ear hair cells (HCs), the mechanoreceptors for perception of sound and balance, can convert the sound or motion into electrochemical signals (Carey and Amin, 2006; Costa et al., 2015). They are terminally differentiated cells and are positioned in the sensory epithelium of the inner ear. The latter grows from the otic placode during embryogenesis (Zhai et al., 2005; Kelley, 2006). Unfortunately, HCs are easily injured by noise, ototoxins, genetic predisposition, and aging and

Abbreviations: ESCs, embryonic stem cells; HCLs, hair cell-like cells; HCs, hair cells; iPSCs, induced pluripotent stem cells; MEFs, mouse embryonic fibroblasts; MET, mesenchymal-to-epithelial transition; OECs, otic epithelial cells; OPCs, otic progenitor cells; SCs, supporting cells; SES, Sox2/Eya1/Six1; TGF- β , transforming growth factor beta.

hardly have a capability to regrow in adult mammals (Schacht, 1986; Dror and Avraham, 2009; Smith et al., 2016). As a result, millions of people worldwide are permanently debilitated by hearing loss and balance problems (Ma et al., 2019). Therefore, development of a novel method of producing new HCs *in vitro* may provide a cell replacement therapy method and serve as a helpful system for our studies of HC biology, disease, and regeneration.

By far, stem cells are believed to be a promising source for cell replacement therapy to treat HC loss (Géléoc and Holt, 2014). For HC regeneration, it has been shown that either embryonic stem cells (ESCs) or induced pluripotent stem cells (iPSCs) could be induced to differentiate into inner ear HCLs (Li et al., 2003; Oshima et al., 2010; Koehler et al., 2017; Oujii et al., 2017). However, clinical application of ESCs is troubled by its possible immune rejection and moral and safety worries. Similarly, iPSCs are also limited in clinical use due to its time-consuming and genetic instability that lead to tumor formation (Lanza, 2007; Knoepfler, 2009). In addition to ESCs and iPSCs, some recent studies showed that HCLs could be obtained from either the differentiation of stem cells in the inner ear or a direct transdifferentiation of supporting cells (SCs) in the inner ear (Zheng and Gao, 2000; White et al., 2006; Liu Q. et al., 2016), suggesting that inner ear stem cells and SCs might be considered sources for clinical research and trial application. However, the use of postnatal inner ear stem cells and SCs still encounters a great challenge attributable to the insufficiency of their supply and conceivable ethical concerns (Burns et al., 2012; Liu Q. et al., 2016). In order to overcome the concerns mentioned above, investigators have focused on seeking for additional appropriate cell reservoir as an alternative source. A number of recent investigations reported that fibroblasts have some distinctive advantages, such as less of ethical concern, convenience, accessibility, fast proliferation, and relative guarantee of safety. They are somatic cells and are capable of further converting to cell type of interest that can be used for future auto-transplantation cell therapy. For instance, overexpression of lineage-specific transcription factors (TFs) can directly convert fibroblasts into some other lineages, including neurons (Vierbuchen et al., 2010; Ambasudhan et al., 2011), hepatocytes (Sekiya and Suzuki, 2011; Huang et al., 2011), cardiomyocytes (Ieda et al., 2010; Fu et al., 2013), Sertoli cells (Buganim et al., 2012), and blood progenitors (Szabo et al., 2010). The converted cells can acquire relevant physiological functions. However, up to now, it remains unclear whether and how mouse fibroblasts can be successfully converted into functional HCs.

Previously, several TFs have been shown to act as determinants for HC fate and to influence HC differentiation during inner ear development (Schimmang, 2013). Inner ear HC differentiation requires *Atoh1* (Zheng and Gao, 2000), as well as *Sox2*, *Eya1*, and *Six1* (hereafter referred to as SES), and the latter three genes are co-expressed in sensory progenitors. Mutations in these four genes cause sensorineural hearing loss (Xu et al., 1999; Zheng and Gao, 2000; Ozaki et al., 2004; Dabdoub et al., 2008; Ahmed et al., 2012). Recent reports indicate that SES proteins interact directly and cooperatively to regulate the *Atoh1* enhancer, leading to expression of *Atoh1* and production of

differentiated HCs. In detail, *Sox2* and *Six1* directly bind to the *Atoh1* enhancer, while the transcriptional coactivator *Eya1* establishes a bridge between *Sox2* and *Six1*. Together, these findings confirm that SES work together with *Atoh1* during HC fate determination in the inner ear (Ahmed et al., 2012; Schimmang, 2013).

In the present study, we applied a stepwise strategy to induce mouse embryonic fibroblasts (MEFs) into HCLs. Firstly, MEFs were obtained and induced initially to undergo mesenchymal-to-epithelial transition (MET) by a small-molecule transforming growth factor beta (TGF- β) inhibitor, SB431542. Subsequently, by using a combination of three TFs SES, the epithelial cells derived from the MEFs were induced to become a population of otic epithelial cells (OECs). These OECs were then capable of differentiating into mechanosensitive sensory HCLs. Importantly, via such sequential steps, the MEF-derived HCLs expressed HC-specific genes, displayed ciliary bundle structures, could be permeated rapidly by FM1-43, and exhibited a transcriptional profile of HC signature based on RNA sequencing analyses. Furthermore, these HCLs were responsive to voltage stimulation. Therefore, we provide in this study a novel stepwise method to successfully convert mouse somatic cells into functional HCLs.

RESULTS

Preparation and Characterization of Mouse Embryonic Fibroblasts

To investigate whether MEFs can be used to convert into inner ear HCs, first, we prepared the primary MEFs from embryonic day 13.5 (E13.5) C57BL/6J mice (Vierbuchen et al., 2010). The head, the limb, the visceral tissues, and all red organs were removed, and the remaining tissue was dissociated and cultivated in Dulbecco's modified Eagle's medium (DMEM) in which we supplemented with 10% fetal bovine serum (FBS) and 1% penicillin (Figure 1A). MEFs were used for the subsequent conversion experiments at passage 2 or 3. To study if the MEFs that we isolated were pure fibroblasts without contamination of any HCs, SCs, or OECs, we characterized them in the cultures by immunofluorescence staining with Vimentin, E-cadherin, Myo7a, P27^{kip}, Pax2, Pax8, Sox2, Jag1, and Sox10 antibodies. As shown in Figure 1B, the MEFs were E-cadherin negative and Vimentin positive. In addition, they were negative to Myo7a, P27^{kip}, Pax2, Pax8, Sox2, Jag1, and Sox10 antibodies, markers of HCs, SCs, or OECs (Figures 1C–G). Thus, the MEFs that we prepared were pure fibroblasts and were not contaminated by HCs, SCs, and OECs.

Transforming Growth Factor Beta Inhibitor Induces Mouse Embryonic Fibroblasts to Undergo a Mesenchymal-To-Epithelial Transition

Considering that fibroblasts and inner ear HCs belong to different cell lineages, we postulated that the conversion of MEFs into inner ear HCs might go through a stepwise manner with an

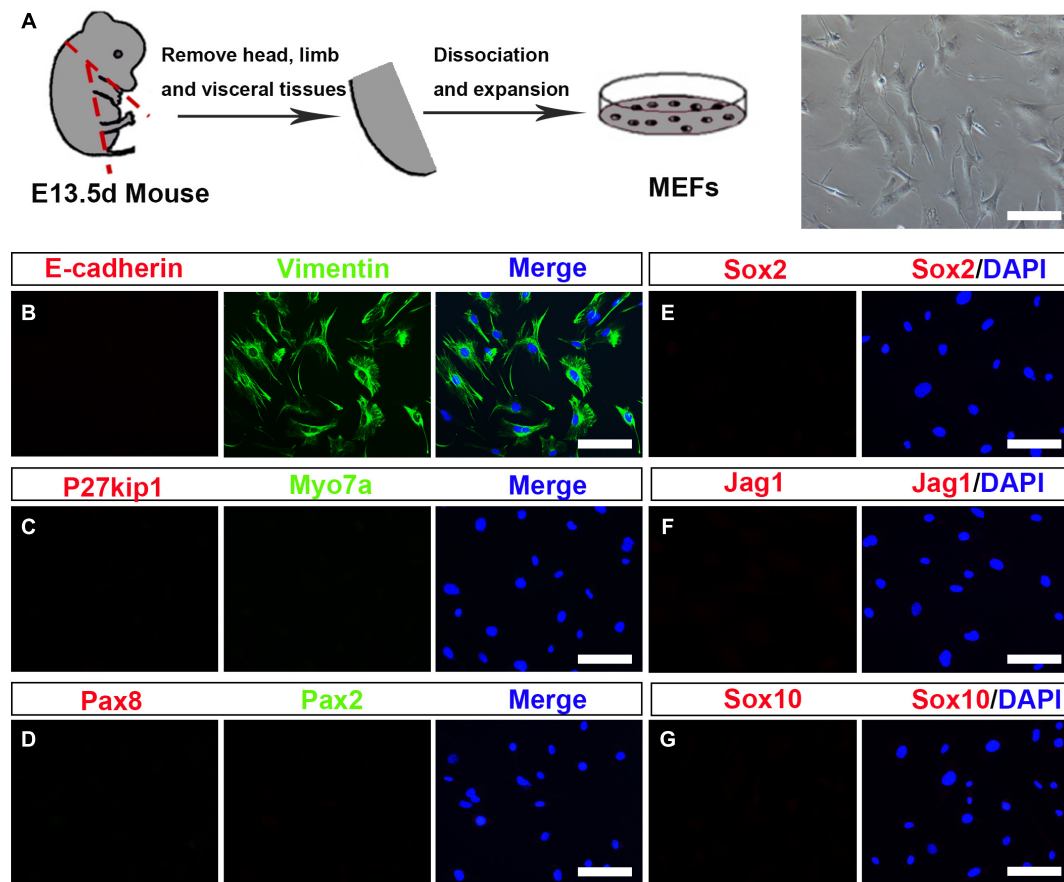


FIGURE 1 | Establishment and characterization of mouse embryonic fibroblasts (MEFs). **(A)** Fibroblasts isolated from mouse embryos were dissociated and cultured under standard fibroblast culture conditions. The fibroblasts were passaged and frozen, and cells passaged at generation 2 or 3 were used for experiments. **(B–G)** Immunostaining of the MEF cells for Vimentin (green) and E-cadherin (red). Hair cells (HCs), supporting cell, and otic epithelial cell (OEC) markers included Myo7a (green), P27^{Kip} (red), Pax2 (green), Pax8 (red), Sox2, Jag1, and Sox10 (scale bar, 25 μ m).

initial MET step. In this regard, we designed our experiment by first inducing the MEFs to become epithelial cells. To achieve this goal, we decided to add a small molecule SB431542 (an inhibitor of TGF- β signaling) to the culture medium, which has been shown to facilitate MET of MEFs and to improve the nuclear reprogramming of mouse fibroblasts (Li et al., 2010). The experimental protocol is described in **Figure 2A**.

To assess the MET of MEFs, we dissociated MEFs and replated them onto poly-L-lysine-coated glass slips in DMEM-containing serum and then replaced with serum-free DMEM/F12 medium plus N2, B27 supplements, and SB431542 (SB) 1 day later. Our quantitative real-time PCR (qRT-PCR) analysis showed an upregulation of E-cadherin gene and a downregulation regulation of Vimentin, a marker for fibroblast, at 3 days post SB treatment in the cultures as compared with the untreated group (**Supplementary Figure 1A**). Such expression pattern became increased at 5 days post SB treatment (**Supplementary Figure 1B**). To determine whether there was a similar expression pattern for E-cadherin and Vimentin proteins, we performed double immunostaining at 5 days post SB treatment in the cultures. As shown in **Supplementary Figure 1C**, while a

considerable number of the cells became E-cadherin positive, many of the cells remained Vimentin positive. In contrast, no E-cadherin-positive cells were seen in the control cultures. At this time point, the E-cadherin staining appeared to be punctate, implying an early stage of MET. To find out whether as time proceeds the MET becomes more complete, we did qRT-PCR analysis for E-cadherin as well as EpCAM and ZO-1, two additional epithelial markers. As shown in **Figure 2B**, the expression of all of the three epithelial marker genes was significantly upregulated as compared with the control cultures. Furthermore, the MEFs with SB treatment exhibited small, compact cell bodies with an epithelial-like morphology (**Figures 2C,D**). These cells also showed positive immunoreactivity to E-cadherin and ZO-1 antibodies (**Figures 2E,F**). In contrast, no such staining was observed in MEFs without SB treatment (**Figures 2G,H**). Moreover, the E-cadherin staining was no longer punctate but rather showed a continuous membrane pattern. Notably, widespread expression of E-cadherin and ZO-1 was only detected in MEFs treated with SB ($46 \pm 5.4\%$ and $48 \pm 2.6\%$ over total cells, respectively) and never seen in MEFs without SB treatment (**Figures 2I,J**).

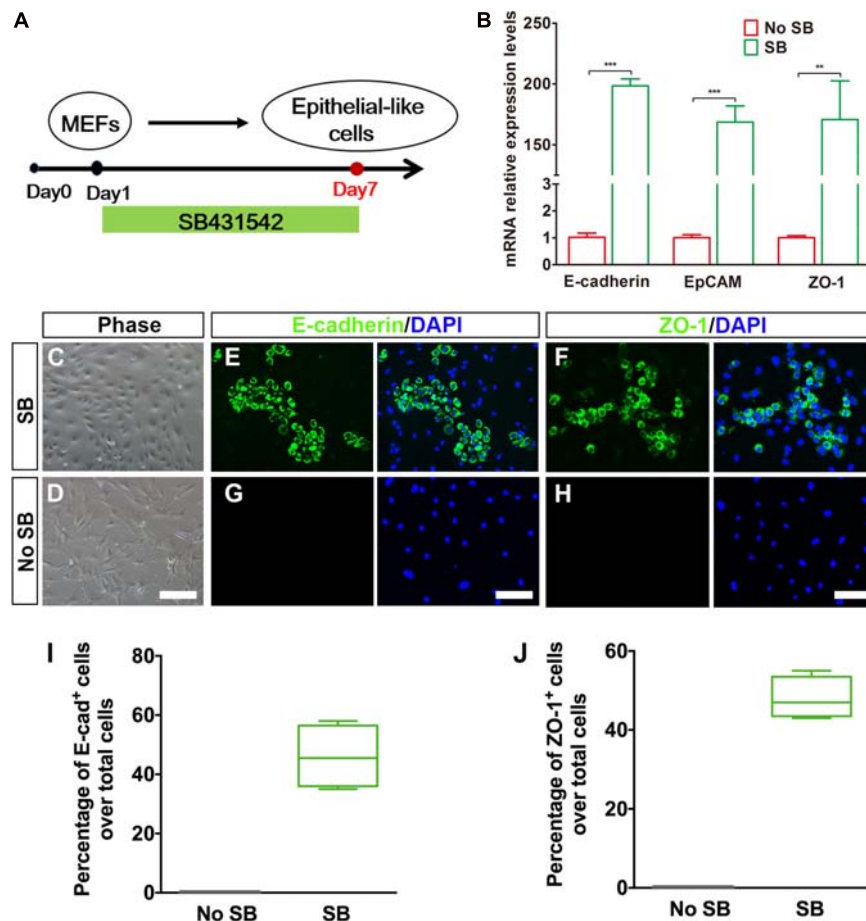


FIGURE 2 | Generation of epithelial-like cells from mouse embryonic fibroblasts (MEFs) by a TGF- β inhibitor. **(A)** An induction protocol describing the SB431542 treatment timeline. **(B)** Quantitative real-time PCR analysis of mRNA levels of E-cadherin, EpCAM, and ZO-1 from MEF-derived epithelial-like cells. MEFs in normal cultures were used as control group, no SB. Data were collected from at least three separate experiments and are shown as means \pm SEM. Statistical significance was tested by Student's *t*-test and expressed as $**p < 0.01$, $***p < 0.001$ compared with the control. **(C,D)** Phase-contrast images of epithelial-like cells (ELCs) and MEFs showing epithelial and mesenchymal cell morphologies, respectively. **(E,F)** Immunostaining analysis of E-cadherin and ZO-1 expression at day 7 in SB-treated cells. Strong upregulation of E-cadherin **(E)** and ZO-1 **(F)** was detected in SB-treated cells. **(G,H)** Immunostaining analysis of E-cadherin and ZO-1 expression at day 7 in no SB treatment cells. No such staining was observed in MEFs without SB treatment. **(I,J)** Frequencies of immunopositive cells for E-cadherin **(I)** and ZO-1 **(J)** in MEF-derived cells with or without SB. Without SB, immunopositivity for E-cadherin and ZO-1 was absent. In contrast, a remarkable number of immunopositive cells were detected in MEF-derived cells with SB. Error bars represent the SEM. $n = 4$ (scale bar, 25 μ m).

Thus, the TGF- β signaling inhibitor facilitates MEFs to gradually undergo a MET so as to form epithelial-like cells.

Conversion of Mouse Embryonic Fibroblast-Derived Epithelial-Like Cells to Otic Epithelial Cells by Transduction of Sox2, Eya1, and Six1

Recent experiments have demonstrated that overexpression of lineage-specific TFs was able to lead to cell-fate changes in various types of somatic cell. For example, Ahmed and colleagues found that a combination of Eya1 and Six1 induces an HC fate in Sox2-expressing non-sensory cells in mouse cochlear explants (Ahmed et al., 2012). In addition, SES are co-expressed in sensory progenitors. If these genes are mutated, an early arrest of otic development can happen in

mice (Xu et al., 1999; Ozaki et al., 2004; Dabdoub et al., 2008; Schimmang, 2013). After considering the TFs that are crucial for HC development and regeneration, we decided to examine whether a combination of SES can program MEF-derived epithelial-like cells to become OECs. To establish a “tunable” SES overexpression system, we first generated doxycycline (Dox)-inducible lentiviruses expressing SES (**Supplementary Figure 2A**). Then we transduced the cultured cells at 7 days post SB treatment with the Dox-inducible SES lentiviruses to generate putative OECs in the presence of Dox. As shown in **Supplementary Figures 2B** and **2C**, qRT-PCR and Western blot analyses indicated that both the SES genes and proteins were significantly overexpressed. Moreover, co-immunostaining for Sox2 and Six1 revealed that Sox2 and Six1 were co-expressed in single cells (**Supplementary Figure 2D**). Notably, the Sox2 staining indicated that the viral infection efficiency was about

43.7% (**Supplementary Figures 2E,F**). In the absence of Dox, no expression of the inducible SES was observed at either the mRNA or protein level, confirming the validity of the tunable SES overexpression.

To evaluate whether OECs could be obtained from MEF-derived epithelial-like cells by overexpression of 3TF, we subjected the MEF-derived epithelial-like cells to a conversion protocol in which Dox treatment was initiated at day 7 and maintained during the following 7 days till day 14, when these cells were collected for analysis (**Figure 3A**). As expected, we found that the induced cells formed colonies at days 7–14 following Dox treatment. Consistent with what was described by Chen W. et al. (2012), the cells in the colonies with Dox treatment showed a flat phenotype with a large amount of cytoplasm and formed epithelioid islands (**Figures 3B,C**). To verify OEC induction, we used antibodies against Pax2 and Pax8 (Hans et al., 2004; Oshima et al., 2010), two markers for OECs, and quantified the numbers of Pax2⁺ cells and Pax8⁺ cells after 7 days of 3TF treatment with or without Dox (**Figures 3D–G**). As a result,

cells without Dox treatment did not express Pax2 and Pax8. By contrast, in the 3TF treatment with Dox group, we observed a remarkable induction of Pax2⁺ cells (36% ± 3.8%) and Pax8⁺ cells (37.8% ± 2.8%) (**Figures 3H,I**). In addition, qRT-PCR analyses also confirmed their extremely high transcript levels, as compared with the group receiving 3TF treatment without Dox (**Figure 3J**). Remarkably, removal of any one or two factors of the 3 TFs reduced the efficiency of OEC induction (**Supplementary Figure 3**). To ascertain that the induced Pax8⁺ cells were indeed epithelial cells, we conducted Pax8 double staining with an epithelial marker E-cadherin. As expected, all of the Pax8⁺ cells were double labeled by the E-cadherin antibody (**Supplementary Figure 4A**). Altogether, these observations suggest that co-expression of SES induces a rapid conversion of MEF-derived epithelial cells into OECs.

Previous studies suggested that during otic development, prior to HC production, there is a formation of the prosensory epithelium where HC progenitors and SCs are generated (Burns and Stone, 2017). To study whether the OECs induced from the

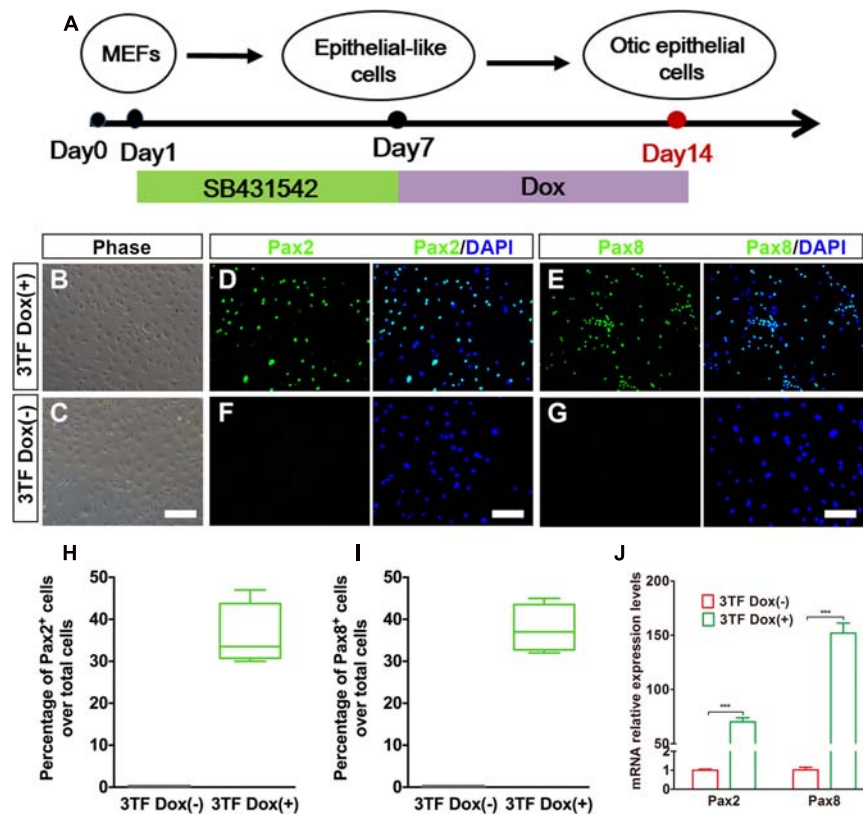


FIGURE 3 | Inducible expression of Six1, Eya1, and Sox2 promotes the conversion of mouse embryonic fibroblast (MEF)-derived epithelial-like cells into otic epithelial cells (OECs). **(A)** MEF induction protocol including the sequential treatment with SB and doxycycline (Dox). **(B,C)** Morphology of OECs (OECs). **(D,E)** Immunostaining analysis of Pax2 and Pax8 expression in MEF-derived epithelial-like cells treated with Dox [3TF Dox (+)]. **(F,G)** Immunostaining analysis of Pax2 and Pax8 expression in MEF-derived epithelial-like cells treated without Dox [3TF Dox (-)]. **(H,I)** Frequencies of immunopositive cells for Pax2 **(H)** and Pax8 **(I)** in MEF-derived cells with or without 3TF Dox. Without Dox, immunopositivity for Pax2 and Pax8 was absent. In contrast, a remarkable number of immunopositive cells were detected in MEF-derived cells with Dox. Error bars represent the SEM. $n = 4$. **(J)** Quantitative real-time PCR analysis of the mRNA levels of OEC genes (Pax2 and Pax8) under different culture conditions. MEF-derived cells cultured without Dox were used as controls. Data were collected from at least three separate experiments and are shown as means ± SEM. Statistical significance was tested by Student's *t*-test and expressed as ** $p < 0.01$, *** $p < 0.001$ compared with the control (scale bar, 25 μ m).

MEFs via the above-mentioned protocol can form prosensory epithelial cells, we performed immunostaining for Sox2, P27^{kip1}, Sox10, and Jag1, markers reminiscent of prosensory epithelial cells in the otic vesicle (Chen and Segil, 1999; Koehler et al., 2013; Wakaoka et al., 2013), in the cultures at days 16–18. Indeed, we observed a significant appearance of cells positive for these genes as compared with the control group (Figure 4A). The percentages of cells immunopositive for Sox2, P27^{kip1}, and Sox10 in 3TF treatment with Dox cells were $34.3 \pm 2.3\%$ (Figure 4B), $28 \pm 1.3\%$ (Figure 4C), and $29.4 \pm 1.5\%$ (Figure 4D), respectively. Furthermore, Sox10⁺Jag1⁺ cells were also seen (Figure 4E). Control cultures not treated with Dox did not express Sox2, P27^{kip1}, Sox10, and Jag1 (Figures 4A–E). Then these genes for prosensory-related markers were also analyzed using qRT-PCR. The data showed that mRNA expression levels of Sox2, P27^{kip1}, Sox10, and Jag1 in cells with Dox were significantly higher than those in cells without Dox ($p < 0.001$), which was in agreement with the results of immunostaining (Figure 4F). In addition, to make sure that the induced Sox2-expressing cells

represented epithelial cells, we performed Sox2 double staining with an epithelial marker E-cadherin. As expected, all of the Sox2-expressing cells were double labeled by the E-cadherin antibody (Supplementary Figure 4B). These results together imply that many of the OECs appear to differentiate further to become prosensory cell-like cells.

Spontaneous Generation of Hair Cell-Like Cells Expressing Multiple Hair Cell Markers and Forming Cilia From Mouse Embryonic Fibroblast-Derived Otic Epithelial Cells

As induction continues, we rendered OECs to a differentiation protocol in which Dox was removed after 7 days of treatment (Figure 5A). We then examined expression of markers for HC such as Myo7a, Calbindin2, or Brn3c to explore whether OECs could give rise to HCLs. Indeed, some of the OECs maintained in the culture for an additional 10 days became

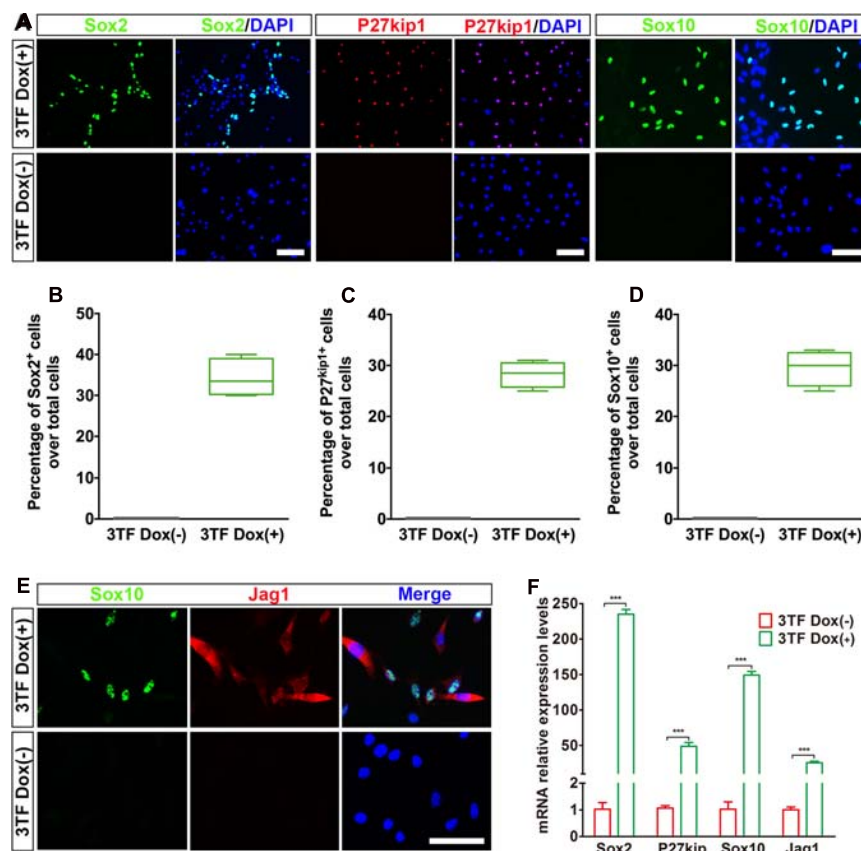


FIGURE 4 | Otic epithelial cells (OECs) induced by Six1, Eya1, and Sox2 can display prosensory cell traits. **(A)** Immunostaining for Sox2, P27^{kip1}, and Sox10 in mouse embryonic fibroblast (MEF)-derived OECs with or without doxycycline (Dox). Without Dox, immunopositivity for Sox2, P27^{kip1}, and Sox10 was absent. In contrast, a remarkable number of immunopositive cells were detected in MEF-derived cells with Dox. **(B)** Frequencies of immunopositive cells for Sox2 in MEF-derived cells with or without Dox ($n = 4$). **(C)** Frequencies of immunopositive cells for P27^{kip1} in MEF-derived cells with or without Dox ($n = 4$). **(D)** Frequencies of immunopositive cells for Sox10 in MEF-derived cells with or without Dox ($n = 5$). **(E)** Double immunostaining of the prosensory cells using anti-Jag1 (red) and anti-Sox10 (green). **(F)** Quantitative real-time PCR analysis of the mRNA levels of prosensory cell genes (Sox2, P27^{kip1}, Jag1, and Sox10) under different culture conditions. MEF-derived cells cultured without Dox were used as controls. Data were collected from at least three separate experiments and are shown as means \pm SEM. Statistical significance was tested by Student's t -test and expressed as $**p < 0.01$, $***p < 0.001$ compared with the control (scale bar, 25 μ m).

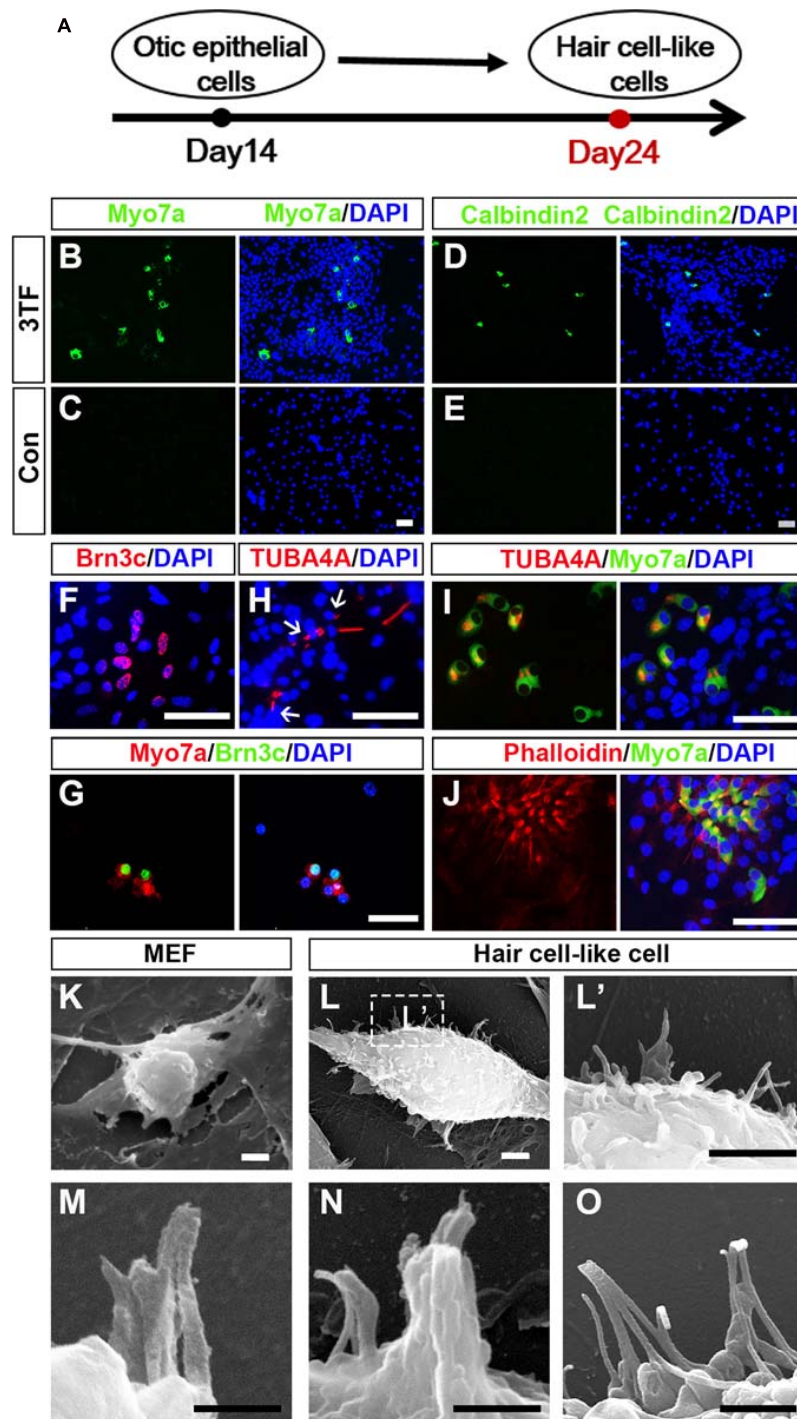


FIGURE 5 | Mouse embryonic fibroblast (MEF)-derived otic epithelial cells (OECs) can give rise to hair cell-like cells (HCLs) exhibiting hair cell markers. **(A)** A schematic differentiation protocol from otic epithelial cells to HCLs. **(B,C)** Immunostaining for Myo7a in MEF-derived HCLs with **(B)** or without 3TF's effect **(C)** at earlier stages. Strong upregulation of Myo7a is detected only in cells with 3TF's effect at earlier stages. **(D,E)** Immunostaining for Calbindin2 in MEF-derived HCLs with **(D)** or without 3TF's effect **(E)** at earlier stages. Strong upregulation of Calbindin2 is detected only in cells with 3TF's effect at earlier stages. **(F)** Immunostaining analysis of Brn3c in HCLs with 3TF's effect at earlier stages. **(G)** Double labeling for Myo7a (red) and Brn3c (green) in HCLs with 3TF's effect at earlier stages. **(H)** The immunostaining with a kinocilium marker, TUBA4A antibody, in HCLs induced by the 3TF at earlier stages. **(I)** Double labeling for Myo7a (green) and TUBA4A (red) in HCLs induced by 3TF at earlier stages. **(J)** Double labeling for Myo7a (green) and Phalloidin (red) in HCLs induced by 3TF at an earlier stage. **(K)** The surface of the MEFs had no cilia. **(L)** Morphology of bundle-like structures protruding from the cell surface of an HCLs, as observed by SEM. **(L')** The boxed regions at high magnification. **(M–O)** Noticeable inter-cilia links existed among the tips of ciliary structures in HCLs. Scale bars, 25 μm for **(B–J)**; 3 μm for **(K–L')**; 500 nm for **(M,N)**; 1 μm for **(O)**.

immunocytochemically positive for Myo7a or Calbindin2 (Figures 5B,D), two HC markers. On average, from 10^4 initially plated cells, approximately 129 ± 39 cells were Myo7a⁺, and 105 ± 21 cells were Calbindin2⁺ ($n = 4$). In sharp contrast, no staining was observed in the cells without 3TF's effect at earlier stages (Figures 5C,E). Furthermore, to confirm that the Myo7a⁺ cells are epithelial cells, we also carried out double staining of Myo7a⁺ cells with an epithelial marker E-cadherin. As expected, all of the Myo7a⁺ cells were double labeled by the E-cadherin antibody (Supplementary Figure 4C). In addition, we found that some cells were also positive for Brn3c (Figure 5F), that is, an HC marker and a TF required for HC survival and maturation (Xiang et al., 1998; Liu Q. et al., 2016). Per 10^4 plated cells, about 153 ± 50 Brn3c⁺ cells were detected ($n = 4$). Notably, under this culture condition, from 10^4 initially plated cells, approximately 18 ± 9 Brn3c⁺Myo7a⁺ cells (Figure 5G) were seen ($n = 3$).

Although these cells displayed many molecular characteristics specific of HCs, it was unclear if these cells had grown ciliary bundle-like structures. To address this issue, we performed immunostaining using an antibody against acetylated- α -Tubulin (TUBA4A), which was reported to label the kinocilium (Koehler et al., 2013, 2017), and indeed observed TUBA4A⁺ cilia in HCs (about 110 ± 27 in per 10^4 plated cells, $n = 4$; Figure 5H). Moreover, these TUBA4A⁺ cells were also Myo7a⁺ cells (Figure 5I). Per 10^4 plated cells, approximately 13 ± 8 TUBA4A⁺ Myo7a⁺ cells were detected ($n = 3$). Consistent with the above-described findings, we performed Phalloidin staining, which is often used to label the stereocilia of HCs (Koehler et al., 2017; McLean et al., 2017). We found that the induced HCLs showed expected Phalloidin staining with a concentration at the tip of the cell, which were also double labeled by Myo7a antibody ($n = 3$) (Figure 5J). In addition, we observed a small subset of Myo7a⁺ cells that formed a rudimentary apical bundle (Oshima et al., 2010; Chen W. et al., 2012; Costa et al., 2015), expressing Espin (Supplementary Figure 5). Furthermore, to provide additional evidence for the formation of the HC unique bundle structures, we examined the surface of the cells at 24 days of culture by scanning electron microscopy (SEM). In agreement with the immunostaining data, SEM revealed that elongated membrane protrusions reminiscent of ciliary bundles were present on the surface of some HCLs compared with control MEFs that did not display any of those structures (Figures 5K–L'). In addition, these putative bundles exhibited diverse arrangements. Importantly, the tips of ciliary bundle-like structures were also linked together (Figures 5M–O), an important feature related to stereociliary bundles (Costa et al., 2015). These results indicated differentiation of MEF-derived OECs to give rise to HCLs that display ciliary bundle-like structures.

As an attempt, we performed induction experiments by culturing the cells under three-dimensional (3D) conditions with a hope that a better HC morphology can be developed (McLean et al., 2017). As shown in Supplementary Figure 6, Myo7a immunostaining revealed that typical pear-shaped HCs were seen, which displayed a big cell body with a large nucleus at the bottom of the cell.

The Hair Cell-Like Cells Generated in the Induction Cultures Acquire Mechanotransduction Channels

To explore whether HCLs expressed functional mechanotransduction channels, we added FM1-43 dye into the culture (Hu and Corwin, 2007). We found that FM1-43 rapidly entered into the Myo7a⁺ cells, indicating that these HCLs behaved like functional HCs (Figure 6A). Moreover, we studied whether the FM1-43⁺ cells respond to mechanical stimulation. We recorded membrane properties of the FM1-43⁺ cells by examining their voltage-dependent currents (Figure 6B). Nineteen FM1-43⁺ cells at day 24 were successfully recorded. Ten of these cells were positive for outward and inward K⁺ currents (IK and IK1) in the presence of KCl in the internal solution (Figures 6C–a–c), and three of these cells expressed inward Ca²⁺ current (I_{Ca}) in the presence of CsCl in the internal solution (Figures 6C–d,e). The analysis of IK, IK1, and I_{Ca} suggests that the cells differentiated from OECs are the hair-cell-like cells (Chen W. et al., 2012). We also detected the electrophysiological profile of MEFs. Outward potassium current could be evoked while no IK1 current was elicited (Figures 6D–a–c). Voltage-gated sodium channel currents were detected with stimulation (Figures 6D–d,e), which could be blocked by 1 μ M tetrodotoxin (TTX) perfusion. Therefore, the capability to take up FM1-43, the morphology of hair bundles, and the electrophysiological properties of HCLs suggested that MEF-derived OECs have differentiated into functional HCs.

The Transcriptional Profiling of Hair Cell-Like Cells Exhibits a Selective Hair Cell Signature

To determine whether the transcriptional profiling of HCLs exhibits a selective HC signature, we carried out RNA-seq analysis of the HCLs at the end of induction compared with MEFs. The MEF-derived HCLs were incubated with FM1-43 dye (5 μ M; Biotium) at room temperature for 10 s and rinsed with the culture medium. Then we obtained the FM1-43⁺ populations of HCLs with green fluorescence for transcriptional profiling by fluorescence-activated cell sorting (FACS) prior to RNA-seq experiments. We particularly focused on some genes known to be functionally relevant to inner ear HC development/function (Costa et al., 2015; Scheffer et al., 2015). Among the 32,007 detected genes in our samples, 15,433 genes showed differential expression. Out of 15,433 genes, 8,562 were upregulated (PADJ < 0.05). Among the 8,562 genes, more than 60 genes known to participate in the formation of HC were significantly upregulated. We then examined the positions of these genes within the ranked list. We found that more than half of them (34 HC-related genes) were positioned among the top 1,500 genes of this ranking (Supplementary Figure 7A and Supplementary Table 2). Moreover, 27 upregulated genes were in the top 1,000, and 14 were in the top 100. Transcripts from well-known HC-related genes such as *Loxhd1*, *Barhl1*, *Ush2a*, *Atoh1*, *Myo15*, *Ush1c*, and *Gfi1* were in the top 100 genes most enriched in HCLs (Figure 6E). Importantly, as shown in Supplementary

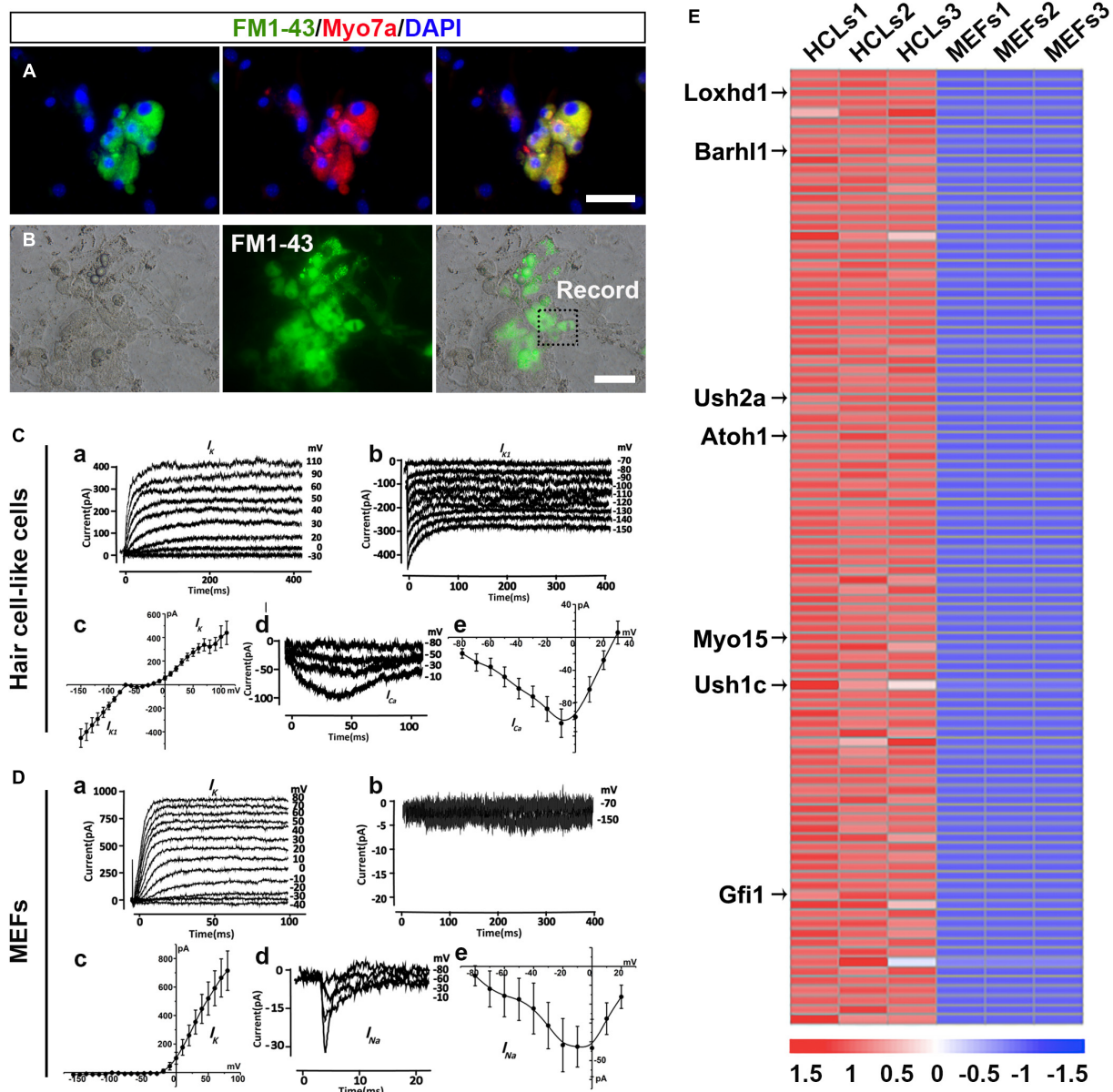


FIGURE 6 | Ciliary structures and electrophysiological properties of hair cell-like cells (HCLs). **(A)** FM1-43⁺ cells co-expressing Myo7a. **(B)** White light image of a recording electrode on an FM1-43⁺ cell. **(C)** Electrophysiological properties of FM1-43⁺ cells. **(a)** The outward potassium channel currents were elicited by 10 voltage steps from the holding potential of -70 mV from mouse embryonic fibroblast (MEF)-derived HCLs ($n = 10$, Peak I_{K1} : 439.89 ± 98.52 pA at 110 mV). **(b)** The inward potassium channel currents were recorded from the holding potential of -70 mV by applying voltage in 10-mV decrements from MEF-derived HCLs ($n = 10$, Peak I_{K1} : -452.74 ± 78.28 pA at -150 mV). The inward and outward potassium channel currents resembled those recorded in pre-hearing mouse cochlear, with HCLs differentiated from human fetal auditory stem cells. **(c)** The average current-voltage (I-V) curve for outward and inward potassium current. **(d)** Example of Ca^{2+} current elicited from MEF-derived HCLs ($n = 3$, Peak I_{Ca} : -104.45 ± 17.18 pA at -10 mV). The hyperpolarized activation range of I_{Ca} indicated the presence of an L-type Ca^{2+} channel containing the Cav1.3 subunit, as previously reported in mammalian cochlear HCs. **(e)** The average current-voltage (I-V) curve of Ca^{2+} . **(D)** Electrophysiological properties of MEFs. **(a)** The outward potassium channel currents were elicited from MEFs ($n = 8$, Peak I_{K1} : 714.97 ± 138.28 pA at 80 mV). **(b)** No obvious inward currents were recorded by applying voltage in 10-mV decrements ($n = 8$). **(c)** The average current-voltage (I-V) curve for outward and inward potassium current. **(d)** Small sodium current was elicited from MEFs in voltage injection in 10-mV increments ($n = 3$, Peak I_{Na} : -43.32 ± 15.24 pA at 0 mV). **(e)** The average current-voltage (I-V) curve of sodium current. **(E)** Heat maps depicting the relative fold changes for the expression of HC-related genes between HCLs and MEFs for the top 100 genes (scale bars, 25 μ m).

Figure 7B, qRT-PCR analysis validated the upregulation of the 14 HC-related genes by the HCLs (Costa et al., 2015; Scheffer et al., 2015). Consistently, the RNA-seq experiment also

revealed a downregulation of several typical mesenchymal genes including Snail1, Snail2, Zeb2, and Vimentin (**Supplementary Figure 8A**), which were also verified by qRT-PCR analysis

(Supplementary Figure 8B). Thus, the transcriptional profiling analysis of HCLs indicates a specific HC signature and further supports the notion that the induced cells are HCLs.

Production Efficiency of Hair Cell-Like Cells Is Enhanced by Wnt Signaling Activation

Given that Wnt signaling activation is important for otic development and HC differentiation *in vivo* and enhances the formation of inner ear organoids *in vitro*, we next examined whether the efficiency of 3TF-induced HC production could be enhanced by addition of a Wnt signaling activator (Chai et al., 2012). We exposed 3TF-derived OECs to 4 days of Dox treatment in a combination with the CHIR99021 (CHIR), a GSK3 β inhibitor that activates the Wnt pathway (Liu X. P. et al., 2016; Koehler et al., 2017). Then, CHIR was kept continuously after Dox was withdrawn (Figure 7A). Remarkably, the numbers of cells immunopositive for Myo7a (Figures 7C,D) in 3TF + CHIR group was significantly higher than the 3TF only group (from 10^4 initially plated cells, approximately 259 ± 33 cells vs. 125 ± 20 in 3TF group, $n = 4$, Figure 7H). Similar results were obtained by immunostaining for Calbindin2 (Figures 7E,G, from 10^4 initially plated cells, approximately 206 ± 23 vs. 99 ± 18 cells, $n = 4$), another HC marker. No Myo7a or Calbindin2-expressing cells were seen in the control group (without 3TF and CHIR treatment, referred here as Con) (Figures 7B,E). In addition, mRNA expression levels of HC genes, including Myo7a, Atoh1, Brn3c, Gfi1, Myo6, Espin, and Calbindin2, were significantly elevated by CHIR treatment in the 3TF-induced OECs (Figure 7H), confirming that CHIR enhances HC production efficiency.

DISCUSSION

Hair cells are located in the inner ear sensory epithelium, which was originated from the otic placode during embryogenesis following a temporospatial program (Kelley, 2006). By mimicking and recapitulating the development of inner ear HCs *in vivo*, we designed our experiments to use a stepwise induction procedure to enable generation of functional HCs from MEFs. This stepwise method includes (1) MET of MEFs into epithelial-like cell; (2) conversion of MEF-derived epithelial-like cells into the OECs via inducible expression of Six1, Eya1, and Sox2; (3) differentiation of OECs into HCLs through an intermediate prosensory epithelial cell step; and (4) improving the production efficiency of HCLs by activating the Wnt pathway. We demonstrated successfully that as time proceeds; with the temporal order of induction, we observed stepwise expression of genes specific for the above-mentioned, related cell types at each of the steps. Therefore, the current study provides a novel strategy to generate inner ear HCs from MEFs.

In addition to verification of expression of HC-specific genes and proteins, the present study also confirmed formation of ciliary bundle-like structures on the surface of the induced HCLs via acetylated- α -Tubulin and Espin immunostaining and SEM. More importantly, our present work also demonstrated that the

induced HCLs expressed functional mechanosensory channels as evidenced by the rapid infiltration of FM1-43 and acquisition of the electrophysiological features. Additional supports include a typical HC morphology in 3D induction cultures and realization of expression of more than 100 HC-selective genes based on the transcriptional profile analysis. Therefore, our stepwise strategy leads to a successful production of HCLs with immunocytochemical, morphological, electrophysiological, and transcriptional signature properties.

It is worth emphasizing that epithelial-to-mesenchymal transition (EMT) and MET are dynamic processes that have been shown to be important for embryogenesis (Chen J. et al., 2012; Liu et al., 2013). While EMT is involved in the formation of iPSCs from fibroblasts (Forte et al., 2017), MET is essential for differentiation of the stem cells into epithelial cell lineages (Li et al., 2010; Shu and Pei, 2014). The present study employed the concept of developmental biology to convert the MEFs into inner ear HCs, by initially switching to a different cell lineage, that is, epithelial cells. Our work is consistent with a previous study in a lower vertebrate system by Cowen and coworkers, reporting that while immortalization of the avian inner ear epithelial SCs can be achieved via an EMT process, differentiation of the immortalized SCs needs go through a MET path (Hu and Corwin, 2007). By addition of a TGF- β signaling inhibitor, SB431542, in the culture for 7 days, many of the MEFs became epithelial-like cells, based on their morphological changes and high expression level of E-cadherin, EpCAM, and ZO-1. The findings in current experiments are in agreement with others, reporting that MET initiates a reprogramming of mouse fibroblasts by suppressing TGF- β signaling (Li et al., 2010). In this way, the MET serves as a first step to recapitulate development process for the conversion of MEFs into inner ear HCs, which involves a switch from one cell lineage to another cell lineage.

Our results reinforce the notion that SES are core TFs of the genetic network participating in HC fate determination and differentiation. Sox2 is a TF that is required for specification of prosensory cells (Dabdoub et al., 2008). For instance, mutant mice that lack Sox2 in the inner ear show a loss of HCs, confirming the requirement for Sox2 in prosensory development (Kiernan et al., 2005). The transcription coactivator phosphatase Eya1 and its cofactor homeodomain protein Six1 are also necessary for HC development. Several studies have indicated inactivation of Eya1 or Six1 leads to an early arrest of otic development in mice (Xu et al., 1999; Ozaki et al., 2004). Moreover, Eya1/Six1 are co-expressed with Sox2 in the inner ear sensory progenitors. Both Atoh-dependent and Atoh-independent pathways are coordinately activated by Eya1/Six1, which in turn induce the expression of Brn3c so as to achieve differentiation of HCs (Ahmed et al., 2012). It is worth noting that even though Sox2 is necessary for the formation of prosensory domain, it also functions as an inhibitor by suppressing the effects of Atoh1 on induction of HC differentiation (Ahmed et al., 2012). To overcome this issue, we utilized a Tet-on gene expression system that enables Dox-inducible expression of SES. In this way, we were able to achieve induction of inner ear HCs that express multiple HC markers and acquire cilia and functions. Although overexpression of GFI1, Pou4f3,

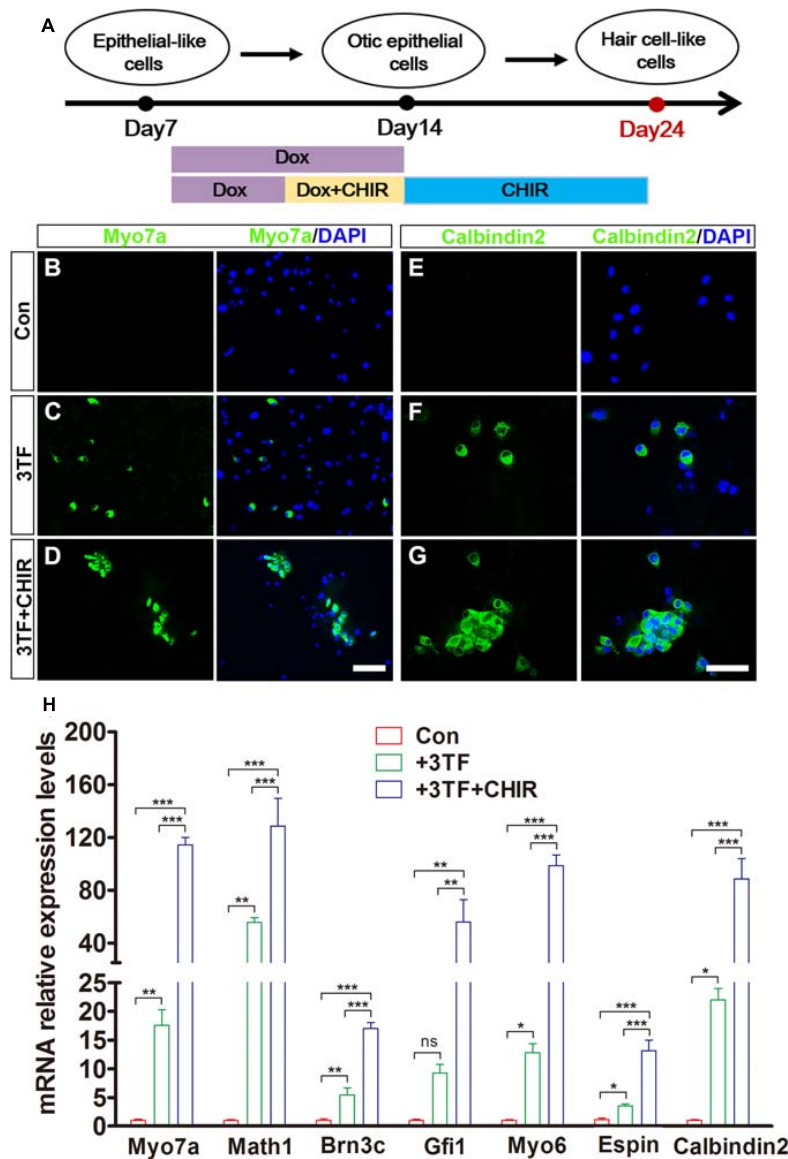


FIGURE 7 | Production efficiency of hair cell-like cells (HCLs) is enhanced by Wnt signaling activation. **(A)** A schematic drawing of the induction procedure from epithelial-like cells (ELCs), including the sequential treatment with doxycycline (Dox) and CHIR. **(B–D)** Immunostaining analysis shows that Myo7a expression is higher in mouse embryonic fibroblast (MEF)-derived HCLs with 3TF + CHIR sequential treatment **(D)** than with 3TF treatment **(C)**. MEF-derived cells cultured without Dox were used as control **(B)**. **(E–G)** Immunostaining analysis shows that Calbindin2 expression is higher in MEF-derived HCLs with 3TF + CHIR sequential treatment **(G)** than with 3TF treatment **(F)**. MEF-derived cells cultured without Dox were used as control **(E)**. **(H)** Quantitative real-time PCR analysis of HC-specific gene expression under different induction conditions. Data are shown as mean \pm SEM ($n = 3$). ns, not significant, * $p < 0.5$, ** $p < 0.01$, *** $p < 0.001$ (scale bars, 25 μ m).

and ATOH1 together has been previously shown to induce conversion of human fibroblasts toward the HC lineage, that approach only allowed generation of cells expressing HC markers but failed to show their functions (Duran Alonso et al., 2018). In our experiments, following the reprogramming of MEFs to epithelial-like cells, transient overexpression of these three TFs in MEF-derived epithelial-like cells with Dox treatment at days 7–14 induced a lineage conversion of epithelial-like cells to OECs (Figure 3). As induction continues, OECs spontaneously differentiate into HCLs expressing multiple HC markers. Furthermore, these induced HCLs grow cilia and

stereociliary bundle-like structures and acquired functional mechanosensory channels. Therefore, our Tet-on tunable gene expression system appears to be important for the maturation and acquisition of the functions of induced HCs.

It is also interesting to point out that activation of Wnt signaling pathway in the present experiments enhanced the HC induction rate, which is consistent with previous studies reporting the involvement of Wnt signaling in the otic progenitor cell (OPC) proliferation and differentiation (Chai et al., 2012). With the use of a Wnt pathway activator, CHIR99021, at the late stage when the OPCs are produced, the HC production rate

is significantly enhanced. These results imply that activation of the Wnt signaling may be considered in future cell replacement therapy for hearing loss.

In conclusion, our study presents a new approach to produce functional inner ear HCs from somatic cells by using a novel stepwise protocol, providing a new working system for illumination of the developmental mechanisms of the HCs in the inner ears. More importantly, this approach might offer a cell replacement therapy for hearing loss in the future. To apply this strategy for the aim of HC regenerative in clinic, it is warranted to determine if human fibroblasts and other somatic cells can be successfully transdifferentiated into functional HCs.

MATERIALS AND METHODS

Fibroblast Isolation and Cell Culture

Mouse embryonic fibroblasts were isolated from C57/BL6 mouse embryos at E13.5. All experiments that we performed were approved by the Ethics Committee at Shanghai Renji Hospital and followed standard established guidelines by Ministry of Health of China. Great attention was paid to remove the head, arms, legs, spinal cord, and internal organs of the embryos. The remaining tissue was dissociated manually in 0.25% trypsin (Sigma), kept at 37°C to obtain a single-cell suspension, and then plated in T75 flasks. MEFs were expanded to two passages or three passages (named as P2 or P3) in DMEM in which we supplemented with 10% FBS, as well as 1% penicillin (Life Technologies) at 37°C. The P2 or P3 MEFs were characterized by immunofluorescence to verify if they were pure without contamination of any HCs, SCs, or OECs using Vimentin, E-cadherin, Myo7a, Brn3c, P27^{kip1}, Sox10, Pax2, Pax8, Sox2, and Jag1. MEFs at P2 or P3 were used to perform the subsequent transdifferentiation experiments.

Three-Dimensional Culture

Two days following transduction with 3TE, the cultured cells were incubated in TrypLE (Gibco) for 5 min at 37°C and collected in 15-ml tubes. After centrifugation for 5 min at 1,000 rpm, the dissociated cells were suspended in DMEM/F12 and strained using a 25-μm cell strainer to produce a single-cell suspension. The cells were then centrifuged again for 5 min at 1,000 rpm and re-suspended in 80:20 Matrigel (growth factor reduced, Corning): DMEM/F12. Then, we placed the Matrigel droplets (30–40 μl) containing the suspended cells in the center of each well of a 48-well plate, one droplet per well. To facilitate Matrigel rapid polymerization, the plate was incubated at 37°C for 15–20 min, after which the droplets were bathed in medium. Media were replaced every other day.

Signaling Molecules and Recombinant Proteins

The following small compounds and recombinant proteins used in the study were as follows: human FGF2 (5–25 ng/ml; PeproTech), TGF-β inhibitor SB431542 (10 μM; Sigma), and GSK3β inhibitor CHIR99021 (3 μM; Selleck).

RNA Preparation, PCR, and Real-Time Quantitative RT-PCR

Total RNAs were prepared from the cells using Zymo Research's Quick-RNA MicroPrep Kit. cDNA was synthesized by reverse transcription with Takara's the PrimeScript RT reagent Kit and oligo (dT) primers based on the manual. Real-time quantitative polymerase chain reaction (qRT-PCR) was performed using Toyobo's SYBR Green method at Applied Biosystems' Prism 7900 HT apparatus. Relative expression of mRNA was calculated by normalization of them to GAPDH mRNA. All the primer pairs were listed in **Supplementary Table 1**.

Immunofluorescence Assay

We used 4% paraformaldehyde to fix cultured cells for 15 min and rinsed three times in phosphate-buffered saline (PBS) for 10 min each. They were infiltrated with 0.3% Triton X-100 for 10 min at room temperature and rinsed three times in PBS. To block non-specific bindings, the preparations were incubated with 10% normal donkey serum and 0.1% Tween 20 in PBS for 1 h. One percent normal donkey serum and 0.1% Tween 2 were added to the primary antibody solution for overnight at 4°C. The primary antibodies used included the following: rabbit anti-Vimentin (1:200, BD Biosciences), mouse anti-E-cadherin (1:200, BD Biosciences), mouse anti-ZO-1 (1:50, Santa Cruz), rabbit anti-Pax2 (1:400, Thermo Scientific), rat anti-Pax8 (1:400, Abcam), goat anti-Jag1 (1:100, Santa Cruz), mouse anti-Sox10 (1:100, eBiosciences), rabbit anti-Sox2 (1:200, Abcam), mouse anti-P27^{kip1} (1:100, Abcam), mouse anti-Brn3c (1:100, Abcam), rabbit anti-Myo7a (1:200, Proteus), mouse anti-acetylated-α-Tubulin (1:100, Sigma), mouse anti-Espin (1:50, Santa Cruz), rabbit anti-Calbindin2 (1:200, ProteinTech). After being washed three times with PBS for 10 min each, Alexa Fluor 488 (1:200, Life Technologies) or 594 (1:400, Life Technologies) conjugated, anti-rabbit, anti-goat, or anti-mouse secondary antibodies (Molecular Probes, Invitrogen) were used to detect primary antibodies. Nuclei were counterstained with 4',6-diamidino-2-phenylindole (DAPI; 1:500, Sigma-Aldrich). After incubation for 1 h at room temperature and being washed three times with PBS, their fluorescence images were captured using inverted fluorescence microscopy or confocal laser scanning microscopy.

Scanning Electron Microscopy

Undifferentiated MEFs and cells differentiated for 24 days were fixed in 2.5% glutaraldehyde that was made in 0.1 M of phosphate buffer (Sigma) overnight at 4°C. After three washes in PBS for 10 min each time and in 1% osmium tetroxide (Sigma) for 60 min each, the preparations were then dehydrated with a graded ethanol series and eventually processed with isoamyl acetate (Aladdin, Shanghai, China) for 20–30 min for critical point drying. Finally, they were examined using a scanning electron microscope (HitachiS-3000N, Japan), operated under a high vacuum at 5–10 kV at a working distance of 7–10 mm.

FM1-43 Uptake Assay

To test whether the MEF-derived HCLs acquired functional mechanotransduction channels, the cultures were incubated with

FM1-43 dye (5 μ M; Biotium) at room temperature for 10 s and rinsed with the culture medium. The preparations were then fixed in 4% paraformaldehyde, counterstained with DAPI, and finally examined under a fluorescence microscope. Moreover, immunofluorescence for Myo7a was processed after FM1-43 dye staining to verify the identity of HCs. Fields were chosen randomly ($n = 15$).

Electrophysiological Recordings

Whole-cell patch-clamp technique was used to record the membrane currents of cells differentiated for 24 days with an amplifier (EPC 10; HEKA Elektronik). PatchMaster software (HEKA) at a Dell computer was used to filter the data at 1–3 kHz and to sample at 3–10 kHz. A vertical pipette puller (PC-10; Narishige) was used to pull patch pipettes from borosilicate capillary glass. The resistance of the electrode was 4–7 M Ω . For I_{K1} , I_K , and I_{Na} acquirement, the patch electrodes were filled with 131 mM of KCl, 3 mM of MgCl₂, 1 mM of EGTA-KOH, 5 mM of Na₂ATP, 5 mM of HEPES, and 10 mM of sodium phosphocreatine (pH 7.3). For I_{Ca} recording, pipette was filled with recording solution (pH 7.3) containing 3 mM of MgCl₂, 131 mM of CsCl, 1 mM of EGTA-KOH, 5 mM of Na₂ATP, 1 μ M of TTX, 5 mM of HEPES, and 10 mM of sodium phosphocreatine. Recording solution contained (in mM) 135 NaCl, 5.8 KCl, 1.3 CaCl₂, 0.9 MgCl₂, 0.7 NaH₂PO₄, 5.6 D-glucose, 10 HEPES, and 2 sodium pyruvate. We performed all recordings with the pH adjusted to 7.3–7.5 at room temperature (20–25°C). Cells used for electrophysiology assay were kept in DMEM/F12 containing FM1-43 for 10 s. The cells labeled with FM1-43 showed green fluorescence in the cytoplasm, which were then used for electrophysiological recordings. The cells were bathed in the external solution and visualized at an inverted phase-contrast microscope (TE-2000U; Nikon). Data were stored on a DELL computer for off-line analysis using Clamp fit and Origin software (Origin Lab). We considered the peak current as the maximum current when it appeared during the step depolarization. Membrane currents were elicited by applying voltage in 10-mV increments or decrements to the holding potential of –70 mV.

RNA Sequencing Analysis

RNA from MEFs and HCLs induced for 24 days was extracted using the TRIzol reagent (Invitrogen). The RNA-seq work was performed by Novogene (Beijing, China). Sequencing libraries were produced using NEBNext® Ultra™ RNA Library Prep Kit for Illumina® (NEB, United States) following the manufacturer's manual, and index codes were added to assign sequences to each sample. Briefly, mRNA was purified by poly-T oligo-attached magnetic beads. The clustering of the index-coded samples was performed on a cBot Cluster Generation System using TruSeq PE Cluster Kit v3-cBot-HS (Illumina) according to the manufacturer's instructions. As for data analysis, differential expression analysis of two groups was conducted using the DESeq2 R package (??). The resulting p-values were adjusted using the Benjamini and Hochberg approach to control the false discovery rate. Genes with an adjusted p -value < 0.05 found

by DESeq2 were regarded as differentially expressed. For each group, three biological replicates were used for the analysis. The data presented in the study are deposited in the (SRA) repository, accession number (PRJNA713364).

Statistical Analysis

All experiments were performed independently with at least three biological replicates. Statistical analysis was performed using the GraphPad Prism software (version 5.0). Data were presented as mean \pm SEM, and statistical significance was performed using Student's t -test and expressed as $p < 0.05$ (*), $p < 0.01$ (**), and $p < 0.001$ (***). The fraction of immunopositive cells among total cells was determined in a double-blinded fashion by observations of approximately 300 cells in each of 10 randomly selected microscopic fields per experiment.

DATA AVAILABILITY STATEMENT

The data presented in the study are deposited in the (SRA) repository, accession number (PRJNA713364).

ETHICS STATEMENT

The animal study was reviewed and approved by Shanghai Renji Hospital and followed standard established guidelines by Ministry of Health of China.

AUTHOR CONTRIBUTIONS

W-QG conceived the concept. QY, HS, and YQ performed the experimental work. QY, HS, YQ, HX, H-BS, and W-QG contributed to the experimental design and data analysis. YQ, WL, LW, YW, ZJ, and S-KY supervised the study. QY, H-BS, and W-QG wrote the manuscript. All authors interpreted the data, discussed the results and approved the final version of the manuscript.

FUNDING

This study was supported by funds from Ministry of Science and Technology of the People's Republic of China (2017YFA0102900 to W-QG), National Natural Science Foundation of China (31571399 to HX, and 81872406 and 81630073 to W-QG), Science and Technology Commission of Shanghai Municipality (20JC147600 to W-QG), 111 project (B21024 to W-QG), and KC Wong Foundation (to W-QG).

SUPPLEMENTARY MATERIAL

The Supplementary Material for this article can be found online at: <https://www.frontiersin.org/articles/10.3389/fcell.2021.672406/full#supplementary-material>

REFERENCES

- Ahmed, M., Wong, E. Y., Sun, J., Xu, J., Wang, F., and Xu, P. X. (2012). Eya1-Six1 interaction is sufficient to induce hair cell fate in the cochlea by activating Atoh1 expression in cooperation with Sox2. *Dev. Cell* 22, 377–390. doi: 10.1016/j.devcel.2011.12.006
- Ambasudhan, R., Talantova, M., Coleman, R., Yuan, X., Zhu, S., Lipton, S. A., et al. (2011). Direct reprogramming of adult human fibroblasts to functional neurons under defined conditions. *Cell Stem Cell* 9, 113–118. doi: 10.1016/j.stem.2011.07.002
- Buganim, Y., Itskovich, E., Hu, Y. C., Cheng, A. W., Ganz, K., Sarkar, S., et al. (2012). Direct reprogramming of fibroblasts into embryonic Sertoli-like cells by defined factors. *Cell Stem Cell* 11, 373–386. doi: 10.1016/j.stem.2012.07.019
- Burns, J. C., and Stone, J. S. (2017). Development and regeneration of vestibular hair cells in mammals. *Semin. Cell Dev. Biol.* 65, 96–105. doi: 10.1016/j.semdcb.2016.11.001
- Burns, J. C., Cox, B. C., Thiede, B. R., Zuo, J., and Corwin, J. T. (2012). In vivo proliferative regeneration of balance hair cells in newborn mice. *J. Neurosci.* 32, 6570–6577. doi: 10.1523/JNEUROSCI.6274-11.2012
- Carey, J., and Amin, N. (2006). Evolutionary changes in the cochlea and labyrinth: solving the problem of sound transmission to the balance organs of the inner ear. *Anat. Rec. A Discov. Mol. Cell Evol. Biol.* 288, 482–489. doi: 10.1002/ar.a.20306
- Chai, R., Kuo, B., Wang, T., Liaw, E. J., Xia, A., Jan, T. A., et al. (2012). Wnt signaling induces proliferation of sensory precursors in the postnatal mouse cochlea. *Proc. Natl. Acad. Sci. U.S.A.* 109, 8167–8172. doi: 10.1073/pnas.1202774109
- Chen, J., Han, Q., and Pei, D. (2012). EMT and MET as paradigms for cell fate switching. *J. Mol. Cell Biol.* 4, 66–69. doi: 10.1093/jmcb/mjr045
- Chen, P., and Segil, N. (1999). p27(Kip1) links cell proliferation to morphogenesis in the developing organ of Corti. *Development* 126, 1581–1590.
- Chen, W., Jongkamonwivat, N., Abbas, L., Eshtan, S. J., Johnson, S. L., Kuhn, S., et al. (2012). Restoration of auditory evoked responses by human ES-cell-derived otic progenitors. *Nature* 490, 278–282. doi: 10.1038/nature11415
- Costa, A., Sanchez-Guardado, L., Juniati, S., Gale, J. E., Daudet, N., and Henrique, D. (2015). Generation of sensory hair cells by genetic programming with a combination of transcription factors. *Development* 142, 1948–1959. doi: 10.1242/dev.119149
- Dabdoub, A., Puligilla, C., Jones, J. M., Fritzsche, B., Cheah, K. S., Pevny, L. H., et al. (2008). Sox2 signaling in prosensory domain specification and subsequent hair cell differentiation in the developing cochlea. *Proc. Natl. Acad. Sci. U.S.A.* 105, 18396–18401. doi: 10.1073/pnas.0808175105
- Dror, A. A., and Avraham, K. B. (2009). Hearing loss: mechanisms revealed by genetics and cell biology. *Annu. Rev. Genet.* 43, 411–437. doi: 10.1146/annurev-genet-102108-134135
- Duran Alonso, M. B., Lopez Hernandez, I., de la Fuente, M. A., Garcia-Sancho, J., Giraldez, F., and Schimmang, T. (2018). Transcription factor induced conversion of human fibroblasts towards the hair cell lineage. *PLoS One* 13:e0200210. doi: 10.1371/journal.pone.0200210
- Forte, E., Chimenti, I., Rosa, P., Angelini, F., Pagano, F., Calogero, A., et al. (2017). EMT/MET at the crossroad of stemness, regeneration and oncogenesis: the Ying-Yang equilibrium recapitulated in cell spheroids. *Cancers (Basel)* 9:98. doi: 10.3390/cancers9080098
- Fu, J. D., Stone, N. R., Liu, L., Spencer, C. I., Qian, L., Hayashi, Y., et al. (2013). Direct reprogramming of human fibroblasts toward a cardiomyocyte-like state. *Stem Cell Rep.* 1, 235–247. doi: 10.1016/j.stemcr.2013.07.005
- Géléoc, G. S., and Holt, J. R. (2014). Sound strategies for hearing restoration. *Science* 344:1241062. doi: 10.1126/science.1241062
- Hans, S., Liu, D., and Westerfield, M. (2004). Pax8 and Pax2a function synergistically in otic specification, downstream of the Foxi1 and Dlx3b transcription factors. *Development* 131, 5091–5102. doi: 10.1242/dev.01346
- Hu, Z., and Corwin, J. T. (2007). Inner ear hair cells produced in vitro by a mesenchymal-to-epithelial transition. *Proc. Natl. Acad. Sci. U.S.A.* 104, 16675–16680. doi: 10.1073/pnas.0704576104
- Huang, P., He, Z., Ji, S., Sun, H., Xiang, D., Liu, C., et al. (2011). Induction of functional hepatocyte-like cells from mouse fibroblasts by defined factors. *Nature* 475, 386–389. doi: 10.1038/nature10116
- Ieda, M., Fu, J. D., Delgado-Olguin, P., Vedantham, V., Hayashi, Y., Bruneau, B. G., et al. (2010). Direct reprogramming of fibroblasts into functional cardio-myocytes by defined factors. *Cell* 142, 375–386. doi: 10.1016/j.cell.2010.07.002
- Kelley, M. W. (2006). Regulation of cell fate in the sensory epithelia of the inner ear. *Nat. Rev. Neurosci.* 7, 837–849. doi: 10.1038/nrn1987
- Kiernan, A. E., Pelling, A. L., Leung, K. K., Tang, A. S., Bell, D. M., Tease, C., et al. (2005). Sox2 is required for sensory organ development in the mammalian inner ear. *Nature* 434, 1031–1035. doi: 10.1038/nature03487
- Knoepfler, P. S. (2009). Deconstructing stem cell tumorigenicity: a roadmap to safe regenerative medicine. *Stem Cells* 27, 1050–1056. doi: 10.1002/stem.37
- Koehler, K. R., Mikosz, A. M., Molosh, A. I., Patel, D., and Hashino, E. (2013). Generation of inner ear sensory epithelia from pluripotent stem cells in 3D culture. *Nature* 500, 217–221. doi: 10.1038/nature12298
- Koehler, K. R., Nie, J., Longworth-Mills, E., Liu, X. P., Lee, J., Holt, J. R., et al. (2017). Generation of inner ear organoids containing functional hair cells from human pluripotent stem cells. *Nat. Biotechnol.* 35, 583–589. doi: 10.1038/nbt.3840
- Lanza, R. (2007). Stem cell breakthrough: don't forget ethics. *Science* 318, 1917–1920. doi: 10.1126/science.318.5858.1865a
- Li, H., Roblin, G., Liu, H., and Heller, S. (2003). Generation of hair cells by stepwise differentiation of embryonic stem cells. *Proc. Natl. Acad. Sci. U.S.A.* 100, 13495–13500. doi: 10.1073/pnas.2334503100
- Li, R., Liang, J., Ni, S., Zhou, T., Qing, X., Li, H., et al. (2010). A mesenchymal-to-epithelial transition initiates and is required for the nuclear reprogramming of mouse fibroblasts. *Cell Stem Cell* 7, 51–63. doi: 10.1016/j.stem.2010.04.014
- Liu, Q., Shen, Y., Chen, J., Ding, J., Tang, Z., Zhang, C., et al. (2016). Induction of functional hair-cell-like cells from mouse cochlear multipotent cells. *Stem Cells Int.* 2016:8197279. doi: 10.1155/2016/8197279
- Liu, X. P., Koehler, K. R., Mikosz, A. M., Hashino, E., and Holt, J. R. (2016). Functional development of mechanosensitive hair cells in stem cell-derived organoids parallels native vestibular hair cells. *Nat. Commun.* 7:11508. doi: 10.1038/ncomms11508
- Liu, X., Sun, H., Qi, J., Wang, L., He, S., Liu, J., et al. (2013). Sequential introduction of reprogramming factors reveals a time-sensitive requirement for individual factors and a sequential EMT-MET mechanism for optimal reprogramming. *Nat. Cell Biol.* 15, 829–838. doi: 10.1038/ncb2765
- Ma, Y., Wise, A. K., Shepherd, R. K., and Richardson, R. T. (2019). New molecular therapies for the treatment of hearing loss. *Pharmacol. Ther.* 200, 190–209. doi: 10.1016/j.pharmthera.2019.05.003
- McLean, W. J., Yin, X., Lu, L., Lenz, D. R., McLean, D., Langer, R., et al. (2017). Clonal expansion of Lgr5-positive cells from mammalian cochlea and high-purity generation of sensory hair cells. *Cell Rep.* 18, 1917–1929. doi: 10.1016/j.jcelrep.2017.01.066
- Oshima, K., Shin, K., Diensthuber, M., Peng, A. W., Ricci, A. J., and Heller, S. (2010). Mechanosensitive hair cell-like cells from embryonic and induced pluripotent stem cells. *Cell* 141, 704–716. doi: 10.1016/j.cell.2010.03.035
- Ouji, Y., Sakagami, M., Omori, H., Higashiyama, S., Kawai, N., Kitahara, T., et al. (2017). Efficient induction of inner ear hair cell-like cells from mouse ES cells using combination of Math1 transfection and conditioned medium from ST2 stromal cells. *Stem Cell Res.* 23, 50–56. doi: 10.1016/j.scr.2017.06.013
- Ozaki, H., Nakamura, K., Funahashi, J., Ikeda, K., Yamada, G., Tokano, H., et al. (2004). Six1 controls patterning of the mouse otic vesicle. *Development* 131, 551–562. doi: 10.1242/dev.00943
- Schacht, J. (1986). Molecular mechanisms of drug-induced hearing loss. *Hear. Res.* 22, 297–304. doi: 10.1016/0378-5955(86)90105-x
- Scheffer, D. I., Shen, J., Corey, D. P., and Chen, Z. Y. (2015). Gene expression by mouse inner ear hair cells during development. *J. Neurosci.* 35, 6366–6380. doi: 10.1523/JNEUROSCI.5126-14.2015
- Schimmang, T. (2013). Transcription factors that control inner ear development and their potential for transdifferentiation and reprogramming. *Hear. Res.* 297, 84–90. doi: 10.1016/j.heares.2012.11.001
- Sekiya, S., and Suzuki, A. (2011). Direct conversion of mouse fibroblasts to hepatocyte-like cells by defined factors. *Nature* 475, 390–393. doi: 10.1038/nature10263
- Shu, X., and Pei, D. (2014). The function and regulation of mesenchymal-to-epithelial transition in somatic cell reprogramming. *Curr. Opin. Genet. Dev.* 28, 32–37. doi: 10.1016/j.gde.2014.08.005
- Smith, M. E., Groves, A. K., and Coffin, A. B. (2016). Editorial: sensory hair cell death and regeneration. *Front. Cell. Neurosci.* 10:208. doi: 10.3389/fncel.2016.00208

- Szabo, E., Rampalli, S., Risueno, R. M., Schnerch, A., Mitchell, R., Fiebig-Comyn, A., et al. (2010). Direct conversion of human fibroblasts to multi lineage blood progenitors. *Nature* 468, 521–526. doi: 10.1038/nature09591
- Vierbuchen, T., Ostermeier, A., Pang, Z. P., Kokubu, Y., Südhof, T. C., and Wernig, M. (2010). Direct conversion of fibroblasts to functional neurons by defined factors. *Nature* 463, 1035–1041. doi: 10.1038/nature08797
- Wakaoka, T., Motohashi, T., Hayashi, H., Kuze, B., Aoki, M., Mizuta, K., et al. (2013). Tracing Sox10-expressing cells elucidates the dynamic development of the mouse inner ear. *Hear. Res.* 302, 17–25. doi: 10.1016/j.heares.2013.05.003
- White, P. M., Doetzlhofer, A., Lee, Y. S., Groves, A. K., and Segil, N. (2006). Mammalian cochlear supporting cells can divide and trans-differentiate into hair cells. *Nature* 441, 984–987. doi: 10.1038/nature04849
- Xiang, M., Gao, W. Q., Hasson, T., and Shin, J. J. (1998). Requirement for Brn-3c in maturation and survival, but not in fate determination of inner ear hair cells. *Development* 125, 3935–3946.
- Xu, P. X., Adams, J., Peters, H., Brown, M. C., Heaney, S., and Maas, R. (1999). Eya1-deficient mice lack ears and kidneys and show abnormal apoptosis of organ primordia. *Nat. Genet.* 23, 113–117. doi: 10.1038/12722
- Zhai, S., Shi, L., Wang, B. E., Zheng, G., Song, W., Hu, Y., et al. (2005). Isolation and culture of hair cell progenitors from postnatal rat cochleae. *J. Neurobiol.* 65, 282–293. doi: 10.1002/neu.20190
- Zheng, J. L., and Gao, W. Q. (2000). Overexpression of Math1 induces robust production of extra hair cells in postnatal rat inner ears. *Nat. Neurosci.* 3, 580–586. doi: 10.1038/75753

Conflict of Interest: The authors declare that the research was conducted in the absence of any commercial or financial relationships that could be construed as a potential conflict of interest.

Copyright © 2021 Yang, Shi, Quan, Chen, Li, Wang, Wang, Ji, Yin, Shi, Xu and Gao. This is an open-access article distributed under the terms of the Creative Commons Attribution License (CC BY). The use, distribution or reproduction in other forums is permitted, provided the original author(s) and the copyright owner(s) are credited and that the original publication in this journal is cited, in accordance with accepted academic practice. No use, distribution or reproduction is permitted which does not comply with these terms.

Advantages of publishing in Frontiers



OPEN ACCESS

Articles are free to read
for greatest visibility
and readership



FAST PUBLICATION

Around 90 days
from submission
to decision



HIGH QUALITY PEER-REVIEW

Rigorous, collaborative,
and constructive
peer-review



TRANSPARENT PEER-REVIEW

Editors and reviewers
acknowledged by name
on published articles

Frontiers

Avenue du Tribunal-Fédéral 34
1005 Lausanne | Switzerland

Visit us: www.frontiersin.org

Contact us: frontiersin.org/about/contact



REPRODUCIBILITY OF RESEARCH

Support open data
and methods to enhance
research reproducibility



DIGITAL PUBLISHING

Articles designed
for optimal readership
across devices



FOLLOW US

@frontiersin



IMPACT METRICS

Advanced article metrics
track visibility across
digital media



EXTENSIVE PROMOTION

Marketing
and promotion
of impactful research



LOOP RESEARCH NETWORK

Our network
increases your
article's readership